VNIVERSITAT DE VALÈNCIA

Dark Matter Phenomenology: Sterile Neutrino Portal and Gravitational Portal in Extra-Dimensions

PhD Thesis

Miguel García Folgado

IFIC - Universitat de València - CSIC
Departamento de Física Teórica
Programa de Doctorado en Física

Under the supervision of

Andrea Donini
Nuria Rius Dionis
Roberto Ruiz de Austri Bazan

Valencia, Marzo 2021

Andrea Donini, Científico titular del Consejo Superior de Investigaciones Científicas,

Nuria Rius Dionis, Catedrática del departamento de Física Teórica de la Universidad de Valencia, y

Roberto Ruiz de Austri Bazan, Científico titular del Consejo Superior de Investigaciones Científicas,

Certifican:

Que la presente memoria, **Dark Matter Phenomenology: Sterile Neutrino Portal and Gravitational Portal in Extra-Dimensions** ha sido realizada bajo su dirección en el Instituto de Física Corpuscular, centro mixto de la Universidad de Valencia y del CSIC, por **Miguel García Folgado**, y constituye su Tesis para optar al grado de Doctor en Ciencias Físicas.

Y para que así conste, en cumplimiento de la legislación vigente, presenta en el Departamento de Física Teórica de la Universidad de Valencia la referida Tesis Doctoral, y firman el presente certificado.

Valencia, a 10 de Diciembre de 2020,

Andrea Donini   Nuria Rius Dionis   Roberto Ruiz de Austri Bazán

Comité Evaluador

Tribunal titular

Dr. Alberto Casas González	Universidad Autónoma de Madrid
Dr. Matthew McCullough	University of Cambridge/CERN
Dr. Verónica Sanz González	Universitat de València

Tribunal suplente

Dr. Arcadi Santamaría Luna	Universitat de València
Dr. David García Cerdeño	Universidad Autónoma de Madrid
Dr. Geraldine Servant	Deutsches Elektronen Synchrotron

A mi familia, amigos y Andrea.
Sin vuestro apoyo incondicional
esta tesis no existiría

It’s a dangerous business
going out your door. You step
onto the road, and if you don’t
keep your feet, there’s no knowing
where you might be swept off to.

J. R. R. Tolkien,
The Lord of the Rings

List of Publications

This PhD thesis is based on the following publications:

- *Probing the sterile neutrino portal to Dark Matter with γ rays* [1],
  Miguel G. Folgado, Germán A. Gómez-Vargas, Nuria Rius and Roberto Ruiz De Austri.
  JCAP **1808** (2018) 002, [`arXiv:1803.08934`].

- *Gravity-mediated Scalar Dark Matter in Warped Extra-Dimensions* [2],
  Miguel G. Folgado, Andrea Donini and Nuria Rius.
  JHEP **01** (2020) 161, [`arXiv:1907.04340`].

- *Gravity-mediated Dark Matter in Clockwork/Linear Dilaton Extra-Dimensions* [3],
  Miguel G. Folgado, Andrea Donini and Nuria Rius.
  JHEP **04** (2020) 036, [`arXiv:1912.02689`].

- *Kaluza-Klein FIMP Dark Matter in Warped Extra-Dimensions* [4],
  Nicolas Bernal, Andrea Donini, Miguel G. Folgado and Nuria Rius.
  JHEP **09** (2020) 142, [`arXiv:2004.14403`].

Other works not included in this thesis are:

- *On the interpretation of non-resonant phenomena at colliders* [5], Miguel G. Folgado and Veronica Sanz. [arXiv:2005.06492].

- *Spin-dependence of Gravity-mediated Dark Matter in Warped Extra-Dimensions* [6], Miguel G. Folgado, Andrea Donini and Nuria Rius. [arXiv:2006.02239].

- *Exploring the political pulse of a country using data science tools* [7], Miguel G. Folgado, Veronica Sanz. [arXiv:2011.10264].

- *Kaluza-Klein FIMP Dark Matter in Clockwork/Linear Dilaton Extra-Dimensions* [8], Nicolas Bernal, Andrea Donini, Miguel G. Folgado and Nuria Rius. [arXiv:2012.10453].

Abbreviations

ΛCDM	The standard cosmological model
AdS	Anti-de-sitter
ATLAS	Spin dependent
ALPs	Axion Like Particles
BBN	Big Bang nucleosintesis
BE	Bose-Einstein
BSM	Beyond the standard model
CC	Electroweak Charged Currents
CDM	Cold dark matter
CERN	Conseil EuropÃĺen pour la Recherche NuclÃĺaire
CFT	conformal field theories
CMB	Cosmic Microwave Background
CMS	Spin dependent
CNNS	coherent neutrino-nucleus scattering
CKM	Cabibbo-Kobayashi-Maskawa matrix
COBE	Cosmic Background Explorer
CP	Charge-conjugate Parity
CPT	Charge-conjugate Parity time

CW/LD	Clockwork/Linear Dilaton
DD	Direct Detection
DRU	Differential rate unit
dSphs	dwarf spheroidal galaxies
ED	Extra-Dimensions
EW	Electroweak
EWSB	Electroweak symmetry breaking
FD	Fermi-Dirac
FIMP	Feebly Interactive Massive Particle
FLRW	Friedman-Lemaître-Robertson-Walker Metric
GC	Galactic Center
GCE	Galactic Center γ-ray Excess
GIM	Glashow-Iliopoulos-Maiani mechanism
HDM	Hot dark matter
ID	Indirect Detection
KK	Kaluza-Klein
LED	Large Extra-Dimensions
LHC	Large hadron collider
LSB	low surface brightness
NC	Electroweak Neutral Currents
NFW	Navarro, Frenk and White
PMNS	Pontecorvo-Maki-Nakagawa-Sakata
QED	Quantum Electrodynamics Detection
QCD	Quantum Chromodynamics

RS	Randall-Sundrum
SD	Spin dependent
SI	Spin independent
SIDM	Self-interactive dark matter
SM	Standard Model
SSB	Spontaneous Symmetry Breaking
SUSY	Supersymmetry
UED	Universal Extra-Dimensions
VEV	Vacuum Expectation Value
WDM	Warm dark matter
WIMP	Weakly Interactive Massive Particle
WMAP	Wilkinson Microwave Anisotropy Probe

List of Figures

List of Tables

Preface

The Standard Model of Fundamental Interactions (SM) represents one of the most precise theories in physics. Among the predictions of the SM we find, for instance, the *anomalous magnetic moment* of the electron $a_e = 0.001159652181643(764)$ [9, 10]. This prediction agrees with the experimental results to more than ten significant digits, the most accurate prediction in the history of physics. However, nowadays we have several evidences that the SM only explains 5% of the matter content of the Universe. The other 95% are composed by the so-called Dark Energy and Dark Matter. As their names suggest, the nature of these two components of the energy/matter content of the Universe is still unclear and represents one of the most important challenges for the particle physicists. In this Thesis we have focused in the study of the phenomenology of one of these mysterious components of the Universe, the Dark Matter. Although we have many evidences of its existence, this new type of matter has not been detected yet. As a consequence, the landscape of the models that can explain the Dark Matter properties is huge. In the present work we propose and study several Dark Matter models, setting limits by using experimental results.

This Thesis is organized in three parts: introduction (Part I), scientific research (Part II) and Resumen de la Tesis (Part III). First, in Part I we provide an overview of the current status of the Dark Matter physics: Chapter 1 explains the fundamental properties of the Standard Model, showing its different open problems. In Chapter 2 we review the standard cosmological model ΛCDM. Chapter 3 summarizes the fundamental properties and evidences of Dark Matter. Chapter 4 deals with the tools needed to understand the thermal evolution of cold relics, which plays a central role in this Thesis. In Chapter 5 we review the Dark Matter experimental landscape, focusing in Direct Detection and Indirect Detection. Chapter

6 discusses the fundamental tools to understand extra-dimensional models. To conclude, in Chapter 7 we summarize the most important results of the publications that compose this Thesis. In Part II we present a collection of the publications done during the research.

Finalmente, la Parte III consiste en un resumen de la Tesis en español. Este resumen está compuesto por dos partes: en la primera parte se explican de forma general las características, evidencias, etc. de la Materia Oscura, mientras que en la segunda parte se resumen los artículos que componen la presente Tesis.

Agradecimientos

Si esta Tesis existe es gracias al apoyo y a la ayuda de toda la gente que me rodea. Me gustaría hacer unos agradecimientos que estén a la altura de todo lo que habéis hecho por mí, pero creo que eso va a ser más difícil que escribir cualquiera de los capítulos que componen este libro. Aunque aún no sé muy bien cómo escribir esta parte, si tengo muy claro por quien empezar. Este trabajo no hubiese sido posible sin la dedicación y la ayuda incondicional de mis directores, Andrea, Nuria y Roberto. Investigar junto a vosotros durante estos cuatro años ha sido todo un placer. Sería imposible cuantificar la gran cantidad de cosas que me habéis enseñado durante este tiempo.

Roberto, te agradezco enormemente tu guía durante las primeras etapas de la Tesis. Gracias al tiempo que trabajamos juntos desarrollé todas mis habilidades con la programación, las cuales valoro muchísimo. Tu dedicación al trabajo siempre me ha parecido impresionante, espero que se me haya quedado algo de tu productividad.

Andrea, aunque solo hemos trabajado juntos durante la segunda mitad del doctorado, has sido un pilar clave en esta Tesis. Desde que empezamos a colaborar has estado pendiente de mí, tus consejos han sido vitales para el desarrollo de todos nuestros proyectos. Tu meticulosa forma de abordar los problemas siempre me ha fascinado, cada vez que hablamos, tu pasión por la física teórica prácticamente se palpa en el ambiente. Espero que se me haya pegado algo de tu forma de trabajar, porque la verdad es que me encanta.

Nuria, tu tiempo y dedicación durante el desarrollo de la Tesis han significado mucho para mí. Siempre con la puerta de tu despacho abierta, dispuesta a hablar de física sea la hora que sea. Me ha encantado la forma en que me has guiado a lo largo de estos años, apoyándome en todo momento y dándome los conocimientos necesarios para llevar a cabo nuestros proyectos, a la vez que me dotabas de autonomía suficiente para desarrollar las ideas por mí mismo. Quiero pensar que el doctorado me ha hecho una persona más independiente y autosuficiente, y eso te lo debo todo a ti, muchas gracias por todo.

Además de a mis directores, me gustaría agradecer también a Nicolás Bernal, con quien he tenido el placer de colaborar en un par de proyectos y de quien he aprendido muchísimo sobre Materia Oscura FIMP, y a Verónica Sanz, que me ha enseñado lo apasionante que puede ser la investigación en temas más allá de la física.

Mis directores no son los únicos que me han ayudado a escribir y corregir esta Tesis, estoy infinitamente agradecido a Andrea, Eva, Iván (desde que te marchaste a Londres se echan tanto de menos nuestros partidos de padel y frontón y nuestras cervezas... ¡Vuelve pronto!), Pablo, Pau y Stefan por echarme una mano con las correcciones ortográficas de los capítulos en inglés, así como a mi hermana, por ayudarme con la ortografía de la parte en español. ¡Muchas gracias a todos! No se que haría sin vosotros (tengo que buscar alguna forma de compensaros esto...).

Aparte de la gente que ha participado activamente en mi investigación, quiero agradecer al resto de miembros del grupo SOM: Olga Mena, Pilar Hernández y Carlos Peña. Muchas gracias por todas las charlas, meetings y discusiones en general. Ha sido genial compartir estos años con vosotros, viviendo vuestra pasión por la física de partículas. Además de por lo mucho que he disfrutado en el grupo, siempre estaré en deuda con vosotros por financiarme el doctorado y por darme la oportunidad de visitar Fermilab y la Universidad de Tokyo (y por los muchos congresos a los que he podido asistir gracias a vosotros), estancias que me han encantado y que han significado mucho para mi a nivel personal. Por supuesto, también estoy muy agradecido de haber compartido esta experiencia con lo miembros más nuevos del grupo, Dani Figueroa y Jacobo López. Muchas gracias Jacobo por haberme dado estabilidad económica durante este último año, gracias a ti he podido finalizar esta Tesis. Finalmente, y no menos importante, quiero agradecer también a los doctorandos y postdocs del grupo: Andrea Caputo, David, Fer, Hector, Jordi, Miguel Escudero, Pablo, Sam, Stefan y Victor. Esta experiencia no hubiese sido lo mismo sin vosotros.

Del mismo modo que agradezco a mi grupo la oportunidad que me han dado permitiéndome hacer las estancias y asistir a diversos congresos, quiero dar las gracias a las universidades que me acogieron en estos eventos. En especial quiero darle las gracias a Pedro Machado, por hacerme sentir en Fermilab como en mi propia casa, y a toda la IPMU en general, por la gran acogida que me dieron en Tokyo. Aparte de en lo profesional, estas dos estancias no hubiesen sido nada a nivel personal de no ser por Brais, con quien viví un montón de aventuras y comí miles de hamburguesas en EEUU (conseguiste contagiarme tu pasión por esta joya gastronómica), y por Pablo, con quien recorrí todo Japón y visité lugares que jamás olvidaré (de no ser por tu iniciativa y tus grandes ansias de viaje la estancia no hubiese sido ni la mitad de lo que fue).

La investigación no ha sido la única labor que he desempeñado durante estos años, también he podido experimentar la docencia, la cual me ha sorprendido muy gratamente. Hasta entrar en el doctorado nunca me planteé siquiera que dar clase pudiese gustarme, pero ha resultado ser una de las actividades que más he disfrutado. Quiero agradecer a Arcadi Santamaría y a Mariam Tórtola, con quienes he tenido el placer de compartir esta experiencia, por toda la autonomía que me han dado y lo mucho que me han enseñado de este bello arte. Así mismo, quiero agradecer a todos los alumnos a los que he dado clase durante este tiempo, no se cuánto habrán aprendido ellos de mí, pero espero que sea comparable a lo mucho que he aprendido yo de ellos.

Durante estos cuatro años he compartido el IFIC con gente genial. En especial me gustaría darle las gracias a Avelino por las muchas oportunidades que me ha dado para hablar y presentar mis trabajos en el journal club, la calidez del hogar siempre es el mejor lugar para practicar charlas y debatir sobre física.

A nivel personal, los años de doctorado me han dejado un montón de experiencias que no cambiaría por nada. Me alegro muchísimo de haber compartido este tiempo con Juan (nuestro año viviendo juntos fue una pasada), Pablo y Stefan, los días en el IFIC no hubiesen sido lo mismo sin

nuestras meriendas y almuerzos. Al igual que no hubiesen sido lo mismo sin las quedadas con vosotros y con Brais, Inma y Lydia (nunca me canso de vivir aventuras contigo, ni lo haré jamas), sois lo mejor que me ha dado el doctorado. Nuestras escapadas a Moixent durante los meses post cuarentena fueron geniales.

Esta Tesis no solo cierra el doctorado, para mi representa el final de una etapa que comenzó hace ya diez años, cuando empecé la carrera. Dicen que los años universitarios se recuerdan siempre como la mejor etapa de la vida, y en mi caso se ha cumplido totalmente. Los amigos que hice durante aquellos años han estado siempre a mi lado, hemos vivido infinidad de cosas juntos y no los cambiaría absolutamente por nada, si aquellos años fueron tan fantasticos es gracias a vosotros. Primero me gustaría agradecer a mis amigos de física, Andrea Gonzalez, Andrés, Iván, Lydia, Marina, Pau y Román, con quienes he vivido viajes, paellas, carnavales, fiestas y, en resumen, un montón de aventuras desde que nos conocimos, y espero seguir haciéndolo siempre, nunca me canso de estar con vosotros. A mis amigas de bioquímica, Eva, Marcela y Carla, hicisteis que aquellas noches de estudio fuesen geniales (en general no muy productivas, pero inmejorables). Y, finalmente, a Laura, tus consejos siempre me han ayudado a seguir adelante. Mi vida como investigador empezó con todos vosotros, no se me ocurre un comienzo mejor.

Ademas de a mi gente de la uni, quiero agradecer a mis amigos del barrio por estar siempre ahí, tanto en los buenos como en los malos momentos. Abraham, Raul y Rover, no podría imaginarme la vida sin vosotros, de hecho hace tanto que estamos juntos que casi ni recuerdo como era todo antes de conoceros. Siempre me he considerado una persona muy afortunada, y es gracias a vosotros. Alba y Victor, aunque nos conocemos de hace menos tiempo también sois vitales para mi, por muy malo que haya sido el día, cuando estoy con vosotros conseguís que se me olvide. Finalmente, me alegro mucho de haberte conocido Bea, siempre consigues que una tarde/noche cualquiera sea genial, por supuesto con un buen café o una cerveza de por medio.

Quiero agradecer también a toda mi familia por apoyarme incondicionalmente y por haber estado a mi lado desde que tengo memoria. En general, le doy las gracias a mis abuelas, abuelos, tías, tíos, primas y primos por todo lo que hemos vivido juntos y por todo el amor y el cariño que me habéis transmitido a lo largo de toda mi vida. A mi madre, por cuidarme desde que tengo uso de razón. Siempre has apostado por mi, a pesar de que al principio me costase encontrar mi camino. A mi padre, no solo por el afecto que me has mostrado durante toda mi vida, también por transmitirme todas tus inquietudes intelectuales sobre astrofísica y cosmología. Todas las historias que me contabas de pequeño sobre la teoría de la relatividad y sobre el tiempo hicieron mella en mi y han acabado convirtiéndome en quien soy. Y finalmente, y para nada menos importante, todo lo contrario, a mi hermana, por su alegría y por aguantarme y quererme siempre tal como soy, con todos mis (muchos) defectos y virtudes.

Por último, quiero darle las gracias a Andrea: desde que nos conocimos has estado siempre ahí, soportando todas mis tonterias, mostrándome siempre todo tu apoyo y amor. Me encanta como eres, la persona más dulce que he conocido, aunque fuerte y dura cuando es necesario (sin ti no se cuánto tiempo hubiese tardado en escribir esta Tesis). No puedo imaginarme la vida sin nuestros paseos, nuestras series y pelis, nuestras cenas y, en definitiva, sin ti.

Después de leer esta parte como cincuenta veces creo que estoy contento con como ha quedado, así que ya, sin más dilación, ¡os dedico esta Tesis!

Contents

Part I

Introduction

Chapter 1

Standard Model of Particles: A Brief Review

Humankind have always tried to understand the great mysteries of the Universe, as well as those of the matter that surrounds us. The Greeks were the first to try to model nature by postulating that all forms of matter can be understood starting from four fundamental elements: water, earth, fire and air. It took thousands of years to refine this description. In the 17th century the first definition of a chemical element was made and after two centuries (1869) the periodic table of the elements was published, which order them according to their chemical properties, with a number of elements very similar to that we know today.

The high number of elements that were known at the beginning of the 20th century led us to think that there had to be a more elementary underlying structure that we did not understand. It was finally Niels Bohr who first proposed the current atomic theory [12–14], in which matter was explained by electrons, protons, and subsequently neutrons. This simplified theory was refined over the years, giving birth to in the Standard Model of Fundamental Interactions (SM).

The model accurately describes nature at the microscopic level using a total of twelve elementary particles that constitute matter at the fundamental level and three force fields. The gravitational field is excluded from

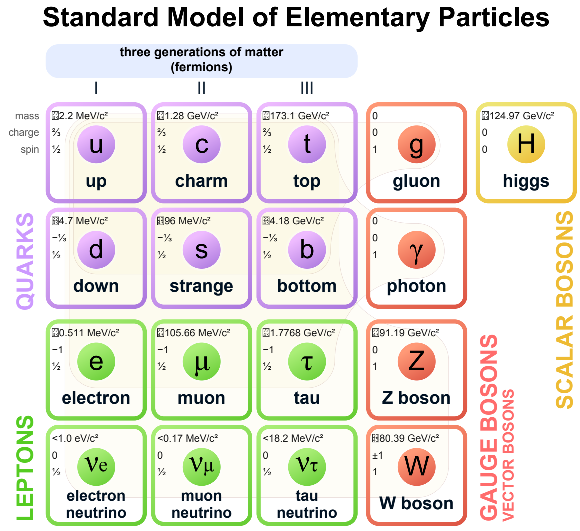

Figure 1.1: *Standard model of particles: Purple, green and red particles represents, respectively, quarks, leptons and gauge bosons. The yellow particle represents the Higgs boson. Image taken from Ref. [11].*

this description since, to this day, the principles of the quantum world and the theory of General Relativity have not been reconciled.

1.1. Particle Content

The Standard Model of particles [15–25] is a relativistic quantum field theory with gauge symmetry $SU(3)_C \times SU(2)_L \times U(1)_Y$ (in the next section we provide a quick justification for the choice of these groups). The model describes with great precision the strong, weak and electromagnetic interactions through the exchange of different spin-1 fields, which constitute the gauge bosons of the theory. The symmetry group $SU(3)_C$ is the one associated with strong interactions, while $SU(2)_L \times U(1)_Y$ is the symmetry group of the Electroweak Theory, that unifies electromagnetic and weak interactions.

The fundamental constituents of matter are fermions, described by the fermionic sector of the Standard Model. It is made up of quarks and leptons, both types of particles separated into three flavour families. Quarks are charged under $SU(3)_C$. As a consequence, each quark appears in the model in three different colours. Leptons can be separated into two kinds of

Particle	**Discovered at**	**Mass**	**charge**	**spin**	**lifetime [s]**
Electron e	Cavendish Laboratory (1897) [26]	510.9989461(31) keV	-1	1/2	Stable
muon μ	Caltech (1937) [27]	105.6583745(24) MeV	-1	1/2	2.2×10^{-6}
tau τ	SLAC (1976) [28]	1776.86(12) MeV	-1	1/2	2.9×10^{-13}
neutrino ν_e	Savannah River Plant (1956) [29]	< 2 eV	0	1/2	Stable
neutrino ν_μ	Brookhaven (1962) [30]	< 2 eV	0	1/2	Stable
neutrino ν_τ	Fermilab (2000) [31]	< 2 eV	0	1/2	Stable
quark u	SLAC (1968) [32, 33]	2.2(5) MeV	2/3	1/2	Stable
quark d	SLAC (1968) [32, 33]	4.7(5) MeV	$-1/3$	1/2	Stable
quark c	Brookhaven & SLAC (1974) [34, 35]	1.275(35) GeV	2/3	1/2	1.1×10^{-12}
quark s	SLAC (1968) [32, 33]	95(9) MeV	$-1/3$	1/2	1.24×10^{-8}
quark t	Fermilab (1995) [36]	173.0(4) GeV	2/3	1/2	4.6×10^{-25}
quark b	Fermilab (1977) [37]	4.18(4) GeV	$-1/3$	1/2	1.3×10^{-12}
photon γ	Washington University (1923) [38]	$< 10^{-18}$ eV	0	1	Stable
gluon G	DESY (1979) [39]	0	0	1	Stable
$W^{\pm}$ boson	CERN (1983) [40, 41]	80.379(12) GeV	± 1	1	3.2×10^{-25}
Z boson	CERN (1983) [42, 43]	91.1876(21) GeV	0	1	2.6×10^{-25}
Higgs boson H	CERN (2012) [44, 45]	125.18(16) GeV	0	0	$> 5.1 \times 10^{-23}$

Table 1.1: Properties of SM particles. Idea taken from [46]. The different data has been extracted from [47]. Up, down and strange quark masses are estimates of so-called *current quark masses*. On the other hand, charm and beauty quark masses are the *running* masses, while the top quark mass comes from direct measurements.

particles: charged leptons and neutrinos (the SM predicts zero mass for the neutrinos). The Standard Model is a chiral gauge theory, in the sense that it treats differently particles with right- and left-handed chiralities, grouping the right-handed in singlets and the left-handed in doublets under the symmetry group $SU(2)_L$. The properties of all these particles are collected in the Review of Particle Physics [47], published and reviewed annually by the Particle Data Group (PDG). To date, no evidence of the existence of right-handed neutrinos has been found, so that they are not included in the model:

$$\begin{aligned}
1^{\text{st}}\,\text{Family} : L_1 &\equiv \begin{pmatrix} \nu_e \\ e^- \end{pmatrix}_L ; \; e_1 \equiv e^-_R \, ; \; Q_1 \equiv \begin{pmatrix} u \\ d \end{pmatrix}_L ; \; U_1 \equiv u_R \, ; \; D_1 \equiv d_R \, , \\
2^{\text{nd}}\,\text{Family} : L_2 &\equiv \begin{pmatrix} \nu_\mu \\ \mu^- \end{pmatrix}_L ; \; e_2 \equiv \mu^-_R \, ; \; Q_2 \equiv \begin{pmatrix} c \\ s \end{pmatrix}_L ; \; U_2 \equiv c_R \, ; \; D_2 \equiv s_R \, , \\
3^{\text{rd}}\,\text{Family} : L_3 &\equiv \begin{pmatrix} \nu_\tau \\ \tau^- \end{pmatrix}_L ; \; e_3 \equiv \tau^-_R \, ; \; Q_3 \equiv \begin{pmatrix} t \\ b \end{pmatrix}_L ; \; U_3 \equiv t_R \, ; \; D_3 \equiv b_R \, .
\end{aligned}$$

The different interactions are mediated by spin-1 particles, the so-called gauge bosons. The electromagnetic and strong interactions are mediated by the photon γ and the gluon G^a (with $a = 1, ..., 8$), respectively, and have an infinite range of interaction, due to the zero mass of the mediators. The weak interactions are mediated by the massive $W^\pm$ and Z bosons; due to the mass of the mediators the weak interaction is a short-range force. Eventually, the only spin-0 particle in the model is the Higgs boson, the most recently discovered components of the SM. The interaction of the Higgs field with the rest of the particles explains the mass generation in the SM. The different properties of particles and mediators of the SM are collected in Tab. 1.1.

1.2. Electroweak Unification: The Election of $SU(2)_L \times U(1)_Y$

Having understood the components of the Standard Model that we observe in experiments, we will try to establish the theoretical framework in which the interactions between the different fermions take place. In order to do this, we must first talk about the choice of the symmetry group.

The description of the weak interactions was one of the great problems of the second half of the 20th century. At that moment, only one gauge theory was known: Quantum Electrodynamics (QED) [48–54] that describes the electromagnetic interactions. The structure of QED is very simple, as the gauge group is $U(1)$, the only mediator is the photon. Its simplicity allows to point out clearly two important characteristics of every gauge theory: on the one hand, the interaction is composed by a gauge field times a fermionic current; on the other hand, the associated charge in QED is the symmetry group generator. However, the observation of the parity violation [55, 56] makes weak interactions totally different from QED.

The election of $SU(2)$ to describe a gauge theory of the weak interaction seems logic: experimentally, we observe three gauge bosons $(W^{\pm}, Z^0)$ and $SU(2)$ has three generators. The weak interaction between charged leptons and neutrons would be described by the Lagrangian

$$\mathcal{L} \propto (J_\mu W^\mu + \text{h.c}) \,, \tag{1.1}$$

with

$$J_\mu \equiv \bar{\nu}_e \gamma_\mu (1 - \gamma_5)\, e \,, \tag{1.2}$$

where J_μ is the weak current and γ_μ and γ_5 are Dirac matrices[1]. The gauge bosons in this group are denoted as $W_i^\mu = (W_1^\mu, W_2^\mu, W_3^\mu)$. This description has several problems, starting with the fact that the term with W_3 is not electrically neutral. On the other hand, the three charges of this Lagrangian (T_1, T_2, T_3) do not form a closed algebra.

[1] There are many books where it is possible to find a complete description of the algebra of these matrices [57, 58], known as Clifford Algebra.

$SU(2)$ can not explain the weak interaction since $m_Z \neq m_W$, but $SU(2) \times U(1)$ can explain it[2] (at the same time that unifies it with the electromagnetic interaction!). The $U(1)$ group of this new theory is different to the $U(1)$ of QED. The conserved charge in this case is not the electrical charge Q. The gauge boson of this new $U(1)$ symmetry group is denoted as B^μ. In order to obtain zero electrical charge for all Lagrangian terms, at the same time that it mixes charged leptons and neutrinos, a complicate structure that differentiate between left- and right-handed fields is needed. The left-handed fields are charged under the $SU(2)$ while the right-handed fields are neutral under this group (for this reason the group is labelled as $SU(2)_L$). This charge is the so-called *weak isospin*, T_3. On the other hand, the charge of the new $U(1)$ group Y receives the name of *hypercharge* and is related with Q and T_3 by $Y = Q - T_3$.

The unification of QED and the weak interactions receives the name of the *Electroweak Theory* [15–17].

1.3. Quantum Chromodynamics (QCD): The Strong Interaction Gauge Group

The gauge theory that describes the strong interactions is called Quantum Chromodynamics (QCD). The fundamental structure of QCD is similar to the QED structure, both are vector theories: left- and right-handed representations are the same. Such as in the QED case, QCD presents a conserved charge called *colour*. The particles that have colour charge in the SM are the quarks while QCD mediators are the gluons, which contrary to the photon also have color. Despite the similarities, QCD has two main properties that makes it totally different to QED. On the one hand, the theory presents color confinement: it is impossible to observe free particles with colour charge. On the other hand, the theory has asymptotic freedom: discovered by David Gross [60] and Frank Wilczek [61] in 1973,

[2]Historically, the election of the group was not clear until the observation of the Z boson mass. If the mass of the three mediators would have been equal, $m_Z = m_W$, the gauge group $O(3)$ [59] could have explained the weak interaction. However, the discovery that m_Z and m_W are related via the Weinberg angle was the key to understand that $SU(2) \times U(1)$ was the correct gauge group.

Particle Name	**Field**	$SU(3)_C \times SU(2)_L \times U(1)_Y$
Quarks left-handed	Q_α	$(3, 2, 1/6)$
Quarks right-handed	U_α	$(3, 1, 1/6)$
	D_α	$(3, 1, -1/3)$
Lepton left-handed	L_α	$(1, 2, -1/2)$
Lepton right-handed	e_α	$(1, 1, -1)$

Table 1.2: Charge of the different SM fermionic components under the gauge fields of the SM $SU(3)_C \times SU(2)_L \times U(1)_Y$. In all fields $\alpha = 1, 2, 3$ represents the family.

this property can be described as a reduction in the strength of interactions between quarks and gluons, going from low to high-energy. This two properties makes Quantum Chromodynamics one of the most complex theories in particle physics, as at low energies the relevant degrees of freedom are not quarks and gluons (that are confined) but colourless mesons and baryons. A complete description of this theory can be found in Ref. [62].

Until the present day, the Electroweak Theory and QCD have not been properly unified. However, both theories can be grouped under the simple group:

$$G = SU(3)_C \times SU(2)_L \times U(1)_Y, \tag{1.3}$$

the gauge symmetry group of the Standard Model. The different charges of the right- and left-handed fermionic fields under the electroweak symmetry group are summarized in Tab. 1.2.

1.4. Standard Model Lagrangian without masses

In the previous section we have established the gauge symmetry group of the theory. The gauge fields of $SU(2)_L \times U(1)_Y$ are $W_i^\mu = (W_1^\mu, W_2^\mu, W_3^\mu)$ and B^μ, while the QCD gauge boson is the gluon G_a^μ, where $(a = 1, ..., 8)$. It is very common to distinguish between two sectors to describe the SM Lagrangian: the gauge sector, that describes the interactions between the different gauge fields, and the fermionic sector, that describes the matter Lagrangian.

The Lagrangian that describes the gauge sector can be written as:

$$\mathcal{L}_{\text{kin,gauge}} = -\frac{1}{4}G^a_{\mu\nu}G^{\mu\nu}_a - \frac{1}{4}W^i_{\mu\nu}W^{\mu\nu}_i - \frac{1}{4}B_{\mu\nu}B^{\mu\nu}\,, \tag{1.4}$$

where, from the gauge fields, the following tensors have been defined

$$\begin{cases} G^a_{\mu\nu} &= \partial_\mu G^a_\nu - \partial_\nu G^a_\mu + g_s f^{abc} G^b_\mu G^c_\nu & a,b,c = 1,...,8\,; \\ W^i_{\mu\nu} &= \partial_\mu W^i_\nu - \partial_\nu W^i_\mu + g\epsilon^{ijk} W^j_\mu W^k_\nu & i,j,k = 1,2,3\,; \\ B_{\mu\nu} &= \partial_\mu B_\nu - \partial_\nu B_\mu\,, \end{cases} \tag{1.5}$$

being (g_s, g, g') the different couplings of each symmetry group of the SM, $SU(3)_C$, $SU(2)_L$ and $U(1)_Y$, respectively. In the above expressions f^{abc} and ϵ^{ijk} are the antisymmetric structure constants of the $SU(3)_C$ and $SU(2)_L$ gauge groups and are defined through the commutators of the different group generators

$$\begin{cases} [\lambda_a, \lambda_b] &= i f^{abc}\lambda_c\,, \\ [\sigma_i, \sigma_j] &= 2i\epsilon^{ijk}\sigma_k\,, \end{cases} \tag{1.6}$$

where λ and σ are the Gell-Mann and Pauli matrices.

The Lagrangian that describes the fermionic content of the Standard Model can be written as

$$\begin{aligned} \mathcal{L}_{\text{kin,fermions}} &= i\sum_\alpha \Big(\bar{Q}_\alpha\gamma^\mu\mathcal{D}_\mu Q_\alpha + \bar{U}_\alpha\gamma^\mu\mathcal{D}_\mu U_\alpha + \bar{D}_\alpha\gamma^\mu\mathcal{D}_\mu D_\alpha \\ &+ \bar{L}_\alpha\gamma^\mu\mathcal{D}_\mu L_\alpha + \bar{e}_\alpha\gamma^\mu\mathcal{D}_\mu e_\alpha\Big)\,, \end{aligned} \tag{1.7}$$

where the sum is over the three flavour families. $\mathcal{D}_\mu$ is the covariant derivative that preserves the gauge invariance of the Lagrangian and γ^μ are the Dirac matrices. The covariant derivative can be written as

$$\mathcal{D}_\mu \equiv \partial_\mu - ig_s\frac{\lambda_a}{2}G^a_\mu - ig\frac{\sigma_i}{2}W^i_\mu - ig'YB_\mu\,, \tag{1.8}$$

where the interaction with a given gauge boson arises only if the matter field is charged under the corresponding group.

With the Lagrangian described in this section, the particle content of the SM is fixed. The problem with this description is that the SM does not accept the existence of masses for any field. On the one hand, left- and right-handed fermions are different with respect to the $SU(2)_L$ gauge group. This fact makes it impossible to write gauge invariant mass terms for the fermions in the Lagrangian. On the other hand, any mass term for the gauge fields is not gauge invariant. As a consequence, all gauge and fermionic fields are massless in the described theory. If the weak theory did not exist, this issues would not affect the description of QED and QCD: in both theories, left- and right-handed representations of the fermions fields are the same and the mediators (gluons and photons) are massless. However, the $SU(2)_L$ description of the weak interaction and the fact that the range of this interaction is finite (which implies massive mediators) points out a problem of the Lagrangian in Eq. 1.4 and 1.7.

In order to understand the problem with the fermion masses we must remember the structure of the electroweak interaction and the different treatment of the right-handed (singlets of $SU(2)_L$) and left-handed (doublets of $SU(2)_L$) fields. The mass terms usually have the form

$$m_\psi \bar{\psi}\psi = m_\psi \left(\psi_L^\dagger \psi_R + \psi_R^\dagger \psi_L \right) . \tag{1.9}$$

As a consequence of the different representation of left- and right-handed fields under the $SU(2)_L$ group, Eq. 1.9 can not be part of the Lagrangian because it explicitly breaks $SU(2)_L$ invariance. For this reason, in Eq. 1.7 these kind of terms are not present.

1.5. The Higgs Mechanism

The scalar sector was the last stone added to the SM at the turn of the beginning of the 21st century. The gauge bosons of the Electroweak Theory have mass. However, gauge invariance forbids explicit mass terms in the Lagrangian. The solution to this problem was proposed by Peter Higgs, Robert Brout, Francois Englert, Gerald Guralnik, Carl Richard Hagen and Tom Kibble in 1962 and developed in what is currently known as the Higgs Mechanism [18–21].

The Higgs Mechanism is based on the idea of the Spontaneous Symmetry Braking (SSB). The symmetry that we have to break is the electroweak symmetry, that has four generators, or four gauge bosons. The final four bosons have to be $(W^{\pm}_{\mu}, Z^0_{\mu})$ and A_μ (the gauge field of QED, the photon), of which three have non-zero mass. On the one hand, the Electroweak Theory mixes the weak neutral currents with the hypercharge one; on the other hand, we know that QED has only one generator. In other words, the Higgs Mechanism must break the electroweak symmetry to QED:

$$SU(2)_L \times U(1)_Y \longrightarrow U(1)_{\text{EM}}\,. \tag{1.10}$$

The idea of the mechanism consists in to add a new scalar field with a non-zero vacuum value that breaks the symmetry, giving masses to the fermions and gauge fields. The question now is, how must be the structure of this new field?

Before starting to describe the Higgs Mechanism it is important to understand the meaning of SSB. According to the Noether theorem [63], each Lagrangian symmetry implies a conserved charge. This theorem was proposed for classical mechanics and is totally valid in quantum mechanics and quantum field theory. However, there are two different ways to realize the theorem in Nature. On the one hand, the most common one is to assume that the vacuum is symmetric under the associated transformation (if Q represents the charge operator, then $Q|0\rangle = 0$). This quantization mechanism is known as Wigner-Weyl quantization [64] and the symmetries that describes are called *exact symmetries*. On the other hand, if the vacuum state is not symmetric under some Lagrangian symmetry ($Q|0\rangle \neq 0$) we say that the symmetry is spontaneously broken. This case is known as Nambu-Goldstone quantization [65, 66] and its most relevant consequence is the prediction of massless bosons associated with the broken symmetry, known as *Goldstone bosons*[3]. More concretely, for each broken generator of the theory a new Goldstone boson appears. Fig. 1.10 shows a representation

[3]The prediction is known as *Goldstone theorem*.

of the implications of this kind of symmetries. Despite the fact that the potential is symmetric under a certain transformation, its vacuum state is not (it presents a non-zero expectation value).

The Higgs Mechanism breaks three generators of the original Electroweak Theory. In order to break the Electroweak Theory as in Eq. 1.10, according to the Goldstone theorem, three massless real scalar fields appear. These fields are *eaten* by the gauge bosons of the Electroweak Theory, becoming on its longitudinal degrees of freedom and providing masses for the particles of the SM. One of this new real scalar fields takes a non-zero *vacuum expectation value* (VEV), providing the structure for the mass terms of the Lagrangian. This field must be electrically neutral. The reason is easy: the electromagnetism is an exact symmetry of the vacuum and, as a consequence, the field that takes the VEV cannot be charged under $U(1)_{\mathrm{EM}}$.

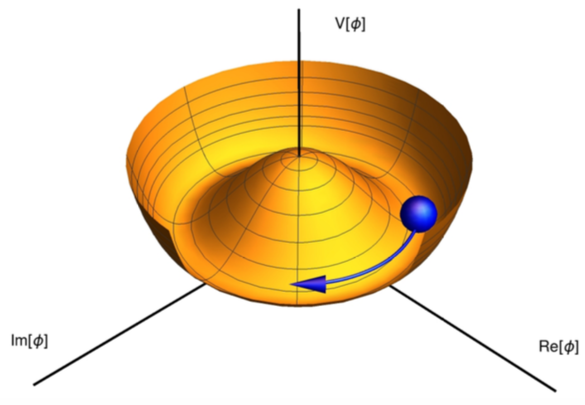

Figure 1.2: *Representation of the Spontaneous symmetry Breaking.*

As the theory does not allow terms like Eq. 1.9 for the fermions, it is necessary that the new field couples to the left-handed doublets of $SU(2)_L$ to generate this kind of mass terms. The minimal candidate that fulfills all requirements is

$$\Phi = \begin{pmatrix} \Phi^+ \\ \Phi^0 \end{pmatrix} = \begin{pmatrix} \Phi^+ \\ \frac{1}{\sqrt{2}}(v + \phi_1 + i\phi_2) \end{pmatrix}, \tag{1.11}$$

where the Φ^+ is a complex scalar field, ϕ_1 and ϕ_2 are real scalar fields and v is the VEV of the Higgs field. The charges of this field under the gauge groups of the SM $SU(3)_C \times SU(2)_L \times U(1)_Y$ are $(1, 2, 1/2)$. The scalar sector of the Lagrangian of the SM takes the form

$$\mathcal{L}_{\rm scalar} = (\mathcal{D}_\mu \Phi)^\dagger (\mathcal{D}^\mu \Phi)^\dagger - \mu_\Phi^2 \Phi^\dagger \Phi - \lambda_4 (\Phi^\dagger \Phi)^2 \,. \tag{1.12}$$

If the mass of this new field is imaginary ($\mu_\Phi^2 < 0$) there will be a VEV different from zero

$$\langle \Phi \rangle = \begin{pmatrix} 0 \\ v/\sqrt{2} \end{pmatrix} = \begin{pmatrix} 0 \\ \sqrt{\dfrac{-\mu_\Phi^2}{2\lambda_4}} \end{pmatrix} \tag{1.13}$$

A clever way to break the symmetry is to use the Kibble parametrization [21]

$$\Phi = \exp\left(i\, \frac{\vec{\sigma}}{2} \cdot \frac{\vec{\theta}}{v} \right) \begin{pmatrix} 0 \\ \dfrac{H+v}{\sqrt{2}} \end{pmatrix} , \tag{1.14}$$

where $\vec{\sigma} = (\sigma_1, \sigma_2, \sigma_3)$ are the Pauli matrices, $\vec{\theta} = (\theta_1, \theta_2, \theta_3)$ are the three real fields (Goldstone bosons) that will be absorbed by gauge bosons after the SSB and H the massive field responsible for the SSB (Higgs boson). Applying the corresponding gauge transformation to Eq. 1.14 the scalar doublet takes the form

$$\Phi = \begin{pmatrix} 0 \\ \dfrac{H+v}{\sqrt{2}} \end{pmatrix} . \tag{1.15}$$

In July of 2012, the hypothesis of the Higgs Mechanism was confirmed with the discovery at CERN, simultaneously by the LHC experiments ATLAS [44] and CMS [45], of a new particle with mass $m_H = 125.3 \pm 0.4$ GeV that coincides in properties with the boson mediator of the Higgs field (a spin-0 particle with positive parity). The data from CDF and D0 collaborations of the Tevatron experiment at Fermilab confirmed the discovery [67].

1.5.1. Gauge Bosons Masses

The mass terms of the gauge fields come from the derivative terms of Eq. 1.12. If we consider the electroweak structure of Eq. 1.8 the derivative term of the Higgs potential is:

$$
\begin{aligned}
(\mathcal{D}_\mu \Phi^\dagger)(\mathcal{D}^\mu \Phi) &= \left| \left(ig\frac{\vec{\sigma}}{2}\vec{W}_\mu + \frac{ig'}{2}B_\mu \right) \Phi \right|^2 \\
&= (v+H)^2 \left(\frac{g^2}{4} W_\mu^+ W^{\mu -} + \frac{g^2}{8\cos^2(\theta_W)} Z_\mu Z^\mu \right) ,
\end{aligned}
\tag{1.16}
$$

where the mass states are given by

$$
W^\pm \equiv \frac{1}{\sqrt{2}} (W_1^\mu \mp i W_2^\mu) \tag{1.17}
$$

and

$$
\begin{pmatrix} A^\mu \\ Z^\mu \end{pmatrix} \equiv \begin{pmatrix} \cos(\theta_W) & \sin(\theta_W) \\ -\sin(\theta_W) & \cos(\theta_W) \end{pmatrix} \begin{pmatrix} B^\mu \\ W_3^\mu \end{pmatrix} , \tag{1.18}
$$

where A^μ represents the gauge field of the photon while $(W_\mu^\pm, Z_\mu)$ are the weak bosons, that acquire masses after the SSB thanks to the VEV of the Higgs field.

The mixing angle between (B^μ, W_3^μ) and (A^μ, Z^μ) is defined as a combination of the g and g' couplings to the gauge groups

$$
\cos(\theta_W) = g/\sqrt{g^2 + g'^2} , \tag{1.19}
$$

and the masses of the gauge bosons are given by the different quadratic terms in Eq. 1.16:

$$
\begin{cases}
m_W = \frac{1}{2} g v , \\
m_Z = \frac{1}{2} v \sqrt{g^2 + g'^2} , \\
m_A = 0 .
\end{cases}
\tag{1.20}
$$

The difference $m_W \neq m_Z$ was the key to understand that $SU(2) \times U(1)$ is the gauge group of the weak interaction. This fact ends the discussions about the possible description of the weak theory using $O(3)$.

1.5.2. Vacuum Expectation Value and Higgs Boson Mass

The mass of the Higgs boson H is given by the non-derivative terms in Eq. 1.12:

$$m_H = \sqrt{2\lambda_4}\, v\,. \tag{1.21}$$

The question now is, how to compute the VEV? The value of this constant is computed using the muon decay channel $\mu \to \nu_\mu + e^- + \bar{\nu}_e$. The prediction

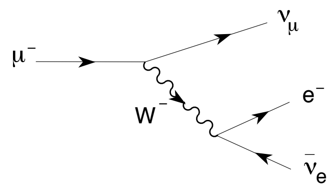

Figure 1.3: *Muon decay channel $\mu \to \nu_\mu + e^- + \bar{\nu}_e$. The prediction of the effective weak theory of this decay, compared with the result of the Electroweak Theory, was used to calculate the VEV.*

of the Electroweak Theory is proportional to $g^2/(8m_W^2)$, while the prediction of the effective weak currents (where the gauge boson has been integrated out) is $G_F/\sqrt{2}$, where $G_F = 1.17 \times 10^{-5}$ GeV represents the Fermi constant. Both prediction must be the same and, as a consequence,

$$v = \frac{1}{\sqrt{\sqrt{2}G_F}} \backsimeq 246\,\text{GeV}\,. \tag{1.22}$$

1.5.3. Fermion Masses

As already commented, the SM does not allow mass terms for the fermion particles. The reason is the difference between the left- and right-handed fields, doublets and singlets of $SU(2)$, respectively. One can analyse the problem using the hypercharge. All terms in the Lagrangian must have zero hypercharge. However, fermionic mass terms have non-zero hypercharge

$$\begin{cases} Y(\bar{Q}_1 D_1) = -1/2\,, \\ Y(\bar{D}_1 Q_1) = 1/2\,. \end{cases} \tag{1.23}$$

Now, in order to give mass to the gauge bosons Z and $W^{\pm}$ we have introduced a new scalar field. The hypercharge of the Higgs field is irrelevant to give mass to the gauge bosons as only the combination $g'Y$ is relevant. However, we can choose $Y(\Phi) = 1/2$ to solve at the same time the fermion mass problem. Therefore, terms like $\bar{Q}_i \Phi D_i$ or $\bar{Q}_i \tilde{\Phi} U_i$ (where $\tilde{\Phi} = i\sigma_2 \Phi^*$) have zero hypercharge and can be part of the Lagrangian. After the SSB, when the Higgs field takes a VEV, mass terms are generated automatically in the Lagrangian

$$\begin{aligned} \bar{Q}_1 \Phi D_1 \,+\, \text{h.c.} \;\; &\xrightarrow[\text{SSB}]{} (\bar{u}_1 \quad \bar{d}_1)_L \begin{pmatrix} 0 \\ \\ v/\sqrt{2} \end{pmatrix} D_1 \,+\, \text{h.c.} \\ &= \frac{v}{\sqrt{2}}\,(d_L^\dagger d_R + d_R^\dagger d_L) = \frac{v}{\sqrt{2}}\,\bar{d}d\,. \end{aligned} \tag{1.24}$$

Once $Y(\Phi)$ is fixed to $1/2$, terms that mix leptons and quarks are not allowed because the hypercharge continues to be different to zero.

One problem of the SM is that we have three different flavour families of fields. This makes it more difficult to write the mass terms. Terms that mix leptons and quarks have non-zero hypercharge and are forbidden, but terms that mix quarks from different flavour families can be part of the Lagrangian, and the same happens for the leptonic terms. As a consequence, the most general Lagrangian that we can build is

$$\mathcal{L}_Y = -\bar{L}_\alpha\, Y^L_{\alpha\beta}\, \Phi\, e_\beta - \bar{Q}_\alpha\, Y^d_{\alpha\beta}\, \Phi\, D_\beta - \bar{Q}_\alpha\, Y^u_{\alpha\,\beta}\, \tilde{\Phi}\, U_\beta + \text{h.c.}\,, \tag{1.25}$$

where $Y_{\alpha\beta}$ are the (3×3) Yukawa matrices.

After the SSB, the Yukawa Lagrangian takes the form:

$$\mathcal{L}_Y = -\frac{H+v}{\sqrt{2}}\left(\bar{e}_{L\alpha}\, Y^L_{\alpha\beta}\, e_{R\beta} + \bar{u}_{L\alpha}\, Y^u_{\alpha\beta}\, u_{R\beta} + \bar{d}_{L\alpha}\, Y^d_{\alpha\beta}\, d_{R\beta} + \text{ h.c.}\right) . \quad (1.26)$$

The Yukawa matrices are not diagonal in general. In order to obtain the mass and interaction eigenstates it is necessary to diagonalise them. First, a redefinition of the fields is needed. For instance, for the leptonic left-handed doublet, $L \to \mathcal{U}_L\, L$. At the end, we need five matrices belonging to global $SU(3)$ flavour group, one per field in Tab. 1.2: $(\mathcal{U}_L,\mathcal{U}_Q,\mathcal{U}_e,\mathcal{U}_u,\mathcal{U}_d)$. Now, we can fix these matrices in order to diagonalise the different Yukawa matrices. For the charged leptons it is an easy task: $\mathcal{M}^L \equiv \mathcal{U}_L^\dagger Y^L \mathcal{U}_e$, we can always find two $SU(3)$ matrices that diagonalise the Yukawa matrix Y^L.

The case of the quarks is more complicate. We can find two matrices to diagonalise Y^u matrix $\mathcal{M}^u \equiv \mathcal{U}_Q^\dagger Y^u \mathcal{U}_u$. The problem appears when we try to do the same for the Y^d matrix, $\tilde{\mathcal{M}}^d \equiv \mathcal{U}_Q^\dagger Y^d \mathcal{U}_d$: the $\mathcal{U}_Q$ matrix has already been fixed to diagonalise Y^u and, as a consequence, it is impossible to diagonalise simultaneously the two Yukawa matrices of the quarks. However, we can chose $\mathcal{U}_d$ in order to get $\tilde{\mathcal{M}}_d = \tilde{\mathcal{M}}_d^\dagger$.

1.5.4. Cabibbo-Kobayashi-Maskawa (CKM) matrix

While the zero mass of the neutrinos always allows to transform the leptonic fields to obtain a diagonal basis, in the quark sector up and down types fields are massive. As a consequence, it is impossible to diagonalise both kind of fields simultaneously keeping the Lagrangian invariant. However, it is possible to introduce a rotation matrix to obtain Y^d diagonal keeping the gauge invariance. After the diagonalization of Y^L and Y^u, Eq. 1.26 can be written as

$$\mathcal{L}_Y = -\left(1+\frac{H}{v}\right)\left(\bar{e}_{L\alpha}\, \mathcal{M}^L_{\alpha\beta}\, e_{R\beta} + \bar{u}_{L\alpha}\, \mathcal{M}^u_{\alpha\beta}\, u_{R\beta} + \bar{d}_{L\alpha}\, \tilde{\mathcal{M}}^d_{\alpha\beta}\, d_{R\beta} + \text{ h.c.}\right) , \quad (1.27)$$

where it has been reabsorbed a factor $v/\sqrt{2}$ in the definition of the matrices. The diagonal matrices are $\mathcal{M}^u = \text{diag}(m_u, m_c, m_t)$ and $\mathcal{M}^L = \text{diag}(m_e, m_\mu, m_\tau)$, while $\tilde{\mathcal{M}}^d$ is an hermitian matrix. One can always find a V matrix that diagonalise $\tilde{\mathcal{M}}^d$. If we assume the presence of this V matrix we can write $\tilde{\mathcal{M}}^d = V\mathcal{M}^d V^\dagger$, where $\mathcal{M}^d = \mathrm{diag}(m_d, m_s, m_b)$. In order to keep the invariance of the Lagrangian it is necessary to rotate the d-type fields

$$\begin{cases} d_R & \rightarrow & V\, d_R\,, \\ d_L & \rightarrow & V\, d_L\,. \end{cases} \tag{1.28}$$

With this new rotation, the d-type fields are diagonals at the same time that we keep diagonal the other two Yukawa matrices. The question now is, what implications have this rotation?

The interaction between $W^{\pm}$, Z and A gauge bosons and the matter fields are determined by the Neutral Currents (NC) and Charged Currents (CC) Lagrangians. The rotations of the $d-$type fields imply that the rotation matrix V appears in the CC Lagrangian. The final interaction is given by

$$\mathcal{L}_{CC} = \frac{g}{\sqrt{2}} W_\mu^+ \left(\bar{u}_{L\alpha}\, \gamma^\mu\, V_{\alpha\beta}\, d_{L\beta} + \bar{\nu}_{L\alpha}\, \gamma^\mu\, e_{L\alpha}\right) + \text{h.c.}\,. \tag{1.29}$$

The rotation matrix $V_{\alpha\beta}$ receives the name of Cabibbo-Kobayashi-Maskawa (CKM) matrix [68, 69] and it is the source of the flavour changing in CC processes.

The NC Lagrangian does not mix the quark flavour, it can be written in compact form

$$\mathcal{L}_{NC} = -\, e\, A_\mu \sum_f\, Q^f\, \bar{f}\, \gamma^\mu\, f \; - \; \frac{e}{\sin(\theta_W)\cos(\theta_W)}\, Z_\mu \sum_f\, \bar{f}\, (v_f - a_f\, \gamma_5)\, f\,, \tag{1.30}$$

where e is the electron charge and the sum is over all the physical fermions. The different a_f and v_f constants depend on each fermion:

$$\begin{cases} a_f & = & \frac{1}{2} T_3^f\,, \\ v_f & = & \frac{1}{2} T_3^f \left[1 - 4|Q^f|\sin^2(\theta_W)\right]\,, \end{cases} \tag{1.31}$$

where T_3^f and Q^f are the isospin and the electrical charge of the fermion f. Notice that in this case, rotating $d \rightarrow Vd$ does not introduces any matrix in NC processes, as they cancel in terms such as $d\,\Gamma d$ (being Γ some combination of Dirac matrices).

1.6. Open Problems of the Standard Model

The Standard Model represents one of the most relevant achievements in physics. It took many years to understand how the microscopic world works. But this is not the end of the story as the SM presents various problems that until the present day have no solution. Examples of open problems in particle physics are the neutrino masses, the hierarchy problem or the strong CP problem. In the rest of this Section we described briefly these topics.

In addition to these problems, there are strong cosmological evidences of the existence of a new kind of matter that does not have the same interaction rules that the particles of the SM. This new kind of matter receives the name of *Dark Matter* (DM). Its phenomenology is still a mystery and it is the main topic of this thesis. The nature and properties of DM will be studied in Chapter 3.

1.6.1. The Hierarchy Problem

There are some hints for the existence of physics beyond the SM (BSM). However, it is unclear at which scale this new physics enters the game. According to the Higgs Mechanism, the new physical scale must be close to the electroweak scale: the technical reason is that the Higgs mass is quadratically sensitive to high scales. If we analyse the Higgs potential (Eq. 1.12), the first order quantum corrections to the mass parameter μ_Φ are given by

$$\delta\mu_\Phi^2 = \frac{\Lambda^2}{32\,\pi^2}\left[-6\,Y_t^2 + \frac{1}{4}\,(9\,g^2 + 3\,g'^2) + 6\lambda_4\right]\,, \tag{1.32}$$

where Λ is the cutoff of the theory, Y_t the top Yukawa coupling and g and g' the electroweak couplings. Since we know the value of the VEV of the Higgs field (Eq. 1.22) and the Higgs mass, we can calculate the value of $\lambda_4 = 0.13$ using Eq. 1.21. If the scale of the new physics is close to the EW scale, the hierarchy problem is not a real problem. However, the landscape of the current experiments in high-energy physics makes us think that these scales are not as close as it should. If the new scale is $\Lambda \gg 1\,\text{TeV}$ the Eq. 1.32 implies $\delta\mu_\Phi^2 \gg \mu_\Phi^2$. If quantum corrections are much larger than the experimentally measured value of μ_Φ, then extremely large, cancellations should be at work. This fact is known as hierarchy problem, a complete revision about this topic can be found in Ref. [70]. Different models to try to solve the hierarchy problem have been proposed in the last decades. The most popular are Supersymmetry (a review can be found in Ref. [71]), technicolor [72–74], composite Higgs [75] and warped extra-dimensions [76, 77].

1.6.2. Strong CP problem

Quantum Chromodynamics predicts the existence of processes with CP violation. However, no violation of the CP-symmetry is observed experimentally. There are no theoretical reasons to preserve this symmetry and, as a consequence, this represents a fine tuning problem.

The absence of any observed violation in strong interactions is a problem because the QCD Lagrangian presents natural terms that break the CP simmetry [78]:

$$\mathcal{L} \supset -\frac{n_f g_s^2 \theta_{CP}}{32\pi^2}\, G_{a\mu\nu}\widetilde{G}^{a\mu\nu}\,, \tag{1.33}$$

where θ_{CP} is the vacuum phase and n_f the number of flavours. This term comes directly from the vacuum QCD structure and it would be absent in presence of massless quarks. The phase is related to the value of the neutral dipole moment [79], whose current limits [80,81] implies that $|\theta_{CP}| < 10^{-10}$.

Different solutions have been proposed to solve the problem, the most popular among them being the one proposed by Roberto D. Peccei and Helen R. Quinn in Ref. [82], introducing a new symmetry $U(1)_{\text{PC}}$. This new symmetry is spontaneously broken generating the Weinberg-Wilczek axion [83, 84] (the Goldstone boson of the broken PQ symmetry). In this scenario, the θ-phase is related with the VEV of a new field and its small value is the consequence of the symmetry breaking at high scales. The value of θ in this approach is determined by irrelevant operators [85, 86].

Different reviews about the strong CP problem and its possible solutions can be found in Refs. [87, 88].

1.6.3. Neutrino Masses: The Seesaw Mechanism

In the Standard Model the neutrinos are massless, but nowadays it is experimentally shown that they have a non-zero mass. In 1957 Bruno Pontecorvo predicted the existence of neutrino oscillations [89], as a consequence of the difference between the interaction (weak) and mass eigenstates. This effect implies non-zero mass for the neutrinos and ever since Pontecorvo predicted its existence, several experiments searched for it and studied their effect [90–106].

There are different mechanisms to generate neutrino masses, for instance add a new right-handed neutrino (N). However, when we add a mass term for the neutrinos with a new state N, singlet under the SM symmetry group, we have the same problem as for the quarks: we need a new matrix to diagonalize charged leptons and neutrino mass matrices simultaneously. The relation between the mass and weak eigenstates can be fixed using the unitary Pontecorvo-Maki-Nakagawa-Sakata (PMNS) matrix $U_{\alpha i}$ [107, 108]:

$$\nu_\alpha = \sum_i U_{\alpha i} \nu_i \,, \tag{1.34}$$

where $\alpha = e, \mu, \tau$ represent the weak eigenstates while $i = 1, 2, 3$ are the mass eigenstates. The PMNS matrix can be parametrized with three mixing angles $(\theta_{12}, \theta_{23}, \theta_{13})$ and a CP-violating Dirac phase δ. The mixing angles are usually refereed to as solar, atmospheric and reactor angles, respectively, because at the kind of experiment where they were measured for the first time. On the other hand, the oscillation lengths are $(\Delta m_{12}, \Delta m_{23}, \Delta m_{13})$. The most recent values of all of these parameters can be found in Ref. [109].

Until this point we only talked about the mixing and oscillation parameters; but what is the mass scale of the neutrinos? The KATRIN experiment puts the upper bound at $\sum m_\nu \lesssim 2.7\,\mathrm{eV}$ at 95% Ref. [110]. Extending the

SM to add neutrino masses is not a complicated task: it is enough to introduce three new fields N that represent the right-handed neutrinos[4]. In that case, an extra term would appear in Eq. 1.25 giving mass to the neutrinos via the Higgs Mechanism, as in the case of quarks and charged leptons. The question now is, if the mechanism to give mass to the neutrinos is the Higgs Mechanism, why the neutrinos masses are so different from the rest of the fundamental particle masses?

The right-handed neutrinos N have a special property that make them different from the rest of the SM particles: they are singlets under all SM gauge groups. This allows the neutrino to be its own antiparticle! While the usual fermions receive the name of Dirac particles, this kind of particles receives the name of Majorana particles [111]. This means that we could add a new extra term to the Lagrangian:

$$\mathcal{L} = -\bar{L}_i Y^{\nu}_{ij} \Phi N_j - \frac{1}{2} N_i^T C^{-1} M^R_{ij} N_j + \text{h.c.}\,, \tag{1.35}$$

where M^R is the 3×3 right-handed neutrino Majorana mass matrix, Y^ν the Yukawa matrix of the neutrinos and C the charge conjugate operator. The *usual* mass of the neutrinos, the so-called Dirac mass, is given by the Yukawa couplings

$$m_D = \frac{v}{\sqrt{2}} Y^\nu\,. \tag{1.36}$$

It is important to keep in mind that we have three flavour families and, as a consequence, m_D is not a parameter, but a 3×3 matrix.

After SSB, the mass matrix of the neutrinos takes the form:

$$\mathcal{M}_\nu = \begin{pmatrix} 0 & m_D \\ m_D^T & M^R \end{pmatrix}, \tag{1.37}$$

As an example, consider the 2×2 case (i.e. for one generator only). In the limit $|m_D| \gg |M^R|$ there is a large hierarchy between the eigenvalues, that are given by $m_\nu \simeq m_D^2/M^R$ and $m_N \simeq M^R$, and approximately corresponds to the eigenvectors of $\nu_1 \backsim \nu_L$ and $\nu_2 \backsim N$. In this way, we could have

[4]Actually, two new fields are sufficient to explain present observations; albeit, with the consequence that the lightest neutrino should be massless.

a *natural* explanation why neutrinos are much lighter than other fermions, even if their Yukawa couplings (and, thus, m_D) are similar. This mechanism receives the name of *seesaw mechanism* type I [112–116], as the larger M_N the smaller m_ν. This is only one of the different seesaw mechanisms able to provide mass to the neutrinos. However, other variants of this mechanism do not need the existence of the right-handed neutrinos.

Complete reviews of different seesaw models can be fond in Ref. [117].

Chapter 2

Introduction to Cosmology: The Homogeneous Universe

2.1. An Expanding Universe: The FLRW Metric

Developing a theory related to the matter of the Universe, regardless of what type the matter is, implies a deep knowledge of the shape of the Universe on large scales. The science that is investigating this is called *cosmology*. Although the word cosmology was used for the first time in 1656 in Thomas Blount's *Glossographia* [118], its origins began long ago. Already the ancient Greeks tried to explain the position and nature of the astronomical objects they observed. At that time notable authors such as Aristoteles and Claudius Ptolemy developed the geocentric model, which placed the Earth as the center of the Universe. Many centuries later, Nicolás Copernicus (1473-1543) developed the heliocentric model, which was strongly supported by Galileo Galilei (1564-1642), laying the first foundations for our current astronomical models. However, the modern cosmology was born during the first half of the 20th century with the discovery of the expansion of the Universe. In 1929 Edwin Hubble found the first evidence of the expansion of the Universe [119]. He observed that all distant galaxies and astronomical objects were moving away from us as

$$z = \frac{\lambda_{\text{observed}} - \lambda_{\text{emitted}}}{\lambda_{\text{emited}}} \backsimeq H_0\, d_L\,. \tag{2.1}$$

This expression is called the *Hubble Law* and establishes a relationship between the *luminosity distance*[1] d_L of some astronomical object with its *redshift*[2] z. At first order, the relation is linear and only depends on the Hubble constant [120]

$$H_0 = 100\, h\, \mathrm{km\, s^{-1}\, Mpc^{-1}} = 67.66 \pm 0.42\, \mathrm{km\, s^{-1}\, Mpc^{-1}}\,, \tag{2.2}$$

where h is the reduced Hubble constant.

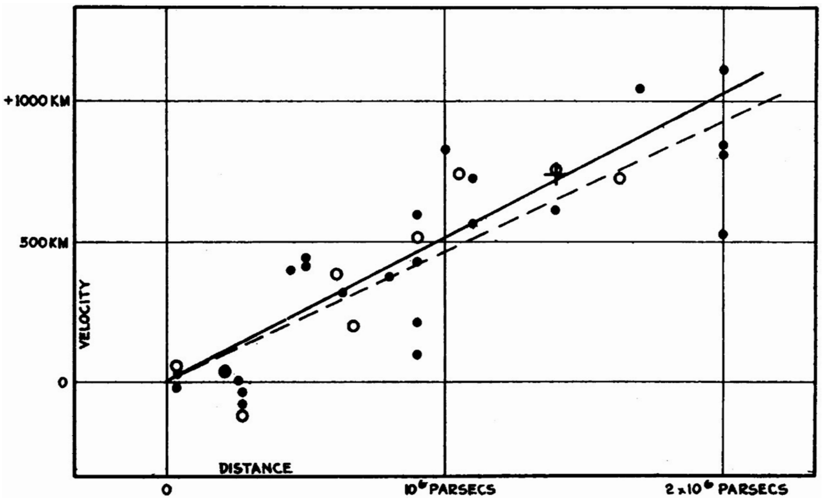

Figure 2.1: *Original figure of [119] showing the results obtained by Edwin Hubble comparing the measurements about the radial velocity of the galaxy with the redshift of 22 different astronomical clusters. The results shown in this figure represent the first proof of the expansion of the Universe.*

The results obtained by Hubble are shown in Fig. 2.1. The original results of Hubble's work analysed 22 different galaxies. Nowadays, we have data of thousands of galaxies and the most part of these shows $z > 0$. This fact is considered an irrefutable proof of the expansion of the Universe. The

[1] Defined as $d_L = 10^{(m-M)/5+1}$, where M is the absolute magnitude while m the apparent magnitude of an astronomical object. The luminosity distance is usually measured in parsecs (pc).

[2] The redshift z is the difference between the observed and the emitted wavelength of the astronomical body.

expansion of the Universe and the assumption that we live in an isotropic and homogeneous Universe[3] lead us to the Big Bang model.

Nowadays, our understanding of the evolution of the Universe is based on the Friedman-Lemaître-Robertson-Walker (FLRW) cosmological model, that describes an isotropic, homogeneous and expanding Universe [122–125] with metric

$$ds^2 = g_{\mu\nu} dx^\mu dx^\nu = dt^2 - a(t)^2 \left[\frac{dr^2}{1 - kr^2} + r^2 d\theta^2 + r^2 \sin^2\theta d\phi \right] , \qquad (2.3)$$

where (t, r, θ, ϕ) are the comoving coordinates and $a(t)$ is the cosmic scale factor. The curvature of the space-time is given by k and can be $+1$, -1 or 0 describing an open, close and flat space-time, respectively.

In order to quantify the expansion of the Universe it is necessary to study the variation of the scale factor $a(t)$. The most convenient way to perform this study is to analyse the so-called expansion rate or Hubble parameter, defined as

$$H \equiv \frac{\dot{a}}{a} , \qquad (2.4)$$

where $\dot{a} = da/dt$. The current value of the Hubble parameter is the Hubble constant, H_0, defined in Eq. 2.2.

2.2. Einstein Field Equations

To understand the evolution of the Universe through the FLRW metric a deep knowledge of General Relativity and the Einstein gravitational field equations is necessary. First proposed in 1915 by Albert Einstein in Ref. [126], the gravitational field equations take the form:

$$G_{\mu\nu} = \frac{8\,\pi\,G}{c^4} T_{\mu\nu} + \Lambda\, g_{\mu\nu} , \qquad (2.5)$$

where $T_{\mu\nu}$ is known as the *energy-momentum* tensor and represents the energy flux and momentum of a matter distribution, Λ is the cosmological constant and $G_{\mu\nu}$ is the unique divergence free tensor which can be built with linear combinations of the space-time metric and its first and second

[3] This is called *cosmological principle* and is backed up by strong evidences [120, 121].

derivatives

$$G_{\mu\nu} \equiv R_{\mu\nu} - \frac{1}{2} g_{\mu\nu} R \,. \tag{2.6}$$

The Einstein field equations form a system of ten coupled differential equations and describe the evolution of the space-time metric tensor $g_{\mu\nu}$ under the influence of the $T_{\mu\nu}$ tensor, and vice-versa. To understand Eq. 2.5, a deep knowledge of the different elements of the differential geometry is needed (see, for instance, Ref. [127]):

$$\begin{cases} \Gamma^{\mu}_{\alpha\beta} &= \frac{1}{2} g^{\mu\nu} \left(-\frac{\partial g_{\alpha\beta}}{\partial x^{\nu}} + \frac{\partial g_{\nu\alpha}}{\partial x^{\beta}} + \frac{\partial g_{\nu\beta}}{\partial x^{\alpha}} \right) & \text{Cristoffel Symbols}\,, \\ R^{\alpha}_{\beta\gamma\sigma} &= \frac{\partial \Gamma^{\alpha}_{\beta\sigma}}{\partial x^{\gamma}} - \frac{\partial \Gamma^{\alpha}_{\gamma\sigma}}{\partial x^{\beta}} + \Gamma^{\mu}_{\beta\sigma}\Gamma^{\alpha}_{\gamma\mu} - \Gamma^{\mu}_{\gamma\sigma}\Gamma^{\alpha}_{\beta\mu} & \text{Riemann Tensor}\,, \\ R_{\sigma\nu} &= R^{\rho}{}_{\sigma\rho\nu} & \text{Ricci Tensor}\,, \\ \mathcal{R} &= R^{\mu}_{\mu} & \text{Scalar Curvature}\,. \end{cases} \tag{2.7}$$

In General Relativity $g_{\mu\nu}$ plays a fundamental role: each solution of the Einstein field equations is characterized by its respective metric, which is defined by the energy density of the Universe. The existence of the last term of Eq. 2.5 has been a topic of debate since Einstein postulated it to give a solution of his equations that predicted a static Universe. In the original formulation of the FLRW model, Λ is supposed to be absent (to get a constant expansion of the Universe). Current cosmology rescued it as a possible explanation of the observed accelerated expansion of the Universe at recent times [128].

2.3. Dynamics of the Universe

The structure of the Universe is fixed by Eq. 2.5. In order to solve this equation it is necessary to know the form of the energy-momentum tensor $T_{\mu\nu}$. Under the assumption of homogeneity and isotropy, the content of the primordial Universe can be described as a perfect fluid, and the energy-momentum tensor can be written as:

$$T^{\mu}{}_{\nu} = p\, g^{\mu}{}_{\nu} + (\rho + p)\, U_{\nu} U^{\mu} \equiv \mathrm{diag}(\rho, -p, -p, -p)\,, \tag{2.8}$$

where $U_\mu \equiv dX^\mu/d\tau$ is the four-velocity of the fluid, ρ the energy density and p the pressure. The energy-momentum conservation principle $dU = -p\, dV$, where $U = \rho V$ is the total energy of the fluid and $V \propto a^3$ the volume, directly implies

$$\frac{d\rho}{dp} + 3\frac{\dot{a}}{a}(\rho + p) = 0\,. \tag{2.9}$$

Eq. 2.9 allows to obtain the relation between the energy density ρ and the scale factor a when the relation between the energy density and the pressure[4] p is known. Most cosmological fluids can be described by a simple time-independent equation of state, where the energy and the pressure are proportional, $p = \omega\rho$, being ω an arbitrary constant. In these cases the energy density can be expressed as $\rho \propto a^{-3(1+\omega)}$.

In order to describe the evolution of the Universe, it is necessary to understand the different components that contribute to the energy-momentum tensor. It is possible to distinguish three different components of the content of the Universe: *matter*, *radiation* and *Dark Energy*. The nature of the first two components is easy to explain: the cosmological definition of matter says that it includes all the different non-relativistic matter species, while radiation includes the relativistic particles.

The third component, the Dark Energy, is a kind of unexplained energy with negative pressure that is necessary to understand our current knowledge about the evolution of the Universe. Quantum field theory predicts the existence of a vacuum energy with negative pressure [129]. This energy can be calculated for the energy-momentum tensor as $T^{\mathrm{vac}}_{\mu\nu} = \rho_{\mathrm{vac}} g_{\mu\nu}$. The problem with this explanation of the Dark Energy nature lies in the fact that there is a large discrepancy between the observed and the calculated energy density

$$\frac{\rho_{\mathrm{vac}}}{\rho_{\mathrm{obs}}} \backsim 10^{120}\,. \tag{2.10}$$

[4]The relation between the pressure and the energy density is called *equation of state*.

This huge discrepancy receives the name of *vacuum catastrophe*[5]. The nature of this component of the Universe is still unclear. The scientific community agrees that it could be related to the cosmological constant, but alternative ideas could also work. A detailed description of the current status of the problem can be found in Ref. [130].

It is possible to distinguish between three different epochs in the evolution of the Universe, depending on whether matter, radiation, or Dark Energy dominates.

$$\begin{cases} p = \frac{1}{3}\rho & \Rightarrow \rho \propto a^{-4} & \text{Radiation Epoch}\,, \\ p = 0 & \Rightarrow \rho \propto a^{-3} & \text{Matter Epoch}\,, \\ p = -\rho & \Rightarrow \rho \propto \text{const.} & \text{Dark Energy Epoch}\,. \end{cases} \tag{2.11}$$

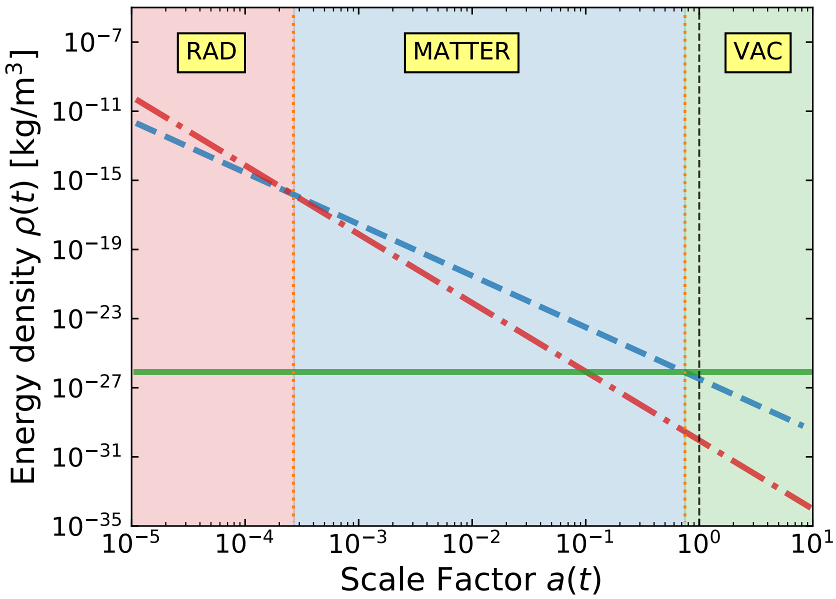

Figure 2.2: *Different epochs of the Universe, depending on which contribution dominates. The red dot-dashed, blue dashed and green solid lines represent the different contributions of radiation, matter and Dark Energy (or vacuum energy), respectively. The black dashed vertical line shows the present moment of the Universe.*

Fig. 2.2 shows the different contributions to the total energy density of the different components of the Universe. The red dot-dashed, blue dashed and green solid lines show, respectively, the radiation, matter and Dark

[5] Also called sometimes *cosmological constant problem*.

Energy contributions. In the early Universe, most parts of the components were relativistic; this era is dominated by the radiation contribution. In the *adolescent* Universe the SM particles, except photons and neutrinos, are non-relativistic, the matter contribution dominates the total energy density. The present moment of the Universe (black-dashed line in Fig. 2.2) is close to the point at which the vacuum contribution begins to dominate over the matter contribution ($z \backsimeq 0.55$). This fact receives the name of *coincidence problem* [131] and its possible anthropic implications have been studied by different authors (see, for instance, Refs. [132, 133]).

2.4. The Friedman Equations

To analyse the evolution of the scale factor it is necessary to simplify the different terms of Eq. 2.5 using the definitions of Eq. 2.7 with the metric of Eq. 2.3 and the form of the energy-momentum tensor that, under the assumption of homogeneity and isotropy, takes the form of Eq. 2.8. The resulting expressions receive the name of Friedman equations

$$\begin{cases} \left(\dfrac{\dot{a}}{a}\right)^2 &= \dfrac{8\pi G}{3}\rho - \dfrac{k}{a^2}\,, \\ \left(\dfrac{\ddot{a}}{a}\right) &= -\dfrac{4\pi G}{3}(\rho + 3p)\,, \end{cases} \tag{2.12}$$

where ρ and p can be understood as the sum of all contributions to the energy density and pressure in the Universe. The first Friedman equation is usually written in terms of the Hubble parameter (Eq. 2.4)

$$H^2 = \frac{8\pi G}{3}\rho - \frac{k}{a^2}\,. \tag{2.13}$$

The flat space case ($k = 0$) in Eq. 2.13 defines the critical case

$$\rho_{\text{crit}} \equiv \frac{3H^2}{8\pi G}\,, \tag{2.14}$$

that can be estimated today using Eq. 2.2 obtaining $\rho_{\text{crit},0} \equiv \rho_{\text{crit}}|_{H=H_0} = 1.9 \times 10^{-29}\, h^2\, \text{g}\, \text{cm}^{-3}$. The critical density is used to define dimensionless density parameters

$$\Omega \equiv \frac{\rho}{\rho_{\rm crit}} \,. \tag{2.15}$$

This is very convenient because the energy densities of the different components of the Universe have enormous values. Since the density parameter Ω is related with k, which describes the curvature of space-time, its value allows to analyse the geometry of the Universe

$$\begin{cases} \Omega > 1 & \text{Closed}\,, \\ \Omega = 0 & \text{Flat}\,, \\ \Omega < 1 & \text{Open}\,. \end{cases} \tag{2.16}$$

The first Friedmann equation (Eq. 2.13) can be written in terms of Ω and the Hubble constant

$$H^2 = H_0^2 \left[\Omega_{\rm r} \left(\frac{a_0}{a}\right)^4 + \Omega_{\rm m} \left(\frac{a_0}{a}\right)^3 + \Omega_k \left(\frac{a_0}{a}\right)^2 + \Omega_\Lambda \right] \,, \tag{2.17}$$

where $\Omega_{\rm r}$, $\Omega_{\rm m}$, Ω_k and Ω_Λ denotes the density parameters of radiation, matter, curvature and vacuum in the present epoch, respectively. In Eq. 2.17 we define the curvature density parameter in the present epoch as $\Omega_k \equiv -k/(a_0 H_0)$. The expression is written in terms of H_0 and a_0, where a_0 represents the scale factor today. It is very common in cosmology to take the normalization for the scale factor $a_0 \equiv 1$. With this normalization, the above expression becomes

$$H^2 = H_0^2 \left(\Omega_{\rm r}\, a^{-4} + \Omega_{\rm m}\, a^{-3} + \Omega_k\, a^{-2} + \Omega_\Lambda \right) \,. \tag{2.18}$$

The question now is, what is the value of these parameters?

2.5. Cosmology in the present days: ΛCDM model

In 1964 Arno Penzias and Robert Woodrow Wilson [137] discovered the *Cosmic Microwave Background* (CMB), a noise, apparently isotropic, in the

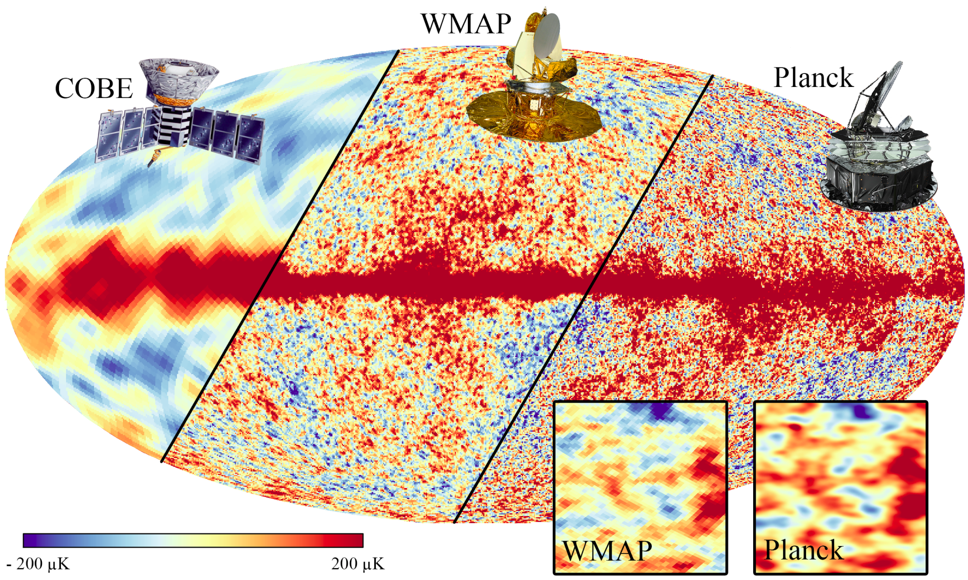

Figure 2.3: *Evolution along the last 30 years of the measurements of the anisotropies in the temperature of the Cosmic Microwave Background. From the left to the right the figure shows the data from COBE (Cosmic Background Explorer) [134], WMAP (Wilkinson Microwave Anisotropy Probe) [135] and Planck [120]. Image taken from [136].*

form of electromagnetic radiation that populates the Universe. Since then, several experiments measured the CMB finding small temperature anisotropies (the evolution of our knowledge about the CMB can be observed in Fig. 2.3) such as the case of COBE (Cosmic Background Explorer) [134], WMAP (Wilkinson Microwave Anisotropy Probe) [135] or Planck [120], the latter being the most accurate measurement today. The CMB discovery confirmed a key prediction of the Big Bang cosmology. Since that moment, the scientific community accepted that the Universe started in a hot and dense state and has been expanding ever since.

The current cosmological model includes a non-vanishing cosmological constant Λ, that represent the Dark Energy or vacuum component of the Universe. As for matter, it assumes that most part of the matter is non-barionic and is mostly composed of *Cold Dark matter*[6] (CDM). The evidence of this fact will be commented in Chapter 3. Respect to the curvature, the model assumes that the Universe is practically flat at large scale. The

[6]See Sect. 3.3 for more details.

Cosmological Parameters Planck 2018	
Expansion	$h = 0.677 \pm 0.004$
Barionic Matter	$\Omega_{\mathrm{b}} h^2 = 0.02242 \pm 0.00014$
Dark Matter	$\Omega_{\mathrm{DM}} h^2 = 0.1193 \pm 0.0009$
Dark Energy	$\Omega_{\Lambda} h^2 = 0.689 \pm 0.006$
Radiation	$\Omega_{\mathrm{r}} h^2 = (9.2 \pm 0.4) \times 10^{-5}$
Curvature	$\Omega_k h^2 = -0.004 \pm 0.015$

Table 2.1: Cosmological parameters published by Planck [120]. These values represent the conclusion of the Experiment.

name of this model that accepts the existence of two new, and unexplained, components of the energy density receives the name of ΛCDM model.

The ΛCDM model is a parametrization of the cosmological measurements. The accuracy of the model depends on the precision of the astrophysical experiments that estimate its parameters. Tab. 2.1 shows the most recent measurements taken by the Planck collaboration of the cosmological parameters. These results show that the most part of the Universe being Dark Energy ($\backsim$ 69%) and Cold Dark Matter ($\backsim$ 26%) while the baryonic matter only represents $\backsim$ 5% of the total energy content. The Dark Energy is still a complete mystery today: the most accepted theory is that is related to the cosmological constant of the Einstein field equations. On the other hand, what is this Dark Matter? This $\backsim$ 26% of the content of the Universe is the main topic of this Thesis.

Chapter 3

About the Nature of Dark Matter

As it was explained in Sect. 2.5, there are unequivocal evidences that point out that the *baryonic* matter (where baryonic in cosmology includes not only baryons, but also all of the SM particles) represents the $\backsim 5\%$ of the energy density of the Universe, while Dark Matter constitutes the $\backsim 26\%$. The implication of this fact is absolutely strong: the SM of fundamental interactions described in Chapter 1 only explains a minuscule portion of the matter of the Universe, the rest is still a mystery. Along this Thesis we try to bring some light over the DM enigma. In order to perform this task it is necessary to understand the nature of this new kind of matter. What are the evidences of DM? is it possible to observe these elusive particles? which is its the nature?

3.1. Dark Matter Evidences

The first observational evidence of the existence of DM date from the early 1930's when Fritz Zwicky measured the velocity dispersion of several galaxies of the Coma Cluster. Zwicky concluded that a bigger amount of matter than the visible one was necessary to keep the galaxy cluster together[1] [139, 140]. Previously to Zwicky, other observations suggesting missing mass in our galaxy were made by Jacobus Cornelius Kapteyn (1922) [141] and by Jan Hendrik Oort (1932) [142].

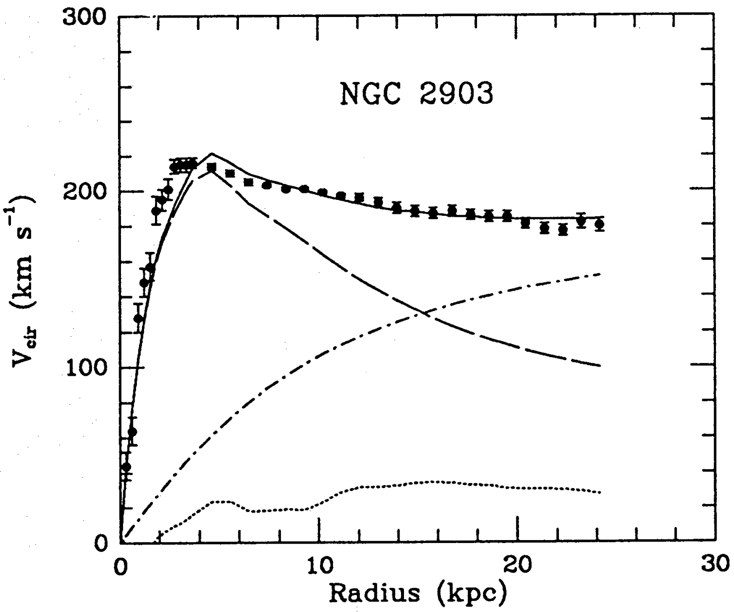

Figure 3.1: *Galaxy rotation curve of NGC 2903 [143]. The solid line represents the data fit of the observed galaxy rotation curve while the dashed, dotted and dash-dotted represent, respectively, the rotation curves of the individual components: the visible components, the gas and the dark halo.*

In the 1960's and 1970's the first astrophysical Dark Matter studies were made. Vera Cooper Rubin, Kent Ford and Ken Freeman measured the velocity rotation curve of different spiral galaxies [144, 145]. In these works they concluded that the velocity rotation curve of the spiral galaxies display an anomalous behaviour contrary to the galaxies luminosity measurements. According to our knowledge about the relation between the luminosity and the mass of the galaxy, if the only kind of matter in it is baryonic, the rotational velocity should follow the dash line in Fig. 3.1. Conversely, as we can understand from the data points in the Figure, the velocity remains almost constant. Since then, many measurements of the velocity rotation curves of several galaxies have been done (see, for instance, Refs. [146, 147]). Nowadays, there are strong evidences that the 95% of the matter content of almost every galaxies is DM.

[1]More precise estimations were made after the first Zwicky observation, using the virial theorem [138].

Galaxy rotation curves were the first solid proof, and probably the most famous, of the DM existence, but are not the only one. Several evidences of the DM content in the Universe have been discovered since Rubin, Ford and Freeman researches, including the fact that the mass of the galaxy clusters is in agreement with the ΛCDM model, supporting the DM theories [148].

One of the ways to estimate the mass of any astronomical body is the *gravitational lensing*. This method uses light that arrives at the Earth emitted by galaxies, clusters, quasar and other astronomical objects. In most cases, these objects are not located close to the Earth, as a consequence, it is quite common the presence of some astronomical bodies along the emitted light path to the Earth. When the light goes through these astronomical objects, according to General Relativity, the gravitational field distorts its propagation. This distortion receives the name of gravitational lensing. The measurement of this effect allows the mass of galaxies, clusters and other astronomical bodies between us and the light source to be estimated. The gravitational lensing measurements of different astronomical objects point to DM predominance in almost every galaxies and clusters [149–152].

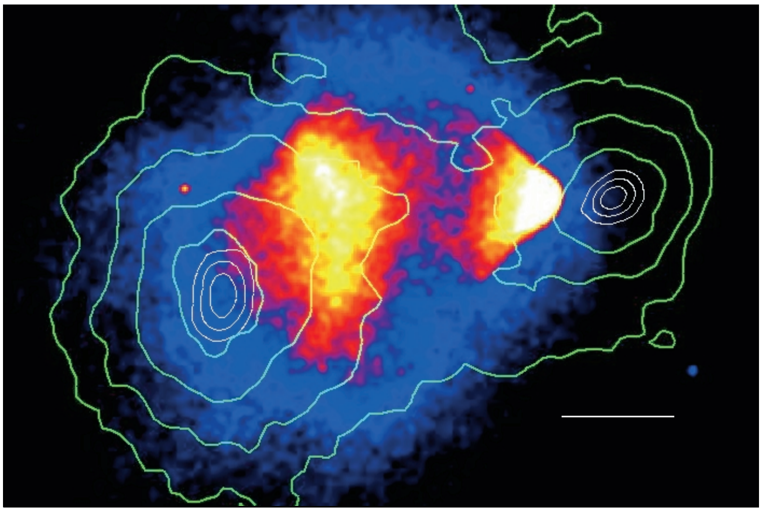

Figure 3.2: *Image taken from [153]. It shows the gas distribution of the Bullet Cluster. Contour lines depict gravitational equipotential lines which indicate the DM location.*

The *Bullet Cluster* is probably the best example of how gravitational lensing proofs the existence of DM. The Bullet Cluster or 1E 0657-56[2] has

[2]The Bullet Cluster is composed by two colliding clusters. Was discovered in 1995 by *Chandra* X-ray [154].

displaced its center of mass with respect to the observed baryonic center of mass. DM models can easily explain this effect. Other alternatives would require a modification of General Relativity [155, 156].

All the evidences illustrated above are astrophysical proofs, but there are several cosmological indications of the existence of DM in agreement with these evidences. The Friedmann equations and General Relativity describe a homogeneous Universe. As a consequence, the galaxies, stars and the rest of the astronomical bodies were originated by small density perturbations after the Big Bang. If had only existed baryonic matter in the early Universe, the presence of galaxies and clusters would not be possible today. In that hypothetical case, the evolution of the primordial density perturbations would not have been sufficient [157–159].

On the other hand, the temperature anisotropies measured in the CMB by COBE, WMAP and Planck [121, 134, 135] absolutely agree with a Universe made of 69% Dark Energy and 31% matter.

In summary, nowadays there are several irrefutable evidences of the existence of DM. It is true that no direct or indirect detection of DM has been until today, but the exceptional predictive power of the ΛCDM cosmological model represents an excellent proof that our Universe is mostly dark.

3.2. Properties of Dark Matter

As it was explained in Sect. 3.1, there are several cosmological and astrophysical evidences of the existence of DM. It is true that, to until now, Dark Matter observations have not been done. As a consequence, the interactions and properties of DM are still unknown. However, the different proofs that we have about its existence allow us to predict some of its properties.

The abundance of DM along the evolution of the Universe is well known: Fig. 3.4 shows the matter and energy content of the Universe today (left) and after the CMB decoupling (right). Nevertheless, the abundance of DM is not the unique property that it is possible to predict with the current data. In this section we explain the mostly accepted DM properties by the scientific community.

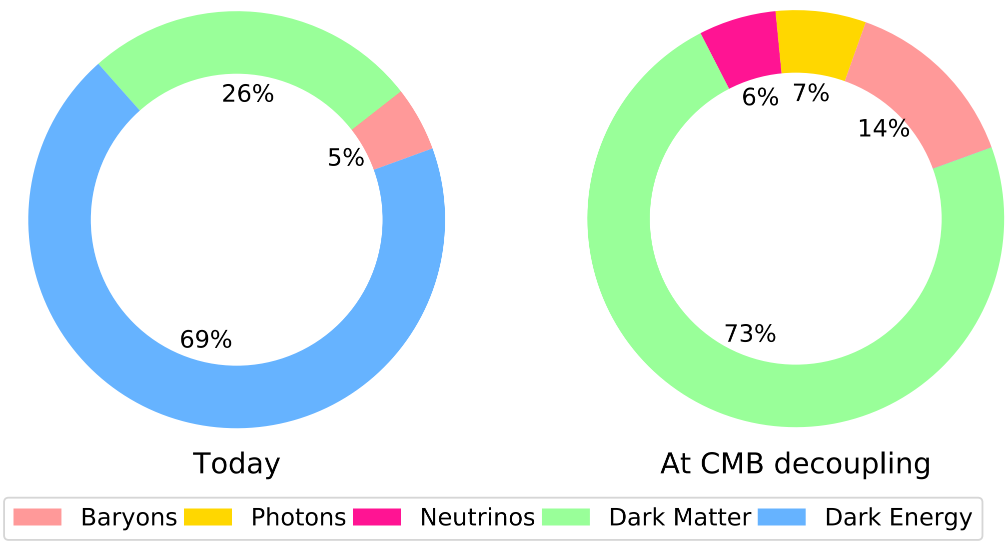

Figure 3.3: *Energy and matter content of the Universe in two different ages. Left: today; Right: at the CMB decoupling.*

3.2.1. DM - SM interactions

Assuming that Dark Matter exists, the first question we must ask is: how does it interact with the rest of the particles? We have clear proofs that DM interacts, at least, through one of the four fundamental forces, the gravitational one. This fact is indisputable: all evidences of the existence of Dark Matter are related to gravitation. Now, what about the other three?

In 1990 strongly interacting DM was proposed [160]; nevertheless, not many years later this option was totally ruled out. The implications of the existence of this Dark Matter type are so strong that even in the Earth heat flow it would be detected [161].

Another Dark Matter theory proposal assumes that DM has electrical charge [162]. However, non-detection of DM and other reasons set strong limits on DM particles with an electric charge, practically ruling out this option. [163]. Consequently, the most accepted hypothesis is that DM is a singlet under the color and electromagnetic SM gauge groups. However, some physicists have speculated about the possibility of having DM composed of particles with a fractional electrical charge, also known as milli-charged particles [164–169]. These kind of DM candidates may have effects in the CMB, setting strong bounds [170]. Besides the CMB, there are other sources of bounds for this type of particles (different constraints are summarized in Ref. [171]).

Regarding the last of the 4 forces, the weak interactions of DM with SM neutrinos are analysed in several works [172–175]. The elusive nature of neutrinos makes it difficult to constrain these kind of interactions. Weakly interacting DM will be reviewed in Sect. 3.5.2.

3.2.2. Dark Matter self-interactions

In Sect. 3.2.1 it were examined the different DM interactions with SM particles. However, what happens with the self-interaction of the DM? The self-interactions of DM have been a subject of debate for many years. Theories with self-interactive Dark Matter (SIDM) were proposed at the end of the last century [176], motivated by the problems generated by the most popular kind of DM, the Cold Dark Matter[3].

However, since DM must explain observations such as the bullet cluster, in order to keep General Relativity, strong bounds are imposed on SIDM [177–181]:

$$\sigma/m \lesssim 10^{-24}\,\mathrm{cm}^2/\mathrm{GeV}. \tag{3.1}$$

3.2.3. Dark Matter stability

If there is a clear property of Dark Matter in which everybody agrees is the DM lifetime. In order to reproduce the current observations of the Dark Matter abundance, any candidate must have a lifetime larger than the age of the Universe, $t_0 = 13.8\,\mathrm{Gyr}$ [120]. Nowadays, DM is part of the content of the Universe as a relic density. If the lifetime condition is not satisfy, Dark Matter would have started to decay after the decoupling moment; therefore, there would be nothing today.

[3]See Sect. 3.3.

3.3. Hot, Warm and Cold Dark Matter

Since Dark Matter is the dominant matter component, the formation of the different structures observed nowadays in the Cosmos is fixed by the random movement of DM in the early times. The DM velocity in the primordial Universe is a function of the distance travelled by the DM particles due to their random motion. The name of this distance is *free streaming length*, λ_{FS}. According to λ_{FS}, DM can be classified into three groups: if λ_{FS} is much smaller than a typical protogalaxy size ($\varnothing \backsim 300\,\mathrm{pc}$), DM is *cold*; if it is much larger *hot* and finally if it is comparable *warm* [182, 183]. In the middle of the 1990's theories of mixed DM became popular, nevertheless today are ruled out. In Fig. 3.4 are represented the structures predicted by the three DM types.

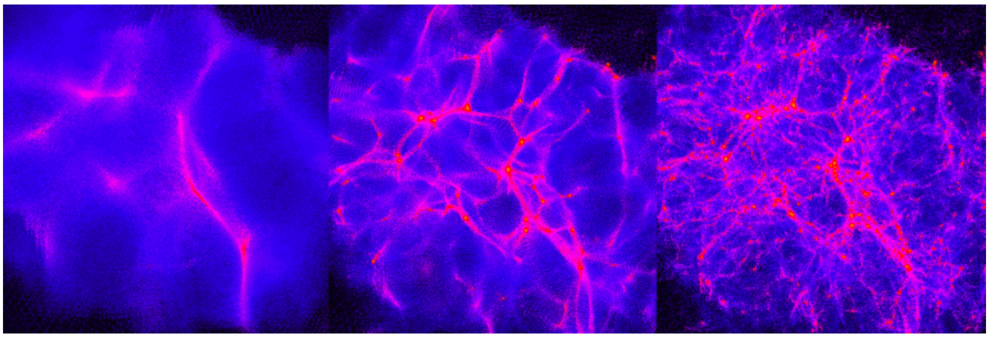

Figure 3.4: *Examples of structure formation with hot (left), warm (middle) and cold (right) Dark Matter. Simulation made by Ben Moore, Zurich University [184].*

Hot Dark Matter (HDM) refers to particles that move with velocity close to the speed of light, like SM neutrinos. The main property of the HDM is that the DM species are relativistic at the time of the structure formation, this implies large damping scales[4]. Nowadays, the HDM is disfavoured by N-body simulations since the Universe predicted by this Dark Matter type is incompatible with the current observations of the structure formation. For a complete description about the HDM problems see Ref. [187].

Cold Dark Matter (CDM) was proposed in 1982 in Refs. [188–190] (the details of the theory were developed in Ref. [191]). Nowadays, CDM is

[4]Photons and baryons are imperfectly coupled and, as a consequence, a series of anisotropy damping are produced in small scale, this effect is the so-called *Silk damping* [185]. Collision-less species that move from areas of higher density to areas of lower density also produce this kind of effects [186].

the most accepted DM model. Its predictions are in agreement with a great number of observations, such as the abundance of clusters at $z \lesssim 1$ and the galaxy-galaxy correlation function. However, in the last years, several discrepancies have been found in CDM scenarios. For example, the CDM models usually predict more *Dwarf Spheroidal Galaxies*[5] (dSphs) than observed ones [192, 193]. In addition to this problem, N-body CDM simulations predict rotation curves for low surface brightness galaxies[6] not compatible with the observations [194–197]. A complete review of CDM can be found in Ref. [198].

In order to alleviate the Cold Dark Matter problems, Warm Dark Matter was proposed (WDM). The larger λ_{FS} of WDM with respect to the CDM ones suppresses the formation of small structures, solving the Dwarf Spheroidal Galaxies problem. In the WDM case, the current DM abundance can be obtained for $\lambda_{\mathrm{FS}} \backsim 0.3\,\mathrm{Mpc}$ [199]. The WDM inhibit the formation of small DM halos at high redshift, that are needed in the star formation processes. This fact, and the observations of the so called *Lyman-α forest*[7], set bounds to the WDM mass.

3.4. Dark Matter distribution in the Galaxy

In previous sections, all properties and proofs of the existence of DM have been explained, as well as the amount of DM that populates our Universe. But how is the DM distributed? is it possible to predict the density profile of DM in our galaxy? The answer is yes!

There are several models that describe the distribution of DM along the Milky Way. The distribution is given by a Dark Matter halo profile model, that relates, for each point, the DM density with the distance between this point and the Galactic Center (GC).

[5] Low-luminosity galaxies with older stellar population.

[6] Low surface brightness galaxies are a diffuse kind of galaxies with a surface brightness that is one magnitude lower than the ambient night sky.

[7] Discovered in 1970 by Roger Lynds with the observations of the quasar 4C 05.34 [200], the Lyman-α forest is a series of absorption lines in electron transition of the neutral hydrogen atom.

Profile Name	**Predicted density** $\rho(r)$	Ref.
NFW	$\frac{\rho_s}{\eta}\,(1+\eta)^{-2}$	[201]
Einasto	$\rho_s\,\exp\left(-\frac{2}{\alpha}\left[(\eta)^{\alpha}-1\right]\right)$	[202, 203]
Isothermal	$\frac{\rho_s}{1+\eta^2}$	[143, 204]
Burkert	$\frac{\rho_s}{(1+\eta)\,(1+\eta^2)}$	[205]
Moore	$\rho_s\,\eta^{-1.16}\,(1+\eta)^{-1.84}$	[206]

Table 3.1: List of the most common Dark Matter halo profiles. We have defined $\eta = r/r_s$ to alleviate the notation. In all profiles there are two parameters that it is necessary to determine with observations: r_s, that represents a typical scale radius, and ρ_s, a typical scale density. The Einasto profile presents an extra parameter, α, that varies from simulation to simulation.

Tab. 3.1 summarizes the most common DM density profiles in the literature. The most common one is the Navarro, Frenk and White (NFW) profile, motivated by N-body simulations. However, recent simulations favour the Einasto profile over the NFW [207,208]. Other models, such as the Isothermal or the Burkert profiles, seem more motivated by the observations of galactic rotation curves. All profiles showed in Tab. 3.1 assume spherical symmetry[8]. A complete discussion about the advantages and disadvantages of different DM density profiles can be found in Ref. [210].

All models present two free parameters[9] (r_s, ρ_s) that must be determined using astrophysical observations of the Milky Way. The two fundamental measurements used to fit these free parameters are the DM density at the Sun location respect to the Galactic Center[10], $\rho_\odot = 0.3 \pm 0.1\,\mathrm{GeV/cm^3}$ [214][11], and the DM contained in 60 kpc, estimated as $M_{60} = 4.7 \times 10^{11} M_\odot$ [216–218].

[8]There are strong evidences in N-body simulations to assume spherical symmetry in the DM halo profiles [209].

[9]The Einasto profile needs an extra parameter, α. This shape parameter varies from simulation to simulation.

[10]Recent measurements determined $R_\odot = 8.33$ kpc [211, 212], in any case, the most extended value for the distance GC-Sun is still $R_\odot = 8.5$ kpc [213].

[11]Measurements of the Sloan Digital Sky Survey estimate $\rho_\odot = 0.46\,\mathrm{GeV/cm^3}$ [215]. However, the most extended value is still $\rho_\odot = 0.3\,\mathrm{GeV/cm^3}$.

Profile	α	r_s [kpc]	ρ_s [GeV/cm^3]
NFW	–	24.42	0.184
Einasto	0.17	28.44	0.033
EinastoB	0.11	35.24	0.021
Isothermal	–	4.38	1.387
Burkert	–	12.67	0.712
Moore	–	30.28	0.105

Table 3.2: Fitted parameter of the Dark Matter halo profiles.

Tab. 3.2 shows the values of the free parameters of the DM halo profile models, which have been taken from Ref. [219]. The Einasto and EinastoB models have the same dependence with the distance to the GC, nevertheless they are completely different in terms of particle inclusion. While in the first one the baryons are not considered, in the second one all SM is present. Fig. 3.5 shows the DM density as a function of the distance r for the different DM halo profile models.

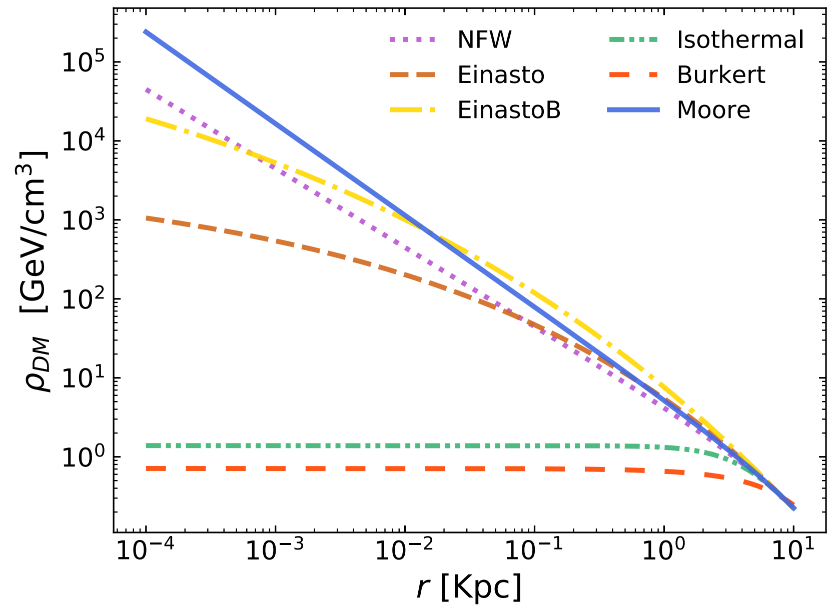

Figure 3.5: *DM density as a function of the radius to the GC for different DM halo profile models.*

3.5. Candidates

Up to this time the evidences and general properties of DM have been explained. The next step is to analyse the possible Dark Matter candidates that would fit the observations. The DM candidates landscape is huge; here we will make a summary of those that are, or have been, most popular. For a complete review about the DM candidates see Ref. [220].

3.5.1. MACHOs

One of the first studied cases was the possibility that the DM was baryonic matter. In this hypothesis DM would consist of small astronomical inert bodies that receive the name of MACHOs[12] [221]. Nowadays, it is known that this kind of DM involves several problems. The current bounds are derived from the microlensing observations causing the exclusion of masses below the solar mass, $M_\odot$ [222, 223]. Besides, since the MACHOs were produced after the BBN, its existence should leave a mark on the abundance of baryons that has not been observed [224].

3.5.2. Weakly interactive massive particles (WIMPs)

One of the most studied Dark Matter candidates is the weakly interactive massive particles (WIMPs). Firstly Proposed by Benjamin W. Lee and Steven Weinberg [225] and studied later in several researches, this kind of particles interact very weakly with the rest of the particles of the SM. In the WIMP paradigm the DM particles were in thermal equilibrium with the SM in the early Universe. When the rate of the interactions between the DM and the SM particles became smaller than the expansion rate of the Universe, the WIMP particles decoupled from the thermal bath leaving a relic abundance that can be observed nowadays[13]. If the WIMP particles are in the GeV-TeV mass range, the interaction scale to obtain the current DM abundance of the Universe is just the electroweak scale [225–228]. This

[12]Massive Astrophysical Compact Halo Objects. This term was coined by the astrophysicist Kim Griest.

[13]This process receives the name of *freeze-out*.

fact, that receives the name of *WIMP miracle*, has motivated the study of these particles during the last 40 years. For instance, in Refs. [1–3, 6] (included in Part II) we have analysed different scenarios where the DM is a WIMP particle. As WIMPs are the main DM candidate studied in the this Thesis, a detailed description of the processes needed to generate the DM abundance in this scenario is provided in Sect. 4.4. Several examples of theories that predict the existence of stable particles at the electroweak scale that can be interpreted as WIMP particles are: SUSY [229–233], UED [234] or little-Higgs theories[14] [235–237].

Until the present day, WIMP searches have been unsuccessful. As a consequence, the possible cross-section of WIMP DM with the SM particles in the mass range $m_{\rm DM} \in [1, 1000]$ GeV is significantly constrained. However, great efforts are being made by the experimental community in this area. Nowadays, there are three fundamental strategies in order to detect WIMP Dark Matter: Direct Detection (DD), Indirect Detection (ID) and collider searches. The DD consists in the detection of DM-nucleus scattering processes. Some DD experiments are, for instance, Xenon1T [238] or PandaX-II [239]. On the other hand, ID experiments try to observe the SM particles that results from the annihilation and decay of particles in the cosmic ray fluxes. Different examples of ID techniques include the detection of γ-rays (such as the Fermi-LAT experiment [240, 241]) or the detection of charged particles (such as AMS-02 [242]). The detection techniques of the WIMP DM are described in detail in Chapter 5. For interesting recent reviews about this topic see Refs. [220, 243–246].

3.5.3. Feebly interactive massive particles (FIMPs)

In order to produce the light elements and the observed structure of the CMB, the SM particles must have been in thermal equilibrium in the early Universe. However, DM may or may not have been part of the same heat bath that the SM. If DM never was in thermal equilibrium with the rest of the particles, the observed DM abundance could be generated via the *freeze-in* mechanism[15] [248–252]. Fig. 3.6 shows the values of the DM

[14] In all cases the stable particle is consequence of a conserved symmetry.

[15] In Sect. 4.5 all the details of the freeze-in production mechanism are explained.

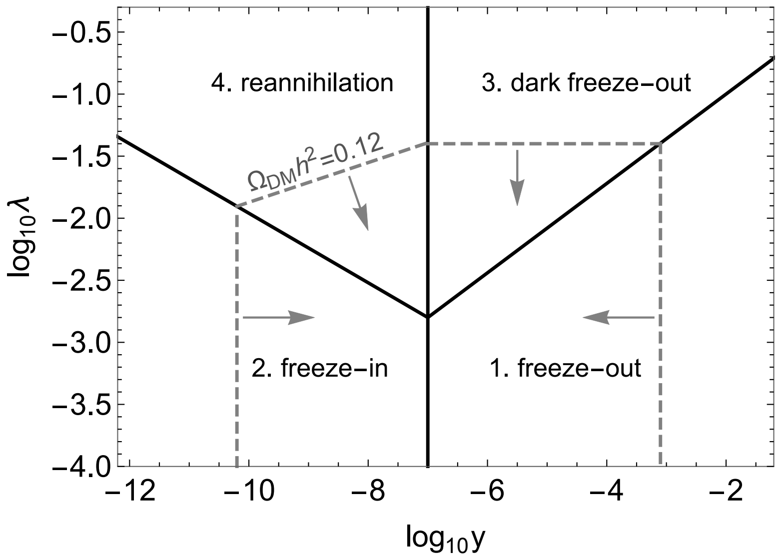

Figure 3.6: *Values of the DM-visible sector coupling (y) and the DM self-interaction coupling (λ) to obtain the correct Dark Matter relic abundance. Image taken from Ref. [247].*

coupling to SM particles (y) and the DM self-coupling (λ) with which it can be obtained the correct relic abundance. While in the WIMP scenario to figure the correct relic abundance the needed interaction scale is the electroweak scale, in this new paradigm the interaction scale is much weaker because the DM particles never reached thermal equilibrium with the SM particles. The name of this new DM candidate is Feebly Interacting Massive Particles (FIMPs) [252]. In Ref. [4] we have considered a FIMP candidate to solve the DM problem.

The detection of FIMP particles is difficult. Since the interaction scale between the SM and the DM candidate is $\log_{10}(y) \in [-10, -7]$, the DD experiments can not impose limits to the scattering cross-section. On the other hand, the signature of the mediators can be searched in the LHC, setting different limits. A summary of the different detection techniques and signals of FIMP Dark Matter can be found in Ref. [247].

3.5.4. Axion Dark Matter

In 1977 Roberto Peccei and Helen Quinn proposed an elegant mechanism to solve the strong CP problem[16] [82]. This mechanism assumes the existence of a new symmetry spontaneously broken. After the SSB of the Peccei-Quinn symmetry, a new light particle appears, the so-called *axion*[17] [253, 254]. QCD non-perturbative effects generate a potential for the axion, giving mass for this particle. The mechanism did not predict the mass of this new light boson, that depends on the scale at which the Peccei-Quinn symmetry is broken.

Axions were very popular in the scientific community since they may solve at the same time both, the strong CP problem and the DM problem. The way to produce the current DM abundance is not related with the thermal mechanism. In this case, it is assumed that the Dark Matter axions were produced in the early Universe as a result of coherent oscillations of the axion field. These oscillations generate bosonic condensates that today would be measured as CDM. The couplings between the Dark Matter axions and the other particles are model dependent and are generally assumed quite small. Nowadays, experimental bounds constrain the original Axion as a DM candidate. If the SSB of the PQ symmetry takes place after inflation, the misalignment angle is fixed, $\theta_{\mathrm{CP}} \backsimeq \pi^2/3$, and the bounds over the mass exclude the axion DM. However, particles that produce the DM abundance through the same mechanism are very dear to the scientific community. The name of these particles is *Axion Like Particles*, ALPs.

Currently, the two most accepted benchmark realizations of the Peccei-Quinn mechanism are the KSVZ [18] [255,256] and DFSZ[19] [257,258] models. The feeble interaction between the axion DM field and the SM particles is also a consequence of the axion small masses, since mass and coupling are

[16]See Sect. 1.6.2 for more details.

[17]The particle was predicted at the same time, independently, by Wilczek and Weinberg. Wilczek was the one who baptised the particle with the name of *axion*, inspired in a detergent brand (see Fig. 3.7), while Weinberg called it *Higglet*. The name that Wilczek gave to the particle became so popular that even Weinberg agreed to adopt it. The origin of the *joke* is that the axion is a pseudoscalar particle, consequently, the symmetry broken is an axial symmetry.

[18]Kim-Shifman-Vainshtein-Zakharov.

[19]Dine-Fischler-Srednicki-Zhitnitsky.

Figure 3.7: *Picture of the detergent in which Wilczek was inspired to name the axion. Surely, the marketing department of the detergent brand never thought that their product would be part of the history of high energy physics.*

inversely proportional:

$$m_a \backsimeq m_\pi \frac{f_\pi}{f_a}\,, \tag{3.2}$$

where m_π and f_π are the pion mass and decay constant, respectively.

The number of experiments that try to find evidences of the existence of axions is enormous. Several experiments base their search in the Primakoff effect[20] [259] such as ADMX [260], HAYSTAC [261], CULTASK [262] and ORGAN [263]. Other experiments, as PVLAS, search changes of the polarized light in a magnetic field [264]. The mentioned experiments are only an infinitesimal example of the large experimental landscape. For more information about the detection and the astrophysical implications of axion DM see Refs. [265–267].

3.5.5. Primordial Black Holes (PBHs)

Primordial Black Holes (PBHs) were firstly proposed in the 1970's in Refs. [268–270]. While the standard Black Holes are the consequence of the gravitational collapse of a star, the PBHs were originated due to the extreme density of the Universe at the beginning of its expansion. Since

[20]The Primakoff effect is the resonant production of neutral mesons via high-energy photons interacting with a nucleus.

PBHs were formed in the very first moments of the Universe, before the BBN, bounds on baryonic matter do not apply to them, became PBHs in a good DM candidate [271, 272].

In order to obtain the correct relic abundance of the DM it is necessary that the PBHs survive until today. As the Primordial Black Holes are not stable[21], a lower bound on their mass exists. If we assume that all DM abundance is due to PBHs, this lower bound is $m_{\mathrm{PBH}} > 3.5\times10^{-17}\,M_{\odot}$ [276]. The idea of PBHs as DM has been revived with the detection of gravitational waves by LIGO [277] since these observations can be explained with two coalescing Primordial Black Holes [278].

[21]PBHs can evaporate through Hawking radiation [273–275].

Chapter 4

Evolution of the Universe: A Thermodynamic Description

In order to understand any form of matter that surrounds us today, we need to ask ourselves which has been its evolution starting from the first moments of the Universe. This is obviously a problem of many bodies that must be statistically analysed. At the beginning of the 20th century it was thought that the Universe was practically empty, except for slight singularities (galaxies, planets, ...) that were completely lost in the immensity of space-time. In the middle of the century, the Cosmic Microwave Background was accidentally discovered. Nowadays, we know that the radiation from the CMB, measured at $T \simeq 2.725$ K [120], is the echo of the first moments after the Big Bang. The existence of a Cosmic Microwave Background is one of the great predictions of cosmological models based on the Big Bang hypothesis, according to which the original Universe was a plasma, at very high temperature, formed by baryons, electrons and photons. As the plasma cooled down, due to the adiabatic expansion of the Universe, the baryons and electrons recombined to form atoms, thus decoupling the photons in equilibrium.

The cooling of the Universe caused the different particles, that populated that hot and inert Universe, to decouple thermodynamically from the plasma until finally a small fraction remained, the CMB that we observe today, and slowly dilutes. Since the primordial Universe can be described as a plasma in thermodynamic equilibrium with good accuracy, developing any evolution model will involve understanding statistical thermodynamics.

4.1. Equilibrium description

4.1.1. Fundamental Thermodynamic Variables

Due to the asymptotic decrease in the strong interaction at high energies/temperatures, we can consider the plasma that formed the primordial Universe as a set of ideal gases in equilibrium with g internal degrees of freedom. The number density n, the energy density ρ and the pressure p of this fluid can be written based on its distribution function in the phase space:

$$\left\{\begin{array}{lcl} n & \equiv & \dfrac{g}{(2\pi)^3}\displaystyle\int_{-\infty}^{\infty} d^3p\, f(\vec{p},t) = \dfrac{g}{2\pi^2}\displaystyle\int_m^{\infty} dE\, E\,(E^2-m^2)^{1/2}\, f(E,T)\,, \\ \rho & \equiv & \dfrac{g}{(2\pi)^3}\displaystyle\int_{-\infty}^{\infty} d^3p\, E(\vec{p})\, f(\vec{p},t) = \dfrac{g}{2\pi^2}\displaystyle\int_m^{\infty} dE\, E^2(E^2-m^2)^{1/2}\, f(E,T)\,, \\ p & \equiv & \dfrac{g}{(2\pi)^3}\displaystyle\int_{-\infty}^{\infty} d^3p\, \dfrac{|\vec{p}|^2}{3E(\vec{p})}\, f(\vec{p},t) = \dfrac{g}{6\pi^2}\displaystyle\int_m^{\infty} dE\,(E^2-m^2)^{3/2}\, f(E,T)\,, \end{array}\right. \tag{4.1}$$

where the distribution function is Fermi-Dirac (FD) or Bose-Einstein (BE), depending on whether we are working with fermions or bosons:

$$f(\vec{p}) = \frac{1}{e^{(E-\mu)/T} \pm 1}\,, \tag{4.2}$$

where μ is the chemical potential of the species. The value of the sign in the denominator corresponds to -1 for the BE case and $+1$ for FD statistics, respectively. In the above expressions $E = \sqrt{|\vec{p}|^2 + m^2}$ represents the energy of a particle with momentum p and mass m. If the species are in chemical equilibrium under the interaction $i + j \longleftrightarrow a + b$, the different chemical potentials associated with the species are related:

$$\mu_i + \mu_j = \mu_a + \mu_b\,. \tag{4.3}$$

The different thermodynamic quantities described in Eq. 4.1 have simple limits when $\mu/T \ll 1$. On the one hand, the different approximations for the $T \gg m$ case are given by:

$$
\begin{aligned}
\rho &= \begin{cases} g\dfrac{7}{8}\dfrac{\pi^2}{30}T^4 & \text{Fermions}\,, \\ g\dfrac{\pi^2}{30}T^4 & \text{Bosons}\,, \end{cases} \\
n &= \begin{cases} g\dfrac{3}{4}\dfrac{\zeta(3)}{\pi^2}T^4 & \text{Fermions}, \\ g\dfrac{\zeta(3)}{\pi^2}T^4 & \text{Bosons}. \end{cases} \\
p &= \rho/3\,,
\end{aligned}
\tag{4.4}
$$

where $\zeta(3) \simeq 1.202$. On the other hand, for the $T \ll m$ case the Maxwell-Boltzmann distribution is a good approach for both, fermions and bosons. In this case, the energy density and the pressure take the following form:

$$
\begin{cases}
n = g\left(\dfrac{mT}{2\pi}\right)^{3/2} e^{-(m-\mu)/T}\,, \\
\rho = \left(\dfrac{3}{2}T + m\right) n\,, \\
p = nT\,.
\end{cases}
\tag{4.5}
$$

In general, the average energy per particle can be obtained as $\langle E\rangle \equiv \rho/n$.

4.1.2. Energy Density of the Universe

The contribution of non-relativistic species to the total energy density is negligible with respect to the relativistic one. As a consequence, during the radiation dominated era the total energy density can be approximated as the radiation energy density, composed by the contribution of all relativistic particles:

$$
\rho \simeq \rho_R = \frac{\pi^2}{30} g_\star T^4\,, \tag{4.6}
$$

where

$$g_\star \equiv \sum_{i=\text{bosons}} g_i \left(\frac{T_i}{T}\right)^4 + \frac{7}{8} \sum_{i=\text{fermions}} g_i \left(\frac{T_i}{T}\right)^4 \tag{4.7}$$

is the effective number of relativistic degrees of freedom of the relativistic species, g_i describes the degrees of freedom of each particle, T_i its temperature and T the temperature of the thermal bath, which coincides with the temperature of the photons.

In general, relativistic species in thermal equilibrium with the photons have $T_i = T \gg m_i$. However, when the temperature of the thermal bath drops below the particle mass m_i, that specie becomes non-relativistic and must be removed from Eq. 4.7. In the epoch where the temperature of the Universe was larger than the top mass m_t, all species were relativistic and $g_\star = 106.75$, its maximum value. Throughout the evolution of the Universe, the temperature decreases and the different particles become non-relativistic, decreasing the total number of relativistic degrees of freedom, until the current value:

$$g_{\star(\text{today})} = 2 + \frac{7}{8} \times 2 \times 3 \times \left(\frac{4}{11}\right)^{4/3} = 3.36\,. \tag{4.8}$$

This value, which remains invariant since e^-e^+ annihilation, takes into account the three neutrino species and photons, the only relativistic particles. Neutrinos decoupled from the thermal bath when $T \backsim 1\,\text{MeV}$, which led to a slightly cooler temperature from then of $T_\nu = (4/11)^{1/3} T_\gamma$ [47]. Under the hypothesis that Eq. 4.6 represents a good approximation to the energy density of the Universe and that large-scale space-time is flat, Friedman's equations (Eq. 2.12) lead to an expression for the Hubble parameter (Eq. 2.4) as a function of the equilibrium temperature of the Universe:

$$H = \sqrt{\frac{8\pi}{3}\frac{\rho}{M_\text{P}}} = \sqrt{\frac{4\,\pi^3}{45}}\sqrt{g_\star}\frac{T^2}{M_\text{P}}\,, \tag{4.9}$$

where $M_\text{P} = 1.22 \times 10^{19}\,\text{GeV}$ is the Planck mass.

4.1.3. Entropy Conservation in the Universe

An analysis of the evolution of any species of particle throughout the expansion of the Universe can be, in principle, complicated. In order to simplify the calculations, it is convenient to work with quantities that are conserved. Within the scope of equilibrium thermodynamics, the most commonly used conserved quantity in a *comoving*[1] volume is the entropy, described by the second principle of thermodynamics:

$$T\,dS = dU + p\,dV = d(\rho V) + p\,dV = d[(\rho + p)V] - V\,dp\,, \tag{4.10}$$

where V is the comoving volume. Using the relation between the pressure and the temperature, $dp/dT = (p+\rho)/T$, Eq. 4.10 is directly integrable:

$$S/V = \frac{p+\rho}{T} \equiv \mathfrak{s}\,, \tag{4.11}$$

where the entropy density $\mathfrak{s}$ is conserved through the expansion of the Universe, $d\mathfrak{s}/dt = 0$. The net transfer of energy in a closed system is null, which means that the total creation and destruction of particles is zero for a Universe in equilibrium. Using Eq. 4.5 the entropy density can be written as

$$\mathfrak{s} = g_{\star\,s}\frac{2\pi^3}{45}T^3\,, \tag{4.12}$$

where

$$g_{\star s} \equiv \sum_{i=\text{bosons}} g_i \left(\frac{T_i}{T}\right)^3 + \frac{7}{8}\sum_{i=\text{fermions}} g_i \left(\frac{T_i}{T}\right)^3 \tag{4.13}$$

is the effective number of degrees of freedom in entropy.

Before neutrino decoupling $g_\star = g_{\star s}$ (all relativistic species were in the thermal bath). When $T \backsim 1$ MeV, before nucleosynthesis, neutrinos decouple from the thermal bath, remaining constant its comoving temperature. At $T \sim 0.5$ MeV, photons are not energetic enough to create $e^\pm$ pairs anymore. Thus, electrons and positrons annihilate, slightly heating the thermal bath and increasing the temperature of the photons. Thenceforth,

[1] The comoving variables are defined in such a way that they are independent of the expansion of the Universe.

the number of relativistic degrees of freedom in entropy becomes

$$g_{\star s(\text{today})} = 2 + \frac{7}{8} \times 2 \times 3 \times \left(\frac{4}{11}\right) = 3.91\,. \tag{4.14}$$

Since then, both $g_\star$ and $g_{\star s}$ remain constant, although differing, since the plasma has been heated up while neutrinos have not. Fig. 4.1 shows the evolution of $g_\star$ and $g_{\star s}$ as a function of the temperature. As can be seen in the Figure, the difference between the degrees of freedom in energy and entropy is only important after the neutrino decoupling. This is due to the fact that neutrinos are the unique species that remains relativistic after its decoupling from the primordial plasma.

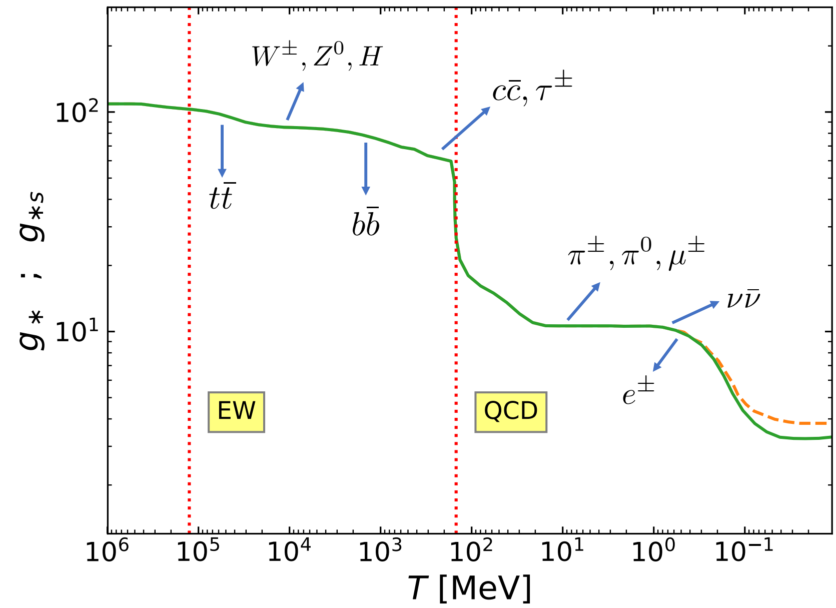

Figure 4.1: *Evolution of the relativistic degrees of freedom in density $g_\star$ (green solid line) and in entropy $g_{\star s}$ (orange dashed line). The red dotted lines show the temperature of the EW and QCD transition. The arrows indicate the moment when each species becomes non-relativistic.*

4.2. Beyond the Equilibrium Description

4.2.1. The Idea of Thermal Decoupling

At the beginning of time, the most part of the constituents of the Universe were in thermal equilibrium. For this reason, a description based on thermodynamic equilibrium is a good approximation of the early thermal history of the Universe. However, if the Universe were actually in complete thermal equilibrium, its current appearance would be that of a gas in equilibrium at the CMB temperature, which is not true. The Universe as we observe it today is the result of a multitude of processes out of equilibrium. A deep knowledge of these processes is the key to understand the evolution of the different particle species that were decoupled from the thermal bath, leaving a little background known today as relic abundances. There are different examples of decoupling from this thermal equilibrium, such as the case of neutrino decoupling, the background radiation, etc.

The problem is therefore reduced to analysing what has been the evolution of the abundance of these particles throughout the history of the Universe and what has been the remnant that they have left. The first task is to understand what equilibrium plasma decoupling actually means. Let's suppose the following $2 \to 2$ reaction:

$$\chi\,\bar{\chi} \longleftrightarrow \psi\bar{\psi}\,, \tag{4.15}$$

where χ represents the particle that will be decoupled (WIMP DM particles, for example) and ψ are the rest of the particles of the primordial plasma. As long as the χ particle is in thermal equilibrium, the reaction given by Eq. 4.15 occurs. The reaction is possible in both directions while the temperature is high enough for the less massive particles to be annihilated giving rise to the more massive ones. The net destruction of χ particles is then null. As the Universe expands, however, the temperature drops until the process can only occur in one direction: there is destruction of χ particles, but there is no creation anymore:

$$\chi\,\bar{\chi} \longrightarrow \psi\bar{\psi}\,. \tag{4.16}$$

At that moment, we say that χ is decoupled from the bath.

The criterion to determine if some kind of particles is coupled or decoupled to the primordial plasma involves the comparison of the interaction rate of the particle, usually called Γ, with the expansion rate of the Universe

(Hubble parameter):

$$\begin{cases} \Gamma > H & \text{(coupled)}\,, \\ \Gamma \lesssim H & \text{(decoupled)}\,. \end{cases} \tag{4.17}$$

The interaction rate is determined by all reactions that keep the species in thermal equilibrium.

After the decoupling, the amount of χ particles falls to the point where the annihilation practically stops. The rest of the thermal bath particles will follow the equilibrium distribution, while the χ species will follow a new distribution function. How is the form of this new distribution function? To determine this it is necessary to understand the Boltzmann equation.

4.2.2. Boltzmann Equation

The evolution of the particle number densities depends on the evolution of the distribution function $f(p^\mu, x^\mu)$ of χ species in phase space, but modelling this mathematically is tricky. Liouville's theorem[2] [280] tell us that the volume of the phase space of a distribution remains constant during the evolution of each particle of the system, as long as the system is collisionless. The theorem can be written in terms of the so-called Liouville operator (or Liouvillian):

$$\hat{L}[f] = 0\,. \tag{4.18}$$

The general covariant form of this operator is given by [226]:

$$\hat{L} = p^\alpha \frac{\partial}{\partial x^\alpha} - \Gamma^\alpha_{\beta\gamma} p^\beta p^\gamma \frac{\partial}{\partial p^\alpha}\,. \tag{4.19}$$

All the gravitational effects of the problem then come from the affine connection of the metric. For the FLRW model, the phase space density is homogeneous and isotropic: this means that $f = f(|\vec{p}|, t)$ (or equivalently $f = f(E, t)$). The Liouville operator in this model takes the following form

$$\hat{L}[f(E,t)] = E\frac{\partial f}{\partial t} - \frac{\dot{a}}{a}|\vec{p}|^2 \frac{\partial f}{\partial E}\,, \tag{4.20}$$

[2] See Ref. [279] for a modern description of the theorem.

where a is the scale factor of the FLRW metric.

In order to describe a system where χ species interacts with the rest of the particles of the SM it is necessary to modify Eq. 4.18 adding the *collision operator*[3] $\hat{C}$:

$$\hat{L}[f] = \hat{C}[f]\,, \tag{4.21}$$

that receives the name of Boltzmann Equation[4] and determines the evolution of the distribution function $f(p^\mu, x^\mu)$ of any species of particles. Using the definition of the number density in terms of the phase space density Eq. 4.1, and integration Eq. 4.21, it is easy to obtain:

$$\frac{dn_\chi}{dt} + 3\frac{\dot{R}}{R}n_\chi = \frac{g}{(2\pi)^3}\int \hat{C}[f]\frac{d^3p}{E}\,, \tag{4.22}$$

where n_χ refers to the numerical density of the χ particle.

In order to solve the equation, the collision term can be derived assuming that the colliding particles are not connected before the collision (the so-called *Stosszahlansatz* or *molecular chaos hypothesis*) [282–284]. Within this hypothesis, Eq. 4.22 can be written as:

$$\begin{aligned}\frac{g}{(2\pi)^3}\int \hat{C}[f]\frac{d^3p_\chi}{E_\chi} &= -\int d\Pi_\chi d\Pi_a d\Pi_b d\Pi_j d\Pi_i \\ &\times (2\pi)^4\delta^4(p_\chi + p_a + p_b - p_i - p_j) \\ &\times \Big[|\mathcal{M}|^2_{\chi+a+b\to i+j} f_a f_b f_\chi (1\pm f_i)(1\pm f_j) \\ &- |\mathcal{M}|^2_{i+j\to\chi+a+b} f_i f_j (1\pm f_a)(1\pm f_b)(1\pm f_\chi)\Big]\,,\end{aligned} \tag{4.23}$$

having used the relativistic kinetic theory (see Ref. [285]). In Eq. 4.23 f_i, f_j, f_a and f_b are the phase space densities of species i, j, a, b; f_χ represents the phase space density of χ (the species that we try to analyse); $\pm$ changes for bosons (+) and for fermions ($-$). Finally, the integration measure is:

$$d\Pi \equiv g\frac{1}{(2\pi)^3}\frac{d^3p}{2E}\,, \tag{4.24}$$

[3]For a derivation of the collision operator in quantum field theory see Ref. [281].

[4]The equation was proposed in 1872 by Ludwig Boltzmann in the context of kinetic theory of gases [282].

where g counts the internal degrees of freedom. For simplicity, Eq. 4.23 is particularized for $\chi + a + b \longleftrightarrow i + j$ case. However, it can be generalized to any number of colliding species.

Two well-motivated approximations can be used in order to simplify Eq. 4.23. The first assumption is CP invariance, that implies

$$|\mathcal{M}|^2_{i+j\to\chi+a+b} = |\mathcal{M}|^2_{\chi+a+b\to i+j} \equiv |\mathcal{M}|^2 \,. \tag{4.25}$$

The second one is to use the Maxwell-Boltzmann statistics for all species, instead than Fermi-Dirac for fermions or Bose-Einstein for bosons. In absence of Bose condensation or Fermi degeneracy, $1 \pm f \backsimeq 1$, $f_i(E_i) = e^{-(E_i-\mu_i)/T}$ can be used for all species in thermal equilibrium. With these approximations, the Boltzmann Equation takes the form

$$\begin{aligned} \dot{n}_\chi + 3Hn_\chi &= -\int d\Pi_\chi \, d\Pi_a \, d\Pi_b \, d\Pi_j \, d\Pi_i \, (2\pi)^4 |\mathcal{M}|^2 \\ &\times \; \delta^4(p_i + p_j - p_\chi - p_a - p_b) \, [f_a f_b f_\chi - f_i f_j] \,, \end{aligned} \tag{4.26}$$

where $H \equiv \dot{a}/a$ is the Hubble rate. Analysing the meaning of the different terms of Eq. 4.26 one finds that while $3Hn_\chi$ is the dilution of the particle density as a consequence of the expansion of the Universe, the right hand side term represents the variation produced by the interactions with the rest of the particles of the plasma.

In the analysis of the Boltzmann Equation it is very common to translate n_χ into the *yield*:

$$Y \equiv \frac{n_\chi}{\mathfrak{s}} \,. \tag{4.27}$$

This quantity takes into account the expansion of the Universe and remains constant throughout its evolution if interactions are absent. As a consequence, the yield only variates with the collision term. The evolution of the yield since the beginning of time is better expressed in terms of temperature rather than time. For this reason, it is common to use the dimensionless variable

$$x \equiv m/T \,, \tag{4.28}$$

where m is some mass scale useful for our problem (typically the mass of the χ species). Under the assumption that the number of relativistic degrees of freedom in energy ($g_\star$) and entropy ($g_{\star s}$) are independent of time, time and x can be related during the radiation dominated epoch as $dt/dx = 1/(Hx)$. Eventually, it is very common to define

$$H(m) = \sqrt{\frac{4\,\pi^3}{45}}\sqrt{g_\star}\frac{m^2}{M_\mathrm{P}}\,, \tag{4.29}$$

related with the Hubble parameter as $H = H(m)/x^2$.

Under the manipulations described above, it is easy to obtain the more usual form of the Boltzmann Equation:

$$\begin{aligned}\frac{dY}{dx} &= -\frac{x}{H(m)\,\mathfrak{s}}\int d\Pi_\chi d\Pi_a d\Pi_b d\Pi_j d\Pi_i (2\pi)^4 |\mathcal{M}|^2 \\ &\times\ \delta^4(p_i + p_j - p_\chi - p_a - p_b)[f_a f_b f_\chi - f_i f_j]\,.\end{aligned} \tag{4.30}$$

4.3. Abundance analysis of the out of equilibrium species

4.3.1. Integrated Boltzmann Equation

The general case of the Boltzmann Equation has been described in Sect. 4.2.2. In this section we study the relic abundance generated by a stable or long-lived particle, the relevant case for the works that compose this Thesis. We can separate the analysis depending on the nature of the interaction: on the one hand, if the particles are stable, only processes $2 \to 2$, such as Eq. 4.15, change the number of χ and $\bar{\chi}$ in a comoving volume. On the other hand, if the particles are unstable, other processes must be considered ($1 \to 2$, the different decays of χ). The description performed in this section follows Ref. [226].

First, we consider a $\chi\bar{\chi} \to \psi\bar{\psi}$ process, where ψ and $\bar{\psi}$ particles represent some SM specie in thermal equilibrium. The distribution functions of these bath particles are given by the equilibrium distribution:

$$\begin{cases} f_\psi &= e^{-E_\psi/T}\,, \\ f_{\bar\psi} &= e^{-E_{\bar\psi}/T}\,. \end{cases} \tag{4.31}$$

The δ-function in Eq. 4.30 implies:

$$E_\chi + E_{\bar\chi} = E_\psi + E_{\bar\psi}\,. \tag{4.32}$$

Using this information, it is easy to obtain:

$$f_\psi f_{\bar\psi} = e^{-(E_\psi+E_{\bar\psi})/T} = e^{-(E_\chi+E_{\bar\chi})/T} = f_\chi^{\rm eq} f_{\bar\chi}^{\rm eq}\,. \tag{4.33}$$

This information allows to simplify Eq. 4.30, obtaining $\left[f_\chi f_{\bar\chi} - f_\psi f_{\bar\psi}\right] = \left[f_\chi f_{\bar\chi} - f_\chi^{\rm eq} f_{\bar\chi}^{\rm eq}\right]$. Defining the thermal average annihilation cross-section for $2 \to 2$ processes:

$$\begin{aligned} \langle\sigma v\rangle &\equiv (n_\chi^{\rm eq})^{-2}\int d\Pi_\chi \Pi_{\bar\chi}\Pi_\psi\Pi_{\bar\psi}(2\pi)^4 \\ &\times\ \delta^4(p_\chi + p_{\bar\chi} - p_\psi - p_{\bar\psi})|\mathcal{M}|^2 e^{-E_\chi/T} e^{-E_{\bar\chi}/T}\,, \end{aligned} \tag{4.34}$$

the Boltzmann Equation takes the form

$$\frac{dY}{dx} = \frac{-x\langle\sigma v\rangle\,\mathfrak{s}}{H(m)}\left(Y^2 - Y_{\rm eq}^2\right)\,, \tag{4.35}$$

where $Y = n_\chi/\mathfrak{s} = n_{\bar\chi}/\mathfrak{s}$ is the yield of χ and $\bar\chi$ particles while $Y_{\rm eq} = n_\chi^{\rm eq}/\mathfrak{s} = n_{\bar\chi}^{\rm eq}/\mathfrak{s}$ is the equilibrium yield. Eventually, in order to obtain the total abundance, it is necessary to sum over all possible annihilation processes. To compute the evolution of the yield, it is necessary to know the abundance of all of the species of the Universe, the so-called equilibrium abundance [228]:

$$Y_{\rm eq} = \frac{45}{4\pi^4}\frac{x^2}{g_{\star s}}K_2(x)\,, \tag{4.36}$$

where $K_2(x)$ is the second modified Bessel function of the second kind, which can be calculated using the following integral [286]:

$$K_n(y) = \frac{\sqrt{\pi}}{(n-1/2)!}\,(y/2)^n \int_1^\infty dt\, e^{-y\,t}\left(t^2-1\right)^{n-1/2} . \qquad (4.37)$$

There are cases in which processes $1 \to 2$ have an important relevance in the evolution of the abundance. In those cases, the Boltzmann Equation must be modified as

$$\frac{dY}{dx} = -\frac{x\,\langle\Gamma\rangle}{H(m)}(Y - Y_{\mathrm{eq}}) , \qquad (4.38)$$

where $\langle\Gamma\rangle$ represents the thermally averaged decay rate. In the most general case, both terms are relevant. The Boltzmann Equation can be written then as:

$$\frac{dY}{dx} = \frac{-x\left[\langle\sigma v\rangle\,\mathfrak{s} + \langle\Gamma\rangle\right]}{H(m)}\left(Y^2 - Y_{\mathrm{eq}}^2\right) . \qquad (4.39)$$

4.3.2. Thermally-Average of Physical Observables

Eq. 4.35 allows obtaining the abundance of some species out of the thermodynamic equilibrium. In order to obtain the yield, it is necessary to evaluate the thermal-averaged annihilation cross-section $\langle\sigma v\rangle$ and decay rate $\langle\Gamma\rangle$. For the $\langle\sigma v\rangle$ case, the first task is to understand what exactly is v. In the non-relativistic case, v is the relative velocity between the two initial particles, defined as $|v_1 - v_2|$. In the relativistic scenario (the most general case) the relative velocity is non-Lorentz invariant. Instead of the classical relative velocity expression, the so-called Møller velocity must be used [287]

$$v_{\mathrm{Møl}} = \left[|\vec{v_1} - \vec{v_2}|^2 - |\vec{v_1} \times \vec{v_2}|^2\right]^{1/2} . \qquad (4.40)$$

Using this expression, the thermal-averaged annihilation cross-section can be written as:

$$\langle\sigma v\rangle = \frac{1}{8m^4 T K_2^2(m/T)} \int_{4m^2}^\infty ds(s-4m^2)\sigma\sqrt{s}K_1(\sqrt{s}/T) \qquad (4.41)$$

where $K_1(y)$ and $K_2(y)$ are the modified Bessel functions of the second kind. On the other hand, the thermally-averaged decay rate $\langle\Gamma\rangle$ can be written as

$$\langle\Gamma\rangle = \Gamma\frac{K_1(x)}{K_2(x)}\,. \tag{4.42}$$

4.4. Freeze-out: WIMP Dark Matter

As it has been commented in Sect. 3.5.2, the WIMP paradigm assumes that the DM was in thermal equilibrium with the rest of the particles of the SM in the early times of the Universe. This kind of DM was first studied by Benjamin W. Lee and Steven Weinberg [225]. Since then, several studies have been done on this scenario. This section aims to understanding how the abundance of the DM is generated for WIMP particles using the Eq. 4.35. The final form of the Boltzmann Equation for $2 \to 2$ processes presented in Sect. 4.3.1 is written as a function of the Hubble rate and the entropy density. Replacing these two functions, the Boltzmann Equation takes the form:

$$\frac{dY}{dx} = -\frac{\lambda}{x^2}\langle\sigma v\rangle\left(Y^2 - Y_{\rm eq}^2\right)\,, \tag{4.43}$$

where

$$\lambda \equiv \sqrt{\frac{\pi}{45}}\,\frac{g_{\star s}}{\sqrt{g_\star}}\,M_{\rm P}\,m_{\rm DM}\,. \tag{4.44}$$

When $x = 0$ the WIMP scenario assumes $Y = Y_{\rm eq}$ (the DM is in thermal equilibrium with the SM species). The expansion of the Universe decreases the rate of the interactions, that for the particular $2 \to 2$ case varies as

$$\Gamma_{\rm an} = n_{\rm eq}\langle\sigma v\rangle\,. \tag{4.45}$$

When $\Gamma_{\rm an} \backsimeq H$, the DM species decouples from the primordial plasma. This occurs at $x = x_{\rm fo}$, the so-called *freeze-out*. Under this hypothesis, it is easy to get an approximated value for $x_{\rm fo}$

$$x_{\rm fo} \backsimeq \log\left[\sqrt{\frac{45}{32\pi^6}}M_{\rm P}\,m_{\rm DM}\sqrt{\frac{x_{\rm fo}}{g_\star}}\langle\sigma v\rangle_{\rm fo}\right]\,, \tag{4.46}$$

where $g_\star$ must be evaluated at the freeze-out and $\langle\sigma v\rangle_{\rm fo} \equiv \langle\sigma v\rangle|_{x=x_{\rm fo}}$. The usual values of $x_{\rm fo}$ in the WIMP scenario are $x_{\rm fo} \backsim 20 - 25$, practically regardless of the DM mass in the GeV-TeV region. After the decoupling, the rate of the interactions becomes negligible, *freezing* the abundance. It is possible to take into account two approximations about the evolution of the yield. On the one hand, the DM before the freeze-out is in thermal equilibrium with the primordial plasma. Therefore, when $x \leq x_{\rm fo}$, the DM yield is equal to the equilibrium yield:

$$Y(x) = Y_{\rm eq}(x). \tag{4.47}$$

On the other hand, after the decoupling, the rate of the interactions decreases to practically zero. This fact implies that the yield remains constant

$$Y(x) = Y(x_{\rm fo}), \tag{4.48}$$

when $x > x_{\rm fo}$.

The background temperature today is $T_\infty = 2.725 \pm 0.001$ K [47] while the observed abundance is given by $Y_\infty = Y_{x\to\infty} \backsimeq Y(x \gg x_{\rm fo})$. The yield is related with the relic density via [288]

$$\Omega_{\rm DM} h^2 = 2.755 \times 10^8 \frac{m_{\rm DM}}{\rm GeV} Y_\infty \,. \tag{4.49}$$

As we have commented in Tab. 2.1, the value of the relic abundance that we observe nowadays is $\Omega_{\rm DM} h^2 = 0.1121 \pm 0.0056$ [120].

In order to solve Eq. 4.43, it is necessary to use different numerical techniques. The annihilation cross-section is, in general, too complicated to obtain an exact solution of the Boltzmann Equation. However, the special conditions of the evolution of the DM abundance in the WIMP scenario allow for an analytical approach to be found. As shown in the right panel of Fig. 4.2, after the freeze-out the DM yield remains constant, while the equilibrium yield falls. Therefore, it is reasonable to neglect $Y_{\rm eq}$ for $x > x_{\rm fo}$. Moreover, $Y = Y_{\rm eq}$ before the freeze out. Under both assumptions

$$\frac{1}{Y_\infty} = \frac{1}{Y_{\rm fo}} + \int_{x_{\rm fo}}^{\infty} \frac{dx}{x^2}\, \lambda \left\langle \sigma v \right\rangle . \tag{4.50}$$

The dependence of λ with x comes from the variation of $g_{\star s}$ and $g_\star$ with the temperature. Taking $g_{\star s}$ and $g_\star$ at the value of $T_{\rm fo}$ and neglecting $1/Y_{\rm fo}$,

$$Y_\infty = \left(\lambda_{\rm fo} \int_{x_{\rm fo}}^{\infty} \frac{dx}{x^2} \langle \sigma v \rangle \right)^{-1} , \tag{4.51}$$

where $\lambda_{\rm fo} \equiv \lambda|_{x=x_{\rm fo}}$.

The relative DM velocity in the WIMP scenario is small, fact which allows to write the cross-section in terms of the relative velocity between the two DM particles of the process. Under this assumption, we can expand the cross-section times v as a power series of v:

$$\sigma v \backsimeq a + b\, v^2 + c\, v^4 + \mathcal{O}(v^6)\,, \tag{4.52}$$

where $v \backsimeq \sqrt{s/m_{\rm DM}^2 - 4}$. The different terms of the expansion represent the s-wave, p-wave and the d-wave contributions, respectively. From Eq. 4.41, we thermally average the above expression [289]

$$\langle \sigma v \rangle = \frac{x^{3/2}}{2\sqrt{\pi}} \int_0^\infty dv\, v^2 (\sigma v) e^{-xv^2/4} \backsimeq a + \frac{6\, b}{x} + \frac{15\, c}{x^2} + \mathcal{O}(1/x^3) \tag{4.53}$$

In the particular case where DM annihilation takes place in s-wave, the thermal-averaged cross-section remains constant and Eq. 4.51 gives a trivial solution for the DM yield:

$$Y_\infty = \frac{x_{\rm fo}}{\langle \sigma v \rangle \lambda_{\rm fo}}\,. \tag{4.54}$$

Thanks to the relation between the yield and the relic density, it is easy to obtain:

$$\Omega_{\rm DM} h^2 = \frac{1.04 \times 10^9\, x_{\rm fo}}{\sqrt{g_{\star s}}\, M_{\rm P} \langle \sigma v \rangle} \,\mathrm{GeV}^{-1}\,. \tag{4.55}$$

Eq. 4.55 assumes that the relativistic degrees of freedom in entropy and energy are equal for the typical decoupling temperatures in the WIMP scenario, $g_\star = g_{\star s} \backsimeq 80 - 100$. The exact value of $x_{\rm fo}$ depends on the mass of the DM particle. However, $x_{\rm fo} \backsim 20 - 30$ in the mass range for which it is possible to describe the DM relic abundance through freeze-out. Therefore, in that range, the relic abundance only depends on the annihilation cross-section, and not directly on the mass.

In general, if $m_{\rm DM} \in [10^{-1}, 10^4]$ GeV, the value of $\langle \sigma v \rangle$ to obtain the correct relic density must be[5] $\langle \sigma v \rangle \sim 2 \times 10^{-26} cm^3/s$. Only small variations of $\langle \sigma v \rangle$ occurs in this mass range [290]. However, the approximation described in Eq. 4.53 is not always valid. There are situations, close to a resonance for instance, where is more convenient solve Eq. 4.43 numerically.

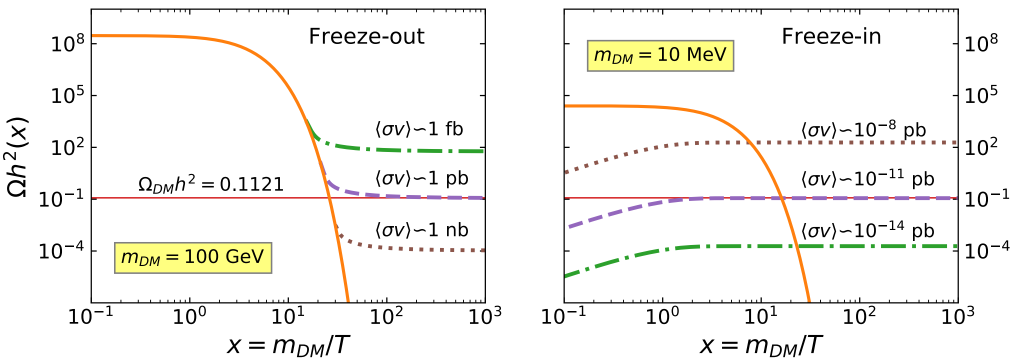

Figure 4.2: *Different examples of the two thermal production mechanisms described in this Chapter. The plots show the abundance Ωh^2 as a function of $x = m_{DM}/T$ for two representatives values of the DM mass. In both plots the red solid horizontal line shows the current DM abundance. Left plot: solution of the Boltzmann Equation 4.43 for different values of the thermal-averaged annihilation cross-section in the freeze-out regime $Y(x_0) = Y_{eq}(x_0)$. The orange solid line represents the abundance associated to the equilibrium distribution for a DM particles with $m_{DM} = 100\, GeV$. The correct relic abundance is reached for $\langle \sigma v \rangle \sim 1\, pb$. Right plot: solution for the freeze-in regime, $Y(x_0) = 0$. In this case, the orange solid line shows the abundance produced by the equilibrium distribution for $m_{DM} = 10\, MeV$.*

Left panel of Fig. 4.2 shows the numerical solution of Eq. 4.43 for different values of the thermal-averaged annihilation cross-section. Independently of the DM mass value, the current value of the DM abundance is reached for $\langle \sigma v \rangle \simeq 2 \times 10^{-26} cm^3/s \backsim 1\, pb$. This value is pretty close to the typical electroweak interaction values: this fact receives the name of *WIMP miracle*.

[5]The conversion factors between the cross-section units are $1\,\mathrm{GeV}^{-2} = 3.89 \times 10^8\,\mathrm{pb} = 1.17 \times 10^{-17}\mathrm{cm}^3/\mathrm{s}$.

4.5. Freeze-in: FIMP Dark Matter

Sect. 4.4 describes the case where the DM and the SM particles were in thermal equilibrium in the early Universe. However, when the visible and DM sectors interact with small couplings, $\backsim \mathcal{O}(10^{-7})$ [247], the interaction rate is too small to reach thermal equilibrium. Therefore, the freeze-out mechanism cannot take place. In this particular case, the abundance of the DM in the early times was negligible:

$$Y(x_0) \backsimeq 0. \tag{4.56}$$

As long as the temperature is high enough, though, the interactions with the SM increases the yield. When the temperature of the Universe decreases, the possibility of generating more DM particles is reduced. As a consequence, the DM *freezes-in* and the yield remains constant until today. This kind of DM receives the name of FIMP[6] (Feebly Interacting Massive Particles) [252]. As we commented in Sect. 4.4, the freeze-out always occur for $x = m_{\rm DM}/T \backsim 20 - 25$. This fact allows finding a typical value of the thermal-averaged cross-section to obtain the correct yield. Unlike WIMP, on the other hand, the FIMP scenario is highly dependent on initial conditions. Therefore, it is not possible to find a model-independent cross-section that reproduces the current relic abundance.

In the freeze-in scenario, the term Y^2 in Eq. 4.35 can always be neglected with respect to the equilibrium one, because the DM never reaches the thermal equilibrium with the primordial bath. As a consequence, the DM abundance before the freeze-in is always smaller than the equilibrium abundance. The Boltzmann Equation for $2 \to 2$ processes can then be simplified as

$$\frac{dY}{dx} = \frac{\lambda}{x^2}\langle\sigma v\rangle \left(Y^2 - Y_{\rm eq}^2\right) \backsimeq -\frac{\lambda\,\langle\sigma v\rangle}{x^2} Y_{\rm eq}^2\,. \tag{4.57}$$

Unlike the freeze-out scenario, where the abundance of the DM decreases with the temperature, the yield of the FIMP increases through the evolution of the thermal history of the Universe, until the freeze-in. The difference between both frameworks produces a minus sign in Eq. 4.57 with respect to

[6] Despite the name was proposed in 2009, the idea was first studied in the late 1990's in Ref. [291].

Eq. 4.35. The right panel of Fig. 4.2 shows the solution of the Boltzmann Equation in the freeze-in scenario for different constant values of the thermal average annihilation cross-section. In contrast to the freeze-out framework, in this case, the interaction must be much smaller to reach the correct relic abundance. In order to solve Eq. 4.57 we take $g_\star = g_{\star s} = 106.75$; this is a direct consequence of the ultra-relativistic nature of DM species in the FIMP regime.

The dependence from the initial conditions makes useful to analyse the main aspects of the freeze-in Eq. 4.35 in terms of the temperature, instead of [7] $x = m_{\rm DM}/T$. Therefore, the Boltzmann Equation can be written as:

$$\frac{dY}{dT} = -\frac{\gamma}{H\,\mathfrak{s}\,T}\left[\left(\frac{Y}{Y_{\rm eq}}\right)^2 - 1\right] \backsimeq \frac{\gamma}{H\,\mathfrak{s}\,T}\,, \tag{4.58}$$

where γ is the interaction rate density, defined for $a \to i + j$ processes as:

$$\gamma_{1\to 2}(T) = \frac{m_a^2 T}{2\pi^2} K_1\left(\frac{m_a}{T}\right)\,; \tag{4.59}$$

and, for $a + b \to i + j$ as:

$$\gamma_{2\to 2}(T) = \frac{T}{64\,\pi^4}\int_{s_{\rm min}}^{\infty} ds\sqrt{s}\sigma_R(s) K_1(\sqrt{s}/T)\,, \tag{4.60}$$

with $s_{\rm min} = {\rm Max}\left[(m_a + m_b)^2, (m_i + m_j)^2\right]$. The reduced cross-section[8] $\sigma_R(s)$ is related to the total annihilation cross-section $\sigma(s)$ via the Källén function[9]:

$$\sigma_R(s) = \frac{2\lambda(s, m_a^2, m_b^2)}{s}\sigma(s)\,. \tag{4.61}$$

Eq. 4.59 and Eq. 4.60 show the interaction rate density for the two kind of processes that can contribute to the DM production in this scenario.

It is easy to integrate Eq. 4.58,

$$Y(T) = \left(\frac{45}{4\pi^3}\right)^{3/2} \frac{2\,M_{\rm P}}{g_{\star s}\sqrt{g_\star}} \int_T^{T_{\rm rh}} \frac{\gamma_{2\to 2}(T)}{T^6}\,, \tag{4.62}$$

[7] Remember that there is a -1 factor between the Boltzmann Equation in terms of T and x, $dx = -(m_{\rm DM}/T^2)\,dT$.

[8] The reduced cross-section represents the cross-section without the flux factors.

[9] Defined as $\lambda(s, m_a^2, m_b^2) = \left[s - (m_a + m_b)^2\right]\left[s - (m_a - m_b)^2\right]$.

where $T_{\rm rh}$ is the *reheating temperature* which, in the approximation of a sudden decay of the *inflaton*[10], corresponds to the maximal temperature reached by the primordial thermal bath. For the previous analysis to be valid, the DM has to be out of chemical equilibrium with the SM bath. One needs to guarantee, therefore, that the interaction rate density is $\gamma \ll n_{\rm eq} H$, which translates into a bound over the reheating temperature.

[10]Hypothetical scalar field responsible of the inflation in the very early universe [292].

Chapter 5

Dark Matter Searches

In Chapter 3 we explained the properties and characteristics of a viable Dark Matter candidate. In Chapter 4 we analysed the WIMP and FIMP scenarios, explaining how the observed DM abundance is generated in the early Universe. However, how can DM particles be detected? In the

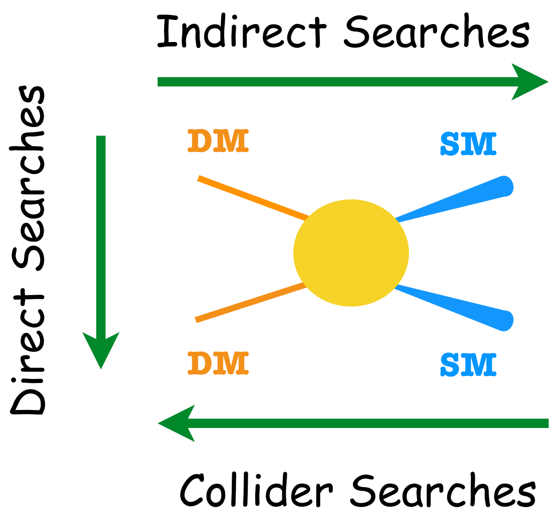

Figure 5.1: *Schematic representation of the different techniques of DM detection. Image taken from [293].*

current particle physics landscape, it is possible to group the detection experiments into three categories: DM production at hadron colliders, such as the LHC [294]; Direct Detection (DD) of DM-nucleus scattering processes in ultra-sensitive low-background experiments [295]; and eventually, Indirect Detection (ID), or the detection of particles generated in Dark Matter annihilation processes [296]. Fig. 5.1 shows a schematic representation of the three detection techniques. Although FIMPs can have similar properties to WIMPs, its coupling to the SM is much more suppressed, hence makes their detection more difficult. Nevertheless, the detection techniques in both cases are the same.

Several experiments are currently trying to detect DM, and identify its nature and interactions beyond gravity. In this Chapter we analyse the current DM detection landscape, focusing on WIMP Dark Matter searches.

5.1. Direct Detection

Nowadays, Direct Detection experiments represents one of the most promising detection techniques of BSM physics. The idea of the DD was first proposed by Mark W. Goodman and Edward Witten [297]. Since the Dark Matter must be electrically neutral, the detection with electromagnetic techniques is impossible. However, the possibility of elastic scattering between the DM and atomic nucleis exist. As the Milky Way is surrounded by a Dark Matter halo, the knowledge about its different astrophysical properties allows us to predict the interaction rate of these DM particles with the detectors located on the Earth.

5.1.1. Basic Ideas

The first derivation of the different formulas presented in this section can be found in Ref. [298]. The following discussion is based on Refs. [299,300]. The most relevant quantity in DD experiments is the *differential rate unit* (DRU) that represents the differential event rate, calculated per counts, kg, day and keV:

$$\frac{dR}{dE_{\rm NR}} = \frac{\rho_0}{m_{\rm N} m_{\rm DM}} \int_{v>v_{\rm min}} v f(v) \frac{d\sigma}{dE_{\rm NR}}(v, E_{\rm NR}) dv \,, \tag{5.1}$$

where m_N is the nucleon mass, $E_{\rm NR}$ is the nuclear recoil energy and σ represents the DM-nucleon scattering cross-section.

Typically, the DM Direct Detection experiments assumes that DM is distributed in an isotropic singular isothermal sphere, $\rho(r) \propto r^{-2}$. The local DM density is then $\rho_{\odot} = \rho|_{r=R_{\odot}}$, where $R_{\odot} = 8.0 \pm 0.5\,\text{Kpc}$ [301] is the approximate distance of the Sun from the Galactic Center. The most common value used in DD experiments for local DM density is given by[1] $\rho_{\odot} = 0.3\,\text{GeV/cm}^3$ [214].

It is common to assume an isotropic and gaussian velocity distribution[2]

$$f(\vec{v}) = \frac{1}{\sqrt{2\pi}\sigma_v}\, e^{|\vec{v}|^2/(2\sigma_v^2)}\,, \tag{5.2}$$

where σ_v represents the velocity dispersion in the DM *gas*. This approximation is called *Standard Halo Profile* and is supported by N-body simulations [302]. The velocity dispersion is related to the total circular velocity of the galaxy by $\sigma_v = \sqrt{3/2}\,v_c$, where $v_c = 220 \pm 20\,\text{km/s}$ [213].

The integral is over all velocities above the minimal velocity required to induce a nuclear recoil. This velocity can be calculated with simple kinematics:

$$v_{\text{min}} = \sqrt{\frac{m_{\text{N}} E_{\text{NR}}}{2\mu^2_{\text{DM-N}}}}\,, \tag{5.3}$$

where $\mu_{\text{DM-N}} \equiv m_N m_{\text{DM}}/(m_N + m_{\text{DM}})$ is the reduced mass of the DM and nucleus system. When the velocity is larger than the escape velocity, $v > v_{\text{esc}} = 544\,\text{km/s}$ [303], the Dark Matter particles escapes from the Dark Matter halo. Therefore, integrating Eq. 5.1 up to the escape velocity is a good approximation.

The total event rate, calculated per kilogram and per day, can be obtained integrating Eq. 5.1 in the range of the possible nuclear recoil energies,

$$R = \int_{E_{\text{NR,low}}}^{E_{\text{NR,high}}} dE_{\text{NR}}\epsilon(E_{\text{NR}})\frac{dR}{dE_{\text{NR}}}\,, \tag{5.4}$$

where $\epsilon(E_{\text{NR}})$ represents the efficiency of the detector. The maximal recoil energy is constraint by the kinematics:

$$E_{\text{NR, high}} = \frac{2\mu_{\text{DM-N}} v^2_{\text{esc}}}{m_{\text{N}}}\,, \tag{5.5}$$

[1]Note, however, that the most recent measurement finds $\rho_{\odot} = 0.46\,\text{GeV/cm}^3$ [215].
[2]Usually called Maxwellian.

while the $E_{\text{NR, low}}$ represents the threshold of the detector.

5.1.2. DM-Nucleus Cross-Section

Eq. 5.4 gives the rate of the interaction per day and per kilogram of DM particles with the detector. All information about the interaction between the nucleus and the DM is given by the DM-nucleus cross-section,

$$\frac{d\sigma}{dE_{\rm NR}} = \left(\frac{d\sigma}{dE_{\rm NR}}\right)_{\rm SI} + \left(\frac{d\sigma}{dE_{\rm NR}}\right)_{\rm SD} , \tag{5.6}$$

that consists of two contributions: Spin-Dependent (SD), the contributions that arise from the DM couplings to the quark axial-vector current, and the Spin-Independent (SI), that comes from the scalar and vector couplings in the Lagrangian.

The DM-nucleus cross-section depends on the DM-nucleon cross-section, that encodes the microscopic information of the collision. The small momentum transfer from the DM to the nucleus, $q = \sqrt{2m_{\rm N}E_{\rm NR}}$, allows us to obtain an expression that relates the microscopic and the macroscopic cross-sections.

5.1.2.1. Spin-Dependent Cross-Section

The SD cross-section depends on the spin of the DM and the angular momentum of the nucleus. For a fermionic[3] DM the expression is given by [299]

$$\left(\frac{d\sigma}{dE_{\rm NR}}\right)_{\rm SD} = \frac{16\,G_F^2\,m_{\rm N}}{\pi v^2}\,\frac{J+1}{J}\,(a_p\langle S_p\rangle + a_n\langle S_n\rangle)^2\,\frac{S(E_{\rm NR})}{S(0)} , \tag{5.7}$$

where $S(E_{\rm NR})$ and $S(0)$ are the form factors, $\langle S_{n,p}\rangle$ are the expectation values of the spin content of the neutron and proton (that can be determined experimentally) and J is the total angular momentum of the nucleus. The

[3]The expression for the spin-1 DM can be found in Ref. [304].

Nucleon	Δ_u	Δ_d	Δ_s
Neutrons	$-0.46(4)$	$0.80(3)$	$-0.12(8)$
Protons	$0.80(3)$	$-0.46(4)$	$-0.12(8)$

Table 5.1: Matrix element of the axial-vector current in a nucleon. The first row represents Δ_q^n while the second represents Δ_q^p. Data taken from [309].

coefficients a_p and a_n are given by

$$\begin{cases} a_p = \sum_{q=u,d,s} \dfrac{\alpha_q^{\mathrm{A}}}{\sqrt{2}G_{\mathrm{F}}} \Delta_q^p \,, \\ a_n = \sum_{q=u,d,s} \dfrac{\alpha_q^{\mathrm{A}}}{\sqrt{2}G_{\mathrm{F}}} \Delta_q^n \,. \end{cases} \tag{5.8}$$

The different α^{A} are the couplings of the DM to the axial-vector quark currents, which are given by the model. On the other hand, the $\Delta_q^{n,p}$ encode the information about the quark spin content of the nucleon and are proportional to $\langle N|\bar{q}\gamma_\mu\gamma_5 q|N\rangle$. These coefficients are usually calculated with two strategies: lattice QCD [305] and experimental nuclear physics techniques [306–308]. The values of $\Delta_q^{n,p}$ are summarized in Tab. 5.1.

5.1.2.2. Spin-Independent Cross-Section

In the zero-momentum transfer approximation [310] Spin Independent contribution is independent of the DM and nucleus angular momentum. The expression is then given by:

$$\left(\frac{d\sigma}{dE_{\mathrm{NR}}}\right)_{\mathrm{SI}} = \frac{2m_{\mathrm{N}}}{\pi v^2}\left(\left[Z\,f^p + (A-Z)\,f^n\,\right]^2 + \frac{B_{\mathrm{N}}^2}{256}\right) F^2(E_{\mathrm{NR}})\,, \tag{5.9}$$

where $B_{\mathrm{N}} \equiv \alpha_u^{\mathrm{V}}(A+Z) + \alpha_d^{\mathrm{V}}(2A-Z)$ is the vector-vector contribution with $\alpha_{u,d}^{\mathrm{V}}$ the vector-vector couplings between the DM and the u and d quarks, (A, Z) the number of neutrons and protons of the nucleus and $F^2(E_{\mathrm{NR}})$ another experimental form factor [311, 312].

Nucleon	f_{TG}	f_{Tu}	f_{Td}	f_{Ts}
Neutrons	0.910(20)	0.013(3)	0.040(10)	0.037(17)
Protons	0.917(19)	0.018(5)	0.027(7)	0.037(17)

Table 5.2: Contributions of the light quarks to the mass of the neutron and proton. The numbers in parentheses are the one-sigma uncertainty. Data taken from [314].

Finally, the $f^{p,n}$ quantities that appear in Eq. 5.9 are

$$\frac{f^{p,n}}{m_{p,n}} = \sum_{q=u,d,s} \frac{\alpha_q^S}{m_q} f_{Tq}^p + \frac{2}{27} f_{TG}^p \sum_{q=u,d,s} \frac{\alpha_q^S}{m_q} . \tag{5.10}$$

The scalar-scalar coupling between the DM and the quarks is given by α_q^{S}. The coefficients $f_{Tq}^{p,n}$ encode the nucleon matrix elements and represent the contribution of each light quark to the nucleon. These coefficients are defined as:

$$f_{Tq}^{p,n} = \frac{m_q}{m_{p,n}} \langle N|\bar{q}q|N\rangle \ , \tag{5.11}$$

and must be calculated using Lattice QCD or experimentally, using measurements of the pion-nucleon sigma term [313]. Finally, $f_{TG}^{p,n}$ represent the gluon contribution to the nucleon mass and is defined as

$$f_{TG}^{p,n} = 1 - \sum_{q=u,d,s} f_{Tq}^{p,n}. \tag{5.12}$$

These different constants are summarized in Tab. 5.2.

For a detailed explanation about the contributions of the light quarks to the mass and the matrix elements of the axial-vector currents see Refs. [315, 316].

5.1.3. Current Status of Direct Detection Landscape

The search for Dark Matter has become one of the great milestones of high-energy physics. However, despite the efforts of many experimental groups, no conclusive direct detection of Dark Matter has ever been made, neither of WIMP particles nor of any other form of Dark Matter[4]. Therefore, currently we only have restrictive experimental bounds on theoretical models.

The first DD experiment started in 1987: Ultralow Background Germanium Spectrometer, with 0.72 kg of high purity germanium crystal [338]. Since then, several experiments have appeared, improving the limits on DD. Nowadays, the landscape of DD is composed of a great number of experiments. The most common are the experiments that use noble gases, like xenon or argon, as a target. Tab. 5.3 summarizes the most important of them, with its different properties.

The different DD experiments represent an important improvement in the detection of the Dark Matter particles, placing strong bounds. On most models, the strongest bounds come from the SI cross-section. Fig. 5.2 shows some of this current limits.

5.2. Indirect Detection

Indirect Detection experiments try to observe the SM products of the annihilation of stable particles in the cosmic rays fluxes. In general, it is possible to distinguish between three kinds of detectable fluxes: charged particles, like electrons and positrons, protons and antiprotons, deuterium and antideuterium; photons and, finally, neutrino fluxes. Since the 1970's, several works appeared trying to find DM signatures. First publications are: in γ-rays [340–343], in positrons fluxes [343–346], in antiproton fluxes [343–347] and in antideuterons fluxes [348–350]. There are several reviews about this topic. In this Thesis we have used Refs. [219, 296].

Information on stable particle fluxes reaching the Earth can be used to constrain DM models under specific conditions. In general, in all BSM

[4]There are some exceptions, such as the case of DAMA/LIBRA experiment, which obtained data compatible with the existence of WIMP particles at specific values of the mass, such as $m_{\rm DM} = 7 - 12$ GeV [317, 318]. The current statistical significance of DAMA/LIBRA signal reaches the 12σ level. However, the annual modulation of the number of detection events found by DAMA/LIBRA is under debate since other experiments, as the experiments like LUX or Xenon1T, do not report any excess in that mass region.

Experiment	**Target**	**Mass [Kg]**	**Laboratory**	**Ref.**
ANAIS-112	NaI	112	Canfranc	[319]
CDEX-10	Ge	10	CJPL	[320]
CDMSLite	Ge	1.4	Soudan	[321]
COSINE-100	NaI	106	YangYang	[322]
CRESST-II	$CaWO_4$	5	LNGS	[323]
CRESST-III	$CaWO_4$	0.024	LNGS	[324]
DAMA/LIBRA-II	NaI	250	LNGS	[325]
Darkside-50	Ar	46	LNGS	[326]
DEAP-3600	Ar	3300	SNOLAB	[327]
DRIFT-II	CF_4	0.14	Boulby	[328]
EDELWEISS	Ge	20	LSM	[329]
LUX	Xe	250	SURF	[330]
NEWS-G	Ne	0.283	SNOLAB	[331]
PandaX-II	Xe	580	CJPL	[239]
PICASSO	C_4F_10	3.0	SNOLAB	[332]
PICO-60	C_3F_8	52	SNOLAB	[333]
SENSEI	Si	9.5×10^{-5}	FNAL	[334]
SuperCDMS	Si	9.3×10^{-4}	SNOLAB	[335]
XENON-100	Xe	62	LNGS	[336]
XENON-1T	Xe	1995	LNGS	[238]
XMASS	Xe	832	Kamioka	[337]

Table 5.3: Current Direct Detection experimental landscape in alphabetic order. The table shows the target, mass in kg and the place of a great part of the current DD experiments. Not all current experiments are included. The different data are extracted from Ref. [295].

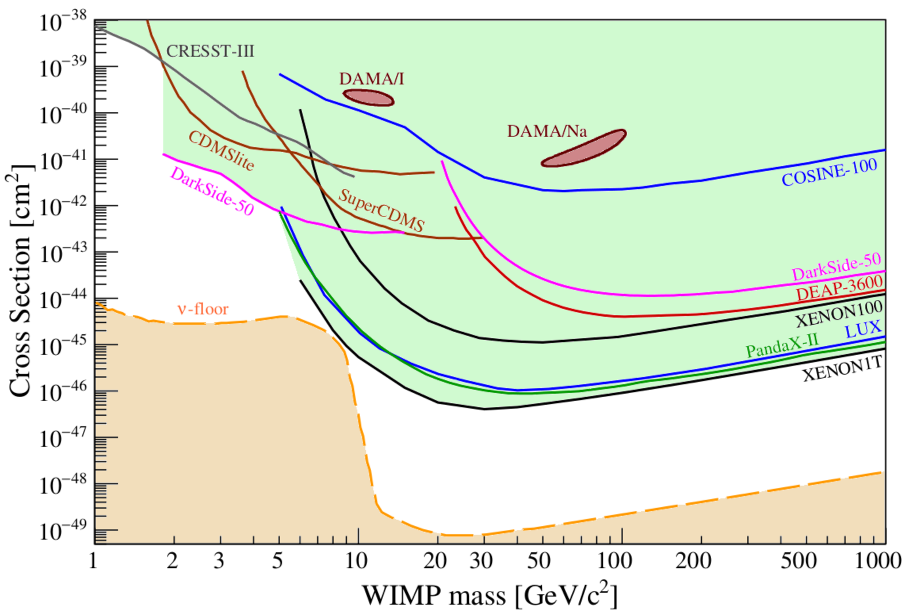

Figure 5.2: *Bounds from Dark Matter Direct Detection SI experiments. The space above the different lines is excluded at 90% confidence level. The two contour red regions represent the DM observation reported by DAMA/LIBRA experiment. The yellow region represents the neutrino floor [339], the parameter space region where the detectors should detect the coherent neutrino-nucleus scattering (CNNS). Image taken from Ref. [295].*

models, the DM can be annihilated into SM particles, resulting, in its final states, in stable particles. If these processes are possible, the signature of the DM annihilations remain in the cosmic rays detected at the Earth. The ID tries to trace the footsteps of these DM annihilations in the stable particle fluxes detected in the experiments. However, not all DM annihilations leave evidences in the cosmic rays. If the annihilation cross-section depends on the relative DM velocity, the contribution of these processes to the stable particle flux will be negligible, since the relative velocity of the DM particles today is small. This situation takes place when the angular momentum of the collision is $l > 0$. According to the velocity dependence, the different annihilation cross-section terms receives the names summarized in Tab. 5.4.

In general, ID is possible in processes that take place in *s-wave*, where the annihilation cross-section is not suppressed by the DM velocity. However, the velocity suppression only affects the indirect signals today. This fact is compatible with the DM production in the early Universe. Indeed, the DM production takes place when DM is relativistic and, as a consequence, the velocity suppression does not prevent reaching the current abundance [228].

Name	l	**Velocity dependence of** $\langle\sigma v\rangle$
s-wave	0	–
p-wave	1	$\langle\sigma v\rangle \propto v^2$
d-wave	2	$\langle\sigma v\rangle \propto v^4$
f-wave	3	$\langle\sigma v\rangle \propto v^6$

Table 5.4: Velocity dependence of the cross-section according to the collision angular momentum l.

5.2.1. Hadrons, leptons and photons spectra

For a given particle physics model, the spectrum of SM particles is not easily calculated. Nowadays, the most efficient way to obtain the different fluxes is to use a specific software, such as those in Refs. [351–355]. Fig. 5.3 shows different examples of spectra generated by annihilation of DM into photons, neutrinos, positrons antideuterons and antiprotons.

In general, the different processes that generate the final SM particle spectrum do not occur close to the Earth, where the detection is produced. As a consequence, it is necessary to propagate the spectrum given by our BSM model. The propagation is strongly dependent on the particle properties and of the cosmic-ray model employed. Indeed, there are different propagation models for photons, neutrinos, positrons, antiprotons and antideuterons. A very useful package to this task is *PPPC4DMID* and can be found in Ref. [219].

5.2.2. Propagation models of charged particles

In this section, we will provide a general benchmark for the propagation of the spectra of differently charged particles. The most common ones are the antiprotons and positrons (both cases will be analysed). For a complete description of deuterium propagation models see Refs. [350, 356, 357].

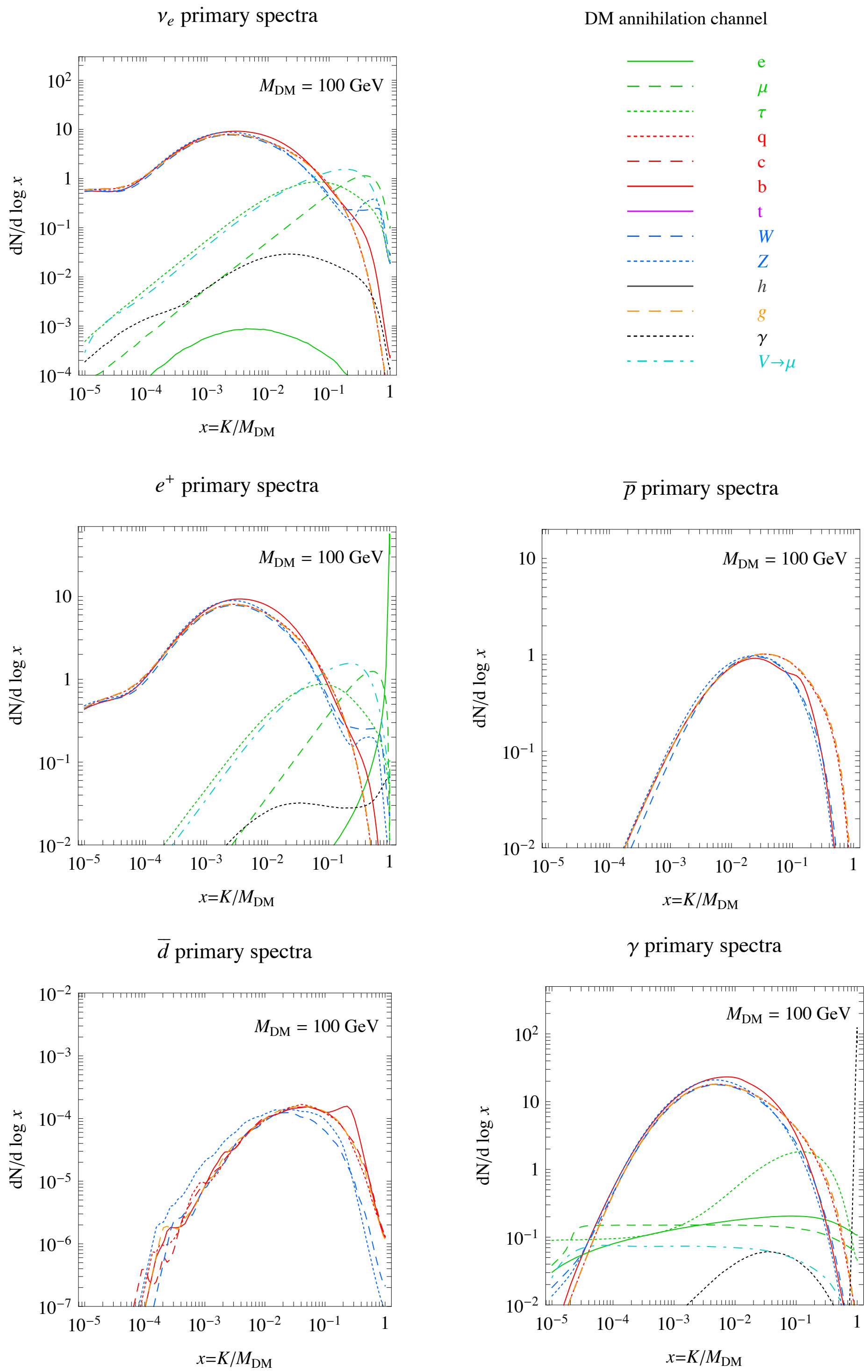

Figure 5.3: *Different examples of SM particles fluxes (from top to bottom, left to right, photons, neutrinos, positrons, antideuterons and antiprotons, respectively) produced by annihilation of two DM particles with m_{DM} = 100 GeV. In all plots K represents the kinetic energy of the final stable states. This examples are taken from Ref. [219].*

Model	δ	$\mathcal{K}_0$ [**kpc^2/Myr**]
Min	0.55	0.00595
Med	0.70	0.0112
Max	0.46	0.0765

Table 5.5: Propagation Coefficients of electrons and positrons through the galaxy. The different data are extracted from Ref. [359].

5.2.2.1. Electrons and positrons

The same formalism is used for electrons and positrons. Therefore in the following expressions we will not distinguish between them. The evolution of the electrons spectrum $f_e \equiv dN_e/dE$ along the galaxy obeys the diffusion loss equation

$$-\nabla\left[\mathcal{K}(\vec{x},E)\,\nabla f_e\right]-\frac{\partial}{\partial E}\left[b(E)\,f_e\right]=Q(\vec{x},E)\,, \tag{5.13}$$

where $Q(\vec{x},E)$ takes into account of all sources, $\mathcal{K}(\vec{x},E)$ is the diffusion coefficient function and $b(E)$ the energy loss coefficient function, that describes the energy lost by charged particles. In general, the diffusion coefficient depends on the position. However, in order to obtain a semi-analytical solution of Eq. 5.13, the spatial dependence is usually neglected in the literature: $\mathcal{K}(E)=\mathcal{K}_0\epsilon^{\delta}$, where $\epsilon\equiv E/\mathrm{GeV}$. In the same way, for high energy $b(\vec{x},E)\backsimeq b(E)\propto E^2$ [358].

The propagation model is defined by the constants $\mathcal{K}_0$ and δ. Moreover, Eq. 5.13 is usually solved in a diffusion region defined by a cylinder that sandwiches the galactic plane. In Tab. 5.5 we summarize the three most used models in the literature. The electron/positron flux Φ_e produced by DM annihilation and decay can be obtained by solving Eq. 5.13:

$$\begin{cases}\dfrac{d\Phi_e}{dE}(E,\vec{x})=\dfrac{v_e}{8\pi b(E,\vec{x})}\left(\dfrac{\rho_\odot}{m_{\rm DM}}\right)^2\displaystyle\sum_f\langle\sigma v\rangle_f\int_E^{m_{\rm DM}}dE_s\frac{dN_e^f}{dE_s}I(E,E_s,\vec{x})\,,\\[2ex] \dfrac{d\Phi_e}{dE}(E,\vec{x})=\dfrac{v_e}{4\pi b(E,\vec{x})}\left(\dfrac{\rho_\odot}{m_{\rm DM}}\right)\displaystyle\sum_f\Gamma_f\int_E^{m_{\rm DM}/2}dE_s\frac{dN_e^f}{dE_s}I(E,E_s,\vec{x})\,,\end{cases} \tag{5.14}$$

Model	δ	$\mathcal{K}_0$ **[kpc^2/Myr]**	$V_{\mathbf{conv}}$ **[km/s]**
Min	0.85	0.0016	13.5
Med	0.70	0.0112	11
Max	0.46	0.0765	5

Table 5.6: Propagation coefficients of protons and antiprotons through the galaxy. The different data are extracted from Ref. [361]

where v_e is the velocity of the electrons, E_s is the particle energy at the production point and $I(E, E_s, \vec{x})$ is the generalized halo function, that encodes all astrophysical information of the propagation. Both $b(E, \vec{x})$ and $I(E, E_s, \vec{x})$ can be calculated for the three models described in Tab. 5.5 with the *PPPC4DMID* package [219].

5.2.2.2. Protons and Antiprotons

Protons and antiprotons are charged particles as positrons and electrons. Therefore, their propagation is defined by differential equation similar to that given Sect. 5.2.2.1. However, it is necessary to include new terms and effects in the model. It is common to find in the literature the expression in cylindrical coordinates (r, z), where z is the distance from the Earth to the source. The equation is given by

$$- \mathcal{K}(K) \cdot \nabla^2 f_p + \frac{\partial}{\partial z} \left[\mathrm{sign}(z) f_p V_{\mathrm{conv}}\right] = Q - 2h\delta(z)\Gamma_{\mathrm{ann}} f_p \tag{5.15}$$

where $f_p \equiv dN_p/dE$, K is the kinetic energy of protons/antiprotons and $\mathcal{K} = \mathcal{K}_0 \beta\, (p/GeV)^\gamma$ is the diffusion function, with $p = \sqrt{K^2 + 2m_p K}$ the momentum and $\beta = v_p/c$ the velocity of the proton/antiproton.

There are two extra terms in Eq. 5.15 with respect to Eq. 5.13. The first one, V_{conv}, is the convective wind, assumed to be constant and directed outward from the galactic plane. The value of V_{conv}, such as δ and $\mathcal{K}_0$, is fixed by the model. The second new term takes into account the annihilation of protons/antiprotons confined in the galactic plane, that has $h = 0.1\,\mathrm{kpc}$ of thickness (see Ref. [360] for more details). Tab. 5.6 summarizes the three most common models for proton/antiproton propagation.

Assuming steady state conditions, the first term in Eq. 5.15 can be neglected, and the equation can be solved analytically [362–365]. Then, the proton/antiproton flux Φ_p due to the DM annihilation and decay is given by

$$\begin{cases} \dfrac{d\Phi_p}{dE}(K) &=& \dfrac{v_p}{8\pi}\left(\dfrac{\rho_\odot}{m_{\rm DM}}\right)^2 R(K)\displaystyle\sum_f \langle\sigma v\rangle_f \dfrac{dN_p^f}{dK}\,, \\ \dfrac{d\Phi_p}{dE}(K) &=& \dfrac{v_p}{4\pi}\left(\dfrac{\rho_\odot}{m_{\rm DM}}\right) R(K)\displaystyle\sum_f \Gamma_f \dfrac{dN_p^f}{dK}\,, \end{cases} \tag{5.16}$$

where $R(K)$ encodes all astrophysical information about the propagation. This function can be approximated with an accuracy better than 6% as

$$\log_{10}\left(\frac{K}{\rm Myr}\right) = a_0 + a_1\,\kappa + a_2\,\kappa^2 + a_3\,\kappa^3 + a_4\,\kappa^4 + a_5\,\kappa^5\,, \tag{5.17}$$

where $\kappa = \log_{10}(K/\text{GeV})$. The a_i coefficients depends on the propagation model (Min, Med, Max) and the DM density profile (the values can be found in Ref. [219]).

Since the mass of the protons/antiprotons is larger than the electron/positron mass, it is necessary to take into account the effect of the solar modulation. A complete description of this effect in the cosmic rays can be found in Ref. [366].

5.2.3. Propagation of Uncharged Particles

Two fluxes of uncharged particles arrive at Earth: neutrinos and photons. Regarding the neutrino flux, the most significant contribution arriving at Earth is generated in the Sun (*solar neutrinos*) or in the Earth's atmosphere (*atmospheric neutrinos*). The weak interaction of the neutrinos with the rest of the particles makes easier their propagation and larger their mean path. However, it is necessary to take into account different effects, such is the case for neutrino oscillations. A complete description of the subtleties of the propagations of neutrinos can be found in Ref. [367].

The other neutral particles that reach the earth are γ-rays. The differential photon flux produced by DM annihilations that arrives at Earth from a window with size $\Delta\Omega$, is given by [219]

$$\frac{d\Phi_\gamma}{dE}(E) = \frac{J}{8\pi m_{\mathrm{DM}}^2}\sum_f \langle\sigma v\rangle_f \frac{N_\gamma^f}{dE}(E)\,, \tag{5.18}$$

where

$$J = \int_{\Delta\Omega} d\Omega \int \rho^2(s) ds \tag{5.19}$$

is called *J-factor* and it encodes all astrophysical information. In other words, the J-factor is the integration of the DM profile along the line of sight. If the γ-rays are generated through DM decay, the flux takes the form

$$\frac{d\Phi_\gamma}{dE}(E) = \frac{J}{4\pi m_{\mathrm{DM}}}\sum_f \Gamma_f \frac{N_\gamma^f}{dE}(E)\,, \tag{5.20}$$

with

$$J = \int_{\Delta\Omega} d\Omega \int \rho(s) ds\,. \tag{5.21}$$

5.2.4. Experimental status of indirect detection: Landscape and limits

The current landscape of ID experiments provides a good source of constraints to the BSM models that include Dark Matter candidates. In this Section, we try to give a general overview of the experimental status.

5.2.4.1. γ-rays searches

The γ-ray search experiments represent the most promising source of bounds in ID. The observation of photons coming from Dwarf Spheroidal Galaxies can be used to set limits in different BSM models. DSphs are objects dominated by DM and, thanks to their high latitude, these astronomical objects suffer from low diffuse γ-ray emission.

In the last years, Fermi-LAT experiment[5] has analysed the photon flux of 15 different dSphs. In general, the Fermi collaboration has studied photons with energies between 500 MeV and 500 GeV [240,241]. It is easy to analyse

[5] The Fermi Large Area Telescope.

the bounds imposed on some BSM models by the dSphs using *gamLike v.1.0* [368].

Although the dSphs are the strongest source of bounds, different advances are being made in the γ-rays coming from the GC and other galaxy groups [369, 370].

5.2.4.2. Charged particle searches

Several experiments have reported the observation of fluxes for positrons and antiprotons. PAMELA has analysed the positron flux coming from the centre of our galaxy [371], whereas AMS-02 did the same analysis but additionally observed the antiproton flux [372–374]. Some DM models predict extra positrons and antiprotons that increase the fluxes predicted by the SM. The SM+BSM flux can be studied and compared using different backgrounds model, allowing to set bounds in specific regions of the parameter space. In the last years, an excess of $\backsimeq 10 - 20$ GeV cosmic-ray antiprotons has been reported by several authors in the data taken by AMS-02 experiment [375–379]. This excess, with a 4.7σ of significance with respect to the background signal [375], has been studied as a DM prove by several authors, some examples can be found in Refs. [380, 381].

In general, the bounds imposed by charged particles are always worse than the bounds from γ-rays or Direct Detection. Their propagation models have many uncertainties and this makes difficult to set robust constraints.

5.2.4.3. Neutrino searches

Most of the neutrinos that reach the Earth are produced in the Sun or in the Earth's atmosphere. DM could be captured by the Sun and annihilate into neutrinos, which would then be detected by different neutrino experiments giving an excess with respect to solar neutrinos due to nuclear reactions in the Sun. However, this is not the only neutrino source: fluxes coming from the GC are looked for, too. Both neutrino fluxes can be used to constrain DM models.

The weak interaction of neutrinos hinders their detection. However, there are several neutrino experiments on Earth making possible the detection of these elusive particles. Nowadays, the two most important neutrino telescopes are KM3Net and IceCube[6].

With Respect to the GC neutrino bounds, the small number of detections in Icecube and Antares makes the bound over DM models due to GC neutrino fluxes $\backsim$ 3 order of magnitude worse than the bounds from γ-rays [382, 383]. However, very competitive bounds from the solar neutrino searches are presented by both experiments [384, 385].

5.2.5. Galactic Center γ-ray Excess (GCE)

The different fluxes explained in the previous sections describe measurements that can be explained using only SM particle. This fact set limits over the DM models. However, there is an unexpected signal detected in the γ-ray data reported by the Fermi-LAT collaboration from the center of the Milky Way, the so-called Galactic Center Excess (GCE). The distribution and morphology of this photon excess is compatible with the predictions about DM annihilation [386–395]. According to the last Fermi-LAT analysis, the GCE is peaked at $\backsim$ 3 GeV.

The physical origin of the GCE is unclear. The DM explanation is not the only one, as the GCE could be caused by the emission of unresolved point sources [396–400] or due to cosmic-ray particles injected in the galactic center region, interacting with the gas or radiation fields [401]. In addition, the nature of the GCE seems different below and above $\backsim$ 10 GeV. The high energy tail may be explained as an extension of the *Fermi bubbles* observed at higher latitudes [400], whereas the low energy excess might be produced by DM annihilation, unresolved *Millisecond Pulsars*, or both.

It is true that the interpretation of the GCE as a signal of DM annihilation is not robust, but currently it can not be ruled out either.

[6] KM3Net is located 2.5 km under the Mediterranean Sea off the coast of Toulon, France (in the same place where ANTARES was located). On the other hand, IceCube is located at the Amundsen-Scott South Pole Station in Antarctica, in the same location that its predecessor AMANDA. In order to suppress the *atmospheric neutrino background*, the neutrino telescopes explore upward-going neutrinos. Therefore, while ANTARES explores the Southern Hemisphere, IceCube explores the Northern.

5.3. Collider Searches

Sect. 5.1 and Sect. 5.2 give an overview about the different techniques of Direct and Indirect DM Detection. In order to complete the DM detection landscape it is necessary to talk about the DM production at colliders. The strongest current bounds come from the searches at LHC. In general, the DM signals at colliders consist on the detection of some missing energy or momentum in the collision. Several reviews can be visited by the reader to expand the brief summary made in this section, for instance Refs. [294, 402–404]

We can distinguish two kind of models analysed at colliders: models where DM couple directly to SM particles and models where do not exist such direct couplings. In the first case, we can find different interesting channels to search for DM. On the one hand, channels related with the Higgs boson have been one of the most promising searches as a consequence of its special role in the electroweak interaction. The current bounds over the invisible decay $\mathrm{Br}(H \to \mathrm{inv})$ imposed by ATLAS and CMS can be found in Refs. [405, 406] and constraints models where DM couple directly to the Higgs. The limits over the DM mass in this case are $m_{\mathrm{DM}} \lesssim m_H/2$. On the other hand, models where DM couple to the Z boson are constrained by the precise measurements in LEP [407]. Analogous to the Higgs case, the limits over this kind of models are $m_{\mathrm{DM}} \lesssim m_Z/2$. The second kind of models is composed by scenarios where DM do not couple directly to the SM particles. In this context, the dijet and dilepton searches [408–412] play an important role when DM interacts with quarks and leptons through BSM mediators. In these cases, strong experimental constraints apply [408–412]. Finally, the study of monojets has important implications in the DM collider searches. In some DM scenarios, it is expected to produce DM at colliders together with QCD jets which set strong bounds, for instance, on DM models with leptophobic and coloured mediators mediators as shown by ATLAS [413] and CMS [414] experiments.

Chapter 6

Extra-Dimensions

6.1. Motivation

To understand the original motivation for the extra dimensions it is necessary to go back to the second half of the 19th century. Between 1860 and 1870 James Clerk Maxwell published his work about the electromagnetic field [415], which represented the unification of the electric and magnetic interactions into the same force, the electromagnetism. The unification of electromagnetism inspired many scientists to try to unify the two interactions that were known at that time: electromagnetism and gravity. In 1916 Einstein published his results on General Relativity [126], the gravitational interaction being fully described as a field theory. The first attempts at unifying electromagnetism and General Relativity came soon. In 1921 Theodor Kaluza presented an extension of the theory of General Relativity into five dimensions [416], with a metric tensor of fifteen components. These fifteen components would be distributed as follows: ten would correspond to the classic 4D metric, explaining gravity; four would represent the potential vector of electromagnetism; finally, the last component would be an unidentified massless scalar field, usually called *radion* or *dilaton*. The equation of motion of the theory provides both the Einstein equations and the Maxwell equations, and identifies the electrical charge with the motion into the fifth dimension.

In 1926, Oskar Klein adds a quantum interpretation to the Kaluza theory[1] [418, 419], imposing the quantization of linear momentum in the fifth dimension. Klein's quantum interpretation gives a solution to the invisibility of the extra-dimension: the new dimension is closed and periodic. Indeed, the characteristic radius of the fifth dimension estimated by Klein was $\backsim 10^{-30}$ cm, which explains the non-observation of the extra-dimension.

The discovery of the weak and strong interactions, and the subsequent electroweak unification, made the original motivation of Kaluza and Klein's theory lost[2]. Years later, in the 1970's, the emergence of string theories [422] revived the extra-dimensional theories in order to obtain a consistent quantum gravity theory. Since the 1990's, theories of extra-dimensions have received much more attention in the scientific community. The Universe being formed by more than 4 dimensions could, for example, give a solution to the hierarchy problem[3]. Also, many extra-dimensional models present natural candidates for Dark Matter, such as the case of the lightest Kaluza-Klein state in Universal Extra Dimensions (UED) [423, 424]. In the extra-dimensional theories it was assumed that the compactification radius of the extra-dimension was of Planck lenght. However, In the 1990's Ignatius Antoniadis in Ref. [425] and Arkani-Hamed, Dimopoulos, and Dvali in Refs. [426–429] proposed the Large Extra Dimensions (LED). In this scenario, the extra-dimension can be *large* of order TeV^{-1}, provided that only gravity propagates along the new dimension. Sect. 6.3 summarizes the fundamental characteristics of LED models.

The space-time described by LED assumes new *flat* dimensions, that is, with the same structure as the other three spatial dimensions already known. This is equivalent to neglect the curvature effects of the gravitational field over the new extra-dimension. The approximation is accurate when the tensions of the branes are small. However, new interesting phenomenology appears when this is not the case and its curvature becomes relevant. These are the so-called Warped Extra-Dimensions scenarios, also known as Randall-Sundrum models after the physicists who proposed them. We review them in Sect. 6.4.

[1]That same year quantum physics began to take its first steps with the publication of the Erwin Schrödinger Equation, Ref. [417].
[2]See, however, the works of Refs. [420, 421].
[3]For a description of the problem see Sect. 1.6.1.

Ever since Lisa Randall and Raman Sundrum proposed their extra-dimensional model, this one and its variants have been the only models of Warped Extra-Dimensions until 2016, when Gian Giudice and Matthew McCullough proposed a new Warped Extra-Dimensional model, the Clockwork/Linear Dilaton (CW/LD) model [430, 431].

In the next Sections we develop the basic concepts of the extra-dimensional models. Several reviews can be found to complete the information of this Chapter, for instance Refs. [70, 432–434].

6.2. Kaluza-Klein Decomposition

The Kaluza-Klein decomposition allows to write the extra-dimensional fields as the sum of a tower of 4D fields. In this section we show the example of the procedure for a scalar field in the 5-dimensional flat space. However, this decomposition is valid as long as we work with a separable metrics.

In the General Relativity 5-dimensional extension, the space-time metric can be written as $ds^2 = g^{(5)}_{MN} dx^M dx^N$. In the rest of the Chapter we use Greek letters when we refer to the classical 4-dimensions $x^\mu = (x^0, x^1, x^2, x^3)$ and to denote the fifth-dimension we use $x^5 = y$. For the 5-dimensional index we use Latin capital letters $x^M = (x^0, x^1, x^2, x^3, y)$. Thereafter, the signature of the metric is understood to be $(1, -1, -1, -1, -1)$.

Let us now consider the specific case of a free real scalar field. The action for a 5-dimensional Minkowski metric can be written as

$$S = \int d^4x \, dy \, \frac{1}{2} \left[(\partial_\mu \phi)^2 - (\partial_y \phi)^2 \right] . \tag{6.1}$$

The equation of motion is then given by $\partial^2_\mu \phi - \partial^2_y \phi = 0$. Imposing the periodic boundary conditions in the extra-dimension, the equation accepts as a solution:

$$\phi(x, y) = \frac{1}{\sqrt{2\pi r_c}} \sum_{n=0}^{\infty} \phi^{(n)}(x) \, e^{i\, n\, y / r_c} , \tag{6.2}$$

Figure 6.1: *Representation of Large Extra-Dimensions 5D space-time.*

where r_c is the compactification radius of the extra-dimension. Using this expression in Eq. 6.1, it is easy to obtain:

$$S = \int d^4x \left[\sum_{n>0} \partial_\mu \phi^{(n)\dagger} \partial^\mu \phi^{(n)} - \frac{n^2}{r_c^2} |\phi^{(n)}|^2 \right] , \tag{6.3}$$

where the 5D field can be written as a sum of infinite 4D massive fields with mass

$$m_n = \frac{n}{r_c} . \tag{6.4}$$

If the 5D field has a mass parameter m_0, the mass spectrum is shifted as $m_n = m_0 + n/r_c$. As we can see, the Kaluza-Klein decomposition is an expansion that transforms a 5D Lagrangian into a 4D Lagrangian with an infinite spectrum of 4D massive particles.

6.3. Large Extra-Dimensions (LED)

The most famous scenario of flat extra dimensions is called Large Extra-Dimensions [425–429]. This model implements one of the fundamental concepts of the modern extra-dimensions, the so-called *branes*. Branes are $(3 + 1)$-dimensional hypersurfaces that can trap fields on their surfaces. The presence of these hypersurfaces implies the existence of fields that only propagate on the brane (4-dimensional fields). In addition to the brane fields, there can also exist fields that freely propagate into the extra-dimensional space (the so-called *bulk*). If the SM is confined in the brane and gravity freely propagates along the bulk, the gravitational interaction is diluted along the extra-dimensional space. Therefore, while the fundamental scale of the higher dimensional gravity (M_D) can be $\mathcal{O}(1)$ TeV, the fundamental scale on the brane is M_{P}. The hierarchy problem then is only an effect of the existence of the extra-dimensions. Fig. 6.1 shows a pictorial representation of the Large Extra-Dimensions 5D space-time.

In order to obtain a relation between both fundamental scales, we assume that the metric of the higher D-dimensional space-time is given by:

$$ds^2 = G^{(D)}_{MN} dx^M dx^N. \tag{6.5}$$

The generalization of the Einstein-Hilbert action to more than 4 dimensions keeps the 4-dimensional structure:

$$S_n = -M_D^{D-2} \int d^D x \sqrt{G^{(D)}} R^{(D)}, \tag{6.6}$$

where $R^{(D)}$ is the Ricci tensor in $D = d + 4$ dimensions. On the other hand, the usual 4-dimensional action is given by

$$S_4 = -M_p^2 \int d^4 x \sqrt{G^{(4)}} R^{(4)}. \tag{6.7}$$

To know how the classical 4-dimensional gravity is contained inside the higher dimensional metric (or equivalently, how the 4-dimensional graviton is contained in the D-dimensional metric) we can expand the 4-dimensional part of the metric:

$$ds^2 = (\eta_{\mu\nu} + h_{\mu\nu}) dx^\mu dx^\nu - r_c^2 d\Omega_d^2, \tag{6.8}$$

where r_c is related to the size of the extra-dimensions (the compactification radius) and $d\Omega_d$ is the line element of the flat extra-dimensional space. The perturbation $h_{\mu\nu}$ represents the 4-dimensional graviton in 5D. Finally, the necessity to reproduce the Newton's law in four dimensions gives a relation between both fundamental scales:

$$M_{\mathrm{P}}^2 = M_D^{D-2} (2\pi r_c)^D. \tag{6.9}$$

Stringent limits for LED models come from the deviations of Newton's law. If we assume $M_D \backsim 1$ TeV (value that solves the hierarchy problem), the distance scale r_c where we found $\mathcal{O}(1)$ deviations order one is given by Eq. 6.9. Tab. 6.1 shows the expected values for r_c as a function of the

Number of extra-dimensions	r_c **[cm]**
$d = 1$	10^{13}
$d = 2$	10^{-2}
$d = 3$	10^{-7}
$d = 4$	10^{-10}
$d = 5$	10^{-12}
$d = 6$	10^{-13}

Table 6.1: LED bounds from deviations of the Newton's law. r_c represents the distance scales where we expect deviations order one.

number of dimensions. It is clear that the one extra-dimension case is totally ruled out because the scale is larger than the size of the Solar System! The effects of the deviation should have been observed in that case. On the other hand, for $d \geq 2$ the LED model solves the hierarchy problem, being r_c compatible with present bounds on deviations from the Newton's law[4] [436].

6.4. Warped Extra-Dimensions

Complementary to the flat case, Warped Extra-Dimensions was proposed, where the new dimensions are curved. This section summarizes the basic concepts of RS scenario, whereas for a complete mathematical description we address to Ref. [2] (included in Part II of this Thesis). For simplicity, we will only study the 5-dimensional case. However, the generalization to D-dimensional bulk can be found in several references (see, for instance, Refs. [70, 432–434]).

6.4.1. The Randall-Sundrum Background

The first steps in these models were given by Lisa Randall and Raman Sundrum at the end of [5] 1990's [76]. The popular Randall-Sundrum scenario

[4] In addition to the limits on deviations from the Newton's law, supernovae and neutron stars are sources of bounds for LED models [435].

[5] An alternative form of the model was published by the same authors shortly after [77].

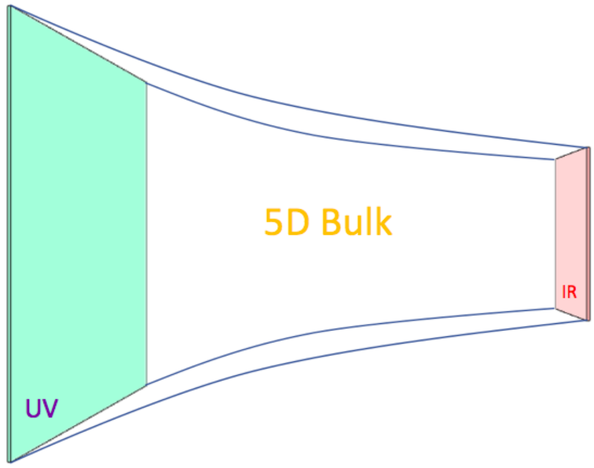

Figure 6.2: *Representation of Randall-Sundrum 5D space-time.*

consider a non-factorizable 5-dimensional metric in the form:

$$ds^2 = e^{-2\sigma(y)}\eta_{\mu\nu}dx^\mu dx^\nu - r_c^2 dy^2 \,, \tag{6.10}$$

where $\sigma(y) = kr_c|y|$ and the signature of the metric is $(+,-,-,-,-)$. In RS scenario r_c is the compactification scale, as in LED, while $k \backsim \mathcal{O}(M_\mathrm{P})$ is the curvature along the 5th-dimension. We impose periodical boundary conditions over the extra dimension, $y = y + 2\pi$, and reflectivity $y = -y$. Therefore, the metric is defined in $0 \le y \le \pi$ region. The resulting space $S_1/\mathbb{Z}_2$ is called *orbifold*. We only consider a slice of the space-time between two branes located conventionally at the two fixed-points of this orbifold, $y = 0$ (the so-called UV-brane) and $y = \pi$ (the IR-brane), with compactification radius r_c. The 5-dimensional space-time is a slice of *anti-de Sitter*[6] (AdS$_5$) space and the exponential factor that multiplies the $\mathcal{M}_4$ Minkowski 4-dimensional space-time is called *warp factor*. Planck mass in this scenario is related with the fundamental M_5 as

$$\bar{M_\mathrm{P}}^2 = \frac{M_5^3}{k}\left[1 - e^{-2k\pi r_c}\right] \,, \tag{6.11}$$

where $\bar{M_\mathrm{P}} = M_\mathrm{P}/\sqrt{8\pi}$ is the reduced Planck mass. Unlike the flat case, in RS M_P and the new fundamental mass parameter M_5 are the same order. Fig. 6.2 shows how the extra-dimension changes along the 5-dimensional

[6]This mathematical space was proposed and studied by Willem de Sitter and Albert Einstein in the 1920's.

bulk. The difference between the fundamental masses of the SM and the Planck Mass is explained by the exponential growth between the IR and the UV branes. The hierarchy problem is then a consequence of the warping of the 5-dimensional space-time.

The original RS model assumes that all fields are confined on the IR-brane, being gravity the only field that can propagate freely along the bulk. While in the classical 4-dimensional space-time the scale of the interactions is the Planck mass, $\bar{M_{\mathrm{P}}}^2$, in RS is given by

$$\Lambda \equiv \bar{M_{\mathrm{P}}} e^{-k\pi r_c} \,. \tag{6.12}$$

Choosing k and r_c such that $\Lambda \ll \bar{M_{\mathrm{P}}}$, the RS scenario can address the hierarchy problem (for $\sigma = kr_c \backsim 10$).

To study in RS scenario the gravitational interaction in the brane we expand the 4-dimensional component metric around the flat space metric:

$$G^{(4)}_{\mu\nu} = e^{-2\sigma}(\eta_{\mu\nu} + \kappa_5 h_{\mu\nu}) \,, \tag{6.13}$$

with $\kappa_5 = 2M_5^{-2/3}$. The 5-dimensional $h_{\mu\nu}$ field play the same role that in the classical space-time linearised gravity, the graviton. This field can be decomposed as a KK-tower of infinite 4-dimensional massive modes in the brane, usually called KK-gravitons. Notice that in the 4-dimensional decomposition of a 5-dimensional metric, two other fields are generally present: the graviphoton, $h_{\mu 5}$ and the graviscalar h_{55}. It has been shown elsewhere [437] that the graviphoton KK-modes are reabsorbed by the (massive) KK-gravitons. On the other hand, the graviscalar field is relevant to stabilize the size of the extra-dimension and it will be discussed in Sect. 6.4.2.

The mass spectrum of the KK-gravitons is given by:

$$m_n = k x_n e^{-k\pi r_c} \,, \tag{6.14}$$

where x_n are the zeros of [7] $J_1(x_n)$. Then, in RS the spacing between two consecutive KK-modes is $\Delta m \backsim k(x_{n-1} - x_n)e^{-k\pi r_c}$. Notice that, for low n, the KK-graviton masses are not equally spaced. This is very different from

[7] J_1 is the first Bessel functions of the first kind. The first zero is $x_1 \approx 3.83$ while the rest can be approximated by $x_n \approx \pi(n + 1/4) + \mathcal{O}(n^{-1})$ [438].

LED where the spacing between the masses of two adjacent KK-modes is $1/r_c^2$. However, for large n, as a consequence of the x_n structure, the spacing becomes approximately constant.

The strongest constraints in RS are given by the resonance searches at LHC, assuming that all fields are located in the IR-brane. Once a KK-graviton resonance is produced, we can study its decay modes in the narrow width approximation. The KK-graviton decay channels that provide the most stringent bound on m_1 and Λ are $pp \to G_1 \to \gamma\gamma$ [439] and $pp \to G_1 \to \ell\ell$ [408].

6.4.2. Size Stabilization: The Goldberger-Wise Mechanism

Stabilizing the size of the extra-dimension to be $y = \pi r_c$ is a complicated task: bosonic quantum loops have a net effect on the border of the extra-dimension such that the extra-dimension itself should shrink to a point (see, e.g., Refs. [440–442]). This feature, in a flat extra-dimension, can only be compensated by fermionic quantum loops and, usually, some supersymmetric framework is invoked to stabilize the radius of the extra-dimension (see, e.g., Ref. [443]). In Randall-Sundrum scenarios, on the other hand, a new mechanism has been considered: if we add a bulk scalar field Φ with a scalar potential $V(\Phi)$ and some ad hoc localized potential terms, $\delta(y = 0)V_{\rm UV}(\Phi)$ and $\delta(y = \pi)V_{\rm IR}(\Phi)$, it is possible to generate an effective potential $V(\varphi)$ for the 4-dimensional field $\varphi = f_{\rm IR}\, e^{-k\pi T}$, where $f_{\rm IR}$ is the IR-brane tension. In order to have a stable background metric in Eq. 6.10 and $\langle T\rangle = r_c$, the condition $f_{\rm IR} = \sqrt{24M_5^3/k}$ must be satisfied. The minimum of this potential can yield the desired value of kr_c without extreme fine-tuning of the parameters [444, 445].

As in the spectrum of the theory there is already a scalar field, the graviscalar $G_{55}^{(5)}$, the Φ field will generically mix with it. The KK-tower of the graviscalar is absent from the low-energy spectrum, as they are eaten by the KK-tower of graviphotons to get a mass (due to the spontaneous breaking of translational invariance caused by the presence of one or more branes). On the other hand, the KK-tower of the field Φ is present, but heavy (see Ref. [446]). The only light field present in the spectrum is a combination of the graviscalar zero-mode and the Φ zero-mode. This field is usually called the *radion*, r. Its mass can be obtained from the effective potential $V(\varphi)$ and is given by

$$m_\varphi^2 = \frac{k^2 v_v^2}{3M_5^3}\,\epsilon^2\, e^{-2\pi k r_c}\,, \tag{6.15}$$

where v_v is the value of Φ at the IR-brane and

$$\epsilon = \frac{m^2}{4k^2}\,, \tag{6.16}$$

with m the mass of the field Φ. Quite generally, $\epsilon \ll 1$ and, therefore, the mass of the radion can be much smaller than the first KK-graviton mass. Notice that m_r is, thus, a new free parameter of the RS model, in addition to m_1 and Λ (or, alternatively, M_5 and k).

6.4.3. AdS/CFT Correspondence and RS Model

In the original Randall-Sundrum scenario (and its subsequent generalizations), the space-time is a slice of the AdS space. AdS_n is a maximally symmetric *Lorentzian manifold*[8] with the peculiarity that presents a constant negative scalar curvature (opposite to a de Sitter space, with positive curvature.). In 1998 the so-called AdS/CFT duality was conjectured, establishing a relationship between quantum gravity theories (like M-theory and string theory) defined in some D-dimensional AdS mathematical space with *conformal field theories* (CFT) living on the boundary of such space. The idea was proposed by Juan Maldacena[9] in Ref. [447]. However, some mathematical aspects were clarified by Steven Gubser, Igor Klebanov, Alexander Polyakov and Edward Witten in Refs. [448, 449]. The AdS/CFT conjecture is also called *holographic duality* because the CFT can be interpreted as a hologram that contains all physical information about the higher-dimensional quantum gravity theory. Fig. 6.3 shows an artistic representation of this duality.

[8] Mathematical space that are described by a *Lorentzian metric*.

[9] Hitherto, in 2020, Maldacena's article is the most cited paper in high-energy physics with 16000 citations!

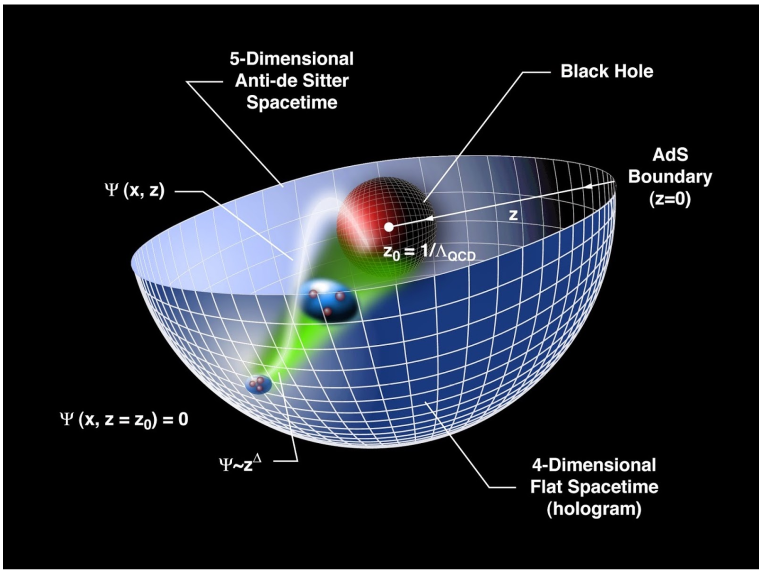

Figure 6.3: *Artistic representation of ADS/CFT correspondence. Image taken from Ref. [450].*

Since AdS/CFT duality was proposed, different authors have studied the implications of this conjecture in RS models. The idea was first explored in the non-compact Randall-Sundrum model[10] [77] (some examples can be found in Refs. [451–455]). Shortly after, the implications of the Maldacena's duality were studied in the original RS model (first publications in this direction include, for instance, Refs. [456, 457]).

A complete review about the ADS/CFT conjecture can be found in Ref. [458].

6.5. Clockwork/Linear Dilaton (CW/LD) Extra-Dimensions

In 2016 Clockwork/Linear Dilaton model was proposed by Gian Giudice and Matthew McCulloug [430, 431]. In this extra-dimensional scenario a KK-graviton tower, with a spacing very similar to that of LED models, starts at a mass gap k with respect to the zero-mode graviton. The fundamental gravitational scale M_5 can be as low as the TeV, where k is typically

[10] Usually called RS2, to distinguish it from original RS model, also called RS1.

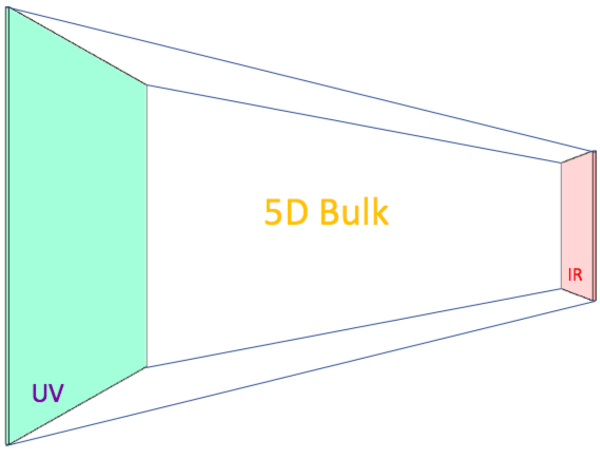

Figure 6.4: *Representation of Clockwork/Linear Dilaton 5D space-time.*

chosen in the GeV to TeV range. In this Section we have summarize the most relevant properties of CW/LD model. A more complete and technical review with all mathematical details can be found in Ref. [3], included in Part II of this Thesis.

Clockwork/Linear Dilaton scenario is defined by the metric:

$$ds^2 = e^{4/3kr_c|y|}\left(\eta_{\mu\nu}dx^\mu dx^\nu - r_c^2\, dy^2\right)\,, \tag{6.17}$$

where the signature of the metric is $(+,-,-,-,-)$. This particular metric was first proposed in the context of *Linear Dilaton* (LD) models and *Little String Theory* (see, *e.g.* Refs. [459–461] and references therein). The metric in Eq. (6.17) implies that the space-time is non-factorizable, as the length scales on our 4-dimensional space-time depending on the particular position in the extra-dimension due to the warping factor $e^{2/3\,kr_c\,|y|}$. Notice, however, that in the limit $k \to 0$ the standard, factorizable, flat LED case is immediately recovered. As for the case of the Randall-Sundrum model, also in the CW/LD scenario the extra-dimension is compactified on a $\mathcal{S}_1/\mathcal{Z}_2$ orbifold (with r_c the compactification radius), and two branes are located at the fixed points of the orbifold, $y=0$ (IR-brane) and at $y=\pi$ (UV-brane). Fig. 6.4 shows the structure of the 5-dimensional CW/LD model. As in the RS case, the hierarchy problem is solved by the growth of the fundamental parameters along the bulk. However, there is a fundamental difference between these two models: the warping factor in Eq. 6.10 multiplies only the four dimensional components, whereas, in the CW/LD case it multiplies all the 5-dimensional metric. The growing then is different in the CW/LD respect to RS, giving a totally different phenomenology [431].

In the minimal scenario, Standard Model fields are located in one of the two branes (usually the IR-brane). The scale k (also called the *clockwork spring*[11]) is the curvature along the 5th-dimension and it can be much smaller than the Planck scale. Being the relation between $\bar{M}_{\rm P}$ and the fundamental gravitational scale M_5 in the CW/LD model:

$$\bar{M}_{\rm P}^{\,2} = \frac{M_5^3}{k}\left(e^{2\pi k r_c} - 1\right) , \tag{6.18}$$

it can be shown that, in order to solve or alleviate the hierarchy problem, k and r_c must satisfy the following relation:

$$k\, r_c = 10 + \frac{1}{2\pi}\,\ln\left(\frac{k}{\rm TeV}\right) - \frac{3}{2\pi}\,\ln\left(\frac{M_5}{10\,{\rm TeV}}\right) . \tag{6.19}$$

For $M_5 = 10$ TeV and r_c saturating the present experimental bound on deviations from the Newton's law, $r_c \sim 100\,\mu$m [462], this relation implies that k could be as small as $k \sim 2$ eV, and KK-graviton modes would therefore be as light as the eV, also. This *extreme* scenario does not differ much from the LED case, but for the important difference that the hierarchy problem could be solved with just one extra-dimension (for LED models, in order to bring M_5 down to the TeV scale, an astronomical lenght r_c is needed and, thus, viable hierarchy-solving LED models start with at least 2 extra-dimensions). In the phenomenological application of the CW/LD model in the literature, however, k is typically chosen above the GeV-scale and, therefore, r_c is accordingly diminished so as to escape direct observation. Notice that, differently from the case of Warped Extra-Dimensions, where scales are all of the order of the Planck scale ($M_5, k \sim \bar{M}_{\rm P}$) or within a few orders of magnitude, in the CW/LD scenario, both the fundamental gravitational scale M_5 and the mass gap k are much closer to the electro-weak scale $\Lambda_{\rm EW}$ than to the Planck scale, as in the LED model.

[11] A term inherited by its rôle in the discrete version of the Clockwork model [430].

Expanding the metric at first order around its static solution, we have:

$$G^{(5)}_{MN} = e^{2/3S}\left(\eta_{MN} + \frac{2}{M_5^{2/3}} h_{MN}\right), \tag{6.20}$$

where $s = 2kr_c|y|$ is the dilaton field. The 4-dimensional component of the 5-dimensional field h_{MN} can be expanded in a Kaluza-Klein tower of 4-dimensional fields (4-dimensional massive gravitons) with masses

$$m_0^2 = 0\,; \qquad m_n^2 = k^2 + \frac{n^2}{r_c^2}\,. \tag{6.21}$$

Instead of $\bar{M}_{\mathrm{P}}$, in CW/LD the scale of the gravitational interactions is enhanced (as it was for RS). Indeed, the scale of the interaction of this KK-gravitons with the particles located in the IR-brane can be $\mathcal{O}$(TeV). This scale is related with the fundamental parameters of the model as

$$\begin{cases} \dfrac{1}{\Lambda_0} = \dfrac{1}{M_{\mathrm{P}}}\,, \\ \dfrac{1}{\Lambda_n} = \dfrac{1}{\sqrt{M_5^3 \pi r_c}}\left(1 + \dfrac{k^2 r_c^2}{n^2}\right)^{-1/2} = \dfrac{1}{\sqrt{M_5^3 \pi r_c}}\left(1 - \dfrac{k^2}{m_n^2}\right)^{1/2}\,, \end{cases} \tag{6.22}$$

from which it is clear that the coupling between KK-graviton modes with $n \neq 0$ is suppressed by the effective scale Λ_n and not by the Planck scale, differently from the LED case and similarly to the Randall-Sundrum one. In the RS scenario this scale is a global parameter (equal for all KK-gravitons). However, in CW/LD each gravitons is coupled different to the brane particles.

Stabilization of the radius of the extra-dimension r_c is always an issue. In the CW/LD scenario, differently from the RS one, we can use the already present bulk dilaton field to stabilize the compactification radius. A complete description of the mechanism can be found in Ref. [3], included in Part II of this Thesis.

As a final comment, In CW/LD scenario the graviton resonances are close enough to considerate a continuum spectrum. This fact allows to constrain the model using non-resonant searches at LHC in $G_1 \to \gamma\gamma$ and $G_1 \to \ell\ell$ channel. [408, 439, 463].

Chapter 7

Summary of the Results

In Chapters 1 to 6 a summary of the most relevant aspects of the Dark Matter and Extra-Dimensions has been made. The aim of the introduction is to offer the tools needed to understand the different models that compose the original works of this Thesis. In this Chapter, on the other hand, we summarize the basic ideas and results of the four papers that constitute the second part of the Thesis. Technical details can be found in the complete articles that are collected in Part II.

7.1. Probing the Sterile Neutrino Portal with γ-rays

One of the most important open problems in high-energy physics is Dark Matter, but, as we commented in Sect. 1.6, it is not the only one. Among the various problems that currently exist in the Standard Model, one of them is the neutrino masses: the model predicts zero mass for them. However, neutrino oscillations was suggested more than half a century ago as a distinctive signature of neutrino masses. This interesting effect, experimentally detected in 1998 [92], consists of a quantum-mechanical oscillation in the leptonic flavor. The phenomenon has deep implications: the effect can only happen if at least one of the three SM neutrino is massive[1]. However, the mass of these particles must be much smaller than the masses of all the other SM particles in order to escape observation. This fact favoured the development of models where the mass of the neutrinos is generated by the so-called *seesaw mechanisms*. In Sect. 1.6.3 a small review about this topic can be found.

The attempt to solve both the Dark Matter and the neutrino mass problems, at the same time[2] led to the development of models with a *sterile neutrino portal to dark matter*. This scenario has been studied by several authors, setting limits on it using Direct Detection [466–468] and Indirect Detection [469–471] experiments. This model is interesting from the point of view of Indirect Detection for several reasons (see Sects. 5.1 and 5.2 for details on DD and ID): on the one hand, Direct Detection does not happen at the lowest order in perturbation theory. As a consequence, the limits on the model due to Direct Detection experiments are worse than in other models. On the other hand, the mixing of sterile neutrinos with active neutrinos causes Dark Matter annihilations to produce photons and charged particles, as a result of several decays. All this makes it the perfect candidate to be studied from the point of view of Indirect Detection, as we have done in Ref. [1].

We analysed a particular model in which, besides the sterile neutrinos, the SM is extended by a dark sector that contains a scalar field ϕ and a fermion Ψ. These fields are both singlets of the SM gauge group but charged under a dark sector symmetry group, $G_{\rm dark}$, such that the combination $\overline{\Psi}\phi$ is a singlet of this hidden symmetry.

The lightest of the two dark particles (ϕ or Ψ) turns out to be stable if all SM particles, as well as the sterile neutrinos, are singlets of $G_{\rm dark}$, irrespective of the nature of the dark group. As a consequence, the stable particle is a good DM candidate. We assume for simplicity that the dark symmetry $G_{\rm dark}$ is a global symmetry at low energies, although we do not expect significant changes in our analysis if it was local.

[1]Despite that the phenomenon could be explained with only one massive neutrino, the observation of the effect in both atmospheric and solar neutrinos needs at least two neutrinos to be explained [464].

[2]The most economical scenario, namely that the sterile neutrinos constitute the DM [465], has been thoroughly studied [244].

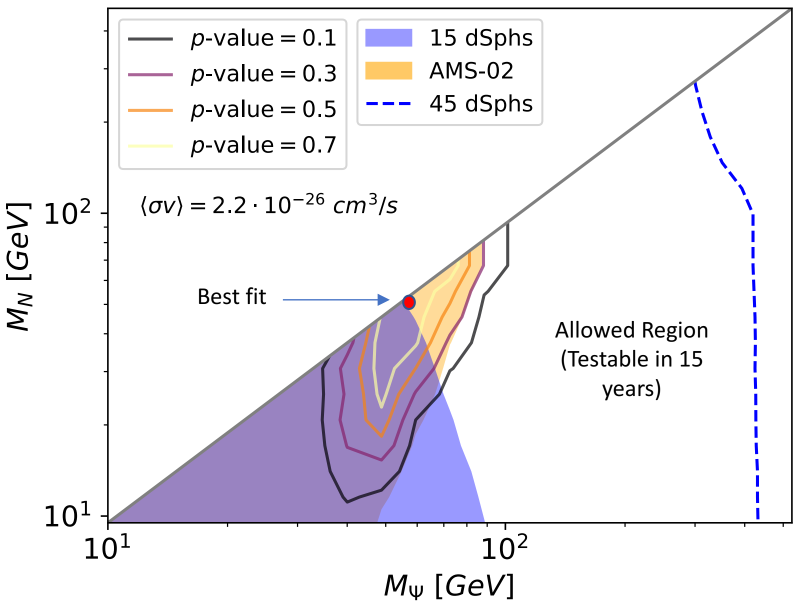

Figure 7.1: *Limits over the sterile neutrino portal to Dark Matter model in the sterile neutrino and DM masses space (M_N, M_ψ). The yellow region shows the antiproton limits, whereas the blue region are the dSphs limits. The different contours represent the region where the GCE can be fitted with its respective p-value (with increasing p-value going from outer to inner contours). Finally, the blue-dashed line shows our prediction about the foreseen future limit from the dSphs in the next 15 years of the Fermi-LAT experiment.*

The most relevant terms in the Lagrangian are given by:

$$\begin{aligned} \mathcal{L} \supset \; & \mu_H^2 H^\dagger H - \lambda_H (H^\dagger H)^2 - \mu_\phi^2 \phi^\dagger \phi - \lambda_\phi (\phi^\dagger \phi)^2 - \lambda_{H\phi} (H^\dagger H)\,(\phi^\dagger \phi) \\ - & \left[\phi \overline{\Psi} (\lambda_a + \lambda_p \gamma_5) N + Y \overline{L}_L H N_R + \text{h.c.} \right] . \end{aligned} \tag{7.1}$$

The Yukawa couplings Y between the right-handed fermions N_R and the SM leptons lead to masses for the active neutrinos after electroweak symmetry breaking, via type-I seesaw mechanism. Although two sterile neutrinos are required to generate the neutrino masses observed in oscillations, at least, in our analysis we consider that only one species is lighter than the DM and therefore relevant for the determination of its relic abundance and indirect searches. The results can be easily extended to the case of two or more sterile neutrinos lighter than the DM. Assuming that the DM is described by the fermionic field Ψ (the analysis would be similar for Dark

Matter being represented by ϕ) the masses of the model fulfill the relation $m_N < m_\Psi < m_\phi$.

Fig. 7.1 shows the final results of our analysis. Fixing the mass of the scalar mediator field such as to obtain the correct relic abundance via the freeze-out mechanism (this means $\langle \sigma\, v \rangle \sim 2 \times 10^{-26} cm^3/s$), the figure shows the different limits from photons and antiprotons in the parameter space (M_N, M_Ψ). As it has been commented in Sect. 5.2.5, the Fermi-LAT experiment has reported a Galaxy-Center γ-ray Excess (GCE). The studied model predicts a photon excess that can be compatible with the GCE in a small region of the parameter space (M_N, M_Ψ). In our analysis we assume that there are two distinct sources for the GCE: one astrophysical, responsible for the high energy tail of the γ-ray spectrum, and DM annihilation, that we considered the only source of the low energy GCE,

$$\Phi = \Phi_{\rm astro} + \Phi_{\rm DM}\,. \tag{7.2}$$

Notice that this astrophysical contribution to the flux is always needed to fit the GCE, independently of the DM model considered. The contour areas in Fig. 7.1 show the region where this fit is possible with different p-values where the outer contours have a lower p-value than the inner contours). However, the extra photons predicted by the model must also be compatible with the rest of measurements made on the different photon fluxes. Specifically, the same experiment performs measurements on the γ-rays from 15 different Dwarf Spheroidal Galaxies[3]. The dark blue-shaded region shows the area of the parameter space where the results obtained are not compatible with these measurements at 90 % C.L.

On the other hand, the model also predicts an increase of antiproton flux. This increase has been compared with the antiproton flux from the galactic center measured by the AMS-02 experiment[4], observing that there are areas in which the predictions of the model would not be compatible with the experimental measurements at 95 % C.L. (light yellow-shaded area in the Figure). However, notice that the antiproton limits are less robust than the dSphs bounds, due to the large astrophysical uncertainties in the

[3]See Sect. 5.2.4.1 for more information about this measurement.

[4]See Sect. 5.2.4.2 for a description of the experimental results and Sect. 5.2.2.2 for the details of the antiprotons propagation along the galaxy.

propagation models of charged particles. Finally, an analysis of the possible impact of future Indirect Detection experiments on the model has also been carried out. Particularly, an improvement in the dSphs data taken by Fermi-LAT is expected and could set strong bounds on the studied model (blue-dashed line). As a final comment, DM models in general, would only marginally solve the GCE, but in our case, the model could be fully tested in the next decade.

7.2. Gravity-mediated Scalar Dark Matter in RS

All the evidence we have today about the existence of Dark Matter is only related to gravitational interaction. This leads us to think about the possibility that Dark Matter particles may only interact gravitationally. In this case, DM would be undetectable by current and future particle physics experiments and it could not be a WIMP, since the gravitational interaction is too weak to produce the observed dark matter abundance through the freeze-out mechanism. However, what would it happen if we lived in more than 4 dimensions? This is the idea that inspired Ref. [2].

In this work we explored the possibility to obtain the current DM abundance, under the assumption that is composed by WIMP scalar particles, only through gravitational interaction and assuming a 5-dimensional RS spacetime. In the described scenario, Dark Matter and the Standard Model live confined in the TeV-brane. Both types of matter interact through gravity, which propagates in the 5-dimensional bulk, and is described in the effective 4-dimensional theory as a tower of massive gravitons (Kaluza-Klein modes).

The model is described using four physical parameters: the scale of the interaction of 4-dimensional massive gravitons with matter, Λ; the mass of the first graviton of the 4-dimensional KK-tower, m_1; the Dark Matter mass, $m_{\rm DM}$; and, the radion mass, m_r. Our analysis shows that when $m_r < m_{\rm DM}$ and, therefore, the annihilation channel into radions is open, the results obtained are largely independent of the particular value of m_r. Regarding the virtual radion-exchange annihilation cross-section into SM particles, it

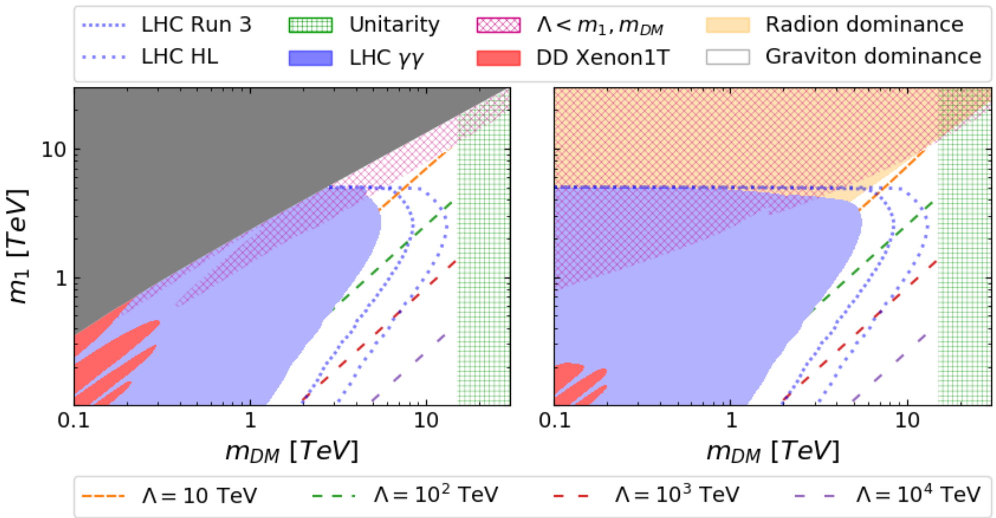

Figure 7.2: *Region of the (m_{DM}, m_1) plane for which $\langle \sigma v \rangle = \langle \sigma_{\rm fo} v \rangle$. Left panel: the radion and the extra-dimension stabilization mechanism play no role in DM phenomenology. Right panel: the extra-dimension length is stabilized with the Goldberger-Wise mechanism, with radion mass $m_r = 100$ GeV. In both panels, the grey area represents the part of the parameter space where it is impossible to achieve the correct relic abundance; the red-meshed area is the region for which the low-energy RS effective theory is untrustable, as $\Lambda < m_1$; the wiggled red area in the lower left corner is the region excluded by DD experiments; the blue area is excluded by resonant KK-graviton searches at the LHC with 36 fb^{-1} at $\sqrt{s} = 13$ TeV; the dotted blue lines represent the expected LHC exclusion bounds at the end of the Run-3 (with ~ 300 fb^{-1}) and at the HL-LHC (with ~ 3000 fb^{-1}); eventually, the green-meshed area on the right is the region where the theoretical unitarity constraints are not fulfilled. In the left panel, the allowed region is represented by the white area, for which $\langle \sigma_{\rm fo} v \rangle$ is obtained through on-shell KK-graviton production. In the right panel, in addition to the white area, within the tiny orange region $\langle \sigma_{\rm fo} v \rangle$ is obtained through on-shell radion production. The dashed lines depicted in the white region represent the values of Λ needed to obtain the correct relic abundance.*

only becomes relevant close to the resonance, $m_{\rm DM} \backsim m_r/2$. Thus, for the study of the phenomenology we fix the radion mass and focus on the remaining parameters.

The method followed for the analysis of the model has been the following: we have first computed the relevant annihilation cross-sections for DM into SM particles and KK-gravitons; then, we have studied a two-dimensional grid with different values of the mass parameters $(m_1, m_{\rm DM})$; for each point on this grid, we have searched for the Λ value to obtain the current DM abundance (for which $\langle \sigma v \rangle \backsimeq \langle \sigma v \rangle_{\rm fo} = 2 \times 10^{-26}\,{\rm cm}^3/{\rm s}$). In this way, for each point the three free parameters $(m_1,\, m_{\rm DM},\, \Lambda)$ are fully defined, which allows us to establish different theoretical and experimental limits on them.

Fig. 7.2 shows the final results of the phenomenological analysis of the model. Following the above strategy, on the left panel the case without radion has been explored, assuming that some alternative method could be found to stabilize the radius of the fifth dimension. In comparison, on the right panel it has been considered that the mass of the radion is $m_r = 100$ GeV (it is important to remember that the phenomenology is not affected by the value of this mass). The dark gray-shaded area is the region where it is not possible to obtain the current DM abundance for any value of Λ, meanwhile the orange area represents the parameter space region where the abundance is achieved thanks to the contributions of radionic interaction channels. The green-meshed area is the region where we found unitarity problems[5], $\sigma > 1/s$. In addition to this limit, there is another theoretical constraint: if $\Lambda < m_{\rm DM}, m_1$ the effective theory that describes the interaction of these quantum fields is not valid (as they should have been integrated out). This occurs in the red-meshed region.

So far, we have summarized the different limits to the model from theoretical reasons. Now we turn to the experimental bounds. The current Direct Detection experiments and the resonance searches in the ATLAS and CMS experiments at the LHC can provide much more information to our analysis. The red areas show the points where the cross-section of DM-nucleon interaction is already excluded by Xenon1T Direct Detection experiment, while the blue area is the one excluded by the resonance searches (KK gravitons searches, in our case) at the LHC. More concretely, the strongest bound comes from searches at the LHC with 36 fb^{-1} at $\sqrt{s} = 13$ TeV in the $\gamma\gamma$ channel. The two dotted lines show our prospect for the LHC-Run-3 (with ~ 300 fb^{-1}) and the HL-LHC (with ~ 3000 fb^{-1}).

The results of this work have been very rich: although similar analysis had already been carried out in the Randall-Sundrum scenario, this is the first paper that takes into account the Dark Matter annihilation channels directly into KK-gravitons in such high regions of mass space (various TeV). Without this annihilation channel, it is not possible to obtain the correct DM relic abundance in this RS scenario. Likewise, a new diagram totally

[5] Dark Matter particles have a small relative velocity, so that $s \simeq m_{\rm DM}^2$. Since to obtain the correct relic abundance $\sigma = \sigma_{\rm fo}$ is needed, then the unitarity limit becomes a restriction directly on the DM mass, $m_{\rm DM}^2 \lesssim 1/\sigma_{\rm fo}$. Therefore, in the mass plane ($m_{\rm DM}$, m_1) this bound appear as a vertical line.

forgotten in the literature has been studied: the annihilation into gravitons without a mediator, coming from the second order expansion of the interaction Lagrangian. Apart from that, it should be noted that this analysis has only been carried out for scalar Dark Matter. However, in Ref. [5], which is currently in publication process, the fermionic and vector Dark Matter cases are analysed. This new study shows that fermionic DM is disfavoured respect to the scalar and vector ones. The reason is that the dominant process (the annihilation directly into gravitons) is more suppress in that case.

7.3. Gravity-mediated Dark Matter in CW/LD

After the analysis of the implications of purely gravitational WIMP Dark Matter in the Randall-Sundrum scenario, the question of what would occur in the recent Clockwork/Linear Dilaton model almost naturally arises. This idea inspired Ref. [3]. CW/LD scenario displays more technical complications than RS: the KK-tower of massive gravitons in this case has a very small separation that makes more complicated the numerical analysis of its phenomenology. A brief review about CW/LD extra-dimensions can be found in Sect. 6.5.

The strategy to analyse the model is the same that we used in the RS case. The main difference with the previous model is the parameters chosen to study the phenomenology. In contrast with RS, in CW/LD the couplings of the massive 4-dimensional gravitons to the rest of the particles are not universal, but depend on the order n of the KK mode. Therefore, it is more useful to characterize the model in terms of M_5 instead of the effective coupling Λ_n, that depends on the particular KK-mode studied. In addition to that, the mass of the first graviton coincides with the value of the curvature along the fifth dimension, $m_1 = k$. In the original RS scenario a stabilization mechanism was absent, and a new scalar field is necessary to stabilize the fifth dimension. On the contrary, in CW/LD the 5-dimensional dilaton field takes this role. Unlike RS, where the radion mass is a new parameter, in this scenario the mass of the radion is also determined by k. However, there are several ways to stabilize the size of the extra-dimension with the dilaton field. The minimal case assumes that the tension of the 4-dimensional branes is infinite. This framework receives the name of *rigid limit* and it is the assumed case in this work. Currently, we are working on the implications of the phenomenology out of the rigid limit [472]. There is another important difference between both frameworks relevant for the phenomenological study: in CW/LD the complete dilaton KK-tower is relevant. In RS the KK tower of the Goldberger-Wise scalar field was present, but heavy [446]. As a consequence, the only light field present in the spectrum in that case was the radion.

Fig. 7.3 shows the results obtained for this scenario, following the same strategy outlined in Sect. 7.2. As in the RS case, M_5 has been fixed to set the current abundance of Dark Matter for each point in the parameter space $(m_{\rm DM}, k)$. The different limits studied are the same as in the RS case: the red-meshed region shows the area where the effective field theory is untrustable, $M_5 < m_{\rm DM}, m_{G_1}$; the green-meshed region represents the area where $\sigma < 1/m_{\rm DM}^2$ and, therefore, suffers from unitarity problems; eventually, the blue-shaded area represents the limits imposed by the LHC. As a consequence of the small separation between the KK-gravitons, the strongest bound imposed by the LHC comes from non-resonant searches in $\gamma\gamma$ channel. Finally, it should be noted that in the CW/LD case the limits imposed by the Direct Detection of Dark Matter exclude very small DM masses and, as a consequence, they do not appear in the Figure.

In this case, three possible Dark Matter particles spin have been analysed: scalar, fermion and vector. The two upper plots correspond to the scalar case without taking into account the radion and the dilaton-tower (left) and taking it into account (right). This is the only case where radion and dilatons play an important role in the phenomenology of the model and therefore it is worth showing what their impact is on the final results. The lower panels correspond to the fermionic case (left) and the vector case (right). In both cases the radion and the dilatons do not play any role. The Figure shows that the fermionic case is disfavoured with respect to the other two: the non-resonant searches at LHC impose strong limits in this case. This fact is because in the fermionic case the dominant channel, the annihilation of Dark Matter directly into KK gravitons, is suppressed.

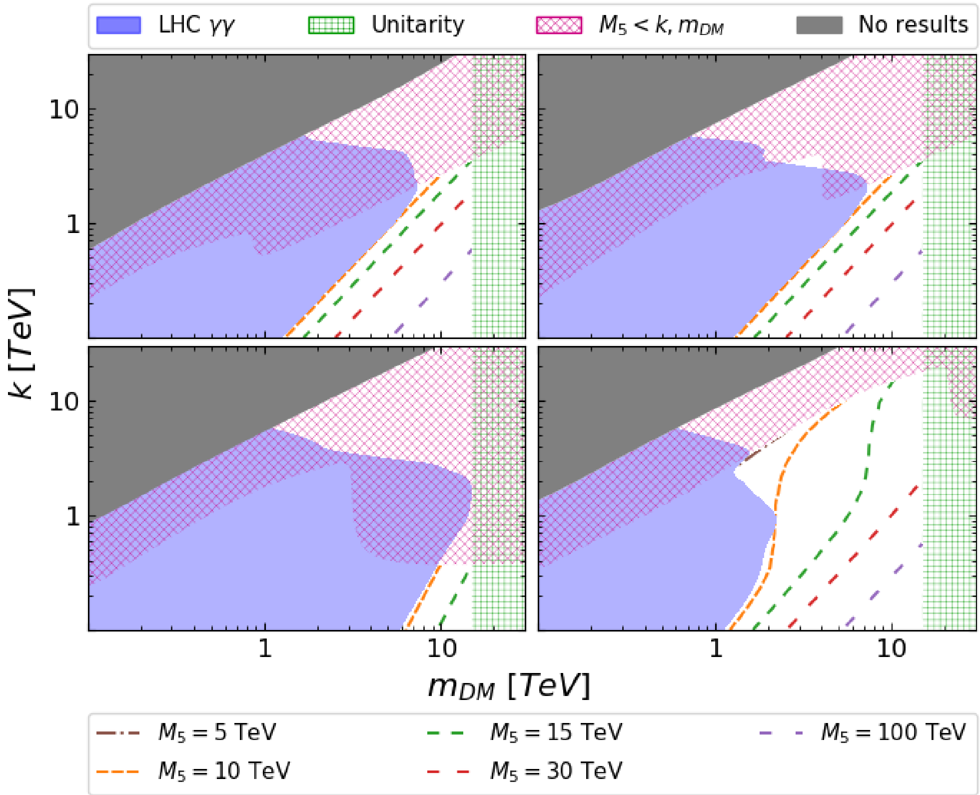

Figure 7.3: *Region of the* $(m_{\rm DM}, k)$ *plane for which* $\langle \sigma v \rangle = \langle \sigma_{\rm fo} v \rangle$. *Upper left panel: scalar DM (unstabilized extra-dimension); Upper right panel: scalar DM (stabilized extra-dimension in the rigid limit); Lower left panel: fermion DM (stabilized extra-dimension in the rigid limit); Lower right panel: vector DM (stabilized extra-dimension in the rigid limit). In all panels, the grey-shaded area represents the part of the parameter space for which it is impossible to achieve the correct relic abundance; the red diagonally-meshed area is the region for which the low-energy CW/LD effective theory is untrustable, as* $M_5 < k, m_{DM}$*; the blue-shaded area is excluded by non-resonant searches at the LHC with 36 fb*$^{-1}$ *at* $\sqrt{s} = 13$ *TeV [431]; eventually, the green vertically-meshed area on the right is the region where the theoretical unitarity constraints are not fulfilled,* $m_{\rm DM} \gtrsim 1/\sqrt{\sigma_{\rm fo}}$. *In all panels, the white area represents the region of the parameter space for which the correct relic abundance is achieved (either through direct KK-graviton and/or radion/KK-dilaton production, as in the case of scalar DM, or through virtual KK-graviton exchange, as for fermion and vector DM) and not excluded by experimental bounds and theoretical constraints. The dashed lines depicted in the white region represent the values of* M_5 *needed to obtain the correct relic abundance.*

As a final comment to gravitational-interacting DM in RS and/or CW/LD scenarios, we can say that in both cases a viable region of the parameter space exists, for the DM masses in the range $[1, 10]$ TeV approximately and for m_1 smaller than $\backsim$ 3 TeV, $\backsim$ 400 GeV and $\backsim$ 10 TeV for the scalar, fermionic and vectorial cases, respectively. Most of the allowed region could be tested by the LHC Run-3 or its high luminosity upgrade. Notice that in the allowed region typically the scale of new physics (either Λ or M_5) is a bit too large to solve the hierarchy problem.

7.4. Kaluza-Klein FIMP Dark Matter in RS

In the three models analysed before it has been considered that the DM is composed by WIMP particles. However, FIMP Dark Matter[6] brings interesting properties for the purely gravitational case. In the last work included in this Thesis we explore the possibility to obtain the DM abundance using gravitational interaction and FIMP particles in the RS scenario [4] (an extension to the CW/LD is in progress). The FIMP case raises very different mathematical and numerical difficulties from the WIMP case: due to the feeble interaction that displays these kind of particles, the mechanism to obtain the DM abundance for FIMP particles is the freeze-in[7], instead of the freeze-out. Indeed, in the WIMP DM case, the abundance is always obtained for $\langle \sigma v \rangle = \langle \sigma_{\rm fo} v \rangle$ for DM masses in the GeV-TeV range. However, in the FIMP scenario the strong dependence of the evolution with the initial conditions makes necessary to solve the Boltzmann Equation, Eq. 4.57, for each point of the parameter space.

In the FIMP case, the abundance also has a strong dependence on a new parameter: the highest temperature of the universe, the so-called *reheating temperature* $T_{\rm rh}$. Due to the complexity of the parameter space, the analysis in this scenario has been performed for a specific value of the Dark Matter mass: $m_{DM} = 1$ MeV. The values of $T_{\rm rh}$ needed to obtain the observed DM relic abundance are shown in Fig. 7.4. The blue-shaded region shows the experimental limits imposed by resonance searches in $pp \to G_1 \to \gamma\,\gamma$ channel at the LHC (and the two expected bounds from the Run-3 and

[6]Described in Sect 3.5.3.
[7]For a complete description of the freeze-in mechanism see Sect. 4.5.

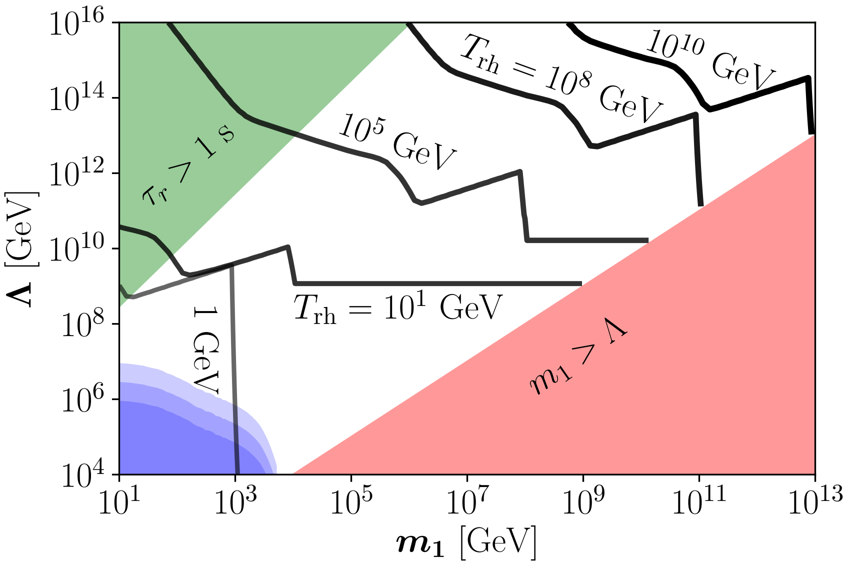

Figure 7.4: Parameter space required to reproduce the observed DM abundance for $m_{\rm DM} = 1$ MeV and $m_r = m_1/10^3$, for several values of the reheating temperature $T_{\rm rh}$. The blue areas are excluded by resonant searches at LHC and represent the current bound and our prospects for the LHC Run-3 and the High-Luminosity LHC in the $\gamma\gamma$ channel [408, 439]. The upper left green corner corresponds to radion lifetimes longer than 1 s. In the lower right red area ($m_1 > \Lambda$) the EFT approach breaks down.

the HL-LHC). The red-shaded area represents the region where the EFT approach breaks down. On the other hand, the upper left green corner corresponds to radion lifetimes higher than 1 s, potentially problematic for BBN (all the KK-graviton states are heavier than the radion and therefore will have naturally shorter lifetimes).

In contrast with the WIMP case, this work shows that the RS model with FIMP is much less constrained, because in order to obtain the correct DM relic abundance via freeze-out Λ can not be larger that 10^4 TeV and $m_1 < 10$ TeV, while the allowed range of these parameters when the DM abundance is set via freeze-in expands over several orders of magnitude. On the other hand, in such regions the model does not solve at all the hierarchy problem.

Bibliography

[1] M. G. Folgado, G. A. Gómez-Vargas, N. Rius and R. Ruiz De Austri, *Probing the sterile neutrino portal to Dark Matter with γ rays*, *JCAP* **1808** (2018) 002, [1803.08934]. Cited on page I, 46, 106, and 331.

[2] M. G. Folgado, A. Donini and N. Rius, *Gravity-mediated Scalar Dark Matter in Warped Extra-Dimensions*, *JHEP* **01** (2020) 161, [1907.04340]. Cited on page I, 46, 94, 109, and 334.

[3] M. G. Folgado, A. Donini and N. Rius, *Gravity-mediated Dark Matter in Clockwork/Linear Dilaton Extra-Dimensions*, *JHEP* **04** (2020) 036, [1912.02689]. Cited on page I, 46, 100, 102, 112, and 337.

[4] N. Bernal, A. Donini, M. G. Folgado and N. Rius, *Kaluza-Klein FIMP Dark Matter in Warped Extra-Dimensions*, *JHEP* **09** (2020) 142, [2004.14403]. Cited on page I, 47, 115, and 340.

[5] M. G. Folgado, A. Donini and N. Rius, *Spin-dependence of Gravity-mediated Dark Matter in Warped Extra-Dimensions*, 2006.02239. Cited on page II, 112, and 337.

[6] M. G. Folgado and V. Sanz, *On the interpretation of non-resonant phenomena at colliders*, 2005.06492. Cited on page II, and 46.

[7] M. G. Folgado and V. Sanz, *Exploring the political pulse of a country using data science tools*, 2020. Cited on page II.

[8] N. Bernal, A. Donini, M. G. Folgado and N. Rius, *FIMP Dark Matter in Clockwork/Linear Dilaton Extra-Dimensions*, 2012.10453. Cited on page II.

[9] T. Aoyama, M. Hayakawa, T. Kinoshita and M. Nio, *Tenth-Order QED Contribution to the Electron g-2 and an Improved Value of the Fine Structure Constant*, *Phys. Rev. Lett.* **109** (2012) 111807, [1205.5368]. Cited on page XI.

[10] T. Aoyama, M. Hayakawa, T. Kinoshita and M. Nio, *Tenth-Order Electron Anomalous Magnetic Moment — Contribution of Diagrams without Closed Lepton Loops*, *Phys. Rev. D* **91** (2015) 033006, [1412.8284]. Cited on page XI.

[11] C. MissMJ, "Standard model of elementary particles." https://commons.wikimedia.org/wiki/File:Standard_Model_of_Elementary_Particles.svg. Cited on page 4, and 312.

[12] N. Bohr, *On the constitution of atoms and molecules, Part I. The binding of electrons by positive nuclei*, . Cited on page 3, and 311.

[13] N. Bohr, *On the constitution of atoms and molecules. Part II. Systems containing only a single nucleus*, . Cited on page 3, and 311.

[14] N. Bohr, *On the constitution of atoms and molecules. Part III. Systems containing several nuclei*, . Cited on page 3, and 311.

[15] S. Weinberg, *A model of leptons*, *Phys. Rev. Lett.* **19** (Nov, 1967) 1264–1266. Cited on page 4, 8, and 312.

[16] S. L. Glashow, *Partial-symmetries of weak interactions*, *Nuclear Physics* **22** (1961) 579 – 588. Cited on page 4, 8, and 312.

[17] A. Salam, *Weak and Electromagnetic Interactions*, *Conf. Proc. C* **680519** (1968) 367–377. Cited on page 4, 8, and 312.

[18] F. Englert and R. Brout, *Broken symmetry and the mass of gauge vector mesons*, *Phys. Rev. Lett.* **13** (Aug, 1964) 321–323. Cited on page 4, 12, 312, and 315.

[19] P. W. Higgs, *Spontaneous symmetry breakdown without massless bosons*, *Phys. Rev.* **145** (May, 1966) 1156–1163. Cited on page 4, 12, 312, and 315.

[20] G. S. Guralnik, C. R. Hagen and T. W. B. Kibble, *Global conservation laws and massless particles*, *Phys. Rev. Lett.* **13** (Nov, 1964) 585–587. Cited on page 4, 12, 312, and 315.

[21] T. W. B. Kibble, *Symmetry breaking in non-abelian gauge theories*, *Phys. Rev.* **155** (Mar, 1967) 1554–1561. Cited on page 4, 12, 14, 312, and 315.

[22] M. Y. Han and Y. Nambu, *Three-triplet model with double* SU(3) *symmetry*, *Phys. Rev.* **139** (Aug, 1965) B1006–B1010. Cited on page 4, and 312.

[23] S. L. Glashow, J. Iliopoulos and L. Maiani, *Weak interactions with lepton-hadron symmetry*, *Phys. Rev. D* **2** (Oct, 1970) 1285–1292. Cited on page 4, and 312.

[24] H. Fritzsch, M. Gell-Mann and H. Leutwyler, *Advantages of the color octet gluon picture*, *Physics Letters B* **47** (1973) 365 – 368. Cited on page 4, and 312.

[25] P. W. Higgs, *Broken symmetries and the masses of gauge bosons*, *Phys. Rev. Lett.* **13** (Oct, 1964) 508–509. Cited on page 4, and 312.

[26] J. Thomson, *Cathode rays*, *Phil. Mag. Ser. 5* **44** (1897) 293–316. Cited on page 5.

[27] J. Street and E. Stevenson, *New Evidence for the Existence of a Particle of Mass Intermediate Between the Proton and Electron*, *Phys. Rev.* **52** (1937) 1003–1004. Cited on page 5.

[28] M. L. Perl et al., *Evidence for Anomalous Lepton Production in e+ - e- Annihilation*, *Phys. Rev. Lett.* **35** (1975) 1489–1492. Cited on page 5.

[29] F. Reines and C. L. Cowan, *The neutrino*, *Nature* **178** (1956) 446–449. Cited on page 5.

[30] G. Danby, J. Gaillard, K. A. Goulianos, L. Lederman, N. B. Mistry, M. Schwartz et al., *Observation of High-Energy Neutrino Reactions and the Existence of Two Kinds of Neutrinos*, *Phys. Rev. Lett.* **9** (1962) 36–44. Cited on page 5.

[31] DONUT collaboration, K. Kodama et al., *Observation of tau neutrino interactions*, *Phys. Lett. B* **504** (2001) 218–224, [hep-ex/0012035]. Cited on page 5.

[32] E598 collaboration, J. Aubert et al., *Experimental Observation of a Heavy Particle J*, *Phys. Rev. Lett.* **33** (1974) 1404–1406. Cited on page 5.

[33] SLAC-SP-017 collaboration, J. Augustin et al., *Discovery of a Narrow Resonance in e^+e^- Annihilation*, *Phys. Rev. Lett.* **33** (1974) 1406–1408. Cited on page 5.

[34] E. D. Bloom et al., *High-Energy Inelastic e p Scattering at 6-Degrees and 10-Degrees*, *Phys. Rev. Lett.* **23** (1969) 930–934. Cited on page 5.

[35] M. Breidenbach, J. I. Friedman, H. W. Kendall, E. D. Bloom, D. Coward, H. DeStaebler et al., *Observed Behavior of Highly Inelastic electron-Proton Scattering*, *Phys. Rev. Lett.* **23** (1969) 935–939. Cited on page 5.

[36] D0 collaboration, S. Abachi et al., *Observation of the top quark*, *Phys. Rev. Lett.* **74** (1995) 2632–2637, [hep-ex/9503003]. Cited on page 5.

[37] S. Herb et al., *Observation of a Dimuon Resonance at 9.5-GeV in 400-GeV Proton-Nucleus Collisions*, *Phys. Rev. Lett.* **39** (1977) 252–255. Cited on page 5.

[38] A. H. Compton, *A Quantum Theory of the Scattering of X-rays by Light Elements*, *Phys. Rev.* **21** (1923) 483–502. Cited on page 5.

[39] PLUTO collaboration, C. Berger et al., *Jet Analysis of the Υ (9.46) Decay Into Charged Hadrons*, *Phys. Lett. B* **82** (1979) 449–455. Cited on page 5.

[40] UA2 collaboration, M. Banner et al., *Observation of Single Isolated Electrons of High Transverse Momentum in Events with Missing Transverse Energy at the CERN anti-p p Collider*, *Phys. Lett. B* **122** (1983) 476–485. Cited on page 5.

[41] UA1 collaboration, G. Arnison et al., *Experimental Observation of Isolated Large Transverse Energy Electrons with Associated Missing Energy at s**(1/2) = 540-GeV*, *Phys. Lett. B* **122** (1983) 103–116. Cited on page 5.

[42] UA2 collaboration, P. Bagnaia et al., *Evidence for $Z^0 \to e^+e^-$ at the CERN $\bar{p}p$ Collider*, *Phys. Lett. B* **129** (1983) 130–140. Cited on page 5.

[43] UA1 collaboration, G. Arnison et al., *Experimental Observation of Lepton Pairs of Invariant Mass Around 95-GeV/c**2 at the CERN SPS Collider*, *Phys. Lett. B* **126** (1983) 398–410. Cited on page 5.

[44] G. Aad, T. Abajyan, B. Abbott, J. Abdallah, S. Abdel Khalek, A. Abdelalim et al., *Observation of a new particle in the search for the standard model higgs boson with the atlas detector at the lhc*, *Physics Letters B* **716** (Sep, 2012) 1?29. Cited on page 5, 14, and 315.

[45] S. Chatrchyan, V. Khachatryan, A. Sirunyan, A. Tumasyan, W. Adam, E. Aguilo et al., *Observation of a new boson at a mass of 125 gev with the cms experiment at the lhc*, *Physics Letters B* **716** (Sep, 2012) 30?61. Cited on page 5, 14, and 315.

[46] G. F. Cottin Buracchio, *Phenomenology of new physics beyond the Standard Model: signals of Supersymmetry with displaced vertices and an extended Higgs sector at colliders*, Aug, 2017. 10.17863/CAM.12237. Cited on page 5.

[47] Particle Data Group collaboration, M. Tanabashi, K. Hagiwara, K. Hikasa, K. Nakamura, Y. Sumino, F. Takahashi et al., *Review of particle physics*, *Phys. Rev. D* **98** (Aug, 2018) 030001. Cited on page 5, 6, 54, and 65.

[48] S. Tomonaga, *On a Relativistically Invariant Formulation of the Quantum Theory of Wave Fields**, *Progress of Theoretical Physics* **1** (08, 1946) 27–42. Cited on page 7, and 315.

[49] Z. Koba, T. Tati and S.-i. Tomonaga, *On a Relativistically Invariant Formulation of the Quantum Theory of Wave Fields. II: Case of*

Interacting Electromagnetic and Electron Fields, *Progress of Theoretical Physics* **2** (10, 1947) 101–116. Cited on page 7, and 315.

[50] S. Kanesawa and S.-i. Tomonaga, *On a Relativistically Invariant Formulation of the Quantum Theory of Wave Fields V*: Case of Interacting Electromagnetic and Meson Fields*, *Progress of Theoretical Physics* **3** (06, 1948) 101–113. Cited on page 7, and 315.

[51] S.-I. Tomonaga and J. R. Oppenheimer, *On infinite field reactions in quantum field theory*, *Phys. Rev.* **74** (Jul, 1948) 224–225. Cited on page 7, and 315.

[52] J. Schwinger, *Quantum electrodynamics. i. a covariant formulation*, *Phys. Rev.* **74** (Nov, 1948) 1439–1461. Cited on page 7, and 315.

[53] R. Feynman, *Space-time approach to nonrelativistic quantum mechanics*, *Rev. Mod. Phys.* **20** (1948) 367–387. Cited on page 7, and 315.

[54] R. Feynman, *Space - time approach to quantum electrodynamics*, *Phys. Rev.* **76** (1949) 769–789. Cited on page 7, and 315.

[55] C. S. Wu, E. Ambler, R. W. Hayward, D. D. Hoppes and R. P. Hudson, *Experimental Test of Parity Conservation in Beta Decay*, *Physical Review* **105** (Feb., 1957) 1413–1415. Cited on page 7.

[56] R. L. Garwin, L. M. Lederman and M. Weinrich, *Observations of the Failure of Conservation of Parity and Charge Conjugation in Meson Decays: the Magnetic Moment of the Free Muon*, *Physical Review* **105** (Feb., 1957) 1415–1417. Cited on page 7.

[57] M. E. Peskin and D. V. Schroeder, *An Introduction to quantum field theory*. Addison-Wesley, Reading, USA, 1995. Cited on page 7.

[58] F. Mandl and G. Shaw, *QUANTUM FIELD THEORY*. 1, 1985. Cited on page 7.

[59] H. Georgi and S. Glashow, *Unity of All Elementary Particle Forces*, *Phys. Rev. Lett.* **32** (1974) 438–441. Cited on page 8.

[60] D. J. Gross and F. Wilczek, *Ultraviolet behavior of non-abelian gauge theories*, *Phys. Rev. Lett.* **30** (Jun, 1973) 1343–1346. Cited on page 8.

[61] H. D. Politzer, *Reliable perturbative results for strong interactions?*, *Phys. Rev. Lett.* **30** (Jun, 1973) 1346–1349. Cited on page 8.

[62] A. Pich, *Aspects of quantum chromodynamics*, in *ICTP Summer School in Particle Physics*, pp. 53–102, 6, 1999. `hep-ph/0001118`. Cited on page 9.

[63] E. Noether, *Invariant variation problems*, *Transport Theory and Statistical Physics* **1** (Jan., 1971) 186–207, [`physics/0503066`]. Cited on page 12.

[64] H. Weyl, *Quantenmechanik und Gruppentheorie*, *Zeitschrift fur Physik* **46** (Nov., 1927) 1–46. Cited on page 12.

[65] Y. Nambu, *Quasi-Particles and Gauge Invariance in the Theory of Superconductivity*, *Physical Review* **117** (Feb., 1960) 648–663. Cited on page 12.

[66] J. Goldstone, *Field Theories with Superconductor Solutions*, *Nuovo Cim.* **19** (1961) 154–164. Cited on page 12.

[67] T. Aaltonen, V. M. Abazov, B. Abbott, B. S. Acharya, M. Adams, T. Adams et al., *Evidence for a particle produced in association with weak bosons and decaying to a bottom-antibottom quark pair in higgs boson searches at the tevatron*, *Physical Review Letters* **109** (Aug, 2012) . Cited on page 14.

[68] N. Cabibbo, *Unitary Symmetry and Leptonic Decays*, *Phys. Rev. Lett.* **10** (1963) 531–533. Cited on page 19.

[69] M. Kobayashi and T. Maskawa, *CP Violation in the Renormalizable Theory of Weak Interaction*, *Prog. Theor. Phys.* **49** (1973) 652–657. Cited on page 19.

[70] C. Csáki, S. Lombardo and O. Telem, *TASI Lectures on Non-supersymmetric BSM Models*, pp. 501–570. WSP, 2018.

1811.04279. 10.1142/9789813233348_0007. Cited on page 21, 91, and 94.

[71] H. E. Haber and L. Stephenson Haskins, *Supersymmetric Theory and Models*, in *Theoretical Advanced Study Institute in Elementary Particle Physics: Anticipating the Next Discoveries in Particle Physics*, pp. 355–499, WSP, 2018. 1712.05926. DOI. Cited on page 21.

[72] S. Weinberg, *Implications of dynamical symmetry breaking*, *Physical Review D* **13** (Feb., 1976) 974–996. Cited on page 21.

[73] S. Weinberg, *Implications of dynamical symmetry breaking: An addendum*, *Physical Review D* **19** (Feb., 1979) 1277–1280. Cited on page 21.

[74] L. Susskind, *Dynamics of spontaneous symmetry breaking in the Weinberg-Salam theory*, *Physical Review D* **20** (Nov., 1979) 2619–2625. Cited on page 21.

[75] D. B. Kaplan and H. Georgi, *SU(2) x U(1) Breaking by Vacuum Misalignment*, *Phys. Lett. B* **136** (1984) 183–186. Cited on page 21.

[76] L. Randall and R. Sundrum, *A Large mass hierarchy from a small extra dimension*, *Phys. Rev. Lett.* **83** (1999) 3370–3373, [hep-ph/9905221]. Cited on page 21, 94, and 325.

[77] L. Randall and R. Sundrum, *An Alternative to compactification*, *Phys. Rev. Lett.* **83** (1999) 4690–4693, [hep-th/9906064]. Cited on page 21, 94, and 99.

[78] R. Peccei and H. R. Quinn, *CP Conservation in the Presence of Instantons*, *Phys. Rev. Lett.* **38** (1977) 1440–1443. Cited on page 21.

[79] R. Crewther, P. Di Vecchia, G. Veneziano and E. Witten, *Chiral Estimate of the Electric Dipole Moment of the Neutron in Quantum Chromodynamics*, *Phys. Lett. B* **88** (1979) 123. Cited on page 21.

[80] M. Pospelov and A. Ritz, *Theta-induced electric dipole moment of the neutron via qcd sum rules*, *Physical Review Letters* **83** (Sep, 1999) 2526?2529. Cited on page 21.

[81] F.-K. Guo, R. Horsley, U.-G. MeiSSner, Y. Nakamura, H. Perlt, P. Rakow et al., *Electric dipole moment of the neutron from2+1flavor lattice qcd*, *Physical Review Letters* **115** (Aug, 2015) . Cited on page 21.

[82] R. D. Peccei and H. R. Quinn, CP *conservation in the presence of pseudoparticles*, *Phys. Rev. Lett.* **38** (Jun, 1977) 1440–1443. Cited on page 21, and 48.

[83] F. Wilczek, *Problem of Strong P and T Invariance in the Presence of Instantons*, *Phys. Rev. Lett.* **40** (1978) 279–282. Cited on page 21.

[84] S. Weinberg, *A New Light Boson?*, *Phys. Rev. Lett.* **40** (1978) 223–226. Cited on page 21.

[85] A. E. Nelson, *Naturally Weak CP Violation*, *Phys. Lett. B* **136** (1984) 387–391. Cited on page 22.

[86] S. M. Barr, *Solving the Strong CP Problem Without the Peccei-Quinn Symmetry*, *Phys. Rev. Lett.* **53** (1984) 329. Cited on page 22.

[87] A. Hook, *TASI Lectures on the Strong CP Problem and Axions*, *PoS* **TASI2018** (2019) 004, [1812.02669]. Cited on page 22.

[88] N. Kaloper and J. Terning, *Landscaping the Strong CP Problem*, *JHEP* **03** (2019) 032, [1710.01740]. Cited on page 22.

[89] B. Pontecorvo, *Mesonium and anti-mesonium*, *Sov. Phys. JETP* **6** (1957) 429. Cited on page 22, and 330.

[90] Kamiokande-II collaboration, K. Hirata et al., *Results from one thousand days of real time directional solar neutrino data*, *Phys. Rev. Lett.* **65** (1990) 1297–1300. Cited on page 22.

[91] Kamiokande-II collaboration, K. Hirata et al., *Observation of a small atmospheric muon-neutrino / electron-neutrino ratio in Kamiokande*, *Phys. Lett. B* **280** (1992) 146–152. Cited on page 22.

[92] Super-Kamiokande collaboration, Y. Fukuda et al., *Evidence for oscillation of atmospheric neutrinos*, *Phys. Rev. Lett.* **81** (1998) 1562–1567, [hep-ex/9807003]. Cited on page 22, 105, and 330.

[93] B. Cleveland, T. Daily, J. Davis, Raymond, J. R. Distel, K. Lande, C. Lee et al., *Measurement of the solar electron neutrino flux with the Homestake chlorine detector*, *Astrophys. J.* **496** (1998) 505–526. Cited on page 22.

[94] GALLEX collaboration, W. Hampel et al., *GALLEX solar neutrino observations: Results for GALLEX IV*, *Phys. Lett. B* **447** (1999) 127–133. Cited on page 22.

[95] SAGE collaboration, J. Abdurashitov et al., *Measurement of the solar neutrino capture rate with gallium metal*, *Phys. Rev. C* **60** (1999) 055801, [astro-ph/9907113]. Cited on page 22.

[96] Super-Kamiokande collaboration, S. Fukuda et al., *Solar B-8 and hep neutrino measurements from 1258 days of Super-Kamiokande data*, *Phys. Rev. Lett.* **86** (2001) 5651–5655, [hep-ex/0103032]. Cited on page 22.

[97] SNO collaboration, Q. Ahmad et al., *Direct evidence for neutrino flavor transformation from neutral current interactions in the Sudbury Neutrino Observatory*, *Phys. Rev. Lett.* **89** (2002) 011301, [nucl-ex/0204008]. Cited on page 22.

[98] GNO collaboration, M. Altmann et al., *Complete results for five years of GNO solar neutrino observations*, *Phys. Lett. B* **616** (2005) 174–190, [hep-ex/0504037]. Cited on page 22.

[99] K2K collaboration, M. Ahn et al., *Measurement of Neutrino Oscillation by the K2K Experiment*, *Phys. Rev. D* **74** (2006) 072003, [hep-ex/0606032]. Cited on page 22.

[100] MINOS collaboration, D. Michael et al., *Observation of muon neutrino disappearance with the MINOS detectors and the NuMI neutrino beam*, *Phys. Rev. Lett.* **97** (2006) 191801, [hep-ex/0607088]. Cited on page 22.

[101] KamLAND collaboration, S. Abe et al., *Precision Measurement of Neutrino Oscillation Parameters with KamLAND*, *Phys. Rev. Lett.* **100** (2008) 221803, [0801.4589]. Cited on page 22.

[102] T2K collaboration, K. Abe et al., *Indication of Electron Neutrino Appearance from an Accelerator-produced Off-axis Muon Neutrino Beam*, *Phys. Rev. Lett.* **107** (2011) 041801, [1106.2822]. Cited on page 22.

[103] Double Chooz collaboration, Y. Abe et al., *Indication of Reactor $\bar{\nu}_e$ Disappearance in the Double Chooz Experiment*, *Phys. Rev. Lett.* **108** (2012) 131801, [1112.6353]. Cited on page 22.

[104] Daya Bay collaboration, F. An et al., *Observation of electron-antineutrino disappearance at Daya Bay*, *Phys. Rev. Lett.* **108** (2012) 171803, [1203.1669]. Cited on page 22.

[105] RENO collaboration, J. Ahn et al., *Observation of Reactor Electron Antineutrino Disappearance in the RENO Experiment*, *Phys. Rev. Lett.* **108** (2012) 191802, [1204.0626]. Cited on page 22.

[106] T2K collaboration, K. Abe et al., *Precise Measurement of the Neutrino Mixing Parameter θ_{23} from Muon Neutrino Disappearance in an Off-Axis Beam*, *Phys. Rev. Lett.* **112** (2014) 181801, [1403.1532]. Cited on page 22.

[107] B. Pontecorvo, *Inverse beta processes and nonconservation of lepton charge*, *Sov. Phys. JETP* **7** (1958) 172–173. Cited on page 22.

[108] Z. Maki, M. Nakagawa and S. Sakata, *Remarks on the unified model of elementary particles*, *Prog. Theor. Phys.* **28** (1962) 870–880. Cited on page 22.

[109] I. Esteban, M. Gonzalez-Garcia, M. Maltoni, I. Martinez-Soler and T. Schwetz, *Updated fit to three neutrino mixing: exploring the accelerator-reactor complementarity*, *JHEP* **01** (2017) 087, [1611.01514]. Cited on page 22.

[110] KATRIN collaboration, M. Aker et al., *Improved Upper Limit on the Neutrino Mass from a Direct Kinematic Method by KATRIN*, *Phys. Rev. Lett.* **123** (2019) 221802, [1909.06048]. Cited on page 22, and 330.

[111] E. Majorana, *Teoria simmetrica dell'elettrone e del positrone*, *Nuovo Cim.* **14** (1937) 171–184. Cited on page 23.

[112] M. Gell-Mann, P. Ramond and R. Slansky, *Complex Spinors and Unified Theories*, *Conf. Proc. C* **790927** (1979) 315–321, [1306.4669]. Cited on page 24, and 330.

[113] R. N. Mohapatra and G. Senjanović, *Neutrino mass and spontaneous parity nonconservation*, *Phys. Rev. Lett.* **44** (Apr, 1980) 912–915. Cited on page 24, and 330.

[114] T. Yanagida, *Horizontal gauge symmetry and masses of neutrinos*, *Conf. Proc.* **C7902131** (1979) 95–99. Cited on page 24, and 330.

[115] S. L. Glashow, *The future of elementary particle physics*, in *Quarks and Leptons* (M. Lévy, J.-L. Basdevant, D. Speiser, J. Weyers, R. Gastmans and M. Jacob, eds.), (Boston, MA), pp. 687–713, Springer US, 1980. Cited on page 24, and 330.

[116] P. Minkowski, *??e? at a rate of one out of 109 muon decays?*, *Physics Letters B* **67** (1977) 421 – 428. Cited on page 24, and 330.

[117] Y. Grossman, *TASI 2002 lectures on neutrinos*, in *Theoretical Advanced Study Institute in Elementary Particle Physics (TASI 2002): Particle Physics and Cosmology: The Quest for Physics Beyond the Standard Model(s)*, pp. 5–48, 5, 2003. hep-ph/0305245. Cited on page 24.

[118] T. Blount, *Glossographia.* Tho. Newcomb; sold by Tho. Flesher, 1681. Cited on page 25.

[119] E. Hubble, *A relation between distance and radial velocity among extra-galactic nebulae*, *Proceedings of the National Academy of Sciences* **15** (1929) 168–173, [https://www.pnas.org/content/15/3/168.full.pdf]. Cited on page 25, and 26.

[120] Planck collaboration, N. Aghanim et al., *Planck 2018 results. VI. Cosmological parameters*, 1807.06209. Cited on page 26, 27, 33, 34, 40, 51, and 65.

[121] Planck collaboration, Y. Akrami et al., *Planck 2018 results. I. Overview and the cosmological legacy of Planck*, `1807.06205`. Cited on page 27, and 38.

[122] A. Friedman, *On the Curvature of space*, *Z. Phys.* **10** (1922) 377–386. Cited on page 27.

[123] A. G. Walker, *On Milne's Theory of World-Structure**, *Proceedings of the London Mathematical Society* **s2-42** (01, 1937) 90–127. Cited on page 27.

[124] A. G. Lemaître, *A Homogeneous Universe of Constant Mass and Increasing Radius accounting for the Radial Velocity of Extra-galactic Nebulæ*, *Monthly Notices of the Royal Astronomical Society* **91** (03, 1931) 483–490. Cited on page 27.

[125] H. Robertson, *Kinematics and World-Structure*, *Astrophys. J.* **82** (1935) 284–301. Cited on page 27.

[126] A. Einstein, *The Foundation of the General Theory of Relativity*, *Annalen Phys.* **49** (1916) 769–822. Cited on page 27, and 89.

[127] S. Weinberg, *Gravitation and Cosmology: Principles and Applications of the General Theory of Relativity.* John Wiley and Sons, New York, 1972. Cited on page 28.

[128] P. Peebles and B. Ratra, *The Cosmological Constant and Dark Energy*, *Rev. Mod. Phys.* **75** (2003) 559–606, [`astro-ph/0207347`]. Cited on page 28.

[129] Y. Zel'dovich, A. Krasinski and Y. Zeldovich, *The Cosmological constant and the theory of elementary particles*, *Sov. Phys. Usp.* **11** (1968) 381–393. Cited on page 29.

[130] J. Martin, *Everything You Always Wanted To Know About The Cosmological Constant Problem (But Were Afraid To Ask)*, *Comptes Rendus Physique* **13** (2012) 566–665, [`1205.3365`]. Cited on page 30.

[131] H. Velten, R. vom Marttens and W. Zimdahl, *Aspects of the cosmological coincidence problem*, *Eur. Phys. J. C* **74** (2014) 3160, [`1410.2509`]. Cited on page 31.

[132] A. Barreira and P. Avelino, *Anthropic versus cosmological solutions to the coincidence problem*, *Phys. Rev. D* **83** (2011) 103001, [`1103.2401`]. Cited on page 31.

[133] J. M. Fedrow and K. Griest, *Anti-Anthropic Solutions to the Cosmic Coincidence Problem*, *JCAP* **01** (2014) 004, [`1309.0849`]. Cited on page 31.

[134] C. Bennett, A. Banday, K. Gorski, G. Hinshaw, P. Jackson, P. Keegstra et al., *Four year COBE DMR cosmic microwave background observations: Maps and basic results*, *Astrophys. J. Lett.* **464** (1996) L1–L4, [`astro-ph/9601067`]. Cited on page 33, and 38.

[135] G. Hinshaw, D. Larson, E. Komatsu, D. N. Spergel, C. L. Bennett, J. Dunkley et al., *Nine-year wilkinson microwave anisotropy probe (wmap) observations: Cosmological parameter results*, *The Astrophysical Journal Supplement Series* **208** (Sep, 2013) 19. Cited on page 33, and 38.

[136] M. Vogelsberger, *Lecture notes in dark matter distribution*, ISAPP 2017: The Dark and Visible Side of the Universe. Cited on page 33.

[137] A. A. Penzias and R. W. Wilson, *A Measurement of excess antenna temperature at 4080-Mc/s*, *Astrophys. J.* **142** (1965) 419–421. Cited on page 32.

[138] S. M. Faber and R. E. Jackson, *Velocity dispersions and mass-to-light ratios for elliptical galaxies.*, *Astrophysical Journal* **204** (Mar., 1976) 668–683. Cited on page 36.

[139] F. Zwicky, *Die Rotverschiebung von extragalaktischen Nebeln*, *Helv. Phys. Acta* **6** (1933) 110–127. Cited on page 36, and 316.

[140] F. Zwicky, *On the Masses of Nebulae and of Clusters of Nebulae*, *Astrophysical Journal* **86** (Oct., 1937) 217. Cited on page 36.

[141] J. Kapteyn, *First Attempt at a Theory of the Arrangement and Motion of the Sidereal System*, *Astrophys. J.* **55** (1922) 302–328. Cited on page 36.

[142] J. H. Oort, *The force exerted by the stellar system in the direction perpendicular to the galactic plane and some related problems*, *bain* **6** (Aug., 1932) 249. Cited on page 36.

[143] K. Begeman, A. Broeils and R. Sanders, *Extended rotation curves of spiral galaxies: Dark haloes and modified dynamics*, *Mon. Not. Roy. Astron. Soc.* **249** (1991) 523. Cited on page 36, and 43.

[144] V. C. Rubin and J. Ford, W. Kent, *Rotation of the Andromeda Nebula from a Spectroscopic Survey of Emission Regions*, *Astrophysical Journal* **159** (Feb., 1970) 379. Cited on page 36, and 316.

[145] K. C. Freeman, *On the Disks of Spiral and S0 Galaxies*, *Astrophysical Journal* **160** (June, 1970) 811. Cited on page 36, and 316.

[146] Y. Sofue and V. Rubin, *Rotation curves of spiral galaxies*, *Ann. Rev. Astron. Astrophys.* **39** (2001) 137–174, [`astro-ph/0010594`]. Cited on page 36.

[147] M. Persic, P. Salucci and F. Stel, *The universal rotation curve of spiral galaxies ? I. The dark matter connection*, *Monthly Notices of the Royal Astronomical Society* **281** (07, 1996) 27–47. Cited on page 36.

[148] S. W. Allen, A. E. Evrard and A. B. Mantz, *Cosmological Parameters from Observations of Galaxy Clusters*, *Annual Review of Astronomy and Astrophysics* **49** (Sept., 2011) 409–470, [`1103.4829`]. Cited on page 37.

[149] A. Taylor, S. Dye, T. J. Broadhurst, N. Benitez and E. van Kampen, *Gravitational lens magnification and the mass of abell 1689*, *Astrophys. J.* **501** (1998) 539, [`astro-ph/9801158`]. Cited on page 37.

[150] X.-P. Wu, T. Chiueh, L.-Z. Fang and Y.-J. Xue, *A comparison of different cluster mass estimates: consistency or discrepancy ?*, *Mon. Not. Roy. Astron. Soc.* **301** (1998) 861, [`astro-ph/9808179`]. Cited on page 37.

[151] P. Natarajan et al., *Mapping substructure in the HST Frontier Fields cluster lenses and in cosmological simulations*, *Mon. Not. Roy. Astron. Soc.* **468** (2017) 1962–1980, [1702.04348]. Cited on page 37.

[152] A. Refregier, *Weak gravitational lensing by large scale structure*, *Ann. Rev. Astron. Astrophys.* **41** (2003) 645–668, [astro-ph/0307212]. Cited on page 37.

[153] D. Clowe, M. Bradac, A. H. Gonzalez, M. Markevitch, S. W. Randall, C. Jones et al., *A direct empirical proof of the existence of dark matter*, *Astrophys. J. Lett.* **648** (2006) L109–L113, [astro-ph/0608407]. Cited on page 37.

[154] W. Tucker, P. Blanco, S. Rappoport, L. David, D. Fabricant, E. Falco et al., *1e0657-56: a contender for the hottest known cluster of galaxies*, *Astrophys. J. Lett.* **496** (1998) L5, [astro-ph/9801120]. Cited on page 37.

[155] D. Clowe, A. Gonzalez and M. Markevitch, *Weak lensing mass reconstruction of the interacting cluster 1E0657-558: Direct evidence for the existence of dark matter*, *Astrophys. J.* **604** (2004) 596–603, [astro-ph/0312273]. Cited on page 38.

[156] M. Markevitch, A. Gonzalez, D. Clowe, A. Vikhlinin, L. David, W. Forman et al., *Direct constraints on the dark matter self-interaction cross-section from the merging galaxy cluster 1E0657-56*, *Astrophys. J.* **606** (2004) 819–824, [astro-ph/0309303]. Cited on page 38.

[157] T. Padmanabhan, *Structure Formation in the Universe.* 1993. Cited on page 38.

[158] P. Peebles, *Growth of the nonbaryonic dark matter theory*, *Nature Astron.* **1** (2017) 0057, [1701.05837]. Cited on page 38.

[159] C. Frenk and S. D. White, *Dark matter and cosmic structure*, *Annalen Phys.* **524** (2012) 507–534, [1210.0544]. Cited on page 38.

[160] G. D. Starkman, A. Gould, R. Esmailzadeh and S. Dimopoulos, *Opening the window on strongly interacting dark matter*, *Phys. Rev. D* **41** (Jun, 1990) 3594–3603. Cited on page 39.

[161] G. D. Mack, J. F. Beacom and G. Bertone, *Towards Closing the Window on Strongly Interacting Dark Matter: Far-Reaching Constraints from Earth's Heat Flow*, *Phys. Rev. D* **76** (2007) 043523, [0705.4298]. Cited on page 39, and 318.

[162] A. De Rújula, S. Glashow and U. Sarid, *Charged dark matter*, *Nuclear Physics B* **333** (1990) 173 – 194. Cited on page 39, and 318.

[163] M. Taoso, G. Bertone and A. Masiero, *Dark Matter Candidates: A Ten-Point Test*, *JCAP* **03** (2008) 022, [0711.4996]. Cited on page 39, and 318.

[164] B. Holdom, *Two U(1)'s and epsilon charge shifts*, Tech. Rep. UTPT-85-30, Toronto Univ. Dept. Phys., Toronto, Ontario, Oct, 1985. Cited on page 39.

[165] B. Holdom, *Oblique electroweak corrections and an extra gauge boson*, *Physics Letters B* **259** (1991) 329 – 334. Cited on page 39.

[166] S. A. Abel, J. Jaeckel, V. V. Khoze and A. Ringwald, *Illuminating the hidden sector of string theory by shining light through a magnetic field*, *Physics Letters B* **666** (Aug, 2008) 66?70. Cited on page 39.

[167] E. Massó and J. Redondo, *Compatibility of cast search with axionlike interpretation of pvlas results*, *Physical Review Letters* **97** (Oct, 2006) . Cited on page 39.

[168] S. Abel and B. Schofield, *Brane?antibrane kinetic mixing, millicharged particles and susy breaking*, *Nuclear Physics B* **685** (May, 2004) 150?170. Cited on page 39.

[169] B. Batell and T. Gherghetta, *Localized u(1) gauge fields, millicharged particles, and holography*, *Physical Review D* **73** (Feb, 2006) . Cited on page 39.

[170] S. L. Dubovsky, D. S. Gorbunov and G. I. Rubtsov, *Narrowing the window for millicharged particles by cmb anisotropy*, *Journal of Experimental and Theoretical Physics Letters* **79** (Jan, 2004) 1?5. Cited on page 39.

[171] S. Davidson, S. Hannestad and G. Raffelt, *Updated bounds on milli-charged particles*, *Journal of High Energy Physics* **2000** (May, 2000) 003?003. Cited on page 40.

[172] C. B?hm, P. Fayet and R. Schaeffer, *Constraining dark matter candidates from structure formation*, *Physics Letters B* **518** (Oct, 2001) 8?14. Cited on page 40.

[173] R. J. Wilkinson, C. B?hm and J. Lesgourgues, *Constraining dark matter-neutrino interactions using the cmb and large-scale structure*, *Journal of Cosmology and Astroparticle Physics* **2014** (May, 2014) 011?011. Cited on page 40.

[174] C. A. Argüelles, A. Kheirandish and A. C. Vincent, *Imaging galactic dark matter with high-energy cosmic neutrinos*, *Physical Review Letters* **119** (Nov, 2017) . Cited on page 40.

[175] A. Olivares-Del Campo, C. B?hm, S. Palomares-Ruiz and S. Pascoli, *Dark matter-neutrino interactions through the lens of their cosmological implications*, *Physical Review D* **97** (Apr, 2018) . Cited on page 40.

[176] D. N. Spergel and P. J. Steinhardt, *Observational evidence for selfinteracting cold dark matter*, *Phys. Rev. Lett.* **84** (2000) 3760–3763, [astro-ph/9909386]. Cited on page 40.

[177] R. Dave, D. N. Spergel, P. J. Steinhardt and B. D. Wandelt, *Halo properties in cosmological simulations of self?interacting cold dark matter*, *The Astrophysical Journal* **547** (Feb, 2001) 574?589. Cited on page 40, and 318.

[178] J. L. Feng, M. Kaplinghat, H. Tu and H.-B. Yu, *Hidden charged dark matter*, *Journal of Cosmology and Astroparticle Physics* **2009** (Jul, 2009) 004?004. Cited on page 40, and 318.

[179] P. Agrawal, F.-Y. Cyr-Racine, L. Randall and J. Scholtz, *Make dark matter charged again*, *Journal of Cosmology and Astroparticle Physics* **2017** (May, 2017) 022?022. Cited on page 40, and 318.

[180] S. W. Randall, M. Markevitch, D. Clowe, A. H. Gonzalez and M. Brada?, *Constraints on the self?interaction cross section of dark matter from numerical simulations of the merging galaxy cluster 1e 0657?56*, *The Astrophysical Journal* **679** (Jun, 2008) 1173?1180. Cited on page 40, and 318.

[181] F. Kahlhoefer, K. Schmidt-Hoberg, M. T. Frandsen and S. Sarkar, *Colliding clusters and dark matter self-interactions*, *Monthly Notices of the Royal Astronomical Society* **437** (Nov, 2013) 2865?2881. Cited on page 40, and 318.

[182] N. Vittorio and J. Silk, *Fine-scale anisotropy of the cosmic microwave background in a universe dominated by cold dark matter*, *Astrophysical Journal* **285** (Oct., 1984) L39–L43. Cited on page 41.

[183] M. Umemura and S. Ikeuchi, *Formation of subgalactic objects within two-component dark matter*, *Astrophysical Journal* **299** (Dec., 1985) 583–592. Cited on page 41.

[184] B. Moore, "Dark matter simulations." `https://www.benmoore.ch`. Cited on page 41.

[185] J. Silk, *Cosmic Black-Body Radiation and Galaxy Formation*, *Astrophysical Journal* **151** (Feb., 1968) 459. Cited on page 41.

[186] J. R. Bond and A. S. Szalay, *The collisionless damping of density fluctuations in an expanding universe*, *Astrophysical Journal* **274** (Nov., 1983) 443–468. Cited on page 41.

[187] J. R. Primack, *Whatever happened to hot dark matter?*, 2001. Cited on page 41, and 318.

[188] P. J. E. Peebles, *Large-scale background temperature and mass fluctuations due to scale-invariant primeval perturbations*, *Astrophysical Journal* **263** (Dec., 1982) L1–L5. Cited on page 41.

[189] J. R. Bond, A. S. Szalay and M. S. Turner, *Formation of Galaxies in a Gravitino-Dominated Universe*, *Physical Review Letters* **48** (June, 1982) 1636–1640. Cited on page 41.

[190] G. R. Blumenthal, H. Pagels and J. R. Primack, *Galaxy formation by dissipationless particles heavier than neutrinos*, *Nature* **299** (Sept., 1982) 37–38. Cited on page 41.

[191] G. R. Blumenthal, S. M. Faber, J. R. Primack and M. J. Rees, *Formation of galaxies and large-scale structure with cold dark matter.*, *Nature* **311** (Oct., 1984) 517–525. Cited on page 41.

[192] A. Klypin, A. V. Kravtsov, O. Valenzuela and F. Prada, *Where are the missing galactic satellites?*, *The Astrophysical Journal* **522** (Sep, 1999) 82?92. Cited on page 42.

[193] B. Moore, S. Ghigna, F. Governato, G. Lake, T. Quinn, J. Stadel et al., *Dark Matter Substructure within Galactic Halos*, *The Astrophysical Journal* **524** (Oct., 1999) L19–L22, [astro-ph/9907411]. Cited on page 42.

[194] R. A. Flores and J. R. Primack, *Observational and theoretical constraints on singular dark matter halos*, *Astrophys. J. Lett.* **427** (1994) L1–4, [astro-ph/9402004]. Cited on page 42.

[195] S. S. McGaugh and W. J. G. de Blok, *Testing the dark matter hypothesis with low surface brightness galaxies and other evidence*, *The Astrophysical Journal* **499** (May, 1998) 41?65. Cited on page 42.

[196] G. Gentile, A. Burkert, P. Salucci, U. Klein and F. Walter, *The dwarf galaxy ddo 47: testing cusps hiding in triaxial halos*, *EAS Publ. Ser.* **20** (2006) 279–280, [astro-ph/0510607]. Cited on page 42.

[197] G. Gentile, P. Salucci, U. Klein, D. Vergani and P. Kalberla, *The cored distribution of dark matter in spiral galaxies*, *Monthly Notices of the Royal Astronomical Society* **351** (Jul, 2004) 903?922. Cited on page 42.

[198] J. R. Primack, *The Nature of dark matter*, *Frascati Phys. Ser.* **24** (2002) 449–474, [astro-ph/0112255]. Cited on page 42.

[199] M. Viel, J. Lesgourgues, M. G. Haehnelt, S. Matarrese and A. Riotto, *Can sterile neutrinos be ruled out as warm dark matter*

candidates?, *Phys. Rev. Lett.* **97** (2006) 071301, [astro-ph/0605706]. Cited on page 42.

[200] P. McDonald, U. Seljak, S. Burles, D. J. Schlegel, D. H. Weinberg, R. Cen et al., *The Lyα Forest Power Spectrum from the Sloan Digital Sky Survey*, *The Astrophysical Journal Supplement Series* **163** (Mar., 2006) 80–109, [astro-ph/0405013]. Cited on page 42.

[201] J. F. Navarro, C. S. Frenk and S. D. White, *The Structure of cold dark matter halos*, *Astrophys. J.* **462** (1996) 563–575, [astro-ph/9508025]. Cited on page 43.

[202] A. W. Graham, D. Merritt, B. Moore, J. Diemand and B. Terzic, *Empirical models for Dark Matter Halos. I. Nonparametric Construction of Density Profiles and Comparison with Parametric Models*, *Astron. J.* **132** (2006) 2685–2700, [astro-ph/0509417]. Cited on page 43.

[203] J. F. Navarro, A. Ludlow, V. Springel, J. Wang, M. Vogelsberger, S. D. White et al., *The Diversity and Similarity of Cold Dark Matter Halos*, *Mon. Not. Roy. Astron. Soc.* **402** (2010) 21, [0810.1522]. Cited on page 43.

[204] J. N. Bahcall and R. Soneira, *The Universe at faint magnetidues. 2. Models for the predicted star counts*, *Astrophys. J. Suppl.* **44** (1980) 73–110. Cited on page 43.

[205] A. Burkert, *The Structure of dark matter halos in dwarf galaxies*, *IAU Symp.* **171** (1996) 175, [astro-ph/9504041]. Cited on page 43.

[206] J. Diemand, B. Moore and J. Stadel, *Convergence and scatter of cluster density profiles*, *Mon. Not. Roy. Astron. Soc.* **353** (2004) 624, [astro-ph/0402267]. Cited on page 43.

[207] J. F. Navarro, E. Hayashi, C. Power, A. R. Jenkins, C. S. Frenk, S. D. M. White et al., *The inner structure of ΛCDM haloes - III. Universality and asymptotic slopes*, *Mon.Not.Roy.Astron.Soc.* **349** (Apr., 2004) 1039–1051, [astro-ph/0311231]. Cited on page 43.

[208] E. Retana-Montenegro, E. Van Hese, G. Gentile, M. Baes and F. Frutos-Alfaro, *Analytical properties of einasto dark matter haloes*, *Astronomy and Astrophysics* **540** (Mar, 2012) A70. Cited on page 43.

[209] Y. Jing and Y. Suto, *Triaxial modeling of halo density profiles with high-resolution N-body simulations*, *Astrophys. J.* **574** (2002) 538, [`astro-ph/0202064`]. Cited on page 43.

[210] W. J. G. de Blok, *The Core-Cusp Problem*, *Advances in Astronomy* **2010** (Jan., 2010) 789293, [`0910.3538`]. Cited on page 43.

[211] J. Bovy, D. W. Hogg and H.-W. Rix, *Galactic masers and the milky way circular velocity*, The Astrophysical Journal **704** (Oct, 2009) 1704?1709. Cited on page 43.

[212] S. Gillessen, F. Eisenhauer, S. Trippe, T. Alexander, R. Genzel, F. Martins et al., *Monitoring stellar orbits around the Massive Black Hole in the Galactic Center*, *Astrophys. J.* **692** (2009) 1075–1109, [`0810.4674`]. Cited on page 43.

[213] F. J. Kerr and D. Lynden-Bell, *Review of galactic constants*, *Mon. Not. Roy. Astron. Soc.* **221** (1986) 1023. Cited on page 43, and 73.

[214] J. Read, *The Local Dark Matter Density*, *J. Phys. G* **41** (2014) 063101, [`1404.1938`]. Cited on page 43, and 73.

[215] S. Sivertsson, H. Silverwood, J. Read, G. Bertone and P. Steger, *The localdark matter density from SDSS-SEGUE G-dwarfs*, *Mon. Not. Roy. Astron. Soc.* **478** (2018) 1677–1693, [`1708.07836`]. Cited on page 43, and 73.

[216] N. Przybilla, A. Tillich, U. Heber and R.-D. Scholz, *Weighing the galactic dark matter halo: A lower mass limit from the fastest halo star known*, *The Astrophysical Journal* **718** (Jun, 2010) 37?42. Cited on page 43.

[217] T. Sakamoto, M. Chiba and T. C. Beers, *The Mass of the Milky Way: Limits from a newly assembled set of halo objects*, *Astron.*

Astrophys. **397** (2003) 899–912, [astro-ph/0210508]. Cited on page 43.

[218] SDSS collaboration, X. Xue et al., *The Milky Way's Circular Velocity Curve to 60 kpc and an Estimate of the Dark Matter Halo Mass from Kinematics of ~2400 SDSS Blue Horizontal Branch Stars*, *Astrophys. J.* **684** (2008) 1143–1158, [0801.1232]. Cited on page 43.

[219] M. Cirelli, G. Corcella, A. Hektor, G. Hutsi, M. Kadastik, P. Panci et al., *PPPC 4 DM ID: A Poor Particle Physicist Cookbook for Dark Matter Indirect Detection*, *JCAP* **03** (2011) 051, [1012.4515]. Cited on page 44, 77, 80, 81, 83, 84, and 85.

[220] H. Baer, K.-Y. Choi, J. E. Kim and L. Roszkowski, *Dark matter production in the early Universe: beyond the thermal WIMP paradigm*, *Phys. Rept.* **555** (2015) 1–60, [1407.0017]. Cited on page 45, and 46.

[221] B. Paczynski, *Gravitational Microlensing by the Galactic Halo*, *The Astrophysical Journal* **304** (May, 1986) 1. Cited on page 45, and 317.

[222] P. Tisserand, L. Le Guillou, C. Afonso, J. N. Albert, J. Andersen, R. Ansari et al., *Limits on the macho content of the galactic halo from the eros-2 survey of the magellanic clouds*, *Astronomy & Astrophysics* **469** (Apr, 2007) 387?404. Cited on page 45.

[223] C. Alcock, R. A. Allsman, D. R. Alves, T. S. Axelrod, A. C. Becker, D. P. Bennett et al., *The macho project: Microlensing results from 5.7 years of large magellanic cloud observations*, *The Astrophysical Journal* **542** (Oct, 2000) 281?307. Cited on page 45.

[224] B. D. Fields, K. Freese and D. S. Graff, *Chemical abundance constraints on white dwarfs as halo dark matter*, *Astrophys. J.* **534** (2000) 265–276, [astro-ph/9904291]. Cited on page 45.

[225] B. W. Lee and S. Weinberg, *Cosmological lower bound on heavy-neutrino masses*, *Phys. Rev. Lett.* **39** (Jul, 1977) 165–168. Cited on page 45, 64, and 319.

[226] E. W. Kolb and M. S. Turner, *The Early Universe*, vol. 69. 1990. Cited on page 45, 58, and 61.

[227] K. Griest and D. Seckel, *Three exceptions in the calculation of relic abundances*, *Phys. Rev. D* **43** (May, 1991) 3191–3203. Cited on page 45.

[228] P. Gondolo and G. Gelmini, *Cosmic abundances of stable particles: Improved analysis*, *Nucl. Phys. B* **360** (1991) 145–179. Cited on page 45, 62, and 79.

[229] S. P. MARTIN, *A supersymmetry primer*, *Advanced Series on Directions in High Energy Physics* (Jul, 1998) 1?98. Cited on page 46.

[230] G. Jungman, M. Kamionkowski and K. Griest, *Supersymmetric dark matter*, *Physics Reports* **267** (Mar, 1996) 195?373. Cited on page 46.

[231] G. Bertone, D. Hooper and J. Silk, *Particle dark matter: evidence, candidates and constraints*, *Physics Reports* **405** (Jan, 2005) 279?390. Cited on page 46.

[232] L. Bergström, *Dark matter evidence, particle physics candidates and detection methods*, *Annalen der Physik* **524** (Aug, 2012) 479?496. Cited on page 46.

[233] L. Roszkowski, E. M. Sessolo and S. Trojanowski, *Wimp dark matter candidates and searches?current status and future prospects*, *Reports on Progress in Physics* **81** (May, 2018) 066201. Cited on page 46.

[234] T. Appelquist, H.-C. Cheng and B. A. Dobrescu, *Bounds on universal extra dimensions*, *Physical Review D* **64** (Aug., 2001) 035002, [`hep-ph/0012100`]. Cited on page 46.

[235] H. Georgi and A. Pais, *Calculability and naturalness in gauge theories*, *Phys. Rev. D* **10** (Jul, 1974) 539–558. Cited on page 46.

[236] S. Weinberg, *Approximate symmetries and pseudo-goldstone bosons*, *Phys. Rev. Lett.* **29** (Dec, 1972) 1698–1701. Cited on page 46.

[237] H. Georgi and A. Pais, *Vacuum symmetry and the pseudo-goldstone phenomenon*, *Phys. Rev. D* **12** (Jul, 1975) 508–512. Cited on page 46.

[238] XENON Collaboration 7 collaboration, E. Aprile, J. Aalbers, F. Agostini, M. Alfonsi, L. Althueser, F. D. Amaro et al., *Dark matter search results from a one ton-year exposure of xenon1t*, *Phys. Rev. Lett.* **121** (Sep, 2018) 111302. Cited on page 46, 78, and 321.

[239] PandaX-II Collaboration collaboration, X. Cui, A. Abdukerim, W. Chen, X. Chen, Y. Chen, B. Dong et al., *Dark matter results from 54-ton-day exposure of pandax-ii experiment*, *Phys. Rev. Lett.* **119** (Oct, 2017) 181302. Cited on page 46, and 78.

[240] Fermi-LAT, DES collaboration, A. Albert et al., *Searching for Dark Matter Annihilation in Recently Discovered Milky Way Satellites with Fermi-LAT*, *Astrophys. J.* **834** (2017) 110, [1611.03184]. Cited on page 46, 85, and 323.

[241] Fermi-LAT collaboration, M. Ackermann et al., *Searching for Dark Matter Annihilation from Milky Way Dwarf Spheroidal Galaxies with Six Years of Fermi Large Area Telescope Data*, *Phys. Rev. Lett.* **115** (2015) 231301, [1503.02641]. Cited on page 46, 85, and 323.

[242] AMS collaboration, N. Tomassetti, *AMS-02 in space: physics results, overview, and challenges*, *Nucl. Part. Phys. Proc.* **265-266** (2015) 245–247, [1511.00052]. Cited on page 46.

[243] M. Klasen, M. Pohl and G. Sigl, *Indirect and direct search for dark matter*, *Prog. Part. Nucl. Phys.* **85** (2015) 1–32, [1507.03800]. Cited on page 46.

[244] M. Drewes et al., *A White Paper on keV Sterile Neutrino Dark Matter*, *JCAP* **01** (2017) 025, [1602.04816]. Cited on page 46, 106, and 330.

[245] J. Alexander et al., *Dark Sectors 2016 Workshop: Community Report*, 8, 2016. 1608.08632. Cited on page 46.

[246] S. Tulin and H.-B. Yu, *Dark Matter Self-interactions and Small Scale Structure*, *Phys. Rept.* **730** (2018) 1–57, [1705.02358]. Cited on page 46.

[247] N. Bernal, M. Heikinheimo, T. Tenkanen, K. Tuominen and V. Vaskonen, *The Dawn of FIMP Dark Matter: A Review of Models and Constraints*, *Int. J. Mod. Phys. A* **32** (2017) 1730023, [1706.07442]. Cited on page 47, and 68.

[248] J. McDonald, *Thermally generated gauge singlet scalars as selfinteracting dark matter*, *Phys. Rev. Lett.* **88** (2002) 091304, [hep-ph/0106249]. Cited on page 46.

[249] K.-Y. Choi and L. Roszkowski, *E-WIMPs*, *AIP Conf. Proc.* **805** (2005) 30–36, [hep-ph/0511003]. Cited on page 46.

[250] A. Kusenko, *Sterile neutrinos, dark matter, and the pulsar velocities in models with a Higgs singlet*, *Phys. Rev. Lett.* **97** (2006) 241301, [hep-ph/0609081]. Cited on page 46.

[251] K. Petraki and A. Kusenko, *Dark-matter sterile neutrinos in models with a gauge singlet in the Higgs sector*, *Phys. Rev. D* **77** (2008) 065014, [0711.4646]. Cited on page 46.

[252] L. J. Hall, K. Jedamzik, J. March-Russell and S. M. West, *Freeze-In Production of FIMP Dark Matter*, *JHEP* **03** (2010) 080, [0911.1120]. Cited on page 46, 47, 68, and 319.

[253] F. Wilczek, *Problem of strong p and t invariance in the presence of instantons*, *Phys. Rev. Lett.* **40** (Jan, 1978) 279–282. Cited on page 48.

[254] S. Weinberg, *A new light boson?*, *Phys. Rev. Lett.* **40** (Jan, 1978) 223–226. Cited on page 48.

[255] J. E. Kim, *Weak-interaction singlet and strong* CP *invariance*, *Phys. Rev. Lett.* **43** (Jul, 1979) 103–107. Cited on page 48.

[256] M. Shifman, A. Vainshtein and V. Zakharov, *Can confinement ensure natural cp invariance of strong interactions?*, *Nuclear Physics B* **166** (1980) 493 – 506. Cited on page 48.

[257] M. Dine, W. Fischler and M. Srednicki, *A simple solution to the strong cp problem with a harmless axion*, *Physics Letters B* **104** (1981) 199 – 202. Cited on page 48.

[258] A. Zhitnitsky, *On Possible Suppression of the Axion Hadron Interactions. (In Russian)*, *Sov. J. Nucl. Phys.* **31** (1980) 260. Cited on page 48.

[259] A. Browman, J. Dewire, B. Gittelman, K. M. Hanson, D. Larson, E. Loh et al., *Decay Width of the Neutral π Meson*, *Physical Review Letters* **33** (Dec., 1974) 1400–1403. Cited on page 49.

[260] S. J. Asztalos, G. Carosi, C. Hagmann, D. Kinion, K. van Bibber, M. Hotz et al., *SQUID-Based Microwave Cavity Search for Dark-Matter Axions*, *Physical Review Letters* **104** (Jan., 2010) 041301, [0910.5914]. Cited on page 49.

[261] B. Brubaker, L. Zhong, Y. Gurevich, S. Cahn, S. Lamoreaux, M. Simanovskaia et al., *First results from a microwave cavity axion search at 24???ev*, *Physical Review Letters* **118** (Feb, 2017) . Cited on page 49.

[262] E. Petrakou, *Haloscope searches for dark matter axions at the center for axion and precision physics research*, *EPJ Web of Conferences* **164** (2017) 01012. Cited on page 49.

[263] B. T. McAllister, G. Flower, J. Kruger, E. N. Ivanov, M. Goryachev, J. Bourhill et al., *The organ experiment: An axion haloscope above 15 ghz*, 2017. Cited on page 49.

[264] L. Maiani, R. Petronzio and E. Zavattini, *Effects of nearly massless, spin-zero particles on light propagation in a magnetic field*, *Physics Letters B* **175** (Aug., 1986) 359–363. Cited on page 49.

[265] S. Borsanyi et al., *Calculation of the axion mass based on high-temperature lattice quantum chromodynamics*, *Nature* **539** (2016) 69–71, [1606.07494]. Cited on page 49.

[266] O. Wantz and E. Shellard, *Axion Cosmology Revisited*, *Phys. Rev. D* **82** (2010) 123508, [0910.1066]. Cited on page 49.

[267] J. E. Kim and G. Carosi, *Axions and the Strong CP Problem*, *Rev. Mod. Phys.* **82** (2010) 557–602, [0807.3125]. Cited on page 49.

[268] B. J. Carr and S. W. Hawking, *Black Holes in the Early Universe*, *Monthly Notices of the Royal Astronomical Society* **168** (08, 1974) 399–415. Cited on page 49, and 319.

[269] B. J. Carr, *The primordial black hole mass spectrum.*, *Astrophysical Journal* **201** (Oct., 1975) 1–19. Cited on page 49, and 319.

[270] S. Hawking, *Gravitationally Collapsed Objects of Very Low Mass*, *Monthly Notices of the Royal Astronomical Society* **152** (04, 1971) 75–78. Cited on page 49, and 319.

[271] G. F. Chapline, *Cosmological effects of primordial black holes*, *Nature* **253** (1975) 251–252. Cited on page 50.

[272] B. Carr, F. Kuhnel and M. Sandstad, *Primordial Black Holes as Dark Matter*, *Phys. Rev. D* **94** (2016) 083504, [1607.06077]. Cited on page 50.

[273] S. Hawking, *Gravitational radiation from colliding black holes*, *Phys. Rev. Lett.* **26** (1971) 1344–1346. Cited on page 50.

[274] S. W. Hawking, *Black hole explosions?*, *Nature* **248** (Mar., 1974) 30–31. Cited on page 50.

[275] S. Hawking, *Particle Creation by Black Holes*, *Commun. Math. Phys.* **43** (1975) 199–220. Cited on page 50.

[276] B. J. Carr, K. Kohri, Y. Sendouda and J. Yokoyama, *New cosmological constraints on primordial black holes*, *Phys. Rev. D* **81** (May, 2010) 104019. Cited on page 50.

[277] B. Abbott, R. Abbott, T. Abbott, M. Abernathy, F. Acernese, K. Ackley et al., *Observation of gravitational waves from a binary black hole merger*, *Physical Review Letters* **116** (Feb, 2016) . Cited on page 50.

[278] S. Bird, I. Cholis, J. B. Muñoz, Y. Ali-Haïmoud, M. Kamionkowski, E. D. Kovetz et al., *Did ligo detect dark matter?*, *Physical Review Letters* **116** (May, 2016) . Cited on page 50.

[279] H. Goldstein, C. Poole and J. Safko, *Classical Mechanics.* Addison Wesley, 2002. Cited on page 58.

[280] J. Liouville, *Note sur la théorie de la variation des constantes arbitraires.*, *Journal de mathématiques pures et appliquées* (1838) 342–349. Cited on page 58.

[281] S. De Groot, W. van Leeuwen and C. van derWert, *Relativistic Kinetic Theory.* North Holland Publishing Co., 1980. Cited on page 59.

[282] L. Boltzmann, *Weitere studien über das wärmegleichgewicht unter gasmolekülen*, 1970. Cited on page 59.

[283] J. Jeans, *The Dynamical Theory of Gases.* Cambridge Library Collection - Physical Sciences. Cambridge University Press, 4 ed., 2009, 10.1017/CBO9780511694370. Cited on page 59.

[284] K. P. N. Murthy, *Ludwig Boltzmann, Transport Equation and the Second Law*, *arXiv e-prints* (Jan., 2006) cond–mat/0601566, [cond-mat/0601566]. Cited on page 59.

[285] O. Sarbach and T. Zannias, *Relativistic Kinetic Theory: An Introduction*, *AIP Conf. Proc.* **1548** (2013) 134–155, [1303.2899]. Cited on page 59.

[286] M. Abramowitz and I. A. Stegun, *Handbook of Mathematical Functions with Formulas, Graphs, and Mathematical Tables.* Dover, New York, ninth dover printing, tenth gpo printing ed., 1964. Cited on page 63.

[287] C. Møller, *General properties of the characteristic matrix in the theory of elementary particles i., k. dan. vidensk. selsk*, *Mat. Fys. Medd* (1945) . Cited on page 63.

[288] G. Gelmini and P. Gondolo, *DM Production Mechanisms*, 1009.3690. Cited on page 65.

[289] S.-M. Choi, H. M. Lee and M.-S. Seo, *Cosmic abundances of SIMP dark matter*, *JHEP* **04** (2017) 154, [1702.07860]. Cited on page 66.

[290] G. Steigman, B. Dasgupta and J. F. Beacom, *Precise Relic WIMP Abundance and its Impact on Searches for Dark Matter Annihilation*, *Phys. Rev. D* **86** (2012) 023506, [`1204.3622`]. Cited on page 67.

[291] D. J. Chung, E. W. Kolb and A. Riotto, *Production of massive particles during reheating*, *Phys. Rev. D* **60** (1999) 063504, [`hep-ph/9809453`]. Cited on page 68, and 320.

[292] A. H. Guth, *The Inflationary Universe: A Possible Solution to the Horizon and Flatness Problems*, *Adv. Ser. Astrophys. Cosmol.* **3** (1987) 139–148. Cited on page 70.

[293] F. Calore, *Lecture notes in dark matter indirect detection*, ISAPP 2017: The Dark and Visible Side of the Universe. Cited on page 71.

[294] F. Kahlhoefer, *Review of LHC Dark Matter Searches*, *Int. J. Mod. Phys. A* **32** (2017) 1730006, [`1702.02430`]. Cited on page 71, and 88.

[295] M. Schumann, *Direct Detection of WIMP Dark Matter: Concepts and Status*, *J. Phys. G* **46** (2019) 103003, [`1903.03026`]. Cited on page 71, 78, and 79.

[296] J. M. Gaskins, *A review of indirect searches for particle dark matter*, *Contemp. Phys.* **57** (2016) 496–525, [`1604.00014`]. Cited on page 72, and 77.

[297] M. W. Goodman and E. Witten, *Detectability of Certain Dark Matter Candidates*, *Phys. Rev. D* **31** (1985) 3059. Cited on page 72, and 321.

[298] J. Lewin and P. Smith, *Review of mathematics, numerical factors, and corrections for dark matter experiments based on elastic nuclear recoil*, *Astropart. Phys.* **6** (1996) 87–112. Cited on page 72.

[299] D. G. Cerdeno and A. M. Green, *Direct detection of WIMPs*, `1002.1912`. Cited on page 72, and 74.

[300] T. Lin, *Dark matter models and direct detection*, *PoS* **333** (2019) 009, [`1904.07915`]. Cited on page 72.

[301] M. Reid, *The distance to the center of the galaxy*, *Ann. Rev. Astron. Astrophys.* **31** (1993) 345–372. Cited on page 73.

[302] M. Kuhlen, M. Vogelsberger and R. Angulo, *Numerical Simulations of the Dark Universe: State of the Art and the Next Decade*, *Phys. Dark Univ.* **1** (2012) 50–93, [1209.5745]. Cited on page 73.

[303] M. C. Smith et al., *The RAVE Survey: Constraining the Local Galactic Escape Speed*, *Mon. Not. Roy. Astron. Soc.* **379** (2007) 755–772, [astro-ph/0611671]. Cited on page 73.

[304] V. Barger, W.-Y. Keung and G. Shaughnessy, *Spin Dependence of Dark Matter Scattering*, *Phys. Rev. D* **78** (2008) 056007, [0806.1962]. Cited on page 74.

[305] QCDSF collaboration, G. S. Bali et al., *Strangeness Contribution to the Proton Spin from Lattice QCD*, *Phys. Rev. Lett.* **108** (2012) 222001, [1112.3354]. Cited on page 75.

[306] COMPASS collaboration, M. Alekseev et al., *Quark helicity distributions from longitudinal spin asymmetries in muon-proton and muon-deuteron scattering*, *Phys. Lett. B* **693** (2010) 227–235, [1007.4061]. Cited on page 75.

[307] COMPASS collaboration, M. Alekseev et al., *The Polarised Valence Quark Distribution from semi-inclusive DIS*, *Phys. Lett. B* **660** (2008) 458–465, [0707.4077]. Cited on page 75.

[308] C. A. Aidala, S. D. Bass, D. Hasch and G. K. Mallot, *The Spin Structure of the Nucleon*, *Rev. Mod. Phys.* **85** (2013) 655–691, [1209.2803]. Cited on page 75.

[309] R. J. Hill and M. P. Solon, *Standard Model anatomy of WIMP dark matter direct detection II: QCD analysis and hadronic matrix elements*, *Phys. Rev. D* **91** (2015) 043505, [1409.8290]. Cited on page 75.

[310] M. I. Gresham and K. M. Zurek, *Effect of nuclear response functions in dark matter direct detection*, *Phys. Rev. D* **89** (2014) 123521, [1401.3739]. Cited on page 75.

[311] J. Engel, *Nuclear form-factors for the scattering of weakly interacting massive particles*, *Phys. Lett. B* **264** (1991) 114–119. Cited on page 75.

[312] R. H. Helm, *Inelastic and Elastic Scattering of 187-Mev Electrons from Selected Even-Even Nuclei*, *Phys. Rev.* **104** (1956) 1466–1475. Cited on page 75.

[313] J. R. Ellis, K. A. Olive and C. Savage, *Hadronic Uncertainties in the Elastic Scattering of Supersymmetric Dark Matter*, *Phys. Rev. D* **77** (2008) 065026, [0801.3656]. Cited on page 76.

[314] J. Ellis, N. Nagata and K. A. Olive, *Uncertainties in WIMP Dark Matter Scattering Revisited*, *Eur. Phys. J. C* **78** (2018) 569, [1805.09795]. Cited on page 76.

[315] F. Bishara, J. Brod, B. Grinstein and J. Zupan, *From quarks to nucleons in dark matter direct detection*, *JHEP* **11** (2017) 059, [1707.06998]. Cited on page 76.

[316] R. Ruiz de Austri and C. Pérez de los Heros, *Impact of nucleon matrix element uncertainties on the interpretation of direct and indirect dark matter search results*, *JCAP* **11** (2013) 049, [1307.6668]. Cited on page 76.

[317] DAMA collaboration, R. Bernabei et al., *First results from DAMA/LIBRA and the combined results with DAMA/NaI*, *Eur. Phys. J. C* **56** (2008) 333–355, [0804.2741]. Cited on page 77, and 321.

[318] DAMA, LIBRA collaboration, R. Bernabei et al., *New results from DAMA/LIBRA*, *Eur. Phys. J. C* **67** (2010) 39–49, [1002.1028]. Cited on page 77, and 321.

[319] J. Amaré et al., *First Results on Dark Matter Annual Modulation from the ANAIS-112 Experiment*, *Phys. Rev. Lett.* **123** (2019) 031301, [1903.03973]. Cited on page 78.

[320] CDEX collaboration, H. Jiang et al., *Limits on Light Weakly Interacting Massive Particles from the First 102.8 kg $\times$ day Data of*

the CDEX-10 Experiment, *Phys. Rev. Lett.* **120** (2018) 241301, [1802.09016]. Cited on page 78.

[321] SuperCDMS collaboration, R. Agnese et al., *Low-mass dark matter search with CDMSlite*, *Phys. Rev. D* **97** (2018) 022002, [1707.01632]. Cited on page 78.

[322] G. Adhikari et al., *Initial Performance of the COSINE-100 Experiment*, *Eur. Phys. J. C* **78** (2018) 107, [1710.05299]. Cited on page 78.

[323] CRESST collaboration, G. Angloher et al., *Results on light dark matter particles with a low-threshold CRESST-II detector*, *Eur. Phys. J. C* **76** (2016) 25, [1509.01515]. Cited on page 78.

[324] CRESST collaboration, A. Abdelhameed et al., *First results from the CRESST-III low-mass dark matter program*, *Phys. Rev. D* **100** (2019) 102002, [1904.00498]. Cited on page 78.

[325] R. Bernabei et al., *First model independent results from DAMA/LIBRA-phase2*, *Nucl. Phys. Atom. Energy* **19** (2018) 307–325, [1805.10486]. Cited on page 78.

[326] DarkSide Collaboration collaboration, P. Agnes, I. F. M. Albuquerque, T. Alexander, A. K. Alton, G. R. Araujo, D. M. Asner et al., *Low-mass dark matter search with the darkside-50 experiment*, *Phys. Rev. Lett.* **121** (Aug, 2018) 081307. Cited on page 78.

[327] DEAP collaboration, R. Ajaj et al., *Search for dark matter with a 231-day exposure of liquid argon using DEAP-3600 at SNOLAB*, *Phys. Rev. D* **100** (2019) 022004, [1902.04048]. Cited on page 78.

[328] DRIFT collaboration, J. Battat et al., *Low Threshold Results and Limits from the DRIFT Directional Dark Matter Detector*, *Astropart. Phys.* **91** (2017) 65–74, [1701.00171]. Cited on page 78.

[329] EDELWEISS collaboration, L. Hehn et al., *Improved EDELWEISS-III sensitivity for low-mass WIMPs using a profile likelihood approach*, *Eur. Phys. J. C* **76** (2016) 548, [1607.03367]. Cited on page 78.

[330] LUX collaboration, D. Akerib et al., *Results from a search for dark matter in the complete LUX exposure*, *Phys. Rev. Lett.* **118** (2017) 021303, [1608.07648]. Cited on page 78, and 321.

[331] NEWS-G collaboration, Q. Arnaud et al., *First results from the NEWS-G direct dark matter search experiment at the LSM*, *Astropart. Phys.* **97** (2018) 54–62, [1706.04934]. Cited on page 78.

[332] E. Behnke et al., *Final Results of the PICASSO Dark Matter Search Experiment*, *Astropart. Phys.* **90** (2017) 85–92, [1611.01499]. Cited on page 78.

[333] PICO collaboration, C. Amole et al., *Dark Matter Search Results from the Complete Exposure of the PICO-60 C_3F_8 Bubble Chamber*, *Phys. Rev. D* **100** (2019) 022001, [1902.04031]. Cited on page 78.

[334] SENSEI Collaboration collaboration, O. Abramoff, L. Barak, I. M. Bloch, L. Chaplinsky, M. Crisler, Dawa et al., *Sensei: Direct-detection constraints on sub-gev dark matter from a shallow underground run using a prototype skipper ccd*, *Phys. Rev. Lett.* **122** (Apr, 2019) 161801. Cited on page 78.

[335] R. Agnese, T. Aralis, T. Aramaki, I. J. Arnquist, E. Azadbakht, W. Baker et al., *First dark matter constraints from a supercdms single-charge sensitive detector*, *Phys. Rev. Lett.* **121** (Aug, 2018) 051301. Cited on page 78.

[336] XENON Collaboration collaboration, E. Aprile, J. Aalbers, F. Agostini, M. Alfonsi, F. D. Amaro, M. Anthony et al., *Xenon100 dark matter results from a combination of 477 live days*, *Phys. Rev. D* **94** (Dec, 2016) 122001. Cited on page 78.

[337] XMASS collaboration, K. Abe et al., *A direct dark matter search in XMASS-I*, *Phys. Lett. B* **789** (2019) 45–53, [1804.02180]. Cited on page 78.

[338] S. Ahlen, F. Avignone, R. Brodzinski, A. Drukier, G. Gelmini and D. Spergel, *Limits on Cold Dark Matter Candidates from an Ultralow Background Germanium Spectrometer*, *Phys. Lett. B* **195** (1987) 603–608. Cited on page 77.

[339] J. Billard, L. Strigari and E. Figueroa-Feliciano, *Implication of neutrino backgrounds on the reach of next generation dark matter direct detection experiments*, *Phys. Rev. D* **89** (2014) 023524, [1307.5458]. Cited on page 79, and 322.

[340] J. E. Gunn, B. W. Lee, I. Lerche, D. N. Schramm and G. Steigman, *Some astrophysical consequences of the existence of a heavy stable neutral lepton.*, *Astrophysical Journal* **223** (Aug., 1978) 1015–1031. Cited on page 77.

[341] F. W. Stecker, *The cosmic gamma -ray background from the annihilation of primordial stable neutral heavy leptons.*, *Astrophysical Journal* **223** (Aug., 1978) 1032–1036. Cited on page 77.

[342] Ya. B. Zeldovich, A. A. Klypin, M. Yu. Khlopov and V. M. Chechetkin, *Astrophysical constraints on the mass of heavy stable neutral leptons*, *Sov. J. Nucl. Phys.* **31** (1980) 664–669. Cited on page 77.

[343] J. R. Ellis, R. Flores, K. Freese, S. Ritz, D. Seckel and J. Silk, *Cosmic Ray Constraints on the Annihilations of Relic Particles in the Galactic Halo*, *Phys. Lett. B* **214** (1988) 403–412. Cited on page 77.

[344] J. Silk and M. Srednicki, *Cosmic-ray antiprotons as a probe of a photino-dominated universe*, *Phys. Rev. Lett.* **53** (Aug, 1984) 624–627. Cited on page 77.

[345] S. Rudaz and F. Stecker, *Cosmic Ray Anti-protons, Positrons and gamma-rays From Halo Dark Matter Annihilation*, *Astrophys. J.* **325** (1988) 16. Cited on page 77.

[346] F. Stecker and A. Tylka, *The Cosmic Ray Anti-proton Spectrum From Dark Matter Annihilation and Its Astrophysical Implications: A New Look*, *Astrophys. J. Lett.* **336** (1989) L51–L54. Cited on page 77.

[347] F. W. Stecker, S. Rudaz and T. F. Walsh, *Galactic antiprotons from photinos*, *Phys. Rev. Lett.* **55** (Dec, 1985) 2622–2625. Cited on page 77.

[348] F. Donato, N. Fornengo and P. Salati, *Anti-deuterons as a signature of supersymmetric dark matter*, *Phys. Rev. D* **62** (2000) 043003, [hep-ph/9904481]. Cited on page 77.

[349] H. Baer and S. Profumo, *Low energy antideuterons: shedding light on dark matter*, *JCAP* **12** (2005) 008, [astro-ph/0510722]. Cited on page 77.

[350] F. Donato, N. Fornengo and D. Maurin, *Antideuteron fluxes from dark matter annihilation in diffusion models*, *Phys. Rev. D* **78** (2008) 043506, [0803.2640]. Cited on page 77, and 80.

[351] A. Alloul, N. D. Christensen, C. Degrande, C. Duhr and B. Fuks, *Feynrules 2.0 ? a complete toolbox for tree-level phenomenology*, *Computer Physics Communications* **185** (Aug, 2014) 2250?2300. Cited on page 80.

[352] T. Sjöstrand, S. Mrenna and P. Skands, *A brief introduction to pythia 8.1*, *Computer Physics Communications* **178** (Jun, 2008) 852?867. Cited on page 80.

[353] J. Alwall, R. Frederix, S. Frixione, V. Hirschi, F. Maltoni, O. Mattelaer et al., *The automated computation of tree-level and next-to-leading order differential cross sections, and their matching to parton shower simulations*, *Journal of High Energy Physics* **2014** (Jul, 2014) . Cited on page 80.

[354] F. Staub, *Exploring new models in all detail withsarah*, *Advances in High Energy Physics* **2015** (2015) 1?126. Cited on page 80.

[355] W. Porod, *Spheno, a program for calculating supersymmetric spectra, susy particle decays and susy particle production at e+e? colliders*, *Computer Physics Communications* **153** (Jun, 2003) 275?315. Cited on page 80.

[356] C. B. Brauninger and M. Cirelli, *Anti-deuterons from heavy Dark Matter*, *Phys. Lett. B* **678** (2009) 20–31, [0904.1165]. Cited on page 80.

[357] M. Kadastik, M. Raidal and A. Strumia, *Enhanced anti-deuteron Dark Matter signal and the implications of PAMELA*, *Phys. Lett. B* **683** (2010) 248–254, [0908.1578]. Cited on page 80.

[358] P. Meade, M. Papucci, A. Strumia and T. Volansky, *Dark Matter Interpretations of the e+- Excesses after FERMI*, *Nucl. Phys. B* **831** (2010) 178–203, [0905.0480]. Cited on page 82.

[359] T. Delahaye, R. Lineros, F. Donato, N. Fornengo and P. Salati, *Positrons from dark matter annihilation in the galactic halo: Theoretical uncertainties*, *Phys. Rev. D* **77** (2008) 063527, [0712.2312]. Cited on page 82.

[360] J. Hisano, S. Matsumoto, O. Saito and M. Senami, *Heavy wino-like neutralino dark matter annihilation into antiparticles*, *Phys. Rev. D* **73** (2006) 055004, [hep-ph/0511118]. Cited on page 83.

[361] F. Donato, N. Fornengo, D. Maurin and P. Salati, *Antiprotons in cosmic rays from neutralino annihilation*, *Phys. Rev. D* **69** (2004) 063501, [astro-ph/0306207]. Cited on page 83.

[362] A. Bottino, F. Donato, N. Fornengo and P. Salati, *Which fraction of the measured cosmic ray anti-protons might be due to neutralino annihilation in the galactic halo?*, *Phys. Rev. D* **58** (1998) 123503, [astro-ph/9804137]. Cited on page 84.

[363] P. Chardonnet, G. Mignola, P. Salati and R. Taillet, *Galactic diffusion and the anti-proton signal of supersymmetric dark matter*, *Phys. Lett. B* **384** (1996) 161–168, [astro-ph/9606174]. Cited on page 84.

[364] D. Maurin, F. Donato, R. Taillet and P. Salati, *Cosmic rays below z=30 in a diffusion model: new constraints on propagation parameters*, *Astrophys. J.* **555** (2001) 585–596, [astro-ph/0101231]. Cited on page 84.

[365] D. Maurin, R. Taillet, F. Donato, P. Salati, A. Barrau and G. Boudoul, *Galactic cosmic ray nuclei as a tool for astroparticle physics*, astro-ph/0212111. Cited on page 84.

[366] L. Gleeson and W. Axford, *Solar Modulation of Galactic Cosmic Rays*, *Astrophys. J.* **154** (1968) 1011. Cited on page 84.

[367] M. Cirelli, N. Fornengo, T. Montaruli, I. A. Sokalski, A. Strumia and F. Vissani, *Spectra of neutrinos from dark matter annihilations*, *Nucl. Phys. B* **727** (2005) 99–138, [hep-ph/0506298]. Cited on page 84.

[368] GAMBIT Dark Matter Workgroup collaboration, T. Bringmann et al., *DarkBit: A GAMBIT module for computing dark matter observables and likelihoods*, *Eur. Phys. J. C* **77** (2017) 831, [1705.07920]. Cited on page 86.

[369] M. Lisanti, S. Mishra-Sharma, N. L. Rodd and B. R. Safdi, *Search for Dark Matter Annihilation in Galaxy Groups*, *Phys. Rev. Lett.* **120** (2018) 101101, [1708.09385]. Cited on page 86.

[370] L. J. Chang, M. Lisanti and S. Mishra-Sharma, *Search for dark matter annihilation in the Milky Way halo*, *Phys. Rev. D* **98** (2018) 123004, [1804.04132]. Cited on page 86.

[371] O. Adriani, G. C. Barbarino, G. A. Bazilevskaya, R. Bellotti, M. Boezio, E. A. Bogomolov et al., *Cosmic-ray electron flux measured by the pamela experiment between 1 and 625 gev*, *Physical Review Letters* **106** (May, 2011) . Cited on page 86.

[372] AMS Collaboration collaboration, M. Aguilar, L. Ali Cavasonza, B. Alpat, G. Ambrosi, L. Arruda, N. Attig et al., *Antiproton flux, antiproton-to-proton flux ratio, and properties of elementary particle fluxes in primary cosmic rays measured with the alpha magnetic spectrometer on the international space station*, *Phys. Rev. Lett.* **117** (Aug, 2016) 091103. Cited on page 86.

[373] AMS Collaboration collaboration, M. Aguilar, D. Aisa, B. Alpat, A. Alvino, G. Ambrosi, K. Andeen et al., *Precision measurement of the $(e^+ + e^-)$ flux in primary cosmic rays from 0.5 gev to 1 tev with the alpha magnetic spectrometer on the international space station*, *Phys. Rev. Lett.* **113** (Nov, 2014) 221102. Cited on page 86.

[374] AMS Collaboration collaboration, L. Accardo, M. Aguilar, D. Aisa, B. Alpat, A. Alvino, G. Ambrosi et al., *High statistics measurement of the positron fraction in primary cosmic rays of 0.5–500 gev with the alpha magnetic spectrometer on the international space station*, *Phys. Rev. Lett.* **113** (Sep, 2014) 121101. Cited on page 86.

[375] A. Cuoco, M. Krämer and M. Korsmeier, *Novel Dark Matter Constraints from Antiprotons in Light of AMS-02*, *Phys. Rev. Lett.* **118** (2017) 191102, [1610.03071]. Cited on page 86.

[376] M.-Y. Cui, Q. Yuan, Y.-L. S. Tsai and Y.-Z. Fan, *Possible dark matter annihilation signal in the AMS-02 antiproton data*, *Phys. Rev. Lett.* **118** (2017) 191101, [1610.03840]. Cited on page 86.

[377] T. Bringmann, M. Vollmann and C. Weniger, *Updated cosmic-ray and radio constraints on light dark matter: Implications for the GeV gamma-ray excess at the Galactic center*, *Phys. Rev. D* **90** (2014) 123001, [1406.6027]. Cited on page 86.

[378] M. Cirelli, D. Gaggero, G. Giesen, M. Taoso and A. Urbano, *Antiproton constraints on the GeV gamma-ray excess: a comprehensive analysis*, *JCAP* **12** (2014) 045, [1407.2173]. Cited on page 86.

[379] D. Hooper, T. Linden and P. Mertsch, *What Does The PAMELA Antiproton Spectrum Tell Us About Dark Matter?*, *JCAP* **03** (2015) 021, [1410.1527]. Cited on page 86.

[380] I. Cholis, T. Linden and D. Hooper, *A Robust Excess in the Cosmic-Ray Antiproton Spectrum: Implications for Annihilating Dark Matter*, *Phys. Rev. D* **99** (2019) 103026, [1903.02549]. Cited on page 86.

[381] M.-Y. Cui, W.-C. Huang, Y.-L. S. Tsai and Q. Yuan, *Consistency test of the AMS-02 antiproton excess with direct detection data based on the effective field theory approach*, *JCAP* **11** (2018) 039, [1805.11590]. Cited on page 86.

[382] IceCube collaboration, M. Aartsen et al., *Search for Neutrinos from Dark Matter Self-Annihilations in the center of the Milky Way with 3 years of IceCube/DeepCore*, *Eur. Phys. J. C* **77** (2017) 627, [1705.08103]. Cited on page 87.

[383] A. Albert et al., *Results from the search for dark matter in the Milky Way with 9 years of data of the ANTARES neutrino telescope*, *Phys. Lett. B* **769** (2017) 249–254, [1612.04595]. Cited on page 87.

[384] ANTARES collaboration, S. Adrian-Martinez et al., *Limits on Dark Matter Annihilation in the Sun using the ANTARES Neutrino Telescope*, *Phys. Lett. B* **759** (2016) 69–74, [1603.02228]. Cited on page 87.

[385] IceCube collaboration, M. Aartsen et al., *Search for annihilating dark matter in the Sun with 3 years of IceCube data*, *Eur. Phys. J. C* **77** (2017) 146, [1612.05949]. Cited on page 87.

[386] L. Goodenough and D. Hooper, *Possible Evidence For Dark Matter Annihilation In The Inner Milky Way From The Fermi Gamma Ray Space Telescope*, *ArXiv e-prints* (Oct., 2009) , [0910.2998]. Cited on page 87, and 323.

[387] Fermi-LAT collaboration, V. Vitale and A. Morselli, *Indirect Search for Dark Matter from the center of the Milky Way with the Fermi-Large Area Telescope*, in *Fermi gamma-ray space telescope. Proceedings, 2nd Fermi Symposium, Washington, USA, November 2-5, 2009*, 2009. 0912.3828. Cited on page 87, and 323.

[388] D. Hooper and L. Goodenough, *Dark Matter Annihilation in The Galactic Center As Seen by the Fermi Gamma Ray Space Telescope*, *Phys. Lett.* **B697** (2011) 412–428, [1010.2752]. Cited on page 87, and 323.

[389] C. Gordon and O. Macias, *Dark Matter and Pulsar Model Constraints from Galactic Center Fermi-LAT Gamma Ray Observations*, *Phys. Rev.* **D88** (2013) 083521, [1306.5725]. Cited on page 87, and 323.

[390] D. Hooper and T. Linden, *On The Origin Of The Gamma Rays From The Galactic Center*, *Phys.Rev.* **D84** (2011) 123005, [1110.0006]. Cited on page 87, and 323.

[391] T. Daylan, D. P. Finkbeiner, D. Hooper, T. Linden, S. K. N. Portillo, N. L. Rodd et al., *The characterization of the gamma-ray signal from the central Milky Way: A case for annihilating dark matter*, *Phys. Dark Univ.* **12** (2016) 1–23, [1402.6703]. Cited on page 87, and 323.

[392] A. Boyarsky, D. Malyshev and O. Ruchayskiy, *A comment on the emission from the Galactic Center as seen by the Fermi telescope*, *Physics Letters B* **705** (Nov., 2011) 165–169, [1012.5839]. Cited on page 87, and 323.

[393] F. Calore, I. Cholis and C. Weniger, *Background model systematics for the Fermi GeV excess*, *JCAP* **3** (Mar., 2015) 038, [1409.0042]. Cited on page 87, and 323.

[394] K. N. Abazajian, N. Canac, S. Horiuchi and M. Kaplinghat, *Astrophysical and Dark Matter Interpretations of Extended Gamma-Ray Emission from the Galactic Center*, *Phys. Rev.* **D90** (2014) 023526, [1402.4090]. Cited on page 87, and 323.

[395] B. Zhou, Y.-F. Liang, X. Huang, X. Li, Y.-Z. Fan, L. Feng et al., *GeV excess in the Milky Way: The role of diffuse galactic gamma-ray emission templates*, *Phys. Rev.* **D91** (2015) 123010, [1406.6948]. Cited on page 87, and 323.

[396] K. N. Abazajian, *The Consistency of Fermi-LAT Observations of the Galactic Center with a Millisecond Pulsar Population in the Central Stellar Cluster*, *JCAP* **03** (2011) 010, [1011.4275]. Cited on page 87.

[397] R. Bartels, S. Krishnamurthy and C. Weniger, *Strong support for the millisecond pulsar origin of the Galactic center GeV excess*, *Phys. Rev. Lett.* **116** (2016) 051102, [1506.05104]. Cited on page 87.

[398] S. K. Lee, M. Lisanti, B. R. Safdi, T. R. Slatyer and W. Xue, *Evidence for Unresolved γ-Ray Point Sources in the Inner Galaxy*,

Phys. Rev. Lett. **116** (2016) 051103, [1506.05124]. Cited on page 87.

[399] Fermi-LAT collaboration, M. Ajello et al., *Characterizing the population of pulsars in the inner Galaxy with the Fermi Large Area Telescope*, 1705.00009. Cited on page 87.

[400] S. Caron, G. A. Gómez-Vargas, L. Hendriks and R. Ruiz de Austri, *Analyzing γ-rays of the Galactic Center with Deep Learning*, *JCAP* **05** (2018) 058, [1708.06706]. Cited on page 87.

[401] I. Cholis, C. Evoli, F. Calore, T. Linden, C. Weniger and D. Hooper, *The Galactic Center GeV Excess from a Series of Leptonic Cosmic-Ray Outbursts*, *JCAP* **12** (2015) 005, [1506.05119]. Cited on page 87.

[402] A. Boveia and C. Doglioni, *Dark Matter Searches at Colliders*, *Ann. Rev. Nucl. Part. Sci.* **68** (2018) 429–459, [1810.12238]. Cited on page 88.

[403] J. Abdallah et al., *Simplified Models for Dark Matter Searches at the LHC*, *Phys. Dark Univ.* **9-10** (2015) 8–23, [1506.03116]. Cited on page 88.

[404] F. Kahlhoefer, K. Schmidt-Hoberg, T. Schwetz and S. Vogl, *Implications of unitarity and gauge invariance for simplified dark matter models*, *JHEP* **02** (2016) 016, [1510.02110]. Cited on page 88.

[405] ATLAS collaboration, M. Aaboud et al., *Combination of searches for invisible Higgs boson decays with the ATLAS experiment*, *Phys. Rev. Lett.* **122** (2019) 231801, [1904.05105]. Cited on page 88.

[406] CMS collaboration, A. M. Sirunyan et al., *Search for invisible decays of a Higgs boson produced through vector boson fusion in proton-proton collisions at $\sqrt{s} = 13$ TeV*, *Phys. Lett. B* **793** (2019) 520–551, [1809.05937]. Cited on page 88.

[407] ALEPH, DELPHI, L3, OPAL, SLD, LEP Electroweak Working Group, SLD Electroweak Group, SLD Heavy

FLAVOUR GROUP collaboration, S. Schael et al., *Precision electroweak measurements on the Z resonance*, *Phys. Rept.* **427** (2006) 257–454, [hep-ex/0509008]. Cited on page 88.

[408] ATLAS collaboration, M. Aaboud et al., *Search for new high-mass phenomena in the dilepton final state using 36 fb?1 of proton-proton collision data at* $\sqrt{s} = 13$ *TeV with the ATLAS detector*, *JHEP* **10** (2017) 182, [1707.02424]. Cited on page 88, 97, 103, and 116.

[409] LHCb collaboration, R. Aaij et al., *Search for Dark Photons Produced in 13 TeV pp Collisions*, *Phys. Rev. Lett.* **120** (2018) 061801, [1710.02867]. Cited on page 88.

[410] R. M. Harris and K. Kousouris, *Searches for Dijet Resonances at Hadron Colliders*, *Int. J. Mod. Phys. A* **26** (2011) 5005–5055, [1110.5302]. Cited on page 88.

[411] ATLAS collaboration, M. Aaboud et al., *Search for new phenomena in dijet events using 37 fb*$^{-1}$ *of pp collision data collected at* $\sqrt{s}$ *=13 TeV with the ATLAS detector*, *Phys. Rev. D* **96** (2017) 052004, [1703.09127]. Cited on page 88.

[412] CMS collaboration, A. M. Sirunyan et al., *Search for dijet resonances in proton–proton collisions at* $\sqrt{s}$ *= 13 TeV and constraints on dark matter and other models*, *Phys. Lett. B* **769** (2017) 520–542, [1611.03568]. Cited on page 88.

[413] ATLAS collaboration, M. Aaboud et al., *Search for dark matter at* $\sqrt{s} = 13$ *TeV in final states containing an energetic photon and large missing transverse momentum with the ATLAS detector*, *Eur. Phys. J. C* **77** (2017) 393, [1704.03848]. Cited on page 88.

[414] CMS collaboration, A. M. Sirunyan et al., *Search for dark matter produced with an energetic jet or a hadronically decaying W or Z boson at* $\sqrt{s} = 13$ *TeV*, *JHEP* **07** (2017) 014, [1703.01651]. Cited on page 88.

[415] J. Maxwell, *A dynamical theory of the electromagnetic field*, *Phil. Trans. Roy. Soc. Lond.* **155** (1865) 459–512. Cited on page 89.

[416] T. Kaluza, *Zum Unitätsproblem der Physik*, *Sitzungsberichte der Königlich Preußischen Akademie der Wissenschaften (Berlin* (Jan., 1921) 966–972. Cited on page 89.

[417] E. Schrödinger, *An undulatory theory of the mechanics of atoms and molecules*, *Phys. Rev.* **28** (Dec, 1926) 1049–1070. Cited on page 90.

[418] O. Klein, *Quantentheorie und fünfdimensionale Relativitätstheorie*, *Zeitschrift fur Physik* **37** (Dec., 1926) 895–906. Cited on page 90.

[419] O. Klein, *The Atomicity of Electricity as a Quantum Theory Law*, *Nature* **118** (Oct., 1926) 516. Cited on page 90.

[420] A. Salam and J. Strathdee, *On Kaluza-Klein Theory*, *Annals Phys.* **141** (1982) 316–352. Cited on page 90.

[421] C. Wetterich, *Kaluza-klein cosmology and the inflationary universe*, *Nuclear Physics B* **252** (1985) 309 – 320. Cited on page 90.

[422] U. Danielsson, *Introduction to string theory*, *Reports on Progress in Physics* **64** (dec, 2000) 51–96. Cited on page 90.

[423] T. Appelquist, H.-C. Cheng and B. A. Dobrescu, *Bounds on universal extra dimensions*, *Phys. Rev. D* **64** (2001) 035002, [`hep-ph/0012100`]. Cited on page 90.

[424] M. T. Arun, D. Choudhury and D. Sachdeva, *Universal Extra Dimensions and the Graviton Portal to Dark Matter*, *JCAP* **10** (2017) 041, [`1703.04985`]. Cited on page 90.

[425] I. Antoniadis, *A Possible new dimension at a few TeV*, *Phys. Lett. B* **246** (1990) 377–384. Cited on page 90, and 92.

[426] I. Antoniadis, S. Dimopoulos and G. Dvali, *Millimeter range forces in superstring theories with weak scale compactification*, *Nucl. Phys. B* **516** (1998) 70–82, [`hep-ph/9710204`]. Cited on page 90, and 92.

[427] N. Arkani-Hamed, S. Dimopoulos and G. Dvali, *The Hierarchy problem and new dimensions at a millimeter*, *Phys. Lett. B* **429** (1998) 263–272, [`hep-ph/9803315`]. Cited on page 90, 92, and 324.

[428] I. Antoniadis, N. Arkani-Hamed, S. Dimopoulos and G. Dvali, *New dimensions at a millimeter to a Fermi and superstrings at a TeV*, *Phys. Lett. B* **436** (1998) 257–263, [hep-ph/9804398]. Cited on page 90, and 92.

[429] N. Arkani-Hamed, S. Dimopoulos and G. Dvali, *Phenomenology, astrophysics and cosmology of theories with submillimeter dimensions and TeV scale quantum gravity*, *Phys. Rev. D* **59** (1999) 086004, [hep-ph/9807344]. Cited on page 90, and 92.

[430] G. F. Giudice and M. McCullough, *A Clockwork Theory*, *JHEP* **02** (2017) 036, [1610.07962]. Cited on page 91, 99, 101, and 327.

[431] G. F. Giudice, Y. Kats, M. McCullough, R. Torre and A. Urbano, *Clockwork/linear dilaton: structure and phenomenology*, *JHEP* **06** (2018) 009, [1711.08437]. Cited on page 91, 99, 101, 114, 327, 338, and 339.

[432] C. Csaki, *TASI lectures on extra dimensions and branes*, in *Theoretical Advanced Study Institute in Elementary Particle Physics (TASI 2002): Particle Physics and Cosmology: The Quest for Physics Beyond the Standard Model(s)*, pp. 605–698, 4, 2004. hep-ph/0404096. Cited on page 91, and 94.

[433] G. D. Kribs, *TASI 2004 lectures on the phenomenology of extra dimensions*, in *Theoretical Advanced Study Institute in Elementary Particle Physics: Physics in $D \geqq 4$*, pp. 633–699, 5, 2006. hep-ph/0605325. Cited on page 91, and 94.

[434] H.-C. Cheng, *Introduction to Extra Dimensions*, in *Theoretical Advanced Study Institute in Elementary Particle Physics: Physics of the Large and the Small*, pp. 125–162, 2011. 1003.1162. DOI. Cited on page 91, and 94.

[435] S. Hannestad and G. G. Raffelt, *Supernova and neutron star limits on large extra dimensions reexamined*, *Phys. Rev. D* **67** (2003) 125008, [hep-ph/0304029]. Cited on page 94.

[436] D. Kapner, T. Cook, E. Adelberger, J. Gundlach, B. R. Heckel, C. Hoyle et al., *Tests of the gravitational inverse-square law below*

the dark-energy length scale, *Phys. Rev. Lett.* **98** (2007) 021101, [hep-ph/0611184]. Cited on page 94.

[437] G. F. Giudice, R. Rattazzi and J. D. Wells, *Quantum gravity and extra dimensions at high-energy colliders*, *Nucl. Phys. B* **544** (1999) 3–38, [hep-ph/9811291]. Cited on page 96.

[438] H. T. Davis and W. J. Kirkham, *A new table of the zeros of the bessel functions* $j_0(x)$ *and* $j_1(x)$ *with corresponding values of* $j_1(x)$ *and* $j_0(x)$, *Bull. Amer. Math. Soc.* **33** (11, 1927) 760–772. Cited on page 96.

[439] ATLAS collaboration, M. Aaboud et al., *Search for new phenomena in high-mass diphoton final states using 37 fb*$^{-1}$ *of proton–proton collisions collected at* $\sqrt{s} = 13$ *TeV with the ATLAS detector*, *Phys. Lett. B* **775** (2017) 105–125, [1707.04147]. Cited on page 97, 103, and 116.

[440] T. Appelquist and A. Chodos, *Quantum Effects in Kaluza-Klein Theories*, *Phys. Rev. Lett.* **50** (1983) 141. Cited on page 97.

[441] T. Appelquist and A. Chodos, *The Quantum Dynamics of Kaluza-Klein Theories*, *Phys. Rev. D* **28** (1983) 772. Cited on page 97.

[442] B. de Wit, M. Luscher and H. Nicolai, *The Supermembrane Is Unstable*, *Nucl. Phys. B* **320** (1989) 135–159. Cited on page 97.

[443] E. Ponton and E. Poppitz, *Casimir energy and radius stabilization in five-dimensional orbifolds and six-dimensional orbifolds*, *JHEP* **06** (2001) 019, [hep-ph/0105021]. Cited on page 97.

[444] W. D. Goldberger and M. B. Wise, *Bulk fields in the Randall-Sundrum compactification scenario*, *Phys. Rev. D* **60** (1999) 107505, [hep-ph/9907218]. Cited on page 97, and 327.

[445] W. D. Goldberger and M. B. Wise, *Modulus stabilization with bulk fields*, *Phys. Rev. Lett.* **83** (1999) 4922–4925, [hep-ph/9907447]. Cited on page 97, and 327.

[446] W. D. Goldberger and M. B. Wise, *Phenomenology of a stabilized modulus*, *Phys. Lett. B* **475** (2000) 275–279, [hep-ph/9911457]. Cited on page 98, and 113.

[447] J. M. Maldacena, *The Large N limit of superconformal field theories and supergravity*, *Int. J. Theor. Phys.* **38** (1999) 1113–1133, [hep-th/9711200]. Cited on page 98.

[448] S. Gubser, I. R. Klebanov and A. M. Polyakov, *Gauge theory correlators from noncritical string theory*, *Phys. Lett. B* **428** (1998) 105–114, [hep-th/9802109]. Cited on page 98.

[449] E. Witten, *Anti-de Sitter space and holography*, *Adv. Theor. Math. Phys.* **2** (1998) 253–291, [hep-th/9802150]. Cited on page 98.

[450] S. J. Brodsky and G. F. de Teramond, *AdS/CFT and Light-Front QCD*, *Subnucl. Ser.* **45** (2009) 139–183, [0802.0514]. Cited on page 99.

[451] S. S. Gubser, *AdS / CFT and gravity*, *Phys. Rev. D* **63** (2001) 084017, [hep-th/9912001]. Cited on page 99.

[452] S. B. Giddings, E. Katz and L. Randall, *Linearized gravity in brane backgrounds*, *JHEP* **03** (2000) 023, [hep-th/0002091]. Cited on page 99.

[453] S. B. Giddings and E. Katz, *Effective theories and black hole production in warped compactifications*, *J. Math. Phys.* **42** (2001) 3082–3102, [hep-th/0009176]. Cited on page 99.

[454] H. L. Verlinde, *Holography and compactification*, *Nucl. Phys. B* **580** (2000) 264–274, [hep-th/9906182]. Cited on page 99.

[455] M. Duff and J. T. Liu, *Complementarity of the Maldacena and Randall-Sundrum pictures*, *Class. Quant. Grav.* **18** (2001) 3207–3214, [hep-th/0003237]. Cited on page 99.

[456] N. Arkani-Hamed, M. Porrati and L. Randall, *Holography and phenomenology*, *JHEP* **08** (2001) 017, [hep-th/0012148]. Cited on page 99.

[457] R. Rattazzi and A. Zaffaroni, *Comments on the holographic picture of the Randall-Sundrum model*, *JHEP* **04** (2001) 021, [hep-th/0012248]. Cited on page 99.

[458] T. Gherghetta, *A Holographic View of Beyond the Standard Model Physics*, in *Theoretical Advanced Study Institute in Elementary Particle Physics: Physics of the Large and the Small*, pp. 165–232, 2011. 1008.2570. DOI. Cited on page 99.

[459] I. Antoniadis, A. Arvanitaki, S. Dimopoulos and A. Giveon, *Phenomenology of TeV Little String Theory from Holography*, *Phys. Rev. Lett.* **108** (2012) 081602, [1102.4043]. Cited on page 100.

[460] M. Baryakhtar, *Graviton Phenomenology of Linear Dilaton Geometries*, *Phys. Rev. D* **85** (2012) 125019, [1202.6674]. Cited on page 100.

[461] P. Cox and T. Gherghetta, *Radion Dynamics and Phenomenology in the Linear Dilaton Model*, *JHEP* **05** (2012) 149, [1203.5870]. Cited on page 100.

[462] E. Adelberger, J. Gundlach, B. Heckel, S. Hoedl and S. Schlamminger, *Torsion balance experiments: A low-energy frontier of particle physics*, *Prog. Part. Nucl. Phys.* **62** (2009) 102–134. Cited on page 101.

[463] CMS collaboration, A. M. Sirunyan et al., *Search for physics beyond the standard model in high-mass diphoton events from proton-proton collisions at $\sqrt{s} = 13$ TeV*, *Phys. Rev. D* **98** (2018) 092001, [1809.00327]. Cited on page 103.

[464] A. Donini, P. Hernandez, J. Lopez-Pavon and M. Maltoni, *Minimal models with light sterile neutrinos*, *JHEP* **07** (2011) 105, [1106.0064]. Cited on page 106.

[465] S. Dodelson and L. M. Widrow, *Sterile-neutrinos as dark matter*, *Phys. Rev. Lett.* **72** (1994) 17–20, [hep-ph/9303287]. Cited on page 106, and 330.

[466] M. Escudero, N. Rius and V. Sanz, *Sterile neutrino portal to Dark Matter I: The $U(1)_{B-L}$ case*, *JHEP* **02** (2017) 045, [1606.01258]. Cited on page 106, and 330.

[467] V. Gonzalez Macias and J. Wudka, *Effective theories for Dark Matter interactions and the neutrino portal paradigm*, *JHEP* **07** (2015) 161, [1506.03825]. Cited on page 106, and 330.

[468] M. Escudero, N. Rius and V. Sanz, *Sterile Neutrino portal to Dark Matter II: Exact Dark symmetry*, *Eur. Phys. J. C* **77** (2017) 397, [1607.02373]. Cited on page 106, and 330.

[469] Y.-L. Tang and S.-h. Zhu, *Dark matter annihilation into right-handed neutrinos and the galactic center gamma-ray excess*, *JHEP* **03** (2016) 043, [1512.02899]. Cited on page 106.

[470] B. Batell, T. Han and B. Shams Es Haghi, *Indirect Detection of Neutrino Portal Dark Matter*, *Phys. Rev. D* **97** (2018) 095020, [1704.08708]. Cited on page 106.

[471] M. D. Campos, F. S. Queiroz, C. E. Yaguna and C. Weniger, *Search for right-handed neutrinos from dark matter annihilation with gamma-rays*, *JCAP* **07** (2017) 016, [1702.06145]. Cited on page 106.

[472] J. Márquez-Hernández, *Radion contribution to gravity-mediated dark matter in Clockwork/linear dilaton extra dimensions out of the rigid limit*, . Cited on page 113.

[473] A. D. Sakharov, *Vacuum quantum fluctuations in curved space and the theory of gravitation*, *Soviet Physics Uspekhi* **34** (may, 1991) 394–394. Cited on page 313.

[474] G. B. Gelmini, *El boson de higgs*, 2014. Cited on page 316.

Part II

Scientific Research

Journal of Cosmology and Astroparticle Physics
An IOP and SISSA journal

Probing the sterile neutrino portal to Dark Matter with γ rays

Miguel G. Folgado,[a] **Germán A. Gómez-Vargas,**[b] **Nuria Rius**[a] **and Roberto Ruiz de Austri**[a]

[a]Departamento de Física Teórica and IFIC, Universidad de Valencia-CSIC, C/ Catedrático José Beltrán, 2, E-46980 Paterna, Spain

[b]Instituto de Astrofísica, Pontificia Universidad Católica de Chile, Avda. Vicuña Mackenna 4860, Santiago, Chile

E-mail: migarfol@ific.uv.es, gggomezv@uc.cl, nuria.rius@ific.uv.es, rruiz@ific.uv.es

Received April 4, 2018
Accepted July 17, 2018
Published August 1, 2018

Abstract. Sterile neutrinos could provide a link between the Standard Model particles and a dark sector, besides generating active neutrino masses via the seesaw mechanism type I. We show that, if dark matter annihilation into sterile neutrinos determines its observed relic abundance, it is possible to explain the Galactic Center γ-ray excess reported by the Fermi-LAT Collaboration as due to an astrophysical component plus dark matter annihilations. We observe that sterile neutrino portal to dark matter provides an impressively good fit, with a p-value of 0.78 in the best fit point, to the Galactic Center γ-ray flux, for DM masses in the range (40-80) GeV and sterile neutrino masses $20\,\mathrm{GeV} \lesssim M_N < M_{\mathrm{DM}}$. Such values are compatible with the limits from Fermi-LAT observations of the dwarfs spheroidal galaxies in the Milky Way halo, which rule out dark matter masses below $\sim 50\,\mathrm{GeV}$ ($90\,\mathrm{GeV}$), for sterile neutrino masses $M_N \lesssim M_{\mathrm{DM}}$ ($M_N \ll M_{\mathrm{DM}}$). We also estimate the impact of AMS-02 anti-proton data on this scenario.

Keywords: dark matter theory, particle physics - cosmology connection, neutrino theory

ArXiv ePrint: 1803.08934

https://doi.org/10.1088/1475-7516/2018/08/002

JCAP08(2018)002

Contents

1 Introduction

Dark matter (DM) and neutrino masses constitute indubitable observational evidence for physics beyond the Standard Model (SM) of fundamental interactions. Thus, the existence of a connection between the new degrees of freedom needed to account for both observations is an exciting possibility to explore. In particular, if DM is a thermal relic of the early Universe and the *seesaw mechanism* is realized to generate neutrino masses, new massive particles are required to solve both problems. The most economical scenario, namely that the sterile neutrinos constitute the DM [1], has been thoroughly studied [2]. Hence we consider in this work a different case: The sterile neutrino portal to DM. In this scenario DM is an SM singlet state that interacts mainly with sterile neutrinos, being such interactions of the right strength to produce the observed DM relic abundance [3–5].

DM interactions with SM particles are very weak to avoid collider and direct detection constraints, although they must reproduce the correct abundance of DM thermally through its annihilation into sterile neutrinos which eventually decay into SM particles. This decay is due to Yukawa couplings of sterile neutrino and leptons which also generate a Majorana mass for the light neutrinos via the type I seesaw mechanism. In general, if DM s-wave interactions dominate the annihilation process, we expect to have indirect detection signals, searches for these signals lead to the most stringent bounds on this scenario [5].

A comprehensive analysis of indirect detection hunts within the sterile neutrino portal to DM has been presented in [6], including constraints from Planck CMB measurements, γ-ray flux collected by the Fermi Large Area Telescope (LAT), and AMS-02 antiproton observations. Indirect signals from solar DM annihilation to long-lived sterile neutrinos have been analyzed in [7]. The primary target for neutral DM annihilation products is the Galactic Center, as we expect there the largest DM concentration in the nearby cosmos. Interestingly, an unexpected signal detected in the gamma-ray data collected by the Fermi LAT from the inner Galaxy, the so-called Galactic Center Excess (GCE). It has created a great excitement because its spectral energy distribution and morphology are consistent with predictions from DM annihilation[8–17]. All those works devoted to analyzing the GCE confirm that its properties strongly depends on the analysis method used to subtract it from the Fermi-LAT data. The variation in the GCE properties with the analysis causes modifications in the models able to explain it. The work in [18] shows that it is possible to account for the GCE obtained in [15] by DM annihilation into sterile neutrinos. In [6] the compatibility of the GCE DM interpretation with the other indirect searches is discussed. The dwarf spheroidal galaxies (dSphs) are pristine targets for DM signals because they lack detectable gamma-ray sources. The authors of [19] use the Fermi-LAT gamma-ray data from dSphs to set limits on DM annihilations into sterile neutrinos.

In this paper we consider a new Fermi-LAT analysis of Pass 8 data on Galactic Center γ-rays presented in [20], and we explore the ability of the DM sterile neutrino portal to account for the GCE, which is peaked at ~ 3 GeV, that is, slightly higher energies than reported in previous analysis. We also derive the limits from dSphs. Although we use a particular realization of the sterile neutrino portal DM, the results of our analysis can be applied to other models, provided the sterile neutrino decays only to SM particles.

The paper is organized as follows. In Sec. 2 we briefly review the sterile neutrino portal scenario, and derive the SM particle spectra from sterile neutrino decays, relevant for the indirect detection constraints on such portal. In Sec. 3 we describe the model independent fit to the GCE, while in Sec. 4 we present the limits from Fermi-LAT dSphs and AMS-02 anti-proton data. We conclude in Sec. 5.

2 Sterile neutrino portal to Dark Matter

Our analysis can be applied to any type of sterile neutrino portal scenario up to the following requirement: The observed DM relic abundance is determined by its interactions with sterile neutrinos, which in turn generate light neutrino masses via the type I seesaw mechanism. For definiteness in this section we consider a very simple realization studied in [5]. Besides the sterile neutrinos, the SM is extended by a dark sector that contains a scalar field ϕ and a fermion Ψ. These fields are both singlets of the SM gauge group but charged under a dark sector symmetry group, G_{dark}, such that the combination $\overline{\Psi}\phi$ is a singlet of this hidden symmetry.

The lighter of the two dark particles (ϕ and Ψ) turns out to be stable if all SM particles, as well as the sterile neutrinos, are singlets of G_{dark}, disregarding the nature of the dark group. The stable particle is a good DM candidate. We assume for simplicity that the dark symmetry G_{dark} is a global symmetry at low energies, although our analysis is equally valid whether it is local.

The relevant terms of the Lagrangian are:

$$\begin{aligned}\mathcal{L} = {} & \mu_H^2 H^\dagger H - \lambda_H (H^\dagger H)^2 - \mu_\phi^2 \phi^\dagger \phi - \lambda_\phi (\phi^\dagger \phi)^2 - \lambda_{H\phi} (H^\dagger H)\,(\phi^\dagger \phi) \\ & - \big(\phi \overline{\Psi} (\lambda_a + \lambda_p \gamma_5) N + Y \overline{L}_L H N_R + \text{h.c.}\big) \end{aligned} \tag{2.1}$$

where we have omitted flavour indexes. The Yukawa couplings Y between the right-handed fermions N_R and the SM leptons lead to masses for the active neutrinos after electroweak symmetry breaking, via type I seesaw mechanism. Although at least two sterile neutrinos are required to generate the neutrino masses observed in oscillations, in our analysis we consider that only one species is lighter than the DM and therefore relevant for the determination of its relic abundance and indirect searches. The results can be easily extended to the case of two or more sterile neutrinos lighter than the DM.

Assuming that the dark fermion Ψ is Majorana and constitutes the DM, its annihilation cross section into sterile neutrinos is given by [1]

$$\sigma v = \frac{(\alpha + \beta\, r_{N\Psi})^2}{4\pi M_\Psi^2} \frac{\sqrt{1 - r_{N\Psi}^2}}{(1 + r_\phi^2 - r_{N\Psi}^2)^2} + \mathcal{O}(v^2) \tag{2.2}$$

where $\alpha = \lambda_s^2 - \lambda_p^2$ and $\beta = \lambda_s^2 + \lambda_p^2$, $r_\phi = M_\phi/M_\Psi$, and $r_{N\Psi} = M_N/M_\Psi$ and v is the relative velocity of the DM particles. In the following, we restrict ourselves to a scalar interaction between the dark fermion and the $N's$, but from eq. (2.2) it is clear that a pseudoscalar coupling $\lambda_p\gamma_5$ leads to the same results. Only a chiral interaction gives rise to reduced indirect detection signals, since for $M_N \ll M_\Psi$ the annihilation cross section is effectively p-wave, and therefore velocity suppressed.

In the scenario presented above it is always possible to obtain the observed DM relic abundance when $M_N < M_\Psi$ in the range $M_\Psi \in$ [1 GeV, 2 TeV] with perturbative couplings $\lambda_s \equiv \lambda \sim 0.01$ - 1 and mediator masses $M_\phi \in$ [1 GeV, 10 TeV] [5]. It is worth noticing that for sufficiently small Yukawa couplings of the sterile neutrinos, it could happen that the DM Ψ and N bath decouple from the SM after the decay of the dark scalar, $T \lesssim M_\phi$, and remain in thermal equilibrium but with a different temperature. In this case, the DM freeze-out leads to a larger relic abundance, so that a larger annihilation cross section (and thus a larger coupling between DM and sterile neutrinos) is needed to reproduce the observed value [21, 22]. In Sec. 4 we will see that the Fermi-LAT data from dSphs can set stringent constraints on these scenarios.

If the scalar ϕ were the DM instead, the corresponding annihilation cross section is very similar to eq.(2.2), including the fact that it becomes velocity suppressed for $M_N \ll M_\phi$ if the DM couplings are chiral. In [5] it has been shown that for scalar DM it is also possible to get the correct relic abundance in a comparable region of the parameter space, therefore our analysis applies to such scenario as well.

The indirect detection signatures depend on the thermally averaged total annihilation cross section, $\langle\sigma v\rangle$ (for a detailed calculation of the thermal average see for instance ref.[23]), and on the energy spectrum of the final SM particles, which is determined by M_Ψ and M_N. Moreover, given a pair of values (M_Ψ, M_N), it is always possible to obtain a certain value of the cross section by appropriately choosing the other two free variables, λ, M_ϕ, with the only limitation of the coupling λ to remain perturbative. Therefore, in the next sections we will consider as free parameters $(\langle\sigma v\rangle, M_\Psi, M_N)$; in this way, our analysis is valid for any other neutrino portal scenario able to reproduce the same annihilation cross section, provided the sterile neutrinos decay only to SM particles.

Light neutrino masses are generated via TeV scale type I seesaw mechanism. We denote ν_α the active neutrinos and N_s the sterile ones. After electroweak symmetry breaking, the neutrino mass matrix in the basis (ν_α, N_s) is given by

$$\mathcal{M}_\nu = \begin{pmatrix} 0 & M_D \\ M_D^T & M_N \end{pmatrix} \tag{2.3}$$

where $M_D = Y v_H/\sqrt{2}$ and $Y_{\alpha s}$ are the Yukawa couplings. The matrix $\mathcal{M}_\nu$ can be diagonalized by a unitary matrix U, so that

$$\mathcal{M}_\nu = U^*\, Diag(M_\nu, M)\, U^\dagger \tag{2.4}$$

[1]Were Ψ a Dirac fermion, the exchange $\alpha \leftrightarrow \beta$ should be performed in eq.(2.2).

where M_ν is the diagonal matrix with the three lightest eigenvalues of $\mathcal{M}_\nu$, of order M_D^2/M_N, and M contains the heavier ones, of order M_N.

The mass eigenstates $\mathbf{n} = (\nu_i, N_h)$ are related to the active and sterile neutrinos, (ν_α, N_s), by

$$\begin{pmatrix} \nu_\alpha \\ N_s \end{pmatrix}_L = U^* \begin{pmatrix} \nu_i \\ N_h \end{pmatrix}_L \ . \tag{2.5}$$

The unitary matrix U can be written as

$$U = \begin{pmatrix} U_{\alpha i} & U_{\alpha h} \\ U_{si} & U_{sh} \end{pmatrix} \tag{2.6}$$

where, at leading order in the seesaw expansion parameter, $\mathcal{O}(M_D/M_N)$:

$$\begin{aligned} U_{\alpha i} &= [U_{PMNS}]_{\alpha i} \qquad U_{sh} = I \\ U_{\alpha h} &= [M_D M_N^{-1}]^*_{\alpha h} \\ U_{si} &= -[M_N^{-1} M_D^T U_{PMNS}]_{si} \ . \end{aligned} \tag{2.7}$$

Notice that at this order the states N_h and N_s coincide, therefore we identify them in the rest of this paper.

Sterile neutrinos are produced in DM annihilations and then decay into SM particles. The decay channels depend on the sterile neutrino mass. Namely if the right-handed neutrino is lighter than the W boson, N will decay through off-shell h, Z, W bosons to three fermions. Since the decay via a virtual h is further suppressed by the small Yukawa couplings of the SM fermions, it is a very good approximation to consider only the processes mediated by virtual W, Z, whose partial widths read [24]:

$$\Gamma(N \to \nu q \bar{q}) = 3\, A C_{NN} [2(a_u^2 + b_u^2) + 3(a_d^2 + b_d^2)] f(z) \tag{2.8}$$

$$\Gamma(N \to 3\nu) = A C_{NN} [\tfrac{3}{4} f(z) + \tfrac{1}{4} g(z,z)] \tag{2.9}$$

$$\Gamma(N \to \ell q \bar{q}) = 6\, A C_{NN} f(w,0) \tag{2.10}$$

$$\Gamma(N \to \nu \ell \bar{\ell}) = A C_{NN} [3(a_e^2 + b_e^2) f(z) + 3 f(w) - 2 a_e g(z,w)] \tag{2.11}$$

where

$$A \equiv \frac{G_F^2 M_N^5}{192\, \pi^3} \ , C_{ij} = \sum_{\alpha=1}^{3} U_{\alpha i} U^*_{\alpha j} \tag{2.12}$$

a_f, b_f are the left and right neutral current couplings of the fermions ($f = q, \ell$), the variables z, w are given by

$$z = (M_N/M_Z)^2 \ , \qquad w = (M_N/M_W)^2 \tag{2.13}$$

and the functions $f(z), f(w,0)$ and $g(z,w)$ can be found in [25].

On the other hand, if $M_N > M_W$ two body decays to SM particles are open, and the corresponding widths are [26]:

$$\Gamma(N \to W^\pm \ell_\alpha^\mp) = \frac{g^2}{64\pi} |U_{\alpha N}|^2 \frac{M_N^3}{M_W^2} \left(1 - \frac{M_W^2}{M_N^2}\right)^2 \left(1 + \frac{2M_W^2}{M_N^2}\right) \tag{2.14}$$

$$\Gamma(N \to Z\, \nu_\alpha) = \frac{g^2}{64\pi c_W^2} |C_{\alpha N}|^2 \frac{M_N^3}{M_Z^2} \left(1 - \frac{M_Z^2}{M_N^2}\right)^2 \left(1 + \frac{2M_Z^2}{M_N^2}\right) \tag{2.15}$$

$$\Gamma(N \to h\, \nu_\alpha) = \frac{g^2}{64\pi} |C_{\alpha N}|^2 \frac{M_N^3}{M_W^2} \left(1 - \frac{M_h^2}{M_N^2}\right)^2 \ . \tag{2.16}$$

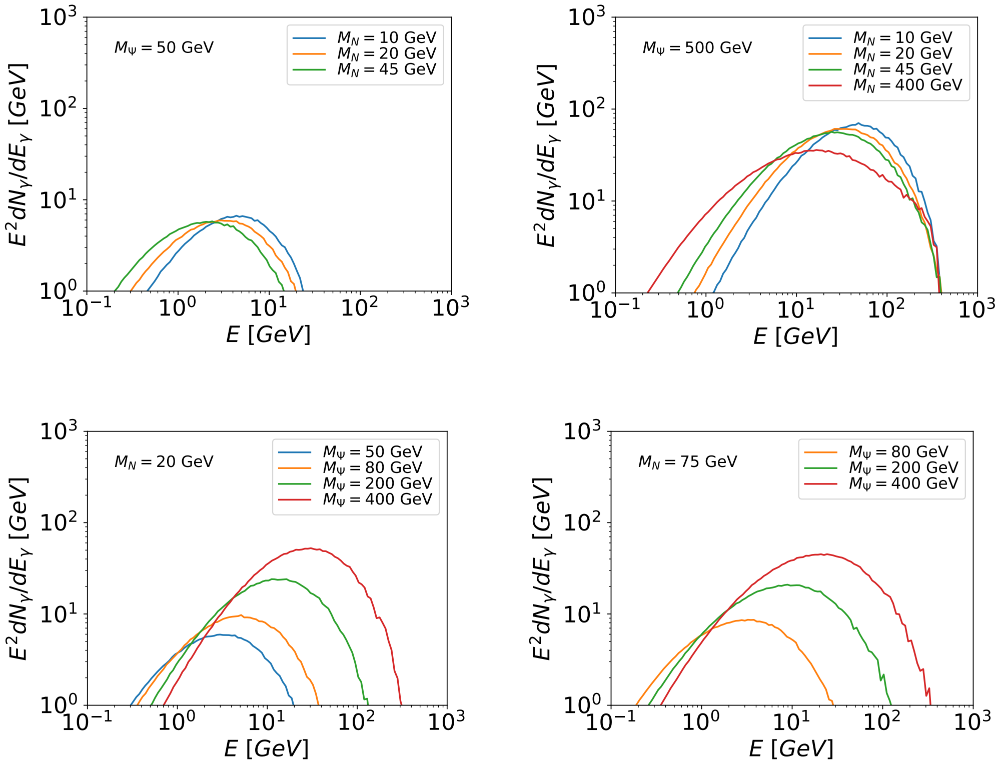

Figure 1. Photon spectrum different DM and sterile neutrino masses. In the upper figures we fix the DM mass and in the lower figures the sterile neutrino one. Low DM masses ($\lesssim$ 80 GeV) can fit the Galactic center excess.

To obtain the final state's SM particle spectrum from DM annihilation into sterile neutrinos, dN/dE, we have used *SPheno v.3.3.8* [27] to determine the decay rates of all the particles, implementing first the model, at the Lagrangian level, using *SARAH v.4.9.1* [28, 29]. Then, we simulate the DM to sterile neutrino annihilation with *MadGraph5 v.2.5* [30], and we use *Pythia v.8.2* [31] to compute the sterile neutrino decays and its parton shower. Our analysis differs from ref.[6] in that they simulate the decay of sterile neutrino to SM particles in the N-rest frame using *SM_HeavyN_NLO* model files [32, 33] and boost the final spectrum to the DM rest frame. We have checked that both methods predict similar photon and anti-particle spectra.

In Fig.1 it is depicted the photon spectrum that we obtain for different DM and N masses: in the upper plots we show the dependence on the sterile neutrino mass for two fixed values of the DM mass, namely $M_{DM} = 50$ GeV, which as we will see in the next section can fit the GCE, and $M_{DM} = 500$ GeV, which do not. We observe that for a given DM mass, the photon spectrum is harder for lighter sterile neutrino.

The reason for this behavior, also observable in the anti-particle spectra, is the boost between the sterile neutrino and DM rest frames, which becomes larger for $M_N \ll M_{DM}$. For instance, an isotropic spectrum with fixed energy E in the sterile neutrino rest frame becomes a box shaped spectrum when boosted to the DM rest frame, of the form [34]

$$\frac{dN}{dE'} = \frac{1}{2\gamma\beta\sqrt{E^2 - m^2}}\,\theta(E' - E_-)\theta(E_+ - E') \tag{2.17}$$

where $E_\pm = \gamma(E \pm \beta\sqrt{E^2 - m^2})$, θ is the Heaviside step function, γ and β are the boost parameters, with $\gamma = m_{DM}/m_N$, and $m = 0$ for the case of photons As a consequence, the more boosted the sterile neutrino, the harder the final spectrum.

In the lower plots the sterile neutrino mass is fixed, and in this case the spectrum is harder for heavier DM mass, as we expected.

In our calculation we have taken only the Yukawa coupling of the sterile neutrino to the first generation of SM leptons non-zero. We have checked that the photon spectrum has little sensitivity to this choice of flavour, in agreement with ref. [19]; thus the photon spectrum from DM annihilation do not provide insight into disentangling the structure of the sterile neutrino Yukawa couplings.

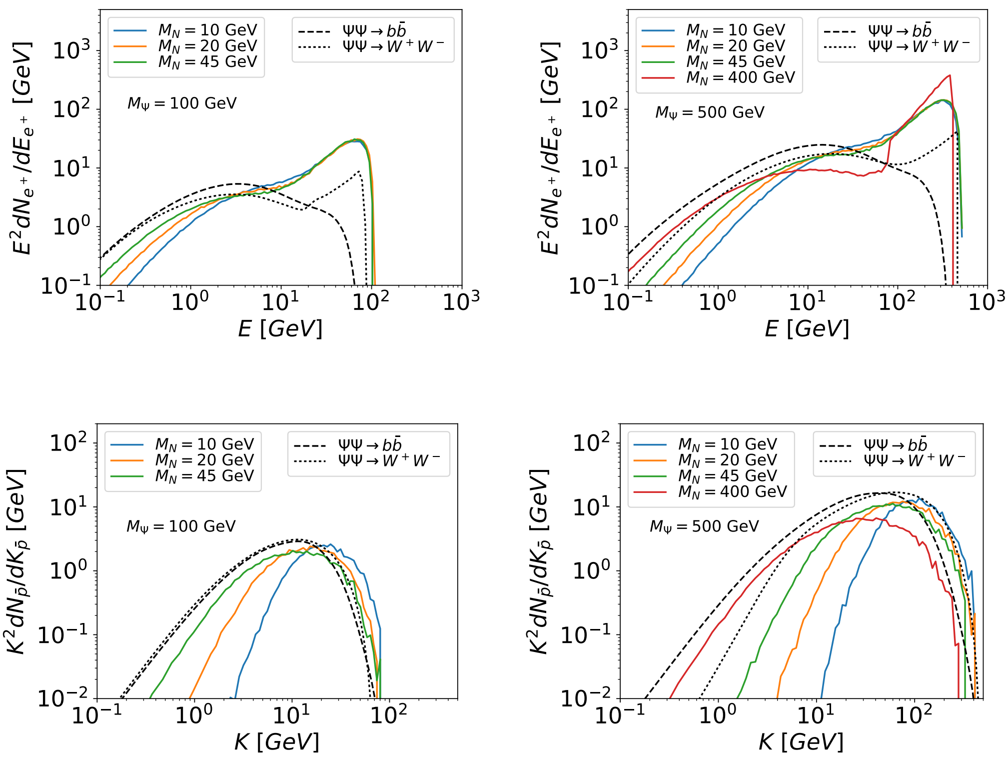

Figure 2. Positron and antiproton spectrum for different DM and sterile neutrino masses compared with a simple case of a DM candidate that annihilates directly to $b\bar{b}$ and W^+W^-.

We have calculated the positron and anti-proton spectra from DM annihilation into sterile neutrinos and its subsequent cascade decay, shown in Fig. 2. While we find that also the anti-proton spectrum is largely insensitive to the flavour structure of the Yukawa couplings, the peak in the electron spectrum at high energies is only present if the sterile neutrino couples to the (e, ν_e) doublet, due to a strong component of the reaction $N \to We$ which occurs only in this case.

In this work we focus on the γ-ray probe for several reasons. First of all, we have found that the positron flux generated in the DM sterile neutrino portal can not account for the positron flux observed, for instance, by PAMELA [35] and AMS-02 [36, 37]. We have used the approximation described in [38] to propagate the positrons and electrons, and obtain the corresponding flux at Earth position. Although the approximation is not very accurate, it is good enough to show that this scenario predicts a positron flux about two orders of magnitude smaller than the measured one, for any value of the DM and N masses; therefore it can not explain the positron excess.

On the other hand, regarding anti-protons, recent analyses of AMS-02 [39] data seem to find an excess over the expected background; however a careful study would require a complete fit of both the cosmic ray propagation and DM parameters, which is beyond the scope of this work. Nevertheless, as an illustration we plot in Fig. 2 the anti-proton spectra for several values of the DM and N masses, together with the spectra corresponding to DM annihilation into WW and $b\bar{b}$ for comparison. In Sec.4 we will also estimate which part of the parameter space could be excluded by AMS-02 anti-proton data.

Finally, light neutrinos are also produced in DM annihilation, and IceCUBE can set constraints on the cross section to neutrinos, but current limits are about three orders of magnitude above the flux predicted within the sterile neutrino portal scenario [4].

Note that one can also constrain the sterile neutrino portal using the CMB anisotropy measurements, which are sensitive to DM annihilation during the cosmic dark ages. Specially if the annihilation products contain energetic electrons and photons, when these particles are injected into the plasma will modify the ionization history, leading to observable changes in the temperature and polarization anisotropies. These constraints have been estimated in [5], and explicitly calculated in [6], and they exclude DM masses below ~ 20 GeV, irrespective of the value of M_N. Therefore, such CMB bounds are weaker than the ones from Fermi-LAT dSphs that we discuss in Sec. 4.

3 Analysis of the Galactic Center gamma-ray Excess within the sterile neutrino portal

The Fermi-LAT has boosted significant advances in our knowledge of the gamma-ray sky over the last few years. Regarding DM properties, if it is a weakly interacting particle (WIMP) we expect that its annihilation in dense regions of the Universe, such as the our Galactic Center or the DM rich dSphs, will produce a significant flux of SM particles. High energy gamma rays are particularly interesting, since the signal can be traced back to the source, providing information about the location of the DM reaction. Several studies of the Fermi-LAT data show that the Galactic center is brighter than predicted by conventional models of interstellar diffuse γ-ray emission [8–17, 40, 41], tuned with Galactic plane data and point source catalogs. In a recent analysis by the Fermi-LAT collaboration [20], it has been found that the GCE is a sub-dominant component (10%) of the observed flux, with a spectral energy distribution peaked at about 3 GeV, slightly shifted towards higher energies than in previous studies. We consider the GCE obtained in the so-called Sample Model of ref. [20], and perform the fits using the covariance matrices derived in [42].

Notice however that the origin of the GCE is still unclear: in addition to the DM explanation, it could be due to the emission of a population of unresolved point sources [43–47], or cosmic-ray particles injected in the Galactic center region, interacting with the gas or radiation fields [48]. In fact, the excess could have different origins below and above ~ 10 GeV [20, 49]: the high energy tail may be due to the extension of the Fermi bubbles observed at higher latitudes, while the lower energy (< 10 GeV) excess might be produced by DM annihilation, unresolved millisecond pulsars, or both. In conclusion, the interpretation of the GCE as a signal of DM annihilation is not robust, but it can not be ruled out either [20, 47].

In general, the interpretation of the low energy GCE as originated by DM annihilation is not easy to reconcile with DM direct detection constraints, since in particular models the region able to reproduce the excess is already excluded by current experiments: for instance in the context of the minimal supersymmetric standard model, DM can only account for a ~ 40 % of the low energy ($E < 10$ GeV) GCE [42]. In our sterile neutrino portal scenario direct detection limits can be easily avoided, provided the mixing angle between the SM Higgs and the dark scalar is small enough; since the relic abundance is determined by the DM annihilation into sterile neutrinos, it is possible to obtain the correct one independently of such mixing. In fact, for this reason DM indirect searches are the most promising way to constrain this scenario. See also [50], where an extended scalar-singlet Higgs portal model is shown to provide an excellent fit to the GC excess, evading strong direct detection constraints by adding a second (heavier) singlet scalar in the dark sector.

In our analysis we assume that there are two distinct sources for the GCE: one astrophysical, responsible for the high energy tail of the γ-ray spectrum, and DM annihilation, that we considerer the only source of the low energy GCE,

$$\Phi = \Phi_{astro} + \Phi_{DM} \ . \tag{3.1}$$

For the astrophysical component, according to the morphological studies of [20] it seems reasonable to consider a continuation to lower Galactic latitudes of the Fermi bubbles. Given that above 10^o in Galactic latitude the spectral shape of the Fermi bubbles is described by a power low times an exponential cut off [51], we assume the same form for the astrophysical contribution to the GCE,

$$\Phi_{astro} = N E^{-\alpha} e^{-E/E_{cut}} \tag{3.2}$$

We leave N, α, E_{cut} as free parameters in the fit, in order to compare with the values $\alpha = 1.9 \pm 0.2$ and cutoff energy $E_{cut} = 110 \pm 50$ GeV from the Fermi bubbles, according to the results of ref. [51].

For the DM component, the differential flux of photons from a window with size $\Delta\Omega$, is given by [52]

$$\frac{d\Phi_\gamma}{dE_\gamma}(E_\gamma) = \frac{J}{8\pi M_{DM}^2} \sum_f \langle \sigma v \rangle_f \frac{dN_\gamma^f}{dE_\gamma}(E_\gamma) \ , \tag{3.3}$$

where the J-factor is an astrophysical factor that only depends of the angle of the window size and the DM density profile:

$$J = \int_{\Delta\Omega} d\Omega \int \rho_{DM}^2(s) ds \tag{3.4}$$

The J-factor is an integral of the DM profile over the line of sight. It is very common to adopt the Navarro, Frenk and White (NFW) profile [53]. In our case this is the best option because we want to compare our results with the Fermi-LAT data of the GCE and the dSphs, and this is the profile used by the Fermi-LAT Collaboration. The functional form of the NFW profile is:

$$\rho_\Psi(r) = \rho_s \left(\frac{r}{r_s}\right)^{-\gamma} \left(1 + \frac{r}{r_s}\right)^{-3+\gamma} , \tag{3.5}$$

where $r_s = 20\ kpc$ is the scale radius and ρ_s is the scale density, which is fixed using data at the location of the Sun: at $r_\odot = 8.5\ Kpc$, the DM density is $\rho_\odot = 0.3\ GeV/cm^3$. We take the central value of γ as determined in [20], $\gamma = 1.25 \pm 0.8$.

In Fig.3 we can see different examples of the photon flux, for the same DM and N masses as in Fig.1 and thermal annihilation cross section, $\langle\sigma v\rangle = 2.2 \times 10^{-26}\ cm^3/s$.

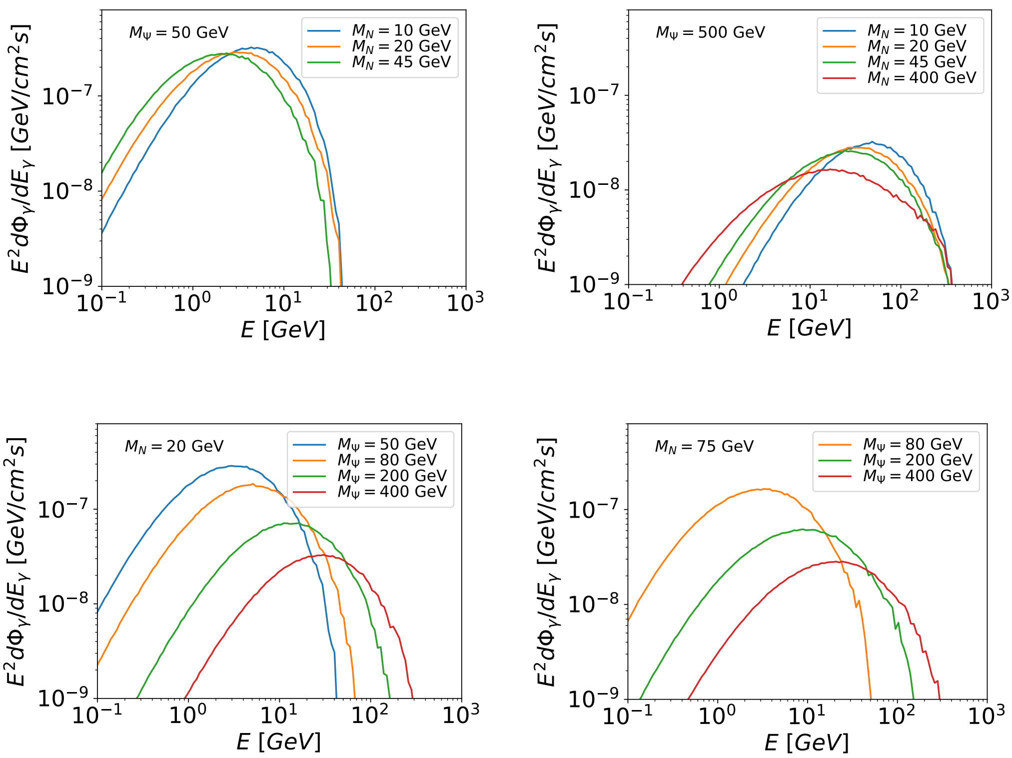

Figure 3. Photon flux for the same points of the parameter space that we chose in figure 1.

We perform a seven parameters fit: N, α, E_{cut} for the astrophysical flux and J, $\langle\sigma v\rangle$, M_Ψ, M_N for the DM contribution. The quality of the fit is evaluated by constructing the χ^2 estimator:

$$\chi^2 = \sum_{i,j} (\Phi_i^{obs} - \Phi_i^m) \Sigma_{i,j}^{-1} (\Phi_j^{obs} - \Phi_j^m) , \tag{3.6}$$

where i is the energy bin label, Φ_i^m is the predicted flux for a model, determined by the six free parameters, Φ_i^{obs} is the flux in the Sample model (light blue points of Fig.5) and $\Sigma_{i,j}^{-1}$ is the inverse of the covariance matrix, calculated in [42]. Thus the derived information on the GCE spectrum in [20] is contained in $\Phi_i^{obs}, \Sigma_{i,j}^{-1}$.

Notice that since the functions used to fit the GCE are not linear, one can not use the reduced χ^2 to calculate p-values. Instead we perform the following procedure [42]:

1. For each point of the DM model, $(\langle\sigma v\rangle, M_\Psi, M_N)$, we vary the astrophysical parameters N, α, E_{cut}, as well as the J-factor to account for its uncertainties [2],so as to find the best fit to the data, Φ_{best}^m.

2. We create a set of 100.000 pseudo-random data normal distributed with mean at Φ_{best}^m, according to $\Sigma_{i,j}^{-1}$.

3. We compute χ^2 between Φ_{best}^m and each of the 100.000 pseudo-random data created in 2.

4. We create a χ^2 distribution using the values from 3.

5. The integrated χ^2 distribution up to the best-fit-χ^2 to the actual data gives the p-value of the model.

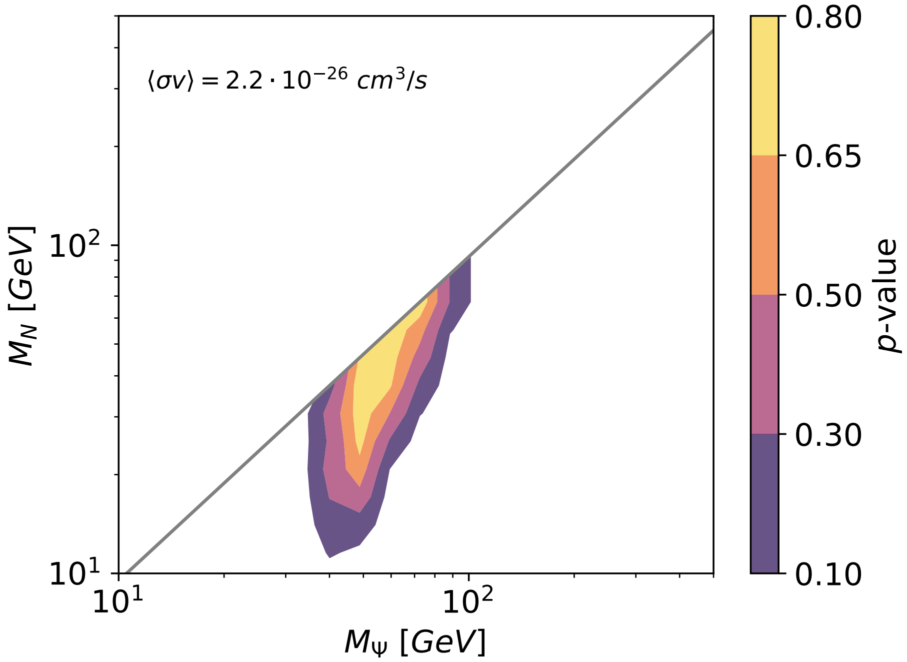

Figure 4. The color shows the parameter space region in which the model predicts a γ-ray flux compatible with the Galactic Center excess for a fixed $\langle\sigma v\rangle = 2.2 \times 10^{-26}\text{cm}^3/\text{s}$. For the fit we use the combined DM and astrophysical components, eq. (3.1).

Due to the uncertainties on the J-factors, there is a degeneracy between J and $\langle\sigma v\rangle$, so that a very good fit can be obtained for $\langle\sigma v\rangle$ in the range $0.2 \lesssim \langle\sigma v\rangle/\langle\sigma v\rangle_{thermal} \lesssim 1.5$. As a result, in the best fit point the value of $\langle\sigma v\rangle$ is not unambiguously determined, and we have

[2]We consider one order of magnitude variation in the J-factors.

chosen to present the results for the thermal one, $\langle\sigma v\rangle_{thermal} = 2.2 \times 10^{-26}\text{cm}^3/\text{s}$ because this is the thermal cross section consistent with the observed DM density.

Fig. 4 shows the different p-values in the (M_Ψ, M_N) plane. Notice that it is only possible to fit the GC excess in the low mass region for the DM particle and the sterile neutrinos, more precisely within the range of mass 30-100 GeV for both particles. From the photon fluxes depicted in Fig. 3 we can see that increasing the sterile neutrino mass leads to less energetic γ-rays, while increasing the DM mass produces the contrary effect, the γ-rays are more energetic. On the other hand, the flux decreases for heavier DM, since there are fewer particles contributing. These features explain the shape of the fitting regions depicted in Fig. 4.

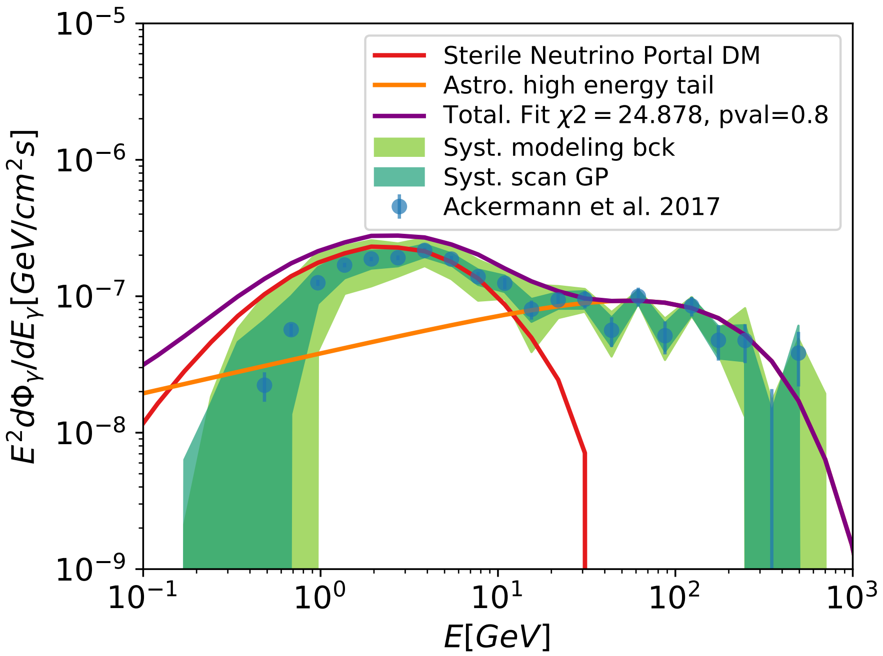

Figure 5. Fit to the GCE spectrum (blue dots) by the combination of a power-law with an exponential cutoff, describing the astrophysical sources (orange line), plus the contribution of DM annihilation, as given by dark matter annihilation into sterile neutrinos (red line). The purple line gives the final prediction of the model. The dark green band represents the diagonal of the covariance matrix due to excesses along the Galactic Plane, obtained using the same procedure as for the GCE [42]. The light green band is the diagonal of the covariance matrix from variations in the GCE due to uncertainties in modelling diffuse emission from ref. [41]

.

As already mentioned, the fit in Fig. 4 used the new GCE data reported by the Fermi-LAT Collaboration [41]. The reference [6] provides an excellent analysis of a previous estimation of the GCE in [15]. We find a larger parameter space allowed to fit the GCE data than in [6] mainly because of the broader systematic uncertainties in the GCE estimation that we used and our inclusion of an extra astrophysical component to model the GCE.

Fig. 5 shows the photon flux for our best fit point of the parameter space. Combining the astrophysical and the DM component, as given in eq. (3.1), we obtain that the best fit point is $(M_\Psi, M_N) = (55.1, 51.4)$ GeV for the DM component. For this point the best values of the astrophysical parameters are $(N, \alpha, E_{cut}) = (3.81 \times 10^{-8}\,\mathrm{GeV}^\alpha, 1.7, 187.8\,\mathrm{GeV})$. We obtain a very good fit, $\chi^2 = 24.9$ for 27 energy bins, which corresponds to a p-value = 0.78.

4 Constraints from indirect detection: gamma rays from dSphs and antiproton data

In the previous section, we have analyzed the photon flux from DM annihilation into sterile neutrinos, and its impact in the GCE. In this section, we will constrain the parameter space with the non-detection of dSphs by the Fermi LAT. Given the large diversity of photon spectra in the DM sterile neutrino portal to DM scenario, see fig. 1, we can not use the limits presented in the Fermi-LAT Collaboration publications, as they are for some particular annihilation channels [54]. Therefore, we use *gamLike v.1.0* [55], a software that evaluates the likelihoods for γ-ray searches using the combined analysis of 15 dSphs from 6 years of Fermi-LAT data, processed with the Pass-8 event-level analysis. *gamLike* calculates the Poisson likelihood following the method described in [56]. First of all we define the J-factor likelihood:

$$\mathcal{L}_J(J_i|J_{obs,i,}, \sigma_i) = \frac{e^{-(\log_{10}(J_i)-\log_{10}(J_{obs,i}))^2/2\sigma_i^2}}{\ln(10) J_{obs,i}\sqrt{2\pi}\sigma_i} \tag{4.1}$$

where $J_{obs,i}$ is the measured J-factor with error σ_i in each dSphs i and J_i is the true J-factor value. We then define the combined likelihood of all dSphs in the form:

$$\mathcal{L}_i(\mu, \theta_i|D_i) = \prod_j \mathcal{L}_i(\mu, \theta_i|\mathcal{D}_{i,j}) \tag{4.2}$$

where μ are the parameters of the DM model, θ_i accounts for the set of nuisance parameters from the LAT study and J-factors of the dSphs, and D_i is the γ-ray data set.

Using these ingredients we perform a test statistic (TS) to obtain 90% C.L. upper limits on the DM annihilation cross section. Such bounds are derived by finding a change in the log-likelihood:

$$TS = -2\ln\frac{\mathcal{L}(\mu_0, \hat{\theta}|\mathcal{D})}{\mathcal{L}(\hat{\mu}, \hat{\theta}|\mathcal{D})} \tag{4.3}$$

where μ_0 are the parameters of the no DM case (when we do not have γ-rays in our model) while $\hat{\mu}$ and $\hat{\theta}$ are the parameters for the point we want to analyze.

If $TS > 2.71$ the parameter space point is excluded because it is not compatible with the background at 90% C.L. Using this method we can find the exclusion line in the plane $M_\Psi - M_N$.

We can see in Fig. 6 the contour limits, corresponding to different $\langle\sigma v\rangle$ values. The region to the left of the corresponding curve is excluded at 90% C.L. We show as a red-dashed line the limit for a thermal annihilation cross-section, which in principle is the one needed to obtain the observed DM relic abundance within the sterile neutrino portal scenario under study. We find that DM masses $M_\Psi < 60$ GeV are excluded, in agreement with [6], a somehow weaker limit than the one obtained in [19].

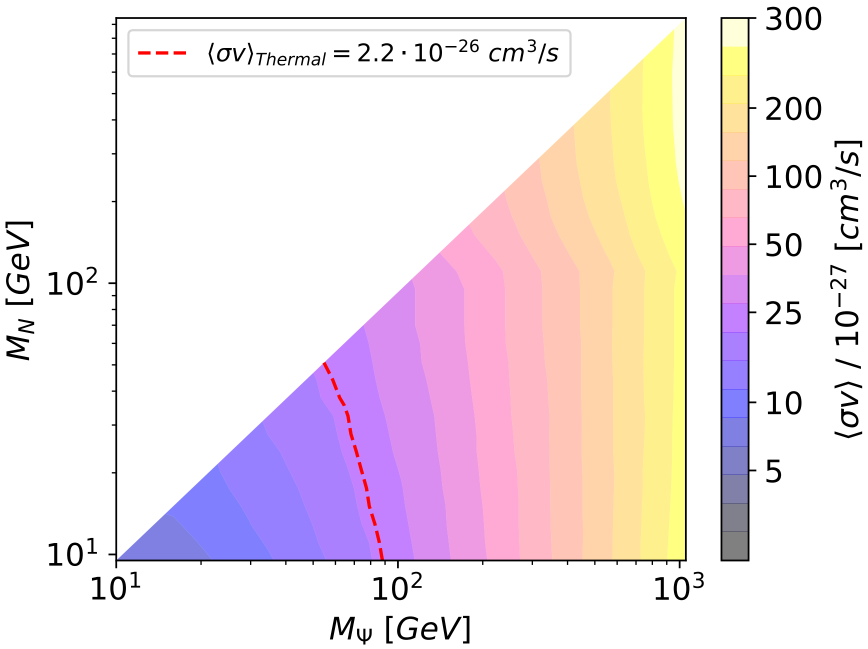

Figure 6. dSphs exclusion limit defined using the compatibility with the background. In this plot the color code shows the constrain for different values of $\langle \sigma v\rangle$.

Note however than in some cases the dark sector (including the sterile neutrino) could be at a different temperature than the SM, so that a larger freeze-out annihilation cross section is required to fit the observed DM abundance [21, 22]. Therefore a larger region of the parameter space (M_Ψ, M_N) is excluded in such cases.

Focusing on the standard thermal annihilation cross-section, we next analyze the impact of the dSphs constraints on our fit of the GCE. In Fig. 8 we plot both results, and we can see that the dSphs limit disfavours the low DM mass region of our fit of the GCE, although a sizable range of (M_Ψ, M_N) able to fit the GCE, remains allowed.

We expect that the sensitivity of the Fermi-LAT telescope will improve significantly in the next years by, among other reasons, the potential discoveries of new ultra-faint dwarf galaxies [57]. Using a similar analysis to [58], we estimate that in 15 years of data taking Fermi-LAT will have 3 times more dSphs discovered (45 dSphs) and considering that the point spread function (PSF) sensitivity for the Fermi-LAT instrument increases approximately as the square-root of the observation time (this is a conservative estimate), the Fermi-LAT constraints will improve by a factor of $(\sqrt{15}/\sqrt{6}) \times 3 \simeq 5$. In Fig. 8 we show the impact of this prospect (dashed blue line): the region to the left of this line will be potentially excluded in the next years by Fermi-LAT, including the GCE fit area (if we assume that all low energy GCE is due to DM annihilation).

Finally, we roughly estimate the effect of anti-proton data from AMS-02 on the sterile neutrino portal allowed parameter space. The derivation of these bounds suffer from large uncertainties, one of them being that the propagation parameters in the traditional MIN-MED-MAX schemes are determined by old Cosmic Ray data, and they are not necessarily guaranteed to describe the current status; indeed for instance the MIN propagation scheme is seriously disfavored [59] by the preliminary anti-proton to proton ratio reported by AMS-02. However, the MED scheme seems to provide a reasonable fit to the data, at least in the low energy region, so we have considered it to assess the region that could be excluded by AMS-02 data. Therefore our results should be taken as an indication of the parameter space that would be excluded by a complete fit of the cosmic ray propagation and DM parameters. We do not attempt here to explain the excess at high anti-proton energies.

We estimate the total flux of anti-protons within our model as the sum of the best fit of the background in the MED scheme [59], $\Phi_{\bar{p},bkg}(K)$, plus the DM contribution, i.e., $\Phi_{\bar{p}}(K_i, M_\Psi, M_N) = \Phi_{\bar{p},bkg}(K_i) + \Phi_{\bar{p},\Psi}(K_i, M_\Psi, M_N)$. Then, we calculate the ratio between this flux and the proton flux data $\Phi_p(K_i)$ from AMS-02 [60], in order to compare it with the last experimental data on the anti-proton-to-proton flux ratio $R(K_i) \pm \sigma_i$, also obtained by the AMS-02 experiment [39].

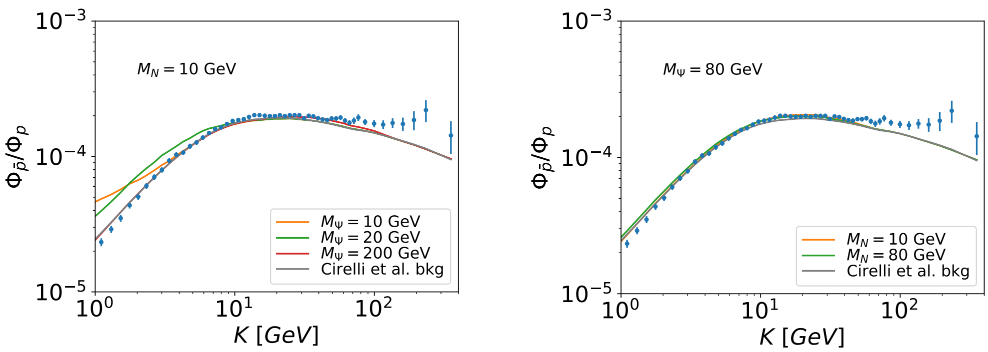

Figure 7. Total anti-proton-to-proton flux ratio for different points of the parameter space compared with the background contribution in the MED propagation scheme (gray line in both plots). Blue dots correspond to AMS-02 data [39]. In the left panel we can see the effect of the variation of M_Ψ, whereas in the right one the effect of the variation of M_N

.

In Fig. 7 we show the anti-proton-to-proton flux ratio from the background (gray line) and for different (M_Ψ, M_N) points as calculated in the MED propagation scheme, together with the recent AMS-02 data. Notice that since the data is in agreement or below the astrophysical background model at low values of the anti-proton kinetic energy K, points of the parameter space leading to larger ratios are disfavored.

Now, for each point of our parameter space $(\langle \sigma v \rangle, M_\Psi, M_N)$ we construct the estimator:

$$\chi^2 = \sum_i \left[\frac{R(K_i) - \Phi_{\bar{p}}(K_i, M_\Psi, M_N))/\Phi_p(K_i)}{\sigma_i} \right]^2 , \tag{4.4}$$

where i denotes the energy bins, and σ_i the corresponding uncertainty on the flux ratio. Denoting χ_0^2 the minimum chi-squared of the background-only case from [59], we can define the limit on $\langle\sigma v\rangle$ for each point (M_Ψ, M_N) using the condition:

$$\chi^2(\langle\sigma v\rangle, M_\Psi, M_N) - \chi_0^2 \leq 4 \tag{4.5}$$

Note that in this derivation we have used the Einasto DM density profile, since it is the one employed by AMS-02.

In Fig. 8 we show the impact of the anti-proton AMS-02 data using the MED propagation scheme on the sterile neutrino portal parameter space. The orange region corresponds to the (M_Ψ, M_N) points for which the limit on $\langle\sigma v\rangle$ obtained in the way described above is $\leq 2.2 \times 10^{-26}\text{cm}^3/\text{s}$. Our results for the MED propagation scheme agree with ref.[6], where a similar analysis has been performed. As noticed there, the constrains from anti-proton are complementary to the dSphs ones, and for a fixed M_Ψ they disfavour the high M_N region of the GCE fit, since heavier sterile neutrinos produce a larger anti-proton flux at low kinetic energies K. However the astrophysical uncertainties are still very large, as has been shown in [6] by using different propagation schemes and DM density profiles, as well as varying the J-factors.

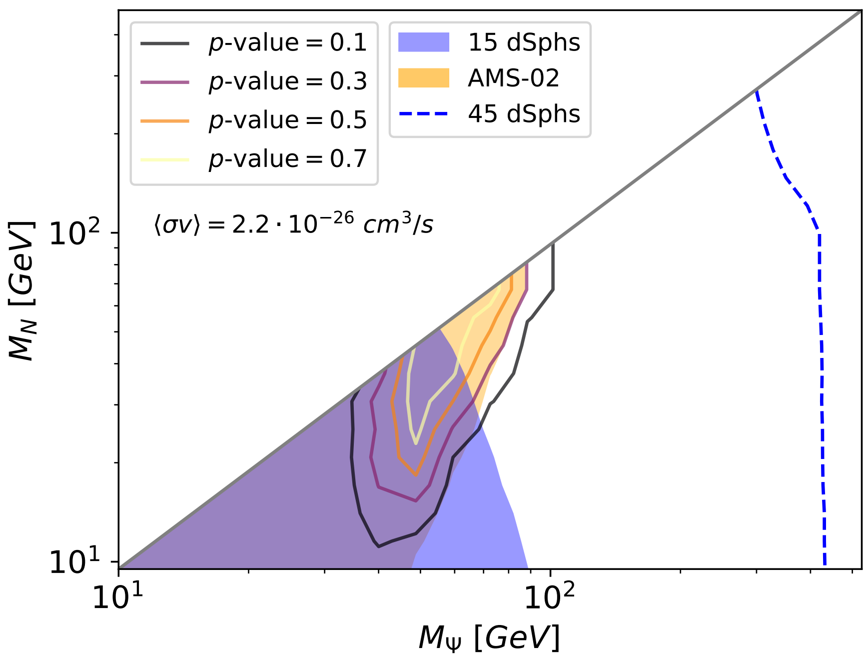

Figure 8. Region of the parameter space that fit the GCE combined with the dSphs and AMS-02 anti-protons constrain for a thermal value of the $\langle\sigma v\rangle$.

5 Conclusions

The DM relic abundance could be determined by the freeze-out of DM interactions with sterile neutrinos, which in turn generate light neutrino masses via the seesaw type I mechanism;

this is the so-called sterile neutrino portal to DM. Generically such scenario is challenging to test at colliders and easily evades DM direct searches. However, it can be probed in DM indirect detection experiments, since the sterile neutrinos copiously produced in DM annihilations will subsequently cascade decay into SM final states due to its mixing with the active neutrinos (unless the annihilation cross section is p-wave and therefore it is velocity suppressed at present).

In this work, we focus on the impact of the new analysis of the Fermi-LAT Collaboration of the Galactic Center region, based on the reprocessed Pass 8 event data, which confirms the existence of a γ-ray excess peaked at ~ 3 GeV. We assume that annihilation of DM into sterile neutrinos is the main contributor to the low energy photon flux of the GCE (photon energy < 10 GeV). The high energy tail of the GCE (> 10 GeV) could be due to an astrophysical component, which we model as a power law with an exponential cut-off, eq. (3.2). Although the interpretation of the GCE as DM annihilation is still under debate, it is worth to explore whether a complete particle physics model can account for it.

We perform a model-independent analysis within the sterile neutrino portal scenario. Indeed, our results only depend on the thermally averaged DM annihilation cross section into sterile neutrinos, which we fix to $\langle\sigma v\rangle = 2.2 \times 10^{-26}\text{cm}^3/s$, and the DM and sterile neutrino masses, (M_Ψ, M_N). Therefore, our analysis can be extended to any model able to reproduce the thermal DM annihilation cross section into sterile neutrinos.

We find that the sterile neutrino portal to DM provides an excellent fit to the GCE: $\chi^2 = 24.9$ for 27 energy bins (p-value = 0.78). The best fit corresponds to $(M_\Psi, M_N) = (55.1, 51.4)$ GeV.

We then check the compatibility of these results with the limits from Fermi-LAT Pass 8 data on the dSphs positions and anti-proton data from AMS-02. Fig. 8 summarizes our main findings. We see that there is a sizeable region in the (M_Ψ, M_N) plane able to contribute significantly to the GCE and allowed by the dSphs constraints. Indeed, the dSphs set an stringent limit which excludes DM masses below ~ 50 GeV (90 GeV), for sterile neutrino masses $M_N \lesssim M_{DM}$ ($M_N \ll M_{DM}$). In particular, the above best-fit point to the GCE is allowed. It is worth noticing that shortly further constraints from a larger number of dSphs may be in tension with the explanation of the GCE, under the assumption that a large fraction of the low energy sector of the GCE (below ≈ 10 GeV) is due to DM annihilation.

On the other hand, using the MED propagation scheme we find that current anti-proton data from AMS-02 already disfavours a large fraction of the (M_Ψ, M_N) region able to account for the GCE; however our analysis is not conclusive, given the large uncertainties in the anti-proton background estimate and propagation parameters.

Acknowledgements

We thank Brian Batell for correspondence about the photon and anti-proton spectrum of sterile neutrino decays. This work has been partially supported by the European Union projects H2020-MSCA-RISE-2015-690575-InvisiblesPlus and H2020-MSCA-ITN-2015/674896-ELUSIVES, by the Spanish MINECO under grants FPA2014-57816-P and SEV-2014-0398, and by Generalitat Valenciana grant PROMETEOII2014/050. The work of GAGV was supported by Programa FONDECYT Postdoctorado under grant 3160153.

References

[1] S. Dodelson and L. M. Widrow, *Sterile-neutrinos as dark matter*, *Phys. Rev. Lett.* **72** (1994) 17–20, [hep-ph/9303287].

[2] R. Adhikari et al., *A White Paper on keV Sterile Neutrino Dark Matter*, *Submitted to: White paper* (2016) , [1602.04816].

[3] M. Pospelov, A. Ritz and M. B. Voloshin, *Secluded WIMP Dark Matter*, *Phys. Lett.* **B662** (2008) 53–61, [0711.4866].

[4] M. Escudero, N. Rius and V. Sanz, *Sterile neutrino portal to Dark Matter I: The $U(1)_{B-L}$ case*, *JHEP* **02** (2017) 045, [1606.01258].

[5] M. Escudero, N. Rius and V. Sanz, *Sterile Neutrino portal to Dark Matter II: Exact Dark symmetry*, *Eur. Phys. J.* **C77** (2017) 397, [1607.02373].

[6] B. Batell, T. Han and B. Shams Es Haghi, *Indirect Detection of Neutrino Portal Dark Matter*, 1704.08708.

[7] R. Allahverdi, Y. Gao, B. Knockel and S. Shalgar, *Indirect Signals from Solar Dark Matter Annihilation to Long-lived Right-handed Neutrinos*, *Phys. Rev.* **D95** (2017) 075001, [1612.03110].

[8] L. Goodenough and D. Hooper, *Possible Evidence For Dark Matter Annihilation In The Inner Milky Way From The Fermi Gamma Ray Space Telescope*, *ArXiv e-prints* (Oct., 2009) , [0910.2998].

[9] Fermi-LAT collaboration, V. Vitale and A. Morselli, *Indirect Search for Dark Matter from the center of the Milky Way with the Fermi-Large Area Telescope*, in *Fermi gamma-ray space telescope. Proceedings, 2nd Fermi Symposium, Washington, USA, November 2-5, 2009*, 2009, 0912.3828, https://inspirehep.net/record/840760/files/arXiv:0912.3828.pdf.

[10] D. Hooper and L. Goodenough, *Dark Matter Annihilation in The Galactic Center As Seen by the Fermi Gamma Ray Space Telescope*, *Phys. Lett.* **B697** (2011) 412–428, [1010.2752].

[11] C. Gordon and O. Macias, *Dark Matter and Pulsar Model Constraints from Galactic Center Fermi-LAT Gamma Ray Observations*, *Phys. Rev.* **D88** (2013) 083521, [1306.5725].

[12] D. Hooper and T. Linden, *On The Origin Of The Gamma Rays From The Galactic Center*, *Phys.Rev.* **D84** (2011) 123005, [1110.0006].

[13] T. Daylan, D. P. Finkbeiner, D. Hooper, T. Linden, S. K. N. Portillo, N. L. Rodd et al., *The characterization of the gamma-ray signal from the central Milky Way: A case for annihilating dark matter*, *Phys. Dark Univ.* **12** (2016) 1–23, [1402.6703].

[14] A. Boyarsky, D. Malyshev and O. Ruchayskiy, *A comment on the emission from the Galactic Center as seen by the Fermi telescope*, *Physics Letters B* **705** (Nov., 2011) 165–169, [1012.5839].

[15] F. Calore, I. Cholis and C. Weniger, *Background model systematics for the Fermi GeV excess*, *JCAP* **3** (Mar., 2015) 038, [1409.0042].

[16] K. N. Abazajian, N. Canac, S. Horiuchi and M. Kaplinghat, *Astrophysical and Dark Matter Interpretations of Extended Gamma-Ray Emission from the Galactic Center*, *Phys. Rev.* **D90** (2014) 023526, [1402.4090].

[17] B. Zhou, Y.-F. Liang, X. Huang, X. Li, Y.-Z. Fan, L. Feng et al., *GeV excess in the Milky Way: The role of diffuse galactic gamma-ray emission templates*, *Phys. Rev.* **D91** (2015) 123010, [1406.6948].

[18] Y.-L. Tang and S.-h. Zhu, *Dark matter annihilation into right-handed neutrinos and the galactic center gamma-ray excess*, *JHEP* **03** (2015) , [1512.02899].

[19] M. D. Campos, F. S. Queiroz, C. E. Yaguna and C. Weniger, *Search for right-handed neutrinos from dark matter annihilation with gamma-rays*, *JCAP* **1707** (2017) 016, [1702.06145].

[20] Fermi-LAT collaboration, M. Ackermann et al., *The Fermi Galactic Center GeV Excess and Implications for Dark Matter*, *Astrophys. J.* **840** (2017) 43, [1704.03910].

[21] Y.-L. Tang and S.-h. Zhu, *Dark Matter Relic Abundance and Light Sterile Neutrinos*, *JHEP* **01** (2017) 025, [1609.07841].

[22] N. Bernal and C. S. Fong, *Hot Leptogenesis from Thermal Dark Matter*, 1707.02988.

[23] P. Gondolo and G. Gelmini, *Cosmic abundances of stable particles: Improved analysis*, *Nucl. Phys.* **B360** (1991) 145–179.

[24] M. C. Gonzalez-Garcia, A. Santamaria and J. W. F. Valle, *Isosinglet Neutral Heavy Lepton Production in Z Decays and Neutrino Mass*, *Nucl. Phys.* **B342** (1990) 108–126.

[25] M. Dittmar, A. Santamaria, M. C. Gonzalez-Garcia and J. W. F. Valle, *Production Mechanisms and Signatures of Isosinglet Neutral Heavy Leptons in Z^0 Decays*, *Nucl. Phys.* **B332** (1990) 1–19.

[26] A. Pilaftsis, *Radiatively induced neutrino masses and large Higgs neutrino couplings in the standard model with Majorana fields*, *Z. Phys.* **C55** (1992) 275–282, [hep-ph/9901206].

[27] W. Porod, *SPheno, a program for calculating supersymmetric spectra, SUSY particle decays and SUSY particle production at e+ e- colliders*, *Comput. Phys. Commun.* **153** (2003) 275–315, [hep-ph/0301101].

[28] F. Staub, *Exploring new models in all detail with SARAH*, *Adv. High Energy Phys.* **2015** (2015) 840780, [1503.04200].

[29] A. Vicente, *Computer tools in particle physics*, 1507.06349.

[30] J. Alwall, R. Frederix, S. Frixione, V. Hirschi, F. Maltoni, O. Mattelaer et al., *The automated computation of tree-level and next-to-leading order differential cross sections, and their matching to parton shower simulations*, *JHEP* **07** (2014) 079, [1405.0301].

[31] T. Sjostrand, S. Mrenna and P. Z. Skands, *A Brief Introduction to PYTHIA 8.1*, *Comput. Phys. Commun.* **178** (2008) 852–867, [0710.3820].

[32] D. Alva, T. Han and R. Ruiz, *Heavy Majorana neutrinos from $W\gamma$ fusion at hadron colliders*, *JHEP* **02** (2015) 072, [1411.7305].

[33] C. Degrande, O. Mattelaer, R. Ruiz and J. Turner, *Fully-Automated Precision Predictions for Heavy Neutrino Production Mechanisms at Hadron Colliders*, *Phys. Rev.* **D94** (2016) 053002, [1602.06957].

[34] P. Agrawal, B. Batell, P. J. Fox and R. Harnik, *WIMPs at the Galactic Center*, *JCAP* **1505** (2015) 011, [1411.2592].

[35] PAMELA collaboration, O. Adriani et al., *The cosmic-ray electron flux measured by the PAMELA experiment between 1 and 625 GeV*, *Phys. Rev. Lett.* **106** (2011) 201101, [1103.2880].

[36] AMS Collaboration collaboration, M. Aguilar, D. Aisa, B. Alpat, A. Alvino, G. Ambrosi, K. Andeen et al., *Precision measurement of the $(e^+ + e^-)$ flux in primary cosmic rays from 0.5 gev to 1 tev with the alpha magnetic spectrometer on the international space station*, *Phys. Rev. Lett.* **113** (Nov, 2014) 221102.

[37] AMS Collaboration collaboration, L. Accardo, M. Aguilar, D. Aisa, B. Alpat, A. Alvino, G. Ambrosi et al., *High statistics measurement of the positron fraction in primary cosmic rays of 0.5˘500 gev with the alpha magnetic spectrometer on the international space station*, *Phys. Rev. Lett.* **113** (Sep, 2014) 121101.

[38] M. Cirelli, G. Corcella, A. Hektor, G. Hutsi, M. Kadastik, P. Panci et al., *PPPC 4 DM ID: A Poor Particle Physicist Cookbook for Dark Matter Indirect Detection*, *JCAP* **1103** (2011) 051, [1012.4515].

[39] AMS Collaboration collaboration, M. Aguilar, L. Ali Cavasonza, B. Alpat, G. Ambrosi, L. Arruda, N. Attig et al., *Antiproton flux, antiproton-to-proton flux ratio, and properties of elementary particle fluxes in primary cosmic rays measured with the alpha magnetic spectrometer on the international space station*, *Phys. Rev. Lett.* **117** (Aug, 2016) 091103.

[40] **Fermi/LAT** Collaboration, *Fermi-LAT Observations of High-Energy Gamma-Ray Emission toward the Galactic Center*, *ApJ* **819** (Mar., 2016) 44, [1511.02938].

[41] Fermi-LAT collaboration, M. Ackermann et al., *The Fermi Galactic Center GeV Excess and Implications for Dark Matter*, *Astrophys. J.* **840** (2017) 43, [1704.03910].

[42] A. Achterberg, M. van Beekveld, S. Caron, G. A. Gomez-Vargas, L. Hendriks and R. Ruiz de Austri, *Implications of the Fermi-LAT Pass 8 Galactic Center excess on supersymmetric dark matter*, *JCAP* **1712** (2017) 040, [1709.10429].

[43] K. N. Abazajian, *The Consistency of Fermi-LAT Observations of the Galactic Center with a Millisecond Pulsar Population in the Central Stellar Cluster*, *JCAP* **1103** (2011) 010, [1011.4275].

[44] R. Bartels, S. Krishnamurthy and C. Weniger, *Strong support for the millisecond pulsar origin of the Galactic center GeV excess*, *Phys. Rev. Lett.* **116** (2016) 051102, [1506.05104].

[45] S. K. Lee, M. Lisanti, B. R. Safdi, T. R. Slatyer and W. Xue, *Evidence for Unresolved γ-Ray Point Sources in the Inner Galaxy*, *Phys. Rev. Lett.* **116** (2016) 051103, [1506.05124].

[46] Fermi-LAT collaboration, M. Ajello et al., *Characterizing the population of pulsars in the inner Galaxy with the Fermi Large Area Telescope*, *Submitted to: Astrophys. J.* (2017) , [1705.00009].

[47] S. Caron, G. A. Gomez-Vargas, L. Hendriks and R. Ruiz de Austri, *Analyzing γ-rays of the Galactic Center with Deep Learning*, *JCAP* **1805** (2018) 058, [1708.06706].

[48] I. Cholis, C. Evoli, F. Calore, T. Linden, C. Weniger and D. Hooper, *The Galactic Center GeV Excess from a Series of Leptonic Cosmic-Ray Outbursts*, *JCAP* **1512** (2015) 005, [1506.05119].

[49] T. Linden, N. L. Rodd, B. R. Safdi and T. R. Slatyer, *High-energy tail of the Galactic Center gamma-ray excess*, *Phys. Rev.* **D94** (2016) 103013, [1604.01026].

[50] J. A. Casas, G. A. Gomez-Vargas, J. M. Moreno, J. Quilis and R. Ruiz de Austri, *Extended Higgs-portal dark matter and the Fermi-LAT Galactic Center Excess*, 1711.10957.

[51] Fermi-LAT collaboration, M. Ackermann et al., *The Spectrum and Morphology of the Fermi Bubbles*, *Astrophys. J.* **793** (2014) 64, [1407.7905].

[52] A. Achterberg, S. Amoroso, S. Caron, L. Hendriks, R. Ruiz de Austri and C. Weniger, *A description of the Galactic Center excess in the Minimal Supersymmetric Standard Model*, *JCAP* **1508** (2015) 006, [1502.05703].

[53] J. F. Navarro, C. S. Frenk and S. D. M. White, *A Universal density profile from hierarchical clustering*, *Astrophys. J.* **490** (1997) 493–508, [astro-ph/9611107].

[54] DES, Fermi-LAT collaboration, A. Albert et al., *Searching for Dark Matter Annihilation in Recently Discovered Milky Way Satellites with Fermi-LAT*, *Astrophys. J.* **834** (2017) 110, [1611.03184].

[55] The GAMBIT Dark Matter Workgroup collaboration, T. Bringmann et al., *DarkBit: A GAMBIT module for computing dark matter observables and likelihoods*, *Eur. Phys. J.* **C77** (2017) 831, [1705.07920].

[56] Fermi-LAT collaboration, M. Ackermann et al., *Searching for Dark Matter Annihilation from Milky Way Dwarf Spheroidal Galaxies with Six Years of Fermi Large Area Telescope Data*, *Phys. Rev. Lett.* **115** (2015) 231301, [1503.02641].

[57] Fermi-LAT collaboration, E. Charles et al., *Sensitivity Projections for Dark Matter Searches with the Fermi Large Area Telescope*, *Phys. Rept.* **636** (2016) 1–46, [1605.02016].

[58] S. Horiuchi, O. Macias, D. Restrepo, A. Rivera, O. Zapata and H. Silverwood, *The Fermi-LAT gamma-ray excess at the Galactic Center in the singlet-doublet fermion dark matter model*, *JCAP* **1603** (2016) 048, [1602.04788].

[59] G. Giesen, M. Boudaud, Y. Génolini, V. Poulin, M. Cirelli, P. Salati et al., *AMS-02 antiprotons, at last! Secondary astrophysical component and immediate implications for Dark Matter*, *JCAP* **1509** (2015) 023, [1504.04276].

[60] AMS Collaboration collaboration, M. Aguilar, D. Aisa, B. Alpat, A. Alvino, G. Ambrosi, K. Andeen et al., *Precision measurement of the proton flux in primary cosmic rays from rigidity 1 gv to 1.8 tv with the alpha magnetic spectrometer on the international space station*, *Phys. Rev. Lett.* **114** (Apr, 2015) 171103.

Published for SISSA by Springer

Received: *July 29, 2019*
Revised: *November 17, 2019*
Accepted: *January 2, 2020*
Published: *January 27, 2020*

Gravity-mediated scalar Dark Matter in warped extra-dimensions

Miguel G. Folgado, Andrea Donini and Nuria Rius

Departamento de Física Teórica and IFIC, Universidad de Valencia-CSIC, C/ Catedrático José Beltrán, 2, E-46980 Paterna, Spain

E-mail: migarfol@ific.uv.es, donini@ific.uv.es, nuria.rius@ific.uv.es

Abstract: We revisit the case of scalar Dark Matter interacting just gravitationally with the Standard Model (SM) particles in an extra-dimensional Randall-Sundrum scenario. We assume that both, the Dark Matter and the Standard Model, are localized in the TeV brane and only interact via gravitational mediators, namely the graviton Kaluza-Klein modes and the radion. We analyze in detail the dark matter annihilation channel into two on-shell KK-gravitons, and contrary to previous studies which overlooked this process, we find that it is possible to obtain the correct relic abundance for dark matter masses in the range [1, 10] TeV even after taking into account the strong bounds from LHC Run II. We also consider the impact of the radion contribution (virtual exchange leading to SM final states as well as on-shell production), which does not significantly change our results. Quite interestingly, a sizeable part of the currently allowed parameter space could be tested by LHC Run III and by the High-Luminosity LHC.

Keywords: Phenomenology of Field Theories in Higher Dimensions

ArXiv ePrint: 1907.04340

https://doi.org/10.1007/JHEP01(2020)161

JHEP01(2020)161

Contents

1 Introduction

The Nature of Dark Matter (DM) is one of the long-standing puzzles that still have to be explained in order to claim that we have a "complete" picture of the Universe. On the one side, both from astrophysical and cosmological data (see, e.g., Ref. [1] and refs. therein), rather clear indications regarding the existence of some kind of matter that gravitates but that does not interact with other particles by any other detectable mean can be gathered. On the other hand, no candidate to fill the rôle of Dark Matter has yet been observed in high-energy experiments at colliders, nor is present in the Standard Model (SM) spectrum. Within SM particles, the only ones that share with Dark Matter the property of being weakly coupled to SM matter are neutrinos. However, experimental searches have shown that neutrinos constitute just a tiny fraction of what is called non-baryonic matter in the Universe energy budget [2]. Most of the suggestions for physics Beyond the Standard Model (BSM), therefore, include one or several possible candidates to be the Dark Matter. Under the assumptions of the "WIMP paradigm" (with "WIMP" standing for "weakly interacting massive particle"), these new particles have in common to be rather heavy and with very weak interactions with SM particles. Two examples of these are the neutralino in supersymmetric extensions of the SM [3] or the lightest Kaluza-Klein particle in Universal Extra-Dimensions [4, 5]. Searches for these heavy particles at the LHC have pushed bounds on the masses of the candidates to the TeV range, a region of the parameter space rather difficult to test for experiments searching for Dark Matter particles interacting directly within the detector (see, e.g., Ref. [6]) or looking at annihilation products of Dark Matter particles [7]. Both for this reason and for the fact that very heavy WIMP's are relatively unnatural in theories that want to solve the hierarchy problem and not only host some Dark Matter candidates, models in which the Dark Matter particles are either "feebly interacting massive particles" (FIMP's) [8] or "axion-like" very light particles (see, e.g., Ref. [9]) have been constructed. As a result, at present a very rich (and complicated) landscape of models explaining the Nature of Dark Matter exists, and experimental searches have to look for very different signals.

In this paper we want to explore in some detail a possibility that was advanced in the literature several times in the last ten to twenty years. The idea is that the interaction between Dark Matter particles and the SM ones, though only gravitational, may be enhanced due to the fact that gravity feels more than the standard $3+1$ space-time dimensions. Extra-dimensional models have been proposed to solve the hierarchy problem, related to the large hierarchy existing between the electro-weak scale, $\Lambda_{\rm EW} \sim 250$ GeV, and the Planck scale, $M_P \sim 10^{19}$ GeV. In all these models, the gravitational interaction strength is generically enhanced with respect to the standard picture since the "true" scale of gravitation is not given by M_P but, rather, by some fundamental scale M_D (where D is the number of dimensions). The two scales, M_P and M_D are connected by some relation that takes into account the geometry of space-time. In so-called *Large Extra-Dimensions* models (LED) [10–14], for example, $M_P^2 = V_d \times M_D^{2+d}$ (where d is the number of extra spatial dimensions). If the extra-dimensions are compactified in a d-dimensional volume V_d, and V_d is sufficiently large, then $M_D \ll M_P$, thus solving or alleviating the hierarchy problem. In *warped extra-dimensions* (also called Randall-Sundrum models) [15, 16], on the other hand, the separation between M_P and M_D is not very large, $M_P^2 = 8\pi(M_D^3/k)\,[1 - \exp(-2\pi r_c k)]$, where k is the curvature of the space-time along the extra-dimension and r_c is the distance between two points in the extra-dimension. However, all physical masses have an exponential suppression with respect to M_P due to the curvature k, $m = \exp(-2\pi r_c k)\,m_0$. In this picture, m_0 is a fundamental mass parameter of order M_P and m is the mass tested by a 4-dimensional observer. In the *ClockWork/Linear Dilaton* model (CW/LD), eventually, the relation between M_P and M_D is a combination of a volume factor, as for LED models, and a curvature factor, as for warped models [17].

The possibility that Dark Matter particles, whatever they be, have an *enhanced* gravitational interaction with SM particles have been studied mainly in the context of warped extra-dimensions. The idea was first advanced in Refs. [18, 19] and subsequently studied in Refs. [20–24]. As already stressed, the Nature of Dark Matter is still unknown. In particular, if new particles are added to the SM spectrum to act as Dark Matter particles, their spin is completely undetermined. In the publications above, therefore, scalar, fermion and vector DM particles have been usually considered. In this paper, on the other hand, we only consider scalar Dark Matter. We have been led to this decision by the fact that, maybe unexpectedly, we have found significant regions of the model parameter space for which the thermal relic abundance can be achieved and that can avoid present experimental bounds and theoretical constraints (in contrast, for example, with the conclusions of Ref. [21]). Interestingly enough, most of the allowed parameter space will be tested by the Run III at the LHC and by its high-luminosity version, the HL-LHC. On the way to achieve the correct relic abundance, we have found some discrepancies with existing literature on the subject when looking for DM annihilation into Kaluza-Klein gravitons. In addition, in order to give a consistent picture of this possibility in the framework of warped extra-dimensions, we have also taken into account the DM annihilation through and to radions within the Goldberger-Wise approach [25], finding that this channel may also give the correct relic abundance, though in a very tiny region of the parameter space difficult to test at the LHC.

In forthcoming publications we plan to extend our study to DM particles with a different spin and explore other extra-dimensional scenarios, such as LED and CW/LD.

The paper is organized as follows: in Sec.2 we outline the theoretical framework, reminding shortly the basic ingredients of warped extra-dimensional scenarios and of how dark matter can be included within this hypothesis; in Sec.3 we show our results for the annihilation cross-sections of scalar DM particles into SM particles, KK-gravitons and/or radions; in Sec.4 we review the present experimental bounds on the Kaluza-Klein graviton mass from LEP and LHC, as well as on the DM mass from direct and indirect search experiments, and we remind the theoretical constraints coming from unitarity violation and effective field theory consistency; in Sec.5 we explore the allowed parameter space such that the correct relic abundance is achieved for scalar DM particles; and, eventually, in Sec.6 we conclude. In the Appendices we give some of the mathematical expressions used in the paper: App. A contains the KK-graviton propagator and polarization tensor; in App. B we provide the Feynman rules for our model; in App. C we give the expressions for the decay amplitudes of the KK-graviton and of the radion; and, eventually, in App. D we give the formulæ for the annihilation cross-sections of dark matter particles into Standard Model particles, KK-gravitons and radions.

2 Theoretical framework

In this Section, we shortly review the Warped Extra-Dimensions scenario (also called Randall-Sundrum model [15]) and introduce our setup to include Dark Matter in the model, we give the relevant formulæ to compute the DM relic abundance and eventually provide the DM annihilation cross-sections into SM particles, Kaluza-Klein gravitons and into radions.

2.1 A short summary on Warped Extra-Dimensions

The popular Randall-Sundrum scenario (from now on RS or RS1 [15], to be distinguished from the scenario called RS2 [16]) consider a non-factorizable 5-dimensional metric in the form:

$$ds^2 = e^{-2\sigma}\eta_{\mu\nu}dx^\mu dx^\nu - r_c^2\, dy^2 \tag{2.1}$$

where $\sigma = kr_c|y|$ and the signature of the metric is $(+,-,-,-,-)$. In this scenario, k is the curvature along the 5th-dimension and it is $\mathcal{O}(M_P)$. The length-scale r_c, on the other hand, is related to the size of the extra-dimension: we only consider a slice of the space-time between two branes located conventionally at the two fixed-points of an orbifold, $y = 0$ (the so-called UV-brane) and $y = \pi$ (the IR-brane). The 5-dimensional space-time is a slice of AdS_5 and the exponential factor that multiplies the $\mathcal{M}_4$ Minkowski 4-dimensional space-time is called the "warp factor". Notice that, in order to have gravity in 4-dimensions, in general $\eta_{\mu\nu} \to g_{\mu\nu}$, with $g_{\mu\nu}$ the 4-dimensional induced metric on the brane.

The action in 5D is:

$$S = S_{\text{gravity}} + S_{\text{IR}} + S_{\text{UV}} \tag{2.2}$$

where

$$S_{\text{gravity}} = \frac{16\pi}{M_5^3}\int d^4x \int_0^\pi r_c dy\sqrt{G^{(5)}}\left[R^{(5)} - 2\Lambda_5\right], \tag{2.3}$$

with M_5 the fundamental gravitational scale, $G^{(5)}_{MN}$ and $R^{(5)}$ the 5-dimensional metric and Ricci scalar, respectively, and Λ_5 the 5-dimensional cosmological constant. As usual, we consider capital latin indices M, N to run over the 5 dimensions and greek indices μ, ν only over 4 dimensions. The Planck mass is related to the fundamental scale M_5 as:

$$\bar{M}_P^2 = \frac{M_5^3}{k}\left(1 - e^{-2k\pi r_c}\right), \tag{2.4}$$

where $\bar{M}_P = M_P/\sqrt{8\pi} = 2.435 \times 10^{18}$ GeV is the reduced Planck mass.

We consider for the two brane actions the following expressions:

$$S_{\text{IR}} = \int d^4x\sqrt{-g}\,\left\{-f_{\text{IR}}^4 + \mathcal{L}_{\text{SM}} + \mathcal{L}_{\text{DM}}\right\} \tag{2.5}$$

and

$$S_{\rm UV} = \int d^4x\sqrt{-g}\,\left\{-f_{\rm UV}^4 + \dots\right\}\,, \tag{2.6}$$

where $f_{\rm IR}, f_{\rm UV}$ are the brane tensions for the two branes. In Randall-Sundrum scenarios, in order to achieve the metric in eq. (2.1) as a classical solution of the Einstein equations, the brane-tension terms in $S_{\rm UV}$ and $S_{\rm IR}$ are chosen such as to cancel the 5-dimensional cosmological constant, $f_{\rm IR}^4 = -f_{\rm UV}^4 = \sqrt{-24M_5^3\,\Lambda_5}$.

Throughout this paper, we consider all the SM and DM fields localized on the IR-brane, whereas on the UV-brane we could have any other physics that is Planck-suppressed. We assume that DM particles only interact with the SM particles gravitationally and, for simplicity, we focus on scalar DM. More complicated DM spectra (with particles of spin higher than zero or with several particles) will not be studied here. Notice that, in 4-dimensions, the gravitational interactions would be enormously suppressed by powers of the Planck mass. However, in an extra-dimensional scenario, the gravitational interaction is actually enhanced: on the IR–brane, in fact, the effective gravitational coupling is $\Lambda = \bar{M}_P \exp\left(-k\pi r_c\right)$, due to the rescaling factor $\sqrt{G^{(5)}}/\sqrt{-g^{(4)}}$. It is easy to see that $\Lambda \ll \bar{M}_P$ even for moderate choices of σ. In particular, for $\sigma = kr_c \sim 10$ the RS scenario can address the hierarchy problem. In general, we will work with $\Lambda = \mathcal{O}(1\,{\rm TeV})$ but not necessarily as low as to solve the hierarchy problem.

Expanding the 4-dimensional component of the metric at first order about its static solution, we have:

$$G_{\mu\nu}^{(5)} = e^{-2\sigma}\left(\eta_{\mu\nu} + \kappa_5 h_{\mu\nu}\right)\,, \tag{2.7}$$

with $\kappa_5 = 2M_5^{-2/3}$. The 5-dimensional field $h_{\mu\nu}$ can be written as a Kaluza-Klein tower of 4-dimensional fields as follows:

$$h_{\mu\nu}(x,y) = \sum h_{\mu\nu}^n(x)\frac{\chi^n(y)}{\sqrt{r_c}}\,. \tag{2.8}$$

The $h_{\mu\nu}^n(x)$ can be interpreted as the KK-excitations of the 4-dimensional graviton. The $\chi^n(y)$ factors are the wavefunctions of the KK-gravitons along the extra-dimension. Notice that in the 4-dimensional decomposition of a 5-dimensional metric, two other fields are generally present: the graviphoton, $G_{\mu 5}^{(5)}$, and the graviscalar $G_{55}^{(5)}$. It has been shown elsewhere [15] that graviphotons are massive due to the breaking of 5-dimensional translational invariance induced by the presence of the branes. On the other hand, the graviscalar field is relevant to stabilize the size of the extra-dimension and it will be discussed below when introducing the *radion*.

The equation of motion for the n-th KK-mode is given by:

$$\left(\eta^{\mu\nu}\partial_\mu\partial_\nu + m_n^2\right)h_{\mu\nu}^n(x) = 0\,, \tag{2.9}$$

where m_n is its mass. Using the Einstein equations we obtain [26]:

$$\frac{-1}{r_c^2}\frac{d}{dy}\left(e^{-4\sigma}\frac{d\chi^n}{dy}\right) = m_n^2 e^{-2\sigma}\chi^n\,. \tag{2.10}$$

from which:

$$\chi^n(y) = \frac{e^{2\sigma(y)}}{N_n} \left[J_2(z_n) + \alpha_n Y_2(z_n) \right] \, , \tag{2.11}$$

being J_2 and Y_2 Bessel functions of order 2 and $z_n(y) = m_n/ke^{\sigma(y)}$. The N_n factor is the n-th KK-mode wavefunction normalization. In the limit $m_n/k \ll 1$ and $e^{k\pi r_c} \gg 1$, the coefficient α_n becomes $\alpha_n \sim x_n^2 \exp(-2k\pi r_c)$, where x_n are the are the roots of the Bessel function J_1, $J_1(x_n) = 0$, and the masses of the KK-graviton modes are given by:

$$m_n = k x_n e^{-k\pi r_c} \, . \tag{2.12}$$

Notice that, for low n, the KK-graviton masses are not equally spaced, as they are proportional to the roots of the Bessel function J_1. This is very different from both the LED and the CW/LD scenarios, however for large n the spacing between KK-graviton modes become so small that all extra-dimensional scenarios eventually coincide, $m_n \sim n/R$ (being R some relevant length scale specific to each scenario).

The normalization factors can be computed imposing that:

$$\int dy e^{-2\sigma} \left[\chi^n \right]^2 = 1 \, . \tag{2.13}$$

In the same approximation as above, i.e. for $m_n/k \ll 1$ and $e^{k\pi r_c} \gg 1$, we get:

$$N_0 = -\frac{1}{\sqrt{k r_c}} \qquad ; \qquad N_n = \frac{1}{\sqrt{2 k r_c}} \, e^{k\pi r_c} \, J_2(x_n) \, . \tag{2.14}$$

Notice the difference between the $n = 0$ mode and the $n > 0$ modes: for $n = 0$, the wave-function at the IR-brane location $y = \pi$ takes the form

$$\chi^0(y = \pi) = \sqrt{k r_c} \left(1 - e^{-2k\pi r_c} \right) = -\sqrt{r_c} \, \frac{M_5^{3/2}}{\bar{M}_P} \, , \tag{2.15}$$

whereas for $n > 0$:

$$\chi^n(y = \pi) = \sqrt{k r_c} \, e^{k\pi r_c} = \sqrt{r_c} \, e^{k\pi r_c} \frac{M_5^{3/2}}{\bar{M}_P} = \sqrt{r_c} \, \frac{M_5^{3/2}}{\Lambda} \tag{2.16}$$

The important difference can be easily understood by looking at the coupling between the energy-momentum tensor and gravity at the location of the IR-brane:

$$\mathcal{L} = -\frac{1}{M_5^{3/2}} T^{\mu\nu}(x) h_{\mu\nu}(x, y = \pi) = -\frac{1}{M_5^{3/2}} T^{\mu\nu}(x) \sum_{n=0} h^n_{\mu\nu} \frac{\chi^n}{\sqrt{r_c}} \, , \tag{2.17}$$

where the only scale is the fundamental gravitational scale M_5. However, if we separate the $n = 0$ and the $n > 0$ modes we get:

$$\mathcal{L} = -\frac{1}{\bar{M}_P} T^{\mu\nu}(x) h^0_{\mu\nu}(x) - \frac{1}{\Lambda} \sum_{n=1} T^{\mu\nu}(x) h^n_{\mu\nu}(x) \, , \tag{2.18}$$

from which is clear that the coupling between KK-graviton modes with $n \neq 0$ is suppressed by the effective scale Λ and not by the Planck scale.

It is useful to remind here the explicit form of the energy-momentum tensor:

$$T_{\mu\nu} = T^{SM}_{\mu\nu} + T^{DM}_{\mu\nu} \,, \tag{2.19}$$

where

$$\begin{aligned} T^{SM}_{\mu\nu} = &\left[\frac{i}{4}\bar{\psi}(\gamma_\mu D_\nu + \gamma_\nu D_\mu)\psi - \frac{i}{4}(\gamma_\mu D_\nu \bar{\psi}\gamma_\mu + D_\mu \bar{\psi}\gamma_\nu)\psi - \eta_{\mu\nu}(\bar{\psi}\gamma^\mu D_\mu \psi - m_\psi \bar{\psi}\psi) + \right.\\ &\left. + \frac{i}{2}\eta_{\mu\nu}\partial^\rho \bar{\psi}\gamma_\rho \psi\right] + \left[\frac{1}{4}\eta_{\mu\nu}F^{\lambda\rho}F_{\lambda\rho} - F_{\mu\lambda}F^{\lambda}{}_{\nu}\right] + \Big[\eta_{\mu\nu}D^\rho H^\dagger D_\rho H + \eta_{\mu\nu}V(H) + \\ &+ D_\mu H^\dagger D_\nu H + D_\nu H^\dagger D_\mu H\Big] \end{aligned}$$

and

$$T^{DM}_{\mu\nu} = \ (\partial_\mu S)(\partial_\nu S) - \frac{1}{2}\eta_{\mu\nu}(\partial^\rho S)(\partial_\rho S) + \frac{1}{2}\eta_{\mu\nu} m_S^2 S^2 \,, \tag{2.20}$$

where we have introduced the scalar singlet field S to represent the DM particle in our scenario.

Notice that a scalar DM particle will also interact with the SM through the so-called "Higgs portal", namely

$$\mathcal{L}_{\rm DM} \supset \lambda_{hS}(H^\dagger H)(S^\dagger S) \ , \tag{2.21}$$

since this term is always allowed. However, such coupling is strongly constrained (see Sect. 2.3), and we neglect its effect in our analysis.

2.2 Adding the radion

Stabilizing the size of the extra-dimension to be $y = \pi r_c$ is a complicated task. In general (see, e.g., Refs. [27–29]) bosonic quantum loops have a net effect on the border of the extra-dimension such that the extra-dimension itself should shrink to a point. This feature, in a flat extra-dimension, can only be compensated by fermionic quantum loops and, usually, some supersymmetric framework is invoked to stabilize the radius of the extra-dimension (see, e.g., Ref. [30]). In Randall-Sundrum scenarios, on the other hand, a new mechanism has been considered: if we add a bulk scalar field Φ with a scalar potential $V(\Phi)$ and some ad hoc localized potential terms, $\delta(y=0)V_{\rm UV}(\Phi)$ and $\delta(y=\pi r_c)V_{\rm IR}(\Phi)$, it is possible to generate an effective potential $V(\varphi)$ for the four-dimensional field $\varphi = f\,\exp{(-k\pi T)}$ (with $f = \sqrt{24M_5^3/k}$ and $\langle T\rangle = r_c$). The minimum of this potential can yield the desired value of kr_c without extreme fine-tuning of the parameters [25, 31].

As in the spectrum of the theory there is already a scalar field, the graviscalar $G^{(5)}_{55}$, the Φ field will generically mix with it. The KK-tower of the graviscalar is absent from the low-energy spectrum, as they are eaten by the KK-tower of graviphotons to get a mass (due to the spontaneous breaking of translational invariance caused by the presence of one or more branes). On the other hand, the KK-tower of the field Φ is present, but heavy (see Ref. [32]). The only light field present in the spectrum is a combination of the graviscalar zero-mode and the Φ zero-mode. This field is usually called the *radion*, r. Its mass can be obtained from the effective potential $V(\varphi)$ and is given by $m_\varphi^2 = k^2 v_v^2/3M_5^3\,\epsilon^2\,\exp(-2\pi k r_c)$, where v_v is the value of Φ at the visible brane and $\epsilon = m^2/4k^2$ (with m the mass of the field Φ). Quite generally $\epsilon \ll 1$ and, therefore, the mass of the radion can be much smaller than the first KK-graviton mass.

The radion, as for the KK-graviton case, interacts with both the DM and SM particles. It couples with matter through the trace of the energy-momentum tensor T [18]. Massless gauge fields do not contribute to the trace of the energy-momentum tensor, but effective couplings are generated from two different sources: quarks and W boson loops and the trace anomaly [33]. Thus the radion Lagrangian takes the following form [32, 34]:

$$\mathcal{L}_r = \frac{1}{2}(\partial_\mu r)(\partial^\mu r) - \frac{1}{2}m_r^2 r^2 + \frac{1}{\sqrt{6}\Lambda} rT + \frac{\alpha_{EM}\, C_{EM}}{8\pi\sqrt{6}\Lambda} r F_{\mu\nu}F^{\mu\nu} + \frac{\alpha_S C_3}{8\pi\sqrt{6}\Lambda} r \sum_a F^a_{\mu\nu}F^{a\mu\nu} \ , \quad (2.22)$$

where $F_{\mu\nu}, F^a_{\mu\nu}$ are the Maxwell and $SU_c(3)$ Yang-Mills tensors, respectively. The C_3 and C_{EM} constants encode all information about the massless gauge boson contributions and are given in App. B.

2.3 The DM Relic Abundance in the Freeze-Out scenario

Experimental data ranging from astrophysical to cosmological scales point out that a significant fraction of the Universe energy appears in the form of a non-baryonic (*i.e.* electromagnetically inert) matter. This component of the Universe energy density is called *Dark Matter* and, in the cosmological "standard model", the ΛCDM, it is usually assumed to be represented by stable (or long-lived) heavy particles (*i.e.* non-relativistic, or "cold"). Within the thermal freeze-out scenario the DM component is supposed to be in thermal equilibrium with the rest of particles in the Early Universe. The evolution of the dark matter number density $n_{\rm DM}$ in this paradigm is governed by the Boltzmann equation [35]:

$$\frac{dn_{\rm DM}}{dt} = -3H(T)\, n_{\rm DM} - \langle \sigma v \rangle \left[n_{\rm DM}^2 - (n_{\rm DM}^{eq})^2 \right] \ , \quad (2.23)$$

where T is the temperature, $H(T)$ is the Hubble parameter as a function of the temperature, and $n_{\rm DM}^{eq}$ is the DM number density at equilibrium (see, *e.g.*, Ref. [35]). The Boltzmann equation is governed by two factors: one proportional to $H(T)$ and the second to the thermally-averaged cross-section, $\langle \sigma v \rangle$. In order for $n_{\rm DM}(T)$ to freeze-out, as the Universe expanded and cooled down the thermally-averaged annihilation cross-section $\langle \sigma v \rangle$ times the number density should fall below $H(T)$. At that moment, DM decouples from the rest of particles leaving an approximately constant number density in the co-moving frame, called relic abundance.

The experimental value of the relic abundance can be computed starting from the DM density in the ΛCDM model. From Ref. [36] we have $\Omega_{\rm CDM} h^2 = 0.1198 \pm 0.0012$, where h parametrizes the present Hubble parameter. Solving eq. (2.23), it can be found the thermally-averaged cross-section at freeze-out $\langle \sigma_{\rm FO}\, v \rangle = 2.2 \times 10^{-26}$ cm^3/s [37]. Notice that for $m_{\rm DM} > 10$ GeV, the relic abundance is insensitive to the value of $m_{\rm DM}$ and therefore the thermally-averaged annihilation cross section $\sigma_{\rm FO}$ needed to obtain the correct relic abundance is not a function of the DM particle mass.

When comparing the prediction of a given model to the expectation in the freeze-out scenario, the key parameter to compute the relic abundance is, thus, $\langle \sigma v \rangle$. In order to obtain this quantity, we must first calculate the total annihilation cross-section of the DM particles (represented in our case by the field S):

$$\sigma_{\rm th} = \sum_{\rm SM} \sigma_{\rm ve}(S\,S \to {\rm SM\,SM}) + \sum_{n=1} \sum_{m=1} \sigma_{GG}(S\,S \to G_n\,G_m) + \sigma_{rr}(S\,S \to r\,r)\,, \tag{2.24}$$

where in the first term, $\sigma_{\rm ve}$ ("ve" stands for "virtual exchange"), we sum over all SM particles. The second term, σ_{GG}, corresponds to DM annihilation into a pair of KK-gravitons, $G_n\,G_m$. Eventually, the third term, σ_{rr}, corresponds to DM annihilation into radions.

If the DM mass m_S is smaller than the mass of the first KK-graviton and of the radion, only the first channel exists. Since in the freeze-out paradigm the DM particles have small relative velocity v when the freeze-out occurs, it is useful to approximate the c.o.m. energy s as $s \sim 4m_S^2$, and keep only the leading order in the so-called *velocity expansion.* Formulæ for the DM annihilation into SM particles within this approximation are given in App. D.

Notice that DM annihilation to SM particles can occur through three possible mediators: the Higgs boson, the KK-tower of gravitons and the radion. The first option, that depends on the coupling introduced in eq. (2.21), has been extensively studied. Current bounds (see for instance [38, 39] for recent analyses) rule out DM masses $m_S \lesssim 500$ GeV (except for the Higgs-funnel region, $m_S \simeq m_h/2$) and future direct detection experiments such as LZ [40] will either find DM or exclude larger masses, up to $\mathcal{O}$(TeV). In the presence of other annihilation channels, as in our case, if LZ does not get any positive signal of DM it will lead to a stringent limit on the Higgs portal coupling λ_{hS}, so that the Higgs boson contribution to DM annihilation into SM particles will be negligible for DM masses at the TeV scale [39, 41]. In the rest of the paper, we will assume that λ_{hS} is small enough so as to be irrelevant in our analysis, and we will not consider this channel any further.

On the other hand, depending on the particular values for the radion mass (determined by the specific features of the bulk and localized scalar potentials) and the KK-graviton masses (fixed by k, M_5 and r_c), radion or KK-graviton exchange can dominate the annihilation amplitude. When computing the contribution of the radion and KK-graviton exchange to the DM annihilation cross-section into SM particles, it is of the uttermost importance to take into account properly the decay width of the radion and of the KK-gravitons, respectively [1]. Notice that the DM annihilation cross-section into SM particles via virtual exchange of KK gravitons is velocity suppressed (d wave), due to the spin 2 of the mediators, while the corresponding one through virtual radion is s wave.

Within the Goldberger-Wise stabilization mechanism, the radion is expected to be lighter than the first KK-graviton mode, so the next channel to open is usually the DM annihilation into radions. The analytic expression for $\sigma_{rr}(S\,S \to r\,r)$ in the approximation $s \sim 4m_S^2$ is given in App. D. It is also s wave.

[1]In the case of the KK-gravitons, due to the breaking of translational invariance in the extra-dimension, the KK-number is not conserved and heavy KK-graviton modes can also decay into lighter KK-gravitons when kinematically allowed. Formulæ for the radion and KK-graviton decays are given in App. C.

Eventually, for DM masses larger than the mass of the first KK-graviton mode, annihilation of DM particles into KK-gravitons becomes possible and the last channel in eq. (2.24) opens. As the KK-number is not conserved due to the presence of the branes in the extra-dimension (that breaks explicitly momentum conservation in the 5th-dimension), any combination of KK-graviton modes is possible when kinematically allowed. Therefore, we must sum over all the modes as long as the condition $2m_S \geq m_{G_n} + m_{G_m}$ is fulfilled. The analytic expression for $\sigma_{GG}(S\,S \to G_n\,G_m)$ at leading order in the velocity expansion is also given in App. D, and it turns out to be s wave as well. Notice that we will not take into account annihilation into zero-modes gravitons, $G_0\,G_0$ or $G_0\,G_n$, as these channels are Planck-suppressed with respect to the production of a pair of massive KK-graviton modes, $G_n\,G_m$.

As the *velocity expansion* approximation may fail in the neighbourghood of resonances and, in the RS model, the virtual graviton exchange cross-section is indeed the result of an infinite sum of KK-graviton modes, we computed the analytical value of $\langle\sigma v\rangle$ using the exact expression from Ref. [42]:

$$\langle\sigma v\rangle = \frac{1}{8m_S^4 T K_2^2(x)} \int_{4m_S^2}^{\infty} ds (s - 4m_S^2)\, \sqrt{s}\, \sigma(s)\, K_1\left(\frac{\sqrt{s}}{T}\right) , \tag{2.25}$$

where K_1 and K_2 are the modified Bessel functions and v is the relative (Møller) velocity of the DM particles.

3 Scalar DM annihilation cross-section in RS

For relatively low DM mass the only open annihilation channel is into SM particles through KK-graviton or radion exchange. Direct production of radions or KK-gravitons in the final state becomes allowed for DM mass $m_S \geq m_{G_1}, m_r$, where m_S and m_{G_1} are the DM and the first KK-graviton masses, respectively.

3.1 Virtual KK-graviton exchange and on-shell KK-graviton production

We plot in Fig. 1 the different KK-graviton contributions to $\langle\sigma v\rangle$ separately, so as to understand clearly the main features.

We consider first the case of DM annihilation into SM particles through KK-graviton exchange, summed over all virtual KK-gravitons, $\sigma_{\text{ve},G}$. This result is shown by the solid (purple) line in Fig. 1 as a function of the DM mass m_S, for the particular choice $\Lambda = 100$ TeV and $m_{G_1} = 1$ TeV. When the DM particle mass is nearly half of one of the KK-graviton masses, $s = 4m_S^2 \sim m_{G_n}^2$, the resonant contribution dominates the cross-section, which abruptly increases. At each of the resonances, $\langle\sigma v\rangle$ depends only marginally on the DM mass m_S and, therefore, we have an approximately constant thermally-averaged maximal cross-section (a small m_S-dependence arises only at very large values of m_S). This contribution was studied in detail in Ref. [21], where it was shown that the resonant enhancement of the cross-section for $m_S \sim m_{G_n}/2$ was not enough to achieve the value of $\langle\sigma_{\text{FO}} v\rangle$ that gives the correct relic abundance, once values of Λ compatible with LHC exclusion bounds were taken into account.

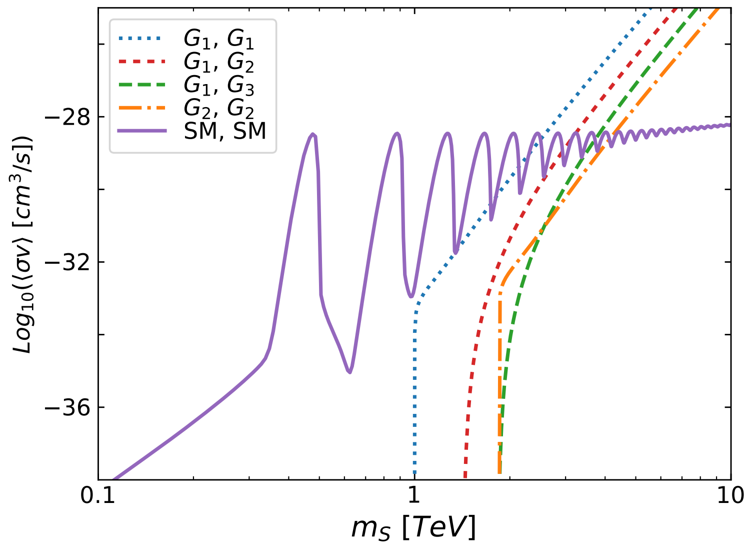

Figure 1. *Contributions to the scalar DM annihilation cross-section due to KK-gravitons, for $\Lambda = 100$ TeV and $m_{G_1} = 1$ TeV, as a function of the DM mass m_S. The solid purple line corresponds to the DM annihilation into SM particles through virtual KK-graviton exchange, $\sigma_{\rm ve,G}$. The non-solid lines correspond to DM annihilation into two KK-gravitons, σ_{GG}: from left to right $SS \to (G_1, G_1), (G_1, G_2), (G_2, G_2)$ and (G_1, G_3), respectively.*

On the other hand, for $m_S \geq m_{G_1}$ DM annihilation into on-shell KK-gravitons becomes possible. Depending on the DM particle mass, production of several KK-graviton modes is allowed. This is represented in Fig. 1 by dashed or dot-dashed lines, where we show the contribution to the DM annihilation cross-section from the channels $SS \to (G_1\,G_1), (G_1\,G_2), (G_2\,G_2)$ and $(G_1\,G_3)$. More channels open for larger values of m_S that however have not been depicted in Fig. 1, where we have decided to show just the lowest-lying ones for the sake of clarity of the plot. Recall that each of the two KK-gravitons can have any KK-number: in particular, it is not forbidden by any symmetry to have $SS \to G_n\,G_m$ with $n \neq m$, as translational invariance in the 5th-dimension is explicitly broken due to the presence of the IR- and UV-branes and the KK-number is not conserved. As it can be seen in the Figure, the contribution of each channel to the total cross-section varies with the DM mass. For example, $SS \to G_2\,G_2$ (orange, dot-dashed line) dominates over $SS \to G_1\,G_3$ (green, dashed line) in a very small range of m_S, whereas the latter takes over for large m_S. Notice that, although KK-graviton production was considered in Ref. [18], the possibility of producing different KK-graviton modes was overlooked there.

In Fig. 2 (left panel) we plot the different Feynman diagrams that contribute to DM annihilation into on-shell KK-gravitons. Diagram (c) was not considered previously in the literature (see, *e.g.*, Ref. [18]). However, it must be taken into account when computing the production of two real gravitons, as the corresponding amplitude is also proportional

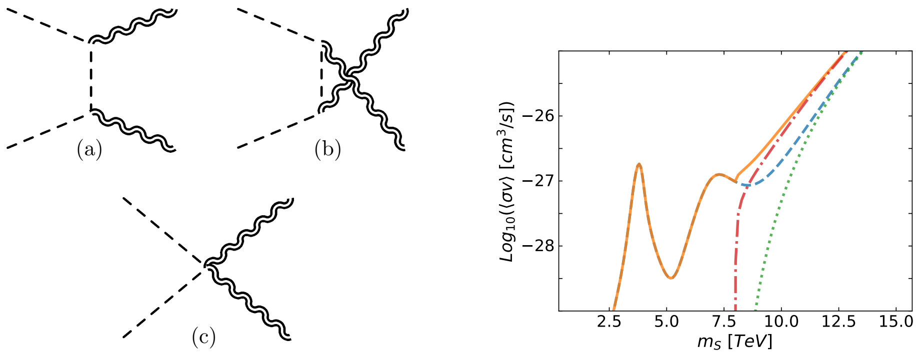

Figure 2. *Left panel: Feynman diagrams corresponding to the different amplitudes that contribute to scalar DM annihilation into two on-shell KK-gravitons at $\mathcal{O}(1/\Lambda^2)$. Diagrams (a) and (b): t- and u-channel DM exchange. Diagram (c): second order expansion of the metric in eq. (2.7). Right panel: Relevance of overlooked contributions to the scalar DM annihilation cross-section for $\Lambda = 10$ TeV and $m_{G_1} = 8$ TeV, as a function of the DM mass m_S. The solid orange (blue dashed) line corresponds to the DM annihilation cross-section through and into KK-gravitons with (without) the contribution to the amplitude from diagram (c). The dot-dashed red (dotted green) line is the DM annihilation cross-section into KK-gravitons, only, with (without) the contribution from diagram (c).*

to $1/\Lambda^2$, the same order as the two other diagrams[2]. The corresponding Feynman rule can be obtained by expanding the metric up to second order about the Minkowski space-time:

$$\mathcal{L} \supset -\frac{1}{2\Lambda^2} \sum_{n=1} T^{\mu\nu}(x) \left(h^{(n)}_{\mu\alpha}(x) h^{(n)}_{\beta\nu}(x) \eta^{\alpha\beta} + h^{(n)}_{\mu\nu}(x) h^{(n)}_{\alpha\beta}(x) \eta^{\alpha\beta} \right) . \tag{3.1}$$

Notice that, if a diagram that should be considered at a given order in $1/\Lambda$ when computing a given process is absent, then the gravitational gauge-invariance of the amplitude is not guaranteed and the cross-section computation is built over slippery ground from a theoretical point of view. The impact of diagram (c) is shown in Fig. 2 (right panel), where we compare the total DM annihilation cross-section through and into KK-gravitons including or not the contribution to the amplitude from this diagram, for a particular choice of $m_{G_1} = 8$ TeV and $\Lambda = 10$ TeV. The solid orange (blue dashed) line is the total DM annihilation cross-section through and into KK-gravitons with (without) diagram (c), whereas the dot-dashed red (dotted green) line is the DM annihilation cross-section into KK-gravitons with (without) diagram (c). It can be seen that, for this particular choice of m_{G_1} and Λ, the difference between the two computations can be as large a one order of magnitude for $m_S \sim 10$ TeV.

In Fig. 3 we eventually show the total contribution of KK-gravitons to $\langle\sigma v\rangle$, summing virtual KK-graviton exchange and KK-graviton direct production with contributions from

[2]Notice that on-shell KK-graviton production through KK-graviton exchange in s-channel only appears when expanding the metric in eq. (2.7) up to third order and, therefore, the corresponding amplitude is suppressed by $1/\Lambda^4$.

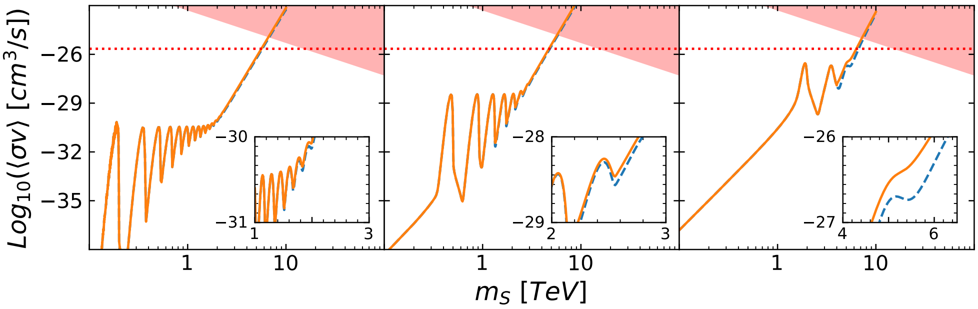

Figure 3. *The thermally-averaged scalar DM annihilation cross-section through virtual KK-graviton exchange and direct production of two KK-gravitons, $\sigma_G = \sigma_{\text{ve},G} + \sigma_{GG}$, as a function of the DM mass m_S. In all panels, the solid orange (blue dashed) lines represent the total cross-section including (not including) mixed KK-graviton production and diagram (c) contribution. The latter case corresponds to Refs. [18] and [21]. In order to appreciate the difference, we have included in all panels a zoomed plot in linear scale for the range of m_S of interest. Left panel: $\Lambda = 1000$ TeV, $m_{G_1} = 400$ GeV; middle panel: $\Lambda = 100$ TeV, $m_{G_1} = 1$ TeV; right panel: $\Lambda = 10$ TeV, $m_{G_1} = 4$ TeV.*

the three diagrams in Fig. 2, $\sigma_G = \sigma_{\text{ve},G} + \sigma_{GG}$. We consider three particular choices of Λ and m_{G_1}: $\Lambda = 1000$ TeV, $m_{G_1} = 400$ GeV (left); $\Lambda = 100$ TeV, $m_{G_1} = 1$ TeV (middle) and $\Lambda = 10$ TeV, $m_{G_1} = 4$ TeV (right). Our result for $\langle\sigma_G v\rangle$ is depicted by the solid (orange) line, and it is compared with the results shown in the literature (in Refs. [18] and [21]), represented by the dashed (blue) line. As it can be seen, our results and those in the literature coincide, but for some small differences at large DM masses, $m_S \in [1, 6]$ TeV, a range shown in the zoomed panel in linear scale. The net effect of mixed KK-gravitons channels and of diagram (c) in Fig. 2 is an increase of the cross-section, that can be as large as a factor two for some specific choices of Λ and m_{G_1}. In all panels, the horizontal red dashed line corresponds to the value of the thermally-averaged cross-section for which the correct relic abundance is achieved, $\langle\sigma_{\text{FO}} v\rangle = 2.2 \times 10^{-26}$ cm^3/s. As it was reported in Ref. [21], $\langle\sigma_{\text{FO}} v\rangle$ is not achievable through KK-graviton exchange since, even for values of m_S such that $s \sim m_{G_n}^2$, the resonant cross-section is way smaller than the required one. This result is general and can be found for any value of Λ and m_{G_n}, not only for the few examples shown in Fig. 3. On the other hand, as reported in Ref. [18], for larger values of m_S, when the two on-shell KK-graviton production channels take over, a cross-section as large as $\langle\sigma_{\text{FO}} v\rangle$ is achievable and the correct relic abundance can be then reproduced. With respect to Ref. [18], the net effect of mixed KK-gravitons production and of diagram (c) is to lower slightly the value of m_S for which $\langle\sigma v\rangle = \langle\sigma_{\text{FO}} v\rangle$. In Fig. 3, the red-shaded area represents the theoretical unitarity bound $\langle\sigma v\rangle \geq 1/s$, where we can no longer trust the theory outlined in Sec.2 and higher-order operators should be taken into account. Notice that, even if in Fig. 3 the "untrustable" region seems to be very near to the value of m_S for which the correct relic abundance can be achieved, it is indeed at least one order of magnitude away, as plots are shown in bi-logarithmic scale.

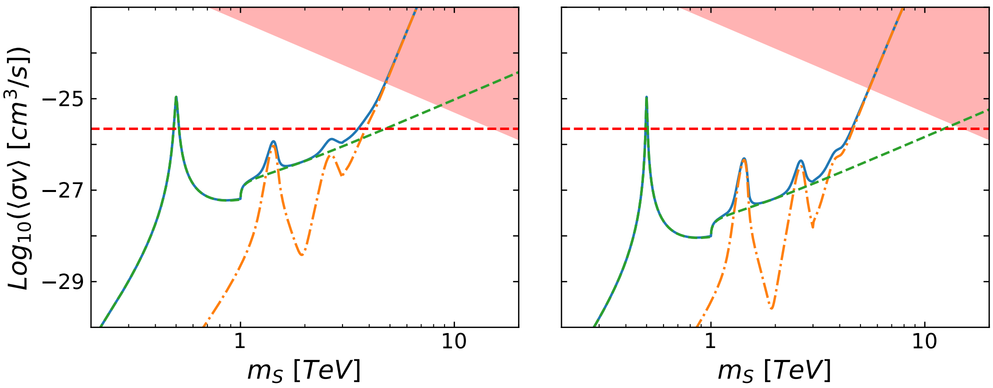

Figure 4. *The thermally-averaged scalar DM annihilation cross-section through virtual radion exchange and direct production of two radions,* $\sigma_r = \sigma_{\mathrm{ve},r} + \sigma_{rr}$ *(green, dashed line), as a function of the DM mass* m_S*, compared with the corresponding cross-section through KK-graviton exchange and production,* σ_G *(orange, dot-dashed line). The sum of the two cross-sections,* $\sigma_r + \sigma_G$*, is represented by the (blue) solid line. Left panel:* $\Lambda = 5$ *TeV,* $m_{G_1} = 3$ *TeV and* $m_r = 1$ *TeV; Right panel:* $\Lambda = 8$ *TeV,* $m_{G_1} = 3$ *TeV and* $m_r = 1$ *TeV.*

3.2 Virtual radion exchange and on-shell radion production

Consider now the case of DM annihilation into SM particles through radion exchange and of direct production of two on-shell radions,

$$\sigma_r = \sigma_{\mathrm{ve},r}(S\,S \to \mathrm{SM\,SM}) + \sigma_{rr}(S\,S \to r\,r)\,. \tag{3.2}$$

The analytic expressions for the two relevant radion channels contributing to σ_r can be found in App. D.2, whereas in App. C.2 we give the radion partial decay widths. It can be seen that radion decay to fermions is proportional to the fermion mass squared, $\Gamma(r \to \psi\,\psi) \propto m_r m_\psi^2/\Lambda^2$, whilst radion decay to bosons (either scalar or vector ones) is $\Gamma(r \to B\,B) \propto m_r^3/\Lambda^2$. Clearly, for radions with $\mathcal{O}(\mathrm{TeV})$ mass bosons decay channels dominate over fermion ones. However, the decay to massive or massless bosons is rather different: the radion decays to photons and gluons at the one-loop level and, therefore, these decay channels are suppressed with respect to decays into massive bosons, which proceed at tree level. In summary, the radion decay width is dominated by $r \to WW, r \to ZZ$ and $r \to HH$ (and $r \to SS$ if kinematically possible).

The two contributions to σ_r are shown in Fig. 4, where we plot σ_r (green, dashed line) as a function of m_S and compare it with σ_G (orange, dot-dashed line). The sum of σ_r and σ_G is represented by the solid (blue) line. The input parameters for these plots are: $m_{G_1} = 3$ TeV and $m_r = 1$ TeV; $\Lambda = 5$ TeV (left panel) and $\Lambda = 8$ TeV (right panel). For these particular choices of m_{G_1}, only a couple of KK-graviton resonances appear in σ_G before two KK-graviton production takes over. Again, the red-shaded area represents the theoretical unitarity bound $\langle\sigma v\rangle \geq 1/s$, where we can no longer trust the theory outlined in Sec.2, whilst the red dashed horizontal line is $\langle\sigma_{\rm FO} v\rangle$. We can see that, generically and differently from the KK-graviton case, the correct relic abundance can be achieved by the resonant virtual radion exchange channel for DM masses around $m_S \sim m_r/2\left[1+\mathcal{O}\left(m_r^2/\Lambda^2\right)\right]$. Since the radion decay width is rather small, for allowed values of Λ and radion masses in the TeV range or below, a significant amount of fine-tuning is needed in order to get the resonant behaviour. In the absence of a theoretical framework to explain the specific required relation between m_S and m_r, we consider difficult to defend this possibility as an appealing scenario to achieve the observed DM relic abundance. On the other hand, as it was the case for the KK-graviton exchange and production shown in Fig. 3, the target value of $\langle\sigma v\rangle$ can be achieved also in the range of DM masses for which radion and/or KK-graviton production dominate the cross-section. For the specific values of m_{G_1}, m_r and Λ shown in Fig. 4 this occurs through KK-graviton production. We have found that this channel dominates in most of the allowed parameter space, while the contribution of radion production is dominant only near the untrustable region $m_{G_1} \sim \Lambda$.

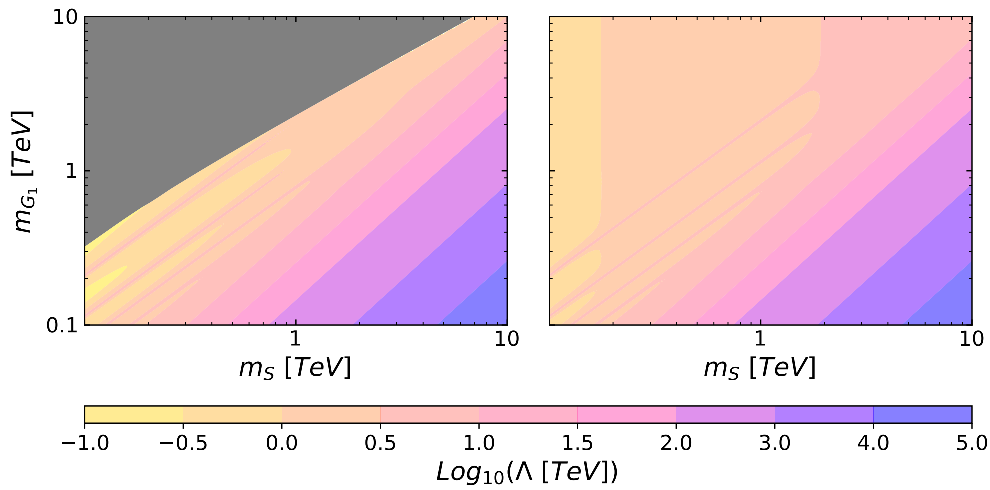

Figure 5. *Values of Λ for which the correct DM relic abundance is obtained in the plane (m_S, m_{G_1}). Left panel: the extra-dimension length is stabilized without using the radion; Right panel: the extra-dimension length is stabilized using the Goldberger-Wise mechanism, with a radion mass $m_r = 100$ GeV. The required Λ ranges from 100 GeV to 10^5 TeV, as shown by the color legend.*

In Fig. 5 we show the values of Λ for which the correct DM relic abundance is obtained in the (m_S, m_{G_1}) plane. In the left panel we assume that the extra-dimension length is stabilized without introducing the radion field. We can see that $\langle\sigma_{\rm FO} v\rangle$ can be achieved in a significant part of the parameter space through KK-graviton production. In order to obtain the target relic abundance $\langle\sigma_{\rm FO} v\rangle$ for $m_S < m_{G_1}$, small values of Λ are needed, usually excluded by LHC data (as we will see in the next section). Eventually, resonant virtual KK-graviton exchange is not enough to achieve $\langle\sigma_{\rm FO} v\rangle$ for $m_S \ll m_{G_1}$ for any value of Λ, as it is depicted by the grey region (in agreement with Ref. [21]).

In the right panel we consider, instead, that the extra-dimension length is stabilized using the Goldberger-Wise mechanism and we introduce a radion with mass $m_r = 100$ GeV. In this case, it is always possible to achieve the correct relic abundance: either through resonant radion exchange for $m_S \sim 50$ GeV (not shown in the plot), through radion production in the region $m_S \leq m_{G_1}$ or, for $m_S > m_{G_1}$, through KK-graviton production.

4 Experimental bounds and theoretical constraints

As we have seen in Fig. 5, in principle the target relic abundance can be achieved in a vast region of the (m_S, m_{G_1}) parameter space, for Λ ranging from 10^{-1} TeV to 10^5 TeV. However, experimental searches for resonances strongly constrain m_{G_1} and Λ. We will summarize here the relevant experimental bounds and see how only a relatively small region of the parameter space is indeed allowed.

4.1 LHC bounds

The strongest constraints are given by the resonance searches at LHC. In our model we have considered two types of particles that could be resonantly produced at the LHC, the KK-gravitons and the radion. In order to quantify the impact of LHC data in our parameter space, first of all we need to compute their production cross-section at the LHC.

The n-th KK-graviton production cross-section at LHC is given by [43]:

$$\sigma_{pp\to G_n}(m_{G_n}) = \frac{\pi}{48\Lambda^2}\left[3\mathcal{L}_{gg}(m^2_{G_n}) + 4\sum_q \mathcal{L}_{q\bar{q}}(m^2_{G_n})\right] , \tag{4.1}$$

with

$$\mathcal{L}_{ij}(\hat{s}) = \frac{\hat{s}}{s}\int_{\hat{s}/s}^1 \frac{dx}{x} f_i(x) f_j\left(\frac{\hat{s}}{xs}\right) . \tag{4.2}$$

In our calculations we use the Parton Distribution Functions (PDF's) $f_i(x)$ at $Q^2 = m^2_{G_n}$ obtained from MSTW2008 at leading-order [44].

Regarding the radion, since the $\bar{q}\,q\,r$ vertex is proportional to the corresponding quark mass, the production cross-section in $p\,p$ collisions at the LHC is dominated by gluon fusion. The gluon-radion interaction is similar to the gluon-Higgs interaction in the SM. We therefore may use the well-known results obtained for the SM Higgs production [45] rescaling the Lagrangian by a factor $3vC_3/(2\sqrt{6}\Lambda)$, where v is the standard model VEV. The final expression is given by:

$$\sigma_{pp\to r}(m_r) = \frac{\alpha_s^2 C_3^2}{1536\pi\Lambda^2}\mathcal{L}_{gg}(m_r^2) . \tag{4.3}$$

In Fig. 6 we show the production cross-sections for $\Lambda = 5$ TeV at $\sqrt{s} = 13$ TeV, where the solid (orange) line stands for $p\,p \to G_1$ and the dashed (purple) line for $p\,p \to r$. It is straightforward to obtain the production cross-sections for a different value of Λ by rescaling this plot. As we can see, the radion production is smaller than graviton production by some orders of magnitude. For this reason, the LHC constraints on the Randall-Sundrum model are dominated by (resonant) KK-graviton searches.

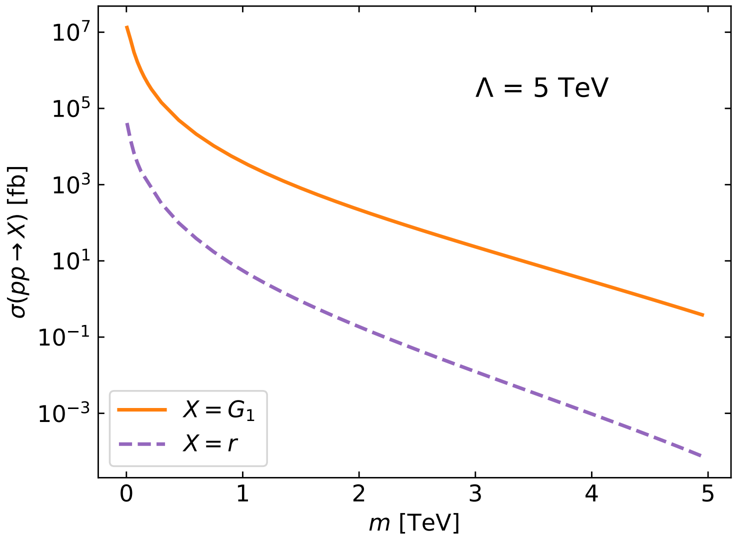

Figure 6. *Theoretical KK-graviton and radion production cross-section at the LHC with* $\sqrt{s} = 13$ *TeV for* $\Lambda = 5$ *TeV.*

The KK-graviton decay channels that provide the stringest bounds on m_{G_1} and Λ are $G_1 \to \gamma\gamma$ [46] and $G_1 \to \ell\ell$ [47]. In Fig. 7 we plot the functional dependence over Λ and m_{G_1} of the cross-section $pp \to \ell\ell$, with $\sigma \times \text{BR}(G_1 \to \ell\ell)$ ranging from 10^2 fb (bottom line) to 10^{-3} fb (top line). Comparing the theoretical expectation with the experimental bounds on $\sigma(pp \to \ell\ell)$ it is possible to draw exclusion regions in the (m_{G_1}, Λ) plane, given by the darker (blue) shaded area. The same can be done using the channel $pp \to \gamma\gamma$, represented by the lighter (light red) shaded area. We can see that the stringest bounds on Λ are set by $pp \to G_1 \to \gamma\gamma$. Notice that experimental exclusion bounds are given for $m_{G_1} \geq 200$ GeV, approximately.

In Fig. 8 we show the statistical uncertainties on the experimental bound on $\sigma(pp \to \ell\ell)$ (left panel) and $\sigma(pp \to \gamma\gamma)$ (right panel), where the yellow and green bands are the bounds at 1σ and 2σ in the (m_{G_1}, Λ) plane, respectively. It can be seen that for low KK-graviton mass the bounds on Λ suffer from a large indetermination: in this range we can only say that Λ should be larger than some value ranging from 50 to 100 TeV, approximately.

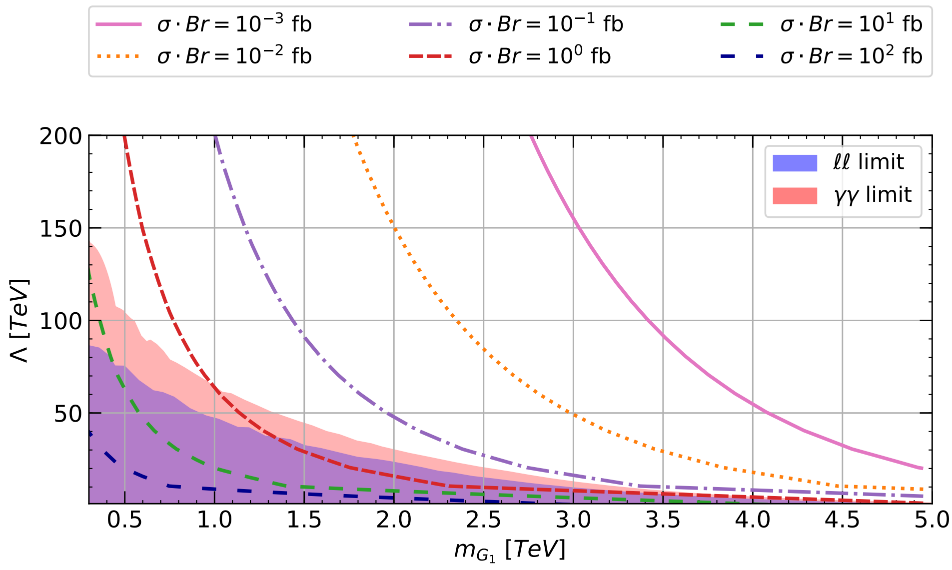

Figure 7. *The exclusion region in the (m_{G_1}, Λ) plane at the LHC Run II with $\sqrt{s} = 13$ TeV and 36 fb^{-1} through resonant production of KK-graviton eventually decaying into leptons (light blue) and photons (light red), from Refs. [46] and [47]. The dashed lines correspond to the functional relation between Λ and m_{G_1} for values of $\sigma(pp \to G_1) \times \mathrm{BR}(G_1 \to \ell\,\ell)$ ranging from 10^2 fb (bottom line) to 10^{-3} fb (top line) as in the legend.*

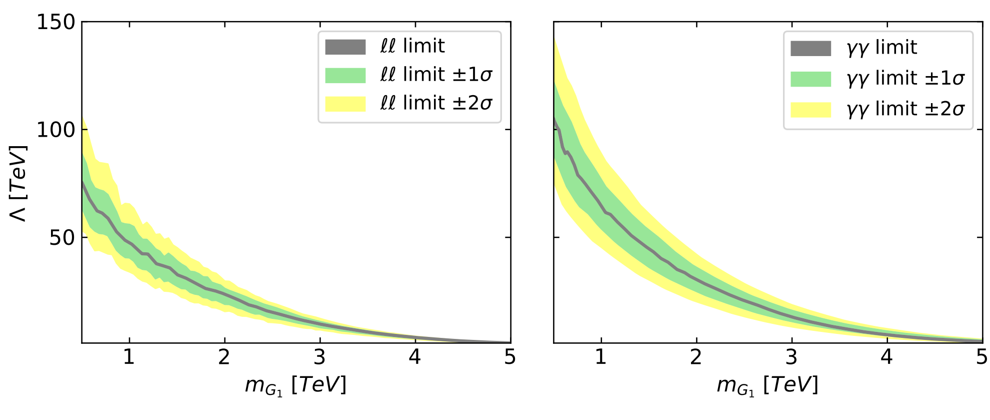

Figure 8. *Bounds over Λ as a function of m_{G_1} from the LHC with $\sqrt{s} = 13$ TeV and 36 fm^{-1}, from Refs. [46] and [47]. Red and blue lines represent the 1σ and 2σ error on the constraint, respectively. The resonance (to be understood as the first KK-graviton mode) eventually decays into leptons (left panel) or into photons (right panel).*

4.2 Direct and Indirect Dark Matter Detection

The total cross-section for spin-independent elastic scattering between dark matter and nuclei reads [24]:

$$\sigma^{\rm SI}_{{\rm DM}-p} = \left[\frac{m_p\, m_S}{A\pi(m_S+m_p)}\right]^2 \left[A f_p^S + (A-Z) f_n^S\right]^2 \ , \tag{4.4}$$

where m_p is the proton mass, while Z and A are the number of protons and the atomic number. The nucleon form factors are given by

$$\begin{cases} f_p^{\rm DM} = \frac{m_S\, m_p}{4 m_{G_1}^2\, \Lambda^2} \left\{ \sum_{q=u,c,d,b,s} 3\left[q(2)+\bar{q}(2)\right] + \sum_{q=u,d,s} \frac{1}{3} f^p_{Tq} \right\} \ , \\ \\ f_n^{\rm DM} = \frac{m_S\, m_p}{4 m_{G_1}^2\, \Lambda^2} \left\{ \sum_{q=u,c,d,b,s} 3\left[q(2)+\bar{q}(2)\right] + \sum_{q=u,d,s} \frac{1}{3} f^n_{Tq} \right\} \ , \end{cases} \tag{4.5}$$

with $q(2)$ the second moment of the quark distribution function

$$q(2) = \int_0^1 dx\; x\; f_q(x) \tag{4.6}$$

and $f^{N=p,n}_{Tq}$ the mass fraction of light quarks in a nucleon: $f^p_{Tu} = 0.023$, $f^p_{Td} = 0.032$ and $f^p_{Ts} = 0.020$ for a proton and $f^n_{Tu} = 0.017$, $f^n_{Td} = 0.041$ and $f^n_{Ts} = 0.020$ for a neutron [48]. The strongest bounds from Direct Detection (DD) Dark Matter searches are found at XENON1T, which uses as target mass ^{129}Xe, ($Z = 54$ and $A - Z = 75$). In order to compute the second moment of the PDF's we have used Ref. [44] and the exclusion curve of XENON1T [49] to set constraints on the (m_S, m_{G_1}, Λ) parameter space. Our results are shown in Fig. 9, where we depict the DD bounds in the (m_S, Λ) plane for two values of m_{G_1}, $m_{G_1} = 250$ GeV (left panel) and $m_{G_1} = 400$ GeV (right panel). Also shown is the dependence of the value of Λ required to achieve the observed relic abundance, $\Lambda_{\rm FO}$, as a function of the scalar DM mass m_S. The resonant behaviour of $\Lambda_{\rm FO}$ for different values of m_S shows that, for low values of m_S and m_{G_1}, the cross-section is dominated by virtual KK-graviton exchange. For larger values of m_S at fixed m_{G_1} production of KK-gravitons takes over and $\Lambda_{\rm FO}$ grows smoothly with m_S. The region of the parameter space excluded by DD experiments is represented by the green-shaded area at the bottom of the two plots. Due to the fact that in the excluded region the dominant channel to achieve $\langle\sigma_{\rm FO} v\rangle$ is KK-graviton virtual exchange, the exclusion bounds will show a characteristic striped pattern (as it will be shown in Fig. 10). We have found, however, that constraints from DD experiments are always much weaker than those obtained at the LHC.

Regarding DM indirect searches, there are several experiments looking for astrophysical signals: for instance, the Fermi-LAT collaboration has analyzed the gamma ray flux arriving at the Earth from Dwarf spheroidal galaxies [50] and the galactic center [51, 52], while AMS-02 has reported data about the positrons [53] and antiprotons [54] coming from the center of the galaxy. These results are relevant for DM models that generate a continuum spectra of different SM particles, such as the RS scenario we are considering. Recall that DM annihilation into a pair of SM particles via KK-graviton exchange is d-wave–suppressed and, therefore, only the annihilation channels into either KK-gravitons or

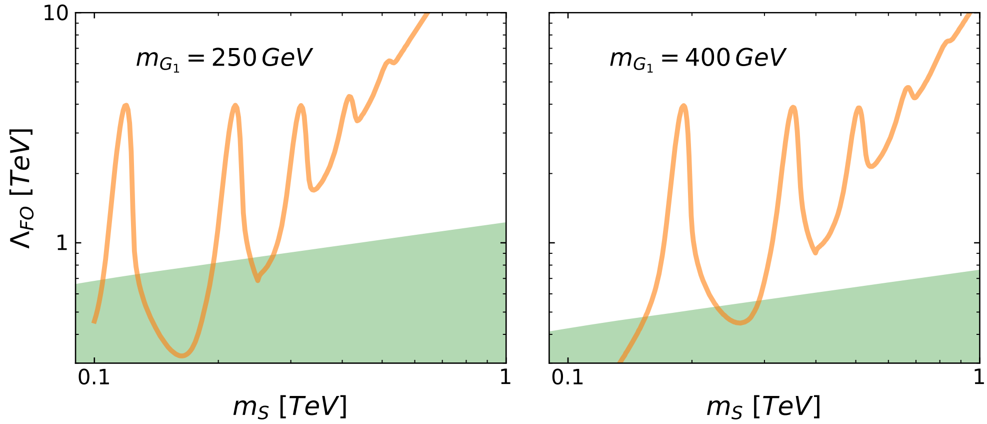

Figure 9. *The DD bounds in the (m_S, Λ) plane for two values of m_{G_1}, represented by the green-shaded area. Also shown is the dependence of $\Lambda_{\rm FO}$ on the scalar DM mass m_S for fixed m_{G_1}, being $\Lambda_{\rm FO}$ the value of Λ for which the freeze-out thermally-averaged cross-section $\langle \sigma_{\rm FO} v \rangle$ is achieved for the chosen values of m_S and m_{G_1}. Left panel: $m_{G_1} = 250$ GeV; Right panel: $m_{G_1} = 400$ GeV.*

radions lead to observable signals. Both of them will then decay into SM particles leading to a continuum spectrum [3]. However, current data from indirect detection experiments allows to constrain DM masses below ~ 100 GeV (provided the annihilation cross-section is not velocity suppressed), while for our case of heavy DM (~ 1 TeV) the limits on the cross-section are well above the required value $\langle \sigma_{\rm FO} v \rangle$. Thus, indirect searches have no impact on the viable parameter space (see however Ref. [19] for other DM scenarios based on RS).

4.3 Theoretical constraints

Besides the experimental limits, there are mainly two theoretical concerns about the validity of our calculations which affect part of the (m_S, m_{G_1}, Λ) parameter space. The first one is related to the fact that we are performing just a tree-level computation of the relevant DM annihilation cross-sections, and we should worry about unitarity issues. In particular, the t-channel annihilation cross-section into a pair of KK-gravitons, $\sigma(SS \to G_n G_m)$, diverges as $m_S^8/(m_{G_n}^4 m_{G_m}^4)$ in the non-relativistic limit $s \simeq m_S^2$, so it is important to check that the effective theory is still unitary. We estimate the unitarity bound as $\sigma < 1/s \simeq 1/m_S^2$, showing as a green-meshed area in Fig. 10 the region in which such bound is not satisfied and therefore our calculation is not fully reliable.

The second theoretical issue refers to the consistency of the effective theory framework: in the Randall-Sundrum scenario, at energies somewhat larger than Λ the KK-gravitons are strongly coupled and the five-dimensional field theory from which we start is no longer valid. We therefore impose that at least $m_{G_1} < \Lambda$ to trust our results[4]. Notice that this

[3]We disregard the fine-tuned possibility of achieving the target DM relic density via resonant radion exchange, as discussed in SSec.ec. 5.

[4]We will see that, in the allowed region, also the relation $m_S < \Lambda$ is fulfilled.

constraint is general for any effective field theory: since we are including the first KK-gravitons in the low energy spectra, for the effective theory to make sense the cut-off scale Λ should be larger than the masses of such states.

5 Achieving the DM relic abundance in RS

We show in this section the allowed parameter space for which the target value of $\langle \sigma v \rangle$ needed to achieve the correct DM relic abundance in the freeze-out scenario, ($\langle \sigma_{\rm FO} v \rangle = 2.2 \times 10^{-26}$ cm^3/s) can be obtained, taking into account both the experimental bounds and the theoretical constraints outlined in Sec. 4.

Our final results are shown in Fig. 10, where we draw the allowed regions of the (m_S, m_{G_1}) plane for which $\langle \sigma v \rangle = \langle \sigma_{\rm FO} v \rangle$. In the left panel, we are agnostic about the extra-dimension length stabilization mechanism, and assume that neither the unspecified mechanism nor the radion have an impact on the DM phenomenology, as would be the case for instance if all the new particles in this sector are heavier than the TeV scale; in the right panel, we take into account the radion and consider the Goldberger-Wise mechanism to stabilize the extra-dimension length. The radion mass in this case can be somewhat smaller than the TeV scale (see Sec. 2.2), and therefore it can be relevant for DM annihilation, as we will discuss below. We show our findings for $m_r = 100$ GeV, but other values of m_r lead to similar results. As a guidance, the dashed lines taken from Fig. 5 represent the values of Λ needed to achieve the relic abundance in a particular point of the (m_S, m_{G_1}) plane. The color legend for the two plots is given in the Figure caption.

5.1 KK-graviton contributions

Let's consider first the case in which the relic abundance is obtained through virtual KK-graviton exchange and/or on-shell KK-graviton production (left panel). We can distinguish two regions of the parameter space:

1. $m_{G_1} > m_S$
   In this regime the DM annihilates via KK-graviton exchange to SM particles, only. As we have seen in Fig. 1, the annihilation cross-section is rather small. The grey shaded area in the plot represents the region of the (m_S, m_{G_1}) plane for which it is not possible to get $\langle \sigma_{\rm FO} v \rangle$. Below this region, in principle we could find a value of Λ low enough to reach the target relic abundance via resonant KK-graviton exchange. This is, however, in conflict with exclusion bounds in the (m_{G_1}, Λ) plane from LHC (see Fig. 7), represented by the darkest (blue) shaded area In addition to the stringent LHC Run II bounds, if the Λ needed to achieve $\langle \sigma_{\rm FO} v \rangle$ for a given m_S is smaller than m_{G_1}, we can no longer trust the RS model as a viable effective low-energy formulation of gravity (diagonal red-meshed area). Therefore, due to the combination of experimental bounds and theoretical constraints, for $m_{G_1} > m_S$ is not possible to obtain $\langle \sigma_{\rm FO} v \rangle$, as it was indeed found in Ref. [21].

2. $m_{G_1} < m_S$
   In this case, although the $S\,S \to {\rm SM\,SM}$ channel is still open, the target cross-section

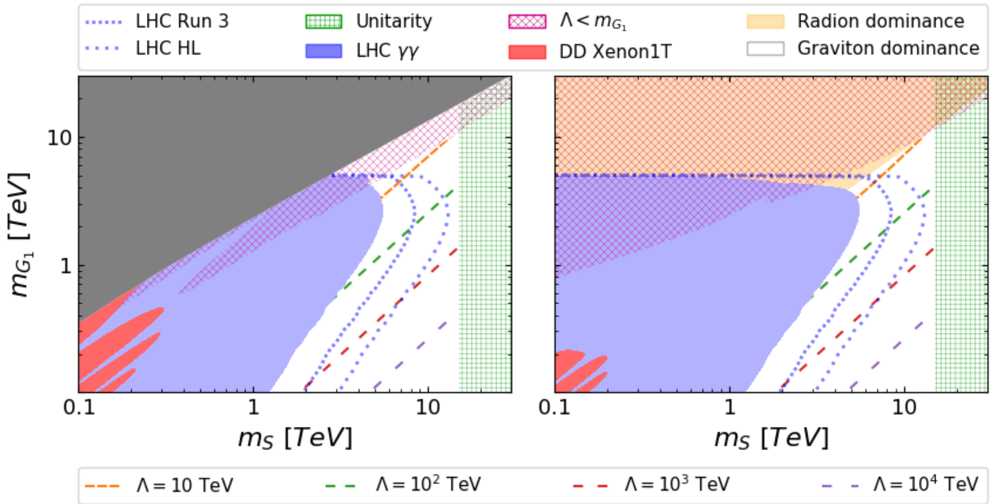

Figure 10. *Region of the (m_S, m_{G_1}) plane for which $\langle\sigma v\rangle = \langle\sigma_{\rm FO} v\rangle$. Left panel: the radion and the extra-dimension stabilization mechanism play no role in DM phenomenology. Right panel: the extra-dimension length is stabilized with the Goldberger-Wise mechanism, with radion mass $m_r = 100$ GeV. In both panels, the grey area represents the part of the parameter space where it is impossible to achieve the correct relic abundance; the red-meshed area is the region for which the low-energy RS effective theory is untrustable, as $\Lambda < m_{G_1}$; the wiggled red area in the lower left corner is the region excluded by DD experiments; the blue area is excluded by resonant KK-graviton searches at the LHC with 36 fb^{-1} at $\sqrt{s} = 13$ TeV; the dotted blue lines represent the expected LHC exclusion bounds at the end of the Run III (with ~ 300 fb^{-1}) and at the HL-LHC (with ~ 3000 fb^{-1}); eventually, the green-meshed area on the right is the region where the theoretical unitarity constraints are not fulfilled. In the left panel, the allowed region is represented by the white area, for which $\langle\sigma_{\rm FO} v\rangle$ is obtained through on-shell KK-graviton production. In the right panel, in addition to the white area, within the tiny orange region $\langle\sigma_{\rm FO} v\rangle$ is obtained through on-shell radion production and virtual radion exchange. The dashed lines depicted in the white region represent the values of Λ needed to obtain the correct relic abundance (as in Fig. 5 of Sec. 3).*

is achievable through production of on-shell KK-gravitons, $S\,S \to G_n\,G_m$. Due to the LHC Run II bounds, the region of the (m_{G_1}, Λ) plane for which we can obtain $\langle\sigma_{\rm FO} v\rangle$ corresponds mainly to the region for which $(m_{G_1}/m_S)^2 \ll 1$. In this region, the value of Λ needed to reach the freeze-out relic abundance is in the range $\Lambda \in [10, 10^4]$ GeV, in agreement with the stringent LHC Run II bounds on Λ for relatively low m_{G_1}. At large values of m_S the theoretical unitarity bound discussed in Sec. 4.3 is relevant and, therefore, m_S cannot be much larger than 10 TeV (vertical green-meshed area). Eventually, the white area represents the region of the parameter space for which the freeze-out scenario can produce the correct DM relic abundance. Notice that most of this region could be tested either by the LHC Run III[5] (with expected 300 fb^{-1}) or

[5]This region could be already partially tested using the complete LHC Run II analysis, with 100 fb^{-1},

by the High-Luminosity LHC (with nominal 3000 fb^{-1}), as shown by the dotted lines depicted in the Figure. Typical values for m_S, m_{G_1} and Λ in the region that would still be allowed after HL-LHC are $m_S \in [3, 15]$ TeV, $m_{G_1} < 1$ TeV and $\Lambda > 10^3$ TeV (although a tiny region around $m_S \sim 10$ TeV with m_{G_1} as large as few TeV with $\Lambda \in [10, 100]$ TeV could also be viable).

The wiggled dark shaded (red) region in the lower left corner is the bound imposed by XENON1T. The peculiar shape of the bound is a consequence of the resonances in the DM annihilation channels via virtual graviton exchange (see Fig. 9). We can see that the DD bounds are much weaker than those from the LHC.

5.2 Radion contribution

Let's consider now the case in which, in addition to virtual KK-graviton exchange and/or on-shell KK-gravitons production, DM could also produce virtual or real radions (right panel). To make easy the comparison with the previous situation, we again consider two regimes:

1. $m_{G_1} > m_S$
   It is always possible to achieve the correct relic abundance through resonant virtual radion exchange and on-shell radion production (see Fig. 4). In the right plot of Fig. 10 the former would occur for $m_S = 50$ GeV, outside the range depicted in the Figure. Being the radion width extremely narrow, this is possible only in presence of a significant fine-tuning of the DM mass m_S and of the radion mass, $2m_S \sim m_r$. In the absence of a theoretical motivation for such a relation between two, in principle, uncorrelated parameters, we consider this mechanism to achieve the target relic abundance not *natural*. In the region considered in the plot, the relic abundance can be also achieved through production of on-shell radions for very low values of Λ. This region is represented by the orange (lightest) shaded area. Most of this region, however, is excluded when asking Λ to be larger than m_{G_1}, as one can see by the diagonal red-meshed area in the plot, $\Lambda < m_{G_1}$. After taking into account the LHC Run II bounds and the limit of validity of the RS model as an effective low-energy theory, a tiny orange-shaded region at $m_S \sim 4$ TeV, $m_{G_1} \sim 5$ TeV and $\Lambda \in [5, 10]$ TeV is still not excluded. Most of it will be tested with the LHC Run III.

2. $m_{G_1} < m_S$
   Since the real KK-graviton production channel, once kinematically open grows very fast as $(m_S/m_{G_1})^8$ (see Fig. 4), it easily dominates the cross-section. Therefore, in this region of the parameter space there are no significant differences with respect to the case in which the radion is absent, discussed in Sec. 5.1.

5.3 Remarks about other setups

In this paper we have focused on the original RS model, in which all the SM particles (and also the DM in our case) are localized on the IR-brane. In the absence of graviton

not included in this paper.

brane localized kinetic terms (BLKT's), within this setup all the SM and DM fields couple to the full tower of KK-graviton excitations with universal strength, Λ^{-1}. As we have seen, the strong bounds from LHC Run II lead to quite large allowed values of Λ ($\gtrsim 10$ TeV), which somehow reintroduce a little hierarchy problem. However many other different configurations have been studied, allowing for some of (or all) the SM fields to propagate in the bulk; for instance, placing gauge bosons and fermions in the bulk has the potential to also explain the hierarchy of fermion masses. Moreover, these extra-dimensional scenarios can be interpreted as strongly-coupled models in four dimensions (see Ref. [18] for details of this duality).

Several of the above possibilities have been already analyzed in the context of gravity-mediated DM that we are addressing, including DM candidates of various spins (0,1/2 and 1). The idea is that the propagation of SM fields in the bulk and the introduction of BLKT's can reduce suitably the coupling of the SM particles to the KK-gravitons, relaxing the LHC bounds and allowing for lower values of Λ which would then satisfy the original motivation of RS models for solving the hierarchy problem. Although to study in detail these alternative RS scenarios is beyond the scope of this paper, we want to comment in this section about the impact of our results on such other models.

In Ref. [21], besides the scenario considered here with all SM and DM fields localized in the IR-brane, two additional benchmark models were studied: 1) SM gauge bosons in the bulk with third generation quarks confined in the IR brane, and all other SM fermions localized close to the UV-brane, so that their couplings to the KK-graviton modes are negligible, and 2) SM fermions localized at various places in the bulk to explain the observed fermion masses and SM gauge bosons propagating also in the bulk. In all scenarios, the Higgs field should remain close to the IR-brane to solve the hierarchy problem, and the DM is also assumed to be localized on the IR-brane. While in none of these setups it was possible to obtain the correct relic density for scalar DM through virtual KK-graviton exchange, the authors did not consider the annihilation channel $SS \to G_n G_m$ nor $SS \to rr$. Since these channels will occur with the same cross-section as in the IR-brane model we analyzed in this paper, it is clear that also in the cases considered in Ref. [21] it would be possible to get the target value $\langle \sigma_{\rm FO} v \rangle$ when $m_S > m_{G_1}$. Actually, it would be easier than in the case considered here, as the LHC bounds on Λ are weaker.

In Ref. [19] two additional setups where analyzed and also confronted with indirect bounds from astrophysical data: model A, which addresses the hierarchy problem with the Higgs and DM localized on the IR-brane and the SM matter on the UV-brane, and model B (that gives up the hierarchy problem) where only DM is localized on the IR-brane while the SM matter and Higgs fields are confined to the UV-brane. In both cases, SM gauge bosons propagate in the bulk, so that there is a hierarchy of couplings of the KK-graviton modes, being of order Λ^{-1} for DM (and the Higgs field in model A) but conveniently suppressed for gauge bosons and negligible for SM matter fields (and the Higgs in model B). As a consequence, the standard radion and KK-graviton searches at LHC do not apply to these models and other searches should be re-interpreted to obtain bounds. Therefore, much lower values of Λ and m_{G_1} would still be allowed and it should be possible to achieve the correct relic abundance for DM masses in a wider range, from few GeV to TeV, in agreement with our results in Fig. 5.

In the dual picture of the RS model, the radion is dual to the dilaton, the Goldstone boson from dilatation symmetry in 4D. The dilaton couplings are fixed by scale invariance, and turn out to have the same structure as the radion couplings at linear order. In Refs. [33, 55], the case in which DM couples to the SM only through a dilaton was studied The authors found that the correct relic abundance can be achieved for light dilaton and DM, since collider bounds from dilaton searches are weaker than for the KK-graviton modes (the dilaton production cross-section is about two - three orders of magnitude smaller than the KK-graviton one, as we can see in Fig. 6). However, as we are studying a consistent gravitational theory and not only the SM plus a dilaton field, the much stringent bounds from KK-gravitons searches do apply.

6 Conclusions

In this paper we have explored the possibility that the observed Dark Matter component in the Universe is represented by some new scalar particle with a mass in the TeV range. This particle interacts with the SM particles only gravitationally (in agreement with non-observation of DM signals at both direct and indirect detection DM experiments). Although this hypothesis would, in principle, mean that the interaction with SM particles is too feeble to reproduce the observed DM relic abundance, we show that this is not the case once this setup is embedded in a warped extra-dimensional space-time, along the ideas of the Randall-Sundrum proposal of Ref. [15]. We consider, therefore, two 4-dimensional branes in a 5-dimensional AdS_5 space-time at a separation r_c, very small compared with present bounds on deviations from Newton's law. On one of the branes, the so-called "IR-brane", both the SM particles and a scalar DM particle are confined, with no particle allowed to escape from the branes to explore the bulk. In this particular extra-dimensional setup, gravitational interaction between particles on the IR-brane, in our case between a scalar DM particle and any of the SM particles, occurs with an amplitude proportional to $1/M_P^2$ when the two particles exchange a graviton zero-mode, but with a suppression factor $1/\Lambda^2$ when they do interact exchanging higher KK-graviton modes. Since Λ can be as low as a few TeV (due to the warping effect induced by the curvature of the space-time along the brane separation), clearly a huge enhancement of the cross-section is possible with respect to standard linearized General Relativity.

Using this mechanism, it was studied in the literature if the observed relic abundance in the Universe can be obtained through resonant KK-graviton exchange via $\sigma(\text{DM}\,\text{DM} \to G_n \to \text{SM}\,\text{SM})$ (for any spin of the DM particle), showing that taking into account the LHC bounds on Λ as a function of the mass of the first KK-graviton, m_{G_1}, it is impossible to achieve the target value of the thermally-averaged cross-section $\langle \sigma_{\text{FO}}\, v \rangle$ for any value of m_{DM} if the DM particle has spin 0 or 1/2 [21]. In Refs. [18–20, 24] it was however shown that, for DM masses larger then the KK-graviton mass, another annihilation channel opens, namely DM annihilation into two (identical) KK-gravitons, $\sigma(\text{DM}\,\text{DM} \to G_n\, G_n)$. In this paper, we have studied the possibility that this channel may give a cross-section large enough to attain the observed relic abundance, for the particular case of a scalar DM particle with mass m_S. We have indeed found that this is the case and that the region of the parameter space for which $\langle \sigma\, v \rangle \sim \langle \sigma_{\rm FO}\, v \rangle$ is typically at m_S of the order of a few TeV, compatible with present direct production searches at the LHC. In the references above some effects were overlooked, though. In particular, a quadratic interaction of the DM particles with KK-gravitons (*i.e.* the existence of a $S\,S\,G_n\,G_m$ vertex when expanding the metric up to second order about the Minkowski metric) was not considered. This amplitude is of the same order in $1/\Lambda$ as the t- and u-channel contributions to $\sigma(\mathrm{DM}\,\mathrm{DM} \to G_n\,G_n)$ considered in the literature and, by increasing the cross-section at large value of the DM mass, lowers the value of m_S needed to achieve the relic abundance at fixed value of m_{G_1}. The same effect is also induced by the possibility of the DM particles annihilating into different KK-gravitons, $\sigma(\mathrm{DM}\,\mathrm{DM} \to G_m\,G_n)$, something allowed since translational invariance along the 5-th dimension is explicitly broken by the presence of the branes. This was also overlooked in the existing literature. These effects and their impact have been discussed extensively in Sec. 3 and App. D.

After having computed the relevant contributions to the cross-section, we have scanned the parameter space of the model (represented by m_S, m_{G_1} and Λ), looking for regions in which the observed relic abundance can be achieved. This region has been eventually compared with experimental bounds from resonant searches at the LHC Run II and from direct and indirect DM detection searches, finding which portion of the allowed parameter space is excluded by data. Eventually, we have studied the theoretical unitarity bounds on the mass of the DM particle and on the validity of the RS model as a consistent low-energy effective theory. Our main result is that a significant portion of the (m_S, m_{G_1}) plane where $m_S > m_{G_1}$ can reproduce the observed relic abundance, for values of Λ ranging from a few to thousands of TeV and $m_S \in [1, 10]$ TeV. Unitarity bounds put a (theoretical) upper limit on the mass of the DM particle and, interestingly enough, most part of the allowed parameter space could therefore be tested by the LHC Run III and by the proposed High-Luminosity LHC.

In the presence of a Goldberger-Wise mechanism to stabilize the separation between the two branes, the radion r is expected to be light, $m_r \lesssim \mathcal{O}(\mathrm{TeV})$, and DM can also annihilate into SM particles via the exchange of a virtual radion and, for $m_S > m_r$, two DM particles can also produce directly two on-shell radions. This has been studied in detail in Sec. 3.2 and App. D.2. Since, contrary to the KK-graviton mass (strongly related to Λ in the RS setup), the radion mass is in practice a free parameter of the model (depending on the unknown details of the scalar potential in the bulk and of some brane-localized terms), it is possible to achieve $\langle \sigma_{\rm FO}\, v \rangle$ for any value of m_S and m_{G_1}, even in the case $m_{G_1} > m_S$, through the resonant radion exchange channel (at the price of introducing a significant, theoretically unappealing, fine-tuning of the DM mass with respect to the radion mass, $2 m_S \sim m_r$) or through on-shell radion production. The region for $m_{G_1} > m_S$, however, is mostly excluded due to the fact that the value of Λ needed to reach the target relic abundance is $\Lambda < m_{G_1}$, a condition that makes untrustable the RS model as a valid effective low-energy theory. Apart from a tiny region for which the two radion on-shell production channel dominates in the cross-section, the rest of the allowed parameter space is similar to that found in the absence of a radion.

Acknowledgements

We thank, Hyun Min Lee, Myeonghun Park and Verónica Sanz for correspondence about the DM annihilation cross-sections into KK-gravitons and radion interactio. This work has been partially supported by the European Union projects H2020-MSCA-RISE-2015 and H2020-MSCA- ITN-2015//674896-ELUSIVES and by the Spanish MINECO under grants FPA2014-57816-P, FPA2017-85985-P and SEV-2014-0398.

A Spin 2 massive graviton

The propagator of the n-th KK-graviton mode, with mass m_n, decay width Γ_n and 4-momentum k in the unitary gauge is:

$$i\Delta^G_{\mu\nu\alpha\beta}(k) = \frac{iP_{\mu\nu\alpha\beta}(k, m_n)}{k^2 - m_n^2 + im_n\Gamma_n}\,, \tag{A.1}$$

where $P_{\mu\nu\alpha\beta}$ is the sum of the polarization tensors $\epsilon^s_{\mu\nu}(k)$ (being s the spin):

$$\begin{aligned} P_{\mu\nu\alpha\beta}(k, m_g) &= \sum_s \epsilon^s_{\mu\nu}(k)\epsilon^s_{\alpha\beta}(k) \\ &= \frac{1}{2}(G_{\mu\alpha}G_{\nu\beta} + G_{\nu\alpha}G_{\mu\beta} - \frac{2}{3}G_{\mu\nu}G_{\alpha\beta}) \end{aligned} \tag{A.2}$$

and

$$G_{\mu\nu} \equiv \eta_{\mu\nu} - \frac{k_\mu k_\nu}{m_n^2}\,. \tag{A.3}$$

The tensor $P_{\mu\nu\alpha\beta}$ must satisfy several conditions for an on-shell graviton $G_{\mu\nu}$, in order to reduce the number of degrees-of-freedom to the physical ones:

$$\eta^{\alpha\beta}P_{\mu\nu\alpha\beta}(k, m_g) = \eta^{\nu\mu}P_{\mu\nu\alpha\beta}(k, m_n) = 0\,, \tag{A.4}$$

$$k^\alpha P_{\mu\nu\alpha\beta}(k, m_g) = k^\beta P_{\mu\nu\alpha\beta}(k, m_g) = k^\mu P_{\mu\nu\alpha\beta}(k, m_g) = k^\nu P_{\mu\nu\alpha\beta}(k, m_g) = 0\,. \tag{A.5}$$

B Feynman rules

We summarize in this Appendix the different Feynman rules corresponding to the couplings of scalar DM particles and of SM particles with KK-gravitons and radions.

B.1 Graviton Feynman rules

The vertex that involves one KK-graviton (with $n \neq 0$) and two scalars of mass m_S is given by:

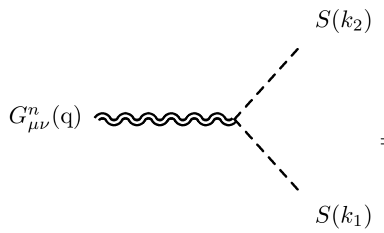

$$= -\frac{i}{\Lambda}\left(m_S^2\eta_{\mu\nu} - C_{\mu\nu\rho\sigma}k_1^\rho k_2^\sigma\right)\,, \tag{B.1}$$

where

$$C_{\mu\nu\alpha\beta} \equiv \eta_{\mu\alpha}\eta_{\nu\beta} + \eta_{\nu\alpha}\eta_{\mu\beta} - \eta_{\mu\nu}\eta_{\alpha\beta} \, . \tag{B.2}$$

This expression can be used for the coupling of both scalar DM and the SM Higgs boson to KK-gravitons.

The Feynman rule corresponding to the interaction of two SM Dirac fermions of mass m_ψ with one KK-graviton is given by:

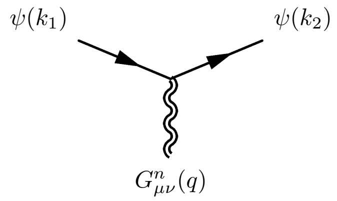

$$= -\frac{i}{4\Lambda}\left[\gamma_\mu\left(k_{2\nu}+k_{1\nu}\right)+\gamma_\nu\left(k_{2\mu}+k_{1\mu}\right) -2\eta_{\mu\nu}\left(\not{k}_2+\not{k}_1-2m_\psi\right)\right] , \tag{B.3}$$

whereas

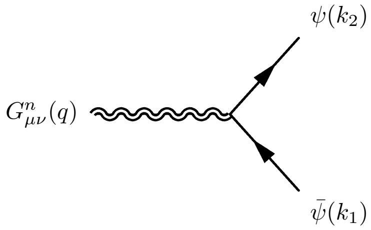

$$= -\frac{i}{4\Lambda}\left[\gamma_\mu\left(k_{2\nu}-k_{1\nu}\right)+\gamma_\nu\left(k_{2\mu}-k_{1\mu}\right) -2\eta_{\mu\nu}\left(\not{k}_2-\not{k}_1-2m_\psi\right)\right] . \tag{B.4}$$

The interaction between two SM gauge bosons of mass m_A and one KK-graviton is given by:

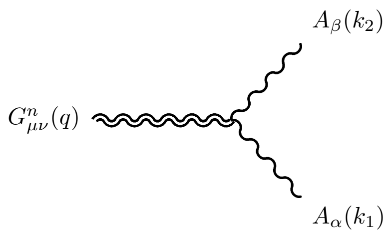

$$= -\frac{i}{\Lambda}\left(m_A^2 C_{\mu\nu\alpha\beta} + W_{\mu\nu\alpha\beta}\right) , \tag{B.5}$$

where

$$W_{\mu\nu\alpha\beta} \equiv B_{\mu\nu\alpha\beta} + B_{\nu\mu\alpha\beta} \tag{B.6}$$

and

$$B_{\mu\nu\alpha\beta} \equiv \eta_{\alpha\beta}k_{1\mu}k_{2\nu}+\eta_{\mu\nu}(k_1\cdot k_2\,\eta_{\alpha\beta}-k_{1\beta}k_{2\nu})-\eta_{\mu\beta}k_{1\nu}k_{2\alpha}+\frac{1}{2}\eta_{\mu\nu}(k_{1\beta}k_{2\alpha}-k_1\cdot k_2\,\eta_{\alpha\beta}) \, . \tag{B.7}$$

Eventually, the interaction between two scalar DM particles and two KK-gravitons (coming from a second order expansion of the metric $g_{\mu\nu}$ about the Minkowski metric $\eta_{\mu\nu}$)

is given by:

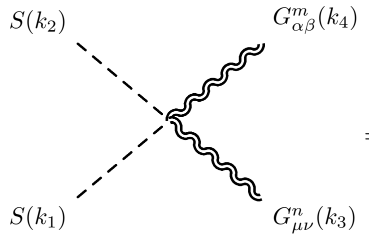

$$= -\frac{i}{\Lambda^2}\eta_{\nu\beta}\left(m_S^2\eta_{\mu\alpha} - C_{\mu\alpha\rho\sigma}k_1^\rho k_2^\sigma\right) . \tag{B.8}$$

The Feynman rules for the $n = 0$ KK-graviton can be obtained by the previous ones by replacing Λ with M_{P}. We do not give here the triple KK-graviton vertex, as it is irrelevant for the phenomenological applications of this paper. The same occurs for the vertices between one KK-graviton and two radions and two KK-gravitons and one radion.

B.2 Radion Feynman rules

The radion field r couples with both the SM and the DM particles with the trace of the energy-momentum tensor, $T = g^{\mu\nu}T_{\mu\nu}$. The only exception are photons and gluons that, being massless, do not contribute to T at tree-level. However, effective couplings of these fields to the radion are generated through quarks and W loops, and the trace anomaly.

The interaction between one radion and two scalar fields (either the DM or the SM Higgs boson) is given by:

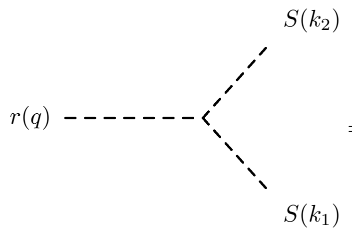

$$= -\frac{2i}{\Lambda\sqrt{6}}\left(2m_S^2 + k_{1\mu}k_2^\mu\right) . \tag{B.9}$$

The vertex that involves the radion and two SM Dirac fermions takes the form:

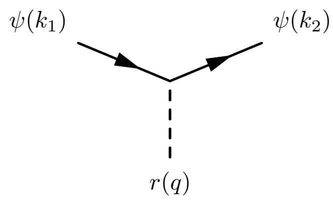

$$= -\frac{i}{2\Lambda\sqrt{6}}\left[8m_\psi - 3\left(\not{k}_2 + \not{k}_1\right)\right] \tag{B.10}$$

and, as in the case of the graviton-fermion-fermion vertex, we have:

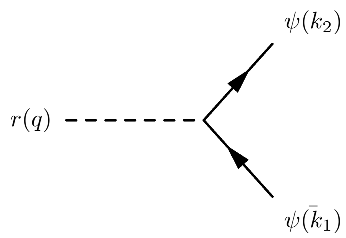

$$= -\frac{i}{2\Lambda\sqrt{6}}\left[8m_\psi - 3\left(\not{k}_2 - \not{k}_1\right)\right] . \tag{B.11}$$

The interaction between two massive SM gauge bosons and one radion is given by:

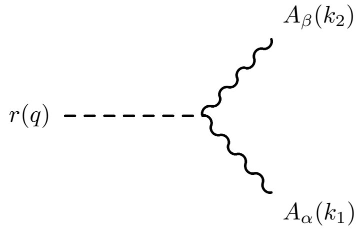

$$= \frac{2i}{\Lambda\sqrt{6}} m_A^2 \eta_{\alpha\beta} \,. \tag{B.12}$$

The Feynman rule corresponding to the interaction between two massless SM gauge bosons and one radion is:

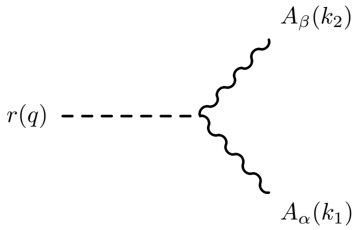

$$= \frac{4i\alpha_i C_i}{8\pi\Lambda\sqrt{6}} \left[\eta_{\mu\nu}(k_1 \cdot k_2) - k_{1\nu} k_{2\mu}\right] \,, \tag{B.13}$$

where $\alpha_i = \alpha_{EM}, \alpha_s$ for the case of the photons or gluons, respectively, and

$$\begin{cases} C_3 & = b_{IR}^{(3)} - b_{UV}^{(3)} + \frac{1}{2}\sum_q F_{1/2}(x_q) \,, \\ & \\ C_{EM} & = b_{IR}^{(EM)} - b_{UV}^{(EM)} + F_1(x_W) - \sum_q N_c Q_q^2 F_{1/2}(x_q) \,, \end{cases} \tag{B.14}$$

with $x_q = 4m_q/m_r$ and $x_W = 4m_w/m_r$. The explicit form of $F_{1/2}$ and the values of the one-loop β-function coefficients b are given by [33]:

$$\begin{cases} F_{1/2}(x) = 2x[1 + (1-x)f(x)], \\ \\ F_1(x) = 2 + 3x + 3x(2-x)f(x), \end{cases} \tag{B.15}$$

$$f(x) = \begin{cases} [\arcsin(1/\sqrt{x})]^2 & x > 1, \\ & \\ -\frac{1}{4}\left[\log\left(\frac{1+\sqrt{x-1}}{1-\sqrt{x-1}}\right) - i\pi\right]^2 & x < 1, \end{cases} \tag{B.16}$$

while $b_{IR}^{(EM)} - b_{UV}^{(EM)} = 11/3$ and $b_{IR}^{(3)} - b_{UV}^{(3)} = -11 + 2n/3$, where n is the number of quarks whose mass is smaller than $m_r/2$.

Eventually, the interaction Lagrangian between the DM and the radion up to second order is given by [6] :

$$\mathcal{L} = \frac{1}{\Lambda\sqrt{6}} r T^{\rm DM} - \frac{1}{12\Lambda^2} r^2 (\partial_\mu S)(\partial\mu S) + \frac{1}{2\Lambda^2} r^2 S^2 \,, \tag{B.17}$$

[6] In the second order interaction terms for the radion, based on [32], we have found some numerical factors that differ from Refs. [18, 34], however such difference will not modify our main results, since the dominant DM annihilation channel in most of the allowed region is into KK-gravitons.

being T^{DM} the trace of the energy-momentum tensor of the DM eq. (2.20). As in the case of the interactions with gravitons, exists a 4-legs interaction term:

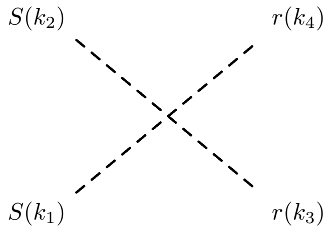

$$= -\frac{i}{3\Lambda^2}\left(6m_S^2 + k_{1\mu}k_2^{\mu}\right) . \tag{B.18}$$

C Decay widths

In this appendix we compute the decay widths of KK-gravitons and of the radion, using the Feynman rules given in App.B.

C.1 KK-graviton decay widths

The KK-graviton can decay into scalar particles (including the Higgs boson, the DM particle, if the mass of the considered KK-graviton is sufficiently large, and the radion), SM fermions, SM gauge bosons and lighter KK-gravitons.

Decay widths of KK-gravitons into SM particles, $\Gamma(G_n \to \mathrm{SM\,SM})$, are all proportional to $1/\Lambda^2$. In particular, the decay width into SM Higgs bosons is given by:

$$\Gamma(G_n \to hh) = \frac{m_n^3}{960\pi\Lambda^2}\left(1 - \frac{4m_h^2}{m_n^2}\right)^{5/2} , \tag{C.1}$$

where m_n is the mass of the n-th KK-graviton (in the main text, this was called m_{G_n}, but we prefer here a shorter notation to increase readability of the formulæ). If $m_n > 2m_S$, the n-th KK-graviton can decay into two DM particles:

$$\Gamma(G \to SS) = \frac{m_n^3}{960\pi\Lambda^2}\left(1 - \frac{4m_S^2}{m_n^2}\right)^{5/2} . \tag{C.2}$$

The decay width of the n-th KK-graviton into SM Dirac fermions is given by:

$$\Gamma(G_n \to \bar{\psi}\psi) = \frac{m_n^3}{160\pi\Lambda^2}\left(1 - \frac{4m_\psi^2}{m_n^2}\right)^{3/2}\left(1 + \frac{8m_\psi^2}{3m_n^2}\right) . \tag{C.3}$$

The decay width of the n-th KK-graviton into two SM massive gauge bosons reads:

$$\begin{cases} \Gamma(G_n \to W^+W^-) = \frac{m_n^3}{480\pi\Lambda^2}\left(1 - \frac{4m_W^2}{m_n^2}\right)^{1/2}\left(13 + \frac{56m_W^2}{m_n^2} + \frac{48m_W^4}{m_n^4}\right) , \\ \Gamma(G_n \to ZZ) = \frac{m_n^3}{960\pi\Lambda^2}\left(1 - \frac{4m_Z^2}{m_n^2}\right)^{1/2}\left(13 + \frac{56m_Z^2}{m_n^2} + \frac{48m_Z^4}{m_n^4}\right) , \end{cases} \tag{C.4}$$

whereas the decay width into massless gauge bosons is:

$$\begin{cases} \Gamma(G_n \to \gamma\gamma) &= \frac{m_n^3}{80\pi\Lambda^2}\,, \\ \\ \Gamma(G_n \to gg) &= \frac{m_n^3}{10\pi\Lambda^2}\,. \end{cases} \tag{C.5}$$

On the other hand, the decay widths of KK-gravitons with KK-number n into lighter KK-gravitons are proportional to $1/\Lambda^6$, as the triple graviton vertex comes from the third order expansion of the metric about the Minskowski spacetime. For this reason, we have not considered these decays when computing the total KK-graviton decay widths. The same happens for the radion: the coupling of the radion with the gravitons arises from the mixing of the radion with the graviscalar h_{55}, that eventually couples with KK-gravitons again with a triple graviton vertex, proportional to $1/\Lambda^3$. Also in this case the decay width $\Gamma(G_n \to r\,r)$ is proportional to $1/\Lambda^6$ and, therefore, negligible.

C.2 Radion decay widths

The decay width of the radion into scalar particles, either the SM Higgs boson or the DM particle if the radion is sufficiently heavy, is given by:

$$\Gamma(r \to hh, SS) = \frac{m_r^3}{192\pi\Lambda^2}\left(1 - \frac{4m_X^2}{m_r^2}\right)^{1/2}\left(1 + \frac{2m_X^2}{m_r^2}\right)^2\,, \tag{C.6}$$

where $m_X = m_h, m_S$ depending on the considered channel.

The radion decay width into SM Dirac fermions is given by:

$$\Gamma(r \to \bar\psi\psi) = \frac{m_r m_\psi^2}{48\pi\Lambda^2}\left(1 - \frac{4m_\psi^2}{m_r^2}\right)^{3/2}\,. \tag{C.7}$$

The radion decay width into SM massive gauge bosons reads:

$$\begin{cases} \Gamma(r \to W^+W^-) &= \frac{m_r^3}{96\pi\Lambda^2}\left(1 - \frac{4m_W^2}{m_r^2}\right)^{1/2}\left(12 - \frac{4m_W^2}{m_r^2} + \frac{m_W^4}{m_r^4}\right)\,, \\ \\ \Gamma(r \to ZZ) &= \frac{m_r^3}{192\pi\Lambda^2}\left(1 - \frac{4m_Z^2}{m_r^2}\right)^{1/2}\left(12 - \frac{4m_Z^2}{m_r^2} + \frac{m_Z^4}{m_r^4}\right)\,, \end{cases} \tag{C.8}$$

whereas the decay width into SM massless gauge bosons is:

$$\begin{cases} \Gamma(r \to \gamma\gamma) &= \frac{\alpha_{EM} C_{EM} m_r^3}{7680\pi\Lambda^2}\,, \\ \\ \Gamma(r \to gg) &= \frac{\alpha_3 C_3 m_r^3}{960\pi\Lambda^2}\,. \end{cases} \tag{C.9}$$

D Annihilation DM Cross section

Since in the freeze-out scenario, DM annihilation occurs at small relative velocity of the two DM particles, it is useful to approximate the Mandelstam variable s as:

$$s \approx m_{dm}^2(4 + v_{rel}^2)\,. \tag{D.1}$$

Within this approximation, the different scalar products for processes in which two DM particles S's annihilate into two SM particles X's, with incoming and outcoming momenta $S(k_1)\,S(k_2) \to X(k_3)\,X(k_4)$, become:

$$\begin{cases} k_1 \cdot k_4 = k_2 \cdot k_3 \approx m_S^2 + \frac{1}{2} m_S^2 \sqrt{1 - \frac{m_X^2}{m_S^2}}\, \cos\theta\, v_{rel} + \frac{1}{4} m_S^2\, v_{rel}^2\,, \\ \\ k_1 \cdot k_3 = k_2 \cdot k_4 \approx m_S^2 - \frac{1}{2} m_S^2 \sqrt{1 - \frac{m_X^2}{m_S^2}}\, \cos\theta\, v_{rel} + \frac{1}{4} m_S^2\, v_{rel}^2\,, \end{cases} \tag{D.2}$$

where

$$\begin{cases} k_1 \cdot k_1 \,=\, k_2 \cdot k_2 = m_S^2\,, \\ \\ k_3 \cdot k_3 \,=\, k_4 \cdot k_4 = m_X^2\,. \end{cases} \tag{D.3}$$

We will always write the annihilation cross-sections at leading order in this velocity expansion.

D.1 Annihilation through and into Gravitons

The annihilation of DM particles into SM particles through virtual KK-graviton exchange occurs in d-wave. In the following expressions, S_{KK} stands for the sum over all KK states:

$$S_{KK} = \frac{1}{\Lambda^2} \sum_{n=1}^{\infty} \frac{1}{s - m_n^2 + i m_n \Gamma_n}\,, \tag{D.4}$$

where m_n is the mass of the n-th KK-graviton.
The annihilation cross-section into two SM Higgs bosons reads:

$$\sigma_g(S\,S \to h\,h) \approx v_{rel}^3 \cdot |S_{KK}|^2 \frac{m_S^6}{720\pi} \left(1 - \frac{m_h^2}{m_S^2}\right)^{5/2}\,. \tag{D.5}$$

The annihilation cross-section into two SM massive gauge bosons is given by:

$$\begin{cases} \sigma_g(S\,S \to W^+\,W^-) \approx v_{rel}^3 \cdot |S_{KK}|^2 \frac{m_S^6}{360\pi} \left(1 - \frac{m_w^2}{m_S^2}\right)^{1/2} \left(13 + \frac{14 m_w^2}{m_S^2} + \frac{3 m_w^4}{m_S^4}\right)\,, \\ \\ \sigma_g(S\,S \to Z\,Z) \qquad \approx v_{rel}^3 \cdot |S_{KK}|^2 \frac{m_S^6}{720\pi} \left(1 - \frac{m_w^2}{m_S^2}\right)^{1/2} \left(13 + \frac{14 m_Z^2}{m_S^2} + \frac{3 m_Z^4}{m_S^4}\right)\,, \end{cases} \tag{D.6}$$

whereas for two massless gauge bosons we have:

$$\begin{cases} \sigma_g(S\,S \to \gamma\,\gamma) \approx v_{rel}^3 \cdot |S_{KK}|^2 \frac{m_S^6}{60\pi}\,, \\ \\ \sigma_g(S\,S \to g\,g) \approx v_{rel}^3 \cdot |S_{KK}|^2 \frac{2 m_S^6}{15\pi}\,. \end{cases} \tag{D.7}$$

Eventually, the annihilation cross-section into two SM fermions is:

$$\sigma_g(S\,S \to \bar{\psi}\,\psi) \approx v_{rel}^3 \cdot |S_{KK}|^2 \frac{m_s^6}{360\pi} \left(1 - \frac{m_\psi^2}{m_s^2}\right)^{3/2} \left(3 + \frac{2 m_\psi^2}{m_s^2}\right)\,. \tag{D.8}$$

As it was shown in Ref. [18], for DM particle masses larger than the mass of a given KK-graviton mode DM particles may annihilate into two KK-gravitons. In the small velocity approximation, the corresponding cross-section is:

$$\sigma_g(S\,S \to G_n\,G_m) \approx v_{rel}^{-1}\left(\frac{A+B+C/4}{9216\pi}\right)\left(\frac{1}{\Lambda^4\,m_{\rm S}^3\,m_{\rm n}^4\,m_{\rm m}^4}\right)\sqrt{\frac{\left(4m_{\rm S}^2+m_{\rm n}^2-m_{\rm m}^2\right)^2}{16m_{\rm S}^2}-m_{\rm n}^2}\,, \tag{D.9}$$

where the three contributions to the cross-section come from the square of the t- and u-channels amplitudes in diagrams (a) and (b) of Fig. 2 (A), the square of the 4-points amplitude in diagram (c) of the same Figure (C) and from the interference between the two classes of diagrams (B), respectively:

$$\begin{cases} A \;=\; \dfrac{\left[-2\,m_{\rm m}^2\left(4\,m_{\rm S}^2+m_{\rm n}^2\right)+\left(m_{\rm n}^2-4\,m_{\rm S}^2\right)^2+m_{\rm m}^4\right]^4}{2\left(4\,m_{\rm S}^2-m_{\rm n}^2-m_{\rm m}^2\right)^2}\,, \\[2ex] B \;=\; \dfrac{\left[-8\,m_{\rm S}^2\left(m_{\rm n}^2+m_{\rm m}^2\right)+16\,m_{\rm S}^4+\left(m_{\rm n}^2-m_{\rm m}^2\right)^2\right]^2}{4\,m_{\rm S}^2-m_{\rm n}^2-m_{\rm m}^2}\left[16\,m_{\rm S}^4\left(m_{\rm n}^2+m_{\rm m}^2\right)\right. \\ \quad \left. -\;8\,m_{\rm S}^2\left(-m_{\rm n}^2\,m_{\rm m}^2+m_{\rm n}^4+m_{\rm m}^4\right)+\left(m_{\rm n}^2-m_{\rm m}^2\right)^2\left(m_{\rm n}^2+m_{\rm m}^2\right)\right]\,, \\[2ex] C \;=\; 256\,m_{\rm S}^8\left(13\,m_{\rm n}^2\,m_{\rm m}^2+2\,m_{\rm n}^4+2\,m_{\rm m}^4\right)-512\,m_{\rm S}^6\left(m_{\rm n}^6+m_{\rm m}^6\right) \\[1ex] \quad +\;32\,m_{\rm S}^4\left(-17\,m_{\rm n}^6\,m_{\rm m}^2+98\,m_{\rm n}^4\,m_{\rm m}^4-17\,m_{\rm n}^2\,m_{\rm m}^6+6\,m_{\rm n}^8+6\,m_{\rm m}^8\right) \\[1ex] \quad -\;32\,m_{\rm S}^2\left(m_{\rm n}^2-m_{\rm m}^2\right)^2\left(m_{\rm n}^6+m_{\rm m}^6\right)+\left(m_{\rm n}^2-m_{\rm m}^2\right)^4\left(13\,m_{\rm n}^2\,m_{\rm m}^2+2\,m_{\rm n}^4+2\,m_{\rm m}^4\right)\,. \end{cases} \tag{D.10}$$

When the two KK-gravitons have the same KK-number, $m = n$, eq. (D.9) simplifies:

$$\begin{aligned}\sigma_g(S\,S \to G_n\,G_n) \approx\; & v_{rel}^{-1}\frac{m_S^2}{576\,\pi\,\Lambda^4}\frac{(1-r)^{1/2}}{r^4(2-r)^2}\left(256-768\,r+968\,r^2-520\,r^3\right.\\ & \left.+\;142\,r^4-52\,r^5+19\,r^6\right)\,,\end{aligned} \tag{D.11}$$

where $r \equiv (m_{\rm n}/m_S)^2$.

D.2 Annihilation through and into Radions

When the distance between the two branes is stabilized using the Goldberger-Wise mechanism, the DM particles can annihilate into SM particles also through virtual radion exchange. The processes involving the radion occur in S-wave and can be more efficient than the exchange of a tower of virtual KK-gravitons, which is in d-wave.

The DM annihilation cross-section into the SM Higgs boson is:

$$\sigma_r(S\,S \to h\,h) \approx v_{rel}^{-1}\frac{m_S^6}{16\,\pi\,\Lambda^4}\,\frac{1}{(s-m_r^2)^2+m_r^2\,\Gamma_r^2}\left(1-\frac{m_h^2}{m_S^2}\right)^{1/2}\left(2+\frac{m_h^2}{m_S^2}\right)^2\,, \tag{D.12}$$

where m_r is the mass of the radion.

The cross-section for DM annihilation into SM massive gauge bosons reads:

$$\begin{cases} \sigma_r(S\,S \to W^+\,W^-) \approx v_{rel}^{-1}\,\frac{m_S^6}{8\,\pi\,\Lambda^4}\,\frac{1}{(s-m_r^2)^2+m_r^2\,\Gamma_r^2}\,\left(1-\frac{m_w^2}{m_S^2}\right)^{1/2}\left(4-\frac{4m_w^2}{m_S^2}+\frac{3\,m_w^4}{m_S^4}\right), \\ \sigma_r(S\,S \to Z\,Z) \qquad \approx v_{rel}^{-1}\,\frac{m_S^6}{16\,\pi\,\Lambda^4}\,\frac{1}{(s-m_r^2)^2+m_r^2\,\Gamma_r^2}\,\left(1-\frac{m_w^2}{m_S^2}\right)^{1/2}\left(4-\frac{4m_Z^2}{m_S^2}+\frac{3\,m_Z^4}{m_S^4}\right). \end{cases} \tag{D.13}$$

The DM annihilation into photons and gluons is proportional to the vertex in eq. (B.13). The corresponding expressions for the cross-sections are:

$$\begin{cases} \sigma_r(S\,S \to \gamma\,\gamma) \approx v_{rel}^{-1}\,\frac{m_S^6\,\alpha_{EM}\,C_{EM}}{32\,\pi^3\,\Lambda^4}\,\frac{1}{(s-m_r^2)^2+m_r^2\,\Gamma_r^2}, \\ \sigma_r(S\,S \to g\,g) \approx v_{rel}^{-1}\,\frac{m_S^6\,\alpha_3\,C_3}{4\,\pi^3\,\Lambda^4}\,\frac{1}{(s-m_r^2)^2+m_r^2\,\Gamma_r^2}. \end{cases} \tag{D.14}$$

Eventually, the DM annihilation cross-section into SM fermions is given by:

$$\sigma_r(S\,S \to \bar\psi\,\psi) \approx v_{rel}^{-1}\,\frac{m_s^4\,m_\psi^2}{4\,\pi\,\Lambda^4}\,\frac{1}{(s-m_r^2)^2+m_r^2\,\Gamma_r^2}\left(1-\frac{m_\psi^2}{m_s^2}\right)^{3/2}. \tag{D.15}$$

As in the case of the graviton, if the mass of the DM is larger than the mass of the radion, then the DM particles can annihilate into two on-shell radions:

$$\sigma_r(S\,S \to r\,r) \approx v_{rel}^{-1}\,\frac{m_S^5\,\sqrt{m_S^2-m_r^2}}{576\,\pi\,\Lambda^4\,\left(m_r^2-2\,m_S^2\right)^2}\left(2+7\,\frac{m_r^2}{m_S^2}\right)^2, \tag{D.16}$$

where we have considered both the u- and t-channels amplitudes and the contribution coming from the 4-legs vertex in eq. (B.18).

References

[1] G. Bertone, D. Hooper and J. Silk, *Particle dark matter: Evidence, candidates and constraints*, *Phys. Rept.* **405** (2005) 279–390, [hep-ph/0404175].

[2] Particle Data Group collaboration, M. Tanabashi et al., *Review of Particle Physics*, *Phys. Rev.* **D98** (2018) 030001.

[3] S. Dimopoulos and H. Georgi, *Softly Broken Supersymmetry and SU(5)*, *Nucl.Phys.* **B193** (1981) 150.

[4] T. Appelquist, H.-C. Cheng and B. A. Dobrescu, *Bounds on universal extra dimensions*, *Phys.Rev.* **D64** (2001) 035002, [hep-ph/0012100].

[5] M. T. Arun, D. Choudhury and D. Sachdeva, *Universal Extra Dimensions and the Graviton Portal to Dark Matter*, *JCAP* **1710** (2017) 041, [1703.04985].

[6] P. Cushman et al., *Working Group Report: WIMP Dark Matter Direct Detection*, in *Proceedings, 2013 Community Summer Study on the Future of U.S. Particle Physics:*

Snowmass on the Mississippi (CSS2013): Minneapolis, MN, USA, July 29-August 6, 2013, 2013, 1310.8327, http://www.slac.stanford.edu/econf/C1307292/docs/CosmicFrontier/WIMPDirect-24.pdf.

[7] M. Cirelli, G. Corcella, A. Hektor, G. Hutsi, M. Kadastik, P. Panci et al., *PPPC 4 DM ID: A Poor Particle Physicist Cookbook for Dark Matter Indirect Detection*, *JCAP* **1103** (2011) 051, [1012.4515].

[8] L. J. Hall, K. Jedamzik, J. March-Russell and S. M. West, *Freeze-In Production of FIMP Dark Matter*, *JHEP* **03** (2010) 080, [0911.1120].

[9] A. G. Dias, A. C. B. Machado, C. C. Nishi, A. Ringwald and P. Vaudrevange, *The Quest for an Intermediate-Scale Accidental Axion and Further ALPs*, *JHEP* **06** (2014) 037, [1403.5760].

[10] I. Antoniadis, *A Possible new dimension at a few TeV*, *Phys. Lett.* **B246** (1990) 377–384.

[11] I. Antoniadis, S. Dimopoulos and G. Dvali, *Millimeter range forces in superstring theories with weak scale compactification*, *Nucl.Phys.* **B516** (1998) 70–82, [hep-ph/9710204].

[12] N. Arkani-Hamed, S. Dimopoulos and G. Dvali, *The Hierarchy problem and new dimensions at a millimeter*, *Phys.Lett.* **B429** (1998) 263–272, [hep-ph/9803315].

[13] I. Antoniadis, N. Arkani-Hamed, S. Dimopoulos and G. Dvali, *New dimensions at a millimeter to a Fermi and superstrings at a TeV*, *Phys.Lett.* **B436** (1998) 257–263, [hep-ph/9804398].

[14] N. Arkani-Hamed, S. Dimopoulos and G. Dvali, *Phenomenology, astrophysics and cosmology of theories with submillimeter dimensions and TeV scale quantum gravity*, *Phys.Rev.* **D59** (1999) 086004, [hep-ph/9807344].

[15] L. Randall and R. Sundrum, *A Large mass hierarchy from a small extra dimension*, *Phys. Rev. Lett.* **83** (1999) 3370–3373, [hep-ph/9905221].

[16] L. Randall and R. Sundrum, *An Alternative to compactification*, *Phys.Rev.Lett.* **83** (1999) 4690–4693, [hep-th/9906064].

[17] G. F. Giudice and M. McCullough, *A Clockwork Theory*, *JHEP* **02** (2017) 036, [1610.07962].

[18] H. M. Lee, M. Park and V. Sanz, *Gravity-mediated (or Composite) Dark Matter*, *Eur. Phys. J.* **C74** (2014) 2715, [1306.4107].

[19] H. M. Lee, M. Park and V. Sanz, *Gravity-mediated (or Composite) Dark Matter Confronts Astrophysical Data*, *JHEP* **05** (2014) 063, [1401.5301].

[20] C. Han, H. M. Lee, M. Park and V. Sanz, *The diphoton resonance as a gravity mediator of dark matter*, *Phys. Lett.* **B755** (2016) 371–379, [1512.06376].

[21] T. D. Rueter, T. G. Rizzo and J. L. Hewett, *Gravity-Mediated Dark Matter Annihilation in the Randall-Sundrum Model*, *JHEP* **10** (2017) 094, [1706.07540].

[22] T. G. Rizzo, *Dark Photons, Kinetic Mixing and Light Dark Matter From 5-D*, in *53rd Rencontres de Moriond on Electroweak Interactions and Unified Theories (Moriond EW 2018) La Thuile, Italy, March 10-17, 2018*, 2018, 1804.03560.

[23] T. G. Rizzo, *Kinetic mixing, dark photons and extra dimensions. Part II: fermionic dark matter*, *JHEP* **10** (2018) 069, [1805.08150].

[24] A. Carrillo-Monteverde, Y.-J. Kang, H. M. Lee, M. Park and V. Sanz, *Dark Matter Direct Detection from new interactions in models with spin-two mediators*, *JHEP* **06** (2018) 037, [1803.02144].

[25] W. D. Goldberger and M. B. Wise, *Modulus stabilization with bulk fields*, *Phys. Rev. Lett.* **83** (1999) 4922–4925, [hep-ph/9907447].

[26] H. Davoudiasl, J. L. Hewett and T. G. Rizzo, *Phenomenology of the Randall-Sundrum Gauge Hierarchy Model*, *Phys. Rev. Lett.* **84** (2000) 2080, [hep-ph/9909255].

[27] T. Appelquist and A. Chodos, *Quantum Effects in Kaluza-Klein Theories*, *Phys.Rev.Lett.* **50** (1983) 141.

[28] T. Appelquist and A. Chodos, *The Quantum Dynamics of Kaluza-Klein Theories*, *Phys.Rev.* **D28** (1983) 772.

[29] B. de Wit, M. Luscher and H. Nicolai, *The Supermembrane Is Unstable*, *Nucl.Phys.* **B320** (1989) 135.

[30] E. Ponton and E. Poppitz, *Casimir energy and radius stabilization in five-dimensional orbifolds and six-dimensional orbifolds*, *JHEP* **06** (2001) 019, [hep-ph/0105021].

[31] W. D. Goldberger and M. B. Wise, *Bulk fields in the Randall-Sundrum compactification scenario*, *Phys. Rev.* **D60** (1999) 107505, [hep-ph/9907218].

[32] W. D. Goldberger and M. B. Wise, *Phenomenology of a stabilized modulus*, *Phys. Lett.* **B475** (2000) 275–279, [hep-ph/9911457].

[33] K. Blum, M. Cliche, C. Csaki and S. J. Lee, *WIMP Dark Matter through the Dilaton Portal*, *JHEP* **03** (2015) 099, [1410.1873].

[34] C. Csaki, M. Graesser, L. Randall and J. Terning, *Cosmology of brane models with radion stabilization*, *Phys. Rev.* **D62** (2000) 045015, [hep-ph/9911406].

[35] E. W. Kolb and M. S. Turner, *The Early Universe*, *Front. Phys.* **69** (1990) 1–547.

[36] Planck collaboration, N. Aghanim et al., *Planck 2018 results. VI. Cosmological parameters*, 1807.06209.

[37] G. Steigman, B. Dasgupta and J. F. Beacom, *Precise Relic WIMP Abundance and its Impact on Searches for Dark Matter Annihilation*, *Phys. Rev.* **D86** (2012) 023506, [1204.3622].

[38] M. Escudero, A. Berlin, D. Hooper and M.-X. Lin, *Toward (Finally!) Ruling Out Z and Higgs Mediated Dark Matter Models*, *JCAP* **1612** (2016) 029, [1609.09079].

[39] J. A. Casas, D. G. Cerde'no, J. M. Moreno and J. Quilis, *Reopening the Higgs portal for single scalar dark matter*, *JHEP* **05** (2017) 036, [1701.08134].

[40] LZ collaboration, D. S. Akerib et al., *LUX-ZEPLIN (LZ) Conceptual Design Report*, 1509.02910.

[41] M. Escudero, N. Rius and V. Sanz, *Sterile Neutrino portal to Dark Matter II: Exact Dark symmetry*, *Eur. Phys. J.* **C77** (2017) 397, [1607.02373].

[42] P. Gondolo and G. Gelmini, *Cosmic abundances of stable particles: Improved analysis*, *Nucl. Phys.* **B360** (1991) 145–179.

[43] G. F. Giudice, Y. Kats, M. McCullough, R. Torre and A. Urbano, *Clockwork/linear dilaton: structure and phenomenology*, *JHEP* **06** (2018) 009, [1711.08437].

[44] A. D. Martin, W. J. Stirling, R. S. Thorne and G. Watt, *Parton distributions for the LHC*, *Eur. Phys. J.* **C63** (2009) 189–285, [0901.0002].

[45] M. Spira, A. Djouadi, D. Graudenz and P. M. Zerwas, *Higgs boson production at the LHC*, *Nucl. Phys.* **B453** (1995) 17–82, [hep-ph/9504378].

[46] ATLAS collaboration, M. Aaboud et al., *Search for new phenomena in high-mass diphoton final states using 37 fb^{-1} of proton–proton collisions collected at $\sqrt{s} = 13$ TeV with the ATLAS detector*, *Phys. Lett.* **B775** (2017) 105–125, [1707.04147].

[47] ATLAS collaboration, T. A. collaboration, *Search for new high-mass phenomena in the dilepton final state using 36.1 fb^{-1} of proton-proton collision data at $\sqrt{s} =$ 13 TeV with the ATLAS detector*, .

[48] J. Hisano, K. Ishiwata, N. Nagata and M. Yamanaka, *Direct Detection of Vector Dark Matter*, *Prog. Theor. Phys.* **126** (2011) 435–456, [1012.5455].

[49] XENON collaboration, E. Aprile et al., *First Dark Matter Search Results from the XENON1T Experiment*, *Phys. Rev. Lett.* **119** (2017) 181301, [1705.06655].

[50] Fermi-LAT, DES collaboration, A. Albert et al., *Searching for Dark Matter Annihilation in Recently Discovered Milky Way Satellites with Fermi-LAT*, *Astrophys. J.* **834** (2017) 110, [1611.03184].

[51] Fermi-LAT collaboration, M. Ajello et al., *Fermi-LAT Observations of High-Energy γ-Ray Emission Toward the Galactic Center*, *Astrophys. J.* **819** (2016) 44, [1511.02938].

[52] Fermi-LAT collaboration, M. Ackermann et al., *The Fermi Galactic Center GeV Excess and Implications for Dark Matter*, *Astrophys. J.* **840** (2017) 43, [1704.03910].

[53] AMS Collaboration collaboration, M. Aguilar, D. Aisa, B. Alpat, A. Alvino, G. Ambrosi, K. Andeen et al., *Precision measurement of the $(e^+ + e^-)$ flux in primary cosmic rays from 0.5 gev to 1 tev with the alpha magnetic spectrometer on the international space station*, *Phys. Rev. Lett.* **113** (Nov, 2014) 221102.

[54] AMS Collaboration collaboration, M. Aguilar, L. Ali Cavasonza, B. Alpat, G. Ambrosi, L. Arruda, N. Attig et al., *Antiproton flux, antiproton-to-proton flux ratio, and properties of elementary particle fluxes in primary cosmic rays measured with the alpha magnetic spectrometer on the international space station*, *Phys. Rev. Lett.* **117** (Aug, 2016) 091103.

[55] Y. Bai, M. Carena and J. Lykken, *Dilaton-assisted Dark Matter*, *Phys. Rev. Lett.* **103** (2009) 261803, [0909.1319].

Published for SISSA by Springer

Received: *December 21, 2019*
Revised: *February 24, 2020*
Accepted: *March 17, 2020*
Published: *April 7, 2020*

Gravity-mediated dark matter in clockwork/linear dilaton extra-dimensions

Miguel G. Folgado, Andrea Donini and Nuria Rius

Departamento de Física Teórica and IFIC, Universidad de Valencia-CSIC, C/ Catedrático José Beltrán 2, E-46980 Paterna, Spain

E-mail: migarfol@ific.uv.es, donini@ific.uv.es, nuria.rius@ific.uv.es

Abstract: We study for the first time the possibility that Dark Matter (represented by particles with spin $0, 1/2$ or 1) interacts gravitationally with Standard Model particles in an extra-dimensional Clockwork/Linear Dilaton model. We assume that both, the Dark Matter and the Standard Model, are localized in the IR-brane and only interact via gravitational mediators, namely the Kaluza-Klein (KK) graviton and the radion/KK-dilaton modes. We analyse in detail the Dark Matter annihilation channel into Standard Model particles and into two on-shell Kaluza-Klein towers (either two KK-gravitons, or two radion/KK-dilatons, or one of each), finding that it is possible to obtain the observed relic abundance via thermal freeze-out for Dark Matter masses in the range $m_{\rm DM} \in [1, 15]$ TeV for a 5-dimensional gravitational scale M_5 ranging from 5 to a few hundreds of TeV, even after taking into account the bounds from LHC Run II and irrespectively of the DM particle spin.

Keywords: Phenomenology of Field Theories in Higher Dimensions, Strings and branes phenomenology

ArXiv ePrint: 1912.02689

https://doi.org/10.1007/JHEP04(2020)036

JHEP04(2020)036

Contents

1 Introduction

The Standard Model of Fundamental Interactions is in a wonderful shape, after the discovery of the Higgs boson in 2012 [1], and it may very well be that a huge energy desert above the TeV will be painstakingly explored till we could get in contact with even a single new particle. However, a reasonable hope can alter this unappealing landscape: there it must be something more than the Standard Model out there, as the Standard Model is not able to explain what Dark Matter is. The Nature of Dark Matter (DM) is, indeed, one of the longest long-standing puzzles to be explained in order to claim that we have a "complete" picture of the Universe. On one side, both from astrophysical and cosmological data (see, e.g., Ref. [2] and refs. therein), rather clear indications regarding the existence of some kind of matter that gravitates but that does not interact with other particles by any other detectable mean can be gathered. On the other hand, no candidate to fill the rôle of DM has yet been observed in high-energy experiments at colliders, nor is present in the Standard Model (SM) spectrum. Extensions of the Standard Model usually do include some DM candidate, a stable (or long-lived, with a lifetime as long as the age of the Universe) particle, with very small or none interaction with Standard Model particles and with particles of its own kind. These states are usually supposed to be rather heavy and are called "WIMP's", or "weakly interacting massive particles". Examples of these are the neutralino in supersymmetric extensions of the SM [3] or the lightest Kaluza-Klein particle in Universal Extra-Dimensions [4]. The typical range of masses for these particles was expected to be $m_{\rm DM} \in [100, 1000]$ GeV. However, searches for these heavy particles at the LHC have pushed bounds on the masses of the candidates above the TeV scale, into the multi-TeV region. Moreover, experiments searching for DM particles through their interactions with a fixed target, or "Direct Detection" (DD) experiments (see, e.g., Ref. [5]) or through their annihilation into Standard Model particles, or "Indirect Detection" (ID) experiments (see, e.g., Ref. [6]) have thoroughly explored the $m_{\rm DM} \in [100, 1000]$ GeV region, pushing constraints on the interaction cross-section between DM and SM particles to very small values. In addition to this, both DD and ID experiments have a rather limited sensitivity above the TeV, as they have been mostly designed to look for $\mathcal{O}(100)$ GeV particles. Other hypotheses have, however, been advanced: DM particles could indeed be "feebly interacting massive particles" (FIMP's) [7], "strongly interacting massive particles" (SIMP's) [8] or "axion-like" very light particles (ALP's) [9]. All of these new proposals try to explore the possibility that DM is made of particles lighter than the expected WIMP range, a region where the exclusion bounds from DD and ID experiments are much weaker.

If we take seriously the possibility that DM is made of $\mathcal{O}(1)$ TeV particles other options can be considered, though. One interesting option is that the interaction between DM and SM particles be only gravitational. Being, however, the gravitational coupling enhanced by the existence of more than 3 spatial dimensions. Several extra-dimensional models have been proposed in the last twenty years to explain a troublesome feature of the Standard

Model, nicknamed as the "Hierarchy Problem", i.e. the large hierarchy between the electroweak scale, $\Lambda_{\rm EW} \sim 250$ GeV, and the Planck scale, $M_P \sim 10^{19}$ GeV. In short, the mass of a scalar particle (the Higgs boson) should be sensitive (through loops) to the scale at which the Standard Model may be replaced by a more fundamental theory. If there is no new physics between the energy frontier reached by the LHC and the Planck scale, then the mass of the Higgs boson should be as large as the latter. Being the experimentally measured mass of the Higgs $m_{\rm H} = \mathcal{O}(\Lambda_{\rm EW})$, either the SM is not an effective theory and it is, after all, the ultimate theory (something not very convincing, as the SM does not explain Dark Matter, Dark Energy, Baryogenesis, the source of neutrino masses and, of course, gravity) or an incredible amount of fine-tuning between loop corrections stabilizes $m_{\rm H}$ at its value. Extra-dimensional models solve the hierarchy problem by either replacing the Planck scale $M_{\rm P}$ with a fundamental gravitational scale $M_{\rm D}$ (being D the number of dimensions) that could be as low as a few TeV (Large Extra-Dimensions models, or LED, see Refs. [10–14]), or by "warping" the space-time such that the effective Planck scale Λ felt by particles of the SM is indeed much smaller than the fundamental scale $M_{\rm D}$, similar to $M_{\rm P}$ (see Refs. [15, 16]), or by a mixture of the two options (see Refs. [17, 18]).

The possibility that Dark Matter particles, whatever they be, may have an *enhanced* gravitational interaction with SM particles has been studied mainly in the context of warped extra-dimensions. The idea was first advanced in Refs. [19, 20] and subsequently studied in Refs. [21–29]. The generic conclusion of these papers was that when all the matter content is localized in the so-called TeV (or infrared brane), after taking into account current LHC bounds it was not possible to achieve the observed Dark Matter relic abundance in warped models for scalar DM particles (whereas this was not the case for fermion and vector Dark Matter). However, an important caveat was that these conclusions were drawn assuming the DM particle being *lighter* than the first Kaluza-Klein graviton mode. In this case, the only kinematically available channel to deplete the Dark Matter density in the Early Universe is the annihilation of two DM particles into two SM particles through virtual KK-graviton exchange. However, in Ref. [30], we performed a check of the literature for the particular case of scalar DM in warped extra-dimensions, finding that as soon as the DM particle is allowed to be *heavier* than the first KK-graviton, annihilation of two DM particles into two KK-gravitons becomes kinematically possible and, through this channel, the observed relic abundance can indeed be achieved in a significant region of the parameter space within the freeze-out scenario. In the same paper, we included previously overlooked contributions to the DM annihilation cross-section, such as the possibility that DM annihilation into any pair of KK-gravitons can occur (regardless of the KK-number of the gravitons), and additional contributions to the thermally-averaged cross-section arising at second order in the expansion of the metric around a background Minkowski 5-dimensional space-time (the correct order to reach, once considering production of two KK-gravitons). Eventually, we also study the impact of a Goldberger-Wise radion [31], both in DM annihilation through virtual radion exchange and through direct production of two radions. The region of the parameter space for which the observed DM relic abundance is achieved in the freeze-out framework corresponds to DM masses in the range $m_{\rm DM} \in [1, 10]$ TeV, with first KK-graviton mass ranging from hundreds of GeV to some TeV. The price to pay to achieve the freeze-out thermally-averaged cross-section is that the scale Λ for which interactions between SM particles and KK-gravitons occur must be larger than 10 TeV, approximately. Therefore, in this scenario, the hierarchy problem cannot be completeley solved and some hierarchy between Λ and $\Lambda_{\rm EW}$ is still present. This is something, however, common to most proposals of new physics aiming at solving the hierarchy problem, as the LHC has found no hint whatsoever of new physics to date. One of the most interesting features of the scenario proposed in Ref. [30] is that a large part of the allowed parameter space could be tested using either the LHC Run III or the HL-LHC data. By the end of the next decade, therefore, only tiny patches of the allowed parameter space should survive in case of no experimental signal, tipically corresponding to DM mass $m_{\rm DM} \sim 10$ TeV, near the theoretical unitarity bounds.

In this paper, we extend the study of DM in an extra-dimensional framework to the case of a 5-dimensional ClockWork/Linear Dilaton (CW/LD) model. This model was proposed in Ref. [17] and its phenomenology at the LHC has been studied in Ref. [18]. In this scenario, a KK-graviton tower with spacing very similar to that of LED models starts at a mass gap k with respect to the zero-mode graviton. The fundamental gravitational scale M_5 can be as low as the TeV, where k is typically chosen in the GeV to TeV range. To our knowledge, this paper is the first attempt to use the CW/LD framework to explain the observed Dark Matter abundance in the Universe. In order to study this possibility, we very much follow the outline of our previous paper on DM in warped extra-dimensions albeit in this case we will consider DM particles with spin 0, 1/2 and 1. Also in this scenario we have found that the freeze-out thermal relic abundance can be achieved in a significant region of the model parameter space, with the DM mass ranging from 1 TeV to approximately 15 TeV, for DM of any spin. The fundamental gravitational scale M_5 needed to achieve the target relic abundance goes from a few TeV to a few hundreds of TeV, thus introducing a little hierarchy problem. Notice that the LHC Run III data and those of the high-luminosity upgrade HL-LHC will be able to test most of this region.

The paper is organized as follows: in Sect. 2 we outline the theoretical framework, reminding shortly the basic ingredients of the ClockWork/Linear Dilaton extra-dimensional scenario and of how dark matter can be included within this hypothesis; in Sect. 3 we show our results for the annihilation cross-sections of DM particles into SM particles, KK-gravitons and radion/KK-dilatons; in Sect. 4 we review the present experimental bounds on the parameters of the model (the fundamental Planck scale M_5, the mass gap k and the DM mass $m_{\rm DM}$) from the LHC and from direct and indirect searches of Dark Matter, and recall the theoretical constraints (coming from unitarity violation and effective field theory consistency); in Sect. 5 we explore the allowed parameter space such that the correct relic abundance is achieved for DM particles; and, eventually, in Sect. 6 we conclude. In the Appendices we give some of the mathematical expressions used in the paper: in App. A we give the Feynman rules for the theory considered here; in App. B we give the expressions for the decay amplitudes of the KK-graviton; in App. C we remind how the sum over KK-modes is carried on; and, eventually, in App. D we give the formulæ relative to the annihilation cross-sections of Dark Matter particles into Standard Model particles, KK-gravitons and radion/KK-dilatons.

2 Theoretical framework

In this Section, we first review the freeze-out mechanism that could produce the observed DM relic abundance in the Universe. We then sketch the basic ingredients of the ClockWork/Linear Dilaton Extra-Dimensions scenario (CW/LD) needed to compute the thermally-averaged DM annihilation cross-section.

2.1 The DM Relic Abundance in the Freeze-Out scenario

The fact that a significant fraction of the Universe energy appears in the form of a non-baryonic (*i.e.* electromagnetically inert) matter is the outcome of experimental data ranging from astrophysical to cosmological scales. This component of the Universe energy density is called *Dark Matter* and, in the cosmological "standard model", the ΛCDM, it is usually assumed to be represented by stable (or long-lived) heavy particles (*i.e.* non-relativistic, or "cold"). Within the thermal DM production scenario, DM particles were in thermal equilibrium with the rest of SM particles in the Early Universe. The DM density is governed by the Boltzmann equation [32]:

$$\frac{dn_{\rm DM}}{dt} = -3H(T)\, n_{\rm DM} - \langle\sigma v\rangle \left[n_{\rm DM}^2 - (n_{\rm DM}^{eq})^2\right] \,, \tag{2.1}$$

with T the temperature and $H(T)$ the Hubble parameter as a function of the temperature. The Boltzmann equation depends on a term proportional to the Hubble expansion rate at temperature T and a term proportional to the thermally-averaged cross-section, $\langle\sigma v\rangle$. To obtain the correct population of DM particles within this scenario, the rate of decay and annihilation of DM particles should be such that, below a certain temperature $T_{\rm FO}$, the DM density $n_{\rm DM}(T)$ "freezes out" and thermal fluctuations cannot any longer modify it. This occurs when $\langle\sigma v\rangle \times n_{\rm DM}$ falls below $H(T)$, DM decouples from the rest of particles and leaves an approximately constant number density in the co-moving frame, called relic abundance. The experimental value of the relic abundance can be derived starting from the DM density in the ΛCDM model. From Ref. [33] we have $\Omega_{\rm CDM}h^2 = 0.1198 \pm 0.0012$, being h the Hubble parameter. Solving eq. (2.1), it can be found for the thermally-averaged cross-section at the freeze-out $\langle\sigma_{\rm FO}\, v\rangle \simeq 2.2 \times 10^{-26}$ cm^3/s [34].

It is very common to compute $\langle\sigma v\rangle$ in a given model in the so-called *velocity expansion* (*i.e.* assuming small relative velocity between the two DM particles). However, this approximation may fail in the neighbourhood of resonances. In the CW/LD model, the virtual graviton exchange cross-section is indeed the result of an infinite sum of KK-graviton modes. For this reason, we computed the value of $\langle\sigma v\rangle$ using the exact expression from Ref. [35]:

$$\langle\sigma v\rangle = \frac{1}{8m_S^4\, T\, K_2^2(x)} \int_{4m_S^2}^{\infty} ds(s - 4m_S^2)\,\sqrt{s}\,\sigma(s)\, K_1\left(\frac{\sqrt{s}}{T}\right) \,, \tag{2.2}$$

being K_1 and K_2 the modified Bessel functions and v the relative velocity between DM particles.

2.2 A short summary on ClockWork/Linear Dilaton Extra-Dimensions

The metric considered in the CW/LD scenario (see Refs. [17, 18]) is:

$$ds^2 = e^{4/3 k r_c |y|} \left(\eta_{\mu\nu} dx^\mu dx^\nu - r_c^2 \, dy^2 \right) , \tag{2.3}$$

where the signature of the metric is $(+, -, -, -, -)$ and, as usual, we use capital latin indices M, N to run over the 5 dimensions and greek indices μ, ν only over 4 dimensions. Notice that we have rescaled the coordinate in the extra-dimension such that y is adimensional. This particular metric was first proposed in the context of *Linear Dilaton* (LD) models and *Little String Theory* (see, *e.g.* Refs. [36–38] and references therein). The metric in eq. (2.3) implies that the space-time is non-factorizable, as the length scales on our 4-dimensional space-time depending on the particular position in the extra-dimension due to the warping factor $\exp(2/3 \, k r_c \, |y|)$. Notice, however, that in the limit $k \to 0$ the standard, factorizable, flat LED case [10–14] is immediately recovered. As for the case of the Randall-Sundrum model, also in the CW/LD scenario the extra-dimension is compactified on a $\mathcal{S}_1/\mathcal{Z}_2$ orbifold (with r_c the compactification radius), and two branes are located at the fixed points of the orbifold, $y = 0$ ("IR" brane) and at $y = \pi$ ("UV" brane). Standard model fields are located in one of the two branes (usually the IR-brane). The scale k, also called the "clockwork spring" (a term inherited by its rôle in the discrete version of the Clockwork model [17]), is the curvature along the 5th-dimension and it can be much smaller than the Planck scale (indeed, it can be as light as a few GeV). Being the relation between $M_{\rm P}$ and the fundamental gravitational scale M_5 in the CW/LD model:

$$M_{\rm P}^2 = \frac{M_5^3}{k} \left(e^{2\pi k r_c} - 1 \right) , \tag{2.4}$$

it can be shown that, in order to solve or alleviate the hierarchy problem, k and r_c must satisfy the following relation:

$$k \, r_c = 10 + \frac{1}{2\pi} \ln \left(\frac{k}{\rm TeV} \right) - \frac{3}{2\pi} \ln \left(\frac{M_5}{10 \, \rm TeV} \right) . \tag{2.5}$$

For $M_5 = 10$ TeV and r_c saturating the present experimental bound on deviations from the Newton's law, $r_c \sim 100 \, \mu$m [39], this relation implies that k could be as small as $k \sim 2$ eV, and KK-graviton modes would therefore be as light as the eV, also. This "extreme" scenario does not differ much from the LED case, but for the important difference that the hierarchy problem could be solved with just one extra-dimension (for LED models, in order to bring M_5 down to the TeV scale, an astronomical lenght r_c is needed and, thus, viable hierarchy-solving LED models start with at least 2 extra-dimensions). In the phenomenological application of the CW/LD model in the literature, however, k is typically chosen above the GeV-scale and, therefore, r_c is accordingly diminished so as to escape direct observation. Notice that, differently from the case of warped extra-dimensions, where scales are all of the order of the Planck scale ($M_5, k \sim M_{\rm P}$) or within a few orders of magnitude, in the CW/LD scenario, both the fundamental gravitational scale M_5 and the mass gap k are much nearer to the electro-weak scale $\Lambda_{\rm EW}$ than to the Planck scale, as in the LED model.

The action in 5D is:

$$S = S_{\text{gravity}} + S_{\text{IR}} + S_{\text{UV}} \tag{2.6}$$

where the gravitational part is, in the Jordan frame:

$$S_{\text{gravity}} = \frac{M_5^3}{2} \int d^4x \int_0^{\pi} r_c dy \sqrt{G^{(5)}}\, e^S \left[R^{(5)} + G^{MN}_{(5)} \partial_M S \partial_N S + 4k^2 \right] , \tag{2.7}$$

with $G^{(5)}_{MN}$ and $R^{(5)}$ the 5-dimensional metric and Ricci scalar, respectively, and S the (dimensionless) dilaton field, $S = 2kr_c|y|$. We consider for the two brane actions the following expressions:

$$S_{\text{IR}} = \int d^4x \sqrt{-g^{(4)}_{\text{IR}}}\, e^S \left\{ -f^4_{\text{IR}} + \mathcal{L}_{\text{SM}} + \mathcal{L}_{\text{DM}} \right\} \tag{2.8}$$

and

$$S_{\text{UV}} = \int d^4x \sqrt{-g^{(4)}_{\text{UV}}}\, e^S \left\{ -f^4_{\text{UV}} + \dots \right\} , \tag{2.9}$$

where $f_{\text{IR}}, f_{\text{UV}}$ are the brane tensions for the two branes and $g^{(4)}_{\text{IR,UV}} = -G^{(5)}/G^{(5)}_{55}$ is the determinant of the induced metric on the IR- and UV-brane, respectively. Throughout the paper, we consider all the SM and DM fields localized on the IR-brane, whereas on the UV-brane we could have any other physics that is Planck-suppressed. We assume that DM particles only interact with the SM particles gravitationally by considering only DM singlets under the SM gauge group. More complicated DM spectra with several particles will also not be studied here.

Notice that the gravitational action is not in its canonical form. Going to the Einstein frame changing $G^{(5)}_{MN} \to \exp(-2/3S) G^{(5)}_{MN}$, we get :

$$\begin{aligned} S_{\text{gravity}} = & \int d^4x \int_0^{\pi} r_c dy \sqrt{-G^{(5)}} \left\{ \frac{M_5^3}{2} \left[R^{(5)} - \frac{1}{3} G^{MN}_{(5)} \partial_M S \partial_N S + 4e^{-\frac{2}{3}S} k^2 \right] \right\} \\ & + \int d^4x \int_0^{\pi} r_c dy \sqrt{-g^{(4)}}\, e^{-\frac{S}{3}} \left\{ \delta(y - y_0) \left[-f^4_{\text{IR}} + \mathcal{L}_{\text{SM}} + \mathcal{L}_{\text{DM}} \right] - \delta(y-\pi) f^4_{\text{UV}} \right\} , \end{aligned} \tag{2.10}$$

where now the gravitational action is the Einstein action and from the kinetic term of the dilaton field we can read out that the physical field must be rescaled as $\left(M_5^{3/2}/\sqrt{3} \right) S$. Eventually, it is important to stress that, in the Einstein frame, the brane action terms still have an exponential dependence $e^{-S/3}$ from the dilaton field. This action has a shift symmetry $S \to S + \text{const}$ in the limit $k \to 0$, that makes a small value of k with respect to M_5 "technically natural" in the 't Hooft sense. Using the action above in the Einstein frame, it can be shown that the metric in eq. (2.3) can be recovered as a classical background if the brane tensions are chosen as:

$$f^4_{\text{IR}} = -f^4_{\text{UV}} = -4k\, M_5^3 \, . \tag{2.11}$$

Notice that, in a pure 4-dimensional scenario, the gravitational interactions would be enormously suppressed by powers of the Planck mass, while in an extra-dimensional one the gravitational interaction is actually enhanced. Expanding the metric at first order around its static solution, we have:

$$G^{(5)}_{MN} = e^{2/3S}(\eta_{MN} + \frac{2}{M_5^{2/3}} h_{MN}) . \tag{2.12}$$

The 4-dimensional component of the 5-dimensional field h_{MN} can be expanded in a Kaluza-Klein tower of 4-dimensional fields as follows:

$$h_{\mu\nu}(x,y) = \sum_{n=0}^{\infty} \frac{1}{\sqrt{\pi r_c}} h^n_{\mu\nu}(x)\, \chi_n(y) . \tag{2.13}$$

The $h^n_{\mu\nu}(x)$ fields are the KK-modes of the 4-dimensional graviton and the $\chi_n(y)$ factors are their wavefunctions. Notice that in the 4-dimensional decomposition of the 5-dimensional metric, two other fields are generally present: the graviphoton, $h_{\mu 5}$, and the graviscalar h_{55}. The KK-tower of the graviscalar is absent from the low-energy spectrum, as they are eaten by the KK-tower of graviphotons to get a mass (due to the spontaneous breaking of translational invariance caused by the presence of one or more branes). These are, in turn, eaten by the KK-gravitons to get a mass (having, thus, five degrees of freedom). The surviving graviphoton zero-mode does not couple with the energy-momentum tensor in the weak gravitational field limit [40], whereas the graviscalar zero-mode will generically mix with the radion needed to stabilize the extra-dimension size.

The eigenfunctions $\chi_n(y)$ can be computed by solving the equation of motion in the extra-dimension of the fields:

$$\left[\partial_y^2 - k^2 r_c^2 + m_n^2 r_c^2\right] e^{k r_c |y|}\, \chi_n(y) = 0 \tag{2.14}$$

with Neumann boundary conditions $\partial_y \chi_n(y) = 0$ at $y = 0$ and π. Normalizing the eigenmodes such that the KK-modes have canonical kinetic terms in 4-dimensions, we get:

$$\begin{cases} \chi_0(y) = \sqrt{\frac{\pi k r_c}{e^{2\pi k r_c} - 1}} \,, \\ \\ \chi_n(y) = \frac{n}{m_n r_c} e^{-k r_c |y|} \left(\frac{k r_c}{n} \sin n|y| + \cos n|y| \right) \,, \end{cases} \tag{2.15}$$

with masses

$$m_0^2 = 0 \, ; \qquad m_n^2 = k^2 + \frac{n^2}{r_c^2} \, . \tag{2.16}$$

At the IR-brane one gets:

$$\mathcal{L} = -\frac{1}{M_5^{3/2}} T^{\mu\nu}(x) h_{\mu\nu}(x, y=0) = -\sum_{n=0} \frac{1}{\Lambda_n} h^n_{\mu\nu}(x)\, T^{\mu\nu}(x) \, , \tag{2.17}$$

where

$$\begin{cases} \frac{1}{\Lambda_0} = \frac{1}{M_{\rm P}} \,, \\ \\ \frac{1}{\Lambda_n} = \frac{1}{\sqrt{M_5^3 \pi r_c}} \left(1 + \frac{k^2 r_c^2}{n^2}\right)^{-1/2} = \frac{1}{\sqrt{M_5^3 \pi r_c}} \left(1 - \frac{k^2}{m_n^2}\right)^{1/2} \qquad n \neq 0 \, , \end{cases} \tag{2.18}$$

from which it is clear that the coupling between KK-graviton modes with $n \neq 0$ is suppressed by the effective scale Λ_n and not by the Planck scale, differently from the LED case and similarly to the Randall-Sundrum one.

It is useful to remind here the explicit form of the energy-momentum tensor for a scalar, fermion and vector field:

$$
\begin{cases}
T^{\Phi}_{\mu\nu} = (\partial_\mu \Phi)^\dagger (\partial_\nu \Phi) + (\partial_\nu \Phi)^\dagger (\partial_\mu \Phi) - \eta_{\mu\nu} \left\{ (\partial_\rho \Phi)^\dagger (\partial\rho \Phi) - m_\Phi^2 \Phi \Phi^\dagger \right\} , \\[2ex]
T^{\psi}_{\mu\nu} = 4 \left[-\eta_{\mu\nu} \left\{ \bar\psi (i\gamma_\rho \partial^\rho - m_\psi)\psi - \frac{1}{2}\partial^\rho (\bar f i \gamma_\nu f) \right\} + \left\{ \frac{1}{2}\bar\psi i \gamma_\mu \partial_\nu \psi - \frac{1}{4}\partial_\mu (\bar\psi i \gamma_\nu \psi) \right. \right. \\[2ex]
\qquad \left. \left. + \ \frac{1}{2}\bar\psi i \gamma_\nu \partial_\mu \psi - \frac{1}{4}\partial_\nu (\bar\psi i \gamma_\mu \psi) \right\} \right] , \\[2ex]
T^{V}_{\mu\nu} = \left[\eta_{\mu\nu} \left\{ \frac{1}{4} \mathbf{F}_{\rho\sigma} \, \mathbf{F}^{\rho\sigma} - \frac{m_V^2}{2} V^\rho V_\rho \right\} - \mathbf{F}^\rho_\mu \, \mathbf{F}_{\nu\rho} + m_V^2 V_\mu V_\nu \right]
\end{cases}
$$

where

$$
\mathbf{F}_{\mu\nu} = F_{\mu\nu} = \partial_\mu V_\nu - \partial_\nu V_\mu \tag{2.19}
$$

for an abelian gauge field and

$$
\mathbf{F}_{\mu\nu} = F^a_{\mu\nu} = \partial_\mu V^a_\nu - \partial_\nu V^a_\mu + g f^{abc} V^b_\mu V^c_\nu \tag{2.20}
$$

for a non-abelian gauge field. In both cases, the expressions above refers to the unitary gauge. For the case of the SM massless gauge fields the expression is $T^V_{\mu\nu} \mid_{m_V=0}$ (whilst we do not specify how the gauge field V_μ gets a mass).

2.3 Introducing the radion

Stabilization of the radius of the extra-dimension r_c is an issue. In general (see, e.g., Refs. [41–43]), bosonic quantum loops have a net effect on the boundaries of the extra-dimension such that the extra-dimension itself should shrink to a point. This feature, in a flat extra-dimension, can only be compensated by fermionic quantum loops and, usually, some supersymmetric framework is invoked to stabilize the radius of the extra-dimension (see, e.g., Ref. [44]). An additional advantage of supersymmetry in the bulk is that the CW/LD background metric may protect eq. (2.11) by fluctuations of the 5-dimensional cosmological constant (see, however, Ref. [45] for a non-supersymmetric clockwork implementation).

In the CW/LD scenario we can use the already present bulk dilaton field S to stabilize the compactification radius. If localized brane interactions generate a potential for S at $y = \pi$, then we could fix the value of the field S at the UV-brane, $S_{\rm UV} = S \mid_\pi$. This is indeed an additional boundary condition that fixes the distance between the two branes to be $\pi k \, r_c = S_{\rm UV}/2$ [17]:

$$
\begin{cases}
S_{\rm IR} = \int d^4x \sqrt{-g^{(4)}_{\rm IR}} \, e^S \left\{ -f^4_{\rm IR} + \frac{\mu_{\rm IR}}{2} (S - S_{\rm IR})^2 + \mathcal{L}_{\rm SM} + \mathcal{L}_{\rm DM} \right\} , \\[2ex]
S_{\rm UV} = \int d^4x \sqrt{-g^{(4)}_{\rm UV}} \, e^S \left\{ -f^4_{\rm UV} + \frac{\mu_{\rm UV}}{2} (S - S_{\rm UV})^2 + \ldots \right\} ,
\end{cases} \tag{2.21}
$$

with $\mu_{\rm IR}$ and $\mu_{\rm UV}$ two parameters with the dimension of a mass. In order to compute the scalar spectrum, we should introduce quantum fluctuations over the background values of $S(x,y) = S_0(y) + \varphi(x,y)$ (where $S_0(y) = 2kr_c|y|$) and of the metric, eq. (2.12). After deriving the Einstein equations for the two scalar degrees of freedom, φ and[1] Φ, and imposing the junction conditions at the boundaries, it can be shown that both satify the following equation of motion:

$$\left[\Box + \frac{1}{r_c^2}\frac{d^2}{dy^2} - k^2\right] e^{kr_c y}\begin{pmatrix}\Phi(x,y)\\ \varphi(x,y)\end{pmatrix} = 0\,. \tag{2.22}$$

Notice that only the combination $v(x,y) = \sqrt{6}e^{kr_c y}M_5^{3/2}\left[\Phi(x,y) - \varphi(x,y)/3\right]$ has a canonical kinetic term.

Expanding Φ and φ over a 4-dimensional plane-waves basis,

$$\Phi(x,y) = \sum_n \Phi_n(y)Q_n(x)\,; \qquad \varphi(x,y) = \sum_n \varphi_n(y)Q_n(x)\,; \qquad \left[\Box - m^2_{\Phi_n}\right]Q_n = 0\,, \tag{2.23}$$

we can eventually derive the scalar fluctuations wave-functions (for example, in Φ):

$$\Phi_n(y) = N_n e^{-kr_c y}\left[\sin(\beta_n y) + \omega_n\cos(\beta_n y)\right]\,, \tag{2.24}$$

with N_n a normalization factor, $\beta_n = m^2_{\Phi_n} - k^2$, and

$$\omega_n = -\frac{3\beta_n\mu_T}{2(k^2+\beta_n^2) + k\mu_T}\,. \tag{2.25}$$

In the so-called *rigid limit*, $\mu_{\rm UV} \to \infty$, the scalar spectrum is given by:

$$\begin{cases} m_r^2 \equiv m^2_{\Phi_0} = \frac{8}{9}k^2\,, \\ \\ m^2_{\Phi_n} = k^2 + \frac{n^2}{r_c^2} \qquad (n \geq 1)\,, \end{cases} \tag{2.26}$$

first obtained in Ref. [46], where we have identified the radion as the lightest state. Out of the rigid limit, the spectrum can be obtained expanding in inverse powers of $\mu_{\rm UV}$, introducing the adimensional parameters $\epsilon_{\rm IR,UV} = 2k/\mu_{\rm IR,UV}$. At first order in the ϵ's,

$$\begin{cases} m_r^2 \equiv m^2_{\Phi_0} = \frac{8}{9}k^2\left(1 - \frac{2\epsilon_{\rm UV}}{9}\right) + \mathcal{O}(\epsilon^2)\,, \\ \\ m^2_{\Phi_n} = k^2 + \frac{n^2}{r_c^2}\left[1 - \frac{6(n^2+k^2r_c^2)(\epsilon_{\rm UV}+\epsilon_{\rm IR})}{9n^2\pi kr_c + \pi k^3 r_c^3}\right] + \mathcal{O}(\epsilon^2)\,. \end{cases} \tag{2.27}$$

There are no massless states for non-vanishing μ's (*i.e.*, when the extra-dimension is stabilized). In the unstabilized regime (for $\mu_{\rm UV}, \mu_{\rm IR} \to 0$), the graviscalar and lowest-lying dilaton mode decouple and we expect two massless modes.

[1] Using the notation of Ref. [38], we call Φ the graviscalar h_{55}. Remember, however, that after compactification the KK-tower of h_{55} is eaten to give a longitudinal component to the KK-tower of gravitons.

The interactions of the radion and of the dilaton KK-tower with SM fields arises [38] from the term:

$$\int d^4x\sqrt{-g^{(4)}}\, e^{-S/3}\left[\mathcal{L}_{\rm SM}+\mathcal{L}_{\rm DM}\right] . \tag{2.28}$$

The main difference between the CW/LD case and the Randall-Sundrum case is that in the former case a dilaton dependence $e^{-S/3}$ is still present in the brane term action going from the Jordan frame to the Einstein frame. On the other hand, the Randall-Sundrum action is already in the Einstein frame (its gravitational action is in the canonical form) and the brane action term couples to gravity minimally, *i.e.* through the $\sqrt{-g^{(4)}}$ coefficient, only.

Expanding the background metric and the dilaton field at first order in quantum fluctuations, we get (after KK-decomposition):

$$\begin{aligned} S_{\rm int} = & -\frac{1}{2}\sum_n \Phi_n(0)\int d^4x\sqrt{-g_0^{(4)}}\left[g_0^{(4)}\right]^{\mu\nu}\left[T^{\rm SM}_{\mu\nu}+T^{\rm DM}_{\mu\nu}\right]Q_n \\ & -\frac{1}{3}\sum_n \varphi_n(0)\int d^4x\sqrt{-g_0^{(4)}}\left[\mathcal{L}_{\rm SM}+\mathcal{L}_{\rm DM}\right]Q_n\,. \end{aligned} \tag{2.29}$$

Notice that the scalar fluctuations of metric AND dilaton couple with 4-dimensional fields through the usual energy-momentum trace and with a direct coupling with the 4-dimensional lagrangian. This is different from the case of the Randall-Sundrum model, where only the first kind of coupling is present, being the radion of purely gravitational origin (see, for example, Ref. [47]). In the CW/LD model, thus, there are two kinds of coupling between the radion and the KK-dilaton fields and the 4-dimensional fields sitting on the IR-brane. Again, at first order in $\epsilon_{\rm UV,IR}$, we get:

$$\begin{cases} \frac{1}{\Lambda^0_\Phi} \equiv \frac{\Phi_0(0)}{2} = \frac{1}{6}\sqrt{\frac{k}{M_5^3}}\left(1+\frac{4}{9}\epsilon_{\rm UV}\right)+\mathcal{O}(\epsilon^2)\,, \\ \\ \frac{1}{\Lambda^n_\Phi} \equiv \frac{\Phi_n(0)}{2} = \frac{2kr_cn}{\sqrt{3\pi M_5^3 r_c}}\left(n^2+k^2r_c^2\right)^{-1/2}\left(9n^2+k^2r_c^2\right)^{-1/2}(1-\epsilon_{\rm UV})+\mathcal{O}(\epsilon^2) \\ \qquad\qquad\quad = \frac{2}{\sqrt{27\pi M_5^3 r_c}}\,\frac{k}{m_{\Phi_n}}\sqrt{\frac{1-\frac{k^2}{m^2_{\Phi_n}}}{1-\frac{8}{9}\frac{k^2}{m^2_{\Phi_n}}}}(1-\epsilon_{\rm UV})+\mathcal{O}(\epsilon^2) \end{cases} \tag{2.30}$$

and

$$\begin{cases} \frac{1}{\Lambda^0_\varphi} \equiv \frac{\varphi_0(0)}{3} = \frac{2}{27}\sqrt{\frac{k}{M_5^3}}\epsilon_{\rm UV}+\mathcal{O}(\epsilon^2)\,, \\ \\ \frac{1}{\Lambda^n_\varphi} \equiv \frac{\varphi_n(0)}{3} = \frac{n}{k\sqrt{3\pi M_5^3 r_c^3}}\left[\frac{\left(n^2+k^2r_c^2\right)}{\left(9n^2+k^2r_c^2\right)}\right]^{1/2}\epsilon_{\rm UV}+\mathcal{O}(\epsilon^2) \end{cases} \tag{2.31}$$

In the rigid limit ($\mu_{\rm UV,IR}\to\infty$) the coupling of dilaton modes with the SM lagrangian vanishes ($1/\Lambda^0_\varphi, 1/\Lambda^n_\varphi \to 0$). In the rest of the paper, we will work in this limit in order to get a sound insight of how the radion and dilaton KK-modes may affect the generation of the freeze-out thermal abundance. A complete study of the impact of scalar perturbations to the DM phenomenology would imply considering general values for $\epsilon_{\rm UV}$ and $\epsilon_{\rm IR}$ and it is beyond the scope of this paper.

A further simplification that we are going to consider is the following: in the presence of a scalar field on the brane (such as the Higgs field), a non-minimal coupling of the scalar with the Ricci scalar is not forbidden by any symmetry. This may arise as a new term in the action:

$$\Delta S_{\rm IR} = \int d^4x \sqrt{-g^{(4)}} e^{\varphi/3} \xi R H^\dagger H \,. \tag{2.32}$$

Such term induces an additional kinetic mixing between the graviscalar Φ_0, the lowest-lying dilaton φ_0 and the Higgs and, therefore, additional couplings with the SM fields. We will neglect this non-minimal coupling in the rest of the paper, taking $\xi = 0$.

Summarizing, in the rigid limit and in the absence of a mixing between the Higgs and the other scalar fields, the scalar perturbation interaction lagrangian with SM and DM particles at first order is:

$$\mathcal{L}_v^{\rm SM} = \sum_{n=0}^{\infty} \frac{1}{\Lambda_\Phi^n} \left[T_{\rm SM} + \frac{\alpha_{EM}\, C_{EM}}{8\pi} F_{\mu\nu} F^{\mu\nu} + \frac{\alpha_S C_3}{8\pi} \sum_a F^a_{\mu\nu} F^{a\mu\nu} \right] v_n \,, \tag{2.33}$$

where $r = v_0$ is the radion field and v_n for $n \geq 1$ is the dilaton KK-tower, and $T_{\rm SM}$ is the trace of the SM energy-momentum tensor. The coefficients of the coupling between scalar perturbations and massless gauge fields are given in App. A.2. Notice that massless gauge fields do not contribute to the trace of the energy-momentum tensor, but they generate effective couplings from two different sources: quarks and W bosons loops contribution and the trace anomaly [48].

2.4 Contributions to $\langle \sigma v \rangle$ in the CW/LD scenario

We are not assuming any particular spin for the DM particle; our only assumptions are that there is just one particle responsible for the whole DM relic abundance and that this particle interacts with the SM only gravitationally. Therefore, in the following we label such particles generically by DM's. The total annihilation cross-section is:

$$\begin{aligned} \sigma_{\rm th} = & \sum_{\rm SM} \sigma_{\rm ve}({\rm DM\,DM} \to {\rm SM\,SM}) + \sum_{n=1} \sum_{m=1} \sigma_{GG}({\rm DM\,DM} \to G_n\, G_m) \\ & + \sum_{n=0} \sum_{m=0} \sigma_{\Phi\Phi}({\rm DM\,DM} \to \Phi_m\, \Phi_n) + \sum_{n=1} \sum_{m=0} \sigma_{G\Phi}({\rm DM\,DM} \to G_n\, \Phi_m) \\ & , \end{aligned} \tag{2.34}$$

where in the first term, $\sigma_{\rm ve}$ ("ve" stands for "virtual exchange"), we sum over all SM particles. The second term, σ_{GG}, corresponds to DM annihilation into KK-gravitons G_n. Notice that we do not consider DM annihilation into zero-mode gravitons G_0, as it is Planck-suppressed. The third term, $\sigma_{\Phi\Phi}$, corresponds to DM annihilation into radions and KK-dilaton modes. Eventually, the fourth term, $\sigma_{G\Phi}$, is the production of one tower of KK-gravitons in association with a tower of radion/KK-dilatons (a channel previously overlooked in the literature on the subject). Notice that the KK-number is not conserved in the second, third and fourth term of eq. (2.34) due to the explicit breaking of momentum conservation in the 5th-dimension induced by the brane terms and, therefore, we must sum over all values of (m, n) as long as the condition $2m_{\rm DM} \geq m_n + m_m$ (being m_n

the mass of the n-th KK-graviton or radion/KK-dilaton) is fulfilled. If the DM mass $m_{\rm DM}$ is smaller than the mass of the first KK-graviton and of the radion, only the first channel is open. Formulæ for the DM annihilation into SM particles through virtual KK-graviton and radion/KK-dilaton exchange are given in App. D in the small relative velocity approximation, expanding the centre-of-mass energy s around $s \simeq 4m_{\rm DM}^2$. Notice that, when computing the contribution of the radion/KK-dilaton exchange and KK-graviton exchange to the annihilation DM cross-section into SM particles, it is of the uttermost importance to take into account properly the decay width of the radion/KK-dilaton and of the KK-gravitons. Formulæ for the radion/KK-dilaton and KK-graviton decays[2] are given in App. B.

If the DM mass is larger than the radion or the first KK-graviton mass[3], $m_{\rm DM} \leq (m_r, m_{G_1})$, the direct production of KK-graviton and/or radion/KK-dilaton towers becomes possible and the other three channels of eq. (2.34) open. The analytic expressions for $\sigma_{GG}({\rm DM\,DM} \to G_m\,G_n)$, $\sigma_{G\Phi}({\rm DM\,DM} \to G_m\,\Phi_n)$ and $\sigma_{\Phi\Phi}({\rm DM\,DM} \to \Phi_m\,\Phi_n)$ in the small relative velocity approximation are given in App. D.

A DM singlet could have other interactions with the SM besides the gravitational one, through several so-called "portals". Such scenarios have been extensively studied in the literature and are strongly constrained (see for instance [49, 50] for recent analyses), so we will neglect those couplings and focus only on the gravitational mediators that have not been previously considered.

3 DM annihilation cross-section in CW/LD model

In this section we study in detail the different contributions to the thermally-averaged DM annihilation cross-section, comparing the results for scalar, fermion and vector DM particles.

As we reminded in the previous section, for relatively low DM particles mass the first annihilation channel to open is the annihilation into SM particles through KK-graviton or radion/KK-dilaton exchange. Differently from the RS case (see Ref. [30]), both the virtual KK-graviton and radion/KK-dilaton exchange cross-sections do not behave as the sum of relatively independent channels with well-separated peaks, one per KK-mode. For the typical values of M_5 and k that may solve the hierarchy problem, in the CW/LD case a huge number of KK-modes must be coherently summed in $\sigma_{\rm ve}({\rm DM\,DM} \to {\rm SM\,SM})$.

In order to understand easily the difference between the cross-sections for scalar, fermion and vector DM particles, we remind in Tab. 1 the dependence of the thermally-averaged annihilation cross-section $\langle \sigma v \rangle$ on the relative velocity v, from App. D. Recall that v acts as a suppression factor and, therefore, the larger the power to which it appears, the smaller the cross-section.

[2]Recall that, due to the breaking of translational invariance in the extra-dimension, the KK-number is not conserved and heavy KK-graviton and KK-dilaton modes can also decay into lighter KK-modes when kinematically allowed.

[3]Notice that, in the rigid limit, both the radion/KK-dilaton and KK-graviton masses only depend on the parameter k and r_c that are chosen to solve the hierarchy problem, differently from the RS scenario where the radion mass is an additional free parameter of the model.

	Scalar	Fermion	Vector
Graviton Virtual Exchange	v^4 (d)	v^2 (p)	v^0 (s)
Radion/Dilatons Virtual Exchange	v^0 (s)	v^2 (p)	v^0 (s)
Annihilation into Gravitons	v^0 (s)	v^0 (s)	v^0 (s)
Annihilation into Radion/Dilatons	v^0 (s)	v^2 (p)	v^0 (s)
Annihilation into Dilaton + Graviton	v^0 (s)	v^0 (s)	v^0 (s)

Table 1. Velocity dependence of the different DM annihilation channels and the corresponding s-, p- or d-wave.

The thermally-averaged virtual exchange cross-section, $\langle \sigma_{\rm ve} v \rangle = \langle (\sigma_{{\rm ve},G} + \sigma_{{\rm ve},\Phi}) v \rangle$, is depicted in Fig. 1 for a scalar (left panel), a fermion (middle panel) and a vector (right panel) DM particle, respectively, for the particular choice $k = 1$ TeV and $M_5 = 7$ TeV [4]. Virtual radion/KK-dilaton exchange is shown with (green) dot-dashed lines, virtual KK-graviton exchange with (blue) solid lines. In all cases, $\sigma_{\rm ve}({\rm DM\,DM} \to {\rm SM\,SM})$ is extremely small below $m_{\rm DM} \sim 500$ GeV, whilst rapidly increasing when $m_{\rm DM}$ approaches half the mass of the lightest mode (the radion). From that point onward, for larger and larger DM masses the cross-section starts to rapidly oscillate crossing threshold after threshold with new KK-modes entering the game. This behaviour can be clearly seen in the dot-dashed lines representing radion/KK-dilaton virtual exchange, where the difference between on-peak and off-peak cross-section can be as large as one order of magnitude. The sum over KK-dilaton modes does not increase the cross-section going to larger DM masses, as interferences from the near-continuum of modes collectively result in a slow decrease of $\sigma_{{\rm ve},\Phi}$ going from $m_{\rm DM} \sim 1$ TeV to $m_{\rm DM} \sim 10$ TeV. The KK-graviton exchange cross-section shows a different behaviour: the difference between on- and off-peak is extremely small, and the sum over virtual KK-graviton modes gives a net (albeit slow) increase of the cross-section going to larger DM masses. These results are common to scalar, fermion and vector DM particles.

In the three panels, we also show the DM annihilation cross-section into real KK-gravitons, represented by an (orange) dashed line, and the freeze-out thermally-averaged cross-section $\langle \sigma_{\rm FO} v \rangle$, represented by the horizontal red-dotted line . The DM annihilation cross-section into two real radion/KK-dilaton towers and into one KK-graviton and one radion/KK-dilaton tower are not shown, as both are much smaller and, therefore, irrelevant. For a scalar or a vector DM particle the real KK-graviton production cross-sections are very similar. This component of the total cross-section takes over both the radion/KK-dilaton and KK-graviton virtual exchange and rapidly dominates the total cross-section for $m_{\rm DM}$ above a few TeVs. On the other hand, the fermion DM real KK-graviton production cross-section is substantially smaller than those for scalar and vector DM particles in the considered range of $m_{\rm DM}$ and its growth with $m_{\rm DM}$ is much slower (the corresponding cross-sections can be found in App. D.1). We can see that, for the considered values of M_5

[4] Although the observed DM relic density can be obtained for lower values of (k, M_5), our choice is motivated by the fact that these are currently allowed by LHC data, as we will see in the next section.

and k, the total fermion DM annihilation cross-section is dominated by virtual KK-graviton exchange up to $m_{\rm DM} \sim 10$ TeV.

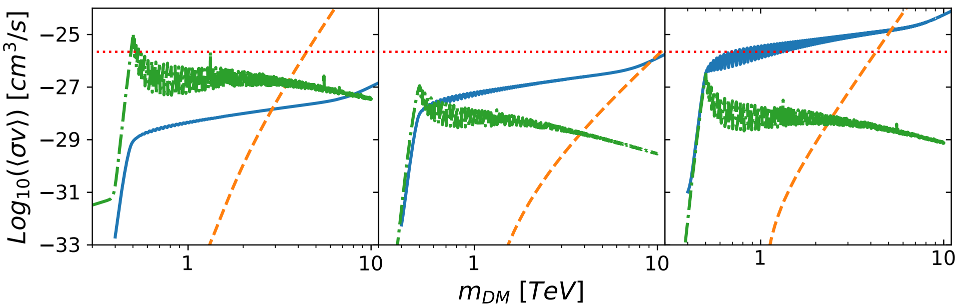

Figure 1. *Comparison of the thermally-averaged DM annihilation cross-section into SM particles through virtual radion/KK-dilaton exchange $\langle\sigma_{{\rm ve},r}v\rangle$ (green dot-dashed lines) and virtual KK-graviton exchange $\langle\sigma_{{\rm ve},G}v\rangle$ (blue solid lines), as a function of the DM particle mass, m_{DM}. Left panel: scalar DM. Middle panel: fermion DM. Right panel: vector DM. In all panels, the orange dashed line represents the thermally-averaged DM annihilation cross-section into KK-gravitons, $\langle\sigma_{GG}v\rangle$, summing over all kinematically allowed KK-gravitons in the final state. The horizontal red-dotted line represents $\langle\sigma_{\rm FO}v\rangle$. The results have been obtained for $M_5 = 7$ TeV and $k = 1$ TeV.*

Comparing the results for different spin of the DM particle, we see that the scalar DM case is the only one where, for relatively low DM masses, the radion/KK-dilaton virtual exchange cross-section actually dominates over the KK-graviton virtual exchange one. The difference between the two contributions can be as large as two orders of magnitude for $m_{\rm DM}$ smaller than a few TeV, whereas the two become comparable for $m_{\rm DM} \sim 10$ TeV (at a scale where, however, the real KK-graviton production has already become the dominant process). In this particular scenario, as it was the case for the RS model, the thermally-averaged virtual KK-graviton exchange cross-section is much lower than $\langle\sigma_{\rm FO}v\rangle$. On the other hand, the virtual radion/KK-dilaton exchange cross-section can actually reach the target value for $m^2_{\rm DM} \sim m^2_r/4$ (*i.e.* $m^2_{\rm DM} = 2/9k^2$ in the rigid limit). For fermion and vector DM particles, this is not the case: the virtual radion/KK-dilaton exchange cross-section is of the same order or smaller than the virtual KK-graviton exchange cross-section[5]. In summary, for the particular choice of k and M_5 shown in Fig. 1, for a scalar DM particle the target freeze-out value $\langle\sigma_{\rm FO}v\rangle$ is achievable either through virtual radion/KK-dilaton exchange for low $m_{\rm DM}$ or via real KK-graviton production for $m_{\rm DM}$ a few TeV; for a fermion DM particle $\langle\sigma_{\rm FO}v\rangle$ is not achieved for $m_{\rm DM} < 10$ TeV; and, for a vector DM particle, the target relic abundance is achieved through virtual KK-graviton exchange for $m_{\rm DM} \sim 1$ TeV (as it was found in the RS scenario [19, 22]).

In Fig. 2 we show the total cross-section involving KK-gravitons, only (summing virtual KK-graviton exchange and KK-graviton production) as a function of the DM particle

[5]This is the combined effect of the different v-dependence according to the DM particle spin and of numerical factors.

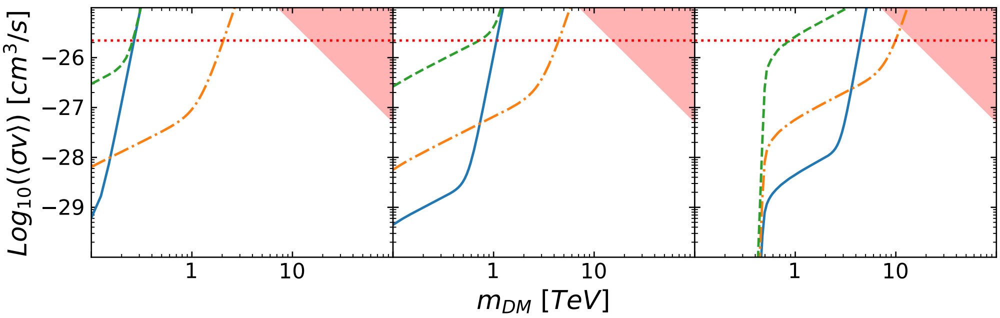

Figure 2. *The thermally-averaged DM annihilation cross-section through virtual KK-graviton exchange and direct production of two KK-gravitons, $\sigma_G = \sigma_{\rm ve,G} + \sigma_{GG}$, as a function of the DM mass m_{DM} for three choices of k: $k = 10$ GeV (left panel); $k = 100$ GeV (middle panel); $k = 1000$ GeV (right panel). In all panels, $M_5 = 7$ TeV. The green dashed, orange dot-dashed and blue solid lines represent $\langle \sigma_G v\rangle$ for a vector, fermion and scalar DM particle, respectively. The red-shaded area represents the theoretical unitarity bound $\sigma \geq 1/s$.*

mass $m_{\rm DM}$ for different choices of k: $k = 10$ GeV (left panel), $k = 100$ GeV (middle panel) and $k = 1$ TeV (right panel). In all cases, $M_5 = 7$ TeV. In all panels, we plot $\langle \sigma_G v\rangle = \langle (\sigma_{\rm ve,G} + \sigma_{GG})\, v\rangle$ for scalar (blue, solid lines), fermionic (orange, dot-dashed lines) and vector (green, dashed lines) DM particles, thus making comparison easier. The red dotted horizontal line shows $\langle \sigma_{\rm FO} v\rangle$. For all choices of k, at very low values of $m_{\rm DM}$ the scalar DM scenario give a much lower thermally-averaged cross-section with respect to the fermion and vector case. It rapidly catches up, though, eventually merging with the vector case. We see that $\langle \sigma_G v\rangle = \langle \sigma_{\rm FO} v\rangle$ at approximately $m_{\rm DM} \sim 10\, k$ for k below the TeV and $m_{\rm DM} = \mathcal{O}(k)$ for k at the TeV in the scalar and vector case. On the other hand, a much larger value of $m_{\rm DM}$ is needed to achieve the freeze-out target value if the DM particle is a fermion. The red-shaded area represents the theoretical unitarity bound $\langle \sigma v\rangle \geq 1/s$, where we can no longer trust the theory outlined in Sect. 2 and higher-order operators should be taken into account.

We have seen that it is relatively easy to achieve the freeze-out relic abundance for DM particles with a mass at the TeV scale or below for $M_5 = 7$ TeV. However, it is important to understand how this scales with M_5 so as to see how much having a DM candidate is compatible with solving the hierarchy problem. This is shown in Fig. 3, where we draw the value of M_5 needed to achieve the freeze-out DM annihilation cross-section $\langle \sigma_{\rm FO} v\rangle$ for a given choice of k and $m_{\rm DM}$. In the top-left panel we show our results for a scalar DM particle using only virtual KK-graviton exchange and real KK-graviton production; in the top-right panel we again show our results for a scalar DM particle, albeit adding the contribution from virtual radion/KK-dilaton exchange and real radion/KK-dilaton production (since we saw in Fig. 1 that for this particular case these contributions are quite relevant); in the bottom-left and bottom-right panels, on the other hand, we show our results for a fermion and a vector DM particle, respectively, taking into account virtual KK-graviton exchange and real KK-graviton production only, as it was previously shown that in both cases the radion/KK-dilaton contribution is sub-dominant. The grey area represents the region of the $(m_{\rm DM}, k)$ plane for which it is not possible to achieve the freeze-out relic abundance. The coloured area is the region for which $\langle\sigma v\rangle$ can be as large as $\langle\sigma_{\rm FO} v\rangle$ for some values of $m_{\rm DM}, k$ and M_5. The colour palette represents the corresponding ranges in M_5. The lowest values of M_5 for which we have $\langle\sigma v\rangle = \langle\sigma_{\rm FO} v\rangle$ are in the hundreds of GeV range, whereas in the lower-right corner of all panels we find values of M_5 are of the order of tens of TeV.

4 Experimental bounds and theoretical constraints

As we have seen in Fig. 3, the target relic abundance can be achieved in a vast region of the $(m_{\rm DM}, k)$ parameter space, if we allow M_5 to vary from 10^{-1} TeV to 10^2 TeV. However, experimental searches strongly constrain k and M_5. We will summarize here the relevant experimental bounds and see how only a relatively small region of the parameter space is allowed, indeed.

4.1 LHC bounds

The strongest constraints are given by the non-resonant searches at LHC. Differently from the results from resonance searches at the LHC [51, 52], data from non-resonant searches are not easily turned into bounds in k and M_5. We will therefore take advantage of the analysis performed in Ref. [18] and of the dedicated analysis from the CMS Collaboration described in Ref. [53]. The two bounds in the (k, M_5) plane are shown in Fig. 4, where the solid blue and dashed red lines represent results from Ref. [18] and Ref. [53], respectively. The orange-shaded area is the region of the parameter space for which the mass of the first KK-graviton m_{G_1} (where $m_{G_1} = k$) is larger than the scale of the theory, M_5. In this region of the parameter space the low-energy gravity effective theory is not trustable (see Sect. 4.3). In the rest of the paper, we have applied the experimental LHC bounds from Ref. [53] as a conservative choice.

4.2 Direct and Indirect Dark Matter Detection

In order to understand the bounds from Direct Detection Dark Matter searches (DD) we need to compute the total cross-section for spin indepedent elastic scattering between Dark Matter and the nuclei [26]:

$$\sigma^{\rm SI}_{{\rm DM}-p} = \left[\frac{m_p\, m_{DM}}{A\pi(m_{DM}+m_p)}\right]^2 \left[A f_p^{DM} + (A-Z) f_n^S\right]^2 \,, \tag{4.1}$$

where m_p is the proton mass, while Z and A are the number of protons and the atomic number. The nucleon form factors are given by the same formula for Dark Matter of any spin (at zero momentum transfer):

$$\begin{cases} f_p^{\rm DM} = \frac{m_{DM}\, m_p}{4 m_{G_1}^2 \Lambda^2} \left\{\sum_{q=u,c,d,b,s} 3\left[q(2)+\bar{q}(2)\right] + \sum_{q=u,d,s} \frac{1}{3} f_{Tq}^p\right\} \,, \\ \\ f_n^{\rm DM} = \frac{m_{DM}\, m_p}{4 m_{G_1}^2 \Lambda^2} \left\{\sum_{q=u,c,d,b,s} 3\left[q(2)+\bar{q}(2)\right] + \sum_{q=u,d,s} \frac{1}{3} f_{Tq}^n\right\} \,, \end{cases} \tag{4.2}$$

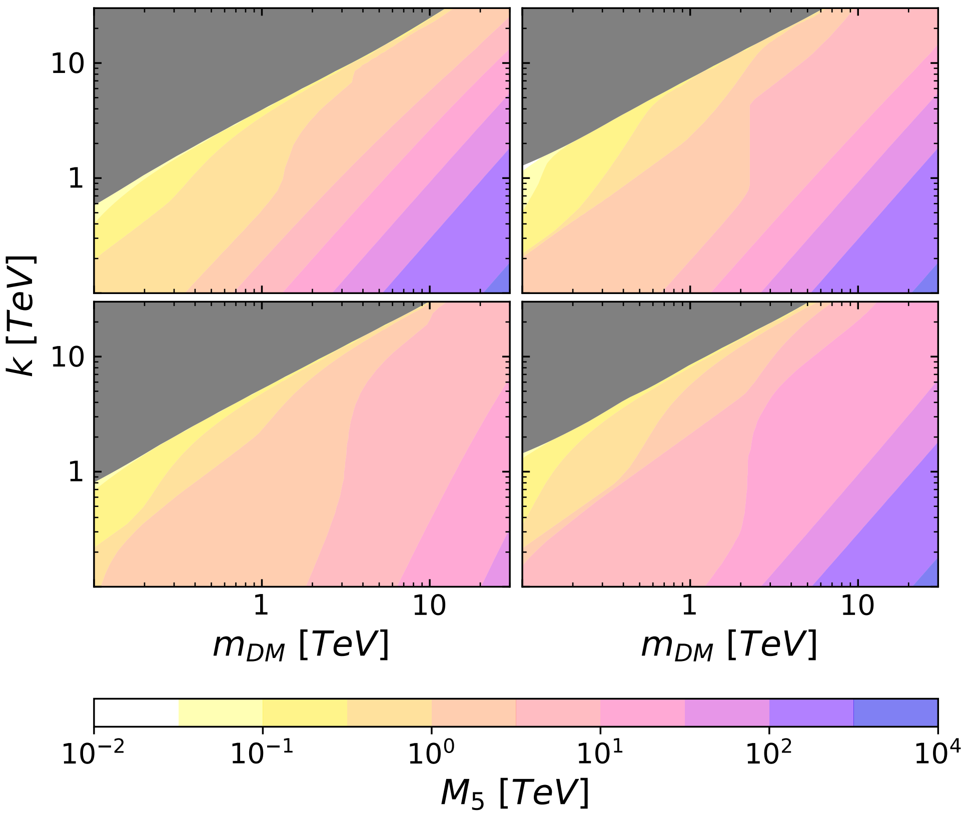

Figure 3. *Values of M_5 for which the correct DM relic abundance is obtained in the plane m_{DM}, k. Top-left panel: Scalar DM particle, virtual KK-graviton exchange and real KK-graviton production only; Top-right panel: Scalar DM particle, virtual KK-graviton exchange and real KK-graviton production together with virtual radion/KK-dilaton exchange and real radion/KK-dilaton production; Bottom-left panel: Fermion DM particle, virtual KK-graviton exchange and real KK-graviton production only; Bottom-right panel: Vector DM particle, virtual KK-graviton exchange and real KK-graviton production only. The required M_5 ranges are shown by the color legend. The grey-shaded area represents the region of the parameter space for which is impossible to reach the freeze-out relic abundance.*

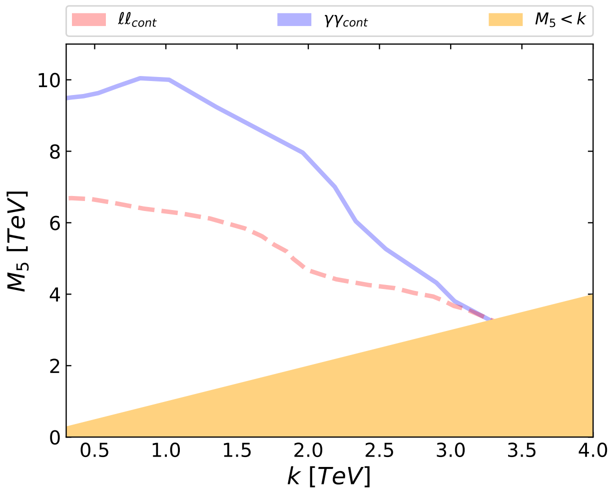

Figure 4. *Bounds in the (k, M_5) plane from non-resonant searches at the LHC with $\sqrt{s} = 13$ TeV and 36 fb^{-1}, from an analysis of ATLAS data [18] (dashed red line) and from the CMS Collaboration results [53] (solid blue line). The orange-shaded area is the region of the parameter space for which $m_{G_1} \geq M_5$.*

with $q(2)$ the second moment of the quark distribution function

$$q(2) = \int_0^1 dx \; x \; f_q(x) \tag{4.3}$$

and $f_{Tq}^{N=p,n}$ the mass fraction of light quarks in a nucleon: $f_{Tu}^p = 0.023$, $f_{Td}^p = 0.032$ and $f_{Ts}^p = 0.020$ for a proton and $f_{Tu}^n = 0.017$, $f_{Td}^n = 0.041$ and $f_{Ts}^n = 0.020$ for a neutron [54].

The strongest bounds come from the XENON1T experiment that uses ^{129}Xe, ($Z = 54$ and $A - Z = 75$) as a target. In our analysis we compute the second moment of the PDF's using Ref. [55] and the exclusion curve of XENON1T [56] to set constraints in the parameter space. In Fig. 5 we show the scale needed to achieve the freeze-out relic abundance, $M_5^{\rm FO}$, as a function of the DM mass $m_{\rm DM}$, for $k = 250$ GeV. The three lines (solid orange, dot-dashed blue and dotted red) correspond to scalar, fermion and vector DM, respectively. The green-shaded area is the experimental bound in the $(m_{\rm DM}, M_5)$ plane from XENON1T. We can see that the bounds imposed by DD only constrain very low values of $m_{\rm DM}$ and they are irrelevant in the range of DM masses considered in the rest of this paper ($m_{\rm DM} \geq 100$ GeV). We have checked that this result is general also for other values of k.

With respect to Indirect Detection Dark Matter searches (ID), several experiments are analysing differents signals. For instance, the Fermi-LAT Collaboration studied the γ-ray flux arriving at Earth from the galactic center [57, 58] and from different Dwarf Spheroidal galaxies [59]. Other experiments detect charged particles instead of photons, as it is the case of AMS-02 that presented data about the positron [60] and anti-proton fluxes coming from the galactic center [61]. These results are relevant in various DM models that can

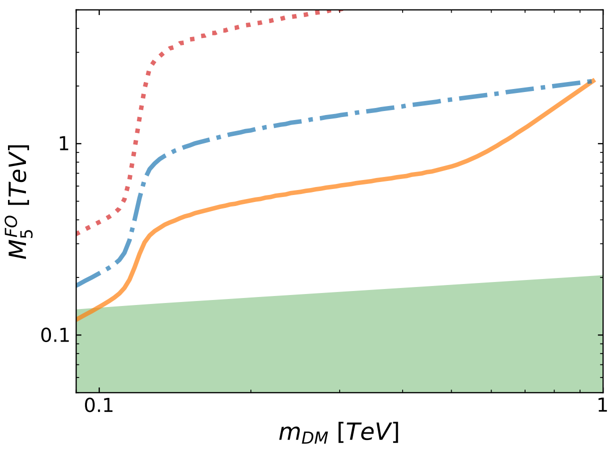

Figure 5. The scale needed to achieve the freeze-out relic abundance, $M_5^{\rm FO}$, as a function of the DM mass $m_{\rm DM}$, for $k = 250$ GeV. Solid orange, dot-dashed blue and dotted red lines correspond to scalar, fermion and vector DM, respectively. The green-shaded area, on the other hand, is the experimental bound in the $(m_{\rm DM}, M_5)$ plane from XENON1T [56].

generate a continuum spectra of SM particles, such as our case. However, current data from ID only allows to constrain DM masses below 100 GeV, a region which is already excluded by LHC data.

4.3 Theoretical constraints

Besides the experimental limits, there are mainly two theoretical concerns about the validity of our calculations which affect part of the $(m_{\rm DM}, k, M_5)$ parameter space. The first one is related to the fact that we are performing just a tree-level computation of the relevant DM annihilation cross-sections, and we should worry about unitarity issues. In particular, the annihilation cross-section into a pair of real KK-gravitons, $\sigma({\rm DM\,DM} \to G_n G_m)$, diverges as $m_{\rm DM}^{10}/(m_{G_n}^4 m_{G_m}^4)$ for scalar and vector DM and as $m_{\rm DM}^6/(m_{G_n}^2 m_{G_m}^2)$ for fermion DM (see eqs. (D.11,D.17) and (D.25) in App. D.1). When the DM mass becomes very large with respect to the KK-graviton masses, it is important to check that the effective theory is still unitary [62]. Asking for the cross-section to be bounded, $\sigma < 1/s \simeq 1/m_{\rm DM}^2$, we got the red-shaded areas shown in Fig. 2. If we combine the unitarity requirement with the request that the freeze-out thermally-averaged cross-section is achieved to get the correct DM relic abundance, we have an upper bound on the DM mass: $m_{\rm DM} \lesssim 1/\sqrt{\sigma_{\rm FO}}$, independently on the parameters that determine the geometry of the space-time, (k and M_5). This will be shown by a vertical line in the $(m_{\rm DM}, k)$ plane in Fig. 6.

The second theoretical issue refers to the consistency of the effective theory framework: in the CW/LD scenario, at energies somewhat larger than M_5 the KK-gravitons are strongly coupled and the five-dimensional field theory from which we start is no longer valid. We therefore impose that at least $m_{G_1} = k < M_5$ to trust our results. Notice that this constraint is general for any effective field theory: since we are including the KK-graviton tower in the low-energy spectrum, for the effective theory to make sense the cut-off scale M_5 should be larger than the masses of such states. For the same reason, we also ask for the Dark Matter mass $m_{\rm DM}$ to be lighter than M_5, $m_{\rm DM} < M_5$, although we will see that, in the allowed region, this requirement is almost always fulfilled.

5 Results

We show in Fig. 6 the allowed parameter space in the $(m_{\rm DM}, k)$ plane for which the target value of $\langle \sigma v \rangle$ needed to achieve the correct DM relic abundance in the freeze-out scenario, ($\langle \sigma_{\rm FO} v \rangle = 2.2 \times 10^{-26}$ cm^3/s), can be obtained, taking into account both the experimental bounds and the theoretical constraints outlined in Sec. 4.

In the upper left panel we show our results for a scalar DM particle, considering only decays into SM particles through virtual KK-graviton exchange or into KK-gravitons. This corresponds to the unstabilized regime, *i.e.* when the coefficients $\mu_{\rm IR}, \mu_{\rm UV}$ of the localized potential terms in eq. (2.21) vanish. In the upper right panel we show our results for scalar DM when the extra-dimension is stabilized in the rigid limit, $\mu_{\rm IR}, \mu_{\rm UV} \to \infty$, and in the absence of non-minimal coupling with gravity, $\xi = 0$ (see Sect. 2 for details). In this case, the annihilation of DM particles occurs through virtual KK-graviton and radion/KK-dilaton exchange into SM particles and through direct KK-graviton and radion/KK-dilaton production. In the bottom left and right panels we show our results for a fermion and a vector DM particle, respectively. In both cases, the radion/KK-dilaton contribution (in the rigid limit with $\xi = 0$) is included but it is irrelevant.

As a guidance, dashed lines taken from Fig. 3 represent the values of M_5 needed to achieve the relic abundance in a particular point of the $(m_{\rm DM}, k)$ plane. The legend for the four plots is given in the Figure caption.

5.1 Scalar Dark Matter

In the case of scalar DM, depicted in the upper left and right panels, virtual KK-graviton exchange is not enough to achieve the freeze-out relic abundance. For this reason, when the extra-dimension is unstabilized (left panel), $\langle \sigma_{\rm FO} v \rangle$ can be obtained only when the KK-graviton production channel opens, as it was the case for the RS scenario [30]. As a consequence, the DM particle mass has to be in a given relation with the mass of the KK-graviton tower and, therefore, a grey region for which it is impossible to achieve $\langle \sigma_{\rm FO} v \rangle$ can be seen. The red diagonally-meshed area represents the region of the parameter space for which the correct relic abundance is achieved with a value of M_5 lower than the mass of the first KK-graviton, $m_{G_1} = k$. Above this line the low-energy effective theory we are using is untrustable, as new dynamical particles in the spectrum are heavier than the scale of the theory. The blue-shaded area represents the excluded region from searches of non-resonant channels at LHC Run II with 36 pb$^-$1 from Ref. [18]. The green vertically-meshed area is the upper bound on the DM mass that must be fulfilled to comply with unitarity.

When the extra-dimension is stabilized (right panel), the virtual radion/KK-dilaton exchange channel may reach the target value for the cross-section for some values of the

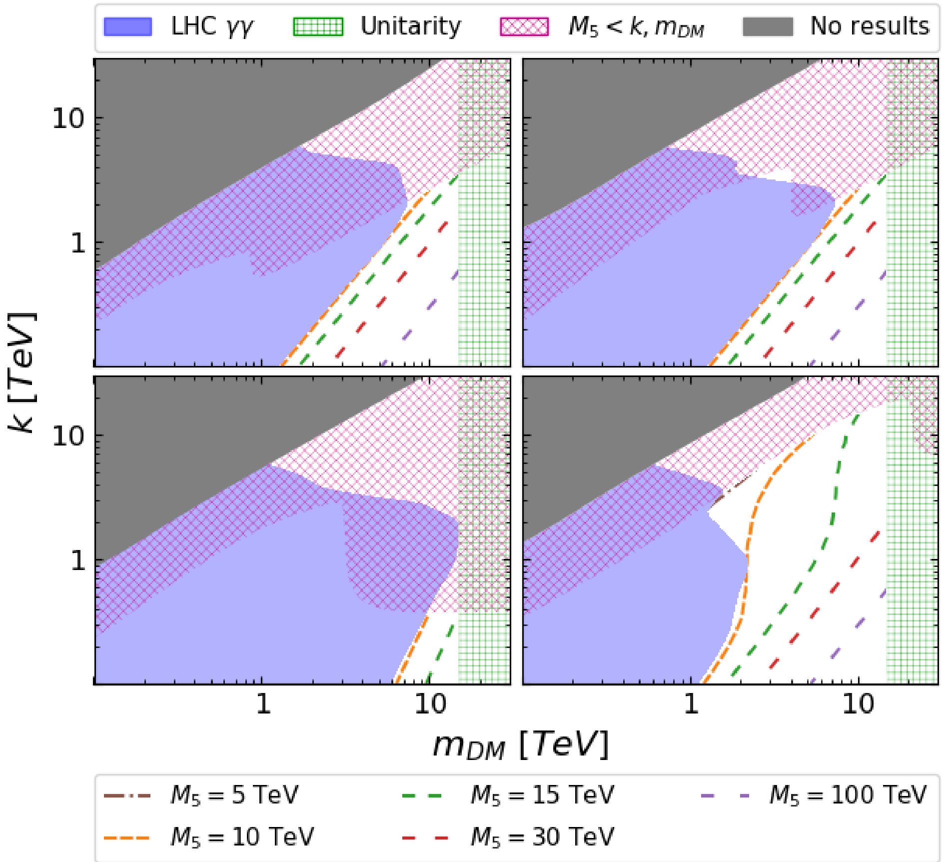

Figure 6. *Region of the* $(m_{\rm DM}, k)$ *plane for which* $\langle \sigma v \rangle = \langle \sigma_{\rm FO} v \rangle$*. Upper left panel: scalar DM (unstabilized extra-dimension); Upper right panel: scalar DM (stabilized extra-dimension in the rigid limit,* $\epsilon_{\rm IR} = \epsilon_{\rm UV} = 0$*, without non-minimal coupling with gravity,* $\xi = 0$*); Lower left panel: fermion DM (stabilized extra-dimension in the rigid limit without non-minimal coupling with gravity); Lower right panel: vector DM (stabilized extra-dimension in the rigid limit without non-minimal coupling with gravity). In all panels, the grey-shaded area represents the part of the parameter space for which it is impossible to achieve the correct relic abundance; the red diagonally-meshed area is the region for which the low-energy CW/LD effective theory is untrustable, as* $M_5 < k$*; the blue-shaded area is excluded by non-resonant searches at the LHC with 36 fb*$^{-1}$ *at* $\sqrt{s} = 13$ *TeV [18]; eventually, the green vertically-meshed area on the right is the region where the theoretical unitarity constraints are not fulfilled,* $m_{\rm DM} \gtrsim 1/\sqrt{\sigma_{\rm FO}}$*. In all panels, the white area represents the region of the parameter space for which the correct relic abundance is achieved (either through direct KK-graviton and/or radion/KK-dilaton production, as in the case of scalar DM, or through virtual KK-graviton exchange, as for fermion and vector DM) and not excluded by experimental bounds and theoretical constraints. The dashed lines depicted in the white region represent the values of* M_5 *needed to obtain the correct relic abundance (from Fig. 3).*

DM mass for which the KK-graviton exchange channel may not (see Fig. 1). Therefore, a grey area is present but it somewhat smaller than in the unstabilized case (differently from the Randall-Sundrum case, where no grey area was found in this case [30]). Most of this region is excluded because the value of M_5 is lower than k and, thus, the effective theory we are using is untrustable (red-meshed region). As a consequence, the allowed region that complies with experimental bounds and theoretical constraints is very similar to the unstabilized case and, roughly speaking, corresponds to $m_{\rm DM} \in [1, 15]$ TeV and $k < 6$ TeV. Within the allowed region, M_5 may vary between 10 TeV's and a few hundreds of TeV's.

5.2 Fermion Dark Matter

The case of fermion DM is depicted in the lower left panel. The meaning of the coloured areas is the same as for the upper panels: the grey area is the region of the parameter space for which is impossible to achieve $\langle \sigma_{\rm FO} v \rangle$; the blue-shaded area corresponds to the LHC Run II exclusion bound [18]; the red diagonally-meshed and green vertically-meshed areas represent theoretical unitarity bounds; and, the white area is the allowed region of the parameter space, where dashed lines represent benchmark values of M_5 useful to understand its scaling. The main difference with the scalar (and vector) DM case is that for fermion DM a rather small region of the parameter space is compatible with all bounds and constraints. This is a consequence of the slower dependence of the direct KK-graviton production cross-section with $m_{\rm DM}$ (see Figs. 1 and 2 and eq. (D.15) in App. D). Eventually, the allowed region that complies with experimental bounds and theoretical constraints corresponds to $m_{\rm DM} \in [4, 15]$ TeV and $k < 1$ TeV. Within the allowed region, M_5 may vary between 10 TeV's and a few tens of TeV's.

5.3 Vector Dark Matter

The case of vector DM is depicted in the lower right panel. The meaning of the coloured areas is the same as for the upper panels: the grey area is the region of the parameter space for which is impossible to achieve $\langle \sigma_{\rm FO} v \rangle$; the blue-shaded area corresponds to the LHC Run II exclusion bound [18]; the red diagonally-meshed and green vertically-meshed areas represent theoretical unitarity bounds; and, the white area is the allowed region of the parameter space, where dashed lines represent benchmark values of M_5 useful to understand its scaling. The main difference with the scalar and fermion DM case is that for vector DM it is possible to achieve the correct relic abundance through the virtual KK-graviton exchange channel, and the requirements on M_5 are less stringent. As a consequence, a rather large region of the parameter space is compatible with all bounds and constraints. The allowed region that complies with experimental bounds and theoretical constraints corresponds to $m_{\rm DM} \in [0.6, 15]$ TeV and k may be as large as ~ 20 TeV. Within the allowed region, M_5 may vary between a 5 TeV's and a few hundreds of TeV's.

6 Conclusions

In this paper we have explored the possibility that the observed Dark Matter component in the Universe is represented by some new particle with mass in the TeV range which interacts with the SM particles only gravitationally, in agreement with non-observation of DM signals at both direct and indirect detection DM experiments. In standard 4-dimensional gravity, the interaction between such DM particles and SM particles would be too feeble to reproduce the observed DM relic abundance. However, we have found that this is not the case once this setup is embedded in a Clockwork/Linear Dilaton scenario, along the ideas of the CW/LD proposal of Refs. [17, 18]. We consider two 4-dimensional branes in a 5-dimensional space-time with non-factorizable CW/LD metric [36] at a separation r_c, very small compared with present bounds on deviations from Newton's law. On one of the branes, the so-called "IR-brane", both the SM particles and a DM particle (with spin $0, 1/2$ or 1) are confined, with no particle allowed to escape from the branes to explore the bulk. It can be shown that gravitational interaction between particles on the IR-brane (in our case between a DM particle and any of the SM particles) occurs with an amplitude proportional to $1/M_{\rm P}^2$ when the two particles exchange a graviton zero-mode, but with a suppression factor $1/\Lambda_n^2$ when they interact exchanging the n-th KK-graviton mode. As the effective coupling Λ_n can be as low as a few TeV (depending on the particular choices of the two parameters that determine the geometry of the space-time, k and M_5), a huge enhancement of the cross-section is then possible with respect to standard linearized General Relativity.

Once fixed the setup we have computed the relevant contributions to the thermally-averaged DM annihilation cross-section $\langle \sigma\, v\rangle$, taking into accont both virtual KK-graviton and radion/KK-dilaton exchange as well as the direct production of radion/KK-dilatons and KK-gravitons. We have then scanned the parameter space of the model (represented by $m_{\rm DM}$, k and M_5), looking for regions in which the observed relic abundance can be achieved, $\langle \sigma\, v\rangle \sim \langle \sigma_{\rm FO}\, v\rangle$. This region has been compared with experimental bounds from resonant searches at the LHC Run II and from direct and indirect DM detection searches, finding which portion of the allowed parameter space is excluded by data. Eventually, we have studied the theoretical unitarity bounds on the mass of the DM particle and on the validity of the CW/LD model as a consistent low-energy effective theory. We have found that the correct relic abundance may be achieved in a significant region of the parameter space, corresponding typically to a DM mass of a few TeV's.

Depending on the spin and the mass of the DM particle, $\langle \sigma_{\rm FO}\, v\rangle$ is reached either through virtual exchange or direct production of radion/KK-dilatons and/or KK-gravitons. For scalar DM particles, we have found that $\langle \sigma_{\rm FO}\, v\rangle$ can be obtained for DM masses in the range $m_{\rm DM} \in [1, 15]$ TeV and $k \lesssim 6$ TeV. In this case the radion/KK-dilaton virtual exchange increases the cross-section for low DM masses (below 1 TeV), thus making possible to achieve $\langle \sigma_{\rm FO}\, v\rangle$ in a much larger portion of the parameter space with respect to the KK-gravitons only case. However, most of this extra region corresponds to values of m_{G_1} larger than M_5 and, thus, in a part of the parameter space where the effective theory is untrustable. As a consequence, we find no difference between the unstabilized case (no radion/KK-dilatons) and the stabilized case in the rigid limit (with radion/KK-dilatons). For fermion DM particles the allowed mass range is somewhat smaller, $m_{\rm DM} \in [4, 15]$ TeV and $k \lesssim 4$ TeV. Eventually, for vector DM particles, the allowed mass range is somewhat larger, $m_{\rm DM} \in [0.6, 15]$ TeV and $k \lesssim 20$ TeV. Notice that the upper limit on the DM mass comes from theoretical unitarity bounds.

Our results for DM in the CW/LD scenario are very similar to those we have found with AdS_5 metric (the so-called Randall-Sundrum model) in Ref. [30], where we studied only the case of scalar DM. In the Randall-Sundrum scenario it was known that, for scalar DM and SM particles localized in the IR brane, it is not possible to achieve $\langle \sigma_{\rm FO}\, v \rangle$ through the virtual KK-graviton or radion exchange channel (see also Refs. [19, 22]). However, we showed that when the DM mass is large enough so that the direct production of KK-gravitons or radions becomes possible, then the correct relic abundance can be achieved for DM particle masses of a few TeV's, much as in the case of the CW/LD model studied here. Notice that the value of M_5 needed to achieve the correct relic abundance in the CW/LD model is $M_5 \in [10, 100]$ TeV, whereas in the Randall-Sundrum scenario the effective coupling Λ needed to achieve the freeze-out was in $\Lambda \in [10, 1000]$ TeV range. In both cases, some hierarchy between the fundamental gravitational scale (either M_5 or Λ) and the electro-weak scale $\Lambda_{\rm EW}$ is needed.

It is worth to emphasize that in both extra-dimensional scenarios, Randall-Sundrum and CW/LD, it is possible to obtain the correct relic abundance via thermal freeze-out with DM masses in the TeV scale, so they are already quite constrained by LHC data. Moreover, most part of the still allowed parameter space may be tested by the LHC Run III and by the proposed High-Luminosity LHC. While the prospects for the Randall-Sundrum were already analysed in Ref. [30], it would be very interesting to explore in detail the limits that these next LHC phases could set on the CW/LD model.

Acknowledgements

We thank Matthew McCullough, Hyun Min Lee and Verónica Sanz for illuminating discussions. This work has been partially supported by the European Union projects H2020-MSCA-RISE-2015 and H2020-MSCA- ITN-2015//674896-ELUSIVES, by the Spanish MINECO under grants FPA2017-85985-P and SEV-2014-0398, and by Generalitat Valenciana through the "plan GenT" program (CIDEGENT/2018/019) and grant PROMETEO/2019/083.

A Feynman rules

We remind in this Appendix the different Feynman rules corresponding to the couplings of DM particles and of SM particles of any spin with KK-gravitons and radion/KK-dilatons.

A.1 Graviton Feynman rules

The vertex that involves one KK-graviton and two scalars S of mass m_S is given by:

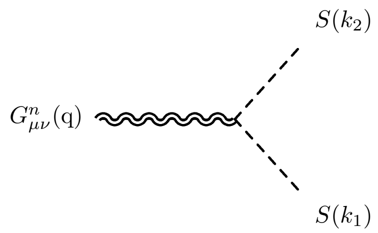

$$= -\frac{i}{\Lambda_n}\left(m_S^2 \eta_{\mu\nu} - C_{\mu\nu\rho\sigma} k_1^\rho k_2^\sigma\right) , \qquad \text{(A.1)}$$

where

$$C_{\mu\nu\alpha\beta} \equiv \eta_{\mu\alpha}\eta_{\nu\beta} + \eta_{\nu\alpha}\eta_{\mu\beta} - \eta_{\mu\nu}\eta_{\alpha\beta}\,. \tag{A.2}$$

This expression can be used for the coupling of both scalar DM and the SM Higgs boson to gravitons.

The vertex that involves one KK-graviton and two fermions ψ of mass m_ψ is given by:

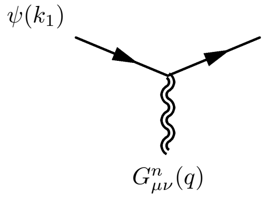

$$= -\frac{i}{4\Lambda_n}\left[\gamma_\mu\left(k_{2\nu}+k_{1\nu}\right)+\gamma_\nu\left(k_{2\mu}+k_{1\mu}\right)\right.$$
$$\left. -2\eta_{\mu\nu}\left(\not{k}_2+\not{k}_1-2m_\psi\right)\right]\,, \tag{A.3}$$

and

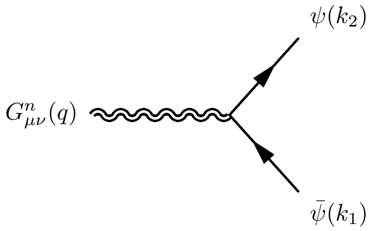

$$= -\frac{i}{4\Lambda_n}\left[\gamma_\mu\left(k_{2\nu}-k_{1\nu}\right)+\gamma_\nu\left(k_{2\mu}-k_{1\mu}\right)\right.$$
$$\left. -2\eta_{\mu\nu}\left(\not{k}_2-\not{k}_1-2m_\psi\right)\right]\,. \tag{A.4}$$

The interaction between two vector bosons V of mass m_V and one KK-graviton is given by:

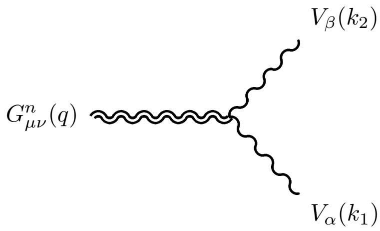

$$= -\frac{i}{\Lambda_n}\left(m_V^2 C_{\mu\nu\alpha\beta} + W_{\mu\nu\alpha\beta}\right)\,, \tag{A.5}$$

where

$$W_{\mu\nu\alpha\beta} \equiv B_{\mu\nu\alpha\beta} + B_{\nu\mu\alpha\beta} \tag{A.6}$$

and

$$\begin{aligned} B_{\mu\nu\alpha\beta} \equiv\ & \eta_{\alpha\beta}k_{1\mu}k_{2\nu} + \eta_{\mu\nu}(k_1\cdot k_2\eta_{\alpha\beta} - k_{1\beta}k_{2\nu}) \\ & -\ \eta_{\mu\beta}k_{1\nu}k_{2\alpha} + \frac{1}{2}\eta_{\mu\nu}(k_{1\beta}k_{2\alpha} - k_1\cdot k_2\eta_{\alpha\beta})\,. \end{aligned} \tag{A.7}$$

Eventually, the interaction between two particles (S, ψ or V_μ depending on their spin) and two KK-gravitons (coming from a second order expansion of the metric $g_{\mu\nu}$ around the Minkowski metric $\eta_{\mu\nu}$) is given by:

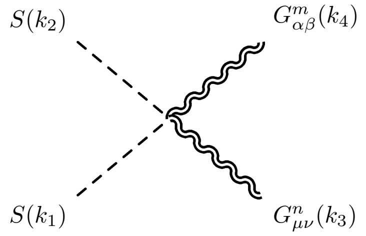

$$= -\frac{i}{\Lambda_n \Lambda_m} \eta_{\nu\beta} \left(m_S^2 \eta_{\mu\alpha} - C_{\mu\alpha\rho\sigma} k_1^\rho k_2^\sigma \right) , \tag{A.8}$$

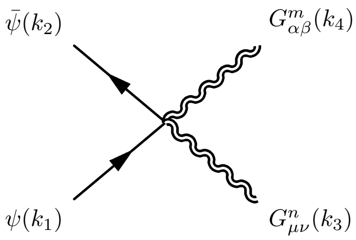

$$\begin{aligned} = &-\frac{i}{\Lambda_n \Lambda_m} \eta_{\nu\beta} \left[\gamma_\mu \left(k_{1\alpha} - k_{2\alpha} \right) + \gamma_\alpha \left(k_{1\mu} - k_{2\mu} \right) \right. \\ &\left. -2\eta_{\mu\alpha} \left(\not{k}_1 - \not{k}_2 - 2m_\psi \right) \right] , \end{aligned} \tag{A.9}$$

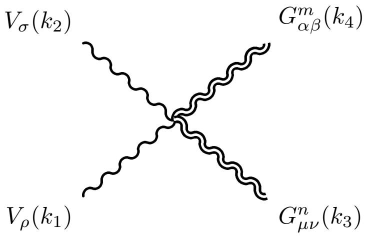

$$= -\frac{i}{\Lambda_n \Lambda_m} \eta_{\nu\beta} \left(m_V^2 C_{\mu\alpha\rho\sigma} + W_{\mu\alpha\rho\sigma} \right) . \tag{A.10}$$

The Feynman rules for the $n = 0$ KK-graviton can be obtained by the previous ones by replacing Λ with $M_{\rm P}$. We do not give here the triple KK-graviton vertex, as it is irrelevant for the phenomenological applications of this paper.

A.2 Radion/KK-dilaton Feynman rules

The radion/KK-dilatons, ϕ_n, couple with particles localized in the IR-brane with the trace of the energy-momentum tensor, $T = g^{\mu\nu} T_{\mu\nu}$ (in the rigid limit with $\xi = 0$, see Sect. 2.3). The only exception are photons and gluons that, being massless, do not contribute to T at tree-level. However, effective couplings of these fields to the radion/KK-dilatons are generated through quarks and W loops, and the trace anomaly.

The interaction between one radion/KK-dilaton and two scalar fields S of mass m_S is given by:

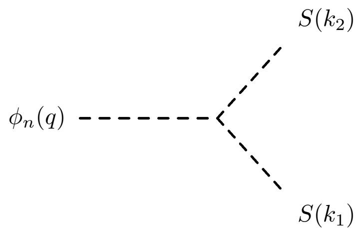

$$= -\frac{2i}{\Lambda_n} \left(2m_S^2 + k_{1\mu} k_2^\mu \right) . \tag{A.11}$$

The vertex that involves one radion/KK-dilaton and two Dirac fermions ψ of mass m_ψ takes the form:

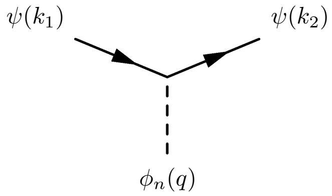

$$= -\frac{i}{2\Lambda_n}\left[8m_\psi - 3\left(\not{k}_2 + \not{k}_1\right)\right] \tag{A.12}$$

and:

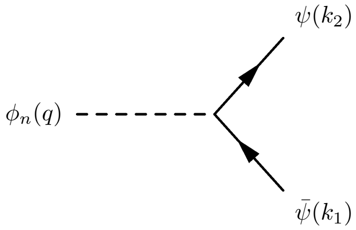

$$= -\frac{i}{2\Lambda_n}\left[8m_\psi - 3\left(\not{k}_2 - \not{k}_1\right)\right] . \tag{A.13}$$

The interaction between two massive vector bosons V of mass m_V and one radion/KK-dilaton is given by:

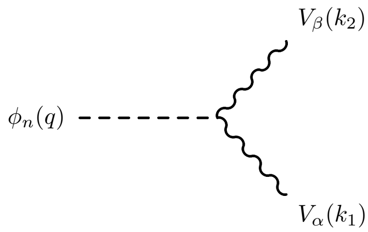

$$= \frac{2i}{\Lambda_n} m_V^2 \eta_{\alpha\beta} , \tag{A.14}$$

whereas the vertex corresponding to the interaction between two massless SM gauge bosons and one radion/KK-dilaton is:

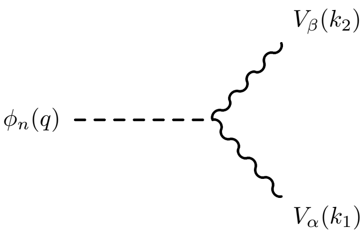

$$= \frac{4i\alpha_i C_i}{8\pi\Lambda_n}\left[\eta_{\mu\nu}(k_1 \cdot k_2) - k_{1\nu}k_{2\mu}\right] , \tag{A.15}$$

where $\alpha_i = \alpha_{EM}, \alpha_s$ for the case of the photons or gluons, respectively, and [48]:

$$\begin{cases} C_3 &= b_{IR}^{(3)} - b_{UV}^{(3)} + \frac{1}{2}\sum_q F_{1/2}(x_q) , \\ \\ C_{EM} &= b_{IR}^{(EM)} - b_{UV}^{(EM)} + F_1(x_W) - \sum_q N_c Q_q^2 F_{1/2}(x_q) , \end{cases} \tag{A.16}$$

with $x_q = 4m_q/m_r$ and $x_W = 4m_w/m_r$. The values of the one-loop β-function coefficients b are $b_{IR}^{(EM)} - b_{UV}^{(EM)} = 11/3$ and $b_{IR}^{(3)} - b_{UV}^{(3)} = -11 + 2n/3$, where n is the number of quarks whose mass is smaller than $m_r/2$. The explicit form of $F_{1/2}$ and F_1 is given by:

$$\begin{cases} F_{1/2}(x) = 2x[1 + (1-x)f(x)], \\ \\ F_1(x) = 2 + 3x + 3x(2-x)f(x), \end{cases} \tag{A.17}$$

with

$$f(x) = \begin{cases} [\arcsin(1/\sqrt{x})]^2 & x > 1, \\ \\ -\frac{1}{4}\left[\log\left(\frac{1+\sqrt{x-1}}{1-\sqrt{x-1}}\right) - i\pi\right]^2 & x < 1. \end{cases} \tag{A.18}$$

Eventually, the 4-legs diagrams are given by:

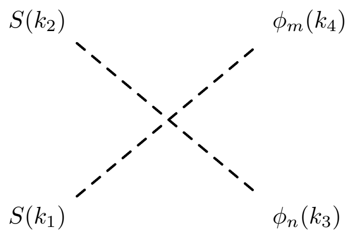

$$= -\frac{i}{3\Lambda^2}\left(6m_S^2 + k_{1\mu}k_2^\mu\right) , \tag{A.19}$$

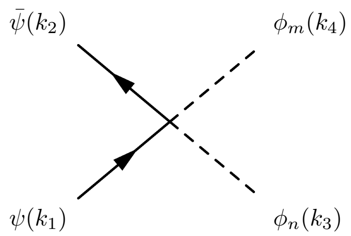

$$= -\frac{i}{2\Lambda_n^2}\left[8m_\psi - 3\left(\not{k}_2 - \not{k}_1\right)\right] \tag{A.20}$$

and

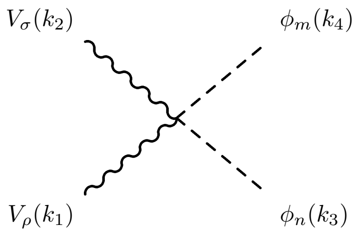

$$= -\frac{2i}{\Lambda_n^2} m_V^2 \eta_{\alpha\beta} \, . \tag{A.21}$$

B Decay widths

In this Appendix we compute the decay widths of KK-gravitons and radion/KK-dilatons, using the Feynman rules given in App. A.

B.1 KK-gravitons decay widths

The KK-graviton can decay into scalar particles (including the Higgs boson, a scalar DM particle and radion/KK-dilatons), fermions (either SM or a fermion DM particle), vector bosons (either massive or massless SM gauge bosons or a vector DM particle) and lighter KK-gravitons.

Decay widths of KK-gravitons into SM particles, $\Gamma(G_n \to \mathrm{SM\,SM})$, are all proportional to $1/\Lambda_n^2$. In particular, the decay width into SM Higgs bosons is given by:

$$\Gamma(G_n \to HH) = \frac{m_n^3}{960\,\pi\,\Lambda_n^2}\left(1 - \frac{4\,m_H^2}{m_n^2}\right)^{5/2}, \tag{B.1}$$

where m_n is the mass of the n-th KK-graviton (in the main text, this was called m_{G_n}, but we prefer here a shorter notation to increase readability of the formulæ).

The decay width of the n-th KK-graviton into SM Dirac fermions is given by:

$$\Gamma(G_n \to \bar\psi\psi) = \frac{m_n^3}{160\,\pi\,\Lambda_n^2}\left(1 - \frac{4\,m_\psi^2}{m_n^2}\right)^{3/2}\left(1 + \frac{8m_\psi^2}{3\,m_n^2}\right). \tag{B.2}$$

The decay width of the n-th KK-graviton into two SM massive gauge bosons reads:

$$\begin{cases} \Gamma(G_n \to W^+W^-) = \frac{13\,m_n^3}{480\,\pi\,\Lambda_n^2}\left(1 - \frac{4\,m_W^2}{m_n^2}\right)^{1/2}\left(1 + \frac{56\,m_W^2}{13\,m_n^2} + \frac{48\,m_W^4}{13\,m_n^4}\right), \\ \\ \Gamma(G_n \to ZZ) \qquad = \frac{13\,m_n^3}{960\,\pi\,\Lambda_n^2}\left(1 - \frac{4\,m_Z^2}{m_n^2}\right)^{1/2}\left(1 + \frac{56\,m_Z^2}{13\,m_n^2} + \frac{48\,m_Z^4}{13\,m_n^4}\right), \end{cases} \tag{B.3}$$

whereas the decay width into SM massless gauge bosons is:

$$\begin{cases} \Gamma(G_n \to \gamma\gamma) = \frac{m_n^3}{80\,\pi\,\Lambda_n^2}, \\ \\ \Gamma(G_n \to gg) = \frac{m_n^3}{10\,\pi\,\Lambda_n^2}. \end{cases} \tag{B.4}$$

Finally, If $m_n > 2m_{DM}$, the n-th KK-graviton can decay into two DM particles:

$$\begin{cases} \Gamma(G_n \to SS) = \frac{m_n^3}{960\,\pi\,\Lambda_n^2}\left(1 - \frac{4\,m_{\rm DM}^2}{m_n^2}\right)^{5/2}, \\ \\ \Gamma(G_n \to \bar\psi\psi) = \frac{m_n^3}{160\,\pi\,\Lambda_n^2}\left(1 - \frac{4\,m_{\rm DM}^2}{m_n^2}\right)^{3/2}\left(1 + \frac{8\,m_{\rm DM}^2}{3\,m_n^2}\right), \\ \\ \Gamma(G_n \to VV) = \frac{13\,m_n^3}{960\,\pi\,\Lambda_n^2}\left(1 - \frac{4\,m_{\rm DM}^2}{m_n^2}\right)^{1/2}\left(1 + \frac{56\,m_{\rm DM}^2}{13\,m_n^2} + \frac{48\,m_{\rm DM}^4}{13\,m_n^4}\right). \end{cases} \tag{B.5}$$

For completeness, we computed the decay of KK-gravitons into KK-gravitons and radion/KK-dilatons, finding that these contributions are totally negligible. For a thorough description of these decays see Ref. [18].

B.2 Radion/KK-dilatons decay widths

The decay width of the radion/KK-dilatons into SM Higgs boson, is given by:

$$\Gamma(\phi_n \to HH) = \frac{m_n^3}{32\,\pi\,\Lambda_n^2}\left(1 - \frac{4\,m_H^2}{m_n^2}\right)^{1/2}\left(1 + \frac{2\,m_H^2}{m_n^2}\right)^2 . \tag{B.6}$$

The radion/KK-dilaton decay width into SM Dirac fermions is given by:

$$\Gamma(\phi_n \to \bar{\psi}\psi) = \frac{m_n m_\psi^2}{8\,\pi\,\Lambda_n^2}\left(1 - \frac{4\,m_\psi^2}{m_n^2}\right)^{3/2} . \tag{B.7}$$

The radion/KK-dilaton decay width into SM massive gauge bosons is:

$$\begin{cases} \Gamma(\phi_n \to W^+W^-) = \frac{3\,m_n^3}{4\,\pi\,\Lambda^2}\left(1 - \frac{4\,m_W^2}{m_n^2}\right)^{1/2}\left(1 - \frac{m_W^2}{3\,m_n^2} + \frac{m_W^4}{12\,m_n^4}\right) , \\ \\ \Gamma(\phi_n \to ZZ) \qquad = \frac{3\,m_n^3}{8\,\pi\,\Lambda^2}\left(1 - \frac{4\,m_Z^2}{m_n^2}\right)^{1/2}\left(1 - \frac{m_Z^2}{3\,m_n^2} + \frac{m_Z^4}{12\,m_n^4}\right) , \end{cases} \tag{B.8}$$

whereas the decay width into SM massless gauge bosons is:

$$\begin{cases} \Gamma(\phi_n \to \gamma\gamma) = \frac{\alpha_{EM}\,C_{EM}\,m_n^3}{1280\pi\Lambda^2} , \\ \\ \Gamma(\phi_n \to gg) = \frac{\alpha_3\,C_3\,m_n^3}{160\pi\Lambda^2} . \end{cases} \tag{B.9}$$

If $m_n > 2m_{DM}$, the n-th radion/KK-dilaton can decay into two DM particles:

$$\begin{cases} \Gamma(\phi_n \to SS) = \frac{m_n^3}{32\,\pi\,\Lambda_n^2}\left(1 - \frac{4m_{\rm DM}^2}{m_n^2}\right)^{1/2}\left(1 + \frac{2\,m_{\rm DM}^2}{m_n^2}\right)^2 , \\ \\ \Gamma(\phi_n \to \bar{\psi}\psi) = \frac{m_n\,m_{\rm DM}^2}{8\,\pi\,\Lambda_n^2}\left(1 - \frac{4\,m_{\rm DM}^2}{m_n^2}\right)^{3/2} , \\ \\ \Gamma(\phi_n \to VV) = \frac{3\,m_n^3}{8\,\pi\,\Lambda^2}\left(1 - \frac{4\,m_{\rm DM}^2}{m_n^2}\right)^{1/2}\left(1 - \frac{m_{\rm DM}^2}{3\,m_n^2} + \frac{m_{\rm DM}^4}{12\,m_n^4}\right) . \end{cases} \tag{B.10}$$

We computed the decay of KK-dilatons into KK-gravitons and radion/KK-dilatons, finding that these contributions are totally negligible, as in the case of KK-gravitons.

C Sums over KK-gravitons and radion/KK-dilatons

In this Appendix we remind the procedure to derive approximated sums over virtual KK-modes following Ref. [18]. In the main text we have mainly shown plots using this approximation. However, we show here the degree of accuracy of the approximated sum comparing it with exact results.

Consider the sum over virtual KK-modes that arise both in virtual KK-graviton or virtual radion/KK-dilaton exchange cross-sections:

$$S_{KK} = \sum_{n=1}^{\infty} \frac{1}{\Lambda_n^2} \frac{1}{s - m_n^2 + i m_n \Gamma_n} , \tag{C.1}$$

where m_n is the mass of the n-th KK-graviton or radion/KK-dilaton and Γ_n its corresponding decay width. If $s > k^2$, the modulus squared of the sum over KK-modes is very well approximated by the sum over the KK-modes moduli squared, as the decay widths of the KK-modes computed in App. B are very small:

$$|S_{KK}|^2 \simeq \sum_{n=1}^{\infty} \frac{1}{\Lambda_n^4} \frac{1}{(s-m_n^2)^2 + m_n^2\Gamma_n^2} \equiv \sum_{n=1}^{\infty} \frac{1}{\Lambda(m_n)^4} \mathcal{F}(m_n)\,, \tag{C.2}$$

with $\mathcal{F}(m_n)$ a function that depends on the mass and the decay width of the virtual KK-modes. We also show explicitly that the n-dependence of Λ_n in eqs. (2.18) and (2.30) arises, indeed, through m_n. The mass difference between two nearby KK-modes, for the typical choices of k and M_5 considered in the paper, is small enough to approximate the sum by an integral in m starting from the mass of the first KK-mode, m_1:

$$|S_{KK}|^2 \approx \int_{m_1}^{\infty} dm \frac{1}{\Lambda(m)^4} \mathcal{F}(m)\, r_c \left(1 - \frac{k^2}{m^2}\right)^{-1/2} . \tag{C.3}$$

Using the narrow-width approximation for $\mathcal{F}(m)$

$$\mathcal{F}(m) \approx \frac{\pi}{\bar{m}\,\Gamma(\bar{m})} \frac{1}{2\sqrt{s}} \delta(\bar{m} - \sqrt{s})\,, \tag{C.4}$$

where $\bar{m}$ corresponds to the mode for which $m_n \sim \sqrt{s}$ (as enforced by the δ-function), eq. (C.2) can be further approximated as:

$$|S_{KK}|^2 \approx \frac{\pi r_c}{2} \frac{1}{\Gamma(\sqrt{s})\Lambda(\sqrt{s})^4} \left[\frac{1}{s}\left(1 - \frac{k^2}{s}\right)^{-1/2}\right] . \tag{C.5}$$

Eq. (C.5) is valid for both, KK-gravitons and radion/KK-dilatons. In the case of KK-gravitons, if we replace Λ_n with the expression in eq. (2.18), we get:

$$|S^g_{KK}|^2 \approx \frac{1}{2\,M_5^6\,\pi\, r_c} \frac{1}{\Gamma_n|_{m_n\sim\sqrt{s}}} \left[\frac{1}{s}\left(1 - \frac{k^2}{s}\right)^{3/2}\right] . \tag{C.6}$$

In the case of radion/KK-dilatons, Λ_n is given by eq. (2.30). Then:

$$|S^r_{KK}|^2 \approx \frac{8}{729 M_5^6 \pi\, r_c} \frac{1}{\Gamma_n|_{m_n\sim\sqrt{s}}} \left[\frac{1}{s}\left(\frac{k^2}{s}\right)^2 \left(1 - \frac{k^2}{s}\right)^{3/2} \left(1 - \frac{8k^2}{9s}\right)^{-2}\right] , \tag{C.7}$$

Notice that these expressions are equivalent to an average over the KK-modes.

In Fig. 7 we show the comparison between the results for $|S^g_{KK}|^2$ using eqs. (C.2) and (C.6) (left panel), as well as the exact thermally-averaged virtual KK-graviton exchange annihilation cross-section $\langle\sigma v\rangle$ versus the approximated one using eq. (C.6) (right panel), for an illustrative choice of M_5 and k, $M_5 = 7$ TeV and $k = 1$ TeV. In the left panel we can see how the sum has a very slow onset for $\sqrt{s} \leq k$ summing over the tails of the Breit-Wigner function representing each KK-mode contribution, followed by a very rapidly oscillating behaviour crossing the KK-mode resonances. The difference between being at

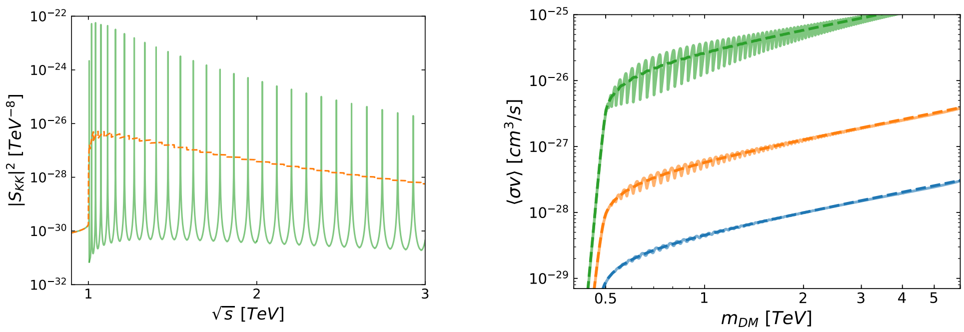

Figure 7. Left panel: the sum $|S_{KK}|^2$ for KK-gravitons with $M_5 = 7$ TeV and $k = 1$ TeV. The green solid and orange dashed lines represent the result using eq. (C.2) and the approximation described in eq. (C.6), respectively. Right panel: the thermally-averaged annihilation cross-section through virtual KK-graviton exchange for scalar (blue), fermion (orange) an vector (green) DM, with $M_5 = 7$ TeV and $k = 1$ TeV. Solid lines stand for the exact result, whereas dashed lines represent the approximated one using eq. (C.6).

the dip between two KK-modes or at the peak can be as large as a factor 10^4. However, the width of each KK-mode resonance is extremely small and, thus, when summing over many KK-modes the approximated sum reproduces correctly the collective behaviour of the system. This is clearly shown in the right panel where we see, that for any spin of the DM particle, the exact and approximated sum within the virtual KK-graviton exchange thermally-averaged annihilation cross-section give the same result.

D Annihilation DM Cross section

In all the expressions of this Appendix we made use of the so-called *velocity expansion* for the DM particles:

$$s \approx m_{\rm DM}^2 (4 + v^2)\,, \tag{D.1}$$

where v is the relative velocity of the two DM particles. Within this approximation, the different scalar products for processes in which two DM particles annihilate into two particles (either SM particles, KK-gravitons or radion/KK-dilatons), with incoming and outcoming momenta $\mathrm{DM}(k_1)\,\mathrm{DM}(k_2) \to \mathrm{Out}(k_3)\,\mathrm{Out}(k_4)$, become:

$$\begin{cases} k_1 \cdot k_4 = k_2 \cdot k_3 \approx m_{\rm DM}^2 + \frac{1}{2} m_{\rm DM}^2 \sqrt{1 - \frac{m_{\rm Out}^2}{m_{\rm DM}^2}} \cos\theta\, v + \frac{1}{4} m_{\rm DM}^2\, v^2\,, \\ \\ k_1 \cdot k_3 = k_2 \cdot k_4 \approx m_{\rm DM}^2 - \frac{1}{2} m_{\rm DM}^2 \sqrt{1 - \frac{m_{\rm Out}^2}{m_{\rm DM}^2}} \cos\theta\, v + \frac{1}{4} m_{\rm DM}^2\, v^2\,, \end{cases} \tag{D.2}$$

where

$$\begin{cases} k_1 \cdot k_1 = k_2 \cdot k_2 = m_{\rm DM}^2\,, \\ \\ k_3 \cdot k_3 = k_4 \cdot k_4 = m_{\rm Out}^2\,. \end{cases} \tag{D.3}$$

D.1 Annihilation through and into KK-gravitons

In the following sections we show the DM annihilation cross-sections through and into KK-gravitons. In all of this expressions S^g_{KK} is the sum over the KK-gravitons given in App. C.

D.1.1 Scalar DM

First we start with the scalar Dark Matter. The annihilation cross-section into two SM Higgs bosons is:

$$\sigma_g(S\,S \to H\,H) \approx v^3\,|S^g_{KK}|^2 \frac{m^6_{\rm DM}}{720\pi}\left(1-\frac{m^2_H}{m^2_{\rm DM}}\right)^{5/2} \tag{D.4}$$

The annihilation cross-section into two SM massive gauge bosons is:

$$\begin{cases} \sigma_g(S\,S \to W^+\,W^-) \approx v^3\,|S^g_{KK}|^2 \frac{13\,m^6_{\rm DM}}{360\pi}\left(1-\frac{m^2_W}{m^2_{\rm DM}}\right)^{1/2}\left(1+\frac{14m^2_W}{13m^2_{\rm DM}}+\frac{3m^4_W}{13m^4_{\rm DM}}\right)\,, \\ \\ \sigma_g(S\,S \to Z\,Z) \qquad \approx v^3\,|S^g_{KK}|^2 \frac{m^6_{13\,\rm DM}}{720\pi}\left(1-\frac{m^2_Z}{m^2_{\rm DM}}\right)^{1/2}\left(1+\frac{14m^2_Z}{13m^2_{\rm DM}}+\frac{3m^4_Z}{13m^4_{\rm DM}}\right)\,, \end{cases} \tag{D.5}$$

whereas for two massless gauge bosons we have:

$$\begin{cases} \sigma_g(S\,S \to \gamma\,\gamma) \approx v^3\,|S^g_{KK}|^2 \frac{2m^6_{\rm DM}}{15\pi}\,, \\ \\ \sigma_g(S\,S \to g\,g) \approx v^3\,|S^g_{KK}|^2 \frac{m^6_{\rm DM}}{60\pi}\,. \end{cases} \tag{D.6}$$

Eventually, the annihilation cross-section into two SM fermions is:

$$\sigma_g(S\,S \to \bar\psi\,\psi) \approx v^3\,|S^g_{KK}|^2 \frac{m^6_{\rm DM}}{120\pi}\left(1-\frac{m^2_\psi}{m^2_{\rm DM}}\right)^{3/2}\left(1+\frac{2m^2_\psi}{3m^2_{\rm DM}}\right)\,. \tag{D.7}$$

As it was shown in Ref. [19], for DM particle masses larger than the mass of a given KK-graviton mode DM particles may annihilate into two KK-gravitons. In the small velocity approximation, the related cross-section is:

$$\begin{aligned} \sigma_g(S\,S \to G_n\,G_m) \approx v^{-1}\left(\frac{A^g_S+B^g_S+C^g_S/4}{18432\,\pi}\right)\left(\frac{1}{\Lambda^2_n\,\Lambda^2_m\,m^2_{\rm DM}\,m^4_{\rm n}\,m^4_{\rm m}}\right) \\ \times\sqrt{\left(1+\frac{m^2_n-m^2_m}{4m^2_{\rm DM}}\right)^2-\frac{m^2_n}{m^2_{\rm DM}}}\,, \end{aligned} \tag{D.8}$$

where the three contributions to the cross-section come from the square of the t- and u-channels amplitudes, the square of the 4-points amplitude from the vertex A.8 and from the interference between the two classes of amplitudes, respectively:

$$\begin{cases} A_S^g = \dfrac{\left[m_{\rm m}^4 - 2\,m_{\rm m}^2\left(4\,m_{\rm DM}^2 + m_{\rm n}^2\right) + \left(m_{\rm n}^2 - 4\,m_{\rm DM}^2\right)^2\right]^4}{2\left(4\,m_{\rm DM}^2 - m_{\rm n}^2 - m_{\rm m}^2\right)^2}\,, \\ B_S^g = \dfrac{\left[16\,m_{\rm DM}^4 - 8\,m_{\rm DM}^2\left(m_{\rm n}^2 + m_{\rm m}^2\right) + \left(m_{\rm n}^2 - m_{\rm m}^2\right)^2\right]^2}{4\,m_{\rm DM}^2 - m_{\rm n}^2 - m_{\rm m}^2}\,\Big[16\,m_{\rm DM}^4\left(m_{\rm n}^2 + m_{\rm m}^2\right) \\ \quad - \; 8\,m_{\rm DM}^2\left(-m_{\rm n}^2\,m_{\rm m}^2 + m_{\rm n}^4 + m_{\rm m}^4\right) + \left(m_{\rm n}^2 - m_{\rm m}^2\right)^2\left(m_{\rm n}^2 + m_{\rm m}^2\right)\Big]\,, \\ C_S^g = 256\,m_{\rm DM}^8\left(13\,m_{\rm n}^2\,m_{\rm m}^2 + 2\,m_{\rm n}^4 + 2\,m_{\rm m}^4\right) - 512\,m_{\rm DM}^6\left(m_{\rm n}^6 + m_{\rm m}^6\right) \\ \quad + \; 32\,m_{\rm DM}^4\left(-17\,m_{\rm n}^6\,m_{\rm m}^2 + 98\,m_{\rm n}^4\,m_{\rm m}^4 - 17\,m_{\rm n}^2\,m_{\rm m}^6 + 6\,m_{\rm n}^8 + 6\,m_{\rm m}^8\right) \\ \quad - \; 32\,m_{\rm DM}^2\left(m_{\rm n}^2 - m_{\rm m}^2\right)^2\left(m_{\rm n}^6 + m_{\rm m}^6\right) \\ \quad + \; \left(m_{\rm n}^2 - m_{\rm m}^2\right)^4\left(13\,m_{\rm n}^2\,m_{\rm m}^2 + 2\,m_{\rm n}^4 + 2\,m_{\rm m}^4\right)\,. \end{cases} \tag{D.9}$$

In the particular case in which the two KK-gravitons have the same KK-number, m = n, eq. (D.8) becomes:

$$\sigma_g(S\,S \to G_n\,G_n) \approx v^{-1}\,\frac{4m_{\rm DM}^2}{9\,\pi\,\Lambda_n^2\Lambda_m^2}\,\frac{(1-r)^{1/2}}{r^4(2-r)^2} \times \left(1 - 3\,r + \frac{121}{32}\,r^2 - \frac{65}{32}\,r^3 + \frac{71}{128}\,r^4 - \frac{13}{64}\,r^5 + \frac{19}{256}\,r^6\right)\,, \tag{D.10}$$

where $r \equiv (m_{\rm n}/m_{\rm DM})^2$.

D.1.2 Fermionic case

If the dark matter is a Dirac fermion (χ) the annihilation into two SM Higgs bosons is:

$$\sigma_g(\bar\chi\,\chi \to H\,H) \approx v\,|S_{KK}^g|^2\,\frac{m_{\rm DM}^6}{144\pi}\left(1 - \frac{m_H^2}{m_{\rm DM}^2}\right)^{5/2} \tag{D.11}$$

The annihilation cross-section into two SM massive gauge bosons is:

$$\begin{cases} \sigma_g(\bar\chi\,\chi \to W^+\,W^-) \approx v\,|S_{KK}^g|^2\,\frac{13m_{\rm DM}^6}{72\pi}\left(1 - \frac{m_W^2}{m_{\rm DM}^2}\right)^{1/2}\left(1 + \frac{14m_W^2}{13m_{\rm DM}^2} + \frac{3m_W^4}{13m_{\rm DM}^4}\right)\,, \\ \sigma_g(\bar\chi\,\chi \to Z\,Z) \qquad \approx v\,|S_{KK}^g|^2\,\frac{13m_{\rm DM}^6}{144\pi}\left(1 - \frac{m_Z^2}{m_{\rm DM}^2}\right)^{1/2}\left(1 + \frac{14m_Z^2}{13m_{\rm DM}^2} + \frac{3m_Z^4}{13m_{\rm DM}^4}\right)\,, \end{cases} \tag{D.12}$$

whereas for two massless gauge bosons we have:

$$\begin{cases} \sigma_g(\bar\chi\,\chi \to \gamma\,\gamma) \approx v\,|S_{KK}^g|^2\,\frac{m_{\rm DM}^6}{12\pi}\,, \\ \sigma_g(\bar\chi\,\chi \to g\,g) \approx v\,|S_{KK}^g|^2\,\frac{2\,m_{\rm DM}^6}{3\pi}\,. \end{cases} \tag{D.13}$$

Eventually, the annihilation cross-section into two SM fermions is:

$$\sigma_g(\bar\chi\,\chi \to \bar\psi\,\psi) \approx v\,|S^g_{KK}|^2\frac{m^6_{\rm DM}}{24\pi}\left(1-\frac{m^2_\psi}{m^2_{\rm DM}}\right)^{3/2}\left(1+\frac{2m^2_\psi}{3m^2_{\rm DM}}\right)\,. \tag{D.14}$$

As in the case of scalar DM if the $m_{DM} > m_{G_1}$ the $\bar\psi\,\psi \to G_n\,G_m$ channel is open:

$$\sigma_g(\bar\chi\,\chi \to G_n\,G_m) \approx v^{-1}\left(\frac{A^g_\chi}{16384\,\pi}\right)\left(\frac{1}{\Lambda^2_n\Lambda^2_m m^2_{\rm DM}m^2_n m^2_m}\right) \times\sqrt{\left(1+\frac{m^2_n-m^2_m}{4m^2_{\rm DM}}\right)^2-\frac{m^2_n}{m^2_{\rm DM}}}\,. \tag{D.15}$$

Notice that, differently from the scalar and vector case, the contribution of the 4-points diagram from the vertex A.9 vanishes ($B^g_\chi = C^g_\chi = 0$). The t- and u-channel contributions give, instead:

$$A^g_\chi = \frac{\left((m^2_n-4m^2_{\rm DM})^2-2m^2_m(4m^2_{\rm DM}+m^2_n)+m^4_m\right)^3}{(m^2_n+m^2_m-4m^2_{\rm DM})^2} \tag{D.16}$$

In the particular case when two KK-gravitons have the same KK-number, m = n, eq. (D.15) becomes:

$$\sigma_g(\bar\chi\,\chi \to G_n\,G_n) \approx v^{-1}\frac{m^2_{\rm DM}}{16\,\pi\,\Lambda^4_n}\frac{(1-r)^{7/2}}{r^2(2-r)^2}\,, \tag{D.17}$$

where[6] $r \equiv (m_{\rm n}/m_{\rm DM})^2$.

D.1.3 Vectorial case

If the dark matter is a spin-1 particle (X) the annihilation into two Higgs bosons is:

$$\sigma_g(X\,X \to H\,H) \approx v^{-1}\,|S^g_{KK}|^2\frac{2m^6_{\rm DM}}{27\pi}\left(1-\frac{m^2_H}{m^2_{\rm DM}}\right)^{5/2} \tag{D.18}$$

The annihilation cross-section into two SM massive gauge bosons is:

$$\begin{cases} \sigma_g(X\,X \to W^+\,W^-) \approx v^{-1}\,|S^g_{KK}|^2\frac{52m^6_{\rm DM}}{27\pi}\left(1-\frac{m^2_W}{m^2_{\rm DM}}\right)^{1/2}\left(1+\frac{14m^2_W}{13m^2_{\rm DM}}+\frac{3m^4_W}{13m^4_{\rm DM}}\right)\,, \\ \sigma_g(X\,X \to Z\,Z) \qquad \approx v^{-1}\,|S^g_{KK}|^2\frac{26m^6_{\rm DM}}{27\pi}\left(1-\frac{m^2_Z}{m^2_{\rm DM}}\right)^{1/2}\left(1+\frac{14m^2_Z}{13m^2_{\rm DM}}+\frac{3m^4_Z}{13m^4_{\rm DM}}\right)\,, \end{cases} \tag{D.19}$$

whereas for two massless gauge bosons we have:

$$\begin{cases} \sigma_g(X\,X \to \gamma\,\gamma) \approx v^{-1}\,|S^g_{KK}|^2\frac{8m^6_{\rm DM}}{9\pi}\,, \\ \sigma_g(X\,X \to g\,g) \approx v^{-1}\,|S^g_{KK}|^2\frac{64\,m^6_{\rm DM}}{9\pi}\,. \end{cases} \tag{D.20}$$

[6]We have found a misprint in Ref. [19]: the cross-section of fermion DM annihilation into two KK-gravitons scales with r^{-2} as in eq. (D.17), and not as r^{-4}, as reported in Ref. [19]. This is relevant when comparing results for scalar and vector DM with respect to those for fermion DM as a function of the DM mass (see Sect. 3).

The annihilation cross-section into two SM fermions is:

$$\sigma_g(X\,X \to \bar{\psi}\,\psi) \approx v^{-1}\,|S^g_{KK}|^2 \frac{12 m_{\rm DM}^6}{27\pi}\left(1 - \frac{m_\psi^2}{m_{\rm DM}^2}\right)^{3/2}\left(1 + \frac{2m_\psi^2}{3m_{\rm DM}^2}\right). \tag{D.21}$$

Eventually, the annihilation into gravitons will be given by:

$$\sigma_g(X\,X \to G_n\,G_m) \approx v^{-1}\left(\frac{A^g_V + B^g_V + C^g_V/2}{331776\pi}\right)\left(\frac{1}{\Lambda_n^2\,\Lambda_m^2\,m_{\rm DM}^2\,m_{\rm n}^4\,m_{\rm m}^4}\right) \times \sqrt{\left(1 + \frac{m_n^2 - m_m^2}{4m_{\rm DM}^2}\right)^2 - \frac{m_n^2}{m_{\rm DM}^2}}\,, \tag{D.22}$$

where:

$$\left\{\begin{array}{l} A^g_V \;=\; \frac{1}{(-4m_{\rm DM}^2+m_n^2+m_m^2)^2}\left[m_{\rm DM}^{16} + 393216\left(m_n^2+m_m^2\right)m_{\rm DM}^{14}\right. \\ \quad -\; 16384\left(-353m_n^2m_m^2 + m_n^4 + m_m^4\right)m_{\rm DM}^{12} \\ \quad -\; \left(m_n^2+m_m^2\right)\left(19m_n^2m_m^2 + m_n^4 + m_m^4\right)m_{\rm DM}^{10} \\ \quad +\; 512\left(2302m_n^6m_m^2 + 3826m_n^4m_m^4 + 2302m_n^2m_m^6 + 205m_n^8 + 205m_m^8\right)m_{\rm DM}^8 \\ \quad -\; \left(m_n^2+m_m^2\right)\left(-430m_n^6m_m^2 - 602m_n^4m_m^4 - 430m_n^2m_m^6 + 7m_n^8 + 7m_m^8\right)m_{\rm DM}^6 \\ \quad -\; \left(1025m_n^{10}m_m^2 + 647m_n^8m_m^4 - 5562m_n^6m_m^6\right. \\ \quad +\; \left.647m_n^4m_m^8 + 1025m_n^2m_m^{10} + 21m_n^{12} + 21m_m^{12}\right)m_{\rm DM}^4 \\ \quad -\; \left(m_n^2-m_m^2\right)^2\left(m_n^2+m_m^2\right)\left(-67m_n^6m_m^2 - 48m_n^4m_m^4 - 67m_n^2m_m^6 + 7m_n^8 + 7m_m^8\right)m_{\rm DM}^2 \\ \quad +\; \left.\left(m_n^2-m_m^2\right)^4\left(208m_n^6m_m^2 + 906m_n^4m_m^4 + 208m_n^2m_m^6 + 51m_n^8 + 51m_m^8\right)\right]\,, \\ \\ B^g_V \;=\; 0\,, \\ \\ C^g_V \;=\; 32768m_{\rm DM}^{12} - 256\left(-135m_m^2m_n^2 + 74m_n^4 + 74m_m^4\right)m_{\rm DM}^8 \\ \quad +\; 512\left(m_n^2+m_m^2\right)\left(-43m_m^2m_n^2 + 17m_n^4 + 17m_m^4\right)m_{\rm DM}^6 \\ \quad -\; 32\left(-13m_m^6m_n^2 - 1166m_m^4m_n^4 - 13m_m^2m_n^6 + 42m_n^8 + 42m_m^8\right)m_{\rm DM}^4 \\ \quad +\; 32\left(m_n^2-m_m^2\right)^2\left(m_n^2+m_m^2\right)\left(5m_m^2m_n^2 + m_n^4 + m_m^4\right)m_{\rm DM}^2 \\ \quad +\; 3\left(m_n^2-m_m^2\right)^4\left(13m_m^2m_n^2 + 2m_n^4 + 2m_m^4\right)\,. \end{array}\right. \tag{D.23}$$

In the particular case in which the two KK-gravitons have the same KK-number, m = n, eq. (D.22) becomes:

$$\sigma_g(X\,X \to G_n\,G_n) \approx v^{-1}\frac{44m_{\rm DM}^2}{81\,\pi\,\Lambda_n^2\Lambda_m^2}\frac{(1-r)^{1/2}}{r^4(2-r)^2} \times \left(1 + \frac{12}{11}\,r + \frac{351}{44}\,r^2 - \frac{777}{44}\,r^3 + \frac{1105}{176}\,r^4 + \frac{181}{88}\,r^5 + \frac{17}{88}\,r^6\right), \tag{D.24}$$

where $r \equiv (m_{\rm n}/m_{\rm DM})^2$.

D.2 Annihilation through and into radion/KK-dilatons

In the following subsections we discuss the different DM annihilation cross sections through and into radion/KK-dilatons, using the approximation for the sums over the radion/KK-dilaton modes described in app.C. The sum over the dilaton states will be represented as S^r_{KK}.

D.2.1 Scalar case

The DM annihilation cross-section into two SM Higgs bosons is:

$$\sigma_r(S\,S \to H\,H) \approx v^{-1}\,|S^r_{KK}|^2 \frac{9\,m^6_{\rm DM}}{\pi}\left(1-\frac{m_H^2}{m^2_{\rm DM}}\right)^{1/2}\left(1+\frac{m_h^2}{2m^2_{\rm DM}}\right)^2 , \tag{D.25}$$

The cross-section for DM annihilation into SM massive gauge bosons is:

$$\begin{cases} \sigma_r(S\,S \to W^+\,W^-) \approx v^{-1}\,|S^r_{KK}|^2\,\frac{18\,m^6_{\rm DM}}{\pi}\left(1-\frac{m_W^2}{m^2_{\rm DM}}\right)^{1/2}\left(1-\frac{m_W^2}{m^2_{\rm DM}}+\frac{3\,m_W^4}{4m^4_{\rm DM}}\right) , \\ \\ \sigma_r(S\,S \to Z\,Z) \qquad \approx v^{-1}\,|S^r_{KK}|^2\,\frac{9\,m^6_{\rm DM}}{\pi}\left(1-\frac{m_Z^2}{m^2_{\rm DM}}\right)^{1/2}\left(1-\frac{m_Z^2}{m^2_{\rm DM}}+\frac{3\,m_Z^4}{4m^4_{\rm DM}}\right) . \end{cases} \tag{D.26}$$

The DM annihilation into photons and gluons is proportional to the vertex in eq. (A.15). The corresponding expressions for the cross-sections are:

$$\begin{cases} \sigma_r(S\,S \to \gamma\,\gamma) \approx v^{-1}\,|S^r_{KK}|^2\,\frac{9\,m^6_{\rm DM}\,\alpha_{EM}\,C_{EM}}{8\,\pi^3} , \\ \\ \sigma_r(S\,S \to g\,g) \approx v^{-1}\,|S^r_{KK}|^2\,\frac{9\,m^6_{\rm DM}\,\alpha_3\,C_3}{\pi^3} . \end{cases} \tag{D.27}$$

The DM annihilation cross-section into SM fermions is given by:

$$\sigma_r(S\,S \to \bar\psi\,\psi) \approx v^{-1}\,|S^r_{KK}|^2\,\frac{9\,m^4_{\rm DM}\,m^2_\psi}{\pi}\left(1-\frac{m^2_\psi}{m^2_{\rm DM}}\right)^{3/2} . \tag{D.28}$$

Eventually, the DM annihilation cross-section into two radion/KK-dilatons is given by:

$$\sigma_g(S\,S \to \phi_n\,\phi_m) \approx v^{-1}\,\frac{A^r_S + B^r_S + C^r_S}{64\pi\Lambda_n^2\Lambda_m^2 m^2_{\rm DM}} \times \sqrt{\left(1+\frac{m_n^2-m_m^2}{4m^2_{\rm DM}}\right)^2 - \frac{m_n^2}{m^2_{\rm DM}}} \tag{D.29}$$

where, as in the case of KK-gravitons, the three contributions to the cross-section come from the square of the t- and u-channels amplitudes (A^r_S), the square of the 4-points amplitude from vertex A.19 (C^r_S) and from the interference between the two classes of diagrams (B^r_S), respectively:

$$\begin{cases} A^r_S = \frac{\left[64m^2_{\rm DM}+(m_n^2-m_m^2)^2\right]^2}{(-4m^2_{\rm DM}+m_n^2+m_m^2)^2} , \\ \\ B^r_S = \frac{28\left[64m_{\rm DM}+(m_n^2-m_m^2)^2\right]}{(-4m^2_{\rm DM}+m_n^2+m_m^2)} , \\ \\ C^r_S = 196\,m^4_{\rm DM} . \end{cases} \tag{D.30}$$

where (m_n, Λ_n) and (m_m, Λ_m) are the masses and coupling of the n-th and m-th radion/KK-dilatons modes, respectively.

D.2.2 Fermionic case

If the Dark Matter is a Dirac fermion (χ) the annihilation into two SM Higgs bosons is:

$$\sigma_r(\bar{\chi}\,\chi \to H\,H) \approx v\,|S^r_{KK}|^2 \frac{m^6_{\rm DM}}{8\,\pi} \left(1 - \frac{m^2_H}{m^2_{\rm DM}}\right)^{1/2} \left(1 + \frac{m^2_H}{2m^2_{\rm DM}}\right)^2 , \tag{D.31}$$

The annihilation cross-section into two SM massive gauge bosons is:

$$\begin{cases} \sigma_r(\bar{\chi}\,\chi \to W^+\,W^-) \approx v\,|S^r_{KK}|^2 \, \frac{m^6_{\rm DM}}{4\,\pi} \left(1 - \frac{m^2_W}{m^2_{\rm DM}}\right)^{1/2} \left(1 - \frac{m^2_W}{m^2_{\rm DM}} + \frac{3\,m^4_W}{4m^4_{\rm DM}}\right) , \\ \\ \sigma_r(\bar{\chi}\,\chi \to Z\,Z) \qquad \approx v\,|S^r_{KK}|^2 \, \frac{m^6_{\rm DM}}{8\,\pi} \left(1 - \frac{m^2_Z}{m^2_{\rm DM}}\right)^{1/2} \left(1 - \frac{m^2_Z}{m^2_{\rm DM}} + \frac{3\,m^4_Z}{4m^4_{\rm DM}}\right) . \end{cases} \tag{D.32}$$

whereas for two massless gauge bosons we have:

$$\begin{cases} \sigma_r(\bar{\chi}\,\chi \to \gamma\,\gamma) \approx v\,|S^r_{KK}|^2 \, \frac{m^6_{\rm DM}\,\alpha_{EM}\,C_{EM}}{16\,\pi^3} , \\ \\ \sigma_r(\bar{\chi}\,\chi \to g\,g) \approx v\,|S^r_{KK}|^2 \, \frac{m^6_{\rm DM}\,\alpha_3\,C_3}{2\,\pi^3} . \end{cases} \tag{D.33}$$

The DM annihilation cross-section into two SM fermions is:

$$\sigma_r(\bar{\chi}\,\chi \to \bar{\psi}\,\psi) \approx v\,|S^r_{KK}|^2 \, \frac{m^4_{\rm DM}\,m^2_\psi}{8\,\pi} \left(1 - \frac{m^2_\psi}{m^2_{\rm DM}}\right)^{3/2} . \tag{D.34}$$

Eventually, the annihilation directly into dilatons is given by:

$$\sigma_g(\bar{\chi}\,\chi \to \phi_n\,\phi_m) \approx v\,\frac{A^r_\chi + B^r_\chi + C^r_\chi}{13824 m^2_{DM}\pi\Lambda^2_n\Lambda^2_m} \sqrt{\left(1 + \frac{m^2_n - m^2_m}{4m^2_{\rm DM}}\right)^2 - \frac{m^2_n}{m^2_{\rm DM}}} \tag{D.35}$$

where:

$$\begin{cases} A^r_\chi = \frac{m^4_{DM}}{(-4m^2_{\rm DM}+m^2_{\rm n}+m^2_{\rm m})^4} \left[4m^6_{\rm m}\left(419m^2_{\rm n} - 1804m^2_{\rm DM}\right)\right. \\ \quad + \; 2m^4_{\rm m}\left(-10312m^2_{\rm DM}m^2_{\rm n} + 21648m^4_{\rm DM} + 3273m^4_{\rm n}\right) \\ \quad - \; 4m^2_{\rm m}\left(1804m^2_{\rm DM} - 419m^2_{\rm n}\right)\left(m^2_{\rm n} - 4m^2_{\rm DM}\right)^2 + 451\left(m^2_{\rm n} - 4m^2_{\rm DM}\right)^4 + \left. 451m^8_{\rm m}\right] , \\ \\ B^r_\chi = 0 , \\ \\ C^r_\chi = 3m^4_{\rm DM} . \end{cases} \tag{D.36}$$

and where (m_n, Λ_n) and (m_m, Λ_m) are the masses and coupling of the n-th and m-th radion/KK-dilatons modes, respectively.

D.2.3 Vectorial case

If the Dark Matter is a spin-1 particle (X) the annihilation into two SM Higgs bosons is:

$$\sigma_r(X\,X \to H\,H) \approx v^{-1}\,|S^r_{KK}|^2 \frac{m^6_{\rm DM}}{3\,\pi} \left(1 - \frac{m^2_H}{m^2_{\rm DM}}\right)^{1/2} \left(1 + \frac{m^2_H}{2m^2_{\rm DM}}\right)^2 , \tag{D.37}$$

The annihilation cross-section into two SM massive gauge bosons is:

$$\begin{cases} \sigma_r(X\,X \to W^+\,W^-) \approx v^{-1}\,|S^r_{KK}|^2\,\frac{4m^2_{\rm DM}\,m^4_W}{3\,\pi}\,\left(1-\frac{m^2_W}{m^2_{\rm DM}}\right)^{1/2}\,\left(1-\frac{3m^2_W}{4m^2_{\rm DM}}+\frac{m^4_W}{8m^4_{\rm DM}}\right)\,, \\ \\ \sigma_r(X\,X \to Z\,Z) \qquad\;\; \approx v^{-1}\,|S^r_{KK}|^2\,\frac{2m^2_{\rm DM}\,m^4_Z}{3\,\pi}\,\left(1-\frac{m^2_Z}{m^2_{\rm DM}}\right)^{1/2}\,\left(1-\frac{3m^2_Z}{4m^2_{\rm DM}}+\frac{m^4_Z}{8m^4_{\rm DM}}\right)\,. \end{cases} \tag{D.38}$$

whereas for two massless gauge bosons we have:

$$\begin{cases} \sigma_r(X\,X \to \gamma\,\gamma) \approx v^{-1}\,|S^r_{KK}|^2\,\frac{3\,m^6_{\rm DM}\,\alpha_{EM}\,C_{EM}}{8\,\pi^3}\,, \\ \\ \sigma_r(X\,X \to g\,g) \;\approx v^{-1}\,|S^r_{KK}|^2\,\frac{3\,m^6_{\rm DM}\,\alpha_3\,C_3}{\pi^3}\,. \end{cases} \tag{D.39}$$

The DM annihilation cross-section into two SM fermions is:

$$\sigma_r(X\,X \to \bar\psi\,\psi) \approx v^{-1}\,|S^r_{KK}|^2\,\frac{m^4_{\rm DM}\,m^2_\psi}{3\,\pi}\,\left(1-\frac{m^2_\psi}{m^2_{\rm DM}}\right)^{3/2}\,. \tag{D.40}$$

Eventually, the annihilation cross-section into two radion/KK-dilatons is given by:

$$\sigma_g(X\,X \;\to \phi_n\,\phi_m) \approx v^{-1}\,\frac{A^r_V+B^r_V+C^r_V}{20736\,\pi\,\Lambda^2_n\,\Lambda^2_m m^2_{\rm DM}}\sqrt{\left(1+\frac{m^2_n-m^2_m}{4m^2_{\rm DM}}\right)^2-\frac{m^2_n}{m^2_{\rm DM}}} \tag{D.41}$$

where:

$$\begin{cases} A^r_V \;= \frac{1}{(-4m^2_{\rm DM}+m^2_n+m^2_m)^2}\left[-512\left(m^2_n+m^2_m\right)m^6_{\rm DM}+128\left(m^4_n+m^4_m\right)m^4_{\rm DM}\right. \\ \qquad\left.-\;16\left(m^2_n-m^2_m\right)^2\left(m^2_n+m^2_m\right)m^2_{\rm DM}+\left(m^2_n-m^2_m\right)^4+1536m^8_{\rm DM}\right]\,, \\ \\ B^r_V \;= 0\,, \\ \\ C^r_V \;= 12m^4_{\rm DM}\,. \end{cases} \tag{D.42}$$

and where (m_n,Λ_n) and (m_m,Λ_m) are the masses and coupling of the n-th and m-th radion/KK-dilatons modes, respectively.

D.3 Annihilation into one KK-graviton and one radion/KK-dilaton

It exists another channel that was not previously considered in the literature: DM annihilation into one KK-graviton and one radion/KK-dilaton. The cross-section for this process is given by the following expressions:

$$
\begin{cases}
\sigma_{gr}(S\,S \to G_n\, r_m) \;\approx v^{-1}\left(\frac{A_S^{gr}}{9216\pi}\right)\left(\frac{1}{\Lambda_{g,n}^2\,\Lambda_{r,m}^2 m_{\rm DM}^2 m_{g,n}^4}\right)\frac{1}{\left(-4m_{\rm DM}^2+m_{g,n}^2+m_{r,m}^2\right)^2} \\
\qquad\qquad\times\sqrt{\left(1+\frac{m_{g,n}^2-m_{r,m}^2}{4m_{\rm DM}^2}\right)^2-\frac{m_{g,n}^2}{m_{\rm DM}^2}}\,, \\
\\
\sigma_{gr}(\bar\chi\,\chi \to G_n\, r_m) \;\approx v^{-1}\left(\frac{A_\chi^{gr}}{576\pi}\right)\left(\frac{1}{\Lambda_{g,n}^2\,\Lambda_{r,m}^2 m_{g,n}^2}\right)\frac{1}{\left(-4m_{\rm DM}^2+m_{g,n}^2+m_{r,m}^2\right)^2} \\
\qquad\qquad\times\sqrt{\left(1+\frac{m_{g,n}^2-m_{r,m}^2}{4m_{\rm DM}^2}\right)^2-\frac{m_{g,n}^2}{m_{\rm DM}^2}}\,, \\
\\
\sigma_{gr}(V\,V \to G_n\, r_m) \approx v^{-1}\left(\frac{A_V^{gr}}{82944\pi}\right)\left(\frac{1}{\Lambda_{g,n}^2\Lambda_{r,m}^2 m_{\rm DM}^2 m_{g,n}^4}\right)\frac{1}{\left(-4m_{\rm DM}^2+m_{g,n}^2+m_{r,m}^2\right)^2} \\
\qquad\qquad\times\sqrt{\left(1+\frac{m_{g,n}^2-m_{r,m}^2}{4m_{\rm DM}^2}\right)^2-\frac{m_{g,n}^2}{m_{\rm DM}^2}}\,,
\end{cases}
$$

where the value of A^{gr} is given by:

$$
\begin{cases}
A_S^{gr} \;=\; \left(m_{g,n}^2-m_{r,m}^2\right)^2\left[-2m_{r,m}^2\left(4m_{\rm DM}^2+m_{g,n}^2\right)+\left(m_{g,n}^2-4m_{\rm DM}^2\right)^2+m_{r,m}^4\right]^2\,, \\
\\
A_\chi^{gr} \;=\; \left(2m_{\rm DM}-m_{g,n}-m_{r,m}\right)\left(2m_{\rm DM}+m_{g,n}-m_{r,m}\right) \\
\quad\times\left(2m_{\rm DM}-m_{g,n}+m_{r,m}\right)\left(2m_{\rm DM}+m_{g,n}+m_{r,m}\right) \\
\quad\times\left[8m_{\rm DM}^2\left(7m_{g,n}^2-3m_{r,m}^2\right)+48m_{\rm DM}^4+3\left(m_{g,n}^2-m_{r,m}^2\right)^2\right]\,, \\
\\
A_V^{gr} \;=\; 4096m_{\rm DM}^{10}\left(3m_{g,n}^2-7m_{r,m}^2\right)+256m_{\rm DM}^8\left(-106m_{g,n}^2m_{r,m}^2+93m_{g,n}^4+53m_{r,m}^4\right) \\
\quad+\,256m_{\rm DM}^6\left(-63m_{g,n}^4m_{r,m}^2+57m_{g,n}^2m_{r,m}^4+67m_{g,n}^6-13m_{r,m}^6\right) \\
\quad+\,64m_{\rm DM}^4\left(m_{g,n}^2-m_{r,m}^2\right)^2\left(-34m_{g,n}^2m_{r,m}^2+17m_{g,n}^4+7m_{r,m}^4\right) \\
\quad+\,32m_{\rm DM}^2\left(m_{g,n}^2-m_{r,m}^2\right)^4\left(4m_{g,n}^2-m_{r,m}^2\right)+24576m_{\rm DM}^{12}+\left(m_{g,n}^2-m_{r,m}^2\right)^6\,.
\end{cases}
\tag{D.43}
$$

In all of these expressions we have used $(m_{g,n}, \Lambda_{g,n})$ and $(m_{r,m}, \Lambda_{r,m})$ for the mass and coupling of the n-th KK-graviton and of the m-th radion/KK-dilaton, respectively. Notice that for this particular channel it does not exists a four-legs vertex.

References

[1] ATLAS collaboration, G. Aad et al., *Observation of a new particle in the search for the Standard Model Higgs boson with the ATLAS detector at the LHC*, *Phys. Lett.* **B716** (2012) 1–29, [1207.7214].

[2] G. Bertone, D. Hooper and J. Silk, *Particle dark matter: Evidence, candidates and constraints*, *Phys. Rept.* **405** (2005) 279–390, [hep-ph/0404175].

[3] S. Dimopoulos and H. Georgi, *Softly Broken Supersymmetry and SU(5)*, *Nucl.Phys.* **B193** (1981) 150.

[4] T. Appelquist, H.-C. Cheng and B. A. Dobrescu, *Bounds on universal extra dimensions*, *Phys.Rev.* **D64** (2001) 035002, [hep-ph/0012100].

[5] P. Cushman et al., *Working Group Report: WIMP Dark Matter Direct Detection*, in *Proceedings, 2013 Community Summer Study on the Future of U.S. Particle Physics: Snowmass on the Mississippi (CSS2013): Minneapolis, MN, USA, July 29-August 6, 2013*, 2013, 1310.8327, http://www.slac.stanford.edu/econf/C1307292/docs/CosmicFrontier/WIMPDirect-24.pdf.

[6] M. Cirelli, G. Corcella, A. Hektor, G. Hutsi, M. Kadastik, P. Panci et al., *PPPC 4 DM ID: A Poor Particle Physicist Cookbook for Dark Matter Indirect Detection*, *JCAP* **1103** (2011) 051, [1012.4515].

[7] L. J. Hall, K. Jedamzik, J. March-Russell and S. M. West, *Freeze-In Production of FIMP Dark Matter*, *JHEP* **03** (2010) 080, [0911.1120].

[8] Y. Hochberg, E. Kuflik, T. Volansky and J. G. Wacker, *Mechanism for Thermal Relic Dark Matter of Strongly Interacting Massive Particles*, *Phys. Rev. Lett.* **113** (2014) 171301, [1402.5143].

[9] A. G. Dias, A. C. B. Machado, C. C. Nishi, A. Ringwald and P. Vaudrevange, *The Quest for an Intermediate-Scale Accidental Axion and Further ALPs*, *JHEP* **06** (2014) 037, [1403.5760].

[10] I. Antoniadis, *A Possible new dimension at a few TeV*, *Phys. Lett.* **B246** (1990) 377–384.

[11] I. Antoniadis, S. Dimopoulos and G. Dvali, *Millimeter range forces in superstring theories with weak scale compactification*, *Nucl.Phys.* **B516** (1998) 70–82, [hep-ph/9710204].

[12] N. Arkani-Hamed, S. Dimopoulos and G. Dvali, *The Hierarchy problem and new dimensions at a millimeter*, *Phys.Lett.* **B429** (1998) 263–272, [hep-ph/9803315].

[13] I. Antoniadis, N. Arkani-Hamed, S. Dimopoulos and G. Dvali, *New dimensions at a millimeter to a Fermi and superstrings at a TeV*, *Phys.Lett.* **B436** (1998) 257–263, [hep-ph/9804398].

[14] N. Arkani-Hamed, S. Dimopoulos and G. Dvali, *Phenomenology, astrophysics and cosmology of theories with submillimeter dimensions and TeV scale quantum gravity*, *Phys.Rev.* **D59** (1999) 086004, [hep-ph/9807344].

[15] L. Randall and R. Sundrum, *A Large mass hierarchy from a small extra dimension*, *Phys. Rev. Lett.* **83** (1999) 3370–3373, [hep-ph/9905221].

[16] L. Randall and R. Sundrum, *An Alternative to compactification*, *Phys.Rev.Lett.* **83** (1999) 4690–4693, [hep-th/9906064].

[17] G. F. Giudice and M. McCullough, *A Clockwork Theory*, *JHEP* **02** (2017) 036, [1610.07962].

[18] G. F. Giudice, Y. Kats, M. McCullough, R. Torre and A. Urbano, *Clockwork/linear dilaton: structure and phenomenology*, *JHEP* **06** (2018) 009, [1711.08437].

[19] H. M. Lee, M. Park and V. Sanz, *Gravity-mediated (or Composite) Dark Matter*, *Eur. Phys. J.* **C74** (2014) 2715, [1306.4107].

[20] H. M. Lee, M. Park and V. Sanz, *Gravity-mediated (or Composite) Dark Matter Confronts Astrophysical Data*, *JHEP* **05** (2014) 063, [1401.5301].

[21] C. Han, H. M. Lee, M. Park and V. Sanz, *The diphoton resonance as a gravity mediator of dark matter*, *Phys. Lett.* **B755** (2016) 371–379, [1512.06376].

[22] T. D. Rueter, T. G. Rizzo and J. L. Hewett, *Gravity-Mediated Dark Matter Annihilation in the Randall-Sundrum Model*, *JHEP* **10** (2017) 094, [1706.07540].

[23] M. Kumar, A. Goyal and R. Islam, *Dark matter in the Randall-Sundrum model*, in *64th Annual Conference of the South African Institute of Physics (SAIP2019) Polokwane, South Africa, July 8-12, 2019*, 2019, 1908.10334.

[24] T. G. Rizzo, *Dark Photons, Kinetic Mixing and Light Dark Matter From 5-D*, in *53rd Rencontres de Moriond on Electroweak Interactions and Unified Theories (Moriond EW 2018) La Thuile, Italy, March 10-17, 2018*, 2018, 1804.03560.

[25] T. G. Rizzo, *Kinetic mixing, dark photons and extra dimensions. Part II: fermionic dark matter*, *JHEP* **10** (2018) 069, [1805.08150].

[26] A. Carrillo-Monteverde, Y.-J. Kang, H. M. Lee, M. Park and V. Sanz, *Dark Matter Direct Detection from new interactions in models with spin-two mediators*, *JHEP* **06** (2018) 037, [1803.02144].

[27] S. Kraml, U. Laa, K. Mawatari and K. Yamashita, *Simplified dark matter models with a spin-2 mediator at the LHC*, *Eur. Phys. J.* **C77** (2017) 326, [1701.07008].

[28] M. T. Arun, D. Choudhury and D. Sachdeva, *Living Orthogonally: Quasi-universal Extra Dimensions*, *JHEP* **01** (2019) 230, [1805.01642].

[29] M. T. Arun, D. Choudhury and D. Sachdeva, *Universal Extra Dimensions and the Graviton Portal to Dark Matter*, *JCAP* **1710** (2017) 041, [1703.04985].

[30] M. G. Folgado, A. Donini and N. Rius, *Gravity-mediated Scalar Dark Matter in Warped Extra-Dimensions*, 1907.04340.

[31] W. D. Goldberger and M. B. Wise, *Modulus stabilization with bulk fields*, *Phys. Rev. Lett.* **83** (1999) 4922–4925, [hep-ph/9907447].

[32] E. W. Kolb and M. S. Turner, *The Early Universe*, *Front. Phys.* **69** (1990) 1–547.

[33] Planck collaboration, N. Aghanim et al., *Planck 2018 results. VI. Cosmological parameters*, 1807.06209.

[34] G. Steigman, B. Dasgupta and J. F. Beacom, *Precise Relic WIMP Abundance and its Impact on Searches for Dark Matter Annihilation*, *Phys. Rev.* **D86** (2012) 023506, [1204.3622].

[35] P. Gondolo and G. Gelmini, *Cosmic abundances of stable particles: Improved analysis*, *Nucl. Phys.* **B360** (1991) 145–179.

[36] I. Antoniadis, A. Arvanitaki, S. Dimopoulos and A. Giveon, *Phenomenology of TeV Little String Theory from Holography*, *Phys. Rev. Lett.* **108** (2012) 081602, [1102.4043].

[37] M. Baryakhtar, *Graviton Phenomenology of Linear Dilaton Geometries*, *Phys. Rev.* **D85** (2012) 125019, [1202.6674].

[38] P. Cox and T. Gherghetta, *Radion Dynamics and Phenomenology in the Linear Dilaton Model*, *JHEP* **05** (2012) 149, [1203.5870].

[39] E. Adelberger, J. Gundlach, B. Heckel, S. Hoedl and S. Schlamminger, *Torsion balance experiments: A low-energy frontier of particle physics*, *Prog.Part.Nucl.Phys.* **62** (2009) 102–134.

[40] G. F. Giudice, R. Rattazzi and J. D. Wells, *Quantum gravity and extra dimensions at high-energy colliders*, *Nucl. Phys.* **B544** (1999) 3–38, [hep-ph/9811291].

[41] T. Appelquist and A. Chodos, *Quantum Effects in Kaluza-Klein Theories*, *Phys.Rev.Lett.* **50** (1983) 141.

[42] T. Appelquist and A. Chodos, *The Quantum Dynamics of Kaluza-Klein Theories*, *Phys.Rev.* **D28** (1983) 772.

[43] B. de Wit, M. Luscher and H. Nicolai, *The Supermembrane Is Unstable*, *Nucl.Phys.* **B320** (1989) 135.

[44] E. Ponton and E. Poppitz, *Casimir energy and radius stabilization in five-dimensional orbifolds and six-dimensional orbifolds*, *JHEP* **06** (2001) 019, [hep-ph/0105021].

[45] D. Teresi, *Clockwork without supersymmetry*, *Phys. Lett.* **B783** (2018) 1–6, [1802.01591].

[46] L. Kofman, J. Martin and M. Peloso, *Exact identification of the radion and its coupling to the observable sector*, *Phys. Rev.* **D70** (2004) 085015, [hep-ph/0401189].

[47] W. D. Goldberger and M. B. Wise, *Phenomenology of a stabilized modulus*, *Phys. Lett.* **B475** (2000) 275–279, [hep-ph/9911457].

[48] K. Blum, M. Cliche, C. Csaki and S. J. Lee, *WIMP Dark Matter through the Dilaton Portal*, *JHEP* **03** (2015) 099, [1410.1873].

[49] M. Escudero, A. Berlin, D. Hooper and M.-X. Lin, *Toward (Finally!) Ruling Out Z and Higgs Mediated Dark Matter Models*, *JCAP* **1612** (2016) 029, [1609.09079].

[50] J. A. Casas, D. G. Cerde'no, J. M. Moreno and J. Quilis, *Reopening the Higgs portal for single scalar dark matter*, *JHEP* **05** (2017) 036, [1701.08134].

[51] ATLAS collaboration, M. Aaboud et al., *Search for new phenomena in high-mass diphoton final states using 37 fb^{-1} of proton–proton collisions collected at $\sqrt{s} = 13$ TeV with the ATLAS detector*, *Phys. Lett.* **B775** (2017) 105–125, [1707.04147].

[52] ATLAS collaboration, T. A. collaboration, *Search for new high-mass phenomena in the dilepton final state using 36.1 fb^{-1} of proton-proton collision data at $\sqrt{s} = 13$ TeV with the ATLAS detector*, .

[53] CMS collaboration, C. Collaboration, *Search for physics beyond the standard model in the high-mass diphoton spectrum at* 13 TeV, .

[54] J. Hisano, K. Ishiwata, N. Nagata and M. Yamanaka, *Direct Detection of Vector Dark Matter*, *Prog. Theor. Phys.* **126** (2011) 435–456, [1012.5455].

[55] A. D. Martin, W. J. Stirling, R. S. Thorne and G. Watt, *Parton distributions for the LHC*, *Eur. Phys. J.* **C63** (2009) 189–285, [0901.0002].

[56] XENON collaboration, E. Aprile et al., *First Dark Matter Search Results from the XENON1T Experiment*, *Phys. Rev. Lett.* **119** (2017) 181301, [1705.06655].

[57] Fermi-LAT collaboration, M. Ajello et al., *Fermi-LAT Observations of High-Energy γ-Ray Emission Toward the Galactic Center*, *Astrophys. J.* **819** (2016) 44, [1511.02938].

[58] Fermi-LAT collaboration, M. Ackermann et al., *The Fermi Galactic Center GeV Excess and Implications for Dark Matter*, *Astrophys. J.* **840** (2017) 43, [1704.03910].

[59] Fermi-LAT, DES collaboration, A. Albert et al., *Searching for Dark Matter Annihilation in Recently Discovered Milky Way Satellites with Fermi-LAT*, *Astrophys. J.* **834** (2017) 110, [1611.03184].

[60] AMS Collaboration collaboration, M. Aguilar, D. Aisa, B. Alpat, A. Alvino, G. Ambrosi, K. Andeen et al., *Precision measurement of the $(e^+ + e^-)$ flux in primary cosmic rays from 0.5 gev to 1 tev with the alpha magnetic spectrometer on the international space station*, *Phys. Rev. Lett.* **113** (Nov, 2014) 221102.

[61] AMS Collaboration collaboration, M. Aguilar, L. Ali Cavasonza, B. Alpat, G. Ambrosi, L. Arruda, N. Attig et al., *Antiproton flux, antiproton-to-proton flux ratio, and properties of elementary particle fluxes in primary cosmic rays measured with the alpha magnetic spectrometer on the international space station*, *Phys. Rev. Lett.* **117** (Aug, 2016) 091103.

[62] F. Kahlhoefer, K. Schmidt-Hoberg, T. Schwetz and S. Vogl, *Implications of unitarity and gauge invariance for simplified dark matter models*, *JHEP* **02** (2016) 016, [1510.02110].

Published for SISSA by Springer

Received: *May 7, 2020*
Accepted: *August 25, 2020*
Published: *September 22, 2020*

Kaluza-Klein FIMP dark matter in warped extra-dimensions

Nicolás Bernal,[a] Andrea Donini,[b] Miguel G. Folgado[b] and Nuria Rius[b]

[a]*Centro de Investigaciones, Universidad Antonio Nariño, Carrera 3 Este # 47A-15, Bogotá, Colombia*

[b]*Instituto de Física Corpuscular, Universidad de Valencia and CSIC, Edificio Institutos Investigación, Catedrático Jose Beltrán 2, Paterna, 46980 Spain*

E-mail: nicolas.bernal@uan.edu.co, donini@ific.uv.es, migarfol@ific.uv.es, nuria.rius@ific.uv.es

Abstract: We study for the first time the case in which Dark Matter (DM) is made of Feebly Interacting Massive Particles (FIMP) interacting just gravitationally with the standard model particles in an extra-dimensional Randall-Sundrum scenario. We assume that both the dark matter and the standard model are localized in the IR-brane and only interact via gravitational mediators, namely the graviton, the Kaluza-Klein gravitons and the radion. We found that in the early Universe DM could be generated via two main processes: the direct freeze-in and the sequential freeze-in. The regions where the observed DM relic abundance is produced are largely compatible with cosmological and collider bounds.

Keywords: Beyond Standard Model, Cosmology of Theories beyond the SM

ArXiv ePrint: 2004.14403

https://doi.org/10.1007/JHEP09(2020)142

Contents

1 Introduction

The nature of Dark Matter (DM) and its interactions remain an open question in our effort to understand the Universe. Up to now, the only evidence about the existence of such dark component is via its gravitational effects. It could well be that DM has no other kind of interaction and, thus, it will be undetectable by current and future particle physics experiments. Moreover, in such a case the reheating temperature needs to be quite high (typically $\gtrsim 10^{16}$ GeV for DM mass of 10 TeV) in order to generate the observed DM relic abundance via a purely gravitational interaction [1–4], given the value of the Planck mass, $m_P \sim 10^{19}$ GeV, which determines its strength.

This is true, however, only if we live in a four-dimensional space-time: in extra-dimensional scenarios, the gravitational interaction may be enhanced, either because the fundamental Planck scale in D dimensions is $m_D \ll m_P$ (as in the case of Large Extra

Dimensions (LED) [5–9]), or due to a warping of the space-time which induces an effective Planck scale Λ in the four-dimensional brane such that $\Lambda \ll m_P$ (as in Randall-Sundrum models (RS) [10, 11]), or by a mixture of the two mechanisms (as it occurs in the more recent ClockWork/Linear Dilaton (CW/LD) model [12–15]). As it is well known, this feature of the extra-dimensional scenarios has been advocated as a solution to the so-called hierarchy problem, i.e., the huge hierarchy between the electroweak scale, $\Lambda_{\rm EW} \sim 250$ GeV, and the Planck scale, which would generate corrections of order of the Planck scale to the Higgs mass. These corrections would destabilize the electroweak scale unless either an enormous amount of fine-tuning is present or the Standard Model (SM) is the ultimate theory, which seems unlikely given the questions that are not explained within this framework (for instance, neutrino masses and baryogenesis, besides DM itself). In the extra-dimensional models mentioned above, the large hierarchy between the electroweak scale and the fundamental (or effective) Planck scale is eliminated, since the latter can be as low as $\mathcal{O}$(TeV).

As a consequence of such lower Planck scale in extra-dimensional models (either fundamental or effective), the gravitational interaction is enhanced, and a DM particle with just such interaction could become a WIMP, that is, a stable or cosmologically long-lived weakly interactive massive particle, with mass typically in the range 100 - 1000 GeV, and whose relic abundance is set via the freeze-out mechanism. This possibility has been thoroughly studied in the framework of the RS scenario [16–25] and in a series of recent papers that study generic spin-2 mediators [26–29]. It has also been considered in the context of the CW/LD model [30].

In this work we again explore the RS framework for DM, yet analyzing a different scenario in which the relic abundance of DM is set via the so-called DM freeze-in production mechanism [31–35] (for a recent review see Ref. [36]). In this case DM is a feebly interacting massive particle (FIMP), so that it never reaches thermal equilibrium with the SM thermal bath, and as a consequence its abundance remains smaller than the equilibrium one along the history of the Universe. More specifically, here we focus on the sub-case of ultraviolet (UV) freeze-in [37] for which the temperature of the thermal bath is always lower than the scale of new physics, which in our model is the effective Planck scale in the 4-dimensional brane, Λ, at which the gravitons become strongly interacting.

In our setup we assume that both the SM and the DM particles are localized in the same 4-dimensional brane, and by definiteness we consider real scalar DM, only. We relax the request for the RS model to solve the hierarchy problem, and allow Λ to vary in a wide range ($\Lambda \in [10^2, 10^{16}]$ GeV) to fully explore the parameter space that could lead to the correct DM relic abundance via freeze-in from a purely phenomenological perspective. In order to have a consistent model, we stabilize the size of the extra-dimension by using the Goldberger-Wise mechanism [38], which generates the required potential for the four-dimensional radion field. Then, besides the interaction through Kaluza-Klein (KK) gravitons, we also take into account that the SM and DM species can interact with the radion. We consider both SM particle annihilation into DM through KK-gravitons and the radion (direct freeze-in), as well as production of DM from out-of-equilibrium KK-gravitons and the radion (sequential freeze-in). We solve numerically the relevant Boltzmann equations in all cases and also provide analytical approximations for the final DM relic abundance in different ranges of the temperature, useful to understand our main results. We always work within the sudden decay approximation for the inflaton, and shortly comment on how our findings would be affected by a non-instantaneous inflaton decay.

We vary the DM mass, radion and KK-graviton masses and the scale Λ, determining the reheating temperature $T_{\rm rh}$ which leads to the correct DM relic abundance in each case, within the validity range of our effective four-dimensional theory. We find that in this scenario the observed DM density can be generated even with a reheating temperature lower than the electroweak scale. Recall that the only constraint on $T_{\rm rh}$ is that it has to be higher than the Big Bang Nucleosynthesis temperature of around a few MeV [39–44].

The outline of the paper is as follows: in Sec. 2 we briefly remind the main features of the RS scenario; Sec. 3 is devoted to the analysis of DM production via freeze-in within our model, both via direct and sequential freeze-in; finally, in Sec. 4 we present our conclusions. Some details on the RS scenario are given in Apps. A and B, whereas the relevant interaction rates used in our calculations are collected in App. C.

2 Theoretical Framework

In this Section, we shortly remind some aspects of the Warped Extra-Dimension scenario (also called Randall-Sundrum model [10]) relevant in the rest of the paper. Some further details on RS scenarios are given in Apps. A and B.

The popular Randall-Sundrum scenario (from now on RS or RS1 [10], to be distinguished from the scenario called RS2 [11]) consider a non-factorizable 5-dimensional metric in the form:

$$ds^2 = e^{-2\sigma}\,\eta_{\mu\nu}\,dx^\mu dx^\nu - r_c^2\,dy^2\,, \tag{2.1}$$

where $\sigma = k\,r_c\,|y|$ and the signature of the metric is $(+,-,-,-,-)$. In this scenario, k is the curvature along the $5^{\rm th}$-dimension and it is $\mathcal{O}\,(M_P)$. The length-scale r_c, on the other hand, is related to the size of the extra-dimension: we only consider a slice of the space-time between two branes located conventionally at the two fixed-points of an orbifold, $y = 0$ (the so-called UV-brane) and $y = \pi$ (the IR-brane). The 5-dimensional space-time is a slice of AdS_5 and the exponential factor that multiplies the $\mathcal{M}_4$ Minkowski 4-dimensional space-time is called the "warp factor".

The action in 5D is:

$$S = S_{\rm gravity} + S_{\rm IR} + S_{\rm UV} \tag{2.2}$$

where

$$S_{\rm gravity} = \frac{16\pi}{M_5^3}\int d^4x\int_0^\pi r_c\,dy\,\sqrt{G^{(5)}}\,\left[R^{(5)} - 2\Lambda_5\right]\,, \tag{2.3}$$

with M_5 the fundamental gravitational scale, $G^{(5)}$ and $R^{(5)}$ the 5-dimensional metric and Ricci scalar, respectively, and Λ_5 the 5-dimensional cosmological constant. As usual, we consider capital Latin indices M, N to run over the 5 dimensions and Greek indices μ, ν only over 4 dimensions. The reduced Planck mass is related to the fundamental scale M_5 as:

$$M_P^2 = \frac{M_5^3}{k}\,\left(1 - e^{-2k\,\pi\,r_c}\right)\,, \tag{2.4}$$

where $M_P = m_P/\sqrt{8\pi} \simeq 2.435 \times 10^{18}$ GeV, being m_P the Planck mass.

We consider for the two brane actions the following expressions:

$$S_{\rm IR} = \int d^4x \sqrt{-g^{(4)}} \, \left[-f_{\rm IR}^4 + \mathcal{L}_{\rm SM} + \mathcal{L}_{\rm DM} \right] \tag{2.5}$$

and

$$S_{\rm UV} = \int d^4x \sqrt{-g^{(4)}} \, \left[-f_{\rm UV}^4 + \dots \right], \tag{2.6}$$

where $f_{\rm IR}$, $f_{\rm UV}$ are the brane tensions for the two branes, $\mathcal{L}_{\rm SM}$ and $\mathcal{L}_{\rm DM}$ the SM and DM Lagrangians densities, respectively. Notice that in 4-dimensions in general $\eta_{\mu\nu}$ is replaced by $g^{(4)}_{\mu\nu}$, the 4-dimensional induced metric on the brane. Dots in eq. (2.6) stand for any possible new physics on the UV brane and, thus, decoupled from us.

In RS scenarios, in order to achieve the metric in eq. (2.1) as a classical solution of the Einstein equations, the brane-tension terms in $S_{\rm UV}$ and $S_{\rm IR}$ are chosen such as to cancel the 5-dimensional cosmological constant, $f_{\rm IR}^4 = -f_{\rm UV}^4 = \sqrt{-24 M_5^3 \Lambda_5}$. Throughout this paper, we consider all the SM and DM fields localized on the IR-brane, whereas on the UV-brane we could have any other physics that is Planck-suppressed. We assume that DM particles only interact with the SM particles gravitationally.[1]

Alternative DM spectra (with particles of spin higher than zero or with several particles) will not be studied here. Notice that, in 4-dimensions, the gravitational interactions would be enormously suppressed by powers of the Planck mass. However, in an extra-dimensional scenario, the gravitational interaction is actually enhanced: on the IR–brane, in fact, the effective gravitational coupling is $\Lambda = M_P \exp(-k\,\pi\, r_c)$, due to the rescaling factor $\sqrt{G^{(5)}}/\sqrt{-g^{(4)}}$. It is easy to see that $\Lambda \ll M_P$ even for moderate choices of σ. In particular, for $\sigma = k\, r_c \simeq 10$ the RS scenario can address the hierarchy problem. From a purely phenomenological perspective, here we will work with $\Lambda = [10^2, 10^{16}]$ GeV, relaxing the requirement that the RS model should provide a solution to the hierarchy problem.

The Kaluza-Klein decomposition of 5-dimensional fields in a RS scenario is shortly reviewed in App. A. The coupling between KK-gravitons and brane matter (being h_{MN} the 5D graviton field and $h_{\mu\nu}$ its 4D component) is:

$$\begin{aligned} \mathcal{L} &= -\frac{1}{M_5^{3/2}} T^{\mu\nu}(x) h_{\mu\nu}(x, y=\pi) = -\frac{1}{M_5^{3/2}} T^{\mu\nu}(x) \sum_{n=0} h^n_{\mu\nu} \frac{\chi^n}{\sqrt{r_c}}\,, \\ &= -\frac{1}{M_P} T^{\mu\nu}(x) h^0_{\mu\nu}(x) - \frac{1}{\Lambda} \sum_{n=1} T^{\mu\nu}(x) h^n_{\mu\nu}(x)\,, \end{aligned} \tag{2.7}$$

from which is clear that the coupling between KK-graviton modes with $n \neq 0$ is suppressed by the effective scale Λ and not by the Planck scale.

Stabilizing the size of the extra-dimension to be $y = \pi\, r_c$ is not easy. Long ago it was shown that bosonic quantum loops have a net effect on the border of the extra-dimension such that the extra-dimension itself should shrink to a point [45–47]. This feature, in a flat extra-dimension, can only be compensated by fermionic quantum loops and, usually, some

[1] If the DM particle is a scalar singlet under the SM gauge group, it will also interact with the SM through its mixing with the Higgs boson.

supersymmetric framework is invoked to stabilize the radius of the extra-dimension (see, e.g., Ref. [48]). A popular mechanism implemented in RS models to stabilize the size of the extra-dimension was proposed in Refs. [38, 49] and can be summarized as follows: if we add a bulk scalar field S with a scalar potential $V(S)$ and some *ad hoc* localized potential terms, $\delta(y=0)V_{\rm UV}(S)$ and $\delta(y=\pi\, r_c)V_{\rm IR}(S)$, it is possible to generate an effective potential $V(\varphi)$ for the four-dimensional field $\varphi = f\, \exp\left(-k\,\pi\, T\right)$ (with $f=\sqrt{24 M_5^3/k}$ and $\langle T\rangle = r_c$). The minimum of this potential can yield the desired value of kr_c without extreme fine-tuning of the parameters.

The S field will generically mix with the graviscalar $G^{(5)}_{55}$ (notice that the KK-tower of the graviscalar is absent from the low-energy spectrum, as they are eaten by the KK-tower of graviphotons to get a mass due to the spontaneous breaking of translational invariance caused by the presence of one or more branes). On the other hand, the KK-tower of the field S is present, but heavy (see Ref. [50]). The only light field present in the spectrum is, then, a combination of the graviscalar zero-mode and the S zero-mode. This field is usually called the *radion*, r. Its mass can be obtained from the effective potential $V(\varphi)$ and is given by $m_\varphi^2 = k^2 v_v^2 / 3 M_5^3\, \epsilon^2\, \exp(-2\pi\, k\, r_c)$, where v_v is the value of S at the visible brane and $\epsilon = m^2/4k^2$ (with m the mass of the field S). Quite generally $\epsilon \ll 1$ and, therefore, the mass of the radion can be much smaller than the first KK-graviton mass.

The radion, as for the KK-graviton case, interacts with both the DM and SM particles. It couples with matter through the trace of the energy-momentum tensor T [16]. Massless gauge fields do not contribute to the trace of the energy-momentum tensor, but effective couplings are generated from two different sources: quarks and W boson loops and the trace anomaly [51]. Thus the radion Lagrangian takes the following form [50, 52]:

$$\mathcal{L}_r = \frac{1}{2}(\partial_\mu r)(\partial^\mu r) - \frac{1}{2} m_r^2 r^2 + \frac{1}{\sqrt{6}\Lambda} r T + \frac{\alpha_{\rm EM}\, C_{\rm EM}}{8\pi\sqrt{6}\Lambda} r F_{\mu\nu}F^{\mu\nu} + \frac{\alpha_S C_3}{8\pi\sqrt{6}\Lambda} r \sum_a F^a_{\mu\nu}F^{a\mu\nu}\,, \quad (2.8)$$

where $F_{\mu\nu}$, $F^a_{\mu\nu}$ are the Maxwell and $SU(3)_c$ Yang-Mills tensors, respectively. Further details on the radion lagrangian can be found in App. B.

Possible couplings between KK-modes of the bulk scalar field S, the DM and SM fields are usually allowed, in the absence of some *ad hoc* bulk symmetry to forbid them. In the rest of the paper we will not include them, since we want to focus on just gravitational mediators (radion and KK-gravitons) between the SM and the dark particles.

Finally, we want to comment about the AdS/CFT correspondence, which suggests a duality between strongly coupled conformal field theories in 4D and weakly coupled gravity in 5D (see, for example, Ref. [53] and refs. therein), also called holography. Within this framework, the extra-dimensional model described above can be interpreted as a strongly interacting theory in which the particles localized at the IR-brane are bound states, while the presence of gravity mediators (KK-gravitons and radion) is a consequence of the conformal symmetry of the composite sector, spontaneously broken by the strong dynamics. The radion is thought to be the Goldstone boson of dilatation symmetry in 4D, i.e., the dilaton, although the dual interpretation of the massive gravitons is not so well understood [16]. The scale Λ in the holographic dual corresponds to the scale of conformal symmetry breaking in 4D.

3 Dark Matter Production in the Early Universe

In Refs. [24, 30] some of us have studied how to reach the observed DM relic abundance in the freeze-out scenario. Freeze-out occurs if the interactions between DM and SM particles are strong enough to bring them into chemical equilibrium. However, if the interaction rates between the visible and the dark sectors were never strong enough, the observed DM relic abundance could still have been produced in the early Universe by non-thermal processes. This is what occurs in the so-called freeze-in mechanism.

The evolution of the DM, radion and KK-gravitons number densities (n, n_r and n_K respectively) is given by a system of coupled Boltzmann equations:

$$\frac{dn}{dt} + 3\,H\,n = -\gamma_{\rm DM\to SM}\left[\left(\frac{n}{n^{\rm eq}}\right)^2 - 1\right] + \gamma^d_{\rm KK\to DM}\left[\frac{n_K}{n_K^{\rm eq}} - \left(\frac{n}{n^{\rm eq}}\right)^2\right], \tag{3.1}$$

$$\begin{aligned}\frac{dn_r}{dt} + 3\,H\,n_r &= -\gamma_{\rm r\to SM}\left[\left(\frac{n_r}{n_r^{\rm eq}}\right)^2 - 1\right] - \gamma^d_{\rm r\to DM}\left[\frac{n_r}{n_r^{\rm eq}} - \left(\frac{n}{n^{\rm eq}}\right)^2\right]\\ &\quad -\gamma^d_{\rm r\to SM}\left[\frac{n_r}{n_r^{\rm eq}} - 1\right],\end{aligned} \tag{3.2}$$

$$\begin{aligned}\frac{dn_K}{dt} + 3\,H\,n_K &= -\gamma_{\rm KK\to SM}\left[\left(\frac{n_K}{n_K^{\rm eq}}\right)^2 - 1\right] - \gamma^d_{\rm KK\to DM}\left[\frac{n_K}{n_K^{\rm eq}} - \left(\frac{n}{n^{\rm eq}}\right)^2\right]\\ &\quad -\gamma^d_{\rm KK\to SM}\left[\frac{n_K}{n_K^{\rm eq}} - 1\right],\end{aligned} \tag{3.3}$$

where H corresponds to the Hubble expansion rate, and $n_i^{\rm eq}$ are the number densities at equilibrium of the species i. Interactions that *only* involve bulk particles, namely KK-gravitons and radions, both in the initial and final states are subdominant due to a strong suppression of $1/\Lambda^8$. The quantity $\gamma_{\Phi\,\to\rm SM}$ is the interaction rate density for the 2-to-2 annihilations of a field Φ (either DM, KK-graviton or radion) into SM particles. Similarly, $\gamma^d_{\Phi\,\to\rm DM}$ and $\gamma^d_{\Phi\,\to\rm SM}$ are the interaction rate densities for the 2-body decay of a field Φ into DM and SM particles, respectively. Let us notice that in this extra-dimensional picture we need a Boltzmann equation like eq. (3.6) for every KK-mode.

A standard way to rewrite the Boltzmann equations is using the dimensionless yield $Y \equiv n/\mathfrak{s}$, with $\mathfrak{s}$ the SM entropy density (not to be confused with the Mandelstam variable s). The SM entropy density is defined, as a function of the temperature, as $\mathfrak{s}(T) = \frac{2\pi^2}{45}\,g_{\star\mathfrak{s}}(T)\,T^3$ (where $g_{\star\mathfrak{s}}(T)$ is the effective number of relativistic degrees of freedom [54]). Equations (3.1) to (3.3) can therefore be rewritten as

$$\frac{dY}{dT} = -\frac{\gamma_{\text{DM}\to\text{SM}}}{H\,\mathfrak{s}\,T}\left[\left(\frac{Y}{Y^{\text{eq}}}\right)^2 - 1\right] + \frac{\gamma^d_{\text{KK}\to\text{DM}}}{H\,\mathfrak{s}\,T}\left[\frac{Y_K}{Y_K^{\text{eq}}} - \left(\frac{Y}{Y^{\text{eq}}}\right)^2\right], \tag{3.4}$$

$$\frac{dY_r}{dT} = -\frac{\gamma_{\text{r}\to\text{SM}}}{H\,\mathfrak{s}\,T}\left[\left(\frac{Y_r}{Y_r^{\text{eq}}}\right)^2 - 1\right] - \frac{\gamma^d_{\text{r}\to\text{DM}}}{H\,\mathfrak{s}\,T}\left[\frac{Y_r}{Y_r^{\text{eq}}} - \left(\frac{Y}{Y^{\text{eq}}}\right)^2\right] - \frac{\gamma^d_{\text{r}\to\text{SM}}}{H\,\mathfrak{s}\,T}\left[\frac{Y_r}{Y_r^{\text{eq}}} - 1\right], \tag{3.5}$$

$$\begin{aligned}\frac{dY_K}{dT} &= -\frac{\gamma_{\text{KK}\to\text{SM}}}{H\,\mathfrak{s}\,T}\left[\left(\frac{Y_K}{Y_K^{\text{eq}}}\right)^2 - 1\right] - \frac{\gamma^d_{\text{KK}\to\text{DM}}}{H\,\mathfrak{s}\,T}\left[\frac{Y_K}{Y_K^{\text{eq}}} - \left(\frac{Y}{Y^{\text{eq}}}\right)^2\right] \\ &\quad - \frac{\gamma^d_{\text{KK}\to\text{SM}}}{H\,\mathfrak{s}\,T}\left[\frac{Y_K}{Y_K^{\text{eq}}} - 1\right].\end{aligned} \tag{3.6}$$

In the freeze-in paradigm DM never gets in thermal equilibrium with the rest of the SM particles of the primordial plasma. It is usually assumed that after inflation the abundance of DM was negligible, and slowly produced via interaction between the SM particles. Along the evolution of the Universe, the DM abundance was generated via two main processes:

1. Direct freeze-in. The DM abundance is generated directly by the annihilation of SM particles via an s-channel exchange of KK-gravitons or a radion.

2. Sequential freeze-in or freeze-in from the dark sector. The DM abundance is generated by decays of KK-gravitons or radions, previously produced by annihilations or inverse decays of SM particles via direct freeze-in. This scenario has been doubted "sequential freeze-in" [55].

Another production channel corresponds to the case in which the DM abundance is set entirely in the hidden sector by 4-to-2 interactions [56–58]. However, such a possibility is sub-dominant due to a strong suppression by higher orders of the scale Λ. It has been also shown that, independently of the nature of DM, it is possible to populate the relic abundance through a freeze-in mechanism via the exchange of a massless spin-2 graviton [1–4]. However, for this mechanism to be dominant, reheating temperatures T_{rh} of the order of 10^{13} GeV for a DM mass of 1 MeV are required. We will see in the following that, in this warped extra-dimensional setup (with KK-gravitons and the radion as additional fields playing the freeze-in mechanism) a much wider range of T_{rh} is indeed possible.

These two main mechanisms previously mentioned, i.e. the direct and the sequential freeze-in, will be described in detail in the following subsections.

3.1 Direct Freeze-in

As it was briefly sketched above, in the case of direct freeze-in the DM abundance n is generated by the annihilation of SM particles via an s-channel exchange of KK-gravitons or a radion.[2] If the production cross-section is small enough to keep DM out of chemical

[2]Another possibility corresponds to the interactions mediated by Higgs bosons. However, we focus here on the extra-dimensional portal ignoring the Higgs one. This can be reached by assuming a quartic coupling $\lambda_{h\chi}$ between the Higgs and the DM such as $\lambda_{h\chi} \ll 10^{-10}$ [59, 60].

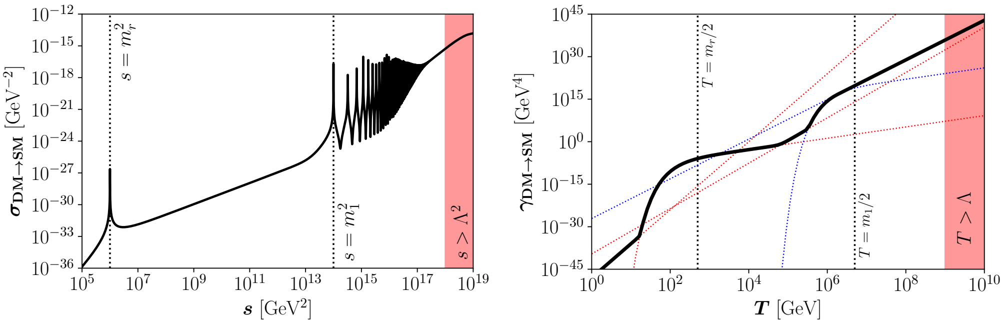

Figure 1. Black solid lines represent the DM annihilation cross section (left panel) and interaction rate density (right panel) for $m_r = 10^3$ GeV, $m_1 = 10^7$ GeV and $\Lambda = 10^9$ GeV. Colored lines depict the analytical approximations of eq. (3.13), where red and blue stand for interactions dominated by the exchange of a radion or a KK-gravitons, respectively. The red-shaded regions on the right of both panels are beyond our EFT approach.

equilibrium with the SM bath, and the evolution of the DM abundance n (or of the yield Y) is largely dominated by the interaction rate density $\gamma_{\text{DM}\to\text{SM}}$, eqs. (3.4) to (3.6) can be simplified to:

$$\frac{dY}{dT} \simeq \frac{\gamma_{\text{DM}\to\text{SM}}}{H\,\mathfrak{s}\,T}\left[\left(\frac{Y}{Y^{\text{eq}}}\right)^2 - 1\right] \simeq -\frac{\gamma_{\text{DM}\to\text{SM}}}{H\,\mathfrak{s}\,T}\,. \tag{3.7}$$

In a Universe dominated by SM radiation the Hubble expansion rate is $H^2 = \frac{\rho_{\text{SM}}}{3\,M_P^2}$, where the SM energy density is $\rho_{\text{SM}}(T) = \frac{\pi^2}{30} g_\star(T)\,T^4$ and $g_\star(T)$ is the effective numbers of relativistic degrees of freedom for the SM radiation [54]. Then, eq. (3.7) becomes:

$$Y(T) \simeq \frac{135}{2\pi^3\,g_{\star\mathfrak{s}}}\sqrt{\frac{10}{g_\star}}\,M_P \int_{T_{\text{rh}}}^{T} \frac{\gamma_{\text{DM}\to\text{SM}}(T)}{T^6}\,dT\,, \tag{3.8}$$

where T_{rh} is the reheating temperature which, in the approximation of a sudden decay of the inflaton, corresponds to the maximal temperature reached by the SM thermal bath. In order to get eq. (3.8) a vanishing initial DM abundance at $T = T_{\text{rh}}$ was assumed and the temperature dependence of $g_\star(T)$ and $g_{\star\mathfrak{s}}(T)$ has been neglected. The asymptotic values $g_\star$ and $g_{\star\mathfrak{s}}$ correspond to the SM values for $T \gg m_t$, $g_\star = g_{\star\mathfrak{s}} = 106.75$ (which take into account all SM degrees of freedom). Since this approximation is reliable for temperatures above the QCD phase transition, we explore the range $T_{\text{rh}} \gtrsim 1$ GeV.

The interaction rate density $\gamma_{\text{DM}\to\text{SM}}$ can be computed from the total DM annihilation cross-section into SM states $\sigma_{\text{DM}\to\text{SM}}$ which, in the limit where the DM and SM particle masses are negligible, can be expressed as:[3]

$$\sigma_{\text{DM}\to\text{SM}}(s) \simeq \frac{49}{1440\pi}\frac{s^3}{\Lambda^4}\left|\sum_{n=1}^{\infty}\frac{1}{s - m_n^2 + i\,m_n\,\Gamma_n}\right|^2 + \frac{s^3}{288\pi\Lambda^4}\frac{1}{(s-m_r^2)^2 + m_r^2\,\Gamma_r^2}\,, \tag{3.9}$$

[3]The details of the individual cross-sections are reported in Appendix C.1.

where the two terms correspond to the exchange of KK-gravitons and the radion, respectively. Left panel of Fig. 1 shows with a solid black line an example of the DM annihilation cross section $\sigma_{\rm DM\to SM}$ for a particular point in the parameter space, $m_r = 10^3$ GeV, $m_1 = 10^7$ GeV and $\Lambda = 10^9$ GeV. Notice that this cross-section is largely independent of the DM mass, m_χ, as long as $m_\chi^2 \ll s$. Then, also the interaction rate density becomes independent of m_χ provided $m_\chi \ll T$. Therefore, in the following we will consider as a benchmark point $m_\chi = 1$ MeV to illustrate our results, but keeping in mind that they can be extended to a wide range of DM masses, typically between the keV and PeV scale. The first peak at $s = m_r^2$ corresponds to the resonant exchange of a radion, whereas the following well-separated peaks correspond to the lightest KK-graviton modes. The non-trivial behavior for $s \gg m_1^2$ is due to the sum over poles and interferences of many different KK mediators. For very large values of the KK-number n, the widths of the KK-graviton resonances become comparable to their mass gap, $\Gamma_n(\sqrt{s}) \simeq \Delta m$. This happens approximately for:

$$s \gtrsim \Lambda^{4/3} \left(\frac{240\,\pi^2\, m_1}{73\, x_1} \right)^{2/3} \,, \tag{3.10}$$

as at large n the KK-modes separation is a constant, $\Delta m \simeq m_1/x_1$, see eq. (A.6). In this regime the resonances overlap and become individually indistinguishable. They eventually merge into one single contribution to the cross-section, as it can be seen in the rightmost region of Fig. 1 (left). Finally, the red-shaded region corresponding to $s > \Lambda^2$ is beyond our EFT approach, being the center-of-mass energy of the process larger than the effective scale of the theory.

In order to solve eq. (3.8), we need to compute the interaction rate density $\gamma_{\rm DM\to SM}$ as a function of the temperature. In general, for the process where two particles $(i,\, j)$ annihilate into two states $(k,\, l)$, the interaction rate density $i + j \to k + l$ is defined as:

$$\gamma(T) = \frac{T}{64\,\pi^4} \int_{s_{\rm min}}^{\infty} ds \sqrt{s}\, \sigma_R(s)\, K_1\left(\frac{\sqrt{s}}{T} \right) \,, \tag{3.11}$$

where $s_{\rm min} \equiv \max\left[(m_i + m_j)^2,\, (m_k + m_l)^2\right]$, σ_R is the reduced cross-section summed over all the degrees of freedom of the initial and final states, and K_1 is the modified Bessel function. σ_R corresponds to the total cross-section $\sigma(s)$ without the flux factor, and can be written as:

$$\sigma_R(s) = 2\, \frac{\left[s - (m_i + m_j)^2\right] \left[s - (m_i - m_j)^2\right]}{s}\, \sigma(s)\,. \tag{3.12}$$

Several useful approximations can be implemented for different ranges of T, such that the interaction rate density $\gamma_{\mathrm{DM}\to\mathrm{SM}}$ for the DM annihilation into SM states becomes:

$$\gamma_{\mathrm{DM}\to\mathrm{SM}}(T) \simeq \begin{cases} \left(\frac{1}{\Lambda^4 m_r^4}\right) T^{12} & \text{for } T \ll \frac{m_r}{2}, \\ 10^{-6} \left(\frac{m_r^8}{\Lambda^4 \Gamma_r}\right) T\, K_1(\frac{m_r}{T}) & \text{for } T \simeq \frac{m_r}{2}, \\ 3 \times 10^{-4} \left(\frac{1}{\Lambda^4}\right) T^8 & \text{for } \frac{m_r}{2} \ll T \ll \frac{m_1}{2}, \\ 10^{-5} \left(\frac{m_1^8}{\Lambda^4 \Gamma_1}\right) T\, K_1\left(\frac{m_1}{T}\right) & \text{for } T \simeq \frac{m_1}{2}, \\ 7 \times 10^{-4} \left(\frac{m_1^2}{\Lambda^4 \Gamma_1}\right) T^7 & \text{for } T \gg \frac{m_1}{2}. \end{cases} \tag{3.13}$$

The right panel of Fig. 1 shows the DM interaction rate density for $m_r = 10^3$ GeV, $m_1 = 10^7$ GeV and $\Lambda = 10^9$ GeV with a black solid line, whose behavior as a function of the temperature can be easily understood using the approximations in eq. (3.13):

- At low temperatures ($T \ll m_r/2$) all the mediators are very heavy and decouple from the low-energy theory; the rate presents a strong temperature dependence, $\gamma \propto T^{12}$, represented by a red-dotted straight line in the plot.
- When $T \simeq m_r/2$, the resonant exchange of a radion dominates and $\gamma \propto T\, K_1(m_r/T)$. This corresponds to the first bump in the plot, again coinciding with a red-dotted (curved) line.
- In the intermediate regime, $m_r/2 \ll T \ll m_1/2$, the temperature is higher than the radion mass but still smaller than all KK states. The interaction is, thus, driven by the exchange of the light radion, with $\gamma \propto T^8$. This is shown by the second straight red-dotted line in the plot, with a slope smaller than the first one (as it is proportional to T^8, compared to T^{12} in the first region).
- We reach then the region in which the KK-gravitons dominance takes over: first, at the peak of the first KK-graviton mode ($T \simeq m_1/2$) for which $\gamma \propto T\, K_1(m_1/T)$, corresponding to the second bump in the plot.
- Eventually, when the increase of the temperature makes heavier KK-graviton states to have a sizable contributions to the rate, with a constructive interference giving a $\gamma \propto T^7$ behavior.

We can see that all the different regimes in T follow extremely well the curved and straight blue- and red-dotted lines, corresponding to the approximate behaviors depicted in eq. (3.13). As for the left panel, the red-shaded region corresponding to $T > \Lambda$ is beyond our EFT approach.

Notice that a big hierarchy between m_r and m_1 was chosen in order to avoid an overlap between the two bumps, such that the five regimes in eq. (3.13) can be clearly seen in the plot. For generic choices in the parameter space, overlap between regions may occur.

Using the approximated expressions of $\gamma_{\rm DM\to SM}$ from eq. (3.13), the Boltzmann equation (3.8) can be analytically solved, finding for the different regions in T:

$$Y_0 \simeq \begin{cases} \frac{3\times10^{-1}}{g_{\star s}}\sqrt{\frac{10}{g_\star}}\left(\frac{M_P}{m_r^4\,\Lambda^4}\right)T_{\rm rh}^7 & \text{for } T_{\rm rh}\ll m_r/2\,,\\ \frac{6.7\times10^{-7}}{g_{\star s}}\sqrt{\frac{10}{g_\star}}\left(\frac{M_P\,m_r^{9/2}}{\Lambda^4\Gamma_r}\right)\left(\frac{4m_r^2+10m_r\,T_{\rm rh}+15T_{\rm rh}^2}{T_{\rm rh}^{5/2}}\right)e^{-\frac{m_r}{T_{\rm rh}}} & \text{for } T_{\rm rh}\simeq m_r/2\,,\\ \frac{2\times10^{-4}}{g_{\star s}}\sqrt{\frac{10}{g_\star}}\left(\frac{M_P}{\Lambda^4}\right)T_{\rm rh}^3 & \text{for } m_r/2\ll T_{\rm rh}\ll m_1/2\,,\\ \frac{6.7\times10^{-6}}{g_{\star s}}\sqrt{\frac{10}{g_\star}}\left(\frac{M_P\,m_1^{9/2}}{\Lambda^4\Gamma_1}\right)\left(\frac{4m_1^2+10m_1\,T_{\rm rh}+15T_{\rm rh}^2}{T_{\rm rh}^{5/2}}\right)e^{-\frac{m_1}{T_{\rm rh}}} & \text{for } T_{\rm rh}\simeq m_1/2\,,\\ \frac{8\times10^{-4}}{g_{\star s}}\sqrt{\frac{10}{g_\star}}\left(\frac{M_P\,m_1^2}{\Lambda^4\,\Gamma_1}\right)T_{\rm rh}^2 & \text{for } T_{\rm rh}\gg m_1/2\,, \end{cases} \tag{3.14}$$

where Y_0 corresponds to the asymptotic value of $Y(T)$ for $T\ll T_{\rm rh}$. The final DM yield in eq. (3.14) has a strong dependence on $T_{\rm rh}$, characteristic of the UV freeze-in production mechanism.

Finally, let us emphasize that for the previous analysis to be valid, the DM has to be out of chemical equilibrium with the SM bath. One needs to guarantee, therefore, that the interaction rate density be $\gamma_{\rm DM\to SM}\ll n^{\rm eq}\,H$, which translates into:

$$T_{\rm rh}\ll\begin{cases} 0.7\left(\frac{g_\star}{10}\right)^{1/14}\left(\frac{\Lambda^4\,m_r^4}{M_P}\right)^{1/7} & \text{for } T_{\rm rh}\ll m_r/2\,,\\ -\frac{2}{7}m_1/W_{-1}\left[-7.8\left(\sqrt{\frac{g_\star}{10}}\frac{\Lambda^4\,\Gamma_r}{m_r^4\,M_P}\right)^{2/7}\right] & \text{for } T_{\rm rh}\simeq m_r/2\,,\\ 7.5\left(\frac{g_\star}{10}\right)^{1/6}\left(\frac{\Lambda^4}{M_P}\right)^{1/3} & \text{for } m_r/2\ll T_{\rm rh}\ll m_1/2\,,\\ -\frac{2}{7}m_1/W_{-1}\left[-4.3\left(\sqrt{\frac{g_\star}{10}}\frac{\Lambda^4\,\Gamma_1}{m_1^4\,M_P}\right)^{2/7}\right] & \text{for } T_{\rm rh}\simeq m_1/2\,,\\ 13.5\left(\frac{g_\star}{10}\right)^{1/4}\sqrt{\frac{\Gamma_1}{M_P}}\,\frac{\Lambda^2}{m_1} & \text{for } T_{\rm rh}\gg m_1/2\,, \end{cases} \tag{3.15}$$

where $W_{-1}[x]$ corresponds to the -1 branch of the Lambert W function computed at x.

Fig. 2 shows the reheating temperature $T_{\rm rh}$ required to reproduce the experimentally observed DM abundance, $\Omega_\chi h^2$, for a fixed value of the DM mass, $m_\chi = 1$ MeV. In the left panel, we show $T_{\rm rh}$ as a function of the first KK-graviton mass, m_1, for fixed $\Lambda = 10^{11}$ GeV; in the right panel, we show $T_{\rm rh}$ as a function of Λ for fixed $m_1 = 10^5$ GeV. The radion mass has been chosen as $m_r = m_1/10^3$ (therefore, it is a variable parameter in the left panel, whereas it is a fixed one in the right panel). In order to compute $T_{\rm rh}$, the DM yield has been held fixed so that $m_\chi\,Y_0 = \Omega_\chi h^2\,\frac{1}{s_0}\,\frac{\rho_c}{h^2}\simeq 4.3\times10^{-10}$ GeV, where $\rho_c\simeq 1.1\times10^{-5}\,h^2$ GeV/cm^3 is the critical energy density, $s_0\simeq 2.9\times10^3$ cm^{-3} is the entropy density at present and $\Omega_\chi h^2\simeq 0.12$ [61]. The gray-shaded areas are the regions where chemical equilibrium with the SM is reached and, therefore, where the freeze-in cannot occur and the analysis performed here is not valid. The black-dotted lines, representing $T_{\rm rh} = m_1/2$ and $T_{\rm rh} = m_r/2$, have been added for reference. Eventually, the red-shaded areas ($m_1 > \Lambda$) represent the regions for which the EFT approach breaks down.

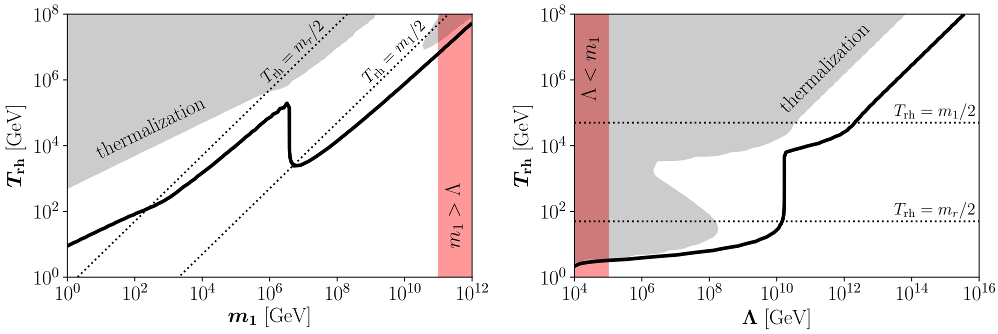

Figure 2. Direct freeze-in: Reheating temperature required to reproduce the experimentally observed DM abundance, $\Omega_\chi h^2$, for $m_\chi = 1$ MeV. Left panel: $T_{\rm rh}$ as a function of m_1 for $\Lambda = 10^{11}$ GeV; right panel: $T_{\rm rh}$ as a function of Λ for $m_1 = 10^5$ GeV. In both panels, the radion mass is $m_r = m_1/10^3$. The gray-shaded areas are the regions where chemical equilibrium with the SM is reached (and freeze-in does not occur), whereas the red-shaded areas are the regions where $m_1 > \Lambda$ and the EFT approach breaks down. Eventually, the two black-dotted lines give a visual understanding of the different regions in eq. (3.14).

For the sake of completeness, notice that the s-channel exchange of a (massless) graviton gives an irreducible contribution to the total DM relic abundance [1–4]. However, due to the large hierarchy $\Lambda \ll M_P$, the contribution of the massless graviton is typically subdominant and can be disregarded. The corresponding interaction rate density is given by:

$$\gamma_{\rm DM\to SM} \simeq 1.9 \times 10^{-4} \frac{T^8}{M_P^4}\,, \tag{3.16}$$

and, therefore, its contribution to the DM yield is:

$$Y_0 \simeq \frac{1.4 \times 10^{-4}}{g_{\star s}} \sqrt{\frac{10}{g_\star}} \left(\frac{T_{\rm rh}}{M_P}\right)^3 . \tag{3.17}$$

We stress that this expression is a function of $T_{\rm rh}$, only, being naturally independent from Λ and the masses of the KK-gravitons and the radion. This contribution, indeed, comes from 4-dimensional gravitons or, in the case considered here, from the long distance (low-energy) limit of 5-dimensional gravitons (corresponding to the KK-graviton zero-mode). For example, for a DM mass $m_\chi = 10$ TeV it would only be relevant for reheating temperatures $T_{\rm rh} \geq 10^{16}$ GeV, *i.e.* well above the range of $T_{\rm rh}$ depicted in Fig. 2.

3.2 Sequential Freeze-in

In this case the DM abundance comes from decays of KK-gravitons or radions, previously produced via the freeze-in mechanism. Such states are mainly generated by 2-to-2 annihilations or inverse decays (2-to-1) of SM particles. We will now review one by one the two possibilities.

3.2.1 Via Annihilations

KK-gravitons and radions with masses below the reheating temperature can be created *on-shell* in the early Universe via annihilations of two SM particles by the freeze-in mechanism. Once created, their decay products may contribute to the total DM relic abundance. In fact, if the production cross-section is small enough to keep KK-gravitons and radions out of chemical equilibrium with the SM bath, and the evolution of the DM yield is largely dominated by their decays, eqs. (3.4) to (3.6) can be simplified to:

$$\begin{aligned}\frac{dY}{dT} &\simeq \frac{\gamma_{\text{KK}\to\text{SM}}}{H\,\mathfrak{s}\,T}\left[\left(\frac{Y_K}{Y_K^{\text{eq}}}\right)^2-1\right]\text{BR}(\text{KK}\to\text{DM})+\frac{\gamma_{\text{r}\to\text{SM}}}{H\,\mathfrak{s}\,T}\left[\left(\frac{Y_r}{Y_r^{\text{eq}}}\right)^2-1\right]\text{BR}(\text{r}\to\text{DM})\\ &\simeq -\frac{1}{H\,\mathfrak{s}\,T}\left[\gamma_{\text{KK}\to\text{SM}}\,\text{BR}(\text{KK}\to\text{DM})+\gamma_{\text{r}\to\text{SM}}\,\text{BR}(\text{r}\to\text{DM})\right], \end{aligned} \tag{3.18}$$

where the rates are:

$$\gamma_{\text{KK}\to\text{SM}}(T) \simeq 4.8\times 10^4\frac{T^{16}}{\Lambda^4 m_n^8} \qquad (\text{for the } n^{\text{th}} \text{ KK-graviton}), \tag{3.19}$$

$$\gamma_{\text{r}\to\text{SM}}(T) \simeq 2.2\times 10^{-4}\frac{T^8}{\Lambda^4}\,. \tag{3.20}$$

Notice that the m_n^{-8} factor in $\gamma_{\text{KK}\,\to\,\text{SM}}$ (and, hence, the strong temperature dependence) comes from the polarization tensor of the KK-gravitons (as it was shown in Refs. [16, 24] for spin-2 massive particles). Such a suppression is not present in the case of radions (that have spin 0). The branching ratios into DM particles are:

$$\text{BR}(\text{KK}\to\text{DM}) \simeq \frac{z_n}{z_n+256}\,, \tag{3.21}$$

$$\text{BR}(\text{r}\to\text{DM}) \simeq \frac{z}{z+37}\,, \tag{3.22}$$

where

$$z_n \equiv \left(1-4\frac{m_\chi^2}{m_n^2}\right)^{5/2}, \tag{3.23}$$

$$z \equiv \sqrt{1-4\frac{m_\chi^2}{m_r^2}}\left(1+2\frac{m_\chi^2}{m_r^2}\right)^2. \tag{3.24}$$

The explicit expressions for annihilation rates and decay widths for KK-gravitons and the radion can be found in Appendix C.

Using a similar procedure to the one used in eq. (3.8) and (3.18), it is possible to find the following analytical solution:

$$Y_0 \simeq \frac{9.5\times 10^3}{g_{\star\mathfrak{s}}}\sqrt{\frac{10}{g_\star}}\frac{M_P}{\Lambda^4 m_1^8}\left(\frac{z_1}{z_1+256}\right)T_{\text{rh}}^{11}+\frac{1.6\times 10^{-4}}{g_{\star\mathfrak{s}}}\sqrt{\frac{10}{g_\star}}\frac{M_P}{\Lambda^4}\left(\frac{z}{z+37}\right)T_{\text{rh}}^{3}\,. \tag{3.25}$$

Notice that in eq. (3.25) only the lightest KK-graviton is taken into account. This is a consequence of the strong suppression with the KK-graviton mass m_n in eq. (3.19). Even if

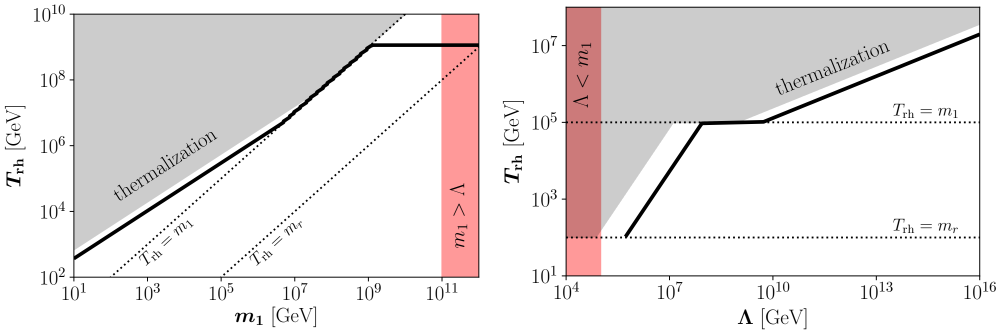

Figure 3. Sequential freeze-in via annihilations: Reheating temperature required to reproduce the experimentally observed DM abundance, $\Omega_\chi h^2$, for $m_\chi = 1$ MeV. Left panel: $T_{\rm rh}$ as a function of m_1 for $\Lambda = 10^{11}$ GeV; right panel: $T_{\rm rh}$ as a function of Λ for $m_1 = 10^5$ GeV. In both panels, the radion mass is $m_r = m_1/10^3$. The gray-shaded areas are the regions where chemical equilibrium with the SM is reached (and freeze-in does not occur), whereas the red-shaded areas are the regions where $m_1 > \Lambda$ and the EFT approach breaks down. Eventually, the two black-dotted lines give a visual understanding of the different regions in eq. (3.25).

all of the KK-gravitons do contribute to the total DM density, the only relevant contribution is given by the lightest state. For the previous analysis to be valid, the KK-gravitons and the radion must be out of chemical equilibrium with the SM bath, which corresponds to the conditions $\gamma_{\rm KK\to SM} \ll n_K^{\rm eq} H$ and $\gamma_{\rm r\to SM} \ll n_r^{\rm eq} H$. The reheating temperature in this limit satisfies the tightest of the following conditions (depending on the mass of the lightest KK-graviton, m_1):

$$T_{\rm rh} \ll \min \left(0.3 \left[\sqrt{\frac{g_\star}{10}} \frac{\Lambda^4 m_1^8}{M_P} \right]^{1/11} ; 8.3 \left[\sqrt{\frac{g_\star}{10}} \frac{\Lambda^4}{M_P} \right]^{1/3} \right). \tag{3.26}$$

Fig. 3 shows the reheating temperature $T_{\rm rh}$ required to reproduce the observed DM abundance for a fixed value of the DM mass, $m_\chi = 1$ MeV. As in Fig. 2, in the left panel we show $T_{\rm rh}$ as a function of the first KK-graviton mass, m_1, for fixed $\Lambda = 10^{11}$ GeV; in the right panel, we show $T_{\rm rh}$ as a function of Λ for fixed $m_1 = 10^5$ GeV. The relation between the radion mass m_r and the lightest KK-graviton mass, m_1 is, again, $m_r = m_1/10^3$. The black-dotted lines indicate $T_{\rm rh} = m_1$ and $T_{\rm rh} = m_r$. Eventually, the gray- and red-shaded areas are the regions where chemical equilibrium with the SM is reached, and where the EFT approach breaks down (as $m_1 > \Lambda$), respectively.

For $T_{\rm rh} < m_r$, on-shell KK gravitons and radions are not produced in the early Universe, and therefore this mechanism can not account for the DM relic abundance. If $m_r < T_{\rm rh} < m_1$, only radions are created. In this region $T_{\rm rh}$ is independent on m_1 (and therefore on m_r) due to the fact that the interaction rate in eq. (3.20) does not depend on m_r, as it can be seen in the left panel of Fig. 3. Now, if $T_{\rm rh} > m_1$ the KK-gravitons are also produced and their decay dominate the DM production. The reheating temperature needed to reproduce the observed value of $\Omega_\chi h^2$ in this region is very near to the border of the gray-shaded area for which the DM is in equilibrium with SM particles and freeze-in does not occurs (remember, though, the log-log scale of the plots).

3.2.2 Via Inverse Decays

Alternatively , frozen-in KK-gravitons and radions are also created *on-shell* via inverse decays of SM particles (a 2-to-1 process), and subsequently they can decay into DM particles. Within the same approximations as in the previous subsection, i.e., assuming that KK-gravitons and radions are produced out of chemical equilibrium from the SM bath via inverse-decays, and the evolution of the DM yield is largely dominated by their decays, eqs. (3.4) to (3.6) can be simplified to:

$$\begin{aligned}\frac{dY}{dT} &\simeq \frac{\gamma^d_{\mathrm{KK}\to\mathrm{SM}}}{H\,\mathfrak{s}\,T}\left[\frac{Y_K}{Y_K^{\mathrm{eq}}}-1\right]\mathrm{BR}(\mathrm{KK}\to\mathrm{DM}) + \frac{\gamma^d_{\mathrm{r}\to\mathrm{SM}}}{H\,\mathfrak{s}\,T}\left[\frac{Y_r}{Y_r^{\mathrm{eq}}}-1\right]\mathrm{BR}(\mathrm{r}\to\mathrm{DM}) \\ &\simeq -\frac{1}{H\,\mathfrak{s}\,T}\left[\gamma^d_{\mathrm{KK}\to\mathrm{SM}}\,\mathrm{BR}(\mathrm{KK}\to\mathrm{DM}) + \gamma^d_{\mathrm{r}\to\mathrm{SM}}\,\mathrm{BR}(\mathrm{r}\to\mathrm{DM})\right], \end{aligned} \tag{3.27}$$

where the interaction rate densities for decays are defined by:

$$\gamma^d(T) = \frac{m^2\,T}{2\pi^2}K_1\left(\frac{m}{T}\right)\Gamma\,, \tag{3.28}$$

with Γ the decay width obtained by summing (rather than averaging) over the degrees of freedom of the decaying particle. Using eqs. (C.19) and (C.21) we get, then:

$$\gamma^d_{\mathrm{KK}\to\mathrm{SM}} \simeq \frac{73}{480\pi^3}\frac{m_n^5\,T}{\Lambda^2}\,K_1\left(\frac{m_n}{T}\right), \tag{3.29}$$

$$\gamma^d_{\mathrm{r}\to\mathrm{SM}} \simeq \frac{37}{384\pi^3}\frac{m_r^5\,T}{\Lambda^2}\,K_1\left(\frac{m_r}{T}\right). \tag{3.30}$$

Eq. (3.27) admits the following approximate analytical solution:

$$Y_0 \simeq \sum_n \frac{5.6\times10^{-2}}{g_{\star\mathfrak{s}}}\sqrt{\frac{10}{g_\star}}\frac{M_P\,m_n}{\Lambda^2}\left(\frac{z_n}{z_n+256}\right) + \frac{3.5\times10^{-2}}{g_{\star\mathfrak{s}}}\sqrt{\frac{10}{g_\star}}\frac{M_P\,m_r}{\Lambda^2}\left(\frac{z}{z+37}\right). \tag{3.31}$$

In this case, most of the DM production happens at $T \simeq m_n/2.5$ and $T \simeq m_r/2.5$ for KK-gravitons and radions, respectively. However, the sum over KK-modes should be performed up to KK-graviton states with mass below the reheating temperature, $m_n < T_{\mathrm{rh}}$. For this reason, the total contribution due to the decay of KK-gravitons explicitly depends on T_{rh} (whereas the second term in eq. (3.31) does not depend on it):

$$Y_0 \simeq \frac{2.2\times10^{-4}}{g_{\star\mathfrak{s}}}\sqrt{\frac{10}{g_\star}}\frac{M_P\,T_{\mathrm{rh}}^2}{m_1\,\Lambda^2} + \frac{3.5\times10^{-2}}{g_{\star\mathfrak{s}}}\sqrt{\frac{10}{g_\star}}\frac{M_P\,m_r}{\Lambda^2}\left(\frac{z}{z+37}\right). \tag{3.32}$$

Again, for the KK-gravitons and the radions to be out of chemical equilibrium with the SM bath one needs to guarantee that $\gamma^d_{\mathrm{KK}\to\mathrm{SM}} \ll n_K^{\mathrm{eq}}\,H$ and $\gamma^d_{\mathrm{r}\to\mathrm{SM}} \ll n_r^{\mathrm{eq}}\,H$. The reheating temperature in this limit satisfies the tightest of the following conditions (depending on the mass of the lightest KK-graviton, m_1):

$$T_{\mathrm{rh}} \ll \min\left(0.34\left[\sqrt{\frac{10}{g_\star}}\,\frac{M_P\,m_1^4}{\Lambda^2}\right]^{1/3};\,0.29\left[\sqrt{\frac{10}{g_\star}}\,\frac{M_P\,m_r^4}{\Lambda^2}\right]^{1/3}\right). \tag{3.33}$$

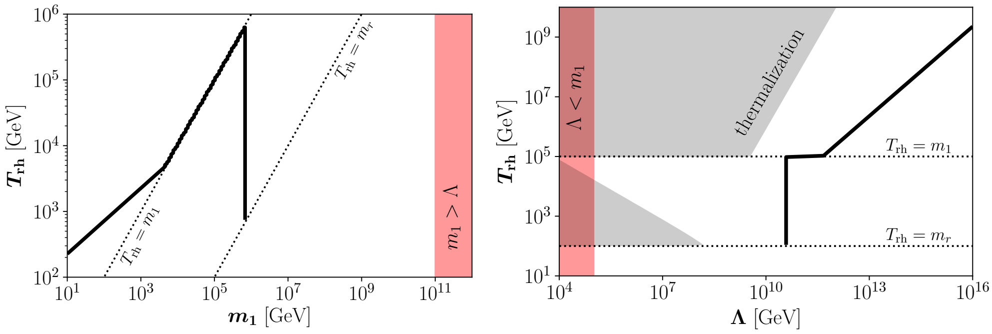

Figure 4. Sequential freeze-in via inverse decays: Reheating temperature required to reproduce the experimentally observed DM abundance, $\Omega_\chi h^2$, for $m_\chi = 1$ MeV. Left panel: $T_{\rm rh}$ as a function of m_1 for $\Lambda = 10^{11}$ GeV; right panel: $T_{\rm rh}$ as a function of Λ for $m_1 = 10^5$ GeV. In both panels, the radion mass is $m_r = m_1/10^3$. The gray-shaded areas are the regions where chemical equilibrium with the SM is reached (and freeze-in does not occur), whereas the red-shaded areas are the regions where $m_1 > \Lambda$ and the EFT approach breaks down. Eventually, the two black-dotted lines give a visual understanding of the different regions in eq. (3.14).

Fig. 4 shows the reheating temperature $T_{\rm rh}$ required to reproduce the observed DM abundance, $\Omega_\chi h^2$, for a fixed value of the DM mass, $m_\chi = 1$ MeV. Again, in the left panel we show $T_{\rm rh}$ as a function of the first KK-graviton mass, m_1, for fixed $\Lambda = 10^{11}$ GeV; in the right panel, we show $T_{\rm rh}$ as a function of Λ for fixed $m_1 = 10^5$ GeV. The radion mass has been chosen as $m_r = m_1/10^3$. The black-dotted lines indicate $T_{\rm rh} = m_1$ and $T_{\rm rh} = m_r$. The gray- and red-shaded areas are the regions where chemical equilibrium with the SM is reached,[4] and where the EFT approach breaks down (as $m_1 > \Lambda$), respectively.

As in the case of sequential freeze-in via annihilation, for $T_{\rm rh} < m_r$ on-shell KK-gravitons and radions are not produced in the early Universe and, therefore, this mechanism can not account for the DM relic abundance below the $T_{\rm rh} = m_r$ black-dotted line. In the region $m_r < T_{\rm rh} < m_1$, only radions are created and, in this case, the DM yield is independent on $T_{\rm rh}$ (as the second term in eq. (3.32) does not depend on $T_{\rm rh}$). This can be clearly seen in Fig. 4. For $T_{\rm rh} > m_1$, the KK-graviton states are also produced. Their decay eventually dominate the DM production and the reheating temperature is proportional to $\sqrt{m_1}$ (left panel) or Λ (right panel).

So far, each individual production channel has been studied separately. Fig. 5 depicts the parameter space favored by the observed DM abundance for $m_\chi = 1$ MeV and $\Lambda = 10^{14}$ GeV as a function of m_1 (upper left panel), or $m_1 = 10^3$ GeV as a function of Λ (upper right panel), taking into account *all* of the three DM production mechanisms described previously (*i.e.* direct production, sequential production via annihilation and sequential production via inverse decay). The thin blue lines correspond to the partial contributions of each of the mechanisms, whereas the black thick line to the total abundance. Eventually,

[4]Notice that in the left panel the gray-shaded area is absent as the region for which the DM is in equilibrium with SM particles is outside of the considered range.

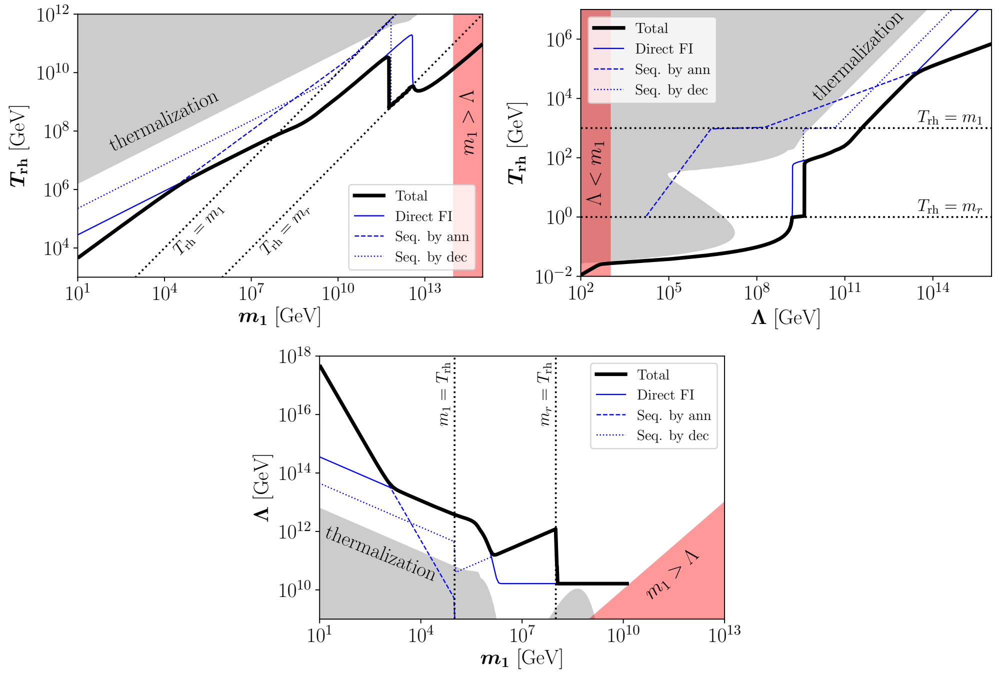

Figure 5. Reheating temperature required to reproduce the experimentally observed DM abundance, $\Omega_\chi h^2$, for $m_\chi = 1$ MeV, taking into account all possible DM production mechanisms (thick black lines). Upper left panel: $T_{\rm rh}$ as a function of m_1 for $\Lambda = 10^{14}$ GeV; Upper right panel: $T_{\rm rh}$ as a function of Λ for $m_1 = 10^3$ GeV; Lower panel: correlation between Λ and m_1 for $T_{\rm rh} = 10^5$ GeV. In all panels, $m_r = m_1/10^3$, whereas as always the gray- and red-shaded areas are the regions where chemical equilibrium with the SM is reached and where the EFT approach breaks down, respectively. The two black-dotted lines represent the conditions $T_{\rm rh} = m_1$ and $T_{\rm rh} = m_r$. The light blue solid, dashed and dotted lines represent the contributions from direct freeze-in, sequential freeze-in via annihilation and sequential freeze-in via inverse decay, respectively (as explained in the legend).

in the lower panel we show the correlation between Λ and m_1 at a fixed value of the reheating temperature required to achieve the observed DM abundance, $T_{\rm rh} = 10^5$ GeV. In all panels, the radion mass is related to the first KK-graviton mass as $m_r = m_1/10^3$. As always, the gray- and red-shaded areas represent the regions where chemical equilibrium between DM and the SM particles is reached and where the EFT breaks down since $m_1 > \Lambda$, respectively.

Finally, in Fig. 6 we show the correlation between Λ and m_1 required to reproduce the observed DM abundance for $m_\chi = 1$ MeV and $m_r = m_1/10^3$ for several representative values of the reheating temperature, $T_{\rm rh} = 1$, 10, 10^5, 10^8 and 10^{10} GeV (notice that the range of Λ plotted in Fig. 6 differs from that in the lower panel of Fig. 5). Let us note that the lines corresponding to $T_{\rm rh} = 1$ and 10 GeV overlap when $m_1 \simeq 10^3$ GeV and $\Lambda \simeq 10^9$ GeV. This can be understood seeing that in that region, the DM relic abundance is mainly generated by sequential freeze-in via inverse decays of the radion and is therefore independent of

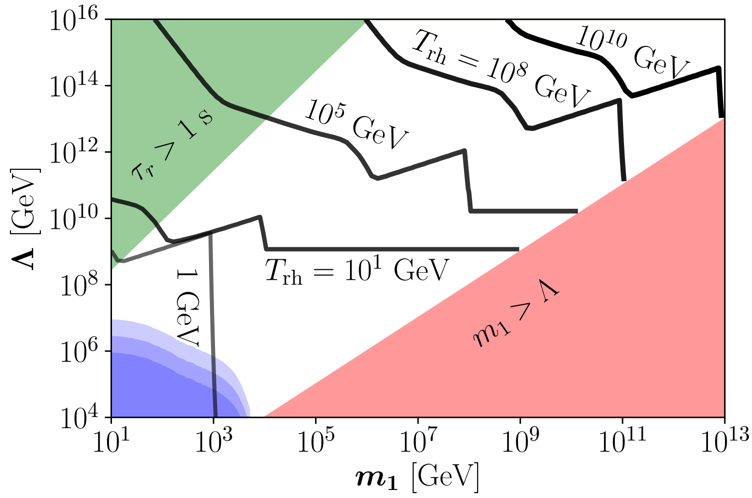

Figure 6. Parameter space required to reproduce the observed DM abundance for $m_\chi = 1$ MeV and $m_r = m_1/10^3$, for several values of $T_{\rm rh}$. The blue areas are excluded by resonant searches at LHC and represent the current bound and our prospects for the LHC Run-3 and the High-Luminosity LHC in the $\gamma\gamma$ channel [62, 63], see text. The green corner corresponds to radion lifetimes longer than 1 s. In the red area ($m_1 > \Lambda$) the EFT approach breaks down.

$T_{\rm rh}$, see eq. (3.31). The red-shaded area, as always, represents the region where the EFT approach breaks down. On the other hand, the upper left green corner corresponds to radion lifetimes higher than 1 s, potentially problematic for BBN (all the KK-graviton states are heavier than the radion and therefore will naturally have shorter lifetimes). Eventually, the blue-shaded regions depict present and future experimental bound coming from resonance searches at the LHC. The proton-proton collision can generate resonant KK-gravitons that later decay into SM particles. ATLAS and CMS put bounds over these processes in $\gamma\gamma$ and lepton-lepton channels as a function of the mass of the resonance (the lightest KK-graviton). These bounds can be translated into limits over Λ as a function of the mass of the first graviton m_1. The present bounds (dark blue) come from the resonant searches at LHC with 36 fb^{-1} [62] and [63], whereas future bounds are estimated assuming 300 fb^{-1} (medium blue) and 3000 fb^{-1} (light blue) for the LHC Run-III and High-Luminosity LHC, respectively. Notice that in this plot we do not show the gray-shaded region for which DM is in equilibrium with SM particles (where freeze-in does not occur), as we should draw a different region for each value of $T_{\rm rh}$.

3.3 Beyond the Sudden Decay Approximation of the Inflaton

While reheating is commonly approximated as an instantaneous event, the decay of the inflaton into SM radiation is a continuous process [64]. Away from this approximation for reheating, the bath temperature may rise to a value $T_{\rm max}$ which exceeds $T_{\rm rh}$ [65]. It is plausible that the DM relic density may be established during this reheating period, in which case its abundance will significantly differ from freeze-in calculations assuming radiation domination. In particular, it has been observed that if the DM is produced during the transition from matter to radiation domination via an interaction rate that scales like $\gamma(T) \propto T^n$, for $n > 12$ the DM abundance is enhanced by a boost factor proportional to $(T_{\max}/T_{\rm rh})^{n-12}$ [66], whereas for $n \leq 12$ the difference between the standard UV freeze-in calculation differ only by an $\mathcal{O}(1)$ factor from calculations taking into account non-instantaneous reheating. More recently, it has been highlighted that the critical mass dimension of the operator at which the instantaneous decay approximation breaks down depend on the equation of state ω, or equivalently, to the shape of the inflationary potential at the reheating epoch [67–69]. Therefore, the exponent of the boost factor becomes $(T_{\max}/T_{\rm rh})^{n-n_c}$ with $n_c \equiv 6 + 2\left(\frac{3-\omega}{1+\omega}\right)$, showing a strong dependence on the equation of state [67]. Subsequent papers have explored the impact of this boost factor in specific models [4, 70–80]. Finally, another way for enhancing the DM abundance occurs in cosmologies where inflation is followed by an epoch dominated by a fluid stiffer than radiation. In such scenarios, even a small radiation abundance, produced for instance by instantaneous preheating effects, will eventually dominate the total energy density of the Universe without the need for a complete inflaton decay. In particular, a strong enhancement if DM production happens via interaction rates with temperature dependence higher that $n_c = 6$ [81].

The present model of KK FIMP DM in warped extra-dimensions features processes where the interaction rate has a particularly strong temperature dependence, the most relevant ones being: *i*) the DM annihilation into SM states for reheating temperatures much lower than the radion mass $\gamma_{\rm DM \to SM}(T) \propto T^{12}$; *ii*) the same process near the resonances $T_{\rm rh} \simeq m_r/2$ and $T_{\rm rh} \simeq m_1/2$, where $\gamma_{\rm DM \to SM}(T) \propto T\, K_1(m_i/T)$ (with m_i being the radion or the lightest KK-graviton mass, respectively); and *iii*) the KK-graviton annihilation into SM particles $\gamma_{\rm KK \to SM}(T) \propto T^{16}$. In these regimes, the non-instantaneous decay of the inflaton is expected to generate a strong boost factor to the DM yield, which translates into a reduction of the reheating temperature required to match the observed DM relic abundance. As the precise determination of such boost factors depends on the details of the inflationary model (in particular on the energy density carried by the inflaton and its equation of state parameter previous to its decay), it is beyond the scope of this study.

4 Conclusions

Dark Matter (DM) is typically assumed to be made of weakly interacting massive particles (WIMPs), produced in the early Universe via the freeze-out mechanism. Freeze-out occurs if the interactions between DM and SM particles are strong enough to bring them into chemical equilibrium. However, if these interaction rates were never strong enough, the observed DM relic abundance could still have been produced by non-thermal processes, like the freeze-in mechanism. In that case, DM is called a feebly interacting massive particle (FIMP).

In a warped extra-dimensional scenario, DM could naturally be a FIMP, if the effective gravitational scale Λ is much higher than the electroweak scale. In this case, DM is produced in two main ways: *i*) promptly by annihilations of SM states via the *s*-channel exchange of KK-gravitons and radions, i.e. the so called *direct freeze-in*, and *ii*) by decays of KK-gravitons or radions, previously produced by annihilations or inverse decays of SM particles via direct freeze-in. This scenario has been doubted *sequential freeze-in*.

In this paper we have systematically studied the different regions of the parameter space that generate the observed DM abundance in the early Universe, within a warped extra-dimensional model . We assume that both the SM and the DM particles are localized in the IR-brane, where the effective four-dimensional Planck scale is given by Λ, which is allowed to vary in a wide phenomenological range, $[10^2,\ 10^{16}]$ GeV, relaxing the requirement for the RS model to solve the hierarchy problem. We also include the radion, using the Goldberger-Wise mechanism [38] to generate the required potential to stabilize the size of the extra dimension. For definiteness, we consider scalar DM and focus on its interactions with gravitational mediators, i.e., the radion, the graviton and the KK-gravitons.

As the interaction rates between the visible and the dark sectors have a strong temperature dependence, the bulk of the DM density is typically produced at the highest temperatures reached by the SM thermal bath, which in the approximation of a sudden decay of the inflaton corresponds to the reheating temperature, $T_{\rm rh}$. This is a characteristic of the so-called UV freeze-in. We found however a case where the DM abundance was mainly produced at much lower temperatures, corresponding to the sequential freeze-in where the radion was generated via inverse decays. In that case the peak of the production happens when the temperature approaches the radion mass, $T \simeq m_r/2.5$.

The possibility of generating the DM relic density within the RS scenario via the usual freeze-out mechanism was analyzed in Refs. [16–22, 25]. After including the DM annihilation channel into KK-gravitons previously disregarded, it was found that even when both SM and DM particles live in the IR-brane there is a region compatible with the experimental and theoretical constraints where it is possible to reach the correct DM relic abundance [24]. The allowed region corresponds to $m_\chi \in [1,\ 15]$ TeV and $\Lambda \in [10,\ 10^4]$ TeV. The upper limit on the DM mass comes from unitarity, while the lower limit is an indirect one, derived from searches at LHC of KK-graviton resonant production, which constrains the scale Λ as a function of the first KK-graviton mass. This bound is very relevant, since it determines the minimum value of the DM mass for which the annihilation channel into the first KK-graviton mode is kinematically open, leading to the observed DM relic density. In the freeze-out scenario, the LHC prospects for the near future exclude most part of the allowed region.

In the present work we find that it is also possible to obtain the correct DM relic abundance in the same RS model via the freeze-in mechanism, for DM masses in a much wider range spanning typically from the keV to the PeV scale, and larger values of the scale Λ than in the freeze-out scenario. This implies that the LHC bounds on the parameter space of the model are weaker than in the freeze-out case. This can be seen in Fig. 6, where we summarize our results in the $(m_1,\ \Lambda)$ plane for the benchmark DM mass $m_\chi = 1$ MeV, finding that only the lower-left corner will be probed by HL-LHC. On the other hand, other constraints are relevant, such as the life-time of the radion, which we require to be larger than 1 s to avoid problems with BBN, and excludes the upper-left corner. The results are not strongly dependent of the radion mass: for this reason we fix $m_r = m_1/10^3$, in agreement with the expectation within the Goldberger-Wise mechanism. We find that the observed DM relic density can be obtained in a wide range of reheating temperatures, $T_{\rm rh} \in [1, 10^{10}]$ GeV. Notice that we find some region of the parameter space for which the observed DM relic abundance is achieved with Λ as low as a few TeV (with lower values excluded by LHC data). In this region, the hierarchy problem is mostly solved, leaving only a remnant little hierarchy to be explained.

Finally, we argued that a more detailed analysis of the present model will require to go beyond the usual approximation where the inflaton decays instantaneously, and therefore the reheat temperature is the maximal temperature reached by the SM thermal bath. This is due to the strong temperature dependence of some interaction rate densities that enter in the determination of the DM relic abundance. A complete analysis must take into account the details of the inflationary model (in particular on the energy density carried by the inflaton and its equation of state parameter previous to its decay), and is therefore beyond the scope of this study.

Acknowledgments

We thank Florian Nortier for valuable discussions. NB thanks the theoretical physics department of University of Valencia and the IFIC for their warm hospitality. This project has received funding from the European Union's Horizon 2020 research and innovation programme under the Marie Skłodowska-Curie grant agreements 674896 and 690575. This work is also supported by the Spanish MINECO Grants SEV-2014-0398 and FPA2017-84543-P, and by Generalitat Valenciana through the "plan GenT" program (CIDEGENT/2018/019) and the grant PROMETEO/2019/083. NB is partially supported by Universidad Antonio Nariño grants 2018204, 2019101 and 2019248. This research made use of IPython [82], Matplotlib [83] and SciPy [84].

A Kaluza-Klein decomposition in the Randall-Sundrum scenario

Any 5-dimensional field $\phi_{\mu\nu}$ can be written as a KK tower of 4-dimensional fields as follows:

$$\phi_{\mu\nu}(x,y) = \sum \phi^n_{\mu\nu}(x) \frac{\chi^n(y)}{\sqrt{r_c}}\,, \tag{A.1}$$

being $\chi^n(y)$ the wave-functions of the KK-modes along the extra-dimension.

The equation of motion for the $n^{\rm th}$ KK-mode is given by:

$$\left(\eta^{\mu\nu}\partial_\mu\partial_\nu + m_n^2\right)\, \phi^n_{\mu\nu}(x) = 0\,, \tag{A.2}$$

where m_n is its mass. Using the Einstein equations we obtain [85]:

$$-\frac{1}{r_c^2}\frac{d}{dy}\left(e^{-4\sigma}\frac{d\chi^n}{dy}\right) = m_n^2\, e^{-2\sigma}\chi^n\,, \tag{A.3}$$

from which:

$$\chi^n(y) = \frac{e^{2\sigma(y)}}{N_n}\left[J_2(z_n) + \alpha_n Y_2(z_n)\right]\,, \tag{A.4}$$

being J_2 and Y_2 Bessel functions of order 2 and $z_n(y) = m_n/ke^{\sigma(y)}$. The N_n factor is the $n^{\rm th}$ KK-mode wave-function normalization. In the limit $m_n/k \ll 1$ and $e^{k\pi r_c} \gg 1$, the coefficient α_n becomes $\alpha_n \simeq x_n^2 \exp(-2k\,\pi\,r_c)$, where x_n are the are the roots of the Bessel function, $J_1(x_n) = 0$, and the masses of the KK-modes are given by:

$$m_n = k\,x_n\,e^{-k\,\pi\,r_c}\,. \tag{A.5}$$

Notice that, for low n, the KK-modes masses are not equally spaced, as they are proportional to the roots of the Bessel function J_1. At large values of n, on the other hand, the roots of the Bessel function become approximately $x_n = \pi\left(n + \frac{1}{4}\right) + \mathcal{O}\left(n^{-1}\right)$. In this limit, the KK-modes masses are approximately equally spaced (as in LED and the CW/LD scenarios) and proportional to a characteristic length scale R such that:

$$m_n \simeq \left(k\,\pi\,e^{-k\,\pi\,r_c}\right) n = \frac{n}{R}\,, \qquad (n \gg 1) \tag{A.6}$$

where $R = x_1/m_1 = 1/(k\pi)e^{k\,\pi\,r_c}$ (with $x_1 = 3.81$) is $\mathcal{O}$ (TeV^{-1}).

The normalization factors can be computed imposing that:

$$\int dy\,e^{-2\sigma}\,[\chi^n]^2 = 1\,. \tag{A.7}$$

In the same approximation as above, i.e. for $m_n/k \ll 1$ and $e^{k\,\pi\,r_c} \gg 1$, we get:

$$N_0 = -\frac{1}{\sqrt{kr_c}} \qquad \text{and} \qquad N_n = \frac{1}{\sqrt{2k\,r_c}}\,e^{k\,\pi\,r_c}\,J_2(x_n)\,. \tag{A.8}$$

Notice the difference between the $n = 0$ mode and the $n > 0$ modes: for $n = 0$, the wave-function at the IR-brane location $y = \pi$ takes the form

$$\chi^0(y = \pi) = \sqrt{k\,r_c}\left(1 - e^{-2k\,\pi\,r_c}\right) = -\sqrt{r_c}\,\frac{M_5^{3/2}}{M_P}\,, \tag{A.9}$$

whereas for $n > 0$:

$$\chi^n(y = \pi) = \sqrt{k\,r_c}\,e^{k\,\pi\,r_c} = \sqrt{r_c}\,e^{k\,\pi\,r_c}\,\frac{M_5^{3/2}}{M_P} = \sqrt{r_c}\,\frac{M_5^{3/2}}{\Lambda}. \tag{A.10}$$

B Radion Lagrangian

As it was already reported in the main text, the radion lagrangian is [50, 52]:

$$\mathcal{L}_r = \frac{1}{2}(\partial_\mu r)(\partial^\mu r) - \frac{1}{2}m_r^2 r^2 + \frac{1}{\sqrt{6}\Lambda} rT + \frac{\alpha_{\rm EM}\,C_{\rm EM}}{8\pi\sqrt{6}\Lambda} rF_{\mu\nu}F^{\mu\nu} + \frac{\alpha_S C_3}{8\pi\sqrt{6}\Lambda} r\sum_a F^a_{\mu\nu}F^{a\mu\nu}\,, \tag{B.1}$$

where $F_{\mu\nu}$, $F^a_{\mu\nu}$ are the Maxwell and $SU(3)_c$ Yang-Mills tensors, respectively. On the other hand, C_3 and $C_{\rm EM}$ encode all information about the massless gauge boson contributions and are given by:

$$C_3 = b_{\rm IR}^{(3)} - b_{\rm UV}^{(3)} + \frac{1}{2}\sum_q F_{1/2}(x_q)\,, \tag{B.2}$$

$$C_{\rm EM} = b_{\rm IR}^{(\rm EM)} - b_{\rm UV}^{(\rm EM)} + F_1(x_W) - \sum_q N_c Q_q^2 F_{1/2}(x_q)\,, \tag{B.3}$$

with $x_q = 4m_q/m_r$ and $x_W = 4m_w/m_r$. The explicit form of $F_{1/2}$ and the values of the one-loop β-function coefficients b are given by [51]:

$$F_{1/2}(x) = 2x[1 + (1-x)f(x)], \tag{B.4}$$
$$F_1(x) = 2 + 3x + 3x(2-x)f(x), \tag{B.5}$$

$$f(x) = \begin{cases} [\arcsin(1/\sqrt{x})]^2 & \text{for } x > 1, \\ -\frac{1}{4}\left[\log\left(\frac{1+\sqrt{x-1}}{1-\sqrt{x-1}}\right) - i\pi\right]^2 & \text{for } x < 1, \end{cases} \tag{B.6}$$

while $b_{\rm IR}^{(\rm EM)} - b_{\rm UV}^{(\rm EM)} = 11/3$ and $b_{\rm IR}^{(3)} - b_{\rm UV}^{(3)} = -11 + 2n/3$, where n is the number of quarks whose mass is smaller than $m_r/2$.

C Relevant Interaction Rates

In this appendix we report the different cross sections and decay widths used in this analysis, for the case of *real scalar* DM. All relevant Feynman rules can be found in Ref. [24].

C.1 Dark Matter Annihilation

In order to analyze the phenomenology of the FIMP DM in the RS model it is necessary to obtain the interaction rates of DM annihilating into SM particles via the s-channel exchange of KK-gravitons or a radion.

C.1.1 Through KK-gravitons

Here we show the different annihilation cross sections of DM χ into SM particles, mediated by the exchange of KK-gravitons. In the following expressions we use the notation S, ψ, V and v for SM scalars, fermions, massive vectors and massless vectors, respectively:

$$\sigma(\chi\chi \to SS) = |S_{\rm KK}|^2 \frac{s^3}{5760\,\pi\Lambda^4}\left(1 - 4\frac{m_\chi^2}{s}\right)^{\frac{3}{2}}\left(1 - 4\frac{m_S^2}{s}\right)^{\frac{5}{2}}, \tag{C.1}$$

$$\sigma(\chi\chi \to \bar{\psi}\psi) = |S_{\rm KK}|^2 \frac{s^3}{2880\,\pi\Lambda^4}\left(1 - 4\frac{m_\psi^2}{s}\right)^{\frac{3}{2}}\left(1 - 4\frac{m_\chi^2}{s}\right)^{\frac{3}{2}}\left(3 + 8\frac{m_\psi^2}{s}\right), \tag{C.2}$$

$$\sigma(\chi\chi \to VV) = |S_{\rm KK}|^2 \frac{s^3}{5760\,\pi\Lambda^4}\left(1 - 4\frac{m_\chi^2}{s}\right)^{\frac{3}{2}}\left(1 - 4\frac{m_V^2}{s}\right)^{\frac{1}{2}}\left(13 + \frac{56 m_V^2}{s} + \frac{48 m_V^4}{s^2}\right), \tag{C.3}$$

$$\sigma(\chi\chi \to vv) = |S_{\rm KK}|^2 \frac{s^3}{480\,\pi\Lambda^4}\left(1 - 4\frac{m_\chi^2}{s}\right)^{\frac{3}{2}}, \tag{C.4}$$

where $S_{\rm KK}$ corresponds to the sum over all KK-graviton propagators:

$$S_{\rm KK} \equiv \sum_{n=1}^{\infty} \frac{1}{s - m_n^2 + i\,m_n\,\Gamma_n}\,. \tag{C.5}$$

C.1.2 Through a Radion

The KK-gravitons are not the only 5-dimensional fields in the bulk. In fact, in order to stabilize the size of the extra-dimension it is necessary to introduce a new scalar field that mixes with the graviscalar. The zero-mode of the KK-tower of this new field receives the name of radion and can mediate the DM annihilations into SM states. The corresponding cross sections are given by:

$$\sigma(\chi\chi \to SS) = \mathcal{P}\frac{s^3}{1152\,\pi\Lambda^4}\sqrt{\frac{s-4m_S^2}{s-4m_\chi^2}}\left(1+2\frac{m_\chi^2}{s}\right)^2\left(1+2\frac{m_S^2}{s}\right)^2, \tag{C.6}$$

$$\sigma(\chi\chi \to \bar{\psi}\psi) = \mathcal{P}\frac{s^2 m_\psi^2}{288\,\pi\Lambda^4}\left(1-4\frac{m_\psi^2}{s}\right)^{\frac{3}{2}}\left(1+2\frac{m_\chi^2}{s}\right)^2\left(1-4\frac{m_\chi^2}{s}\right)^{-\frac{1}{2}}, \tag{C.7}$$

$$\sigma(\chi\chi \to VV) = \mathcal{P}\frac{s^3}{1152\,\pi\Lambda^4}\sqrt{\frac{s-4m_V^2}{s-4m_\chi^2}}\left(1-4\frac{m_V^2}{s}+12\frac{m_V^4}{s^2}\right), \tag{C.8}$$

$$\sigma(\chi\chi \to vv) = \mathcal{P}\frac{s^3\,\alpha_i^2\,C_i^2}{9216\,\pi^3\Lambda^4}\left(1+2\frac{m_\chi^2}{s}\right)^2\left(1-4\frac{m_\chi^2}{s}\right)^{-\frac{1}{2}}, \tag{C.9}$$

where $\mathcal{P} \equiv \left[(s-m_r^2)^2 + m_r^2\,\Gamma_r^2\right]^{-1}$ is the radion propagator. For the SM massless vectors the vertex is generated by the trace anomaly and, therefore, the cross sections are proportional to $\alpha_{\rm EM}$ and $C_{\rm EM}$ for the photon case, and to α_3 and C_3 for the gluon case, as given in eqs. (B.2) and (B.3).

C.2 KK-graviton Annihilation

For the sequential freeze-in we are interested in processes that involve KK-graviton G_n annihilations into SM particles. The corresponding cross-sections can be approximated by:

$$\sigma(G_n G_n \to SS) \simeq \frac{1}{96000\,\pi}\frac{s^5}{\Lambda^4 m_n^8}, \tag{C.10}$$

$$\sigma(G_n G_n \to \bar{\psi}\psi) \simeq \frac{1}{604800\,\pi}\frac{s^5}{\Lambda^4 m_n^8}, \tag{C.11}$$

$$\sigma(G_n G_n \to VV) \simeq \sigma(G_n G_n \to vv) \simeq \frac{19}{28800\,\pi}\frac{s^5}{\Lambda^4 m_n^8}. \tag{C.12}$$

Therefore, the total annihilation cross section for the $n^{\rm th}$ KK-graviton into SM states becomes:

$$\sigma_{\rm KK\to SM}(s) \simeq \frac{8\times 10^{-3}}{\pi}\frac{s^5}{\Lambda^4 m_n^8}. \tag{C.13}$$

C.3 Radion Annihilation

A second contribution to sequential freeze in comes from the annihilation of a pair of radions into SM particles, and is given by:

$$\sigma(rr \to SS) \simeq \frac{1}{540\,\pi}\frac{s}{\Lambda^4}\,, \tag{C.14}$$

$$\sigma(rr \to \bar{\psi}\psi) \simeq \frac{25}{64\,\pi}\frac{m_\psi^2}{\Lambda^4}\,, \tag{C.15}$$

$$\sigma(rr \to VV) \simeq \frac{1}{1152\,\pi}\frac{s}{\Lambda^4}\,, \tag{C.16}$$

$$\sigma(rr \to vv) = 0\,. \tag{C.17}$$

The total annihilation cross section of radions into SM states becomes:

$$\sigma_{\mathrm{r}\to\mathrm{SM}}(s) \simeq \frac{9\times 10^{-3}}{\pi}\frac{s}{\Lambda^4}\,, \tag{C.18}$$

where the contribution of SM fermions is highly suppressed by their masses and was therefore neglected. Notice that eqs. (C.13) and (C.18) do not scale in the same way with the center-of-mass energy s, due to their different dependence on the masses. In particular, the m^{-8} factor in eq. (C.13) comes from the polarization tensor of the KK-gravitons (spin-2 massive particles) and is not present in the case of radions (spin-0).

C.4 KK-graviton Decays

KK-gravitons can decay into both SM and DM particles. The corresponding decay widths are:

$$\Gamma_{\mathrm{KK}\to\mathrm{SM}} \simeq \frac{73}{240\,\pi}\frac{m_n^3}{\Lambda^2}\,, \tag{C.19}$$

$$\Gamma_{\mathrm{KK}\to\mathrm{DM}} = \frac{m_n^3}{960\,\pi\Lambda^2}\left(1-4\frac{m_\chi^2}{m_n^2}\right)^{5/2}\,, \tag{C.20}$$

where all SM masses were neglected for simplicity.

C.5 Radion Decays

Eventually, the decay widths of radions into SM and DM particles are:

$$\Gamma_{\mathrm{r}\to\mathrm{SM}} \simeq \frac{37 m_r^3}{192\,\pi\Lambda^2}\,, \tag{C.21}$$

$$\Gamma_{\mathrm{r}\to\mathrm{DM}} = \frac{m_r^3}{192\,\pi\Lambda^2}\left(1-4\frac{m_\chi^2}{m_r^2}\right)^{\frac{1}{2}}\left(1+2\frac{m_\chi^2}{m_r^2}\right)^2\,, \tag{C.22}$$

where again all SM masses were neglected for simplicity.

References

[1] M. Garny, M. Sandora and M. S. Sloth, *Planckian Interacting Massive Particles as Dark Matter*, *Phys. Rev. Lett.* **116** (2016) 101302, [1511.03278].

[2] Y. Tang and Y.-L. Wu, *On Thermal Gravitational Contribution to Particle Production and Dark Matter*, *Phys. Lett. B* **774** (2017) 676–681, [1708.05138].

[3] M. Garny, A. Palessandro, M. Sandora and M. S. Sloth, *Theory and Phenomenology of Planckian Interacting Massive Particles as Dark Matter*, *JCAP* **02** (2018) 027, [1709.09688].

[4] N. Bernal, M. Dutra, Y. Mambrini, K. Olive, M. Peloso and M. Pierre, *Spin-2 Portal Dark Matter*, *Phys. Rev.* **D97** (2018) 115020, [1803.01866].

[5] I. Antoniadis, *A Possible new dimension at a few TeV*, *Phys. Lett.* **B246** (1990) 377–384.

[6] I. Antoniadis, S. Dimopoulos and G. Dvali, *Millimeter range forces in superstring theories with weak scale compactification*, *Nucl.Phys.* **B516** (1998) 70–82, [hep-ph/9710204].

[7] N. Arkani-Hamed, S. Dimopoulos and G. Dvali, *The Hierarchy problem and new dimensions at a millimeter*, *Phys.Lett.* **B429** (1998) 263–272, [hep-ph/9803315].

[8] I. Antoniadis, N. Arkani-Hamed, S. Dimopoulos and G. Dvali, *New dimensions at a millimeter to a Fermi and superstrings at a TeV*, *Phys.Lett.* **B436** (1998) 257–263, [hep-ph/9804398].

[9] N. Arkani-Hamed, S. Dimopoulos and G. Dvali, *Phenomenology, astrophysics and cosmology of theories with submillimeter dimensions and TeV scale quantum gravity*, *Phys.Rev.* **D59** (1999) 086004, [hep-ph/9807344].

[10] L. Randall and R. Sundrum, *A Large mass hierarchy from a small extra dimension*, *Phys. Rev. Lett.* **83** (1999) 3370–3373, [hep-ph/9905221].

[11] L. Randall and R. Sundrum, *An Alternative to compactification*, *Phys. Rev. Lett.* **83** (1999) 4690–4693, [hep-th/9906064].

[12] I. Antoniadis, A. Arvanitaki, S. Dimopoulos and A. Giveon, *Phenomenology of TeV Little String Theory from Holography*, *Phys. Rev. Lett.* **108** (2012) 081602, [1102.4043].

[13] P. Cox and T. Gherghetta, *Radion Dynamics and Phenomenology in the Linear Dilaton Model*, *JHEP* **05** (2012) 149, [1203.5870].

[14] G. F. Giudice and M. McCullough, *A Clockwork Theory*, *JHEP* **02** (2017) 036, [1610.07962].

[15] G. F. Giudice, Y. Kats, M. McCullough, R. Torre and A. Urbano, *Clockwork/linear dilaton: structure and phenomenology*, *JHEP* **06** (2018) 009, [1711.08437].

[16] H. M. Lee, M. Park and V. Sanz, *Gravity-mediated (or Composite) Dark Matter*, *Eur. Phys. J.* **C74** (2014) 2715, [1306.4107].

[17] H. M. Lee, M. Park and V. Sanz, *Gravity-mediated (or Composite) Dark Matter Confronts Astrophysical Data*, *JHEP* **05** (2014) 063, [1401.5301].

[18] C. Han, H. M. Lee, M. Park and V. Sanz, *The diphoton resonance as a gravity mediator of dark matter*, *Phys. Lett.* **B755** (2016) 371–379, [1512.06376].

[19] T. D. Rueter, T. G. Rizzo and J. L. Hewett, *Gravity-Mediated Dark Matter Annihilation in the Randall-Sundrum Model*, *JHEP* **10** (2017) 094, [1706.07540].

[20] T. G. Rizzo, *Kinetic mixing, dark photons and an extra dimension. Part I*, *JHEP* **07** (2018) 118, [1801.08525].

[21] A. Carrillo-Monteverde, Y.-J. Kang, H. M. Lee, M. Park and V. Sanz, *Dark Matter Direct Detection from new interactions in models with spin-two mediators*, *JHEP* **06** (2018) 037, [1803.02144].

[22] T. G. Rizzo, *Kinetic mixing, dark photons and extra dimensions. Part II: fermionic dark matter*, *JHEP* **10** (2018) 069, [1805.08150].

[23] P. Brax, S. Fichet and P. Tanedo, *The Warped Dark Sector*, *Phys. Lett. B* **798** (2019) 135012, [1906.02199].

[24] M. G. Folgado, A. Donini and N. Rius, *Gravity-mediated Scalar Dark Matter in Warped Extra-Dimensions*, *JHEP* **01** (2020) 161, [1907.04340].

[25] M. Kumar, A. Goyal and R. Islam, *Dark matter in the Randall-Sundrum model*, in *64^{th} Annual Conference of the South African Institute of Physics (SAIP2019) Polokwane, South Africa, July 8-12, 2019*, 2019, 1908.10334.

[26] Y.-J. Kang and H. M. Lee, *Lightening Gravity-Mediated Dark Matter*, *Eur. Phys. J. C* **80** (2020) 602, [2001.04868].

[27] R. S. Chivukula, D. Foren, K. A. Mohan, D. Sengupta and E. H. Simmons, *Massive Spin-2 Scattering Amplitudes in Extra-Dimensional Theories*, *Phys. Rev. D* **101** (2020) 075013, [2002.12458].

[28] Y.-J. Kang and H. M. Lee, *Dark matter self-interactions from spin-2 mediators*, 2002.12779.

[29] Y.-J. Kang and H. M. Lee, *Effective theory for self-interacting dark matter and massive spin-2 mediators*, 2003.09290.

[30] M. G. Folgado, A. Donini and N. Rius, *Gravity-mediated Dark Matter in Clockwork/Linear Dilaton Extra-Dimensions*, *JHEP* **04** (2020) 036, [1912.02689].

[31] J. McDonald, *Thermally generated gauge singlet scalars as selfinteracting dark matter*, *Phys.Rev.Lett.* **88** (2002) 091304, [hep-ph/0106249].

[32] K.-Y. Choi and L. Roszkowski, *E-WIMPs*, *AIP Conf. Proc.* **805** (2006) 30–36, [hep-ph/0511003].

[33] A. Kusenko, *Sterile neutrinos, dark matter, and the pulsar velocities in models with a Higgs singlet*, *Phys. Rev. Lett.* **97** (2006) 241301, [hep-ph/0609081].

[34] K. Petraki and A. Kusenko, *Dark-matter sterile neutrinos in models with a gauge singlet in the Higgs sector*, *Phys. Rev.* **D77** (2008) 065014, [0711.4646].

[35] L. J. Hall, K. Jedamzik, J. March-Russell and S. M. West, *Freeze-In Production of FIMP Dark Matter*, *JHEP* **1003** (2010) 080, [0911.1120].

[36] N. Bernal, M. Heikinheimo, T. Tenkanen, K. Tuominen and V. Vaskonen, *The Dawn of FIMP Dark Matter: A Review of Models and Constraints*, *Int. J. Mod. Phys.* **A32** (2017) 1730023, [1706.07442].

[37] F. Elahi, C. Kolda and J. Unwin, *UltraViolet Freeze-in*, *JHEP* **03** (2015) 048, [1410.6157].

[38] W. D. Goldberger and M. B. Wise, *Modulus stabilization with bulk fields*, *Phys. Rev. Lett.* **83** (1999) 4922–4925, [hep-ph/9907447].

[39] S. Sarkar, *Big bang nucleosynthesis and physics beyond the standard model*, *Rept. Prog. Phys.* **59** (1996) 1493–1610, [hep-ph/9602260].

[40] M. Kawasaki, K. Kohri and N. Sugiyama, *MeV scale reheating temperature and thermalization of neutrino background*, *Phys. Rev.* **D62** (2000) 023506, [astro-ph/0002127].

[41] S. Hannestad, *What is the lowest possible reheating temperature?*, *Phys. Rev.* **D70** (2004) 043506, [astro-ph/0403291].

[42] F. De Bernardis, L. Pagano and A. Melchiorri, *New constraints on the reheating temperature of the universe after WMAP-5*, *Astropart. Phys.* **30** (2008) 192–195.

[43] P. F. de Salas, M. Lattanzi, G. Mangano, G. Miele, S. Pastor and O. Pisanti, *Bounds on very low reheating scenarios after Planck*, *Phys. Rev.* **D92** (2015) 123534, [1511.00672].

[44] T. Hasegawa, N. Hiroshima, K. Kohri, R. S. Hansen, T. Tram and S. Hannestad, *MeV-scale reheating temperature and thermalization of oscillating neutrinos by radiative and hadronic decays of massive particles*, *JCAP* **12** (2019) 012, [1908.10189].

[45] T. Appelquist and A. Chodos, *Quantum Effects in Kaluza-Klein Theories*, *Phys. Rev. Lett.* **50** (1983) 141.

[46] T. Appelquist and A. Chodos, *The Quantum Dynamics of Kaluza-Klein Theories*, *Phys. Rev.* **D28** (1983) 772.

[47] B. de Wit, M. Luscher and H. Nicolai, *The Supermembrane Is Unstable*, *Nucl. Phys.* **B320** (1989) 135–159.

[48] E. Pontón and E. Poppitz, *Casimir energy and radius stabilization in five-dimensional orbifolds and six-dimensional orbifolds*, *JHEP* **06** (2001) 019, [hep-ph/0105021].

[49] W. D. Goldberger and M. B. Wise, *Bulk fields in the Randall-Sundrum compactification scenario*, *Phys. Rev.* **D60** (1999) 107505, [hep-ph/9907218].

[50] W. D. Goldberger and M. B. Wise, *Phenomenology of a stabilized modulus*, *Phys. Lett.* **B475** (2000) 275–279, [hep-ph/9911457].

[51] K. Blum, M. Cliche, C. Csáki and S. J. Lee, *WIMP Dark Matter through the Dilaton Portal*, *JHEP* **03** (2015) 099, [1410.1873].

[52] C. Csáki, M. Graesser, L. Randall and J. Terning, *Cosmology of brane models with radion stabilization*, *Phys. Rev.* **D62** (2000) 045015, [hep-ph/9911406].

[53] O. Aharony, S. S. Gubser, J. M. Maldacena, H. Ooguri and Y. Oz, *Large N field theories, string theory and gravity*, *Phys. Rept.* **323** (2000) 183–386, [hep-th/9905111].

[54] M. Drees, F. Hajkarim and E. R. Schmitz, *The Effects of QCD Equation of State on the Relic Density of WIMP Dark Matter*, *JCAP* **1506** (2015) 025, [1503.03513].

[55] T. Hambye, M. H. G. Tytgat, J. Vandecasteele and L. Vanderheyden, *Dark matter from dark photons: a taxonomy of dark matter production*, *Phys. Rev.* **D100** (2019) 095018, [1908.09864].

[56] N. Bernal and X. Chu, $\mathbb{Z}_2$ *SIMP Dark Matter*, *JCAP* **1601** (2016) 006, [1510.08527].

[57] N. Bernal, X. Chu and J. Pradler, *Simply split strongly interacting massive particles*, *Phys. Rev.* **D95** (2017) 115023, [1702.04906].

[58] N. Bernal, *Boosting Freeze-in through Thermalization*, 2005.08988.

[59] C. E. Yaguna, *The Singlet Scalar as FIMP Dark Matter*, *JHEP* **08** (2011) 060, [1105.1654].

[60] N. Bernal, C. Cosme, T. Tenkanen and V. Vaskonen, *Scalar singlet dark matter in non-standard cosmologies*, *Eur. Phys. J.* **C79** (2019) 30, [1806.11122].

[61] Planck collaboration, N. Aghanim et al., *Planck 2018 results. VI. Cosmological parameters*, 1807.06209.

[62] ATLAS collaboration, M. Aaboud et al., *Search for new high-mass phenomena in the dilepton final state using 36 fb^{-1} of proton-proton collision data at $\sqrt{s} = 13$ TeV with the ATLAS detector*, *JHEP* **10** (2017) 182, [1707.02424].

[63] ATLAS collaboration, M. Aaboud et al., *Search for new phenomena in high-mass diphoton final states using 37 fb^{-1} of proton–proton collisions collected at $\sqrt{s} = 13$ TeV with the ATLAS detector*, *Phys. Lett.* **B775** (2017) 105–125, [1707.04147].

[64] R. J. Scherrer and M. S. Turner, *Decaying Particles Do Not Heat Up the Universe*, *Phys. Rev.* **D31** (1985) 681.

[65] G. F. Giudice, E. W. Kolb and A. Riotto, *Largest temperature of the radiation era and its cosmological implications*, *Phys. Rev.* **D64** (2001) 023508, [hep-ph/0005123].

[66] M. A. G. Garcia, Y. Mambrini, K. A. Olive and M. Peloso, *Enhancement of the Dark Matter Abundance Before Reheating: Applications to Gravitino Dark Matter*, *Phys. Rev.* **D96** (2017) 103510, [1709.01549].

[67] N. Bernal, F. Elahi, C. Maldonado and J. Unwin, *Ultraviolet Freeze-in and Non-Standard Cosmologies*, *JCAP* **1911** (2019) 026, [1909.07992].

[68] M. A. Garcia, K. Kaneta, Y. Mambrini and K. A. Olive, *Reheating and Post-inflationary Production of Dark Matter*, *Phys. Rev. D* **101** (2020) 123507, [2004.08404].

[69] N. Bernal, J. Rubio and H. Veermäe, *UV Freeze-in in Starobinsky Inflation*, 2006.02442.

[70] S.-L. Chen and Z. Kang, *On UltraViolet Freeze-in Dark Matter during Reheating*, *JCAP* **1805** (2018) 036, [1711.02556].

[71] G. Bhattacharyya, M. Dutra, Y. Mambrini and M. Pierre, *Freezing-in dark matter through a heavy invisible Z'*, *Phys. Rev.* **D98** (2018) 035038, [1806.00016].

[72] D. Chowdhury, E. Dudas, M. Dutra and Y. Mambrini, *Moduli Portal Dark Matter*, *Phys. Rev.* **D99** (2019) 095028, [1811.01947].

[73] K. Kaneta, Y. Mambrini and K. A. Olive, *Radiative production of nonthermal dark matter*, *Phys. Rev.* **D99** (2019) 063508, [1901.04449].

[74] A. Banerjee, G. Bhattacharyya, D. Chowdhury and Y. Mambrini, *Dark matter seeping through dynamic gauge kinetic mixing*, *JCAP* **1912** (2019) 009, [1905.11407].

[75] P. Chanda, S. Hamdan and J. Unwin, *Reviving Z and Higgs Mediated Dark Matter Models in Matter Dominated Freeze-out*, *JCAP* **2001** (2020) 034, [1911.02616].

[76] V. Baules, N. Okada and S. Okada, *Braneworld Cosmological Effect on Freeze-in Dark Matter Density and Lifetime Frontier*, 1911.05344.

[77] M. Dutra, *Freeze-in production of dark matter through spin-1 and spin-2 portals*, in *PoS(LeptonPhoton2019)076*, 2019, 1911.11844.

[78] M. Dutra, *The moduli portal to dark matter particles*, in *11th International Symposium on Quantum Theory and Symmetries (QTS2019) Montreal, Canada, July 1-5, 2019*, 2019, 1911.11862.

[79] D. Mahanta and D. Borah, *TeV Scale Leptogenesis with Dark Matter in Non-standard Cosmology*, *JCAP* **04** (2020) 032, [1912.09726].

[80] C. Cosme, M. Dutra, T. Ma, Y. Wu and L. Yang, *Neutrino Portal to FIMP Dark Matter with an Early Matter Era*, 2003.01723.

[81] N. Bernal, J. Rubio and H. Veermäe, *Boosting Ultraviolet Freeze-in in NO Models*, *JCAP* **06** (2020) 047, [2004.13706].

[82] F. Pérez and B. E. Granger, *IPython: A System for Interactive Scientific Computing*, *Comput. Sci. Eng.* **9** (2007) 21–29.

[83] J. D. Hunter, *Matplotlib: A 2D Graphics Environment*, *Comput. Sci. Eng.* **9** (2007) 90–95.

[84] E. Jones, T. Oliphant, P. Peterson et al., *SciPy: Open source scientific tools for Python*, 2001–.

[85] H. Davoudiasl, J. L. Hewett and T. G. Rizzo, *Phenomenology of the Randall-Sundrum Gauge Hierarchy Model*, *Phys. Rev. Lett.* **84** (2000) 2080, [hep-ph/9909255].

Parte III

Resumen de la Tesis

Capítulo 8

Resumen de la Tesis

8.1. Motivación Histórica

Desde tiempos inmemoriales, uno de los más profundos deseos del ser humano ha sido descubrir la composición última de la materia que nos rodea. Ya los primeros escritos griegos hablan sobre la modelización de la naturaleza en base a cuatro elementos fundamentales; a saber, agua, tierra, fuego y viento. El paso de los siglos afinó mucho más esta prematura descripción. En el siglo XVII, se sintetizó por primera vez un elemento químico[1], y tan solo dos siglos después (1869), ya existía una tabla periódica de los elementos, un claro reflejo de nuestro anhelo por encontrar orden en el caos.

El elevado número de elementos descubiertos en el siglo XX motivó la búsqueda de una estructura mucho más fundamental, aún totalmente desconocida. Fue Niels Bohr quien dió forma a esta idea, al sentar las bases de la teoría atómica actual [12–14], apoyándose en los modelos atómicos propuestos previamente por Joseph John Thomson y Ernest Rutherford. Su elegante modelo explicaba toda forma de materia utilizando únicamente tres tipos de partículas: neutrones y protones, que componían el núcleo de los diferentes elementos atómicos, y electrones, los cuales orbitaban alrededor de dichos núcleos con energías cuantizadas. Los átomos quedaban descritos

[1] En 1669 el alquimista Hennig Brand sintetizó por accidente fósforo, bautizándolo con este nombre por el brillo que desprendía.

pues como pequeños sistemas planetarios, solo que las fuerzas implicadas en su estabilidad eran totalmente diferentes a la gravitatoria.

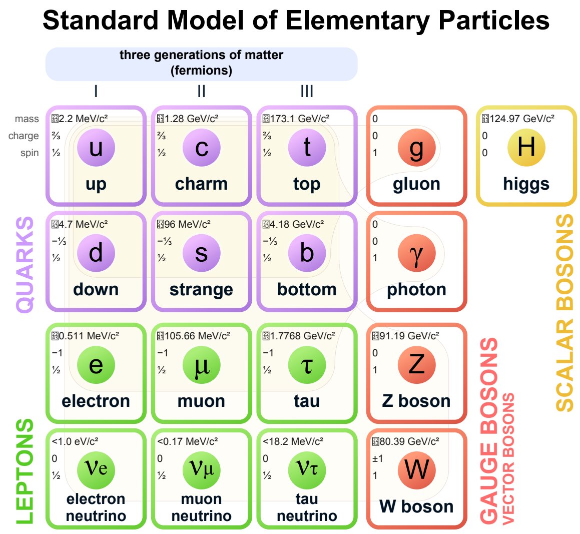

Figura 8.1: *Modelo Estándar de las interacciones fundamentales: las partículas moradas, verdes y rojas representan, respectivamente, los quarks, leptones y bosones de gauge. Por otro lado, la amarilla representa el Bosón de Higgs. Imagen tomada de Ref. [11].*

A lo largo del siglo XX el desarrollo de la mecánica cuántica cambió totalmente la forma de entender el mundo microscópico. A la fuerza gravitatoria y electromagnetica se le sumaron dos nuevas interacciones: débil y fuerte. Por otro lado, los protones y neutrones, que en el modelo de Bohr eran constituyentes fundamentales de la materia, pasaron a ser partículas compuestas por quarks, mientras una nueva plétora de partículas eran descubiertas gracias a los rayos cósmicos y a la construcción de nuevos experimentos y detectores. El resultado último de toda la revolución cuántica fue el Modelo Estándar de la física de partículas [15–25], esquematizado en la Fig. 8.1. El modelo describe la naturaleza a nivel microscópico utilizando un total de doce partículas elementales, o campos, y cuatro tipos de interacción. Los éxitos del Modelo Estándar fueron totalmente rotundos, con él se han realizado las predicciones más precisas de la historia de la ciencia. No obstante, tiene ciertas limitaciones, como el hecho de que es incapaz de describir la gravedad cuántica. En el Capitulo 1 se ha realizado una exposición detallada del modelo, profundizando en sus predicciones y fallos.

Hoy, casi medio siglo después de que fuese propuesto, sabemos que el Modelo Estandar únicamente es capaz de explicar el 5 % del contenido del

Universo, el 95 % restante continua envuelto en un halo de misterio. Observaciones astrofísicas y cosmológicas indican que el 26 % del Universo está compuesto por un nuevo tipo de materia cosmológicamente estable que no emite luz, y que no puede identificarse con ninguna de las partículas del Modelo Estándar. Esta curiosa característica inspiró su nombre, *Materia Oscura*. El resto del Universo es aún más enigmático si cabe. Actualmente se cree que está compuesto por algún tipo de energía que explicaría la expansión acelerada del Universo, pero esto es otra historia muy diferente a la de la Materia Oscura y queda lejos de los objetivos del trabajo aquí realizado.

La motivación de esta Tesis es intentar arrojar algo de luz sobre ese gran porcentaje de materia que nuestra ciencia actual no ha sido capaz de explicar, haciéndola un poco menos oscura de lo que su nombre indica.

8.2. El Modelo Estándar de las Interacciones Fundamentales: La Piedra Angular de la Física de Altas Energías

En esta sección vamos a realizar un breve resumen de los conceptos más importantes del Modelo Estándar (en el Capitulo 1 se han explicado todos los detalles técnicos del mismo). El Modelo Estándar de la física de partículas[2] es una teoría cuántica de campos con simetría gauge de los grupos unitarios $SU(3)_C \times SU(2)_L \times U(1)_Y$. El modelo describe con gran precisión tres de las cuatro interacciones fundamentales que existen en la naturaleza: débil, electromagnética y fuerte. La complejidad de la estructura de la interacción gravitatoria hace que sea muy complicado describirla como una teoría de campos gauge, actualmente se trabaja activamente en el tema[3]. El resto de las interacciones fundamentales quedan descritas con gran preci-

[2] Típicamente abreviado como SM, del inglés Standard Model.

[3] Algunos autores defienden que quizá el origen de la interacción gravitatoria sea totalmente diferente al resto de fuerzas fundamentales. La gravedad emergente (propuesta por Andrei Sakharov en 1967, el artículo original en inglés puede encontrarse en Ref. [473]), por ejemplo, sugiere que dicha interacción no es más que el residuo de una serie de grados de libertad aún desconocidos, tal como la mecánica de fluidos, que deriva de la mecánica estadística.

sión por el modelo mediante el intercambio de diferentes campos de spin 1, que constituyen el sector gauge de la teoría. Mientras que el grupo $SU(3)_C$ se asocia a la interacción fuerte, los grupos $SU(2)_L \times U(1)_Y$ describen la interacción electrodébil[4]

Las partículas de spin 1, o bosones, describen las interacciones del modelo, en tanto que los constituyentes fundamentales de la materia son los fermiones, partículas de spin 1/2: quarks y leptones. Curiosamente, la naturaleza replica los fermiones en 3 familias casi idénticas, únicamente diferenciadas por las masas de sus constituyentes:

$$1^{\text{st}}\,\text{Family} : L_1 \equiv \begin{pmatrix} \nu_e \\ e^- \end{pmatrix}_L ; e_1 \equiv e^-_R ; Q_1 \equiv \begin{pmatrix} u \\ d \end{pmatrix}_L ; U_1 \equiv u_R ; D_1 \equiv d_R ,$$
$$2^{\text{nd}}\,\text{Family} : L_2 \equiv \begin{pmatrix} \nu_\mu \\ \mu^- \end{pmatrix}_L ; e_2 \equiv \mu^-_R ; Q_2 \equiv \begin{pmatrix} c \\ s \end{pmatrix}_L ; U_2 \equiv c_R ; D_2 \equiv s_R ,$$
$$3^{\text{rd}}\,\text{Family} : L_3 \equiv \begin{pmatrix} \nu_\tau \\ \tau^- \end{pmatrix}_L ; e_3 \equiv \tau^-_R ; Q_3 \equiv \begin{pmatrix} t \\ b \end{pmatrix}_L ; U_3 \equiv t_R ; D_3 \equiv b_R .$$

Por otro lado, el modelo trata de forma diferente a partículas con quiralidad dextrógira y levógira, agrupando las primeras en singletes y las segundas en dobletes de $SU(2)_L$. De este modo, los quarks y leptones levógiros vienen representados por Q_i (compuesto por los quarks tipo *up* y tipo *down*, con cargas eléctricas $+2/3$ y $-1/3$ de la carga fundamental del electrón, respectivamente) y L_i (compuesto por los leptones cargados y los neutrinos, con cargas eléctricas -1 y 0, respectivamente). Por otro lado, los quarks dextrógiros están representados por los singletes U_i y D_i, mientras que los leptones cargados dextrógiros vienen dados por e_i. Los neutrinos dextrógiros no están incluidos en el modelo original, aunque hay muchas líneas de investigación abiertas en la actualidad sobre la posibilidad de su existencia.

Aparte de todo lo comentado, el modelo incluye un campo de spin 0, el campo de Higgs. Los bosones gauge de la teoría débil, es decir Z y $W^\pm$, tie-

[4]Las interacciones electromagnéticas y débiles fueron unificadas en los años 70 por Sheldon Lee Glashow, Abdus Salam y Steven Weinberg.

nen masa. Este hecho parecía incompatible con la construcción de un modelo basado en simetrías ya que la invariancia gauge prohíbe términos de masa para los bosones gauge. Por ello, fue necesario desarrollar un mecanismo que dotase de masa a estas partículas. La solución a este problema llegó de la mano de Robert Brout, Francois Englert, Gerald Guralnik, Carl Richard Hagen, Peter Higgs y Tom Kibble (en estricto orden alfabético), constituyendo lo que popularmente se conoce como *mecanismo de Higgs* [18–21].

La idea del mecanismo de Higgs se basa en la *ruptura espontánea de la simetría*[5] (SSB) y consiste en agregar a la teoría un campo complejo escalar doblete de $SU(2)_L$:

$$\Phi = \begin{pmatrix} \Phi^+ \\ \Phi^0 \end{pmatrix} = \begin{pmatrix} \Phi^+ \\ \frac{1}{\sqrt{2}}(v + \phi_1 + i\phi_2) \end{pmatrix}. \tag{8.1}$$

Este peculiar campo presenta lo que se conoce como *valor esperado de vacío*[6] (VEV) no nulo en su componente neutra, produciendo de este modo una ruptura de la simetría electrodébil (que no es una simetría exacta del vacío) y dando como resultado la simetría electromagnética[7],

$$SU(2)_L \times U(1)_Y \longrightarrow U(1)_{QED}. \tag{8.2}$$

Durante la SSB, tanto la parte cargada del doblete como la parte imaginaria de la componente neutra son absorbidos como grados de libertad longitudinales por los bosones gauge de la teoría, los cuales pasan a comportarse como bosones masivos. Por otro lado, la parte real del campo cargado, ϕ_1, se queda presente en el espectro de partículas del Modelo Estándar como una partícula de spin 0, el popular *bosón de Higgs*, que fue detectado en 2012 por los experimentos ATLAS [44] y CMS del LHC [45], confirmando el modelo.

Las representaciones de los fermiones del Modelo Estándar bajo el grupo $SU(2)_L \times U(1)_Y$ no presentan simetría quiral, necesaria para que los corres-

[5]Del inglés *Spontaneous Symmetry Breaking.*
[6]Del inglés de *Vacuum Expectation Value.*
[7]La abreviación QED viene de *Quantum Electrodynamics* [48–54], nombre que recibe la teoría gauge que describe la interacción electromagnética.

pondientes términos de masa puedan aparecer en el lagrangiano del modelo. No obstante, el mecanismo de Higgs soluciona este problema ya que bajo el grupo $U(1)_{\mathrm{QED}}$ si que presentan dicha simetría. En consecuencia, después de la SSB, el VEV del campo de Higgs permite la formación de los términos de masa para estas partículas.

Para una exposición detallada y completa del Modelo Estándar en español ver Ref. [474].

8.3. La Necesidad de la Materia Oscura

Como ya hemos comentado, el Modelo Estandar de partículas solo puede explicar un porcentaje pequeño de la materia que nos rodea, conocida como *bariónica*[8]. El resto de materia que puebla el Universo recibe el nombre de Materia Oscura. A pesar de que este exótico tipo de materia es un activo campo de estudio en la actualidad, los primeros indicadores de su existencia son ya casi centenarios [139]. No obstante, las primeras pruebas sólidas se las debemos a los trabajos de Vera Cooper Rubin, Kent Ford y Ken Freeman, llevados a cabo allá por los años 60 [144, 145].

8.3.1. Evidencias de la Existencia de Materia Oscura

La evidencia más clara que tenemos a día de hoy de la existencia de la Materia Oscura son las curvas de rotación de las galaxias. El contenido en masa de una galaxia puede medirse en base a su luminosidad, mediante técnicas astrofísicas. De este modo, tenemos una clara idea de cuanta materia bariónica hay en una determinada galaxia y como está distribuida dentro de ella. Conocida la masa de la galaxia, la velocidad de rotación de un objeto situado a una distancia R del centro de la misma puede determinarse a partir de las leyes de Kepler[9]. De acuerdo con esto, la distribución de materia bariónica observada nos indica que la velocidad de rotación debería disminuir conforme nos acercamos al borde galáctico. Sin embargo, medidas

[8] Nombre que recibe la materia descrita por el Modelo Estándar.

[9] $v = \sqrt{MG/R}$, donde M es la masa contenida en la esfera de radio R y G la constante de gravitación universal.

directas sobre la velocidad de rotación indican lo contrario: en la mayoría de los casos esta velocidad de rotación permanece constante.

Las curvas de rotación de las galaxias son la evidencia más famosa de la existencia de este exótico tipo de materia, pero no la única. La teoría de la Relatividad General predice que el campo gravitatorio producido por un gran cúmulo de materia es capaz de desviar los rayos de luz, el conocido como efecto *lente gravitatoria*. De este modo, puede utilizarse la luz procedente de galaxias lejanas para, mediante ciertos estudios sobre la trayectoria de los haces de luz, determinar la cantidad de materia que hay en los cúmulos de galaxias situados en su trayectoria. Este análisis confirma la presencia de Materia Oscura en la mayoría de cúmulos de galaxias estudiados.

Aparte de las evidencias astrofísicas, hay también evidencias cosmológicas que confirman la existencia de la Materia Oscura. En la Sec. 3.1 se ha realizado una breve descripción de todas ellas.

8.3.2. Características Fundamentales

A pesar de las evidencias de su existencia, a día de hoy aún no se ha realizado ninguna observación directa de la Materia Oscura. No obstante, podemos inferir mucho acerca de su naturaleza:

- La Materia Oscura debe ser no bariónica: algunos candidatos bariónicos han sido propuestos a lo largo de los años, como es el caso de los MACHOs[10] [221]. No obstante, los límites sobre esta clase de modelos son tan fuertes en la actualidad que están prácticamente descartados en su totalidad.
- Debe ser *fría* o *cálida*: según la distancia recorrida, como consecuencia de movimientos aleatorios, por las partículas de Materia Oscura en el Universo primigenio, podemos catalogarla en tres grandes grupos: *calinte*, *cálida* y *fría*. Si la distancia recorrida es mayor, igual o menor que el tamaño de una protogalaxia (unos 100 años luz), la Materia Oscura será caliente, cálida o fría, respectivamente. En la actualidad se han realizado numerosas simulaciones numéricas de la evolución del

[10] Del inglés *Massive Compact Halo Objects*.

Universo con diferentes tipos de materia. Si la Materia Oscura fuese caliente, de acuerdo con estas simulaciones, el Universo tendría un aspecto muy diferente al que conocemos hoy en día [187].

- Debe colisionar muy débilmente consigo misma: el motivo de esto es que recientes observaciones astrofísicas, tales como las realizadas sobre el conocido como *cúmulo bala*[11], imponen restricciones a la autointeracción de la Materia Oscura [177–181]:

$$\sigma/m \lesssim 10^{-24}\,\mathrm{cm}^2/\mathrm{GeV}. \tag{8.3}$$

- Débilmente interactiva con la materia bariónica: aparte de la interacción gravitatoria, la única interacción posible que podría llegar a tener la Materia Oscura es la débil. Respecto a lo que al electromagnetismo se refiere, las diversas implicaciones que supone la existencia de Materia Oscura cargada han sido profundamente estudiadas en la literatura [162], descartando prácticamente esta opción por motivos experimentales[12] [163]. Por otro lado, de existir la Materia Oscura fuertemente interactiva[13], ésta dejaría huella incluso en el flujo de calor terrestre [161]. Las fuertes implicaciones de este tipo de candidatos hacen que esten excluidos casi en su totalidad.

- Debe ser estable: la Materia Oscura que observamos hoy en día en el Universo es prácticamente un fósil térmico: es el remanente de la que la que componía el Universo primigenio. La única forma de que ese remanente haya sobrevivido hasta nuestros días es que la Materia Oscura sea estable o, en su defecto, que su vida media sea mayor que la edad del Universo.

En la Sec. 3.2 se ha realizado un estudio mucho más profundo de todas estas propiedades.

[11] Este curioso cúmulo es el resultado de dos cúmulos actualmente en colisión. En él se observa un efecto muy exótico, el centro de masas del cúmulo resultante se encuentra desplazado. Esta característica solo puede ser explicada mediante la existencia de grandes cantidades de Materia Oscura en su composición. La alternativa requeriría una modificación de las leyes más fundamentales de la dinámica relativista.

[12] En la actualidad las técnicas de detección de partículas cargadas son tan avanzadas que de existir la Materia Oscura eléctricamente cargada, esta ya debería haber sido observada.

[13] Fuertemente en el sentido de interacción a través de la interacción fuerte.

8.3.3. Candidatos Estudiados

Hasta el momento hemos hablado de las diferentes evidencias y características de la Materia Oscura. Pero ¿cuál es su naturaleza? En el escenario científico actual se han propuesto muchos candidatos a Materia Oscura, desde todo tipo de partículas con interacciones parecidas a las que ya conocemos, hasta candidatos altamente exóticos como agujeros negros primigenios [268–270]. Todo esto ha sido detallado en la Sec. 3.5. En este resumen únicamente hablaremos sobre los dos candidatos estudiados en esta Tesis: las partículas WIMP [225] y las FIMP [252].

8.3.3.1. Materia Oscura tipo WIMP

Las partículas WIMP[14] son partículas con masas típicamente desde el GeV hasta varios TeV. Este candidato se basa en la suposición de que las partículas de Materia Oscura se encontraban en equilibrio térmico con el resto de partículas del Modelo Estándar en el Universo primigenio. La abundancia que observamos en la actualidad sería pues el resultado de un proceso denominado *freeze-out*.

Para entender bien el concepto de *freeze-out*, debemos remontarnos a los primeros instantes del Universo, justo después del Big Bang. En aquella época, los átomos no existían, las diferentes partículas que poblaban el Universo se encontraban en un equilibrio continuo de aniquilación/producción, formando un plasma de altísima temperatura. Poco a poco, el Universo fue expandiéndose, enfriando dicho plasma. El enfriamiento del Universo provocó que algunos de los procesos que mantenían este equilibrio dejasen de tener lugar, desacoplando de este modo las diferentes especies de partículas de este *caldo* primigenio.

Cuando la temperatura del Universo fue demasiado baja como para que la creación de partículas de Materia Oscura fuese posible, está se desacopló del *caldo* primigenio. Como consecuencia, la abundancia de estas partículas comenzó a disminuir, hasta que fue tan pequeña que la probabilidad de que dos partículas de Materia Oscura se encontrasen y se aniquilasen se volvió

[14]Su nombre deriva del inglés *Weakly Interactive Massive Particles*, es decir, partículas masivas débilmente interactivas.

prácticamente nula. A dicha temperatura, conocida como temperatura de *freeze-out*, la abundancia de Materia Oscura superviviente se convirtió en un leve remanente, un mero fósil térmico, que ha llegado hasta nuestros días.

Este candidato a Materia Oscura ha gozado de gran acogida por los físicos teóricos desde que fuese propuesto alla por los años 70. El motivo de tal popularidad es que en el rango de masas mencionado, curiosamente, para reproducir la abundancia de Materia Oscura actual, se necesita que la interacción entre ésta y las partículas del Modelo Estándar sea justo del orden de la interacción electrodébil. Hecho, cuanto menos sorprendente, que se conoce como *Milagro WIMP*. En este rango de masas la sección eficaz necesaria para conseguir dicha abundancia es prácticamente independiente del valor de la masa de la partícula WIMP,

$$\langle \sigma v \rangle \simeq 2 \times 10^{-26}\,\mathrm{cm}^3/\mathrm{s} \backsim 1\,\mathrm{pb}\,. \tag{8.4}$$

Los detalles matemáticos y técnicos de este candidato a Materia Oscura se encuentran explicados en la Sec. 4.4.

8.3.3.2. Materia Oscura tipo FIMP

Complementariamente al caso WIMP, existe la Materia Oscura tipo FIMP[15] la cual jamás llegó al equilibrio térmico con el resto de partículas del Modelo Estándar. En este escenario la Materia Oscura fue producida por diversos procesos durante la época de enfriamiento del Universo, después del Big Bang, siendo nula en el origen de los tiempos. Cuando la temperatura del Universo fue suficientemente baja, esta producción se congeló, dejando un remanente que ha llegado hasta nuestros días. Este mecanismo de producción recibe el nombre de *freeze-in*[16] y está detallado en la Sec. 4.5.

La Materia Oscura FIMP no ha llegado a alcanzar la popularidad de la Materia Oscura tipo WIMP. Hay varios motivos para ello pero el principal es que debido a su baja intensidad de interacción es muy dificil buscar pruebas experimentales de su existencia.

[15]Nombre que deriva del ingles *Feebly Interactive Massive Particle*.

[16]El mecanismo de producción fue propuesto en Ref. [291]. Aunque en aquella época ni el mecanismo se conocía por dicho nombre, ni el candidato como FIMP.

8.4. Detección de Materia Oscura

Como hemos comentado en la Sec. 3.1, y resumido en Sec. 8.3.1, tenemos muchas evidencias de la existencia de a Materia Oscura. No obstante, no se ha conseguido realizar ninguna observación directa de estas elusivas partículas[17]. A pesar de esto, las técnicas de detección de Materia Oscura han avanzado mucho en los últimos años, poniendo cotas cada vez más restrictivas a la existencia de estas partículas aparentemente invisibles. Dentro del gran abanico de experimentos de detección, estos pueden clasificarse en dos grandes grupos: la *Detección Directa*[18] DD y la *Deteccion Indirecta*[19] ID.

8.4.1. Detección Directa

La idea de la Detección Directa (cuyos detalles técnicos se discuten en profundidad en la Sec. 5.1) fue propuesta por primera vez por Mark Goodman y Edward Witten [297]. Como la Materia Oscura no presenta cargas eléctricas, es imposible detectarla mediante técnicas electromagnéticas. No obstante, la existencia de colisiones entre la DM y los núcleos atómicos abre una puerta para su observación directa.

En general, esta clase de detecciones se realizan en experimentos ubicados bajo tierra. Ejemplos notables son Xenon1T [238] o LUX [330], los cuales están compuestos por grandes cantidades de Xenón. La colisión de la Materia Oscura con los átomos de Xenón produciría una excitación de estos últimos, que finalmente se traduciría en la emisión de un fotón. Hasta el momento, no se ha realizado ninguna detección en dichos experimentos, lo cual pone fuertes límites sobre los modelos de Materia Oscura, haciendo que los escenarios más simples y *naturales* estén prácticamente descartados.

[17] Existe una llamativa excepción: el experimento DAMA/Libra ha medido variaciones en la modulación solar que pueden ser interpretadas como Materia Oscura [317, 318]. No obstante, esta señal no está libre de controversia entre la comunidad científica ya que ningún otro experimento ha reportado absolutamente nada en el rango de masas en el que DAMA/Libra mide dicha señal.

[18] Del ingles *Direct Detection.*

[19] Del ingles *Indirect Detection.*

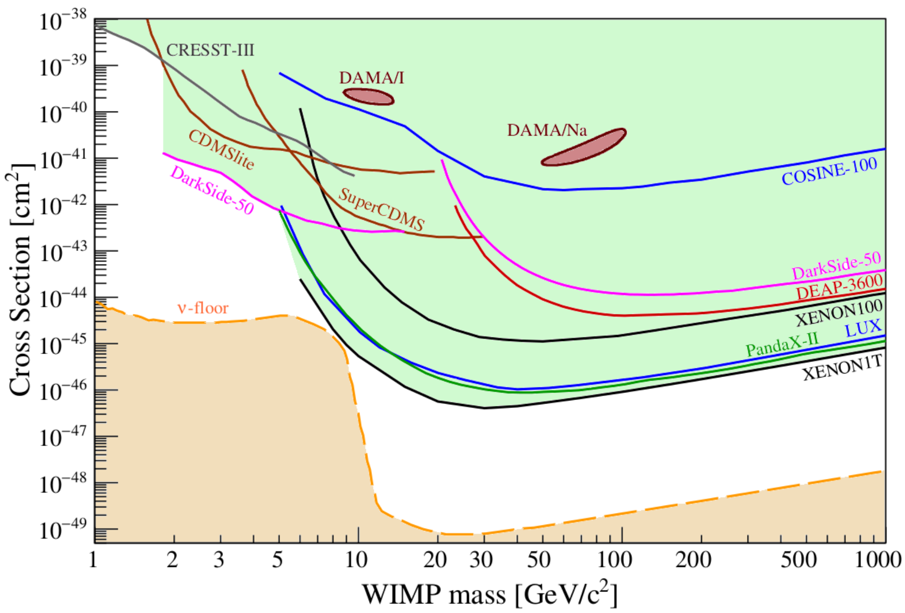

Figura 8.2: *Límites actuales a la sección eficaz de interacción de Materia Oscura con nucleones. La región verde está excluida por los experimentos de Detección Directa con un 90 % de intervalo de confianza. Las dos zonas rojas muestran las regiones en las que DAMA/LIBRA afirma haber observado Materia Oscura. La zona amarilla representa el suelo de neutrinos [339].*

Uno puede hacerse una idea del panorama actual de estos experimentos mirando la Fig. 8.2. En ella, la zona verde muestra los valores de la sección eficaz de Detección Directa, como función de la masa de la Materia Oscura, que ya han sido descartados por los experimentos. Por otro lado, para hacernos una idea de magnitud de la zona ya eliminada, podemos mirar lo cerca que se encuentra de ella la región amarilla. Esta región muestra lo que se conoce como *suelo de neutrinos*[20] [339] y representa la sección eficaz para la que los experimentos de detección comenzarán a observar colisiones producidas por los neutrinos. Realizar exclusiones mediante experimentos de Detección Directa en esta región es complicado, puesto que la señal de ambos tipos de colisión es indistinta. Las dos regiones rojas muestran las observaciones de DAMA/LIBRA en zonas totalmente excluidas por el resto de experimentos.

[20] En ingles conocido como *neutrino floor*.

8.4.2. Detección Indirecta

La observación directa de las colisiones de las partículas de Materia Oscura con los núcleos atómicos no es la única técnica para detectarla. Diferentes experimentos astronómicos llevan años intentando observar los posibles productos de las aniquilaciones de las partículas de Materia Oscura en los rayos cósmicos que nos llegan a la Tierra. Es posible distinguir entre tres tipos de flujos de partículas: fotones, neutrinos y partículas cargadas (como electrones, positrones, etc).

En general, de los diferentes flujos de partículas que llegan a la Tierra, los resultados más prometedores (en lo que a Materia Oscura se refiere) vienen de los fotones. Desde 2008 la colaboración Fermi-LAT analiza el flujo de fotones procedente de diferentes *galaxias enanas* [240, 241]. Hasta el momento el estudio se restringe a 15 ejemplares y por el momento los resultados no muestran ningún exceso en el flujo analizado que no pueda ser explicado por el Modelo Estándar de partículas. Esto pone cotas a modelos de nueva física en los cuales la Materia Oscura pueda aniquilarse a partículas que finalmente se desintegren en fotones, generalmente en el rango de masas $m_{\rm DM} \in (0{,}5, 500)$ GeV. No obstante, desde 2009 el mismo experimento ha estado reportando un exceso inexplicable de fotones procedente del centro galáctico[21]. Aunque su origen aún es desconocido, este exceso, que se observa a una energía ~ 3 GeV, puede ser explicado por diferentes modelos de Materia Oscura.

Por otro lado, las señales procedentes de flujos de antipartículas cargadas acotan de una forma mucho menos restrictiva los modelos de Materia Oscura. El problema con esta clase de flujos es su propagación desde el punto en el que son generados hasta la Tierra (donde finalmente los detectamos). Hoy en día existen diversos modelos para ello, pero su precisión aún tiene que ser perfeccionada para que los límites impuestos por esta clase de flujos sean realmente restrictivos.

En la Sec. 5.2 se ha realizado un análisis exhaustivo de la Detección Indirecta de Materia Oscura.

[21] Popularmente conocido como *Galactic Center γ-ray excess* (GCE) [386–395].

8.5. Dimensiones Extra

De entre las cuatro fuerzas fundamentales de la naturaleza, no cabe ninguna duda de que la gravedad es la más complicada de entender a nivel cuántico. A pesar de los muchos esfuerzos por parte de la comunidad científica, aún no tenemos una teoría cuántica para describirla. Por otro lado, la gravedad es la más débil de las interacciones fundamentales. Tal es el caso, que de existir nueva física a la escala gravitatoria, el Modelo Estándar se enfrentaría a un serio problema: las correcciones a la masa del bosón de Higgs son muy sensibles a la escala de la nueva física. Teniendo en cuenta la diferencia entre la escala de Planck[22] y la escala electrodébil, de aparecer nueva física a la escala gravitatoria las correcciones a la masa del Higgs serían enormes, requiriendo cancelaciones ajustadas entre distintos órdenes de teoría de perturbaciones para explicar el valor medido. A este fenómeno se le conoce como *problema de la jerarquía* (para un analisis más detallado del problema mirar la Sec. 1.6.1). Entre las diversas propuestas que se han realizado para intentar resolver este problema se encuentran las dimensiones extra.

8.5.1. Dimensiones Extra *Grandes* (LED)

El primer modelo de dimensiones extra que se propuso para dar solución al problema de la jerarquía fue *Large Extra-Dimensions* (LED) [427]. En este escenario se asume que las nuevas dimensiones tienen una forma similar a las tres espaciales ya conocidas, es decir, presentarían un aspecto plano. De acuerdo con el modelo LED, el tamaño de estas nuevas dimensiones sería finito o, en otras palabras, estarían compactificadas. Por otro lado, mientras que la gravedad se propaga libremente por el espacio 5-dimensional, el resto de campos del Modelo Estándar se encuentran confinados en unas hipersuperficies 4-dimensionales denominadas *branas*. Este hecho hace que la gravedad se diluya a través de las dimensiones extra, haciendo que en la brana (donde nosotros vivimos confinados) su intensidad parezca anómalamente débil. De este modo, la escala de la gravitación, que para nosotros es $M_{\mathrm{P}} = 1{,}22 \times 10^{19}$ GeV, en el espacio extra-dimensional completo sería M_D.

[22]La escala de la interacción gravitatoria.

Ambas escalas están relacionadas a través del radio de compactificación de las dimensiones extra (r_c):

$$M_{\mathrm{P}}^2 = M_D^{D-2}(2\pi r_c)^D. \tag{8.5}$$

Para el caso particular de 5 dimensiones, el espacio-tiempo queda definido en este modelo por la métrica:

$$ds^2 = \eta_{\mu\nu}dx^\mu dx^\nu + r_c^2 dy^2, \tag{8.6}$$

Donde la dimensión extra está representada por y. Este parámetro puede escogerse de manera que $M_5 \backsim$ TeV, resolviendo así el problema de la jerarquía. No obstante, si imponemos esta condición, el modelo LED 5-dimensional está excluido totalmente a día de hoy: agregar una única dimensión extra en LED predice correcciones de la ley de la gravitación universal que podrían observarse en distancias parecidas al tamaño del Sistema Solar. No obstante, aunque el modelo esté excluido para una única dimensión extra, con dos o más dimensiones es posible resolver el problema de la jerarquía sin entrar en contradicciones con la ley de la gravitación universal.

8.5.2. Dimensiones Extra Deformadas: Modelo de Randall-Sundrum

A pesar de que los modelos LED presentan diversos problemas, pusieron la semilla para modelos futuros muy interesantes. El caso más popular es el modelo propuesto por Lisa Randall y Raman Sundrum a finales de los años 90, conocido como *dimensiones extra deformadas* o *modelo de Randall-Sundrum* (RS) [76]. En dicho modelo, las nuevas dimensiones presentan curvatura, a diferencia de LED, donde eran planas. En el modelo original de RS el espacio extra-dimensional está delimitado por dos branas. Todos los campos de materia viven atrapados en una de ellas (brana *infrarroja* (IR), también llamada brana del TeV), mientras que la otra brana se encuentra vacía (brana *ultravioleta* (UV) o de Planck). Por otro lado, la gravedad se propaga libremente por el espacio extra-dimensional (comúnmente conocido como *bulk*). La geometría del modelo hace que los diferentes parámetros fundamentales con dimensión de masa sufran un proceso de deformación exponencial a lo largo del bulk, resolviendo así el problema de la jerarquía.

Concretamente, para el caso 5-dimensional (una única dimensión extra), la métrica que definiría este espacio tiempo vendría dada por

$$ds^2 = e^{-2kR|y|}\eta_{\mu\nu}dx^\mu dx^\nu - r_c^2 dy\,, \tag{8.7}$$

Donde k es la curvatura a lo largo de la dimensión extra y r_c su radio de compactificación. El factor exponencial que multiplica la parte 4-dimensional de la métrica recibe el nombre de factor de deformación. M_5 y M_{P} quedarían entonces relacionados mediante los dos parámetros libres de la teoría:

$$\bar{M_{\mathrm{P}}}^2 = \frac{M_5}{k}\left(1 - e^{-2k\pi r_c}\right)\,. \tag{8.8}$$

Vemos que hay una clara diferencia con el modelo LED: en RS $M_5 \backsimeq M_{\mathrm{P}}$. Sin embargo, la modificación que sufren los parámetros medidos en la brana IR, debido a la presencia del factor de deformación, resuelve el problema de la jerarquía para $k\,r_c \backsim 10$.

En RS la gravedad puede describirse a través del intercambio de gravitones no masivos 5-dimensionales, los cuales surgen de perturbaciones sobre la componente 4-dimensional de la métrica

$$G^{(4)}_{\mu\nu} = e^{-2kr_c|y|}(\eta_{\mu\nu} + 2M_5^{-2/3}h_{\mu\nu})\,. \tag{8.9}$$

La proyección de este campo 5-dimensional sobre las branas es equivalente a una torre de gravitones 4-dimensionales masivos, comúnmente conocidos como modos de Kaluza-Klein (KK). La escala efectiva de la interacción de estos gravitones 4-dimensionales con los campos confinados en la brana IR viene dada por

$$\Lambda \equiv \bar{M_{\mathrm{P}}} e^{-k\pi r_c}\,. \tag{8.10}$$

Por otro lado, cada gravitón de esta torre de partículas tiene una masa diferente que dependerá de los parámetros libres (k, r_c) del modelo y de su respectivo orden dentro de la torre. No obstante, establecida la masa del primer gravitón m_1, la masa del resto de gravitones queda totalmente fijada. La fenomenología de los modelos de RS puede ser descrita mediante los parámetros (Λ, m_1), en lugar de (k, r_c). Este hecho puede ser muy útil debido a su relación con observables fenomenológicos.

El modelo asume que la distancia entre las branas está fijada, pero no aporta ningún mecanismo para estabilizar este parámetro dinámicamente. La solución a este problema fue propuesta por Walter D. Goldberger y Mark B. Wise [444, 445]. Este mecanismo utiliza un nuevo campo escalar que se propaga libremente por el *bulk*, sometido a unos potenciales localizados en las branas. Por otro lado, el nuevo campo escalar se mezcla con el ya presente en el *bulk*, el graviescalar $G^{(5)}_{55}$ (el cual emerge de las perturbaciones sobre la parte 5-dimensional de la métrica). Al campo resultante de esta mezcla se le conoce como radión. Los mínimos de los potenciales en la brana IR y UV son diferentes, lo que genera un valor esperado de vacío para el radión. El tamaño de la quinta dimensión (r_c) está entonces relacionado con este valor esperado de vacio. La masa del radión no está determianda por los parámetros del modelo original, y representa un nuevo grado de libertad.

El modelo de RS ha gozado de gran popularidad desde que fue propuesto a finales de los 90's. La literatura sobre modelos de física más allá del Modelo Estándar desarrollados en este escenario es inmensa. En la Sec. 6.4 se ha realizado un análisis de los detalles técnicos del modelo.

8.5.3. Dimensiones extra tipo *Clockwork/Linear Dilaton*

Durante casi dos décadas lo modelos de RS fueron los únicos que resolvían el problema de la jerarquía mediante la introducción de dimensiones con curvatura. No obstante, en 2016 Gian Giudice y Matthew McCullough propusieron un nuevo modelo de dimensiones extra curvadas. Este nuevo modelo, propuesto en Ref. [430] y cuya fenomenología fue estudiada en Ref. [431], se conoce con el nombre de *Clockwork/Linear Dilaton* (CW/LD).

Dicho modelo, que fue encontrado como límite continuo de los modelos *Clockwork* discretos, puede caracterizarse a traves de la métrica:

$$ds^2 = e^{4/3kr_c|y|} \left(\eta_{\mu\nu} dx^\mu dx^\nu - r_c^2\, dy^2 \right) , \tag{8.11}$$

donde k y r_c representan la curvatura y el radio de compactificación de la quinta dimensión, respectivamente. Para determinados valores de los parámetros libres, el modelo es capaz de resolver el problema de la jerarquía.

El modelo CW/LD guarda ciertas similitudes con RS. En ambos casos el espacio 5-dimensional está delimitado por las branas IR y UV. El caso mínimo implica tener todo el Modelos Estándar confinado en la brana IR, mientras que la gravedad se propaga libremente por el bulk 5-dimensional. Sin embargo, hay diferencias notables con RS. En primer lugar, la relación entre M_5 y M_P en CW/LD viene dada por

$$M_\mathrm{P}^2 = \frac{M_5^3}{k}\left(e^{2\pi r_c} - 1\right) , \tag{8.12}$$

pudiendo ser esta del orden del TeV (al igual que en el caso LED). Por otro lado, el acoplamiento de los modos de Kaluza-Klein de los gravitones a las partículas localizadas en la brana es diferente para cada gravitón:

$$\frac{1}{\Lambda_n} = \frac{1}{\sqrt{M_5^3 \pi r_c}}\left(1 + \frac{k^2 r_c^2}{n^2}\right)^{-1/2} = \frac{1}{\sqrt{M_5^3 \pi r_c}}\left(1 - \frac{k^2}{m_n^2}\right)^{1/2} . \tag{8.13}$$

Este hecho hace que describir la fenomenología en base a Λ_n no sea tan útil como en RS. Otra diferencia notable es que hay una relación muy interesante entre el valor de la curvatura k y la masa del primer gravitón m_1, haciendo que ambos parámetros sean prácticamente idénticos.

En el caso CW/LD, el modelo original ya incluye un campo escalar que estabiliza el tamaño de la quinta dimension, el campo de dilatación (*dilaton*), $S = 2kr_c|y|$, de la métrica. La existencia de unos potenciales en las branas IR y UV permite fijar la posición de las branas de un modo similar a como se hacía en RS.

8.6. Metodología Utilizada

Antes de ponernos a hablar sobre los cuatro proyectos que conforman la presente Tesis, es necesario comentar las diferentes técnicas (tanto a nivel analítico como numérico) utilizadas en el desarrollo de los mismos.

A nivel analítico, la complejidad de los problemas estudiados ha requerido un profundo conocimiento de la teoría cuántica de campos. Se han utilizado los desarrollos perturbativos de dicha teoría para obtener las diferentes probabilidades de interacción utilizadas posteriormente en los estudios fenomenológicos. Los modelos aquí estudiados asumen Materia Oscura tipo WIMP y FIMP. En ambos casos, la evolución de la abundancia de Materia Oscura a lo largo de la historia térmica del Universo requiere resolver la Ecuación de Boltzman, que determina la evolución de sistemas fuera del equilibrio térmico. Por otro lado, se ha trabajado con dos modelos de dimensiones extra: Randall-Sundrum y Clockwork/Linear Dilatón. La fenomenología estudiada sobre estos modelos ha requerido un análisis exhaustivo de ambos escenarios.

Desde un punto de vista numérico, toda la fenomenología ha sido estudiada mediante lenguaje *C++*, mientras que su representación a nivel gráfico ha sido obtenida utilizando *python*. El análisis de la Detección Indirecta de Materia Oscura realizado en uno de los modelos estudiados ha requerido el uso de software más específico: *micrOMEGAs*, *SARAH*, *gamlike*, *pythia* y *MadGraph*. Por otro lado, todo el estudio de la Ecuación de Boltzman en los cuatro modelos se ha realizado mediante métodos numéricos implementados en lenguaje *C++*.

Finalmente, el enfoque fenomenológico que presenta esta Tesis ha implicado un contacto continuo con datos experimentales. El tratamiento de estos datos, así como las diferentes cotas de exclusión que han puesto sobre los diferentes modelos estudiados, ha requerido un uso de diversas técnicas estadísticas. Se han utilizado diferentes distribuciones de probabilidad (tales como la conocida χ^2), técnicas de Monte Carlo, etc.

8.7. Resultados y conclusiones de la Tesis

En está sección, vamos a realizar un breve resumen de los proyectos que conforman esta Tesis. Todos ellos pueden encontrarse completos en la Parte II.

8.7.1. Estudio de la Detección Indirecta del Modelo de *Portal de Neutrinos Estériles*

Uno de los grandes problemas abiertos en física de altas energías es la Materia Oscura, pero desde luego no es el único. Entre los diversos problemas que existen actualmente en el Modelo Estándar de partículas, uno de los más importantes es la masa de los neutrinos. El modelo predice una masa nula para ellos, no obstante, hace ya más de medio siglo se predijo un efecto denominado *oscilaciones de neutrinos* [89]. Este curioso fenómeno, que fue confirmado experimentalmente en 1999 [92], consiste en una oscilación en el sabor leptónico de los neutrinos. Las implicaciones de este hecho son muy profundas ya que únicamente puede suceder si al menos uno de los tres sabores de neutrinos es masivo[23]. No obstante, las cotas experimentales impuestas a la masa de estas partículas prácticamente invisibles son tan fuertes que su masa debe ser muy pequeña[24]. Este hecho potenció el desarrollo de modelos en los que la masa de los neutrinos era generada por mecanismos de tipo *balancín*[25] [112–116]. Hay diferentes versiones de estos modelos, en el *tipo I*, por ejemplo, se asume la existencia de neutrinos dextrógiros muy masivos que justifican la pequeña masa de los neutrinos del Modelo Estándar. La mezcla de los neutrinos levógiros con los dextrogiros da como resultado los autoestados de masa, prediciendo neutrinos con masas muy grandes y muy pequeñas.

La posibilidad de que el problema de la Materia Oscura y de la masa de los neutrinos estén relacionados motivó el desarrollo del conocido como[26] *portal de neutrinos estériles a Materia Oscura* [466–468]. Este modelo se ha estudiado por diversos autores, acotándolo utilizando la Detección Directa de Materia Oscura. No obstante, es un modelo muy interesante desde el punto de vista de la Detección Indirecta por varios motivos. Por un lado, la Detección Directa en este escenario no sucede al orden más bajo en teoría

[23] A pesar de que el fenómeno podría explicarse con un solo neutrino masivo, la observación del fenomeno tanto en neutrinos atmosfericos como solares requiere que al menos dos de los tres sabores de neutrinos sean masivos.

[24] El límite actual más fuerte viene dado por el experimento *Karlsruhe Tritio Neutrino* (KATRIN) [110].

[25] Modelo *seesaw* en inglés.

[26] El escenario más económico, la posibilidad de que los neutrinos estériles sean la Materia Oscura, fue propuesto en Ref. [465]. A día de hoy, esta posibilidad ha sido fuertemente estudiada y prácticamente descartada [244].

de perturbaciones de la teoría cuántica de campos. Este hecho hace que sus señales de Detección Directa sean bajas que en otros modelos, empeorando así los límites impuestos. Por otro lado, la conexión de los neutrinos estériles con los neutrinos activos hace que las aniquilaciones de Materia Oscura produzcan, como resultado de diversas desintegraciones, excesos de fotones y partículas cargadas. Todo esto lo convierte en el candidato perfecto para ser estudiado desde el punto de vista de la Detección Indirecta, tal como se ha llevado a cabo en la Ref. [1].

En este trabajo hemos analizado un modelo particular en el que, además de los neutrinos estériles, se asume la existencia de dos nuevos campos: uno escalar ϕ y otro fermionico Ψ. Estos campos son ambos singletes del Modelo Estándar, no obstante, están cargados respecto a un nuevo grupo de simetría, $G_{\rm dark}$, de tal forma que la combinación $\overline{\Psi}\phi$ es singlete de este nuevo grupo de simetría.

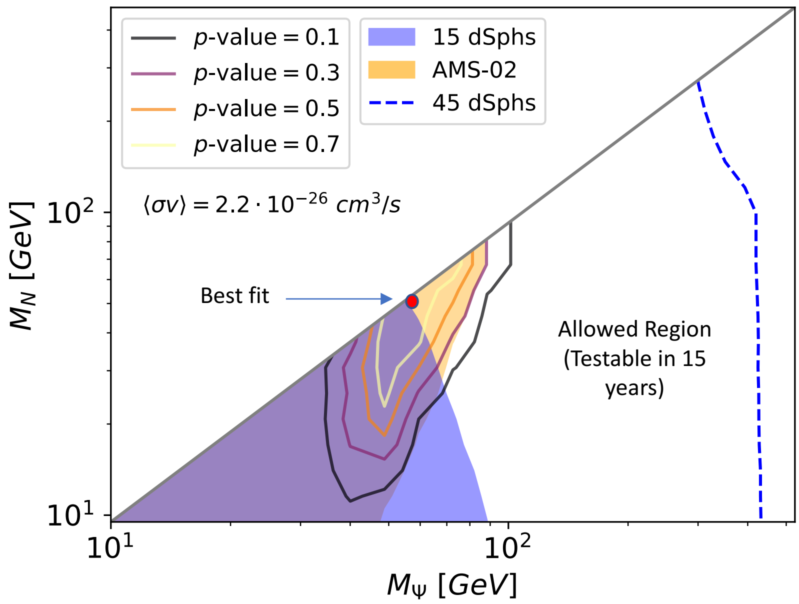

Figura 8.3: *Límites sobre el portal de neutrinos estériles en el espacio de masas. La región amarilla muestra los límites impuestos por los antiprotones mientras que la región azul son los límites impuestos por los fotones procedentes de las galaxias enanas. Los diferentes contornos muestran la zona en la que el modelo es capaz de reproducir el GCE. La línea discontinua azul muestra nuestra predicción sobre el límite de las galaxias enanas para los próximos 15 años.*

La más ligera de estas nuevas partículas *oscuras* (ϕ y Ψ) es estable si todas las particulas del Modelo Estándar, así como los neutrinos esteriles, son singletes de G_{dark}, independientemente de la naturaleza de este grupo de simetría. Como consecuencia, debido a su estabilidad esta partícula es un buen candidato a Materia Oscura. Por simplicidad, asumimos que G_{dark} es una simetría global a baja enería, en cualquier caso no esperamos cambios significantes en nuestro analisis fenomenológico si esta fuese local.

Los terminos más relevantes en el lagrangiano vienen dados por:

$$\begin{aligned}\mathcal{L} &= \mu_H^2 H^\dagger H - \lambda_H (H^\dagger H)^2 - \mu_\phi^2 \phi^\dagger \phi - \lambda_\phi (\phi^\dagger \phi)^2 - \lambda_{H\phi} (H^\dagger H)\,(\phi^\dagger \phi) \\ &- \left(\phi \overline{\Psi} (\lambda_a + \lambda_p \gamma_5) N + Y \overline{L}_L H N_R + \text{h.c.}\right) .\end{aligned} \tag{8.14}$$

Los acoplamientos de Yukawa Y entre los neutrinos dextrógiros N_R y el doblete leptónico del Modelo Estándar genera las masas para los neutrinos activos después de la ruptura espontanea de la simetría, a traves del mecanismo *balancín* de tipo I. Si bien se requieren al menos dos neutrinos estériles para generar las masas de neutrinos observadas en las oscilaciones, en nuestro análisis consideramos que solo una especie es más ligera que la Materia Oscura y, por lo tanto, relevante para la determinación de su abundancia y búsquedas indirectas. No obstante, los resultados son fáclmtente extendibles al caso en el que tenemos dos o más neutrinos estériles más ligeros que la Materia Oscura. Bajo el supuesto de que la Materia Oscura es descrita por Ψ (el análisis es igualmente valido en el caso de que la Materia Oscura sea ϕ) las masas del modelo cumplen la relación $m_N < m_\Psi < m_\phi$.

La Fig. 8.3 muestra los resultados finales de nuestro análisis. Fijando la masa del mediador escalar para obtener la abundancia de Materia Oscura mediante el mecanismo *freeze-out* (es decir $\langle \sigma\, v \rangle \sim 2 \times 10^{-26} cm^3/s$), la figura muestra los diferentes limites impuestos por las búsquedas de fotones y antiprotones en el espacio de masas (M_N, M_Ψ). Como ya hemos comentado, el experimento Fermi-LAT ha reportado un exceso de fotones inexplicable procedente del centro galáctico (GCE). El modelo estudiado predice un pequeño exceso de fotones que podría ser compatible con el GCE en ciertas zonas del espacio de parámetros. En nuestro analisis hemos asumidoque existen dos fuentes diferentes para el GCE: una astrofísica, responsable de la zona de alta energía del espectro de fotones, y otra procedente de las aniquilaciones de Materia Oscura, la cual explicaría la zona de baja energía del exceso,

$$\Phi = \Phi_{\rm astro} + \Phi_{\rm DM}\,. \tag{8.15}$$

Esta contribución astrofísica al flujo de fotones es siempre necesaria para reproducir el GCE, independientemente del modelo de Materia Oscura considerado. La zona en la que puede realizarse el ajuste del exceso de fotones del centro galactico está delimitada por los diferentes contornos que se observan en la figura (en la leyenda está indicado el p-valor asociado a cada contorno). No obstante, este aumento de fotones predicho por el modelo tiene que ser compatible también con el resto de medidas realizadas sobre los diferentes flujos de fotones. En concreto, el mismo experimento realiza medidas sobre los fotones procedentes de 15 galaxias enanas[27], la región sombreada en azul muestra la zona del espacio de parámetros de la teoría en la cual los resultados obtenidos no son compatibles con dichas mediciones al 90 % de intervalo de confianza.

Por otro lado, el modelo también predice un aumento del flujo de antiprotones. Este aumento se ha comparado con el flujo de antiprotones procedente del centro galáctico, el cual es medido en la actualidad por el experimento AMS-02.Los resultados obtenidos muestran que existen zonas en las cuales las predicciones del modelo no serían compatibles al 95 % de intervalo de confianza con lo observado experimentalmente (zona sombreada en amarillo en la figura). Por último, también se ha realizado un análisis del posible impacto de los resultados futuros el experimento Fermi-LAT. Basandonos en la mejora experimentada por la colaboración, hemos estimado que en 15 años se habrán detectado 45 galaxias enanas nuevas. Este hecho podría poner fuertes cotas al modelo estudiado (línea azul discontinua). Como comentario final, podemos decir que algunos modelos de Materia Oscura son capaces de explicar el exceso de fotones del centro galactico parcialmente[28]. En concreto, el modelo aquí estudiado consigue reproducirlo con una precisión muy alta. No obstante, los resultados futuros del experimento Fermi-LAT podrían excluir casi por completo la región del espacio de parámetros en la cual el GCE puede ser explicado por el modelo.

[27]Galaxias compuesta por varios millones de estrellas. En contraposición tenemos las galaxias normales, compuestas por varios miles de millones.

[28]Hasta el momento todos los modelos necesitan asumir que parte del exceso es consecuencia a fenomenos astrofísicos.

8.7.2. Materia Oscura Escalar Mediada por Gravedad en Dimensiones Extra Deformadas

Todas las evidencias que tenemos hoy en día acerca de la existencia de la Materia Oscura están relacionadas con la interacción gravitatoria. Este hecho induce a pensar en la posibilidad de que las partículas de Materia Oscura únicamente interactúen gravitatoriamente. Esta idea tan natural ha sido explorada ya para los candidatos de tipo WIMP sin demasiado exito: la intensidad de la interacción gravitatoria es muy débil y hace imposible obtener la cantidad de abundancia de Materia Oscura que se observa en la actualidad (al menos en el escenario WIMP). No obstante, ¿que ocurre si pensamos en más de 4 dimensiones? Esta es la idea que inspiró la Ref. [2].

En dicho artículo tratamos de explorar si es posible obtener la abundancia de Materia Oscura actual, asumiendo que es de tipo WIMP escalar, únicamente mediante interacción gravitatoria y bajo el supuesto de un Universo 5-dimensional de tipo Randall-Sundrum. En el escenario descrito, la Materia Oscura y el Modelo Estándar viven confinados en la brana infrarroja. Ambos tipos de materia interactúan únicamente a través de la gravedad, cuya proyección sobre la brana IR es equivalente a una torre de gravitones 4-dimensionales masivos (torre de Kaluza-Klein).

El modelo queda descrito en base a cuatro parámetros físicos: la escala de la interacción de los gravitones 4-dimensionales con la materia, Λ; la masa del primer gravitón de la torre de KK, m_1; la masa del candidato a Materia Oscura, $m_{\rm DM}$ y la masa del radión, m_r. Nuestro estudio muestra que cuando $m_r < m_{\rm DM}$ y, en consecuencia, el canal de aniquilación a radiones esta abierto, el valor de m_r es prácticamente irrelevante para la fenomenología. Respecto a la aniquilación de la Materia Oscura a partículas del Modelo Estandar a traves del intercambio de radiones virtuales, esta sección eficaz únicamente es relevante cerca de la resonancia $m_{\rm DM} \backsim m_r/2$. Por lo tanto, en el estudio fenomenológico realizado hemos fijado la masa del radion y nos hemos centrado en el resto de parámetros libres del modelo.

El método seguido para el análisis del modelo ha sido la construcción de una malla bidimensional con diferentes valores de los parámetros $(m_{G_1}, m_{\rm DM})$. Para cada uno de los puntos de este mallado hemos buscado

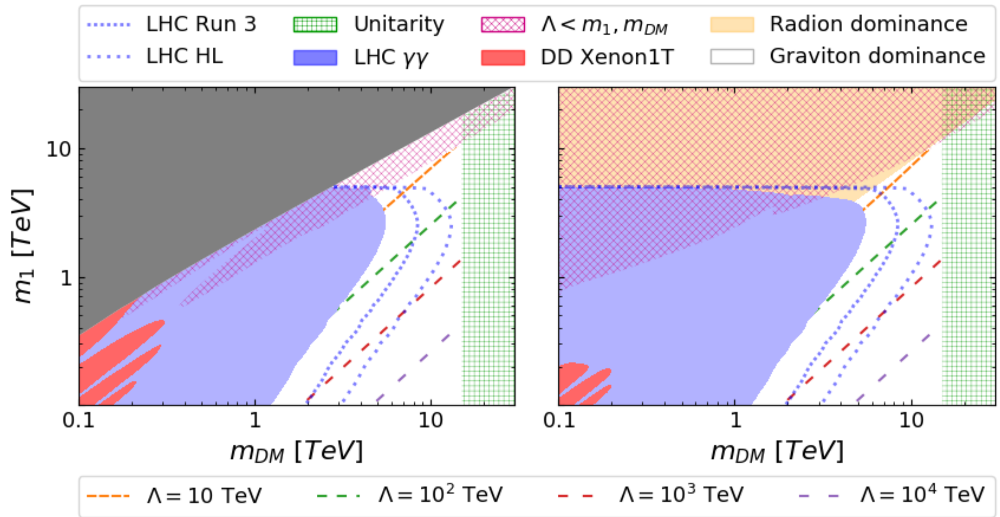

Figura 8.4: *Región en el plano* (m_{DM}, m_1) *para la cual* $\langle \sigma v \rangle = \langle \sigma_{\text{fo}} v \rangle$. *La gráfica de la izquierda muestra el caso sin radión, mientras que en la de la derecha se ha considerado* $m_r = 100$ *GeV. Las líneas discontinuas muestran los diferentes valores de* Λ *en el plano* (m_{DM}, m_1) *para los cuales se consigue la abundancia actual de Materia Oscura. La zona gris muestra la región en la cual es imposible conseguir la abundancia de Materia Oscura, independientemente del valor de* Λ. *Por otro lado, la región naranja nos indica los puntos en los que la abundancia se consigue gracias a los canales de interacción en los que interviene el radión. Respecto a los límites sobre el modelo: la zona de cuadraditos verde representa el límite de unitariedad; la zona de cuadraditos rosa representa la zona en la que la teoría efectiva deja de tener validez, es decir* $\Lambda < m_1$; *la zona roja representa los límites impuestos por el experimento Xenon1T sobre la sección eficaz de Detección Directa; la región azul es la zona eliminada por las búsquedas de resonancias en el LHC usando los datos de 36 fb*$^{-1}$ *at* $\sqrt{s} = 13$ *TeV. Finalmente, las líneas punteadas son las predicciones de exclusión para las fases Run-III (con* ~ 300 *fb*$^{-1}$*) y High Luminosity (con* ~ 3000 *fb*$^{-1}$*) del LHC.*

si existe algún valor de Λ para el cual se obtiene la abundancia de Materia Oscura actual (es decir, para $\langle \sigma v \rangle \backsimeq \langle \sigma v \rangle_{\text{fo}} = 2 \times 10^{-26}\,\text{cm}^3/\text{s}$). De este modo, para cada punto del mallado los tres parámetros libres $(m_1, m_{\text{DM}}, \Lambda)$ quedan totalmente definidos. Este análisis nos permite establecer diferentes límites teóricos y experimentales en el espacio de masas del modelo.

En la Fig. 8.4 pueden verse los resultados finales del análisis fenomenológico sobre el modelo. En la parte izquierda se ha explorado el caso sin radión, asumiendo que podría encontrarse algún método alternativo para estabilizar el radio de la quinta dimensión. Por otro lado, en la parte derecha se ha considerado que la masa del radión es $m_r = 100$ GeV (es importante recordar que la fenomenología no se ve afectada por el valor de esta masa). La zona sombreada en gris es la región en la que no es posible obtener la abundancia actual de Materia Oscura para ningún valor de Λ, mientras que la zona naranja representa la región del espacio de parámetros en la que la abundancia se consigue gracias a las contribuciones de los canales de interacción radiónicos. La zona sombreada con cuadraditos verdes se conoce como límite de unitariedad y representa el punto a partir del cual la sección eficaz de interacción es tan alta que la teoría de campos deja de tener sentido, esto sucede para[29] $\sigma > 1/s$. Además de este límite, existe otra restriccion teórica: si $\Lambda < m_{\rm DM}, m_1$ la teoría efectiva que describe la interacción de estos campos cuánticos deja de tener sentido (ya que deberían estar integrados). Esto ocurre en la región de cuadraditos rosa.

Hasta el momento, hemos hablado de las diferentes restricciones al modelo por motivos teóricos, pero estos no son los únicos límites que pueden establecerse: los actuales experimentos de Detección Directa y las búsquedas de resonancias en los experimentos ATLAS y CMS del LHC pueden aportar mucha información a nuestro análisis. De este modo, las zonas sombreadas en rojo representan los puntos en los que la sección eficaz de Detección Directa está ya excluida por los actuales experimentos. Por otro lado, la zona azul es la excluida por las búsquedas de resonancias (gravitones 4-dimensionales en nuestro caso) en el LHC, se han utilizado los datos tomados a $\sqrt{s} = 13$ TeV con 36 fb^{-1} en el canal $\gamma\gamma$. Las dos líneas punteadas muestran nuestra predicción sobre los límites futuros que serán impuestos por el LHC después de las futuras fases *Run-3* (con $\sim$ 300 fb^{-1}) y *High Luminosity* (con $\sim$ 3000 fb^{-1}), en el caso de que no se detecte ninguna resonancia.

El estudio realizado muestra que, en las regiones no excluidas del espacio de parámetros, la fenomenología está dominada por los canales de interacción relacionados con los gravitones. En dichas regiones, de acuerdo con nuestro análisis, los canales de interacción radiónicos siempre son subdominantes. Para ser más exactos, la abundancia se consigue gracias a la aniquilación de Materia Oscura directamente en gravitones.

[29]En el escenario WIMP las partículas de Materia Oscura tienen una velocidad relativa muy pequeña. Este hecho implica que $s \simeq m_{\rm DM}^2(4+v_{\rm rel}^2)$, donde $v_{\rm rel} \ll 1$ es la velocidad relativa de las partículas de Materia Oscura. Además, para conseguir la abundancia de Materia Oscura observada en la actualidad debe cumplirse $\sigma = \sigma_{\rm fo}$. Como consecuencia, este límite se convierte en un límite sobre la masa de la Materia Oscura $m_{\rm DM}^2 \lesssim 1/\sigma_{\rm fo}$. Por lo tanto, enel plano de masas ($m_{\rm DM}$, m_1) la zona excluida por unitariedad aparece como una linea vertical.

Aunque ya se habían realizado análisis similares en Randall-Sundrum, este trabajo es el primero que tiene en cuenta los canales de aniquilación de Materia Oscura directamente a gravitones en regiones tan altas del espacio de masas (varios TeV). Así mismo, se ha estudiado un diagrama totalmente olvidado en la literatura hasta el momento: la aniquilación a gravitones sin mediador, procedente del desarrollo a segundo orden del lagrangiano de interacción. Aunque el impacto de este diagrama sobre la fenomenología no cambia drásticamente los resultados, debe ser añadido por consistencia ya que es del mismo orden que el resto de diagramas estudiados. Por otro lado, cabe destacar que este análisis únicamente se ha realizado para Materia Oscura escalar. No obstante, en la Ref. [5] que está actualmente en trámites de publicación, se analizan los casos de Materia Oscura fermiónica y vectorial. En este estudio se ve que la Materia Oscura de tipo fermionico está claramente desfavorecida respecto a la escalar y vectorial ya que el canal dominante (la aniquilación directamente a gravitones) está más suprimido que en el resto de casos.

8.7.3. Materia Oscura Mediada por Gravedad en Dimensiones Extra Tipo *Clockwork/Linear Dilaton*

Analizadas las implicaciones de la existencia de Materia Oscura tipo WIMP con interacciones puramente gravitatoria en el escenario de Randall-Sundrum, la pregunta de que ocurriría en el novedoso Clockwork/Linear Dilatón casi surge de forma natural. Esta idea inspiró la Ref. [3]. La estructura de este escenario es diferente a la que teníamos en RS: la torre de KK de gravitones masivos en este caso tiene una separación muy pequeña y variable. Este hecho dificulta en gran medida el análisis numérico de su fenomenología.

A nivel conceptual, la estrategia para abordar el modelo es idéntica a la empleada en el caso RS. La gran diferencia con el modelo anterior son los parámetros elegidos para estudiar la fenomenología. En CW/LD los acoplamientos de los gravitones 4-dimensionales masivos al resto de partículas dependen del orden del gravitón dentro de la torre. Por ello, es más útil caracterizar el modelo en función de M_5 directamente, en lugar de usar los acoplamientos efectivos Λ_n de los gravitones 4-dimensionales. Por otro lado, la masa del primer gravitón coincide prácticamente con el valor de la curvatura a lo largo de la quinta dimensión $m_1 = k$. Otra diferencia notable entre ambos escenarios es la estabilización del tamaño de la dimensión extra. En RS es necesario introducir un nuevo campos escalar en el *bulk* con el fin de estabilizar dinamicamente r_c. En cambio, en CW/LD el dilatón presente en la métrica puede utilizarse para escribir los potenciales en la brana y estabilizar así el tamaño de la quinta dimensión. En este caso, la masa del radión (modo cero de la torre de dilatones 4-dimensionales) está fijada por los parámetros fundamentales del modelo (ya que deriva directamente de la métrica). No obstante, hay diferentes formas de realizar la estabilización usando el dilatón, el caso más simple es asumir que la tensión de las branas es infinita. Este escenario, recibe el nombre de límite rigido.

La Fig. 8.5 muestra los diferentes límites obtenidos para este escenario. Análogamente al caso RS, M_5 se ha utilizado para fijar la abundancia actual de Materia Oscura para cada punto del espacio $(m_{\rm DM}, k)$. Los diferentes límites estudiados son los mismos que en el caso anterior: la región de cuadraditos rosa muestra los límites de la teoría efectiva $(M_5 < k, m_{\rm DM})$, la región de cuadraditos verdes el límite de unitariedad $(m_{\rm DM} \gtrsim 1/\sqrt{\sigma_{\rm fo}})$ y, finalmente, la zona sombreada en azul los límites impuestos por el LHC. En el caso de los límites experimentales, debido a la proximidad de las resonancias en la torre de gravitones, el límite más estricto impuesto por el LHC viene de las búsquedas en el espectro continuo de energías, en lugar de las búsquedas de resonancias. Estos límites han sido calculados usando los datos de 36 fb^{-1} a $\sqrt{s} = 13$ TeV para el canal $\gamma\gamma$ [431]. Finalmente, cabe destacar que, en este caso, los límites impuestos por las búsquedas de Detección Directa de Materia Oscura corresponden a valores de $(m_{\rm DM}, k)$ menores que los mostrados en la Figura.

Otra diferencia notable con el caso RS es que aquí no solo hay que considerar el radión en la fenomenología, si no también toda la torre de KK de los dilatones. No obstante, en CW/LD el radión y los dilatones derivan directamente de la métrica del modelo, no es necesario un mecanismo externo para estabilizar el tamaño de la quinta dimensión. Este hecho hace que la masa de los mismos este intrínsecamente ligada a los parámetros fundamen-

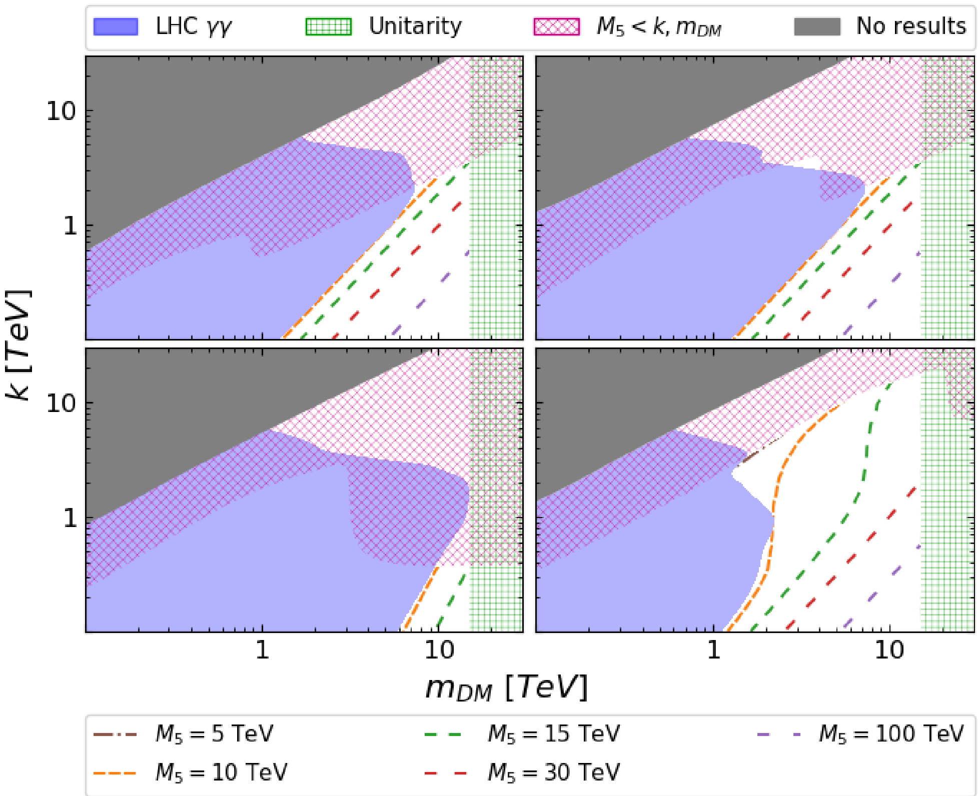

Figura 8.5: *Región en el plano $(m_{\rm DM}, k)$ para la cual $\langle\sigma v\rangle = \langle\sigma_{\rm fo} v\rangle$. Las gráficas superiores muestran los resultados para el caso de Materia Oscura escalar, la inferior izquierda el caso fermiónico y la inferior derecha el vectorial. La gráfica superior izquierda muestra las diferentes zonas de exclusión teniendo en cuenta únicamente la interacción con gravitones. Por otro lado, en la gráfica superior derecha se han considerado ambas, la interacción mediante gravitones y mediante dilatones, para el caso de Materia Oscura escalar. En los casos fermiónico y vectorial no se muestra el caso sin dilatones ya que la contribución de los mismos es despreciable y no varía los resultados. Las líneas discontínuas muestran los diferentes valores de M_5 en el plano (m_{DM}, k) para los cuales se consigue la abundancia actual de Materia Oscura, mientras que la zona gris muestra la región en la cual es imposible conseguir dicha abundancia, independientemente del valor de M_5. Respecto a los límites sobre el modelo: la zona de cuadraditos verde representa el límite de unitariedad ($m_{\rm DM} \gtrsim 1/\sqrt{\sigma_{\rm fo}}$); la región de cuadraditos rosa representa el área en la que la teoría efectiva deja de tener validez ($M_5 < k, m_{DM}$) y, finalmente, la región azul representa los límites impuestos por las búsquedas no-resonantes en el LHC usando los datos de 36 fb^{-1} a $\sqrt{s} = 13$ TeV para el canal $\gamma\gamma$ [431].*

tales del modelo, sin agregar de este modo ningún grado nuevo de libertad al espacio de parámetros de la teoría.

En este trabajo se han analizado los tres posibles tipos de Materia Oscura: escalar, fermiónica y vectorial. Las dos figuras superiores corresponden al caso escalar sin tener en cuenta la torre de radión y dilatones (izquierda) y teniéndola en cuenta (derecha), respectivamente. Este es el único caso en el que los dilatones juegan un papel importante en la fenomenología del modelo y por ello merece la pena mostrar cuál es su impacto sobre los resultados finales. Las gráficas inferiores corresponden al caso fermiónico (izquierda) y al caso vectorial (derecha). Se puede ver claramente que el caso fermiónico está desfavorecido respecto a los otros dos. Este hecho se debe a que en el caso fermiónico el canal dominante, la aniquilación de Materia Oscura directamente a gravitones, sufre una supresión debido al momento angular total.

El análisis llevado a cabo en este trabajo representa el primer estudio fenomenológico del modelo CW/LD con presencia de Materia Oscura. Los resultados anteriores, al igual que en RS, son prometedores en el sentido de que toda la región no excluida podrá ser analizada en los próximos años por el LHC. Como comentario final sobre la Materia Oscura tipo WIMP púramente gravitatoria, podemos decir que en ambos escenarios es posible reproducir la abundancia actual en el rango $m_{\rm DM} \in [1, 10]$ TeV. No obstante, los valores necesarios, tanto de Λ en RS como de M_5 en CW/LD, para ello son excesivamente grandes como para resolver el problema de la jerarquía.

8.7.4. Materia Oscura FIMP en Dimensiones Extra Deformadas

Hasta el momento, todos los modelos analizados consideran partículas tipo WIMP. No obstante, la Materia Oscura tipo FIMP es muy interesante para el caso en el que la interacción es puramente gravitatoria. En el último proyecto incluido en esta Tesis hemos explorado la posibilidad de reproducir la abundancia de Materia Oscura actual utilizando partículas FIMP en un escenario tipo RS [4]. Este caso plantea complicaciones matemáticas y numéricas muy diferentes al caso WIMP. Entre estos problemas, el más importante es que la abundancia final predicha por el modelo depende en gran medida de las condiciones iniciales. Este hecho hace que, mientras que en el caso WIMP[30] la abundancia actual se reproduce para un valor constante de la sección eficaz de interacción ($\langle \sigma v \rangle = \langle \sigma_{\rm fo} v \rangle$), en el caso FIMP es necesario resolver siempre la ecuación diferencial que determina su evolución, la conocida como ecuación de Boltzmann.

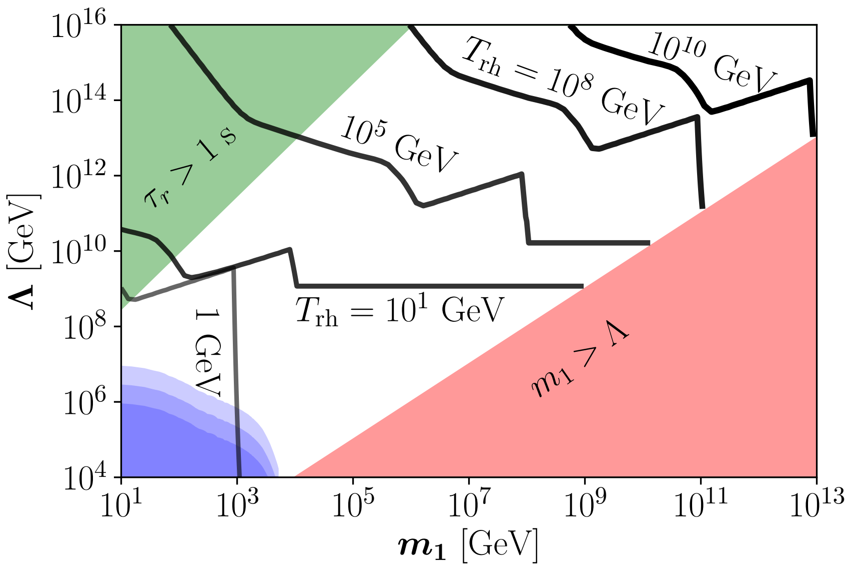

Figura 8.6: *Valores de la temperatura de reheating (lineas negras) para los cuales un determinado valor de la escala de interacción en la brana y la masa del primer graviton reproducen la abundancia de Materia Oscura actual para $m_{DM} = 1$ MeV y $m_r = m_1/10^3$. La zona azul representa la región excluida por las búsquedas de resonancias del LHC. La región roja muestra el límite de la teoría efectiva $m_1 > \Lambda$. Finalmente, la región verde muestra la zona en la que el valor de la vida media del radión entra en conflicto con las observaciones de la Nucleosíntesis del Big Bang.*

Por otro lado, aquí la abundancia también tiene una fuerte dependencia con un nuevo parámetro: la temperatura máxima del Universo, conocida como temperatura de *reheating* ($T_{\rm rh}$). Debido a la complejidad del espacio de parámetros, el analisis en este escenario se ha llevado a cabo para un valor determinado de la masa de la Materia Oscura: $m_{DM} = 1$ MeV, no obstante, los resultados son similares para otros valores m_{DM}. En la Fig. 8.6 se muestran los valores necesarios de la temperatura de reheating para obtener la abundancia observada. La región azul sombreada muestra los límites experimentales impuestos por las búsquedas de resonancias en el

[30] Como consecuencia del *milagro WIMP*.

canal $pp \to G_1 \to \gamma\gamma$ en el LHC (y las dos predicciones para las futuras etapas del experimento). Por otro lado, los límites teóricos en este escenario vienen determinados por la validez de la teoría efectiva (región roja) y la *Nucleosíntesis del Big Bang*. Este último límite se traduce en una restricción sobre la vida media de los gravitones y del radión: si la $\tau > 1$ s se podrían producir modificaciones en las observaciones sobre la Nucleosíntesis del Big Bang que deberían estar reflejadas en los datos experimentales actuales. En los modelos analizados anteriormente, este límte no aparecia ya que la vida media de los gravitones y radion/dilatones siempre era mayor que 1 segundo.

A la vista de los resultados obtenidos, vemos que el caso FIMP está mucho menos excluido que el caso WIMP en el escenarios de RS y que la abundancia de Materia Oscura actual se consigue en una gran región muy amplia del espacio de parámetros. A pesar de ello, los valores obtenidos para los parámetros libres de la teoría están lejos de resolver el problema de la jerarquía. Por otro lado, los experimentos actuales aún no son capaces de explorar los parámetros típicos de los modelos FIMP. No obstante, el hecho de que los modelos de Materia Oscura tipo FIMP sean capaces de explicar la abundancia actual en un rango del espacio de parámetros tan amplio es una gran motivación para el futuro desarrollo de experimentos. Actualmente estamos trabajando en el estudio análogo para el caso CW/LD.

8.7.5. Conclusión

Nuestro escaso conocimiento acerca de la naturaleza de la Materia Oscura hace que el conjunto de modelos que pueden explicar las evidencias actuales sea enorme. Esta Tesis ha contribuido a explorar parte de estos modelos y acotar un poco más lo que sabemos de ella, estudiando la fenomenología de diferentes candidatos. En general, los resultados obtenidos hacen que esperemos con ansia los resultados de los experimentos futuros, tanto en materia de Detección Indirecta, como en búsquedas del LHC. La relevancia de estos futuros datos es tal que en los próximos años la existencia de los candidatos de tipo WIMP puede verse corroborada o seriamente comprometida. Por otro lado, la débil interacción de los candidatos de tipo FIMP hace que su futuro experimental sea bastante más incierto. Como comentario final, es cierto que los modelos aquí estudiados representan una ínfima parte de todo el abanico de posibilidades existentes en la actualidad para explicar este escurridizo tipo de materia. No obstante, espero que hayan arrojado algo de luz sobre tan oscuro misterio.